

UNIVERSITY OF OKLAHOMA

GRADUATE COLLEGE

CONCISE SYNTHESIS METHODS TO AMINOSTEROLS AND STEROL N-  
GLYCOSIDES FOR THE DEVELOPMENT OF NEW OSW-1-DERIVED  
SCAFFOLDS

A DISSERTATION

SUBMITTED TO THE GRADUATE FACULTY

in partial fulfillment of the requirements for the

Degree of

DOCTOR OF PHILOSOPHY

By

CORI A. MALINKY  
Norman, Oklahoma  
2020

CONCISE SYNTHESIS METHODS TO AMINOSTEROLS AND STEROL N-  
GLYCOSIDES FOR THE DEVELOPMENT OF NEW OSW-1-DERIVED  
SCAFFOLDS

A DISSERTATION APPROVED FOR THE  
DEPARTMENT OF CHEMISTRY AND BIOCHEMISTRY

BY THE COMMITTEE CONSISTING OF

Dr. Anthony Burgett, Chair

Dr. Edgar O'Rear

Dr. Daniel Glatzhofer

Dr. Adam Duerfeldt

Dr. Bayrammurad Saparov

© Copyright by CORI MALINKY, 2020  
All Rights Reserved.

*To my loving wife and best friend, Becky, whom without I could not continue to be a dreamer of dreams. To my mother, my sister, and my father, I offer this as evidence that every good deed contributes to a good outcome.*

## **Acknowledgements**

This adventure began in the summer before my official start date, with Dr. Anthony Burgett accepting me into his lab. At the beginning of this dissertation, I want to thank him for the mentorship he has provided; thank you for all the times you helped me believe in myself and provided a consistent example of patience. I would also like to thank my graduate committee, Dr. Edgar O'Rear, Dr. Daniel Glatzhofer, Dr. Adam Duerfeldt, and Dr. Bayram Saparov, for their advice and wisdom throughout this tremulant adventure.

I would like to especially thank Dr. Anh Le-McClain for being my partner-in-crime and for teaching my hands to be steady and my head to be clear while doing lab work. A special thanks to Ryan Bensen, Zack Severance, and Gianni Manginelli for following this adventure with me and providing a sense of brotherhood.

Finally, I would like to thank all the core-faculty members within the department, Dr. Steven Foster and Dr. Doug Powell, who have provided me with above-and-beyond training. A special thank you to Dr. Susan Nimmo, for teaching me everything I know about NMR and for all the advice you have given me. Lastly, I would like to thank Dr. Catherine Mintler for your excellent edits of my personal essays to the Tillman Foundation and for helping me articulate the story behind this adventure.

## Table of Contents

Acknowledgements .....	v
List of Tables .....	x
List of Figures .....	xiii
Abstract .....	xxiv
Chapter 1: Introduction to the oxysterol-binding protein family and the natural product compound OSW-1 .....	1
1.1. Oxysterol-Binding Protein (OSBP/ORPs) Family .....	2
1.1.1. Identification of oxysterol-Binding Proteins (OSBP/ORPs) as possible druggable therapeutic targets .....	2
1.1.2. Oxysterol-binding protein (OSBP/ORPs) family characteristics: .....	3
1.1.3. Oxysterol-binding proteins as druggable therapeutic targets .....	5
1.1.4. Potential targeting of Oxysterol-Binding Protein (OSBP) for prophylactic antiviral drug development .....	6
1.1.5. Precision targeting of OSBP-related protein 4 (ORP4) as anticancer agent .....	8
1.2. Overview of synthesis and biological activity of OSW-1-derived analogs .....	9
1.2.1. OSW-1 derived analogs consisting of side chain and D-ring modifications .....	10
1.2.2. OSW-1 analogs consisting of acyl modifications .....	24
1.2.3. OSW-1 analogs consisting of disaccharide modifications .....	32
1.2.4. Summary of OSW-1 reported SAR and drug development potential .....	40
1.2.5. Objective and relevance of this body of work .....	41

Chapter 2: New methods for formation of aminosterols and N-glycosides: a concise synthesis of C22-N-glycoside-linked OSW-1-derived compound .....	43
2.1. Introduction .....	44
2.2. Results:.....	46
2.2.1. Predicted model of OSW-1 as it exists within the OSBP/ORP oxysterol binding pocket.....	46
2.2.2. Binding-model guided development of a new simplified, E-ring OSW-1 scaffold through a three-component synthesis approach. ....	51
2.2.3. Overview of the new OSW-1-related chemistry research performed .....	53
2.2.4. A concise route for the synthesis of C22-aminosterols:.....	55
2.3. Discussion.....	81
2.4. Conclusions and future work.....	85
2.5. Experimental and supplemental information.....	86
Chapter 3: A convenient two-component approach to functionalized 22-aminosterols .....	167
3.1. Introduction .....	168
3.1.1. Importance of developing approaches and methods toward aminosterol scaffolds.....	169
3.1.2. The ene and Prins reactions.....	170
3.1.3. Lewis acid effects on the imino-ene and aza-Prins reactions .....	173
3.2. Results.....	175
3.2.1. Atypical synthesis of functionalized N-alkyl aryl sulfonyl imines .....	175
3.2.2. Two-component approach to functionalized 22-aminosterols.....	178

3.2.3. Probing mechanism of imino-ene/aza-Prins reaction through Lewis acid screening.....	180
3.3. Discussion.....	182
3.4. Conclusions and future work.....	185
3.5. Experimental and supporting information.....	186
Chapter 4: Structure-activity relationships of ligand binding to oxysterol-binding protein (OSBP) and OSBP-related protein 4 (ORP4).....	
4.1. Introduction .....	223
4.1.4. Oxysterol derivation to better define OSBP/ORP ligand binding .....	223
4.2. Results:.....	225
4.2.5. Synthesis of structurally modified oxysterol derivatives .....	225
4.2.6. OSBP and ORP4 binding activity of structurally modified oxysterol side chain derivatives .....	226
4.3. Discussion.....	228
4.4. Conclusions and future work.....	229
4.5. Experimental and supporting information.....	229
Chapter 5: Synthesis of characterization of Oxysterol-binding protein (OSBP) targeting anti-viral compound, TTP-8307.....	
5.1. Introduction .....	263
5.1.1. TTP-8307 as OSBP-targeting anti-viral compound .....	263
5.2. Results.....	263
5.2.2. Synthesis and first full characterization of TTP .....	263



5.2.3. Synthesis and characterization of oxazole containing TTP-8307 derivative	266
5.3. Discussion	267
5.3.4. Mechanistic analysis of imidazole and oxazole under Radziszweski	
reaction conditions	267
5.4. Conclusions and future work	270
5.5. Experimental and supporting information	270
Chapter 6: Closing remarks and future work	294
6.1. Development of three-component approach to OSW-1-derived scaffolds	295
6.2. Future development of three-component approach to OSW-1-derived scaffolds	
	297
List of Compounds	299
References	301
Vitae	323

## List of Tables

Table 1-1. OSW-1 derived analogs consisting of side chain derivatization for SAR studies on various cell lines, reported as growth inhibitory binding constant ( $GI_{50}$ ) values in nM concentration. C20 is in *S*-configuration unless otherwise noted.  $TCS_{50}$  = tumor cell survival. %GI = percent growth inhibition. Literature references reported next to the entry number. AGS = stomach cancer cell line. 7404 = liver carcinoma cells. CEM = T-lymphoblastic leukemia cell line. MDAMB231 = breast carcinoma cell line. MCF7 = breast carcinoma cell line. K562 = chronic myelogenous leukemia cell line. ARN8 = melanoma cell line. G361 = malignant melanoma cell line. HeLa = epitheloid carcinoma cell line. Jurkat T = human T cell lymphoblast-like cell. HOS = osteosarcoma cell line. A549 = lung carcinoma cell line. NIH3T3 = mouse fibroblast. P388 = mouse leukemia. RKO = colon carcinoma. .... 13

Table 1-2. OSW-1 derived analogs consisting of acyl derivatization for SAR studies on various cell lines with phenotypic results reported as growth inhibitory binding ( $GI_{50}$ ) values in nM concentration. C20 is in *S*-configuration unless otherwise noted. MDAMB231 = breast carcinoma cell line. Jurkat T = human T cell lymphoblast-like cell. CRL1999 = human aorta fibroblast cell line..... 26

Table 1-3. OSW-1 derived analogs consisting of modifications to the disaccharide for SAR studies with phenotypic response reported as growth inhibitory binding ( $GI_{50}$ ) values in nM concentration. C20 is in *S*-configuration unless otherwise noted.  $*TCS_{50}$  = tumor cell survival.  $**\%GI$  = percent growth inhibition. CEM = T-lymphoblastic leukemia cell line. MCF7 = breast carcinoma cell line. K562 = chronic myelogenous leukemia cell line. ARN8 = melanoma cell line. G361 = malignant melanoma cell line.

HeLa = epitheloid carcinoma cell line. Jurkat T = human T cell lymphoblast-like cell.	
HOS = osteosarcoma cell line. A549 = lung carcinoma cell line. NIH3T3 = mouse fibroblast. P388 = mouse leukemia. RKO = colon carcinoma. ....	34
Table 2-1. Mitsunobu reaction on 22-hydroxy sterol using aryl sulfonyl amide nucleophiles. DTBAD stands for di-tertbutyl azodicarboxamide. ....	61
Table 2-2. Imine and reductive amination reaction conditions to transform 22-keto cholesterol (2.27) into C22-amino cholesterol.....	63
Table 2-3. Optimization screening campaign of Fukuyama-Mitsunobu reaction for N-glycosylation. The amine (1) shown is 22-aminosterol with either Ns or DNs protecting groups. Disaccharide is <i>LArb-Xyl</i> -disaccharide. DTBAD stands for di-tertbutyl azodicarboxamide and TMAD stands for trimethyl azodicarboxyldiamide. ....	73
Table 4. qNOESY correlations of selective 1D-NOESY irradiations of Compound 2.29 <sup>112</sup> .....	120
Table 6.....	163
Table 3-1. Effect of various Lewis acids on product ratios formed from imino-Ene and aza-Prins mechanism pathways, arranged in Order of increasing zwitterionic character (CT/e value) as calculated by Yang, Q., et. al. <sup>152</sup> .....	181
Table 8. Crystal data and structure refinement for homoallylic tosyl amine with pentyl side chain.....	214
Table 4-1. [ <sup>3</sup> H]-25-OHC competitive binding K <sub>i</sub> values for OSBP and ORP4 of OHC Endogenous ligands as generated by Zack Severance. *indicates non-sigmoidal. ....	227
<b>Table 2.</b> Crystal data and structure refinement for ( <i>R</i> )-n-octyl-pregnenolol, <b>4.17</b> . ....	252
<b>Table 3.</b> Crystal data and structure refinement for ( <i>R</i> )-n-octyl-pregnenolol, <b>4.8</b> . ....	256

Table 5-1. <sup>1</sup> H-NMR, <sup>13</sup> C-NMR, COSY, and HSQC characterization of TTP-8307 (5). *HSQC correlation not observed for C16-H16 because of the coupling constant of imidazole being outside of the NMR acquisition parameters. ....	265
Table 16. <sup>1</sup> H-NMR, <sup>13</sup> C-NMR, COSY, & HSQC characterization of TTP-8307 (5.1). *HSQC correlation not observed for C16-H16 because of the coupling constant of imidazole being outside of the NMR acquisition parameters. <sup>192</sup> .....	283
<b>Table 3. TTP (5.1)</b> , Tabulated multi-chromatogram analysis. At 280 nm, concentration of TTP (5.1) is 98.3%. At 254 nm, concentration of TTP (5.1) is 95.8% .....	289

## List of Figures

Figure 1-1. Structurally diverse small molecules that interact with both OSBP and ORP4 to prevent viral replication and cancer cell proliferation, respectfully. Schweinfurthin A, binds OSBP with ~40-fold higher affinity than ORP4. LYZ-81 shows ORP4 specificity. *GI <sub>50</sub> values from NCI-60 human cancer cell line cytotoxicity panel 2	
Figure 1-2 OSBP and ORP4 Protein Domain Sequence and Homology Diagram: A) OSBP Protein Sequence and Domains; (PH = Pleckstrin Homology domain); B) OSBP/ORP4 Protein Sequence Alignment/ Similarities (Diagram produced through standard protein sequence analysis) .....	3
Figure 1-3. Component nomenclature of OSW-1 and overview of structure-activity relationship (SAR) studies. ....	9
Figure 2-1: Two-dimensional representation of natural product OSW-1 (3 $\beta$ ,16 $\beta$ ,17 $\alpha$ -trihydroxycholest-5-en-22-one 16-O-(2''-O-4-methoxybenzoyl- $\beta$ -D-xylopyranosyl)-(1'-->3')-(2'-O-acetyl- $\alpha$ -L-arabinopyranoside), including official numbering of all carbon atoms. ....	44
Figure 2-2. Possible docked OSW-1 structure within computationally modeled OSBP structure. The OSBP protein structure is computationally rendered from yeast OSBP/ORP crystal structures. This figure was created in collaboration with Dr. Christina Bourne at the University of Oklahoma. ....	47
Scheme 2-3. A. Space filling model of OSW-1 in aqueous environment as it exists within the ORD binding pocket. B. The putative hydrogen bonding network of OSW-1 as facilitated by arabinose C2-acetate leading to conformational selectivity. ....	49

Scheme 2-4. A. Structural modifications of OSW-1 as guided and developed by the putative binding model of OSW-1 as it exists within the oxysterol-binding pocket. New fused and spiro E-ring azacycle OSW-1-derived scaffolds are proposed. B. Proposed three-component approach for rapid analog development of azacycle E-ring scaffolds. C. Proposed incremental changes to disaccharide replacement with arylsulfonyl building blocks in which varying substituents can be added to Y, Z, or R <sub>1-3</sub> for SAR studies. ....	52
Figure 2-5. Overview of new OSW-1 related chemistry research which highlights methods to synthesis 22-aminosterol (2.3) and glycosylation methodology of the 22-aminosterols (2.5). ....	54
Scheme 2-6. C3 protection strategy employing TriBot protecting agent. A. Classic Williamson ether conditions afforded no products. B. TriBot benzylating agent employed to benzyl protect C3-hydroxyl. C. TriBot-PM, <i>para</i> -methoxy benzylating agent employed to PMB protect C3-hydroxyl. D. Generation of TriBot benzylating reagent. E. Generation of TriBot-PM, paramethoxyl benzylating reagent. ....	56
Figure 2-7. Total synthesis of C22- <i>O</i> -glycoside OSW-1-derived scaffold (2.6). ....	57
Figure 2-8. Various synthesis pathways attempted to generate 4-methylpentanal.....	59
Figure 2-9. Total synthesis of C22- <i>N</i> -glycoside linked OSW-1-derived scaffold. ....	66
Figure 2-10. Measured bond distances as determined through qNOSEY; used to determine C20 and C22 stereochemistry. ....	67
Figure 2-11. Synthesis of <i>L</i> -arabinose residue over 7 steps.....	68
Figure 2-12. Synthesis of <i>D</i> -xylose imidate residue over 10 steps. ....	69

Figure 2-13. Synthesis of disaccharide imidate through Schmitt glycosylation of <i>L</i> -arabinose and <i>D</i> -xylose imidate.....	69
Figure 2-14. Proposed mechanism of Fukuyama-Mitsunobu reaction for <i>N</i> -glycosylation between steroidal amine and disaccharide. A. Formation of the betaine, subsequent formation of the phosphoazadicarboxamide and glycosyl acceptor, and functionalization of the disaccharide to become the glycosyl donor. B. Desired nucleophilic attack to form the desired glycoside. C. Unfavorable nucleophilic attack by the betaine to form the side-product glycoside. D. Undesired formation of the <i>O</i> -glycoside product which was not observed in this reaction. ....	76
Figure 2-15. <sup>1</sup> H-NMR of 4-methylpentanol (2.16) in DMSO- <i>d</i> <sub>6</sub> . ....	90
Figure 2-16. <sup>13</sup> C-NMR of 4-methylpentanol (2.16) in DMSO- <i>d</i> <sub>6</sub> . ....	91
Figure 2-17. <sup>1</sup> H-NMR of crude 4-methylpentanal (2.17) in DMSO- <i>d</i> <sub>6</sub> . ....	93
Figure 2-18. <sup>13</sup> C-NMR of crude 4-methylpentanal (2.17) in DMSO- <i>d</i> <sub>6</sub> . ....	94
Figure 2-19. <sup>1</sup> H-NMR of ethyltriphenylphosphonium bromide in chloroform- <i>d</i> .....	96
Figure 2-20. <sup>1</sup> H-NMR of TriBot-PM (2.23) in chloroform- <i>d</i> .....	98
Figure 2-21. <sup>13</sup> C-NMR of TriBot-PM (2.23) in chloroform- <i>d</i> .....	99
Figure 2-22. <sup>1</sup> H-NMR of Compound 2.13 in chloroform- <i>d</i> .....	101
Figure 2-23. <sup>1</sup> H-NMR of Compound 2.14 with trace impurity in chloroform- <i>d</i> .....	103
Figure 2-24. <sup>13</sup> C-NMR of Compound 2.14 with trace impurity, in chloroform- <i>d</i> . ....	104
Figure 2-25. <sup>1</sup> H-NMR of Compound 2.18 as a diastereomeric mixture in chloroform- <i>d</i> . .....	106
Figure 2-26. <sup>13</sup> C-NMR of Compound 2.18 as a diastereomeric mixture in chloroform- <i>d</i> with trace amounts of an oxa-E-ring side product.....	107

Figure 2-27. <sup>1</sup> H-NMR of Compound 2.27 in chloroform- <i>d</i> .....	109
Figure 2-28. <sup>1</sup> H-NMR of Compound 2.28 in chloroform- <i>d</i> .....	111
Figure 2-29. <sup>13</sup> C-NMR of Compound 2.28 in chloroform- <i>d</i> .....	112
Figure 2-30. <sup>1</sup> H-NMR of Compound 2.29 in chloroform- <i>d</i> .....	114
Figure 2-31. <sup>13</sup> C-NMR of Compound 2.29 in chloroform- <i>d</i> .....	115
Figure 2-32. COSY of Compound 2.29 in chloroform- <i>d</i> .....	116
Figure 2-33. HSQC-AD of Compound 2.29 in chloroform- <i>d</i> .....	117
Figure 2-34. 1D-NOESY selective irradiation of H22, of Compound 2.29 in chloroform- <i>d</i> . ....	118
Figure 2-35. 1D-NOESY selective irradiation of H23', of Compound 2.29 in chloroform- <i>d</i> . ....	119
Figure 2-36. <sup>1</sup> H-NMR of Compound 2.30 in chloroform- <i>d</i> .....	122
Figure 2-37. <sup>13</sup> C-NMR of Compound 2.30 in acetonitrile- <i>d</i> <sub>3</sub> . ....	123
Figure 2-38. <sup>1</sup> H-NMR of final L-arabinose (2.24) in chloroform- <i>d</i> . ....	125
Figure 2-39. <sup>1</sup> H-NMR of xylose imidate (2.25) in chloroform- <i>d</i> .....	127
Figure 2-40. <sup>1</sup> H-NMR of protected disaccharide in chloroform- <i>d</i> . ....	129
Figure 2-41. <sup>1</sup> H-NMR of Compound 2.26 in chloroform- <i>d</i> .....	131
Figure 2-42. <sup>1</sup> H-NMR of Compound 2.19 in chloroform- <i>d</i> .....	133
Figure 2-43. <sup>1</sup> H-NMR of Compound 2.38.a in chloroform- <i>d</i> . ....	136
Figure 2-44. <sup>13</sup> C-NMR of Compound 2.38.a in chloroform- <i>d</i> .....	137
Figure 2-45. HSQC-AD of Compound 2.38.a in chloroform- <i>d</i> .....	138
Figure 2-46. <sup>1</sup> H-NMR of Compound 2.38.b in chloroform- <i>d</i> .....	139
Figure 2-47. <sup>1</sup> H-NMR of $\alpha$ -anomer C22-O-Glycoside (2.6) in acetonitrile- <i>d</i> <sub>3</sub> . ....	141



Figure 2-48. $^{13}\text{C}$ -NMR of $\alpha$ -anomer C22-O-Glycoside (2.6) in acetonitrile- $d_3$ . .....	142
Figure 2-49. HSCQ-AD of $\alpha$ -anomer C22-O-Glycoside (2.6) in acetonitrile- $d_3$ . .....	143
Figure 2-50. Compound 2.6, HRMS (+ESI, 180V, rt: 0.815 min): calcd for $\text{C}_{47}\text{H}_{68}\text{O}_{13}$ + $\text{Na}^+$ - $[\text{M}+\text{H}]^+$ : 863.45631; found 863.4529, $\Delta\text{ppm}= 3.95\text{ppm}$ .....	144
Figure 2-51. Compound 2.6, HRMS (+ESI, 180V, rt: 0.815 min): calcd for $\text{C}_{47}\text{H}_{68}\text{O}_{13}$ + $\text{Na}^+$ - $[\text{M}+\text{H}]^+$ : 863.45631; found 863.4529, $\Delta\text{ppm}= 3.95\text{ppm}$ .....	145
Figure 2-52. $^1\text{H}$ -NMR of the mixture of Compound 2.31.A ( $\alpha$ -anomer) and Compound 2.31.B ( $\beta$ -anomer) in acetonitrile- $d_3$ .....	150
Figure 2-53. $^1\text{H}$ -NMR of Compound 2.31.A ( $\alpha$ -anomer) in acetonitrile- $d_3$ . .....	151
Figure 2-54. $^1\text{H}$ -NMR of Compound 2.31.B ( $\beta$ -anomer) in acetonitrile- $d_3$ . .....	152
Figure 2-56. $^1\text{H}$ -NMR of Compound 2.32.a ( $\alpha$ -anomer) in Methanol- $d_4$ . .....	154
Figure 2-57. HSQC of $\alpha$ -anomer glycoside Compound 2.32.a ( $\alpha$ -anomer) in Methanol- $d_4$ . .....	155
Figure 2-58. Compound 2.32.a ( $\alpha$ -anomer), HRMS (+ESI, 180V, rt: 0.896 min): calcd for $\text{C}_{53}\text{H}_{71}\text{N}_3\text{O}_{18}\text{S}$ + $\text{Na}^+$ - $[\text{M}+\text{Na}]^+$ : 1092.4357; found 1092.4338, $-1.7 \Delta \text{ppm}$ . .....	156
Figure 2-59. Compound 2.32.a ( $\alpha$ -anomer),HRMS (+ESI, 180V, rt: 0.896 min): calcd for $\text{C}_{53}\text{H}_{71}\text{N}_3\text{O}_{18}\text{S}$ + $\text{Na}^+$ - $[\text{M}+\text{Na}]^+$ : 1092.4357; found 1092.4338, $-1.7 \Delta \text{ppm}$ .....	157
Figure 2-60. $^1\text{H}$ -NMR of Compound 2.32.b ( $\beta$ -anomer) in acetonitrile- $d_3$ . .....	159
Figure 2-55. $^1\text{H}$ -NMR of the mixture of Compound 2.32.A ( $\alpha$ -anomer) and Compound 2.32.B ( $\beta$ -anomer) in acetonitrile- $d_3$ .....	161
Figure 2-61. $^1\text{H}$ -NMR of C22-N-Glycoside OSW-1 derived analog (2.33) in 10:1 acetonitrile- $d_3$ /methanol- $d_4$ . .....	164

Figure 2-62. HSQC of C22-N-Glycoside OSW-1 derived analog (2.33) in 10:1 acetonitrile- <i>d</i> <sub>3</sub> /methanol- <i>d</i> <sub>4</sub> . .....	165
Figure 3-1. Proposed mechanistic pathways of the imino-ene (A) and aza-prins (B and C) reactions to obtain homoallylic and hydroxylated 22-aminosterol products. Activation energies computationally calculated by Yang, Q., et. al. <sup>152</sup> .....	171
Figure 3-2. Formation of functionalized <i>N</i> -aryl alkyl imines of various electron donating and electron withdrawing properties. Isohexylimine yields (Entries H-J) are reported after two steps from isohexanol. ....	176
Figure 3-3. A. Preliminary imino-ene/aza-Prins reaction using BF <sub>3</sub> -Et <sub>2</sub> O with 97% conversion of pregnadiene to hydroxylated and homoallylic 22-aminosterol scaffolds. B. Mixture of homoallylic, hydroxylated, and rearranged products afforded during the reaction of various imines to pregnadiene in the presence of BF <sub>3</sub> -Et <sub>2</sub> O. ....	178
Figure 3-4. <sup>1</sup> H-NMR of N-(1-tosylpentyl)- <i>p</i> -toluenesulfonamide (Figure 3-2; Entry A) in chloroform- <i>d</i> . ....	189
Figure 3-5. <sup>13</sup> C-NMR of N-(1-tosylpentyl)- <i>p</i> -toluenesulfonamide (Figure 3-2; Entry A) in chloroform- <i>d</i> . ....	190
Figure 3-6. <sup>1</sup> H-NMR of N-(1-tosylpentyl)- <i>p</i> -methoxybenzenesulfonamide (Figure 3-2; Entry B) in chloroform- <i>d</i> . ....	191
Figure 3-7. <sup>13</sup> C-NMR of N-(1-tosylpentyl)- <i>p</i> -methoxybenzenesulfonamide (Figure 3-2; Entry B) in chloroform- <i>d</i> . ....	192
Figure 3-8. <sup>1</sup> H-NMR of N-(1-tosylpentyl)- <i>p</i> -chlorobenzenesulfonamide (Figure 3-2; Entry C) in chloroform- <i>d</i> . ....	193

Figure 3-9. <sup>13</sup> C-NMR of N-(1-tosylpentyl)-p-chlorobenzenesulfonamide (Figure 3-2; Entry C) in chloroform- <i>d</i> .....	194
Figure 3-10. <sup>1</sup> H-NMR of N-(1-tosylpentyl)-p-nitrobenzenesulfonamide (Figure 3-2; Entry D) in chloroform- <i>d</i> .....	195
Figure 3-11. <sup>1</sup> H-NMR of N-(1-tosylpentyl)-1-naphthalenesulfonamide (Figure 3-2; Entry E) in acetone- <i>d</i> <sub>6</sub> .....	196
Figure 3-12. <sup>1</sup> H-NMR of -(4-methyl-1-tosylpentyl)-p-toluenesulfonamide (Figure 3-2; Entry H) in chloroform- <i>d</i> .....	197
Figure 3-13. <sup>1</sup> H-NMR of N-(4-methyl-1-tosylpentyl)-p-nitrobenzenesulfonamide (Figure 3-2; Entry I) in chloroform- <i>d</i> .....	198
Figure 3-14. <sup>1</sup> H-NMR of (E)-N-(pentylidene)-p-toluenesulfonamide (Figure 3-2; Entry A) in chloroform- <i>d</i> .....	200
Figure 3-15. <sup>1</sup> H-NMR of (E)-N-(pentylidene)-p-nitrobenzenesulfonamide (Figure 3-2; Entry D) in acetone- <i>d</i> <sub>6</sub> .....	201
Figure 3-16. <sup>1</sup> H-NMR of (E)-N-(4-methylpentylidene)-p-toluenesulfonamide (Figure 3-2; Entry H) in chloroform- <i>d</i> .....	202
Figure 3-17. <sup>13</sup> C-NMR of (E)-N-(4-methylpentylidene)-p-toluenesulfonamide (Figure 3-2; Entry H) in chloroform- <i>d</i> .....	203
Figure 3-18. <sup>1</sup> H-NMR of Compound 3.5 in chloroform- <i>d</i> .....	209
Figure 3-19. <sup>13</sup> C-NMR of Compound 3.5 in chloroform- <i>d</i> .....	210
Figure 3-20. COSY of Compound 3.5 in chloroform- <i>d</i> .....	211
Figure 3-21. HSQC of Compound 3.5 in chloroform- <i>d</i> .....	212
Figure 3-22. Crystal structure of Compound 3.5.....	213

Figure 3-23. <sup>1</sup> H-NMR of Compound 3.6 in chloroform- <i>d</i> .....	216
Figure 3-24. <sup>13</sup> C-NMR of Compound 3.6 in chloroform- <i>d</i> .....	217
Figure 3-25. COSY of Compound 3.6 in chloroform- <i>d</i> .....	218
Figure 3-26. HSQC of Compound 3.6 in chloroform- <i>d</i> . ....	219
Figure 3-27. <sup>1</sup> H-NMR of Compound 3.7 in chloroform- <i>d</i> .....	220
Figure 4-1. A. General synthetic route to generate alkyl pregnenolol analogs from pregnenolone acetate. B. Generated pregnenolol analogs consisting of changes to the alkyl side-chain component by varying the lengths and branching points. C. Commercially purchased hydroxy cholesterols. ....	224
Figure 4-2. A. General synthetic route to generate 22-hydroxy oxysterol analogs from pregnenolone B. Synthesized ( <i>R</i> )-22-hydroxy oxysterol of varying side chain length and branching.....	225
Figure 4-3. Saponification of commercially available pregnenolone acetate to pregnenolone.....	229
Figure 4-4. General synthesis of 20-hydroxycholesterol analogs via Grignard reaction .....	230
Figure 4-5. Synthesis of stereoisomers Compound 4.4 and Compound 4.5; Grignard reagent was generated <i>in situ</i> . ....	231
Figure 4-6. Synthesis of stereoisomers Compounds 4.6 and 4.7.....	232
Figure 4-7. Synthesis of Compound 4.8 and 4.9. ....	233
Figure 4-8. Synthesis of Compound 4.11.....	233
Figure 4-9. Synthesis of Compound 4.12.....	234
Figure 4-10. <sup>1</sup> H-NMR of starting material pregnenolone in chloroform- <i>d</i> .....	235

Figure 4-11. $^{13}\text{C}$ -NMR of starting material Pregnenolone in chloroform- <i>d</i> . .....	236
Figure 4-12. $^1\text{H}$ -NMR of ( <i>S</i> )-ethyl-pregnenolol analog (4.5) in chloroform- <i>d</i> . .....	237
Figure 4-13. $^{13}\text{C}$ -NMR of ( <i>S</i> )-ethyl-pregnenolol analog (4.5) in chloroform- <i>d</i> . .....	238
Figure 4-14. $^1\text{H}$ -NMR of ( <i>S</i> )-ethyl-pregnenolol analog (4.5) in chloroform- <i>d</i> . .....	239
Figure 4-15. $^{13}\text{C}$ -NMR of ( <i>R</i> )-ethyl-pregnenolol analog (4.4) in chloroform- <i>d</i> . .....	240
Figure 4-16. $^1\text{H}$ -NMR of ( <i>S</i> )-isobutyl-pregnenolol analog (4.7) in chloroform- <i>d</i> . .....	241
Figure 4-17. $^{13}\text{C}$ -NMR of ( <i>S</i> )-isobutyl-pregnenolol analog (4.7) in chloroform- <i>d</i> . .....	242
Figure 4-18. HRMS (+ESI) of 4.7: calculated $\text{C}_{25}\text{H}_{44}\text{O}_2$ 2+ [M + 2H <sup>+</sup> ]: 376.334679 m/z, observed 376.2618 m/z, $\Delta\text{ppm} = 193$ ppm, a significant difference as the compound did not ionize well. ....	243
Figure 4-19. HRMS (+ESI) of Compound 4.7: calculated $\text{C}_{25}\text{H}_{41}\text{O}$ + [M – OH <sup>-</sup> ]: 357.315192 m/z, observed 357.3155m/z, $\Delta\text{ppm} = 0.86$ ppm .....	244
Figure 4-20. $^1\text{H}$ -NMR of ( <i>R</i> )-isobutyl-pregnenolol analog (4.6) in chloroform- <i>d</i> . .....	245
Figure 4-21. $^{13}\text{C}$ -NMR of ( <i>R</i> )-isobutyl-pregnenolol analog (4.6) in chloroform- <i>d</i> . .....	246
Figure 4-22. HRMS (+ESI) of Compound 4.6: calculated $\text{C}_{25}\text{H}_{41}\text{O}$ + [M – OH <sup>-</sup> ]: 357.315192 m/z, observed 357.3156m/z, $\Delta\text{ppm} = 1.14$ ppm .....	247
Figure 4-23. HRMS (+ESI) of Compound 4.6: calculated $\text{C}_{25}\text{H}_{44}\text{O}_2$ 2+ [M + 2H <sup>+</sup> ]: 376.334679 m/z, observed 376.2595 m/z, $\Delta = 197$ ppm, a significant difference as the compound did not ionize well. ....	248
Figure 4-24. $^1\text{H}$ -NMR of ( <i>S</i> )-n-octyl-pregnenolol analog (4.9) in chloroform- <i>d</i> . .....	249
Figure 4-25. $^{13}\text{C}$ -NMR of ( <i>S</i> )-n-octyl-pregnenolol analog (4.9) in chloroform- <i>d</i> . .....	250
Figure 4-26. Crystal structure of ( <i>R</i> )-n-octyl-pregnenolol, 4.17. ....	251
Figure 4-27. $^1\text{H}$ -NMR of ( <i>R</i> )-n-octyl-pregnenolol analog (4.8) in chloroform- <i>d</i> . .....	253

Figure 4-28. <sup>13</sup> C-NMR of ( <i>R</i> )-n-octyl-pregnenolol analog (4.8) in chloroform- <i>d</i> . .....	254
Figure 4-29. Crystal structure of ( <i>R</i> )-n-octyl-pregnenolol, 4.8.....	255
Figure 4-30. <sup>1</sup> H-NMR of ( <i>S</i> )-n-octyl-pregnenolol analog (4.9) in 10:1 chloroform- <i>d</i> : acetone- <i>d</i> <sub>6</sub> .....	257
Figure 4-31. <sup>13</sup> C-NMR of ( <i>S</i> )-n-octyl-pregnenolol analog (4.9) in 10:1 chloroform- <i>d</i> : acetone- <i>d</i> <sub>6</sub> .....	258
Figure 4-32. <sup>1</sup> H-NMR of ( <i>S</i> )-n-butyl-pregnenolol analog (4.12) in chloroform- <i>d</i> .....	259
Figure 4-33. <sup>13</sup> C-NMR of ( <i>S</i> )-n-butyl-pregnenolol analog (4.12) in chloroform- <i>d</i> . ....	260
Figure 5-1. Four step linear synthesis of OSBP targeting anti-viral compound, TTP- 8307. ....	264
Figure 5-2. Mechanism of possible Radziszweski reactions to form A) imidazole containing TTP-8307, and B) oxazole containing TTP-8307.....	268
Figure 5-3. Synthesis of TTP-8307 (5.1) compound.....	270
Figure 5-4. <sup>1</sup> H-NMR of amide (5.4) in chloroform- <i>d</i> . ....	272
Figure 5-5. Compound 5.4, HRMS (-ESI) of compound 5.4: calculated C <sub>17</sub> H <sub>16</sub> FNO <sub>2</sub> - H+ [M - H <sup>+</sup> ]: 284.1092 m/z, observed 284.1089 m/z, Δ = 1.1 ppm. ....	273
Figure 5-6. <sup>1</sup> H-NMR of alpha mono brominated amide (5.5) in chloroform- <i>d</i> .....	275
Figure 5-7. <sup>13</sup> C-NMR of alpha mono brominated amide (5.5) in chloroform- <i>d</i> .....	276
Figure 5-8. HSQC correlations of alpha mono brominated amide (5.5) in chloroform- <i>d</i> . .....	277
Figure 5-9. Compound 5.5, HRMS (-ESI) of compound 5.3: calculated C <sub>17</sub> H <sub>16</sub> BrFNO <sub>2</sub> -H+ [M - H <sup>+</sup> ]: 365.02497 m/z, observed 362.0196 m/z, Δppm = 0.28 ppm. ....	278

Figure 5-10. <sup>1</sup> H-NMR of Compound 5.7 in chloroform- <i>d</i> .....	280
Figure 5-11. HRMS (-ESI) of Compound 5.7: calculated C <sub>27</sub> H <sub>21</sub> FN <sub>2</sub> O <sub>4</sub> -H <sup>+</sup> [M - H <sup>+</sup> ]: 455.1413 m/z, observed 455.1417 m/z, Δ = 0.88 ppm.....	281
Figure 5-12. <sup>1</sup> H-NMR of TTP (5.1) in methanol- <i>d</i> <sub>4</sub> .....	284
Figure 5-13. <sup>13</sup> C-NMR of TTP (5.1) in methanol- <i>d</i> <sub>4</sub> .....	285
Figure 5-14. TTP (5.1), HRMS (+ESI) of TTP-8307 (5): calculated C <sub>27</sub> H <sub>21</sub> FN <sub>4</sub> O [M + H <sup>+</sup> ]: 437.1772 m/z, observed 437.1761 m/z, Δppm = 2.5 ppm. ....	286
Figure 5-15. COSY correlation of TTP (5.1) in methanol- <i>d</i> <sub>4</sub> .....	287
Figure 5-16. HSQC correlation of TTP (5.1) in methanol- <i>d</i> <sub>4</sub> .....	288
Figure 5-17. Multi-Chromatogram analysis of TTP-8307 (5.1) at max absorbance 280nm (shown in blue) and 254nm (shown in red). ....	289
Figure 5-18. HNMR of oxazole containing TTP derivative (5.8) in acetone- <i>d</i> <sub>6</sub> .....	291
Figure 5-19. Compound 5.8, HRMS (+ESI): calculated C <sub>27</sub> H <sub>20</sub> FN <sub>3</sub> O <sub>2</sub> [M <sup>+</sup> ] 438.1612 m/z, found 438.1630 m/z Δppm = 4.0 ppm.....	292
Scheme 6-1. Future pathway of the three-component approach to azacyclic E-ring OSW-1-derived scaffolds.....	298

## Abstract

The cholestane glycoside natural product compound OSW-1 has both broad spectrum antiviral activity and potent antiproliferative activity. OSW-1 is a high affinity ligand of both oxysterol-binding protein (OSBP) and OSBP-related protein 4 (ORP4). OSBP has been implicated in viral disease replication, and ORP4 has been shown to play a critical role in cancer cell survival. The synthesis and structural complexity of OSW-1, in combination with its indiscriminate targeting of both OSBP and ORP4, have limited its drug development and the study of its molecular pharmacology. Herein, a new, three-component synthesis approach (i.e. steroid component, side-chain component, and disaccharide component) to produce E-ring azacycle OSW-1-scaffolds was development and pursued. Identification of the new E-ring azacycle OSW-1 scaffold was guided by the development of a putative molecular model of OSW-1 interacting within the oxysterol-binding protein pocket. The new three-component approach to new E-ring azacycle OSW-1-derived scaffolds required the development of two new synthetic methods. The first method required a direct and easily diversified route to 22-aminosterols. A direct, tunable two-component stereoselective formation of either C16-C17-ene-22-aminosterol or 17-hydroxyl-22-aminosterol, using an imino-ene/aza-Prins reaction, was successfully developed. The mechanism of this Lewis acid-mediated imino-ene/aza-Prins reaction was explored. The second new method required for the three-component approach to OSW-1-scaffolds was the development of a novel amine glycosylation method. An atypical application of the Fukuyama-Mitsunobu reaction was successfully developed into an aminosterol N-glycosylation method that affords high yields of coupled 22-aminosterol and the OSW-1 arabinose-xylose-disaccharide. The



new reaction methods developed can be generally used to access other aminosterol scaffolds and aminoglycoside carbohydrate-containing compounds. These new methods were used to synthesize a new C-22-aminoglycosylated OSW-1 analog, demonstrating the application of these methods in the synthesis of a complex molecular target. The newly developed methods have laid the fundamental groundwork of the three-component approach to produce E-ring azacycle OSW-1 scaffolds. These new scaffolds will be pursued in the future to rapidly produce new analog compounds for antiviral and anticancer drug development.

**Chapter 1: Introduction to the oxysterol-binding protein family and  
the natural product compound OSW-1**

## 1.1. Oxysterol-Binding Protein (OSBP/ORPs) Family

### 1.1.1. Identification of oxysterol-Binding Proteins (OSBP/ORPs) as possible druggable therapeutic targets

In 2011, a class of potent anti-proliferative natural product compounds, including the cholestane glycoside OSW-1 (**Figure 1-1; 1.1**), cephalostatin 1 (**Figure 1-1; 1.2**), and schweinfurthin A (**Figure 1-1; 1.3**) were recognized to function through targeting the OSBP/ORP protein family.<sup>1-3</sup> These three compounds share a cellular target based on similar cytotoxicity profiles against the NCI-60 human cancer cell line panel.<sup>2,3</sup> Identification of oxysterol-binding protein (OSBP) and OSBP-related protein-4 (ORP4) was done through an affinity purification/proteomic analysis of OSW-1 affinity resin.<sup>1</sup> OSBP and ORP4 are the only two members of the OSBP/ORP family demonstrated to interact with the OSW-1 compound.<sup>4</sup> The identification of OSBP and ORP4 as the

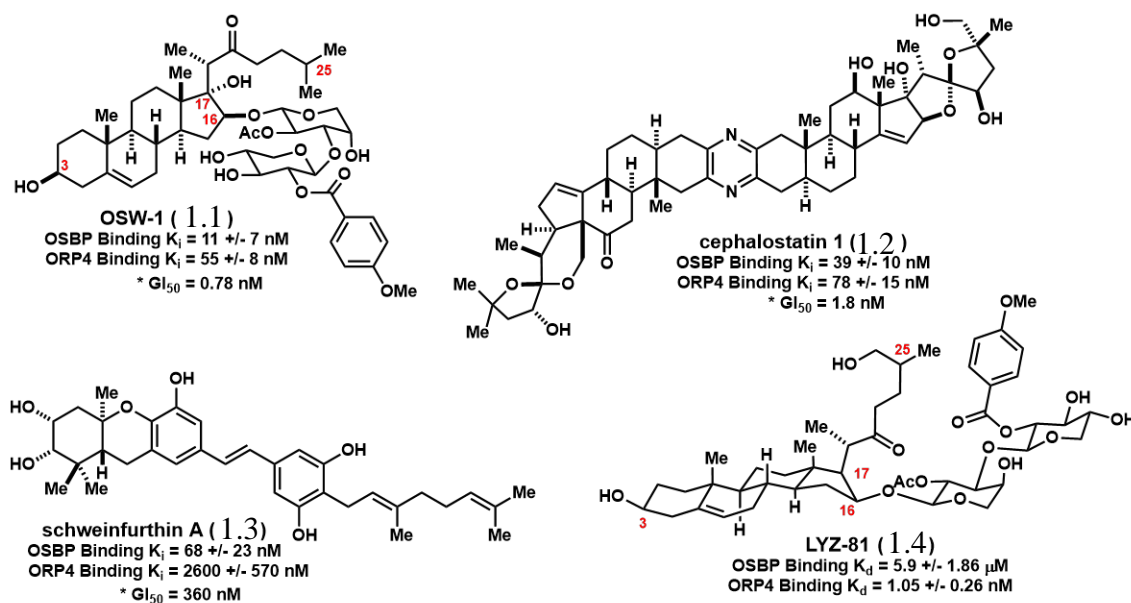


**Figure 1-1.** Structurally diverse small molecules that interact with both OSBP and ORP4 to prevent viral replication and cancer cell proliferation, respectively. Schweinfurthin A, binds OSBP with ~40-fold higher affinity than ORP4. LYZ-81 shows ORP4 specificity. \* $GI_{50}$  values from NCI-60 human cancer cell line cytotoxicity panel.

cellular targets of OSW-1 (**1.1**) has been confirmed by various research groups in pursuit of unrelated projects.<sup>5-9</sup> This extensive evidence, from a multitude of unaffiliated sources, show that OSW-1 (**Figure 1-1; 1.1**) is a potent anti-proliferative, high affinity ligand of OSBP and ORP4.<sup>1,10,11</sup>

**1.1.2. Oxysterol-binding protein (OSBP/ORPs) family characteristics:**

The oxysterol-binding proteins (OSBP/ORPs) are a conserved lipid transfer protein (LTP) family expressed in all eukaryotes that have been identified as critical mediators of cellular and human disease biology.<sup>1,12</sup> The OSBP/ORP family are non-enzymatic,

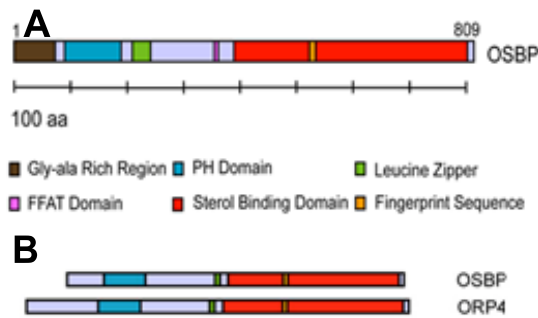


**Figure 1-2** OSBP and ORP4 Protein Domain Sequence and Homology Diagram: A) OSBP Protein Sequence and Domains; (PH = Pleckstrin Homology domain); B) OSBP/ORP4 Protein Sequence Alignment/ Similarities (Diagram produced through standard protein sequence analysis).

cytoplasmic ligand-binding proteins that transport and regulate the metabolism of oxysterols, cholesterols, and, for some family members, phospholipids, within a conserved hydrophobic binding pocket named the OSBP-related domain (ORD) within literature and will be referred to as the ligand-

binding domain (ORD) within this work.<sup>1,12-14</sup> In addition to OSBP, there are 11 other OSBP-related proteins (ORPs) that share the conserved ORD (**Figure 1-2**).<sup>13,14</sup> The OSBP/ORPs possess additional membrane-targeting motifs which allow for the delivery of membrane-lipid specific signaling pairs, however, the cellular functions of the individual OSBP/ORPs remain poorly defined. The overlapping functions or

redundancies shared by individual OSBP/ORP family members render them difficult to study.<sup>1,12,14,15</sup>

The general function of this lipid transfer protein (LTP) family seems to link the ability of the conserved sterol binding domain to bind small lipid molecules and then translate this into specific sensory and/or function through membrane-targeted delivery.<sup>12,15</sup> The intracellular transportation of lipids allows for a unique and complex network of organelle function and regulatory communication to exist.<sup>14</sup> Although vascular transport and membrane fusion constitute a large portion of the lipid transportation, localized movement is mediated by LTPs which facilitate protein-specific delivery of lipids.<sup>14</sup>

No full length OSBP/ORP protein structures have been reported. However, there are multiple reports of yeast OSBP homolog ORDs (i.e. *Osh* proteins) which have been co-crystalized with various ligands bound.<sup>16-19</sup> Most recently, crystal structures were determined for ORP subfamily 2 members, ORP1-ORD and ORP2-ORD, complexed with cholesterol and PI(4,5)P<sub>2</sub>, respectively.<sup>16,20-23</sup> Studying this protein family is further complicated by to the lack of structural definition of the proteins. Although these structures are not full length, they reveal a significant amount of how ligands interact within the OSBP/ORP binding pocket.<sup>16,20-23</sup> Both the yeast and mammalian ORPs revealed that sterols bind in a largely hydrophobic tunnel within the ORD, with the C3-sterol hydroxyl at the bottom of the pocket, and the sterol side chain extended at the top of the ORD, possibly interacting with a putative lid region.<sup>21,24</sup> The existing partial OSBP/ORP homologs only provide partial insight to ligand binding to the ORD and provide no insight to the role and function of the rest of the protein outside of the ORD.

### 1.1.3. Oxysterol-binding proteins as druggable therapeutic targets

OSBP and ORP4 are the only two members of the OSBP/ORP family demonstrated to interact with natural product compound OSW-1.<sup>1-3</sup> OSW-1 is a high affinity ligand of OSBP and ORP4, exhibiting an inhibition binding constant ( $K_i$ ) of 11 nM for OSBP and 55 nM for ORP4 (**Figure 1-1**).<sup>1</sup> ORP4 is the closest related protein to OSBP which shares 59% overall sequence identity, including 68% sequence identity in the sterol binding domain (**Figure 1-2**).<sup>1,12-14</sup> Despite the sequence similarity, there is extensive evidence these two proteins have different biological roles within the human body. OSBP is reported to be localized at the membrane contact site between the ER and Golgi where the protein coORDinates the cross-transfer of PI4P and cholesterol.<sup>5,25-27</sup> OSBP is expressed ubiquitously in all tissues. The PH and FFAT domains alter OSBP cellular localization upon binding of ligands to the C-terminal ligand binding domain.<sup>1,13,14,28</sup> OSBP binding partners, including several regulatory proteins, have been reported.<sup>13,14</sup> In comparison, ORP4 is only reported in some types of tissues such as retina, testes, and parts of the brain.<sup>13,28</sup> In immortalized cell lines and leukemia,<sup>12</sup> ORP4 is highly expressed and drives proliferation.<sup>29-31</sup> ORP4 has been reported to be selectively overexpressed in T-cell acute lymphoblastic leukemia (T-ALL) cells isolated from patients, and ORP4 is critical for the T-ALL cell proliferation through the mediation of cellular calcium homeostasis and bioenergetics of infected cells.<sup>32-35</sup> Additionally, ORP4 has recently been reported to transfer phosphoinositide-2-phosphate (PIP<sub>2</sub>) from the plasma membrane to PLC $\beta$ 3 to trigger pro-growth cell signaling pathways.<sup>30,31</sup> The expression and localization pattern differences between OSBP and ORP4 are evidence of different biological roles.

Although OSBP and ORP4 bind many ligands with similar affinity<sup>1</sup>, such as 25-hydroxycholesterol (25-HC) and OSW-1, OSBP and ORP4 also exhibit ligand binding selectivity.<sup>1</sup> Natural product schweinfurthin A (**Figure 1-1; 1.3**) is reported to have a GI<sub>50</sub>=360 nM in the NCI-60 cancer cell line screening panel.<sup>1</sup> Schweinfurthin A binds OSBP with ~40-fold higher affinity than ORP4, measured as K<sub>i</sub> values competing against 25-hydroxycholesterol; OSBP K<sub>i</sub>= 68 +/- 23 nM and ORP4 K<sub>i</sub> 2600 +/- 750 nM, respectfully.<sup>1</sup> More recently, an OSW-1 derived compound, LYZ-81 (**Figure 1-1; 1.4**) is reported to be a high affinity ORP4 binder with 6000 fold higher selectivity for ORP4 over OSBP.<sup>30</sup> LYZ-81 is reported to eradicate leukemia stem cells *in vitro* and *in vivo*.<sup>30,36</sup> LYZ-81 differs from OSW-1 by the presence of a C26-hydroxyl.<sup>30</sup> The reported ORP4 selectivity in LYZ-81 is direct evidence that OSW-1-derived compounds are capable of specific targeting of OSBP or ORP4. This extensive evidence suggests that OSBP proteins can be selectively targeted through small molecule precision therapeutic development of OSW-1.

#### **1.1.4. Potential targeting of Oxysterol-Binding Protein (OSBP) for prophylactic antiviral drug development**

OSBP is a critical mediator in the replication of multiple clinically important human pathogens belonging to the *Enterovirus* genus.<sup>8,9,37</sup> Human viral pathogens belonging to the genus *Enterovirus* are ubiquitous and are established public health menaces, causing significant societal morbidity and mortality. *Enterovirus* genus pathogens cause a spectrum of diseases including the common cold, acute respiratory infections and pneumonias, myocardial infections, hand, foot and mouth disease (HFMD), acute hemorrhagic conjunctivitis, and the paralytic condition acute flaccid

myelitis.<sup>37-41</sup> Furthermore, OSBP has been reported as a critical mediator of coronavirus,<sup>8,42</sup> hepatitis C virus (HCV),<sup>6,43</sup> encephalomyocarditis (EMCV),<sup>44</sup> dengue virus,<sup>45</sup> and Zika virus.<sup>45</sup> The high mutability and large spectrum of serotypes limit vaccine and antiviral therapeutic development for these viral pathogens.<sup>37-41</sup> However, OSBP has recently emerged as a human protein vital for the replication of these RNA viruses.<sup>46-48</sup> OSBP has been reported as critical in the formation of viral replication organelle structures, which form at the ER-Golgi interface.<sup>46-48</sup> Replication organelles are critical for the reproduction of *Enterovirus* genera viruses as well as other classes of viruses.<sup>37,47</sup> One model shows OSBP as executing a critical lipid transport function at membrane contact sites between the ER and Golgi.<sup>5,26,49</sup> OSBP transports cholesterol from the ER to the Golgi, while counter-transporting phosphoinositide-4-phosphate (PI4P) from the Golgi to the ER.<sup>5,26,49</sup> In this role, OSBP mediates the necessary movement and regulation of the lipids between organelles.<sup>5,26,49</sup>

Multiple independent studies have established the antiviral activity of OSBP-targeting small molecules, including the OSW-1 compound.<sup>8,9,37,50-52</sup> Our research group has demonstrated that short-term exposure of low doses of OSW-1 induces reduction of cellular OSBP level by 90% and the reduction is inherited in multiple generations of cells after OSW-1 treatment.<sup>10</sup> The observed prophylactic reduction of cellular OSBP levels was found to be unique to OSW-1 through methodical biological evaluation of structurally-diverse small molecules (OSW-1, itraconazole, T-001270HEV2, and TTP-8307) that had been reported to exert antiviral biological response through targeting of OSBP.<sup>11</sup> This suggests that OSW-1 has potential as a preventative antiviral treatment through the targeting of OSBP.<sup>10,11</sup>



### 1.1.5. Precision targeting of OSBP-related protein 4 (ORP4) as anticancer agent

The expression and cellular function of ORP4 are important drivers of cancer cell proliferation and cancer cell viability.<sup>32-34</sup> ORP4 expression is normally localized to tissue within parts of the brain, heart, and testis.<sup>32-35</sup> Since ORP4 has such limited expression in normal tissue, ORP4 expression in blood cells was identified as a potential early warning sign of cancer in patients.<sup>32</sup> ORP4 was then identified as a general biomarker for the detection of solid-tumor dissemination in peripheral blood and lymph nodes.<sup>32</sup> Recently, ORP4 is determined to be selectively expressed in T-Cell acute lymphoblastic leukemia (T-ALL) cancer cells in patients.<sup>35</sup> The increased concentration of ORP4 can then be detected within the blood stream making it an excellent biomarker of T-ALL cancer cells.<sup>32-35</sup> ORP4 was reported to be required for a T-ALL cells, chronic lymphocytic leukemia (CLLs) cells, and leukemia stem cells to utilize oxidative phosphorylation within the mitochondria as a source of ATP.<sup>35</sup> A model has been reported that shows ORP4 playing a critical role in regulating cancer cell ATP production by complexing with phospholipase C (PLC) to maintain cellular calcium release and bioenergetics.<sup>35</sup>

The small-molecule precision targeting of ORP4 is a potential route for the development of novel lead compounds for the treatment of T-ALL, and potentially other cancers.<sup>1,32-35</sup> OSW-1 and the OSW-1 analog LYZ-87, have been shown to be efficacious in leukemia animal models.<sup>30</sup> As an antiproliferative, high-affinity ligand for ORP4, the natural product OSW-1 (**Figure 1-1; 1.1**) is an obvious starting point for ORP4 drug development.

## 1.2. Overview of synthesis and biological activity of OSW-1-derived analogs

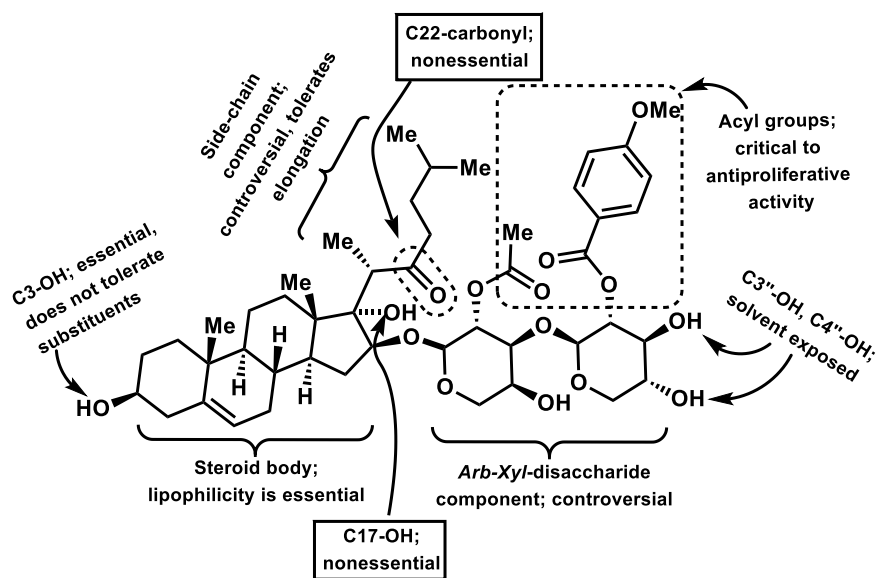


**Figure 1-3.** Component nomenclature of OSW-1 and overview of structure-activity relationship (SAR) studies.

Due to its potent antiproliferative activity and the more recently discovered antiviral activity, OSW-1 has been the target of extensive research.<sup>53,54</sup> Many OSW-1 analogs, including closely related natural product compounds (**Figure 1-1**), have been accessed and tested for biological activity.<sup>53,54</sup> The first reported analogs are natural product saponins that were isolated with OSW-1 from the bulbs of *Ornithogalum saundersiae* in 1992.<sup>54,55</sup> Shortly thereafter, the first OSW-1 total synthesis was reported by Yu's group from the Shanghai Institute in 1999.<sup>53,54</sup> The OSW-1 total syntheses allowed for new OSW-1 derivatives to be accessed. Over twenty years of research on OSW-1 has produced multiple total synthesis approaches and the production of nearly 100 OSW-1 analog compounds (**Table 1-1, 1-2, and 1-3**). However, few of these compounds have been tested for binding interactions with OSBP and ORP4, and much of the biological activity of the OSW-1 analogs were reported against inconsistent cell lines. Due to these limitations, only partial insight into the OSW-1 structure activity relationships (SAR) can

be gained from the previous OSW-1 analogs.<sup>10,11,53,54,56</sup> The existing OSW-1 analogs can largely be divided into three main categories: 1) sidechain and D-ring analogs, 2) acyl variation analogs, and 3) disaccharide analogs.

### **1.2.1.OSW-1 derived analogs consisting of side chain and D-ring modifications**

The first series of OSW-1 side chain analogs were developed via total synthesis using alkyl Grignard reagents attacking the C22-position of ketosterol (**Table 1-1; Entries 6-20**).<sup>57,58</sup> Although these structures were reported, for unclear reasons, not all of them seemed to have been biologically evaluated.<sup>57,58</sup> Truncation of the side chain (**Entries 6-10**) resulted in reduced cytotoxicity except for **Entry 9** which was more potent than OSW-1.<sup>58-60</sup> Extension and modified branching of the alkyl side chain appears to result in lower cytotoxicity, but not enough data was provided for conclusive SAR results (**Entries 13-15**).<sup>58-60</sup> Alterations of C22 oxidation drastically impacted inhibition of cancer cell growth (**Entries 11 and 12**).<sup>59,60</sup> Complete reduction of C22 resulted in an increase in growth inhibition (**Entry 10**) whereas C22-hydroxy analog resulted in a 30-fold reduction of growth inhibition (**Entry 11**).<sup>59,60</sup> Within the report by Morzycki and Wojtkielewicz's group, OSW-1 analogs with linear side chains exhibited reduced growth inhibition.<sup>59</sup>

Shortly after the first reported total synthesis, new total synthesis approaches to OSW-1 were communicated by multiple groups.<sup>61-63</sup> These syntheses further facilitated the generation of OSW-1 derived analogs with modified heteroatom-containing side chains.<sup>61-63</sup> Morzycki's synthesis elaborated the steroidal skeleton side chain via Peterson olefination which could then undergo acyl substitution to various ester-containing side chains.<sup>61</sup> Yu's improved synthesis utilized a similar approach whereby an ester side-chain

functional handle was established via aldol reaction and could be further derivatized through acyl substitutions.<sup>63</sup> **Entries 21-36** were made accessible because of these developed techniques in total synthesis. The majority of these analogs replaced the typical iso-amyl ketone with various alkyl-22-ester derivatives. Generally, this structural modification did not have a significant impact on anticancer activity, as most evident by **Entry 22**, which has a modest 10-fold decrease in potency across three cell lines.<sup>62,64</sup>

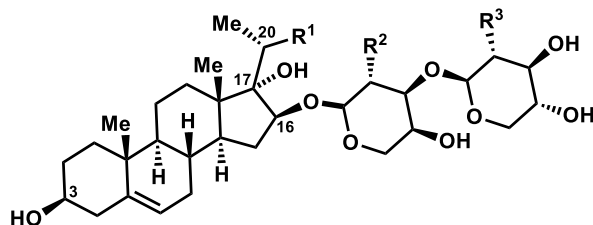
Extension of the side chain afforded conflicting results as shown in **Entries 23, 27, 29, 34, and 35**.<sup>62,64</sup> In **Entries 23, 27, and 34**, only the Jurkat T cell line was affected. In the other cases, multiple cell lines were affected. OSW-1 heteroatom side chain analogs (**Entries 22, 25, 31 and 32**) and the Weinreb amide analog (**Entry 33**) showed equivalent potency in HeLa and Jurkat T cell lines but, the thioester (**Entry 31**) and amide (**Entry 32**) suffered a 20-fold potency decrease in MCF-7 cell lines.<sup>62,64</sup> Comparison of **Entries 21-23** (C20-*S*-epimers) with **Entries 24-26** (C20-*R*-epimers), show a surprising impact on cell line dependent potency.<sup>62,64</sup> **Entries 21-23** (C20-*S*-epimers) are more potent within Jurkat T cell lines, whereas **Entries 24-26** (C20-*R*-epimers) are more potent in MCF-7 cell lines.<sup>62,64</sup> Potency within HeLa cells were not reported for **Entries 21-23** (C20-*S*-epimers).

In 2003, another OSW-1 synthesis was reported that began with natural product diosgenin, eventually leading to the synthesis of OSW-1 derived analog, LYZ-81 (**Figure 1-1, Compound 1.4**).<sup>30,65</sup> Through precise opening of the E/F-spiro-ketal, functional C26-hydroxyl analogs and E-ring-furans became accessible.<sup>36,66</sup> **Entries 37-41** are the only reported analogs of this variety to date.<sup>30,36,67,68</sup> The bioactivity of **Entry 37** (LYZ-81, see also, **Section 1.1.1 Compound 1.4**) and **38** were not fully realized until 2019

when it was revealed to selectively eliminate leukemia stem cells *in vitro* and *in vivo* via ORP4 inhibition.<sup>30</sup> The SAR of C22 ketone is once again revealed as unimportant to potent biological activity when comparing **Entry 37** and **38**.<sup>30,36,67,68</sup> No other C26-hydroxyl bearing OSW-1 derived scaffolds have been reported.<sup>69</sup>

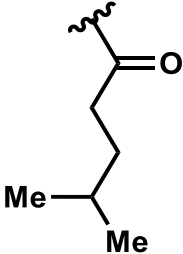
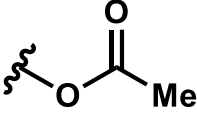
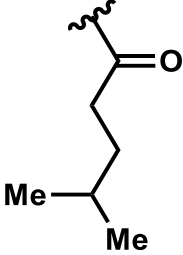
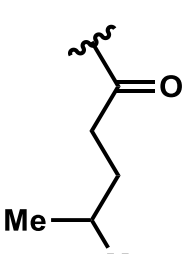
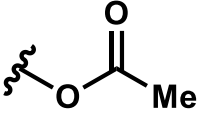
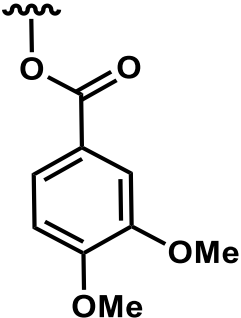
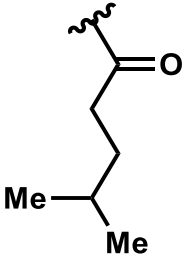
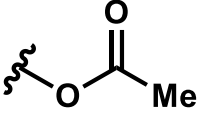
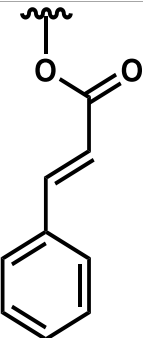
Further exploitation of the synthetic methods available produced three series of side chain ester analogs with saturated (**Entries 42-47**), unsaturated, (**Entries 48-51**) and aromatic (**Entries 52** and **53**) side-chain derivatives.<sup>68</sup> Providing more conclusive evidence than previous studies, **Entries 42-47** did not show significant impact on potency when the side chain was extended.<sup>68</sup> Varying positions of unsaturated alkyl chain (**Entries 48-51**) did not have a significant impact on antiproliferative activity.<sup>68</sup> Replacement of the alkyl chain with aromatic systems afforded a 100-fold decrease in potency.<sup>68</sup> Through comparison of cytotoxicity within normal BJ human fibroblast cell lines, the OSW\_1 ester side chain analogs have the highest selectivity between cancer cells and normal cells.<sup>68</sup>

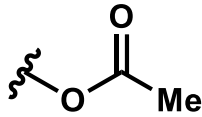
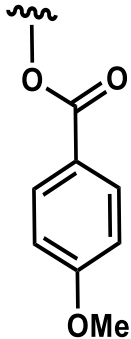
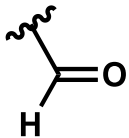
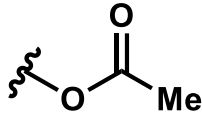
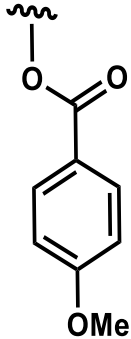
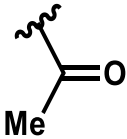
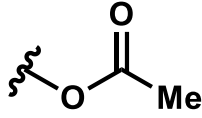
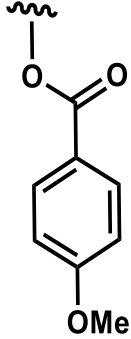
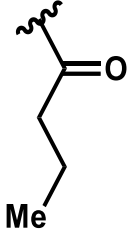
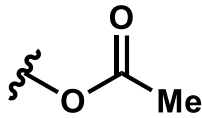
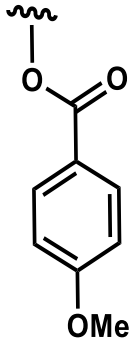
In summary, the side-chain component of OSW-1 is biologically active but tolerates various changes in length, aliphatic branching, and heteroatom replacements.<sup>69</sup> Truncation of the side chain to a C22- ethyl ketone negatively effects potency but elongations of the aliphatic side chain are well tolerated.<sup>69</sup> Changes to the oxidation states of the C22 and C23 carbons, as well as heteroatom replacement at these positions, are well tolerated and exhibit similar potency across multiple cancer cell lines to OSW-1.<sup>62,64</sup> Importantly, no OSBP or ORP4 binding data of the discussed OSW-1 analogs (**Table 1-1**) have been reported.<sup>69</sup> All results have been reported as phenotypic antiproliferative outcomes which leaves a degree of uncertainty to the value of these studies.



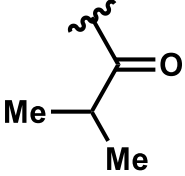
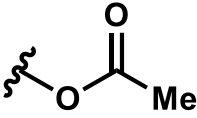
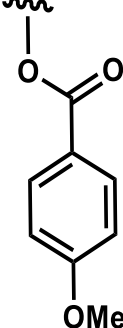
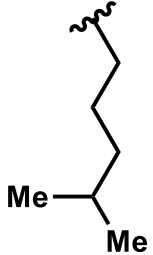
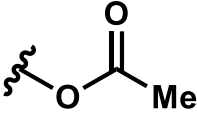
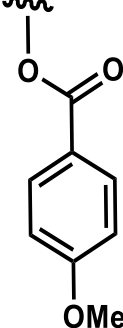
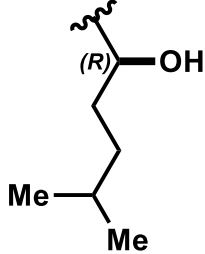
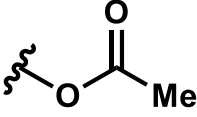
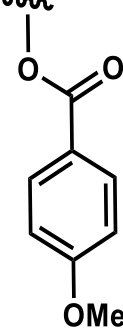
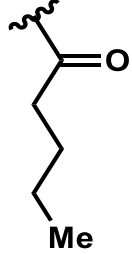
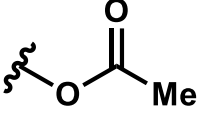
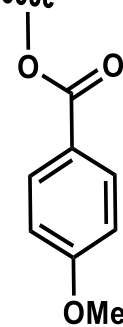
**Table 1-1.** OSW-1 derived analogs consisting of side chain derivatization for SAR studies on various cell lines, reported as growth inhibitory binding constant ( $GI_{50}$ ) values in nM concentration. C20 is in *S*-configuration unless otherwise noted.  $TCS_{50}$  = tumor cell survival. %GI = percent growth inhibition. Literature references reported next to the entry number. AGS = stomach cancer cell line. 7404 = liver carcinoma cells. CEM = T-lymphoblastic leukemia cell line. MDAMB231 = breast carcinoma cell line. MCF7 = breast carcinoma cell line. K562 = chronic myelogenous leukemia cell line. ARN8 = melanoma cell line. G361 = malignant melanoma cell line. HeLa = epitheloid carcinoma cell line. Jurkat T = human T cell lymphoblast-like cell. HOS = osteosarcoma cell line. A549 = lung carcinoma cell line. NIH3T3 = mouse fibroblast. P388 = mouse leukemia. RKO = colon carcinoma.

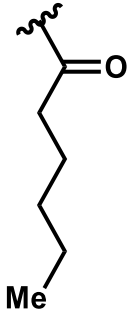
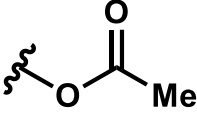
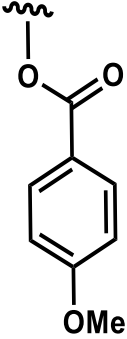
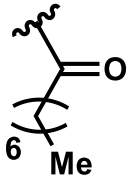
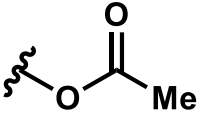
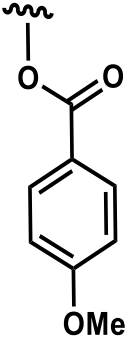
Entry	Ref.	R <sup>1</sup>	R <sup>2</sup>	R <sup>3</sup>	GI <sub>50</sub> (nM)
1.	All within tables				<p><b>OSW-1</b>            HL60: 0.25            CEM: 0.3,            MCF7: 2.4,            Jurkat T: 2.2            G361: 1000,            HeLa: 3.4,            HOS 8200,            A559: 270,            T98: 70,            HCT116:8400,            BJ: 0.2</p> <p><b>*TCS<sub>50</sub></b>            CEM: 0.3,            MCF7: 50,            K562: 0.8,            ARN8: 4.            G361: 1000,            HeLa: 8,            HOS 40,            A559: 0.5,            NIH3T3: &gt;50k</p>

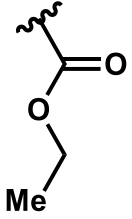
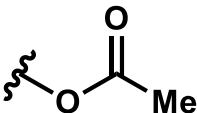
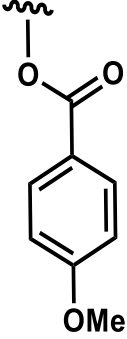
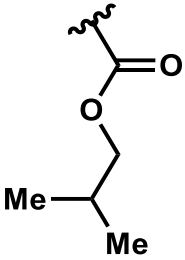
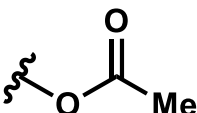
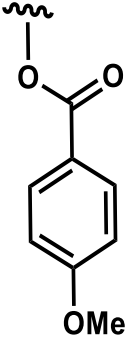
					***%GIP388, A549: 100% @ 1000, 100, & 10 nM,
2.	54,55			-H	Not tested
3.	54,55		-H	-H	HL60: 190
4.	54,55				HL60: 0.20
5.	54,55				HL60: 0.29

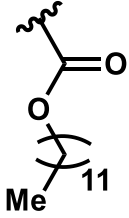
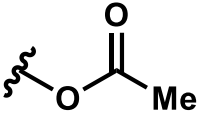
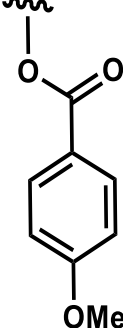
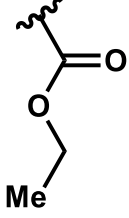
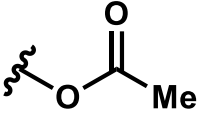
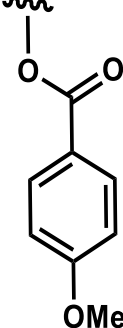
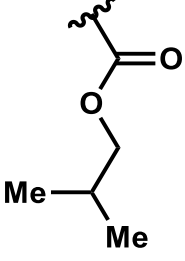
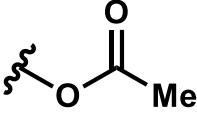
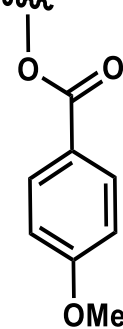
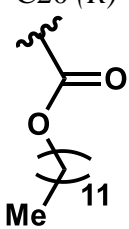
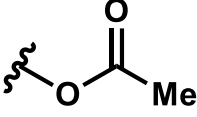
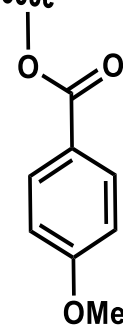
6.	58	-Me			*TCS <sub>50</sub> CEM: 1300, MCF7: 18200, K562: 5100, ARN8: 6800. G361: 9300, HeLa: 6400, HOS 17400, A559: 3200, NIH3T3: >50k
7.	59				Not tested
8.	60				AGS: 6980, A7404: 2900, MCF7: 6610
9.	58-60				*TCS <sub>50</sub> : MCF7: 90, HeLa: 12, <sup>58</sup>  AGS: 1920, A7404: 32, MCF7: 20 <sup>60</sup>

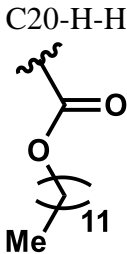
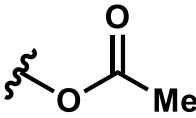
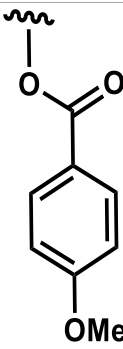
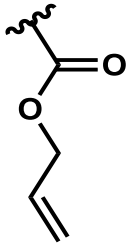
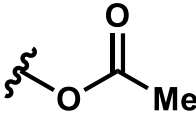
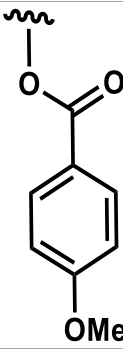
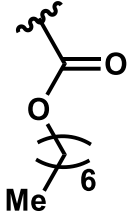
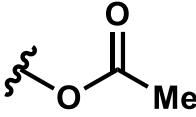
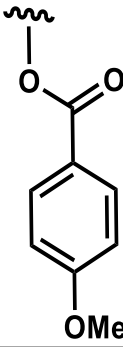
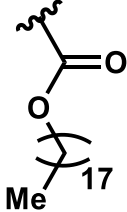
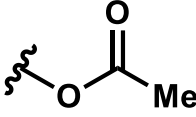
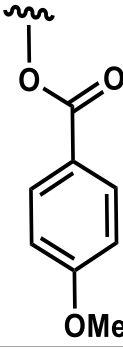


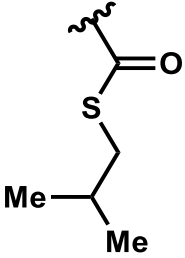
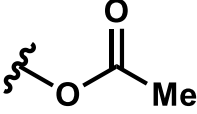
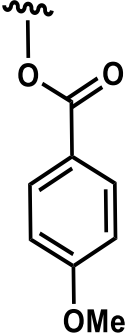
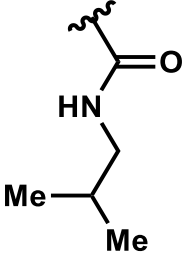
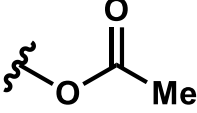
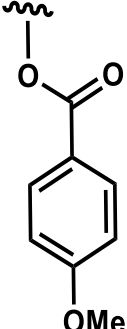
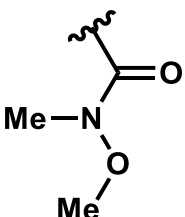
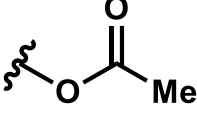
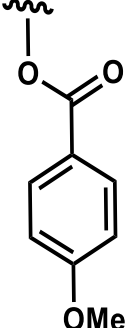
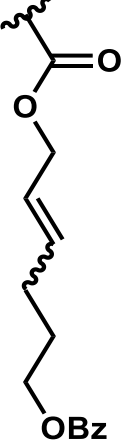
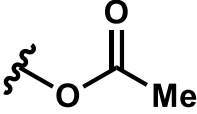
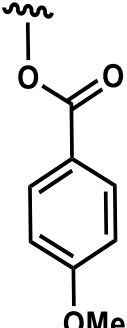
10.	59				Not tested
11.	60				AGS: 1380, A7404: 63, MCF7: 60
12.	60				AGS: 7260, A7404: 1860, MCF7: 1790
13.	59				MCF-7: >10000

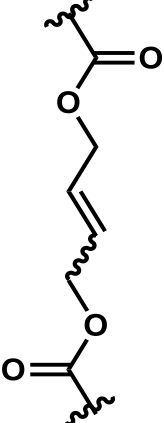
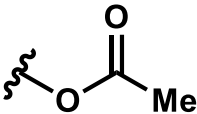
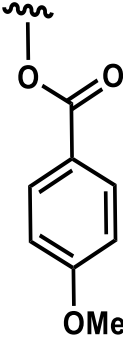
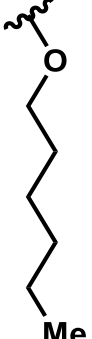
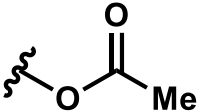
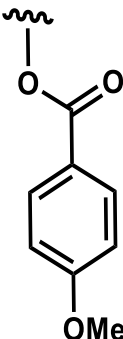
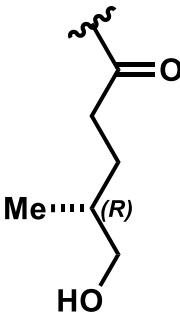
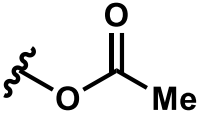
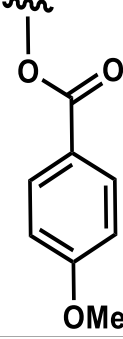
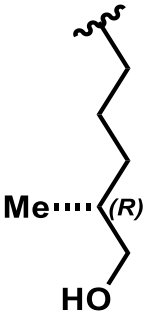
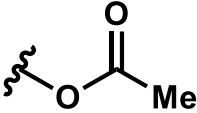
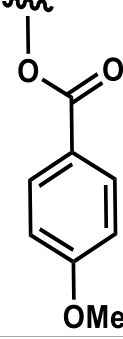
14.	59				MCF-7: >10000
15.	59				Not tested

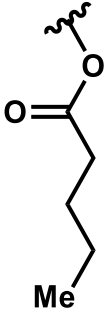
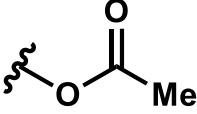
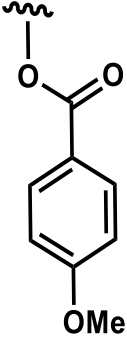
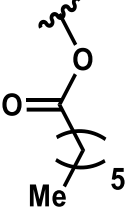
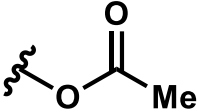
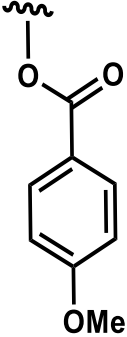
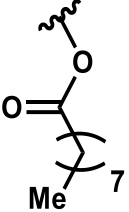
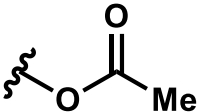
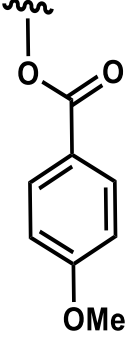
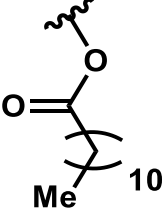
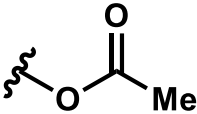
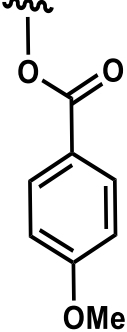
21.	62,64				AGS: 3100 7404: 31 MCF-7: 310
22.	62,64				AGS: 11820, 7404: 30, MCF-7: 900 HeLa: 230, Jurkat T: 5.3

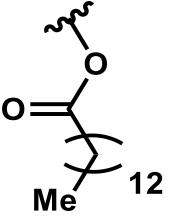
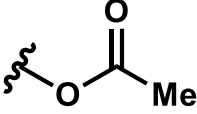
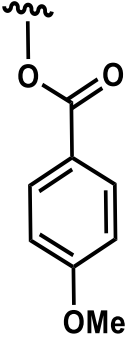
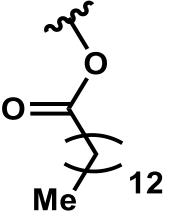
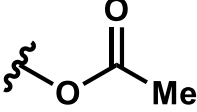
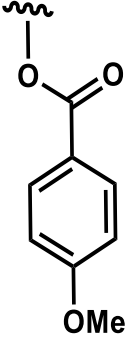
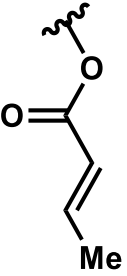
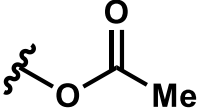
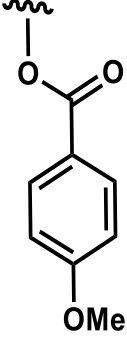
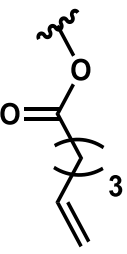
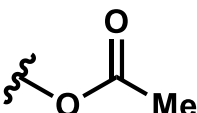
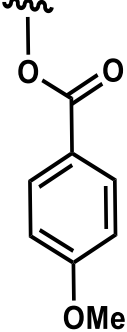
23.	62,64				AGS: 400 7404: 4 MCF-7: 52
24.	64	C20 ( <i>R</i> ) 			HeLa: 34, Jurkat T: 42, MCF-7: 130
25.	64	C20 ( <i>R</i> ) 			HeLa: 34, Jurkat T: 42, MCF-7: 130
26.	64	C20 ( <i>R</i> ) 			Not tested

27.	64	<p>C20-H-H</p> 			<p>HeLa: 10000, Jurkat T: 73, MCF-7: 1400</p>
28.	64				<p>HeLa: 65, Jurkat T: 2.7, MCF7: 100</p>
29.	64				<p>HeLa: 2, Jurkat T: 1.4, MCF-7: 2600</p>
30.	64				<p>HeLa: &gt;10000, Jurkat T: &gt;10000, MCF-7: &gt;1000</p>

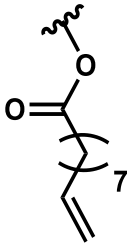
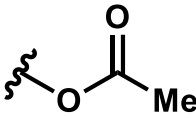
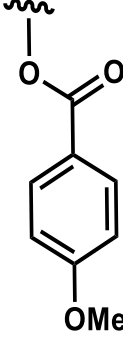
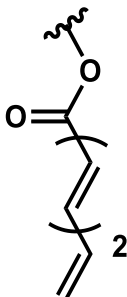
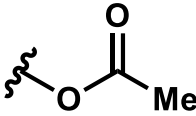
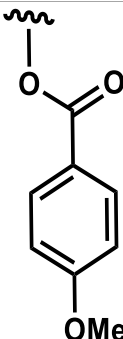
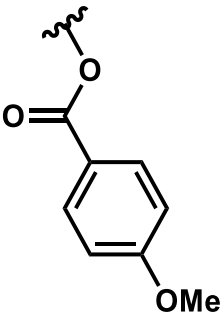
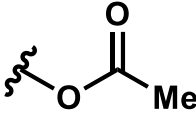
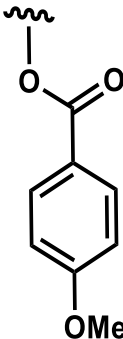
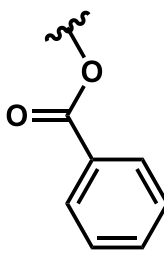
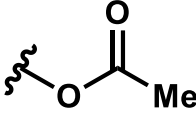
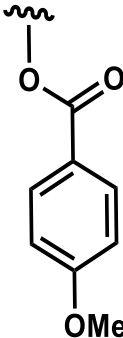
31.	64				<p>HeLa: 1.3, Jurkat T: 0.9, MCF-7: 5200</p>
32.	64				<p>HeLa: 8.4, Jurkat T: 5.3, MCF-7: 1800</p>
33.	64				<p>HeLa: 12, Jurkat T: 35, MCF-7: 16500</p>
34.	64				<p>HeLa: 40, Jurkat T: 3.0, MCF-7: 190</p>

35.	64				HeLa: 70, Jurkat T: 66, MCF-7: 280
36.	SBF-1 58				*TCS <sub>50</sub> CEM: <200, MCF7: 860, K562: <400, ARN8: <400. G361: 1900, HeLa: 350, HOS 1800, A559: <200, NIH3T3: >50k
37.	30,36				HCT-8: 23, BEL7402: 39 BGC823: 2.3, A2780: 73, A549: 46
38.	67				HCT8: 70, BEL7402: 23, BGC823: 2.0, A2780: 6.0, A549: 9.3

42.	68				<p>CEM: 60, MCF7: 500, G361: 390, HeLa: 170, A5490: 160, BJ: 500</p>
43.	68				<p>CEM: 10, MCF7: 400, G361: 1280, HeLa: 30, A5490: 20, BJ: 600</p>
44.	68				<p>CEM: 7.2, MCF7: 26, G361: 15, HeLa: 47, HOS: 2800, A5490: 590, T98: 11, HCT116: 4900 BJ: 600</p>
45.	68				<p>CEM: 6.3, MCF7: 21, G361: 8, HeLa: 42, HOS: 1900, A5490: 930, T98: 7, HCT116: 2800 BJ: 5</p>

46.	68				CEM: 16, MCF7: 48, G361: 30, HeLa: 67, HOS: 2700, A5490: 720, T98: 28, HCT116: 2800 BJ: 83
47.	68				CEM: 58, MCF7: 195, G361: 300, HeLa: 435, HOS:>50000, A5490: 550, T98: 210, HCT116:>50000 BJ: 80
48.	68				CEM: 340, MCF7: 840, G361: 890, HeLa: 1940, HOS:>50000, A5490: 550, T98: 940, HCT116:>50000 BJ: 230
49.	68				CEM: 21, MCF7: 54, G361: 44, HeLa: 61, HOS: 6500, A5490: 840, T98: 43, HCT116:11000 BJ: 20



50.	68				CEM: 6.1, MCF7: 29, G361: 6.7, HeLa: 103, HOS:1940, A5490: 600, T98: 7, HCT116:2600 BJ: 3
51.	68				CEM: 70, MCF7: 700, G361: 1660, HeLa: 240, A5490: 170, BJ: 100
52.	68				CEM: 70, MCF7: 700, G361: 1660, HeLa: 240, A5490: 170, BJ: 100
53.	68				CEM: 57, MCF7: 410, G361: 170, HeLa: 340, HOS:5400, A5490: 570, T98: 55, HCT116: 5000 BJ: 39

### 1.2.2. OSW-1 analogs consisting of acyl modifications

The numerous hydroxyl groups present on OSW-1 are obvious positions for structural variation through acylation. The C2-arabinose acetate group and the C2-xylose benzoate are important for OSW-1 cytotoxicity and binding to OSBP and ORP4.<sup>69</sup> Multiple

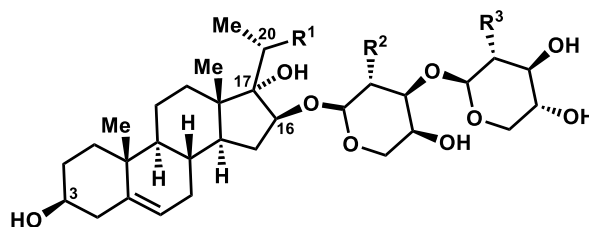
methods to selectively derivatize specific OSW-1 hydroxyls have been reported<sup>1,70</sup> The majority of these selective acylations focused on derivatization of the xylose C3-OH and C4-OH positions; these will be covered in detail in the following section. In 2019 the Yu group reported an extensive SAR campaign consisting of 25 different acylation analogs.<sup>56</sup> Each analog was generated separately through the established total synthesis methods.<sup>57,60,62,64,71,72</sup> These acyl analogs were tested for growth inhibition against human a T-cell lymphoblastic cell lines (i.e. Jurkat T) and a breast cancer carcinoma cell lines (i.e. MDA-MB-231), as well as the non-cancer control, human aorta fibroblast cell line, CRL1999.<sup>56</sup>

The C2-arabinose acetate group and the C2-xylose benzoate are important for OSW-1 cytotoxicity and binding to OSBP and ORP4.<sup>69</sup> These acyl groups can be enzymatically cleaved in cells, potentially inactivating the compound. Replacement of the xylose C3-benzoate ester with an amide prevents that cleavage.<sup>69</sup> Xylose C3-acyl amide analogs were made through late stage derivatization.<sup>69</sup> Replacement of the C3-benzoate ester with an amide allowed for the generation of multiple amide derivatives. (**Table 1-2, Entries 1-25**). It is important to note, the azide containing side chain had not been previously studied but, as discussed in **Section 1.2.1**, elongation of the side chain is tolerated.<sup>69</sup> **Entry 1** has the same *para*-methoxybenzoate group as OSW-1 and showed the strongest activity against Jurkat T cell lines with a 0.11 nM IC<sub>50</sub>, 40-fold more potent than SBF-1 (**Table 1-1, Entry 36**).<sup>56</sup>

Short aliphatic acyl amides on the C3-xylose (**Entries 2-4**) were comparable to OSW-1 in antiproliferative activity.<sup>56</sup> However, increased branching of the amide group resulted in lower potency (**Entries 5 and 6**). With the exception of **Entries 22 and 23**, all xylose-

amide analogs made, were equally cytotoxic in normal-CRL1999 cell lines, which suggests the *para*-methoxybenzoate is a critical component in the potential anticancer activity.

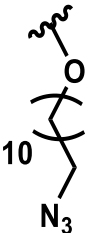
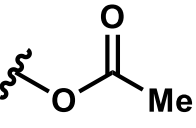
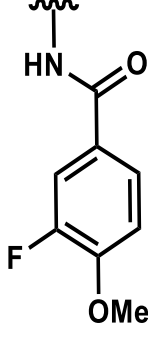
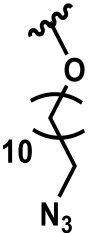
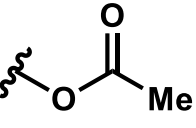
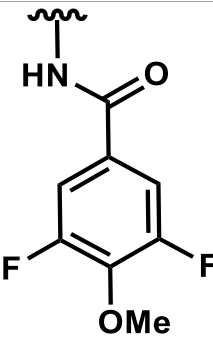
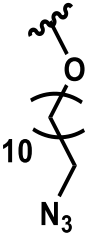
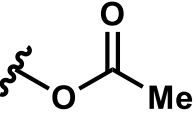
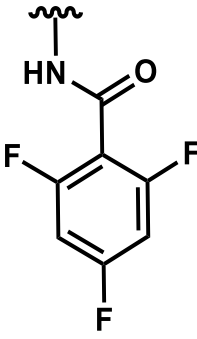
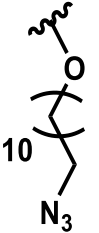
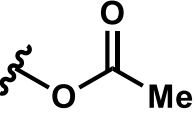
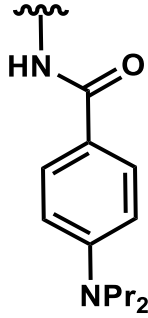
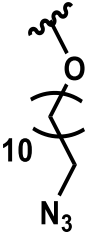
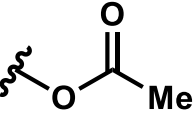
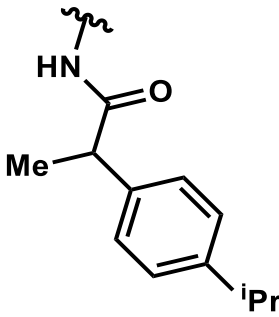
Few OSW-1 analogs with changes to the C2-arabinose acetate component have been reported (Section 1.2.3, Table 1-3, Entries 11, 12, and 13).



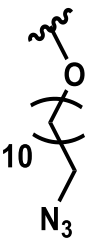
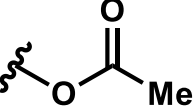
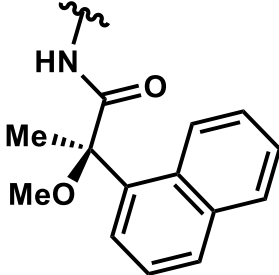
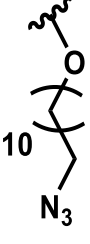
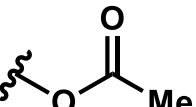
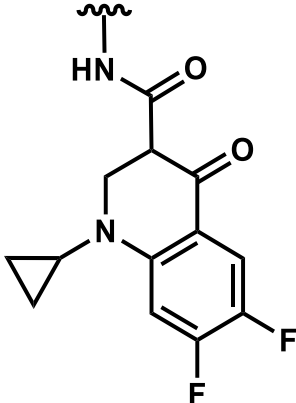
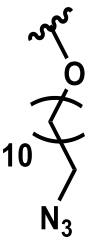
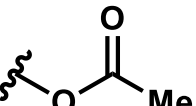
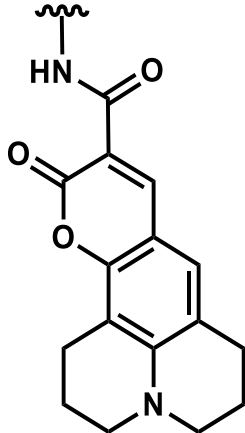
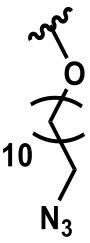
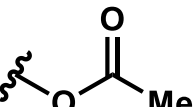
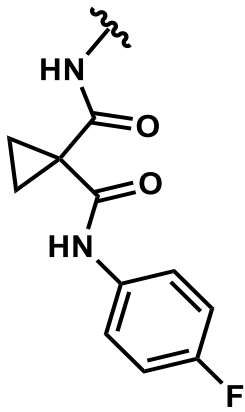
**Table 1-2.** OSW-1 derived analogs consisting of acyl derivatization for SAR studies on various cell lines with phenotypic results reported as growth inhibitory binding (GI<sub>50</sub>) values in nM concentration. C20 is in *S*-configuration unless otherwise noted. MDAMB231 = breast carcinoma cell line. Jurkat T = human T cell lymphoblast-like cell. CRL1999 = human aorta fibroblast cell line.

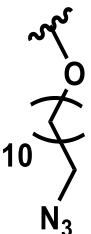
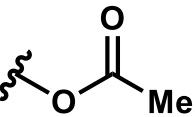
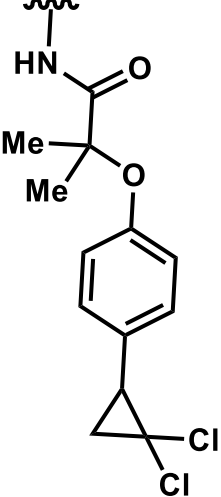
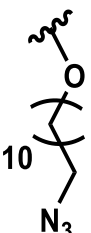
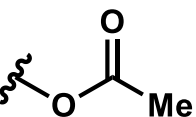
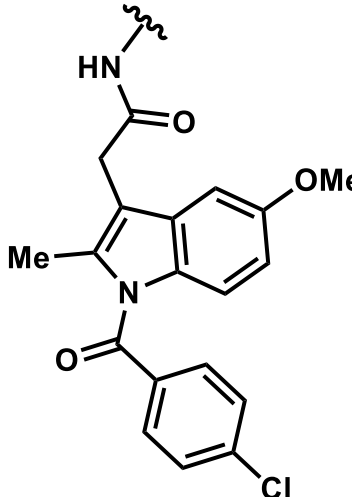
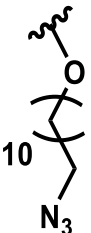
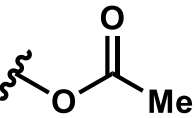
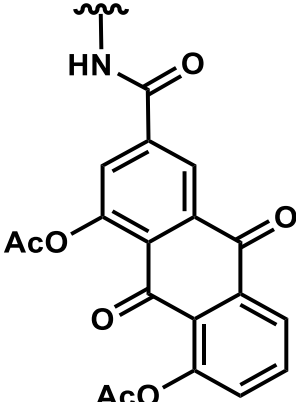
Entry	Ref.	R <sup>1</sup>	R <sup>2</sup>	R <sup>3</sup>	GI <sub>50</sub> (nM)
1.	56				Jurkat: 0.11, MDAMB231: 0.51, CRL1999: 0.40
2.	56				Jurkat: 6.56, MDAMB231: 2.43, CRL1999: N/A
3.	56				Jurkat: 5.57, MDAMB231: 0.85, CRL1999: N/A

4.	56				Jurkat: 162, MDAMB231: 24.8, CRL1999: N/A
5.	56				Jurkat: 153, MDAMB231: 136, CRL1999: N/A
6.	56				Jurkat: 7.10, MDAMB231: 27.0, CRL1999: 12.0
7.	56				Jurkat: 1.8, MDAMB231: 3.7, CRL1999: 11.0
8.	56				Jurkat: 7.26, MDAMB231: 0.88, CRL1999: N/A

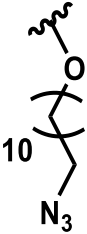
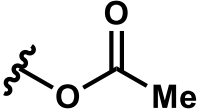
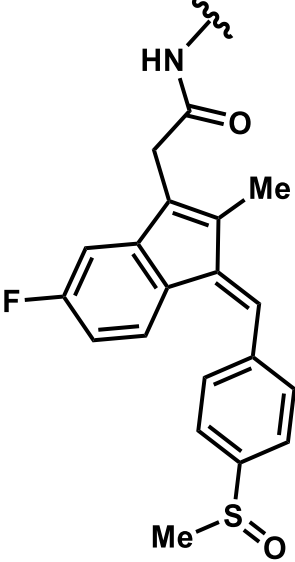
9.	56				Jurkat: 0.59, MDAMB231: 0.75, CRL1999: 0.72
10.	56				Jurkat: 0.44, MDAMB231: 0.76, CRL1999: 1.50
11.	56				Jurkat: 0.46, MDAMB231: 1.40, CRL1999: 0.68
12.	56				Jurkat: 1.00, MDAMB231: 4.10, CRL1999: 4.40
13.	56				Jurkat: 164, MDAMB231: 33.7, CRL1999: N/A

14.	56				Jurkat: 8.60, MDAMB231: 11.0, CRL1999: 56.0
15.	56				Jurkat: 29.0, MDAMB231: 69.0, CRL1999: 220
16.	56				Jurkat: 2.50, MDAMB231: 7.90, CRL1999: 11.0
17.	56				Jurkat: 0.75, MDAMB231: 0.64, CRL1999: 1.40

18.	56				<p>Jurkat: 24.0, MDAMB231: 56.0, CRL1999: 130</p>
19.	56				<p>Jurkat: 3.50, MDAMB231: 6.00, CRL1999: 9.00</p>
20.	56				<p>Jurkat: 6.80, MDAMB231: 6.90, CRL1999: 23.0</p>
21.	56				<p>Jurkat: 3.50, MDAMB231: 6.00, CRL1999: 9.00</p>

22.	56	 <p>Chemical structure of a dendronized azide: a central carbon atom bonded to a nitrogen atom (N<sub>3</sub>), a methyl group (Me), and a dendronized oxygen atom (represented by a wavy line and an oxygen atom).</p>	 <p>Chemical structure of a methyl ester: a wavy line connected to an oxygen atom, which is bonded to a carbonyl group (C=O) and a methyl group (Me).</p>	 <p>Chemical structure of a dendronized amide: a wavy line connected to an NH group, which is bonded to a carbonyl group (C=O). This carbonyl is further bonded to a carbon atom that is also bonded to two methyl groups (Me) and an oxygen atom. The oxygen atom is part of an ether linkage to a para-substituted benzene ring, which is in turn connected to a dichloromethyl group (a carbon atom bonded to two chlorine atoms, Cl).</p>	Jurkat: 83.0, MDAMB231: 260, CRL1999: 2950
23.	56	 <p>Chemical structure of a dendronized azide: a central carbon atom bonded to a nitrogen atom (N<sub>3</sub>), a methyl group (Me), and a dendronized oxygen atom (represented by a wavy line and an oxygen atom).</p>	 <p>Chemical structure of a methyl ester: a wavy line connected to an oxygen atom, which is bonded to a carbonyl group (C=O) and a methyl group (Me).</p>	 <p>Chemical structure of a dendronized amide: a wavy line connected to an NH group, which is bonded to a carbonyl group (C=O). This carbonyl is further bonded to a carbon atom that is also bonded to a methyl group (Me) and a benzimidazole ring system. The benzimidazole ring has a methoxy group (OMe) at the 6-position and is connected to a para-substituted benzene ring with a chlorine atom (Cl). The benzimidazole ring is also bonded to a carbonyl group (C=O) which is further bonded to a para-substituted benzene ring with a chlorine atom (Cl).</p>	Jurkat: 20.0, MDAMB231: 39.0, CRL1999: 30.0
24.	56	 <p>Chemical structure of a dendronized azide: a central carbon atom bonded to a nitrogen atom (N<sub>3</sub>), a methyl group (Me), and a dendronized oxygen atom (represented by a wavy line and an oxygen atom).</p>	 <p>Chemical structure of a methyl ester: a wavy line connected to an oxygen atom, which is bonded to a carbonyl group (C=O) and a methyl group (Me).</p>	 <p>Chemical structure of a dendronized amide: a wavy line connected to an NH group, which is bonded to a carbonyl group (C=O). This carbonyl is further bonded to a carbon atom that is also bonded to an acetoxy group (AcO) and a benzimidazole ring system. The benzimidazole ring has another acetoxy group (AcO) at the 6-position and is connected to a benzene ring with a carbonyl group (C=O). The benzimidazole ring is also bonded to a carbonyl group (C=O) which is further bonded to a benzene ring with an acetoxy group (AcO).</p>	Jurkat: 2.4, MDAMB231: 4.70, CRL1999: 18.0



25.	56				<p>Jurkat: 5.40, MDAMB231: 10.0, CRL1999: 160</p>
-----	----	---	---	--	---

### 1.2.3.OSW-1 analogs consisting of disaccharide modifications

There have been four main studies performed on OSW-1 disaccharide modifications (**Table 1-3**). Each study reported a drastic loss in inhibitory activity through the changes made to the disaccharide.<sup>69</sup> In many of these studies, other structural changes were made in addition to the disaccharide modifications.<sup>69</sup> These studies have been conducted on scaffolds consisting of different side-chain components and/or other minor structural modifications (**Table 1-3**). The first study investigated the truncation of the disaccharide into monosaccharide containing analogs of L-arabinose and D-xylose (**Entries 1 and 2**, respectfully).<sup>59</sup> Interestingly, truncation to monosaccharides resulted in a 100-fold decrease in potency in comparison to OSW-1 but still possessed bioactivity (**Entries 1 and 2**).<sup>59</sup>

A more elaborate study focused on replacement of the xylose residue with a simplified benzoate-containing component. The *para*-methoxybenzoate has been shown to be critical in binding OSBP and ORP4 and the antiproliferative activity.<sup>69</sup> **Entries 3-10** sought to replace the xylose residue with an alkyl benzoate.<sup>72</sup> **Entries 3-5** contained the

typical arabinose C3-OAc but **Entries 6-10** contained a new acyl group, 4-methoxy benzoate.<sup>72</sup> All of these compounds were inactive in the three cell lines tested.<sup>72</sup>

Another study explored the use of maltose in place of both arabinose and xylose in an attempt to simplify the overall synthesis.<sup>73</sup> **Entries 11-13** were generated, and all three of these compounds were inactive in the seven cell lines tested.<sup>73</sup> It is important to note that these three analogs are all missing the biologically important arabinose C2-acetate.<sup>73</sup> As discussed in **Section 1.2.1**, loss of the acetate drastically lowers the potency.<sup>69</sup>

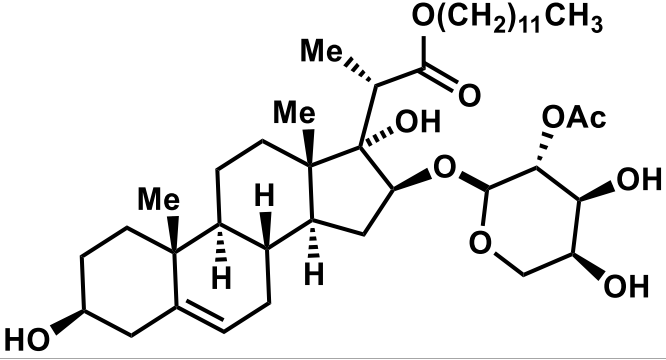
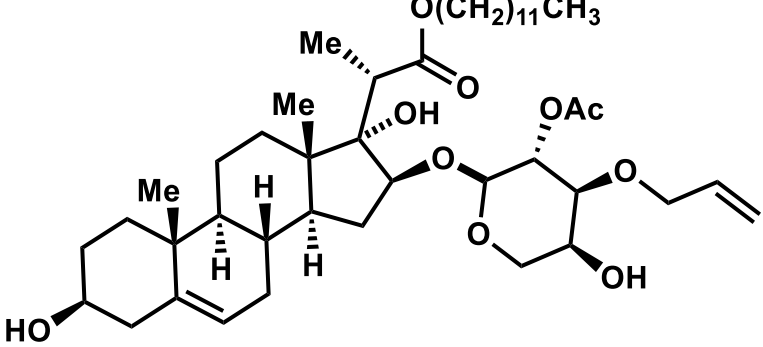
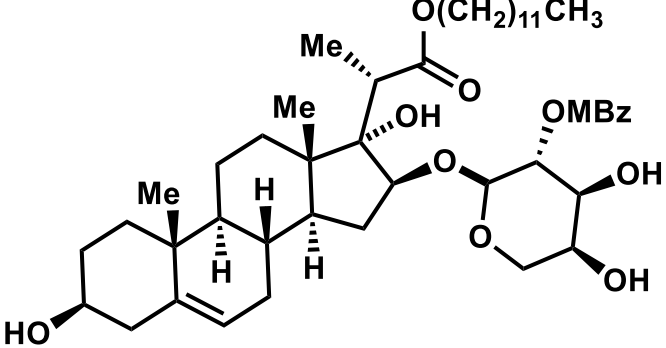
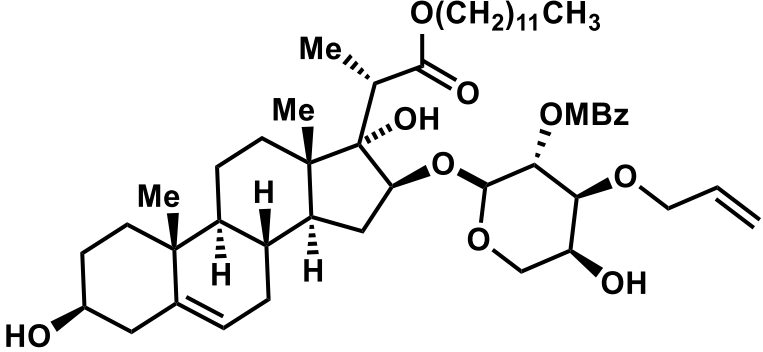
Experimentation to relocate the Arb-Xyl-disaccharide linkage from 1 → 3 to 1 → 4 resulted in a dramatic decrease in growth inhibitory activity (**Entries 14-19**).<sup>74</sup> **Entries 14** and **16** consist of the natural 1 → 3 Arb-Xyl-disaccharide linkage and bare a C22-hydroxide.<sup>74</sup> As discussed in **Section 1.2.1**, C22(*R*)-hydroxy analogs resulted in decreased potency.<sup>60,69</sup> Interestingly, **Entries 14** and **16** both possess a C22(*S*)-hydroxyl and are reported to have nanomolar IC<sub>50</sub> values across eight cell lines, which suggests stereo specificity within the OSW-1 binding interaction at the C22-hydroxy position.<sup>74</sup>

OSW-1 analogs with O-glycosylated linkages at different positions on the structure, such as the side chain, have also been reported (**Table 1-3, Entries 20-25**).<sup>36,58,59,71</sup> The six side-chain O-glycosides were significantly less active than OSW-1,<sup>36,58,59,71</sup> but provide critical insight into the degrees of freedom of the side chain component.

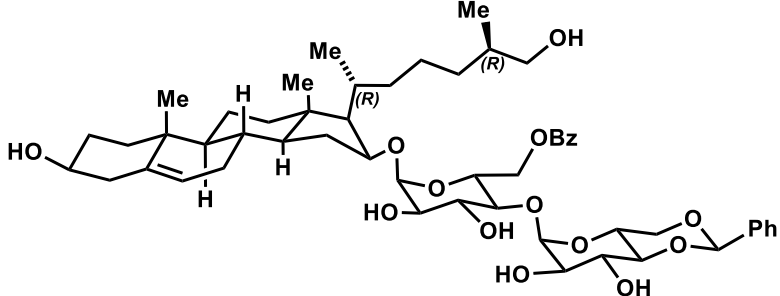
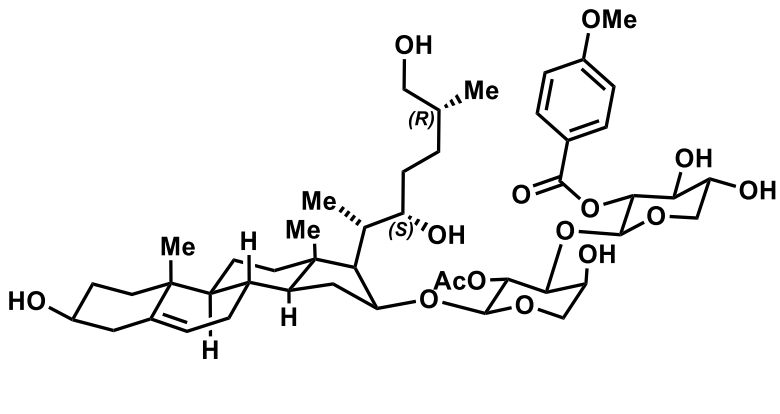
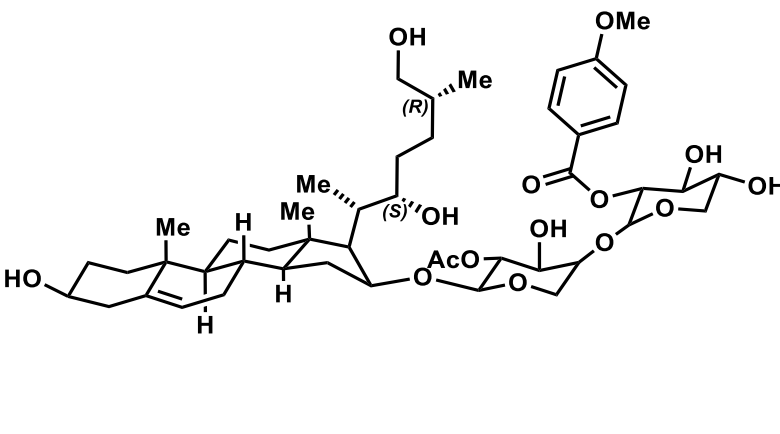
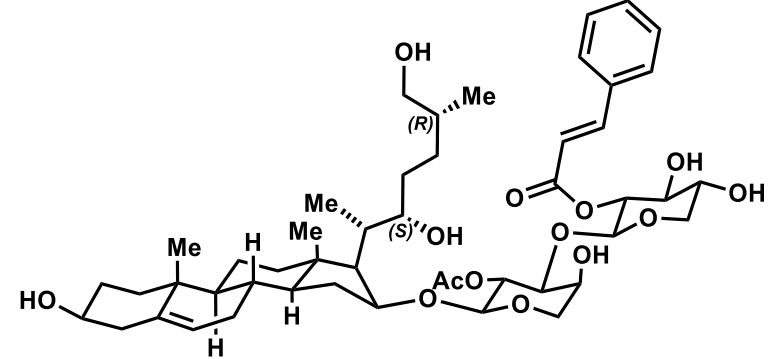
As discussed in **Section 1.2.2**, many methods have been developed for selective acylation of the xylose C3-OH and C4-OH positions of OSW-1.<sup>70</sup> Acylation of these positions is well tolerated<sup>4</sup> and have frequently been used to attach various photocages,<sup>75</sup> fluorophores,<sup>22,76,77</sup> and linkers.<sup>4,22,70</sup> These analogs are not shown here but provide critical evidence that the xylose C3-OH and C4-OH positions tolerate bulky substituents.

**Table 1-3.** OSW-1 derived analogs consisting of modifications to the disaccharide for SAR studies with phenotypic response reported as growth inhibitory binding ( $GI_{50}$ ) values in nM concentration. C20 is in *S*-configuration unless otherwise noted. \* $TCS_{50}$  = tumor cell survival. \*\*%GI = percent growth inhibition. CEM = T-lymphoblastic leukemia cell line. MCF7 = breast carcinoma cell line. K562 = chronic myelogenous leukemia cell line. ARN8 = melanoma cell line. G361 = malignant melanoma cell line. HeLa = epitheloid carcinoma cell line. Jurkat T = human T cell lymphoblast-like cell. HOS = osteosarcoma cell line. A549 = lung carcinoma cell line. NIH3T3 = mouse fibroblast. P388 = mouse leukemia. RKO = colon carcinoma.

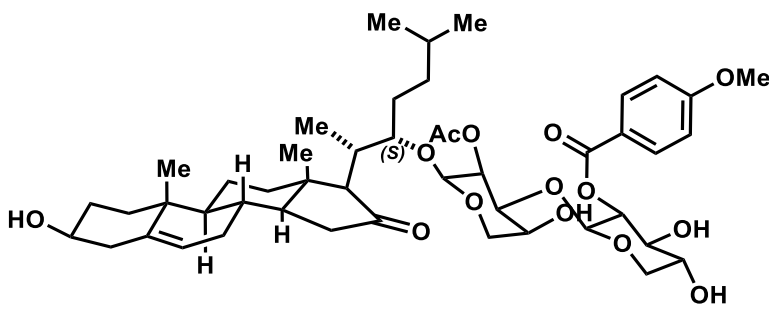
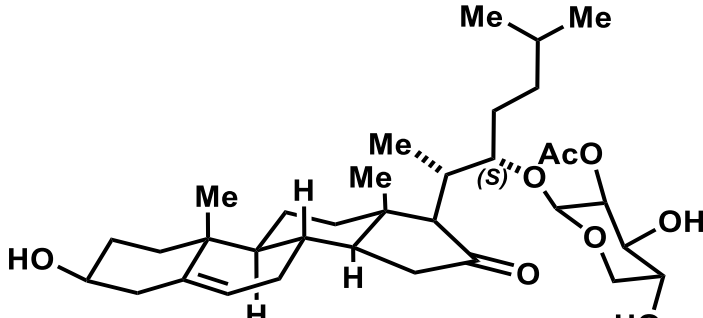
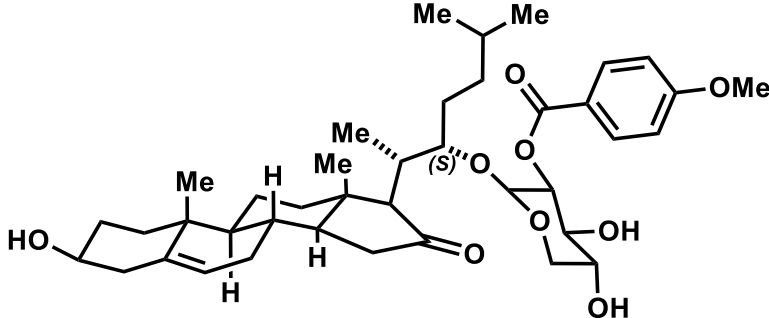
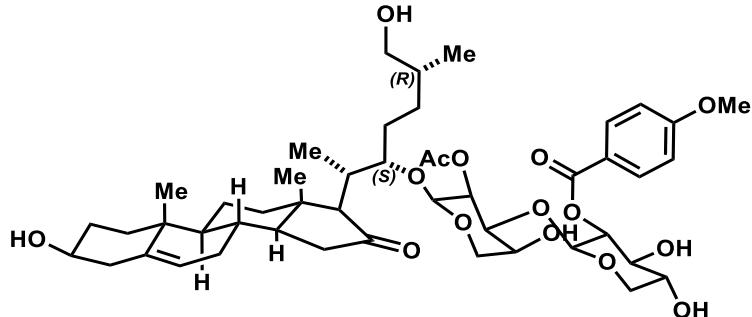
Entry	Ref.	Structure	$GI_{50}$ (nM)
1.	59		* $TCS_{50}$ CEM: 200, MCF7: 1300, K562: 430, ARN8: 1950. G361: 2200, HeLa: 570, HOS 4200, A559: 4200, NIH3T3: >50k
2	59		* $TCS_{50}$ CEM: 1000, MCF7: 3500, K562: 1800, ARN8: 1500. G361: 3500, HeLa: 230, HOS 7200, A559: 7200, NIH3T3: >50k
3.	72		RKO, Jurkat T, HeLa: >10000

4.	72		RKO: >10000, Jurkat T: 78, HeLa: 1200
5.	72		RKO: 1700, Jurkat T: >10000, HeLa: 1100
6.	72		RKO, Jurkat T, HeLa: >10000
7.	72		RKO, Jurkat T, HeLa: >10000

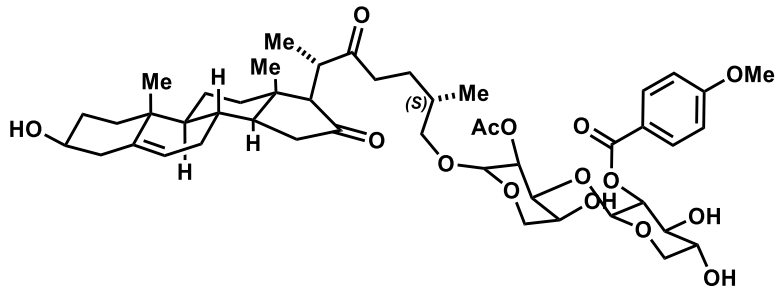
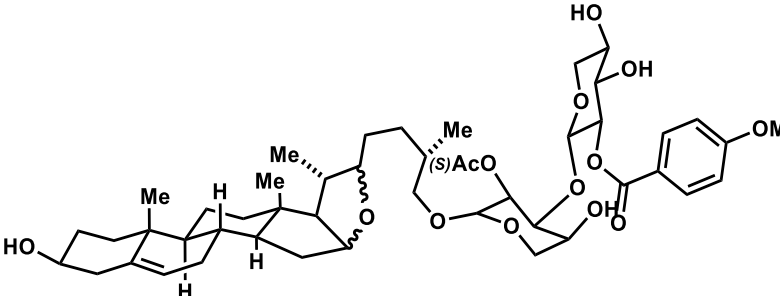
8	72	<p>The structure shows a steroid nucleus with a hydroxyl group at C3, methyl groups at C10 and C13, and a double bond at C5. At C17, there is a side chain containing a methyl group, a hydroxyl group, and a long alkyl chain <math>O(CH_2)_{11}CH_3</math>. The C14 position is linked to a pyranose sugar ring, which is further substituted with a benzoyl group (OMBz) and a hydroxyl group.</p>	RKO, Jurkat T, HeLa: >10000
9	72	<p>The structure is similar to compound 8, but the sugar moiety at C14 is substituted with a benzoyl group (OMBz), a hydroxyl group, and a long chain <math>(CH_2)_8OMBz</math>.</p>	RKO, Jurkat T, HeLa: >10000
10	72	<p>The structure is similar to compound 8, but the sugar moiety at C14 is substituted with a benzoyl group (OMBz), a hydroxyl group, and an ester group <math>EtO-C(=O)-CH=CH-</math>.</p>	RKO, Jurkat T, HeLa: >10000
11	73	<p>The structure shows a steroid nucleus with a hydroxyl group at C3, methyl groups at C10, C13, and C14, and a double bond at C5. At C17, there is a side chain with methyl groups at C18 and C19, and a hydroxyl group at C20. The C14 position is linked to a complex sugar moiety with multiple hydroxyl groups, a benzoyl group (OBn), and a phenyl group (Ph).</p>	A2780, BEL7402, HCT8, KB, BGC823, HeLa, A549: >10000
12	73	<p>The structure is similar to compound 11, but the sugar moiety at C14 is substituted with a benzoyl group (OBz) instead of OBn.</p>	A2780, BEL7402, HCT8, KB, BGC823, HeLa, A549: >10000

13.	73		<p>A2780, BEL7402, HCT8, KB, BGC823, HeLa, A549: &gt;10000</p>
14.	74		<p>HCT116: 8.6, MDAMB23 1: 15, A375: 38, BGC823: 27, ACHN: 30, SW1990: 710, A2780: 0.12, HepG2: 150</p>
15.	74		<p>HCT116: 24000, MDAMB23 1: 24000, A375: 18000, BGC823: 27000, ACHN: 28000, SW1990: &gt;50000, A2780: 190, HepG2: 23000</p>
16.	74		<p>HCT116: 5.3, MDAMB23 1: 0.12, A375: 45, BGC823: 0.68, ACHN: 2.6, SW1990: 26,</p>

			A2780: 00.71, HepG2: 160
17.	74		HCT116: >50000, MDAMB23 1: 2600, A375: 20000, BGC823: 37000, ACHN: >50000, SW1990: >50000, A2780: 22000, HepG2: >50000
18.	74		HCT116: 0.43, NCIH1975: 0.12, Capan2: 24, SW1990: 13, SKNSH: 1.2, BGC823: 0.021, HepG2: 0.0012
19.	74		HCT116: >1000, NCIH1975: >1000, Capan2: >1000, SW1990: >1000, SKNSH: >1000, BGC823: >1000, HepG2: >1000

20.	58,5 9		<p>*TCS<sub>50</sub>  CEM: 280,  MCF7:  3400, K562:  430, ARN8:  500.  G361:  14400,  HeLa: 1000,  HOS 11700,  A559: 480,  NIH3T3:  &gt;50k</p>
21.	58,5 9		Not tested
22.	58,5 9		Not tested
23.	36		<p>HCT-8:  BEL7402:  BGC823:  A2780:  A549:  &gt;10000</p>



24.	71		<b>**%GI P388:</b> 100 @ 1000 nM, 96.9 @ 100 nM, 15.9 @ 10 nM <b>A549:</b> 98.5 @ 1000 nM, 39.7 @ 100 nM, 0 @ 10 nM
25.	71		<b>**%GI P388:</b> 83.8 @ 1000 nM, 100 @ 100 nM, 3.7 @ 10 nM <b>A549:</b> 98.7 @ 1000 nM, 88.7 @ 100 nM, 0 @ 10 nM

#### 1.2.4. Summary of OSW-1 reported SAR and drug development potential

OSW-1 is a high-affinity binder of both OSBP and ORP4 with especially potent antiproliferative activity.<sup>4</sup> OSW-1 has been recently tested in mouse leukemia models and shown to have high efficacy and acceptable toxicity, even after daily dosing for several weeks.<sup>35</sup> This provides an important indication of OSW-1 and OSW-1-derived compounds as potential lead compounds. In addition to OSW-1's antiproliferative activity, OSW-1 was recently discovered to have potent broad-spectrum antiviral activity.<sup>1,10,11,54</sup> These two disease relevant biological activities of OSW-1 suggest the compound has drug development potential.

The evaluation of OSW-1 SAR was based on two major biological activity: 1) cytotoxicity and 2) binding to OSBP and ORP4. Most of the reported OSW-1 studies have focused on the cytotoxicity of OSW-1 analogs. However, the OSW-1 cytotoxicity was reported in many different studies over two decades, often in different cell lines

measured with different methods.<sup>69</sup> A more reliable measurement for SAR is obtained through measuring binding of OSW-1 analogs to OSBP or ORP4. Our lab and a few others have conducted OSW-1 and OSW-1 analog binding to OSBP and ORP4.<sup>1,10,11</sup> These SAR studies have contributed to our model of OSW-1 interacting within the putative binding pocket of OSBP and ORP4 (**Section 2.2.1, Scheme 2-4**).<sup>1,10,11</sup>

The described SAR studies the putative OSW-1 pharmacophore. An overview of the OSW-1 SAR studies suggests four main critical structural features of OSW-1 biological activity: 1) the sterol C3-OH does not tolerate additional substituents; 2) the side-chain component tolerates elongation but not truncation and the C22-carbonyl group is not required; 3) the arabinose C2-acetate is critical for antiproliferative activity but few SAR campaigns have studied this in detail; and 4) the xylose C2-benzoate component is important and requires a isostere, such as a benzyl amide, to maintain activity.

### **1.2.5. Objective and relevance of this body of work**

Despite its potential therapeutic value, OSW-1 requires further development for two main reason; 1) OSW-1 does not discriminate between OSBP and ORP4 which may lead to potential off-target effects, potentially being cytotoxic,<sup>1</sup> and 2) the structural and synthetic complexity of OSW-1 make it difficult to produce at scale and have stifled further development (*vide infra* **Section 2.1**).<sup>69</sup>

Our putative identification of the OSW-1 pharmacophore will guide the structural modifications to make new classes of OSW-1 analogs for biological testing and potential drug development. The new OSW-1-scaffold, designed based on our OSW-1 SAR model, will be able to incorporate new functionality for enhanced pharmacokinetic (PK) and

pharmacodynamic (PD) properties. The objective of this research has been in developing a simplified synthesis to generate lead compounds of therapeutic value from the OSW-1 structure. The new OSW-1-analogs made possible by the new OSW-1 scaffold will allow for the testing of our proposal OSW-1 SAR model and for the identification of new lead compounds for anticancer and antiviral drug development.

Towards the development of new OSW-1-derived scaffolds, new synthetic routes to 22-aminosterols and an atypical application of the Fukuyama-Mitsunobu reaction to achieve steroidal *N*-glycosylation are reported. The pioneered synthetic routes to aminosterols provide a new approach to generate these scaffolds that was otherwise lacking within the literature (see **Section 2.2.4.4** and **Chapter 3**).<sup>78-83</sup> The atypical application of the Fukuyama-Mitsunobu reaction to achieve *N*-glycosylation further widens the utility of the already established *N*-alkylation method by optimizing conditions for complex molecular scaffolds that was not readily available within the literature (see **Section 2.2.4.7**). These new synthetic routes and optimized methods provide access to complex molecular scaffolds containing aminosterol and *N*-glycosides that were previously inaccessible.

## Chapter 2: New methods for formation of aminosterols and N-glycosides: a concise synthesis of C22-N-glycoside-linked OSW-1-derived compound

**Abstract:** The cholestane glycoside saponin natural product OSW-1 is a potent antiviral and anticancer compound. The OSW-1 antiviral activity is due to its high-affinity binding to oxysterol-binding protein (OSBP). The OSW-1 anticancer activity is due to its high-affinity binding to OSBP-related protein 4 (ORP4). The synthesis and structural complexity of OSW-1, in combination of indiscriminate targeting to both OSBP and ORP4, have limited the study of OSW-1 molecular pharmacology and potential drug development. Herein, the development of a molecular model of OSW-1 interaction within the oxysterol-binding pocket is presented. This model led to the development of a new, three-component approach to develop E-ring azacycle OSW-1 analogs. This work describes the development of new methods to produce 22-aminosterols for rapid assembly of the OSW-1 steroid core and side chain, also the use of a novel Fukuyama-Mitsunobu-glycosylation method to produce a C22-N-glycoside OSW-1 derivative. The synthesis of the C22-N-glycoside OSW-1 derivative is the first example, of which I am aware, of the synthesis of an N-aminosterol glycoside compound. The new synthesis and developed methods produce aminosterol scaffolds readily accessible for the derivation of complex molecular targets, such as OSW-1, and provides a useful N-glycosylation method for use in complex molecule synthesis.

**Contributions:** All of the experimental compounds reported in this chapter I produced. Much of the research reported in this chapter was done in collaboration with Dr. Anh Le-McClain, who was a senior graduate student in our research group. Dr. Le-McClain pioneered the oxo-Ene reaction and Fukuyama-Mitsunobu-glycosylation reactions (**Section 2.2.3**). I further developed these initial efforts into optimized and useful reactions, and I also studied the mechanism of these reactions in detail. Mr. Robert Fogle, a graduate student in our research group, assisted with the *D*-xylose synthesis (**Figure 2-12**). Mr. Gianni Manginelli, an undergraduate researcher in our lab, and Mr. Jorge Rivera-Berrios, a graduate student in our lab, assisted with the synthesis of steroid starting materials. Mr. Zack Severance and Mr. Ryan Bensen, both graduate students in our lab, performed all biological assays, most notably, competitive binding assays for the SAR campaign. The development of the OSW-1 SAR model (**Section 2.2.2**) was a joint effort of the members of the Burgett research group, with some additional help from the structural biology research group of Dr. Christina Bourne, in our department at the University of Oklahoma.

## 2.1. Introduction

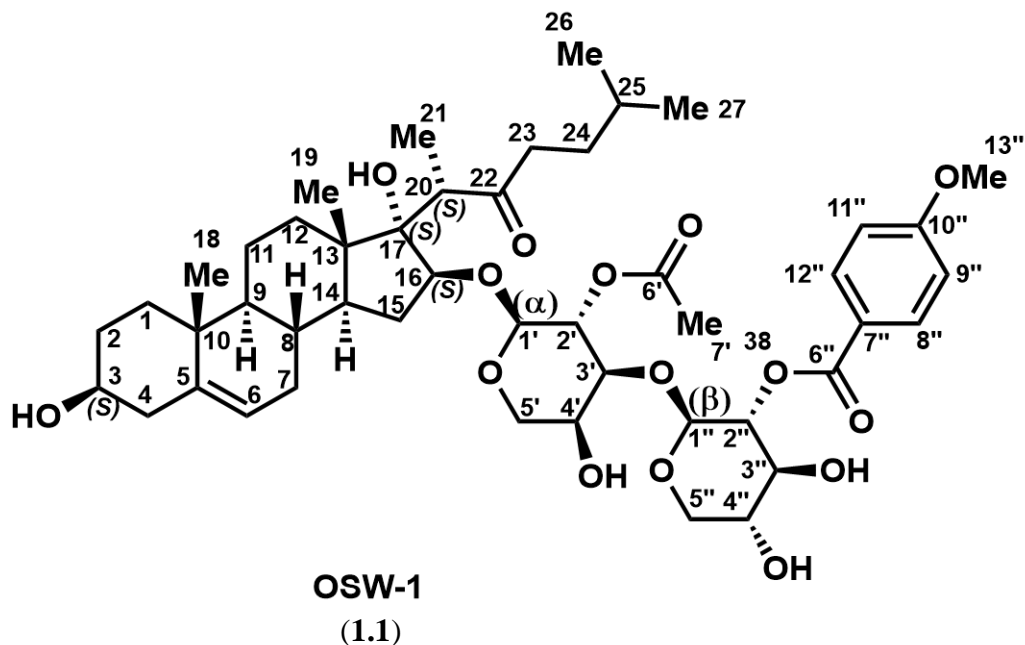


**Figure 2-1:** Two-dimensional representation of natural product OSW-1 (3 $\beta$ ,16 $\beta$ ,17 $\alpha$ -trihydroxycholest-5-en-22-one 16-O-(2''-O-4-methoxybenzoyl- $\beta$ -D-xylopyranosyl)-(1'-->3')-(2'-O-acetyl- $\alpha$ -L-arabinopyranoside), including official numbering of all carbon atoms.

Oxysterol-binding protein (OSBP) and OSBP-related protein 4 (ORP4) are novel potential drug targets for antiviral and anticancer therapeutic development, respectfully (see **Section 1.1**).<sup>1</sup> The natural product, OSW-1 (**Figure 2-1**; **Compound 1.1**) is a high-affinity ligand of both OSBP and ORP4, and OSW-1 has been shown to be a potent antiviral and antiproliferative compound (see **Section 1.1**). Due to its activity, OSW-1 is a potential chemical probe to study both OSBP and ORP4 cellular functions.<sup>1-3</sup> The non-discriminating affinity of OSW-1 for both OSBP and ORP4 limits its usefulness as a drug candidate, but its potent bioactivity (see **Figure 1-1**) makes it an excellent starting point for development of new antiviral and new precision anticancer agents. There is extensive evidence that OSBP and ORP4 can be selectively targeted by small molecules (see **Section 1.1.3**),<sup>1,30,36</sup> but there has not been a systematic program to produce OSBP-

selective antiviral compounds and ORP4-targeting precision anticancer compounds from OSW-1 derived scaffolds.

Multiple OSW-1 total syntheses have been reported,<sup>36,56,62,68–70,74–77,84–86</sup> and various OSW-1 derived analogs have been generated.<sup>57,63,64,87–89</sup> Despite these extensive synthetic efforts, an effective means to generate OSW-1 derived scaffolds for biological studies of interest have yet to be realized. The structural complexity of the OSW-1 natural product has required laborious and complex total syntheses. Such complexity narrows the synthesis flexibility necessary to rapidly and easily generate libraries of OSW-1-derived compounds necessary for potential drug development and biological studies. The general approach within the reported total syntheses of OSW-1 is characterized by elaboration and oxidation of the steroidal body which is then merged with a functionalized Arb-Xyl-disaccharide via a Schmitt glycosylation.<sup>69</sup> The published total syntheses require approximately seven steps to generate the oxidized sterol, including a critical and low yielding osmium tetroxide oxidation step (~40% yield).<sup>69</sup> 17 steps are required to generate the disaccharide.<sup>69</sup> These two components are then merged in a low yielding Schmidt glycosylation step (~50%) followed by subsequent deprotection.<sup>57,63,89</sup>

Beyond the length and limitations of the published total syntheses of OSW-1, the communicated syntheses do not facilitate easy modifications or deviations to be made to the OSW-1 structure. The published approaches are variations on the same strategy of combining the oxidized sterol body with a disaccharide component through the same glycosylation reaction,<sup>36,56,62,68–70,74–77,84–86</sup> and therefore the developed total syntheses of OSW-1 have a stringent scope not suitable to develop a systematic program to discover and create new types of OSW-1 derived scaffolds.

Herein, an investigation into simplified OSW-1 derived scaffolds for chemical biology elucidation and therapeutic targeting of OSBP and ORP4 proteins is reported. We developed a model of OSW-1 structure activity relationship (SAR) binding to OSBP and ORP4 based on our binding results of OSW-1 analogs and our homology modeling of OSW-1 bound to predicted OSBP and ORP4 sterol binding domains. The developed OSW-1 SAR binding model was the design basis for a new strategy to produce simplified OSW-1 scaffolds. The proposed new OSW-1 scaffolds are planned to form through a convergent three-component synthesis approach, combining a steroidal body component, a sterol side-chain component, and a disaccharide components (**Scheme 2-4**). These three components are envisioned to be combined to form an azacycle E-ring OSW-1-derived scaffold (**Scheme 2-4**). The three component azacycle E-ring strategy will facilitate structural alterations of each component for derivation. This approach required the development of new synthetic methods to generate C22-aminosterols and to perform *N*-glycosylation of the aminosterols. A Fukuyama-Mitsunobu-glycosylation method to attach the disaccharide to the C22-aminosterols was created. The newly developed methods and approaches will provide synthetic access to OSW-1 derived scaffolds and will also be general methods to access other aminosterol compounds and aminoglycoside carbohydrate-containing compounds.

## **2.2. Results:**

### **2.2.1. Predicted model of OSW-1 as it exists within the OSBP/ORP oxysterol binding pocket**

We have developed a model of OSW-1 as it exists within the OSBP/ORP binding pocket (**Scheme 2-3**). This predicted model is based on: 1) a thorough and detailed

literature investigation of the antiproliferative activity of OSW-1 analogs, as discussed in **Section 1.2**,<sup>23,30,70</sup> 2) our own calculated OSW-1 docked structure in an OSBP and ORP4 sterol binding domain predicted from modeling to solved OSBP/ORP homology

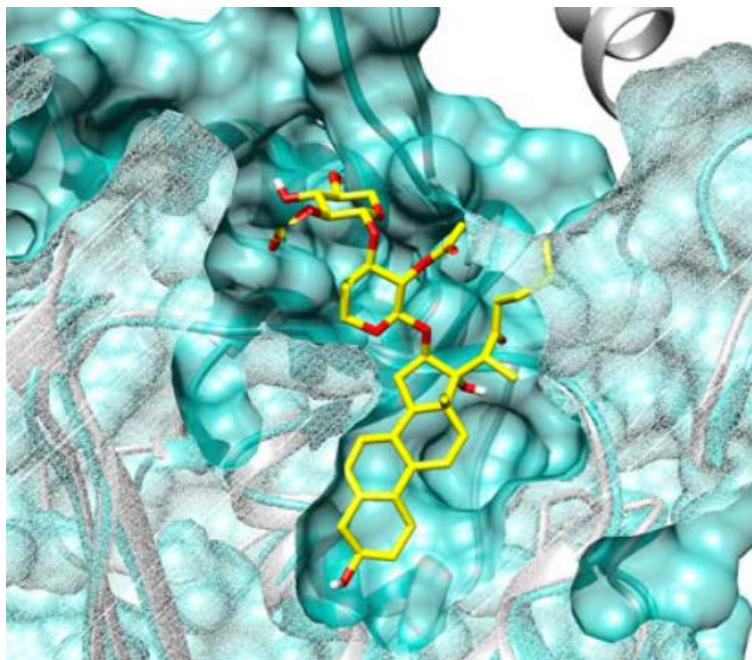


**Figure 2-2.** Possible docked OSW-1 structure within computationally modeled OSBP structure. The OSBP protein structure is computationally rendered from yeast OSBP/ORP crystal structures. This figure was created in collaboration with Dr. Christina Bourne at the University of Oklahoma.

structures (**Figure 2-2**, done by the Bourne research group),<sup>20,21,24</sup> and 3) our OSW-1 and OSW-1 analog SAR binding results to OSBP and ORP4.

Our developed model provided critical insight in identifying the biologically important structural features of OSW-1 and provided a foundation for the design of new OSW-1 derived scaffolds. The

major elements of our predicted model of OSW-1 bound to OSBP and ORP4 sterol binding domain are as follows.

- **C3-Hydroxy**: Although no protein structure of OSBP and ORP4 have been reported, yeast OSBP-related domains (ORD) homologs, which encompass the conserved ligand binding domain, have been co-crystallized with various steroidal ligands (**Section 1.1**).<sup>16,20,21,24</sup> The co-crystallized structures revealed that sterols bind in a

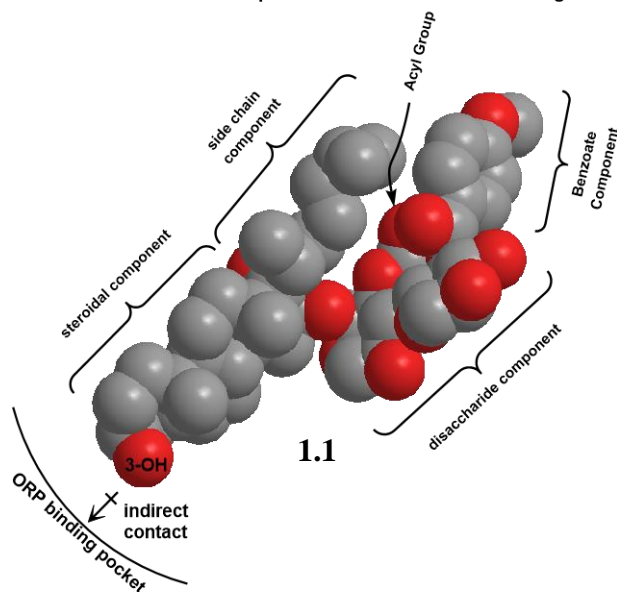


largely hydrophobic tunnel, with the C3-hydroxyl at the bottom of the pocket, while the sterol side chain extends to the top of the tunnel to interact with a putative lid region of the ORD.<sup>16,19–21,24</sup> Analogously, in our model (**Figure 2-2**), the hydrophobic steroidal ring-structure of OSW-1 binds with the 3-hydroxyl buried into the OSBP/ORP hydrophobic tunnel, which is formed by the conserved sterol binding domain (**Figure 1-2**). Our model suggests that the C3-hydroxyl position does not make direct contact with residues within this domain but can flexibly interact with the protein through water molecule mediated interactions.<sup>23,90</sup> SAR studies of the C3-hydroxyl revealed that the presence of sterically large tert-butyl dimethyl silyl (TBS) group at this position was not tolerated for OSBP or ORP4 binding.<sup>85</sup>

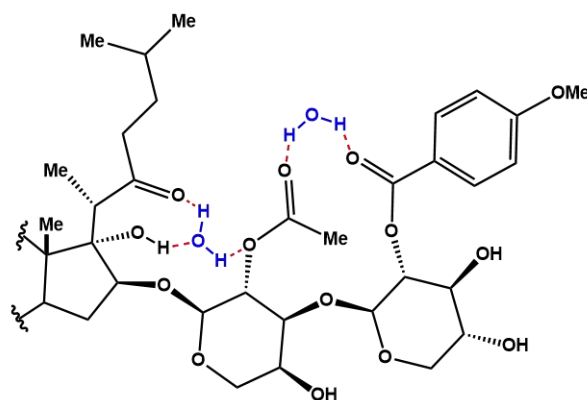
- **Structural tolerance of D-ring and side chain:** Multiple oxysterols (cholesterol<sup>19–21</sup>, 25-hydroxycholesterol,<sup>16</sup> 20-hydroxycholesterol,<sup>19</sup> ergosterol,<sup>19,20</sup> dehydroergosterol<sup>19,20</sup>) have been crystallized in the yeast homolog ORD<sup>16,19–21,24</sup> which is evidence that structural variability from the steroidal D-ring to the side-chain component are well tolerated (see **Section 1.2.1**.) Our SAR studies revealed that hydroxylation at different positions on the side chain of oxysterols (i.e. C-20 or, C-25) is well tolerated for interactions with OSBP and ORP4, but variation of the alkyl carbon skeleton from the isohexyl group is not well tolerated (see **Chapter 4**).
- **Disaccharide as a putative spacer unit:** In our model, the disaccharide serves as a polar spacer unit between the sterol and the biologically-important benzoate component.<sup>72,91</sup> The model, as supported within the literature (see **Section 1.2**), suggests the disaccharide makes minimal contact to the OSBP/ORP4 protein directly.<sup>23,90</sup> This is evident by the structurally-diverse small molecules lacking

saccharides that are known high-affinity ligands of OSBP and ORP4 (**Figure 1-1**), such as, cephalostatin 1 (**1.2**) schweinfurthen A (**1.3**). Truncation of the disaccharide component of OSW-1 to a monosaccharide results in a 100-fold decrease in antiproliferative activity (see **Section 1.2**).<sup>59</sup> Importantly, substituents off the xylose C4-hydroxyl position and, to a lesser extent, the C3-hydroxyl position, are well tolerated within the OSBP/ORP binding pocket.<sup>1,75,76</sup> The xylosyl C3- and C4-

**A. Conformation within an aqueous environment of ORD binding domain**



**B. Hydrogen bonding network leading to conformation**



**Scheme 2-3. A.** Space filling model of OSW-1 in aqueous environment as it exists within the ORD binding pocket. **B.** The putative hydrogen bonding network of OSW-1 as facilitated by arabinose C2-acetate leading to conformational selectivity.

hydroxyl substituents have been used to attach functional groups, including linkers and fluorescent tags while maintaining biological activity.<sup>1,22,70,75,76</sup> This suggests these xylose positions are likely solvent exposed when OSW-1 is bound to OSBP and ORP4 and are not critical in binding activity.

Our SAR studies show that removal of the acyl groups, including the xylosyl-C2- *para*-

methoxybenzoate group (PMB) significantly reduces compound binding to OSBP and ORP4 and its biological activity.<sup>54,55</sup> OSW-1-related natural product compounds with minimal structural variations of the benzoate group, including dimethoxy and cinnamoyl benzoates, are reported to have comparable growth inhibitory activity to OSW-1 for cancer cell lines (see **Section 1.2.2**).<sup>56,69</sup> Substitution of the xylosyl-C2-hydroxyl is limited to aryl carbonyl groups and does not tolerate sterically bulky substituents.<sup>56</sup> Additionally, transformation of the PMB ester bond to an amide bond is reported to induce a modest increase in cytotoxicity potency (**Section 1.2.2**).<sup>56</sup>

This developed model suggests the disaccharide is a polar spacer unit between the critical sterol and benzoate component, and that the main structural purpose of the disaccharide is to appropriately orientate the sterol and benzoate components in relation to each other for interaction with OSBP and ORP4. The calculated OSW-1 docked structure within OSBP (**Figure 2-2**) does not accurately depict the putative orientation of the acyl groups and side-chain components as our results and literature have described them. An accurate depiction of the spatial orientation of the acyl groups and side-chain components in relation to each other is depicted in **Scheme 2-3**.

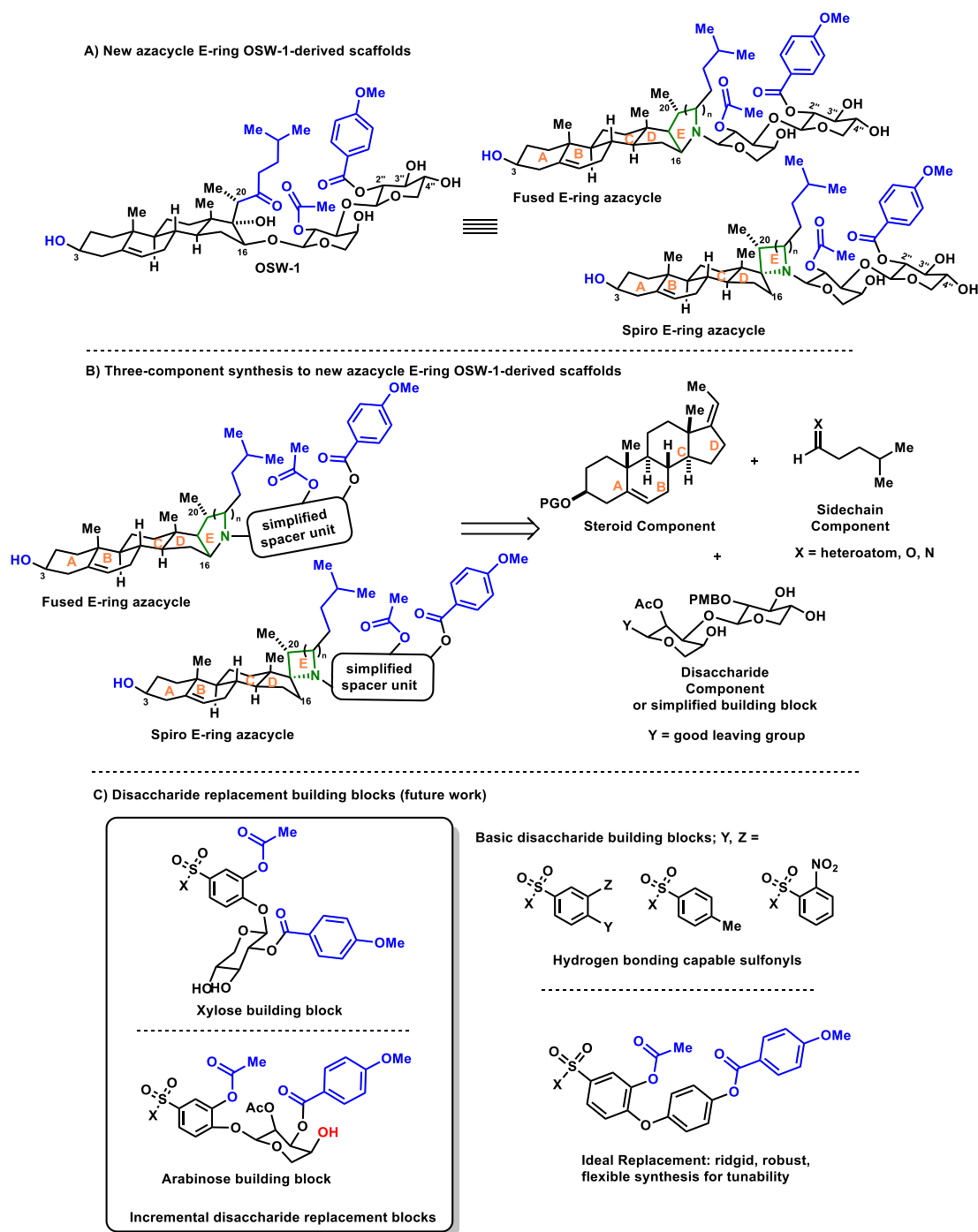
- **OSW-1 conformation controlled by putative hydrogen bonding network:** Our analysis of the OSW-1 structure suggests a specific OSW-1 conformation is preferentially adopted through an intramolecular hydrogen bonding network (**Scheme 2-3**). The hydrogen bonding network is suggested by the atomic distances between the C17 hydroxyl, C22 ketone, arabinose-C2 acetate, and xylose-C3 benzoate.<sup>23,90</sup> The hydrogen bonding network places the benzoate component, acyl group, and

sidechain in relatively close proximity, protruding away from the sterol in a parallel fashion (**Scheme 2-3**). Based on the reported co-crystallized OSBP homologue structures, these components may interact with the putative lid region of the protein.<sup>16,19–21,24</sup>

This hypothesized OSW-1 hydrogen bonding model is supported by a significant loss of OSBP/ORP4 binding affinity and cytotoxicity in analog compounds lacking the arabinose-C2 acetate and the xylose-C3 benzoate.<sup>23,90</sup> Importantly, no arabinose-C2 deacetylated OSW-1 derivatives still possessing the benzoate component have been reported.<sup>69</sup> Within our model, the arabinose-C2 acetate group is the key bridge in the intramolecular hydrogen bonding-network between the sterol hydrogen bonding participants and the xylose-C3 benzoate (**Scheme 2-3. B.**).<sup>23,90</sup> Deacetylation disrupts that hydrogen bonding network and the preferred conformation, resulting in a loss of OSBP and ORP4 binding and cytotoxicity (see **Section 1.2**).<sup>23,90</sup>

### **2.2.2. Binding-model guided development of a new simplified, E-ring OSW-1 scaffold through a three-component synthesis approach.**

Our model of OSW-1 as it exists within the OSBP/ORP binding pocket suggests two important features for the development of new OSW-1 scaffolds: 1) the disaccharide serves as a spacer and linker unit between the sterol and the critical benzoate component, and 2) a hydrogen bonding network between the D-ring of the sterol, the side chain, and the arabinose acetate facilitates a rigid OSW-1 conformation well-suited for OSBP and ORP4 binding. Based on this developed model, we envisioned an OSW-1-derived structure including an azacycle E-ring bridge unit that connects the steroidal component, the side-chain component, and the disaccharide component (**Scheme 2-4. A.**). The



**Scheme 2-4. A.** Structural modifications of OSW-1 as guided and developed by the putative binding model of OSW-1 as it exists within the oxysterol-binding pocket. New fused and spiro E-ring azacycle OSW-1-derived scaffolds are proposed. **B.** Proposed three-component approach for rapid analog development of azacycle E-ring scaffolds. **C.** Proposed incremental changes to disaccharide replacement with arylsulfonyl building blocks in which varying substituents can be added to Y, Z, or R<sub>1-3</sub> for SAR studies.

azacycle E-ring would build upon the steroidal body component to connect the side-chain

component and the disaccharide or disaccharide building block components (**Scheme 2-4. B.**). In addition to bringing the three-components together, the azacycle E-ring introduces a new dimension of subtle modifications with respect to sidechain and disaccharide orientations, which can be tuned in three dimensions by manipulation of E-ring size and the fused- or spiro-cyclic ring connections. The new E-ring azacycle bridge will mimic the putative intramolecular hydrogen bonding network present in the disaccharide component of OSW-1 and will reduce the degrees of freedom, especially of the side chain.

In our model, the disaccharide mainly serves as a spacer unit between the sterol and the xylose-C2 benzoate, and therefore, the disaccharide should be able to be replaced by a simpler, more easily accessed spacer unit. The ideal disaccharide replacement will be simple, rigid, and robust, and will provide highly manipulatable scaffolds for effective orientation of the sterol and the critical benzoate group (**Scheme 2-4. C.**).

This three-component azacycle E-ring approach reduces the OSW-1 analog structural and synthesis complexity by circumventing the tedious oxysterol and disaccharide constructions, while also removing the low yielding, late-stage Schmidt glycosylation. This three-component synthetic approach efficiently orientates the biologically critical structural components of OSW-1 in a high-atom-economy structure to afford simplified molecular targets for the biological elucidation and therapeutic targeting of OSBP and ORP4.

### **2.2.3. Overview of the new OSW-1-related chemistry research performed**

Herein the development of a concise route to C22-functionalized aminosterols and the development of a novel application of a Fukuyama-Mitsunobu-glycosylation method to link the 22-aminosterol with the OSW-1 disaccharide are reported. These

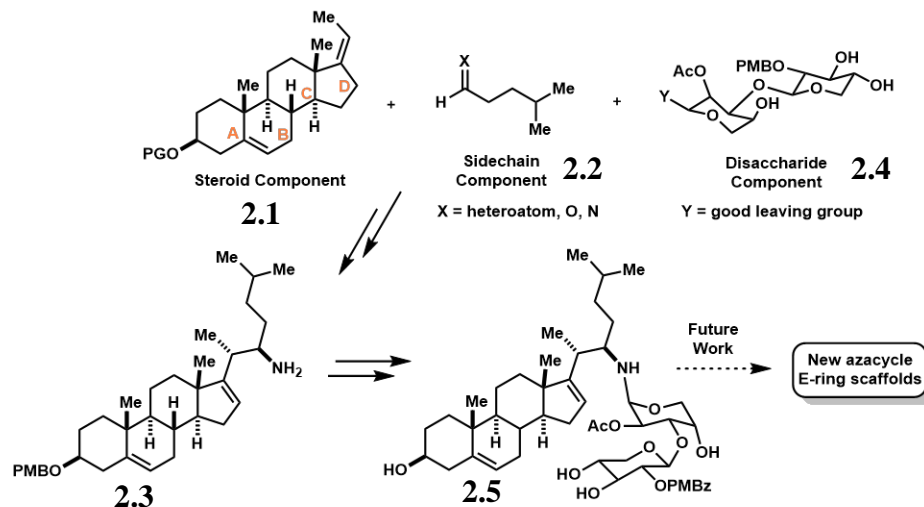


**Figure 2-5.** Overview of new OSW-1 related chemistry research which highlights methods to synthesis 22-aminosterol (**2.3**) and glycosylation methodology of the 22-aminosterols (**2.5**).

accomplishments produced to two new OSW-1 analogs containing C22-glycoside linkages: C22-O-disaccharide and C22-N-disaccharide OSW-1 analogs. These two new analogs, and the associated new methodology, are important steps towards a fully elaborated three-component approach to make the E-ring azacycle OSW-1 derived scaffolds. Synthesis of new OSW-1 analogs through development of a three-component approach.

The three-component approach for the synthesis of OSW-1 analogs as described in **Section 2.2.2**, will combine an oxidized sterol, alkyl side chains, and the disaccharide. In this work, I describe methods to produce and combine these three components and pioneer the foundation of this approach for OSW-1 analog development by producing two new OSW-1 analog compounds, C22-O-Disaccharide and C22-N-Disaccharide. Access to steroid component (**Figure 2-5; 2.1**) required development and optimization of methods to protect the sterol C3-hydroxyl, which is a surprisingly difficult task that required atypical methods. Additionally, access to the correct OSW-1 sidechain

component (**Figure 2-5; 2.2**) prior to being merged with steroid body, required development of a reduction/oxidation sequence. A new synthetic route to aminosterols (**Figure 2-5; 2.3**) were developed as literature procedure for preparation these scaffolds are surprisingly scarce. Through an oxidation/reduction sequence, 22-hydroxysterol was transformed into 22-aminosterol (**Figure 2-5; 2.3**). Additionally, failed reaction sequences to obtain aminosterol (**2.3**), are also reported. Finally, the OSW-1 disaccharide was prepared, and a novel glycosylation method was developed through unique application of a Fukuyama-Mitsunobu to glycosylate aminosterol (**Figure 2-5; 2.5**)

#### **2.2.4. A concise route for the synthesis of C22-aminosterols:**

##### **2.2.4.1. C3-Sterol protection using the TriBot triazine reagent:**

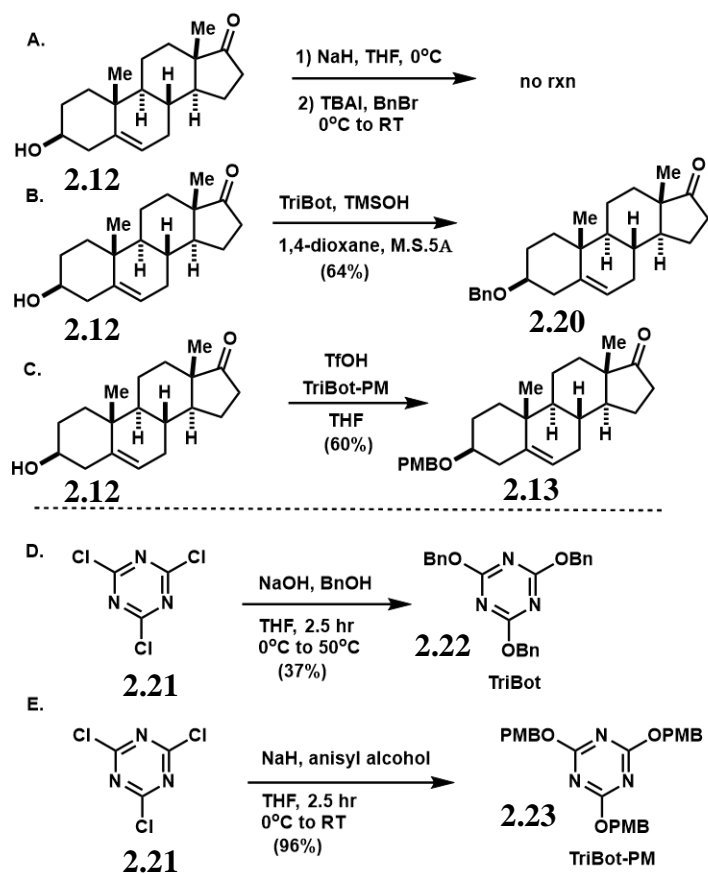
The sterol component synthesis began with protecting the C3-hydroxyl of commercially available *trans*-dehydroandrosterone (**Figure 2-7; 2.12**). Use of an aryl protecting group, such as benzyl or *para*-methoxybenzyl, was of importance to facilitate easier reaction monitoring via TLC under UV visualization and to mitigate undesired reactivity, especially during the Lewis acid catalyzed ene reaction (

**Figure 2-77**). C3-silyl and C3-acetate protecting groups were found to be unstable to the Lewis acid ene conditions. The C3-hydroxyl is well known to be less reactive than typical secondary hydroxyls, and often, yields of protecting this sterol group are much lower than expected.<sup>92-94</sup> The inherent difficulty associated with the C3-hydroxyl as a nucleophile is shown by the unsuccessful benzylation of this position using typical phase transfer etherification conditions, as shown in **Scheme 2-6.A**.

To overcome the difficulty in benzyl protection of the C3-hydroxyl, a lesser known benzylating reagent, TriBot (**Scheme 2-6.B, D, 2.22, 2.23**) was employed.<sup>95,96</sup> TriBot is



an electron deficient triazinedione, established for acid catalyzed benzylation of nucleophiles.<sup>95,96</sup> Variations of TriBot have been developed to install protecting groups other than benzyl, including tert-butylation, p-methoxy benzylation, allylation, and amidation.<sup>96-100</sup> TriBot was generated from cyanuric chloride (**2.21**) and benzyl alcohol in the presence of sodium hydroxide in a 37% yield (**Scheme 2-6. D.**). The C3-hydroxyl was then benzylated using TriBot (**2.22**) in the presence of trifluoro methane sulfonic acid



**Scheme 2-6.** C3 protection strategy employing TriBot protecting agent. **A.** Classic Williamson ether conditions afforded no products. **B.** TriBot benzylating agent employed to benzyl protect C3-hydroxyl. **C.** TriBot-PM, *para*-methoxy benzylating agent employed to PMB protect C3-hydroxyl. **D.** Generation of TriBot benzylating reagent. **E.** Generation of TriBot-PM, paramethoxyl benzylating reagent.

(**Scheme 2-6. C.**). The product was, **2.13**, purified away from the resulting cyanuric by-products through recrystallization at a consistent 60% yield, including on multigram scale.<sup>95,96</sup> In anticipation of eventual deprotection of the final compound, newly developed protecting strategy was adapted to install *para*-methoxy benzyl group (PMB) (**Scheme 2-6. Compound 2.13**). The OSW-1 disaccharide also used PMB groups and use of

PMB at the C3-sterol position would facilitate a single global PMB deprotection at the end-stage of the synthesis. The PMB-protected sterols could also be purified on multi-gram scale via recrystallization. Overall, the TriBot-PM protection strategy affords milder reaction conditions, bypasses column chromatography, and affords comparable yields to previous methods for C3-sterol protection.<sup>92-94</sup> This is the first account of steroid C3-hydroxyl protections using TriBot-based benzyl and PMB and will be generally useful in similar sterol syntheses.

#### 2.2.4.2. Synthesis of complete sterol component through developed ene reaction:

Complete synthesis of the OSW-1 sterol skeleton was planned through direct introduction of the sterol side chain as an alkyl aldehyde through an ene reaction. This proved to be unexpectedly difficult because the 4-methyl pentanal side chain component

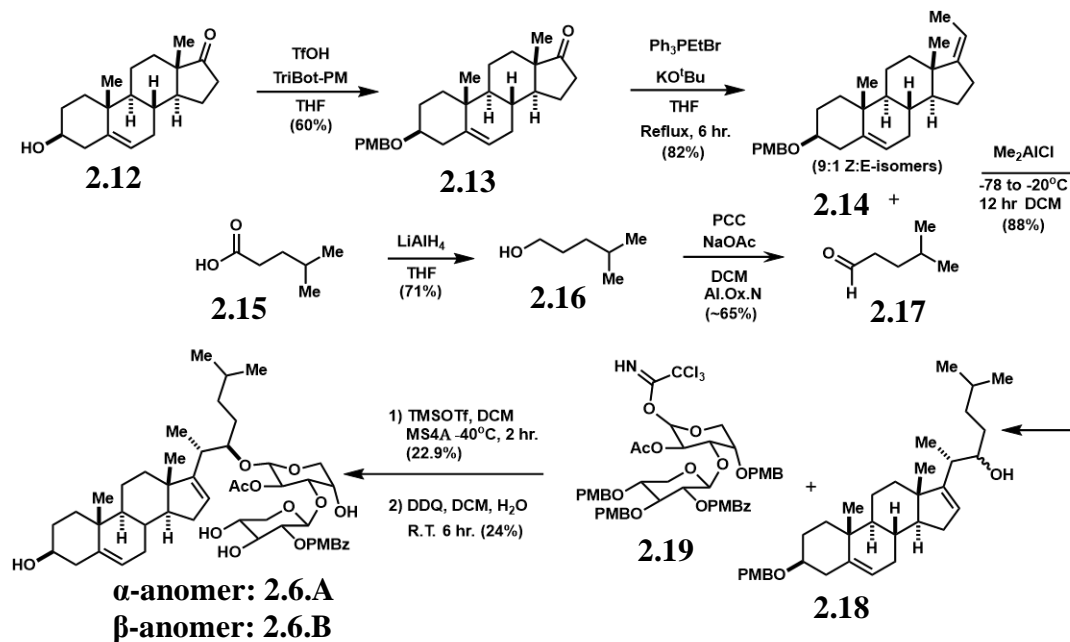


**Figure 2-7.** Total synthesis of C22-O-glycoside OSW-1-derived scaffold (2.6).

(2.17) was not readily available and the limited literature procedures describing its synthesis were not reproducible in my hands. Synthesis of 4-methyl pentanal (**Figure 2-**

**7; 2.17**) required a reduction/oxidation sequence and stringent purification conditions. Method development to merge the alkyl aldehyde (**2.17**) with functionalized steroid (**2.14**) proceeded smoothly. This is the first account of elaboration to the full sterol skeleton in a single step.

The PMB protected dehydroandrosterone (**Figure 2-7; 2.13**) underwent Wittig olefination to produce PMB protected pregnadiene (**2.14**), with 9:1 Z:E-isomers of the exocyclic olefin, at an 82% yield on multigram scale. Exocyclic sterol olefin (**2.14**) could then be combined with alkyl aldehydes of varying length and branching through a developed ene reaction.<sup>84</sup> However, to obtain the desired isohexyl side chain, 4-methyl pentanal (**Figure 2-8, Compound 2.17**) was needed, and access to this aldehyde provided an unexpected challenge. 4-methyl pentanal (**2.17**), is not commercially available, although various isomeric aldehydes were commercially available. During the course of my studies, 4-methyl pentanal was determined to have a stability of a few hours, and the compound was not stable to silica gel chromatography or distillation.

I anticipated accessing 4-methyl pentanal (**Figure 2-7; 2.17**) in a straightforward two step synthesis from commercially available 4-methyl pentanoic acid via reduction followed by oxidation however, this required extensive reaction and purification development.

Four different synthetic routes were attempted to synthesize 4-methyl pentanal (**2.17**) from 4-methyl pentanoic acid (**Figure 2-8; 2.15**) esterification followed by DIBAL reduction; 2) Weinreb-amide synthesis followed by reduction; 3) reduction followed by Swern oxidation; and 4) reduction followed by PCC oxidation. The DIBAL reduction of the corresponding ester only produced over-reduced alcohol (**2.16**). The Weinreb-amide

approach was expected to have the added benefit of long-term amide stability prior to hydride reduction. Although generation of the 4-methyl pentyl Weinreb amide proceeded with ease at quantitative yields, no product was ever obtained upon reduction. This is presumably due to purification issues that were later resolved. The third route to generate 4-methyl pentanal (**2.17**) was via Swern oxidation at cryogenic temperatures and only produced trace amounts of the desired aldehyde (**2.17**) after extensive optimization. Any

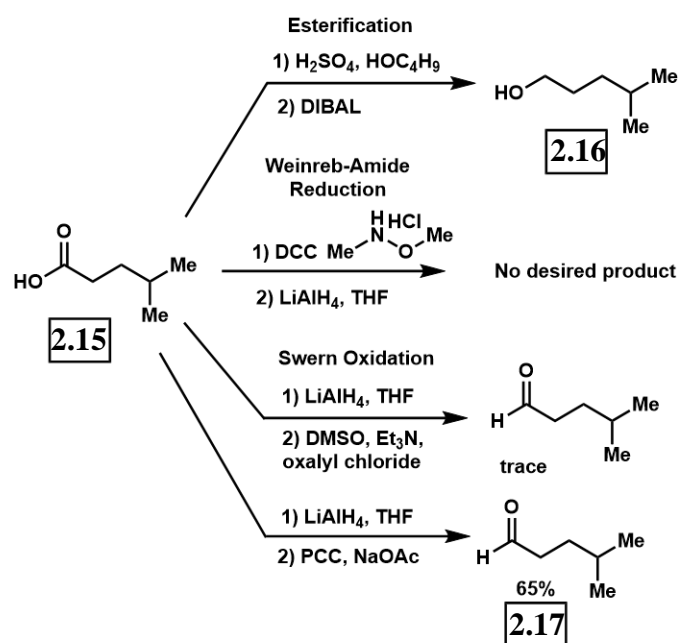


**Figure 2-8.** Various synthesis pathways attempted to generate 4-methylpentanal.

loss of temperature control led to known oxalyl chloride side-products that could not be separated from the desired product.

Finally, a pyridinium chlorochromate oxidation (PCC) was employed to obtain 4-methyl pentanal (**2.17**) from 4-methyl pentanol (**2.16**) in modest

yields. The desired compound was not stable during distillation purification, and the compound degraded on silica gel. Screening of purification conditions revealed that compound chromatographic purification could be achieved using a 1:1 mixture of oven-dried silica and neutral aluminum oxide as the stationary phase, with DCM as mobile phase. This purification was beneficial as it filtered off all chromate reagents and purified

the desired for immediate use. This is the first detailed account of 4-methyl pentanal being synthesized and facilitated the synthesis of multi-gram of aldehyde to be generated.

Having synthesized both steroid (**Figure 2-7; 2.14**) and side-chain components (**Figure 2-7; 2.17**), the next step was to merge these motifs to generate C22-hydroxy sterol(**2.18**) which was accessible through an established Lewis-acid mediated ene reaction.<sup>101</sup> PMB protected pregnadiene (**Figure 2-7; 2.14**) was reacted with 4-methyl pentanal (**Figure 2-7; 2.17**) in the presence of dimethyl aluminum chloride. My optimized conditions in the ene reaction proceeded at a reproducible 88% yield and produced exclusively (*S*)-configuration at the C20 position<sup>83</sup> and a racemic mixture of (*R/S*) 22-hydroxysterol stereoisomers (**Figure 2-7; 2.18**) on multigram scale. The stereospecificity of the C20-position of 22-hydroxysterol (**Figure 2-7; 2.18**) is presumably because only the *Z*-isomer reacted.

This ene reaction, producing the 22-hydroxysterol product provided a convenient branching point for the synthesis of other steroidal molecular targets. Through the ene reaction different alkyl aldehydes could be reacted with pregnadiene to afford sterol skeletons of varying side-chain lengths and functionalities. Additionally, the 22-hydroxysterol product (**Figure 2-7; 2.18**) contains a C16-C17 olefin and C22-hydroxyl group, both of which provide functional handles to exploit for derivation.

#### **2.2.4.3. Unsuccessful attempts to install the C22-aminosterol functionality**

The C22-position appears to be unreactive to the majority of nitrogen nucleophiles, presumably due to steric hinderance. Due to this lack of reactivity, it was challenging to establish the desired C22 amine functionality. Mitsunobu amination of C22-hydroxy

sterol and reductive amination of C22-oxycholesterol investigated and found to be unsuccessful in introducing an amine at the C22-sterol position.

**Table 2-1.** Mitsunobu reaction on 22-hydroxy sterol using aryl sulfonyl amide nucleophiles. DTBAD stands for di-tertbutyl azodicarboxamide.

Entry	Amine (1), Equiv.	Substrate		Conditions	Order of Addition	Results
		(2), 1 Equiv.				
1	NsNH <sub>2</sub> , 1.5 equiv.	2.18		Ph <sub>3</sub> P (2.47 equiv.), DEAD (3 equiv.), THF, RT	1,2 into Ph <sub>3</sub> P, DEAD	NR
2	NsNHBoc, 1.5 equiv	2.18		Ph <sub>3</sub> P (2.47 equiv.), DEAD (3 equiv.), THF, RT	1,2 into Ph <sub>3</sub> P, DEAD	NR
3	NsNHBoc, 1.5 equiv	2.18		Ph <sub>3</sub> P (2.47 equiv.), DEAD (3 equiv.), THF, RT	2 then 1 into Ph <sub>3</sub> P, DEAD	NR
4	NsNHBoc, 1.5 equiv	2.18		Ph <sub>3</sub> P (2.47 equiv.), DIAD (3 equiv.), THF, RT	2 then 1 into Ph <sub>3</sub> P, DEAD	NR
5	NsNHBoc, 1.5 equiv	2.18		Ph <sub>3</sub> P (2.47 equiv.), DIAD (3 equiv.), THF, RT	1 then 2 into Ph <sub>3</sub> P, DEAD	NR
6	NsNHBoc, 1.5 equiv	2.18		Ph <sub>3</sub> P (2.47 equiv.), DIAD (3 equiv.), THF, 60°C	All added then dissolved	NR
7	NsNHBoc, 1.5 equiv	2.18		Ph <sub>3</sub> P (2.47 equiv.), DIAD (3 equiv.), THF, 60°C	DIAD into 1, 2, Ph <sub>3</sub> P	NR
8	Phthalamide 1.1 equiv	2.18		Ph <sub>3</sub> P (1.1 equiv.), DEAD (1.1 equiv.), THF, RT	All added then dissolved	NR
9	DNsNH <sub>2</sub> , 1.4 equiv	2.18		Ph <sub>2</sub> PyP (4 equiv.), DTBAD (4 equiv.), THF, 5°C to 77°C	DTBAD into 1, 2, Ph <sub>2</sub> PyP	NR

Unsuccessful Mitsunobu amination of C22-hydroxy cholesterol: Use of a Mitsunobu reaction to introduce an amine at the C22-position of 22-hydroxy sterol(2.18) was investigated and unsuccessful. The Mitsunobu reaction to aminate secondary alcohols is well established<sup>102–104</sup> and has been successfully performed on similar steroid

compounds<sup>103,105,106</sup> Aryl sulfonyl amides are commonly used as latent amine nucleophiles in these reactions due to their acidity and respective nucleophilicity.<sup>102</sup> Mitsunobu conditions were screened using aryl sulfonyl amides as nucleophiles in an attempt to produce a similar compound to **2.30**. This reaction screening began with nosyl amide and C22-hydroxyl cholesterol (**2.18**) under typical Mitsunobu conditions (**Entry 1**). Although nosyl amides have a ~10 pKa acidity,<sup>107</sup> it was possible that stubborn electrophile, **2.18**, required an even more acidic nucleophile to participate in the reaction. The nosyl amide was then protected as Boc carbamate to further lower the acidity below 7 pKa (**Entries 2-7**), and a screening campaign commenced. **Entries 2** and **3** varied Order of addition without any product formation which indicated the azodicarboxamide might not be reactive enough. **Entries 4-7** varied Order of addition using DIAD as the azodicarboxamide however, still no product formed. **Entry 8** was then attempted according to a review article which uses phthalimides to overcome particularly challenging Mitsunobu reactions<sup>108</sup> but without success. The optimized Fukuyama-Mitsunobu glycosylation conditions developed (*vide infra*, **Section 2.2.3**) were also unsuccessful, presumably because the developed conditions are designed to render the alcohol species less reactive. Although this transformation would have been advantageous in the overall synthesis, it was abandoned because all of these conditions failed to transform C22-hydroxy cholesterol.

Unsuccessful reductive amination of C22-hydroxy cholesterol: Since direct displacement of the C22-hydroxy sterol(**2.18**) to form C22-amino cholesterol (**2.29**) failed, a reductive amination sequence using sulfonamide nucleophiles was attempted. First, C22-hydroxy sterol(**2.18**) was oxidized to C22-keto cholesterol (**2.27**) using PDC.<sup>57</sup> As shown in **Table**

**2-2**, C22-keto cholesterol (**2.27**) was then subjected to various conditions for imine formation and/or reductive aminations, based on a similar reductive amination approaches for cycloalk-2-2-enones.<sup>109</sup> Initial efforts used imine formation conditions that I had previously optimized on pregnenolone acetate (**Entries 1-3**). However, unlike pregnanolone acetate, C22-keto cholesterol failed to react. Further screening based on literature precedent of various titanium Lewis acids<sup>109</sup> and reductive aminations<sup>110</sup> (**Entries 4-8, 10-21**) afforded no desired product. Often, especially in the case of titanium tetraethoxide, the PMB protecting group was cleaved (**Entries 4, 20, and 21**). **Entry 10** showed trace amounts of product however, these results were not reproducible and optimization to afford reproducible product formation was unsuccessful. It was possible that the nitrogen nucleophilicity was deactivated by the aryl sulfonyl group, and so methyl sulfonamide (i.e. mesyl group, Ms) was used in place of tosyl sulfonamide (**Entries 22-24**) but was unsuccessful.<sup>111</sup>

**Table 2-2.** Imine and reductive amination reaction conditions to transform 22-keto cholesterol (**2.27**) into C22-amino cholesterol.

Entry	Steroid (1), 1 Equiv.	Amine (2), 3 Equiv.	Conditions	Notes	Results
1	2.27	TsNH <sub>2</sub> , 3 equiv.	TiCl <sub>4</sub> (3 equiv.), toluene, 150°C	-	NR
2	2.27	TsNH <sub>2</sub> , 3 equiv.	TiCl <sub>4</sub> (2 equiv.), toluene & MeCN, 150°C	-	NR
3	2.27	TsNH <sub>2</sub> , 3 equiv.	BF <sub>3</sub> Et <sub>2</sub> O (1 equiv.), toluene, 75°C	-	NR
4	2.27	TsNH <sub>2</sub> , 3 equiv.	TiCl <sub>4</sub> (1 equiv.), Ti(OEt) <sub>4</sub> (3 equiv.) toluene, 150°C	Et <sub>3</sub> N quench	C3-deprotected product



5	C22-keto Cholesterol	TsNH <sub>2</sub> , 3 equiv.	TiCl <sub>4</sub> (1 equiv.), Ti(OEt) <sub>4</sub> (3 equiv.) toluene, 150°C	Et <sub>3</sub> N quench	NR
6	2.27	TsNH <sub>2</sub> , 3 equiv.	Ti(OEt) <sub>4</sub> (3 equiv.) toluene, 150°C	-	NR
7	C22-keto Cholesterol	TsNH <sub>2</sub> , 3 equiv.	TiCl <sub>4</sub> (1 equiv.), Ti(OEt) <sub>4</sub> (3 equiv.) toluene, 150°C	NaCNBH 3 addition	Imine may have formed but no product observed
8	2.27	TsNH <sub>2</sub> , 3 equiv.	TiCl <sub>4</sub> (3 equiv.), toluene, 150°C	Acid + amine refluxed before steroid addition	NR
9	2.27	TsNH <sub>2</sub> , 3 equiv.	AcOH (3 equiv.), toluene, 150°C	NaCNBH 3 addition	NR
10	2.27	TsNH <sub>2</sub> , 3 equiv.	TiCl <sub>4</sub> (1 equiv.), toluene, 24°C	Acid +steroid then amine	Possible trace
11	2.27	TsNH <sub>2</sub> , 10 equiv.	TiCl <sub>4</sub> (1 equiv.), toluene, 24°C	-	NR
12	2.27	TsNH <sub>2</sub> , 3 equiv.	TiCl <sub>4</sub> (1 equiv.), toluene, 24°C	NaCNBH 3 addition	NR
13	2.27	TsNH <sub>2</sub> , 10 equiv.	TiCl <sub>4</sub> (1 equiv.), toluene, 24°C	NaCNBH 3 addition	NR
14	2.27	TsNH <sub>2</sub> , 10 equiv.	TiCl <sub>4</sub> (1 equiv.), toluene, 24°C	NaBH(O Ac) <sub>3</sub> addition	NR
15	2.27	TsNH <sub>2</sub> , 30 equiv.	TiCl <sub>4</sub> (1 equiv.), toluene, 24°C	NaCNBH 3 addition	NR
16	2.27	TsNH <sub>2</sub> , 30 equiv.	TiCl <sub>4</sub> (1 equiv.), toluene, 24°C	NaBH(O Ac) <sub>3</sub> addition	Possible trace

17	2.27	TsNH <sub>2</sub> , 30 equiv.	Ti(OEt) <sub>4</sub> (1 equiv.), DCM, 24°C	NaCNBH <sub>3</sub> addition	NR
18	2.27	TsNH <sub>2</sub> , 30 equiv.	Ti(O <sup>i</sup> Pr) <sub>4</sub> (1 equiv.), DCM, 24°C	NaCNBH <sub>3</sub> addition	NR
19	2.27	TsNH <sub>2</sub> , 30 equiv.	TiCl <sub>4</sub> (1 equiv.), DCM, 24°C	NaBH(OAc) <sub>3</sub> addition	NR
20	2.27	TsNH <sub>2</sub> , 5 equiv.	Ti(OEt) <sub>4</sub> (10 equiv.), <i>neat</i> , 90°C	-	C3-deprotected product
21	2.27	TsNH <sub>2</sub> , 7 equiv.	Ti(OEt) <sub>4</sub> (20 equiv.), <i>neat</i> , 90°C	-	C3-deprotected product
22	2.27	MsNH <sub>2</sub> , 10 equiv.	TiCl <sub>4</sub> (1 equiv.), DCM, 24°C	-	degradation
23	2.27	MsNH <sub>2</sub> , 10 equiv.	NaOAc-3H <sub>2</sub> O (10 equiv.), EtOH, 90°C <sup>111</sup>	-	NR
24	2.27	MsNH <sub>2</sub> , 7 equiv.	Ti(O <sup>i</sup> Pr) <sub>4</sub> (20 equiv.), <i>neat</i> , 90°C	-	NR

#### 2.2.4.4. Successful introduction of C22-aminosterol functionality

Achieving the synthesis of the C22-*N*-glycoside OSW-1 analog required the exploration of new methods and approaches to aminosterols and amino glycosylation in the context of complex molecule synthesis. As shown in **Figure 2-9**, the total synthesis of C22-*N*-glycoside linked OSW-1 derivative (**Compound 2.7**) began through elaboration of the 22-hydroxy sterol (**2.18**) to a 22-aminosterol (**2.29**)

To install the C22 amine group, 22-hydroxy sterol (**Figure 2-9; 2.18**) underwent a sequence of oxidations and reductions, as shown in **Figure 2-9**. First, 22-hydroxy sterol (**2.18**) was subjected to PDC oxidation conditions to generate 22-keto cholesterol (**Figure 2-9; 2.27**) at a 75% yield.<sup>57</sup> 22-keto cholesterol (**2.27**) was then reacted with hydroxy ammonium chloride in the presence of sodium acetate hexahydrate at 75°C to

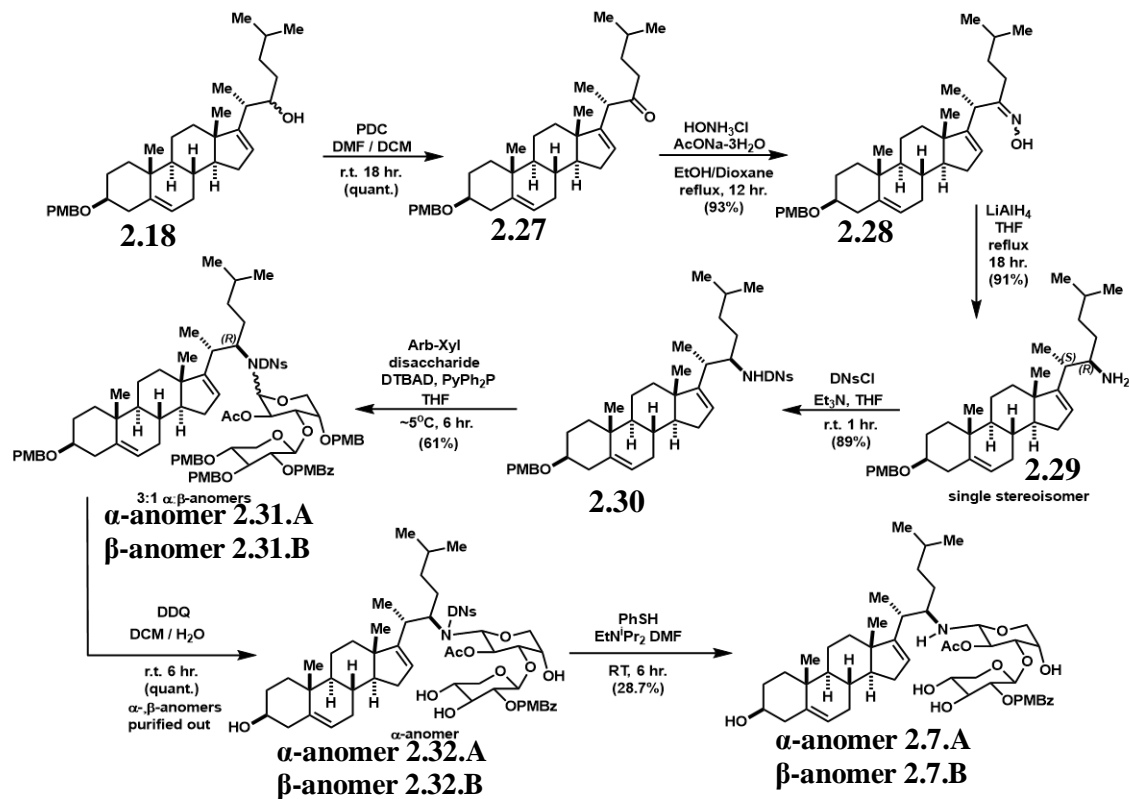


**Figure 2-9.** Total synthesis of C22-N-glycoside linked OSW-1-derived scaffold.

produce steroidal oxime (**2.28**) in quantitative yield (~98%). The afforded oxime (**Figure 2-9; 2.28**) was then reduced with refluxing lithium aluminum hydride to produce a stereoisomeric ratio of 99:1 C22(*R*):C22(*S*), 22-amino cholesterol (**Figure 2-9; 2.29**) at ~90% yield.

Stereochemical assignments were determined via qNOESY.<sup>112–114</sup> qNOESY is a method of conformational and stereochemical determination that has recently been developed to measure the interproton distances of both rigid<sup>112–114</sup> and flexible<sup>115–118</sup> small molecules via nuclear Overhauser enhancement. Using nothing more than a known bond distance between two hydrogens of a methylene atom (H23' and H23'') set at 1.76Å), the spatial distances between neighboring hydrogens can be extrapolated from NOESY spectra, reportedly with high accuracy within a few percent of their true

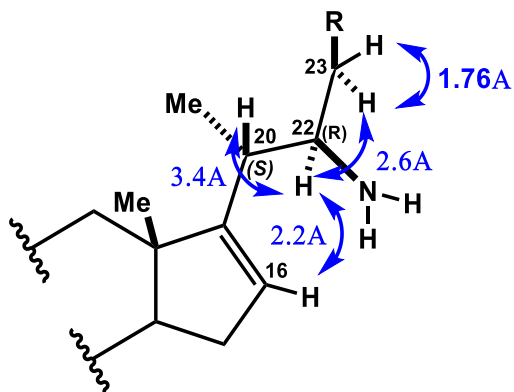


**Figure 2-10.** Measured bond distances as determined through qNOESY; used to determine C20 and C22 stereochemistry.

values.<sup>112-114</sup> As shown in Figure 2-10, the distance between H23' and H23'' for 22-amino cholesterol (**Figure 2-9; 2.29**) was set at 1.76 Å. This was done by taking the integral values of the 1D-NOESY correlation between H23' and H23'' and normalizing it to 1.76 Å. Then through numerous 1D-NOESY spectra, integral values of the neighboring hydrogens were

obtained. These integral values were then plugged into an excel template provided by Dr. Suzan Nimmo. This template processed the data using the newly developed Soloman equations to produce the spatial bond distances shown in **Figure 2-10**.

Previous attempts to uncover the stereochemical configuration of saponin-C22 position included an exhaustive conformational search within literature in combination with computational analysis of local stereochemical minima.<sup>58</sup> These efforts resulted in a qualitative assessment and deemed qNOESY inaccessible to saponin structure due to indirect NOE effects which were believed to render methylene bond distances inconsistent.<sup>58</sup> At the time, this was further complicated by the flexibility of the sterol side chain which was believed to render qNOESY inaccurate. However, modernization of the qNOESY technique has accounted for these inconsistencies and inaccuracies within the calculations, and are reported to provide high accuracy spatial distances within < 3% error.<sup>112-118</sup>

My development of a synthetic route to 22-amino cholesterol (**Figure 2-9; 2.29**) provides a straightforward and high yielding route to aminosterols which has substantial advantages over previously published routes. The difficulties of this transformation provide insight into the lack of reported side-chain aminosterol synthetic methods and approaches. Through successfully obtaining 22-amino cholesterol (**Figure 2-9; 2.29**), a variety of other side-chain aminosterols become accessible through modification/manipulation of the C16-C17 olefin and/or the various C22 functional groups presented.

#### 2.2.4.5. Synthesis of arabinose-xylose disaccharide:

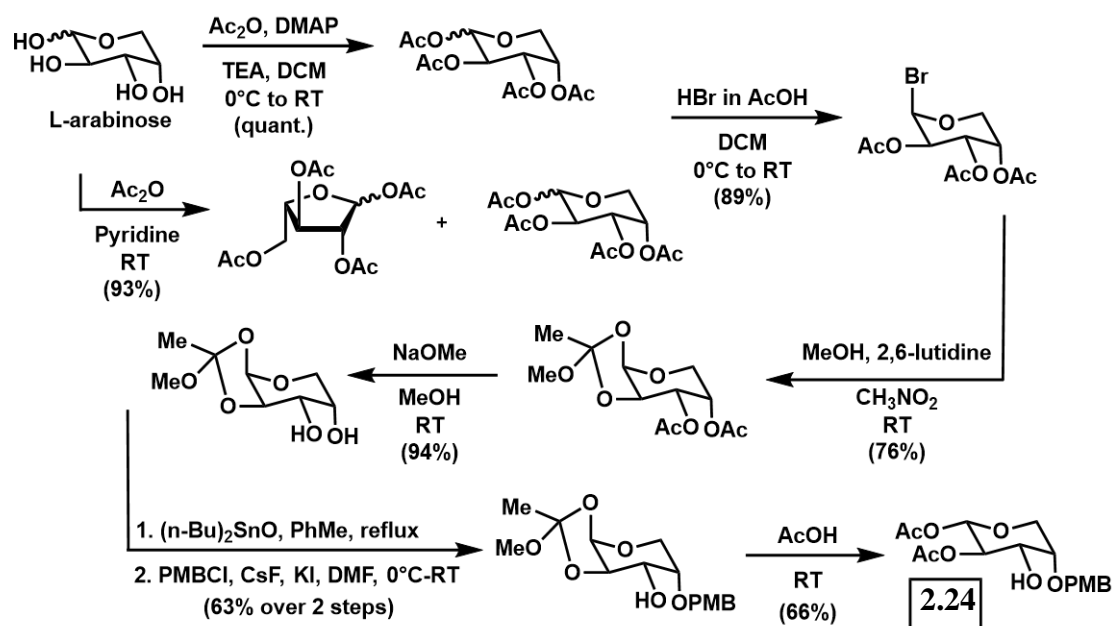


**Figure 2-11.** Synthesis of *L*-arabinose residue over 7 steps.

With synthetic access to 22-hydroxy sterol (**Figure 2-7; 2.18**) and 22-amino cholesterol (**Figure 2-9; 2.29**), the next step was to synthesize the disaccharide component (**2.26**). The disaccharide was synthesized in three stages as previously described.<sup>84</sup> As shown in Figure 2-11, functionalized *L*-arabinose (**2.24**) was synthesized

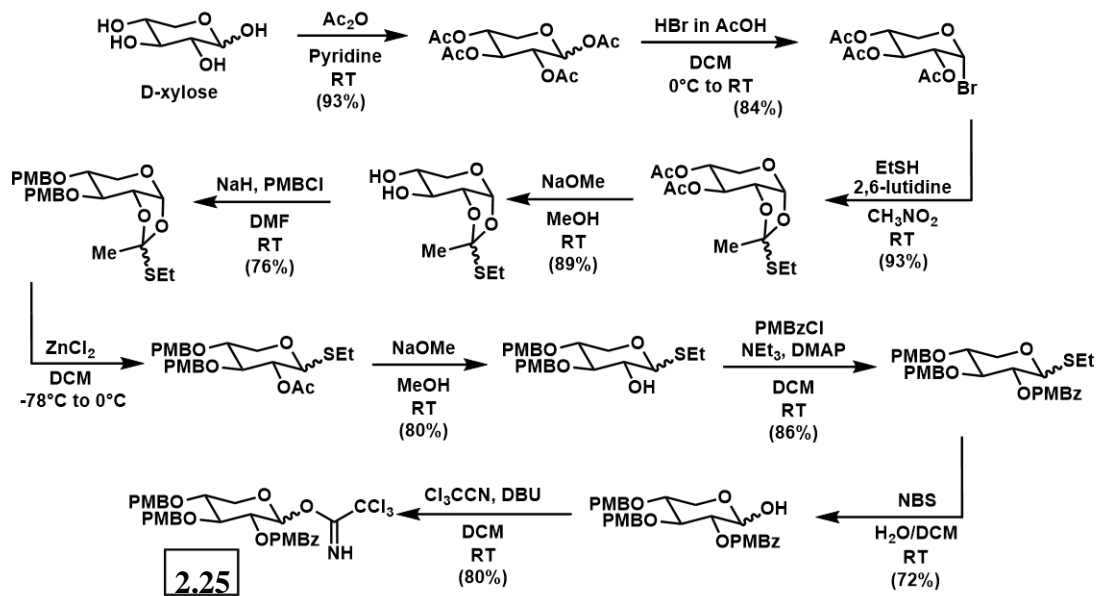


**Figure 2-12.** Synthesis of *D*-xylose imidate residue over 10 steps. on multigram scale over seven steps.<sup>84</sup> Then, as shown in Figure 2-12, functionalized *D*-xylose imidate (**2.25**) was synthesized on multigram scale over 10 steps.<sup>84</sup> Lastly, *L*-arabinose (**2.24**) and *D*-xylose imidate (**2.25**) were coupled through a Schmitt glycosylation, as shown in Figure 2-13. A single  $\beta$ -anomer is produced due to anchimeric assistance of the neighboring acetyl which blocks nucleophilic attack to the axial position.<sup>69</sup> During the Schmidt glycosylation, the neighboring acetyl attacks the oxonium at the C2 in the axial position to stabilize the positive charge, thereby preventing

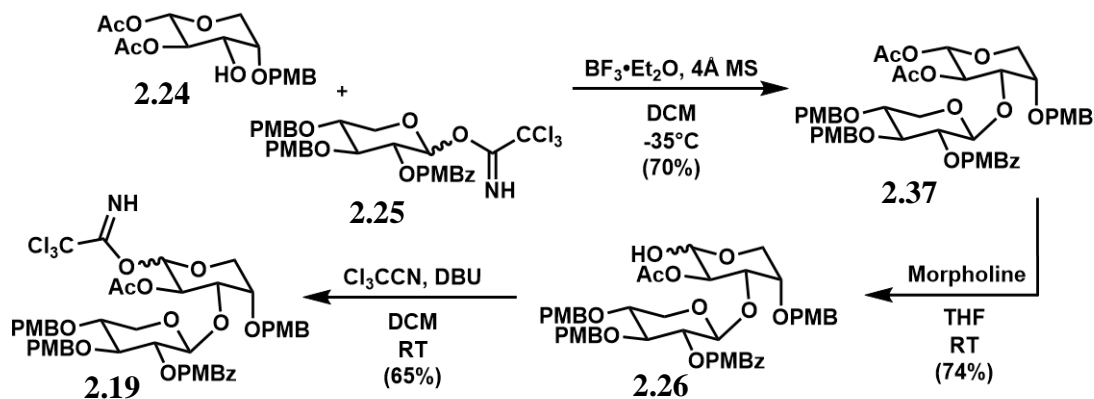


**Figure 2-13.** Synthesis of disaccharide imidate through Schmitt glycosylation of *L*-arabinose and *D*-xylose imidate.

formation of the  $\alpha$ -anomer.<sup>119</sup> This disaccharide was then prepared for a second Schmitt glycosylation to the steroid by transforming it into imidate, **2.19**. This imidate is shelf-stable for months if completely dried and stored at -20°C which allowed for multigram quantities of **2.19** to be generated.

#### 2.2.4.6. Total synthesis of C22-O-Glycoside linked OSW-1 derivative

22-hydroxy sterol (**Figure 2-7; 2.18**) and disaccharide imidate (**Figure 2-7; 2.19**) were then merged together via a Schmitt glycosylation. Using standard conditions for the Schmidt glycosylation reaction, 22-hydroxy sterol (**Figure 2-7; 2.18**) was reacted with disaccharide imidate (**Figure 2-7; 2.19**) in the presence of a catalytic amount of trimethylsilyl trifluoromethanesulfonate at -40°C for two hours to generate a mixture of  $\alpha$  and  $\beta$ -anomers.<sup>69</sup> Interestingly, only the 22(*R*)-hydroxy cholesterol reacted under Schmitt glycosylation conditions to produce 10:1  $\alpha/\beta$ - ratio of **Compounds 2.31.A** (10.1 mg) and **2.31.B product** (1.6 mg) at a low 18.8% overall yield upon HPLC purification. The **Compound 2.31.A** ( $\alpha$ -anomer) was assigned using diagnostic <sup>1</sup>H and <sup>13</sup>C chemical shifts (**Figure 2-7**).<sup>120</sup> The preference for **Compound 2.31.A** ( $\alpha$ -anomer) was expected, based on the anchimeric assistance of the neighboring acetate group.<sup>119</sup> The C22-O-Glycoside linked OSW-1 derived analog (**Figure 2-7; 2.1.A**) was completed through global PMB deprotection of **Compound 2.31.A** ( $\alpha$ -anomer) which was carried out under established DDQ deprotection reaction conditions.<sup>89</sup> Crude material purified via high pressure liquid chromatography mass spectrometry (HPLC-MS) using Shimadzu instrumentation equipped with Luna 5  $\mu$ m C8(2) 100Å column and gradient mobile phase of 98% to 100% acetonitrile to 0.1% formic acid/water. 1.5 mg of **Compound 2.1.A** ( $\alpha$ -

anomer) was synthesized at a 23% yield over 5 linear steps from *trans*-dehydroandrosterone.

Biological evaluation of C22-*O*-Glycoside  $\alpha$ -anomer (

**Figure 2-7, Compound 2.1**) commenced using a well-established radioactive 25-hydroxy cholesterol ( $[^3\text{H}]$ -25-OHC) competitive binding assay against OSBP and ORP4.<sup>11</sup> Unfortunately, this analog did not exhibit competitive binding to OSBP or ORP4. C22-*O*-Glycoside  $\beta$ -anomer produced insufficient material for testing. The failure of **Compound 2.6** to bind is consistent with the reports of other OSW-1 glycosylated side-chain analogs being inactive (see **Section 1.2.3**).

#### **2.2.4.7. Development of a Fukuyama-Mitsunobu reaction for the formation of *N*-sterol glycosides**

The total synthesis of C22-*N*-glycoside (**Section 2.2.4.8**) required a novel approach for successful aminosterol glycosylation because there are few reports of non-peptide complex molecules containing amino glycoside bonds.<sup>121–129</sup> The total synthesis of C22-*N*-glycoside OSW-1 compound is the first report of an aminosterol glycoside, to my knowledge. The rarity of the sterol aminoglycoside is perhaps related to the difficulty I encountered in attempting to glycosylate the 22-aminosterol (see **Section 2.2.4.3**). To overcome the inability of the established amino glycosylation methods, I developed a novel variant of the Fukuyama-Mitsunobu for glycosylation.

In the total synthesis of OSW-1, a Schmitt glycosylation reaction is used to merge the aglycone and disaccharide components and this was successfully implemented in the synthesis of C22-*O*-glycoside OSW-1 analog (



**Figure 2-7, Compound 2.6).** As previously described by our research group,<sup>84</sup> Schmitt glycosylation of 22-aminosterol (**2.29**) to disaccharide (**2.26**) did not afford the desired *N*-glycosylated product. The failure of this reaction is presumably due to the amine being significantly more Lewis basic than the disaccharide imidate, causing the Lewis acid to be sequestered by the amine. *In situ* transformation of 22-aminosterol (**2.29**) into an ammonium-salt then subjecting to Schmitt glycosylation conditions afforded no product formation either. Alternatively, *N*-glycosylation methods that drew inspiration from aromatic amine and amino acid *N*-glycosylation methods were tried on 22-aminosterol without product formation.<sup>130–135</sup>

Further analysis of the literature suggested that the C22-amine would need to be functionalized to facilitate glycosylation. We were however, limited with the type of amine functionalization that could be considered. The C22-amine is fairly unreactive and sterically hindered, limiting its reactivity. Any functionalization of the C22 amine would have to be easily removed in the late stage, coupled product. The total synthesis of aurantioside G by Schobert et. al. introduced the idea of using a Fukuyama-Mitsunobu glycosylation reaction.<sup>125</sup> In the total synthesis of aurantioside G, Fukuyama-Mitsunobu glycosylation is implemented to couple an *o*-nitrobenzene sulfonyl (*o*Nos, Ns) amino acid and monosaccharide. The Fukuyama variation of the Mitsunobu reaction, utilizes an *o*Nos group to lower the pKa of the amine below 13 thereby facilitating sulfonamide participation in the Mitsunobu reaction. The *o*Nos group is commonly used as a protecting group, allowing for convenient and selective deprotections under mild conditions.<sup>104,136,137</sup> The C22-aminosterol (**2.29**) material was then *o*Nos protected under basic conditions to afford 22-*NNs*-aminosterol in acceptable yields.

A method development campaign was undertaken to identify Fukuyama-Mitsunobu reaction conditions capable of successfully forming C22-*N*-glycoside linkages (**Table 2-3**). The Mitsunobu conditions screening (**Table 2-3; Entries 1-7**) began with triphenyl phosphine and di-isopropyl azodicarboxamide, classic Mitsunobu conditions.<sup>104,136,137</sup> These initial studies used a simplified sugar motif, monosaccharide arabinose, instead of the Arb-Xyl-disaccharide.

**Table 2-3.** Optimization screening campaign of Fukuyama-Mitsunobu reaction for *N*-glycosylation. The amine (1) shown is 22-aminosterol with either Ns or DNs protecting groups. Disaccharide is *L*Arb-Xyl-disaccharide. DTBAD stands for di-tertbutyl azodicarboxamide and TMAD stands for trimethyl azodicarboxyldiamide.

Entry	Amine (1), Equiv.	Sugar (2), Equiv.	Conditions	Order of Addition	Results
1	NHNs, 1	arabinose, 2.5	Ph <sub>3</sub> P (2.5 equiv.), DIAD (2.5 equiv.), THF, -78°C to RT	1,2 into Ph <sub>3</sub> P, DIAD	Trace
2	NHNs, 1	arabinose, 2.5	Ph <sub>3</sub> P (2.5 equiv.), DIAD (2.5 equiv.), THF, 0°C to RT	1,2 into Ph <sub>3</sub> P, DIAD	Trace
3	NHNs, 1	arabinose, 5	Ph <sub>3</sub> P (10 equiv.), DIAD (10 equiv.), THF, 0°C to RT	1,2 into Ph <sub>3</sub> P, DIAD	Trace
4	NHNs, 1	arabinose, 3	Ph <sub>3</sub> P (2.5 equiv.), DIAD (2.5 equiv.), THF, 0°C to RT	1,2 into Ph <sub>3</sub> P, DIAD	Trace
5	NHNs, 1	arabinose, 3	Ph <sub>3</sub> P (4 equiv.), DIAD (4 equiv.), THF, -78°C to 60°C	1,2 into Ph <sub>3</sub> P, DIAD	Trace
6	NHNs, 1	Disaccharide, 1.2	Ph <sub>3</sub> P (4 equiv.), DIAD (4 equiv.), THF, -40°C to RT	1,2 into Ph <sub>3</sub> P, DIAD	NR, side- product only
7	NHNs, 1	Disaccharide, 1.3	Ph <sub>3</sub> P (2 equiv.), DIAD (2 equiv.), THF, -40°C to RT	1,2 into Ph <sub>3</sub> P, DIAD	Trace
8	NHNs, 1	Disaccharide, 1.7	(Ph <sub>3</sub> P) <sub>n</sub> (4 equiv.), DIAD (4 equiv.), THF, -40°C to RT	1,2 into (Ph <sub>3</sub> P) <sub>n</sub> , DIAD	NR, side- product only

9	NHNs, 1.2	Disaccharide, 1.0	(Ph <sub>3</sub> P) <sub>n</sub> (2 equiv.), DIAD (1.5 equiv.), THF, -40°C to RT	1,2 into (Ph <sub>3</sub> P) <sub>n</sub> , DIAD	NR, side-product only
10	NHNs, 1	Disaccharide, 1.7	(Ph <sub>3</sub> P) <sub>n</sub> (4 equiv.), TMAD (4 equiv.), THF, RT	1,2 into (Ph <sub>3</sub> P) <sub>n</sub> , TMAD	NR, side-product only
11	NHNs, 1	Disaccharide, 1.2	Ph <sub>3</sub> P (4 equiv.), TMAD (4 equiv.), THF, RT	1,2 into Ph <sub>3</sub> P, TMAD	NR, side-product only
12	NHNs, 1	Disaccharide, 1.2	<sup>n</sup> Bu <sub>3</sub> P (4 equiv.), TMAD (4 equiv.), THF, -40°C to RT	1,2 into <sup>n</sup> Bu <sub>3</sub> P, TMAD	Trace
13	NHNs, 1	Disaccharide, 1.2	<sup>n</sup> Bu <sub>3</sub> P (1.5 equiv.), TMAD (1.5 equiv.), THF, 0°C to RT	TMAD sol <sup>n</sup> into 1, 2, Ph <sub>3</sub> P	NR, side-product only
14	NHNs, 1	Disaccharide, 1.2	<sup>n</sup> Bu <sub>3</sub> P (4 equiv.), TMAD (4 equiv.), MeBn, -40°C to RT	1,2 into <sup>n</sup> Bu <sub>3</sub> P, TMAD	Trace
15	NHNs, 1	Disaccharide, 1.2	Ph <sub>2</sub> PyP (4 equiv.), TMAD (4 equiv.), DCM, RT	1,2 into Ph <sub>2</sub> PyP, TMAD	NR, side-product only
16	NHNs, 1	Disaccharide, 1.2	Ph <sub>2</sub> PyP (4 equiv.), DTBAD (4 equiv.), DCM, RT	1,2 into Ph <sub>2</sub> PyP, TMAD	Trace
17	NHNs, 1	Disaccharide, 1.2	Ph <sub>2</sub> PyP (4 equiv.), DTBAD (4 + 2 equiv.), DCM, 0°C to RT	1,2 into Ph <sub>2</sub> PyP, TMAD	Trace
18	NHNs, 1	Disaccharide, 1.2	Ph <sub>2</sub> PyP (4 equiv.), DTBAD (4 equiv.), DCM, -40°C to RT	DTBAD sol <sup>n</sup> into 1, 2, Ph <sub>2</sub> PyP	Trace
19	NHNs, 1	Disaccharide, 1.2	Ph <sub>2</sub> PyP (2 equiv.), DTBAD (2 equiv.), DCM, 0°C to RT	DTBAD sol <sup>n</sup> into 1, 2, Ph <sub>2</sub> PyP	~20% BORSM
20	NHNs, 1	Disaccharide, 1.2	Ph <sub>2</sub> PyP (2 equiv.), DTBAD (2 equiv.), DCM, -10°C to RT	DTBAD sol <sup>n</sup> into 1, 2, Ph <sub>2</sub> PyP	~20% BORSM
21	NHNs, 1	Disaccharide, 1.2	Ph <sub>2</sub> PyP (2.5 equiv.), DTBAD (2.5 equiv.), DCM, -10°C to RT	DTBAD sol <sup>n</sup> into 1, 2, Ph <sub>2</sub> PyP	~8% BORSM

22	NHNs, 1	Disaccharide, 1.2	Ph <sub>2</sub> PyP (2.5 equiv.), DTBAD (2.5 equiv.), DCM, -10°C to RT	1,2 into Ph <sub>2</sub> PyP, DTBAD	~11% BORSM
23	NHNs, 1	Disaccharide, 1.2	Ph <sub>2</sub> PyP (2 equiv.), DTBAD (2 equiv.), DCM, -10°C to RT	DTBAD sol <sup>n</sup> into 1, 2, Ph <sub>2</sub> PyP	~13% BORSM
24	NHNs, 1	Disaccharide, 1.2	Ph <sub>2</sub> PyP (2 equiv.), DTBAD (2 equiv.), THF, 0°C to RT	1, DTBAD into 2, Ph <sub>2</sub> PyP	~15% BORSM
25	NHNs, 1	Disaccharide, 1.2	Ph <sub>2</sub> PyP (2 equiv.), DTBAD (2 equiv.), THF, 0°C to RT	DTBAD sol <sup>n</sup> into 1, 2, Ph <sub>2</sub> PyP	~25% BORSM
26	NHNs, 1	Disaccharide, 1.2	Ph <sub>2</sub> PyP (1.2 + 1 equiv.), TBAD (2 + 1.5 equiv.), THF, 0°C to RT	DTBAD sol <sup>n</sup> into 1, 2, Ph <sub>2</sub> PyP	~35% BORSM
27	NHNs, 1	Disaccharide, 1.2	Ph <sub>2</sub> PyP (2 equiv.), DTBAD (2 equiv.), THF, 0°C to RT	DTBAD sol <sup>n</sup> into 1, 2, Ph <sub>2</sub> PyP	~14% BORSM
28	NHDNs, 1	Disaccharide, 1.2	Ph <sub>2</sub> PyP (2.2 equiv.), DTBAD (2 equiv.), THF, 0°C to RT	DTBAD sol <sup>n</sup> into 1, 2, Ph <sub>2</sub> PyP	~44% product yield
29	NHDNs, 1	Disaccharide, 1.4	Ph <sub>2</sub> PyP (4 equiv.), DTBAD (4 equiv.), THF, ~5°C	DTBAD sol <sup>n</sup> into 1, 2, Ph <sub>2</sub> PyP	~61% product yield

The complex product mixture from **Entries 1-7** produced separation and characterization challenges. **Entry 6** marked the first glycosylated product clearly isolated and characterized. However, the identified glycosylated product was the unwanted disaccharide azodicarboxamide. In an attempt to prevent this side-reaction, various equivalence of phosphine and azodicarboxamide were investigated (**Entries 7-9**). The phosphine reagents were also varied to employ more sterically-hindered azodicarboxamides (**Entries 9-14**). None of these changes seemed to make a significant

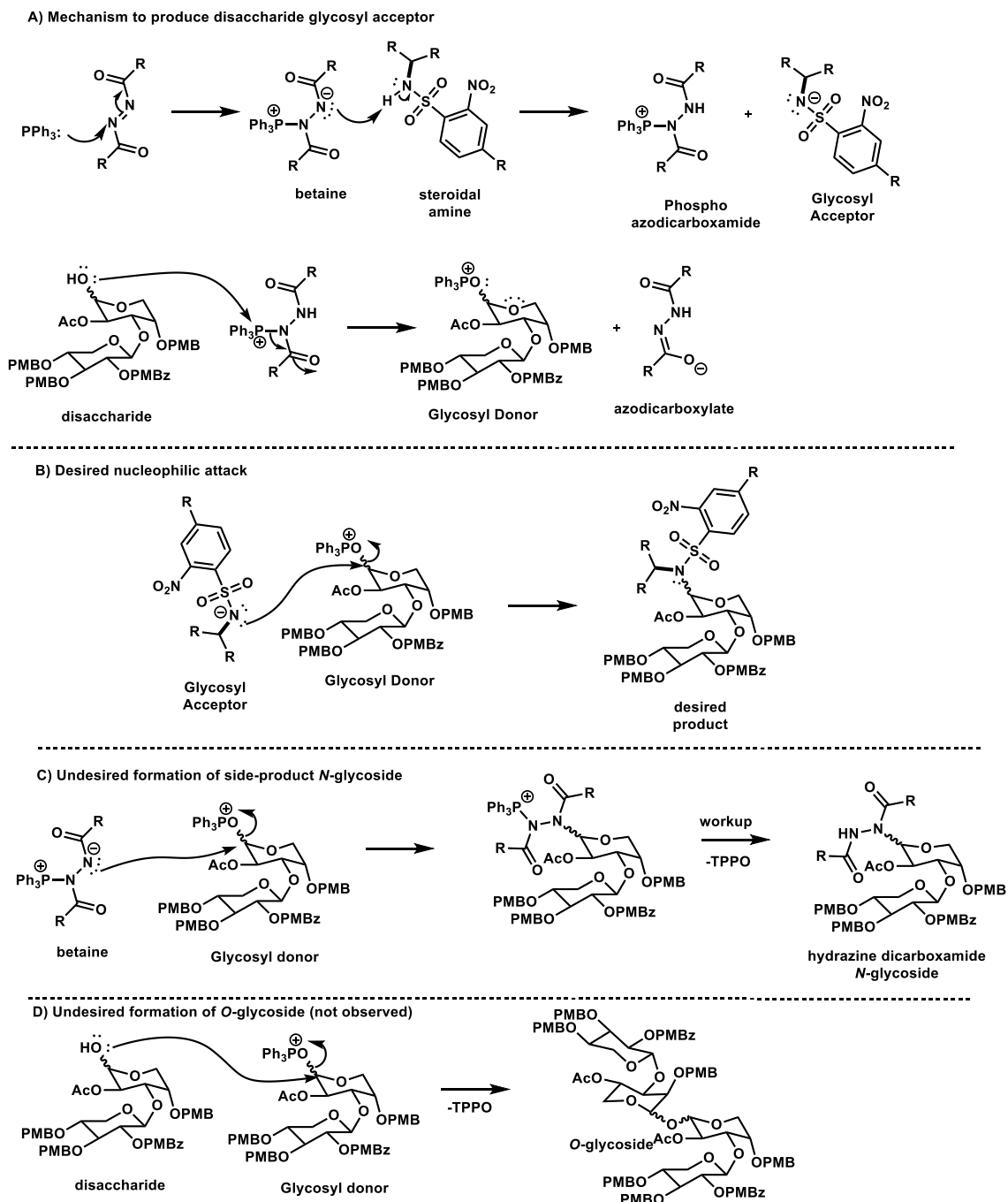


**Figure 2-14.** Proposed mechanism of Fukuyama-Mitsunobu reaction for *N*-glycosylation between steroidal amine and disaccharide. **A.** Formation of the betaine, subsequent formation of the phosphoazodicarboxamide and glycosyl acceptor, and functionalization of the disaccharide to become the glycosyl donor. **B.** Desired nucleophilic attack to form the desired glycoside. **C.** Unfavorable nucleophilic attack by the betaine to form the side-product glycoside. **D.** Undesired formation of the *O*-glycoside product which was not observed in this reaction.

difference; the azodicarboxylate consistently out competed the steroidal amine.

Additionally, purification of the desired product was challenging due to triphenyl phosphine oxide (TPPO) and the glycosylated side product. Having compiled a reaction portfolio of simple reaction condition alterations, a thorough analysis of the Fukuyama-Mitsunobu mechanism was necessary.

The proposed mechanism of the Fukuyama-Mitsunobu glycosylation (**Figure 2-14**) proceeds through first forming a betaine between the phosphine and azaodicarboxylate reagents. Once formed, the betaine subsequently deprotonates the Nos-aminosterol. Nosyl sulfonamides have an estimated pKa of ~10 whereas the disaccharide hemiacetal pKa is ~ 15.<sup>107,138,139</sup> The resulting phospho azodicarboxamide has a pka of ~20.<sup>139</sup> The disaccharide hemiacetal then attacks the phosphine, ejecting azodicarboxamide, and creating the glycosyl acceptor. The glycosyl acceptor is then nucleophilically attacked by either the aminosterol (**Figure 2-14. B.**) or the azodicarboxylate (**Figure 2-14. C.**). Upon attack by the aminosterol on the glycosyl donor, the desired glycoside is formed. If the phosphazodicarboxylate outcompetes the aminosterol and attacks the glycosyl donor instead, the unwanted hydrazine byproduct is formed (**Figure 2. C.**). It is also plausible for starting material, disaccharide to nucleophilically attack the phosphonium activated disaccharide (glycosyl donor) to form an O-glycoside product however, in no instances was this product observed (**Figure 2. D.**).

Four main insights can be concluded from the proposed mechanism. First, the Nos-protected aminosterol must be deprotonated in order to out compete the phosphoazodicarboxamide as a nucleophile. Therefore, a more acidic Nos-protected aminosterol would promote its deprotonation and therefore its nucleophilicity. The second insight is that the sterics of the azodicarboxamide greatly affect its potential as a

glycosyl acceptor. Greater steric hinderance presumably would result in less side-product glycoside formation. The third significant insight is that phosphine electronics have a significant impact on betaine formation and stability. The fourth and final insight, obtained through many experimental outcomes, is that the C22-aminosterol is rather unreactive, limiting its participating as a glycosyl acceptor.

These mechanistic insights led to testing lesser known reagents in the Fukuyama-Mitsunobu-glycosylation reaction: ditertbutyl azodicarboxamide (DTBAD) and diphenyl pyridylphosphine (Ph<sub>2</sub>PPy). Initial reaction screening of these enhanced Mitsunobu reagents proved mildly successful (**Table 2-3 ; Entries 15-19**). These Mitsunobu reagents were described by Jorgensen and Miller, et. al. and had the added benefit of being easily removed via acidic workup.<sup>121</sup> As previously stated, purification and isolation of glycoside products was further complicated by the generation of TPPO and hydrazine by-products. One of the advantages of DTBAD and Ph<sub>2</sub>PPy was that a simple acidic workup procedure removed these by-products from the crude mixture thereby facilitating an easier purification. From a mechanistic perspective, DTBAD has more steric bulk than previous dicarboxamides which rendered it less nucleophilic. Furthermore, Ph<sub>2</sub>PPy contains a pyridine ring which contributed to greater stability of uncharged phosphine however, the species becomes less stable in its cationic state. Presumably, this slows the formation of glycosyl acceptors within the reaction thereby preventing undesired glycoside products. These enhanced Fukuyama-Mitsunobu conditions alleviated purification difficulties and prevented unwanted product formation.

In addition to changing the reagents, altering the Order-of-addition of reaction components and reaction temperature produced a ~20% yield BORSM (**Table 2-3;**

**Entries 15-19**). Reaction temperatures from 0°C to room temperature (**Table 2-3; Entries 18, 19**) and slow addition of the azadicarboxamide reagent to the other reaction components (**Table 2-3; Entries 17** compared to **Entry 19**) increased the yield to ~20% yield BORSM. Further changes to temperature control (**Table 2-3; Entries 20-27**) did not afford increase product formation. These results suggested that Nos-protected aminosterol was insufficiently nucleophile to outcompete the phosphoazodicarboxamide, and that the C22-aminosterol required changes in functionalization, to enhance its acidity within the Fukuyama-Mitsunobu-glycosylation reaction. The desired functionality was accomplished through use of the 2,4-dinitrobenzene sulfonyl (*o,p*NOS, DN<sub>s</sub>) amino protecting group.

Changing the protecting group of C22-aminosterol (**2.29**) from *ortho*-nitro benzene sulfonamide (*o*Nos, N<sub>s</sub>) to 2,4-dinitro benzene sulfonamide (*o,p*DNOS, DN<sub>s</sub>) (

**Figure 2-9, Compound 2.30**) rendered the glycosyl acceptor more acidic in the Fukuyama-Mitsunobu reaction while facilitating an even milder deprotection strategy. The DN<sub>s</sub>-aminosterol afforded a gratifying boost in product from ~25% BORSM to 44% product yield (**Table 2-3; Entries 28 & 29**)! Further optimization focused on fine tuning temperature control. The temperature control study revealed that temperatures lower than 0°C afforded only desired product but in unsatisfactory yields, whereas temperatures at or greater than 10°C afforded more side-product than desired product. The best product yields are afforded at ~5°C where there seems to be enough energy to produce the betaine and glycosyl donor (as shown in **Figure 2-14. A.**) but not enough for phospho azodicarboxamide to be readily available as a glycosyl acceptor. The highest recorded yield was achieved at ~5 °C for 4 hours and afforded a ~61% yield of desired product in



a 3:1  $\alpha$ : $\beta$ -anomeric ratio, <10% yield of undesired side product, with no starting material recovered (**Table 2-3; Entry 29**).

#### **2.2.4.8. Total synthesis of C22-N-glycoside linked OSW-1 derivative**

22-aminosterol (**Figure 2-9; 2.29**) was dinitrobenzene sulfonyl (DNs) protected using 2,4-dinitrobenzene sulfonyl chloride in the presence of triethyl amine to arrive at compound, **2.30 (Figure 2-9)**, in relatively high yields (~90%). Glycosylation was then carried out to merge disaccharide (**Figure 2-9; 2.26**) to the DNs-protected C22-aminosterol (**Figure 2-9; 2.30**) using the optimized Fukuyama-Mitsunobu conditions (**Section 2.2.4.7**). To a stirring solution of (**Figure 2-9; 2.30**), disaccharide (**Figure 2-9; 2.26**), and diphenyl pyridylphosphine in THF at 5°C was added ditertbutyl azodicarboxamide as a dilute solution over several hours. These strict electronic and sterically hindered conditions were necessary to render **2.30** reactive enough to outcompete azodicarboxamide and prevent intermolecular glycosylation between disaccharides. After extensive methodology development and optimization, the desired glycoside was obtained with a 61% product yield (**Figure 2-9; 2.30**) and 3:1  $\alpha$ : $\beta$ -anomeric product ratio. **Compounds 2.31.A** ( $\alpha$ -anomer) and **Compound 2.31.B** ( $\beta$ -anomer) were isolated and individual anomers were carried forward.

The last synthetic sequence comprised of two deprotections: DDQ treatment to cleave four PMB groups followed by Fukuyama conditions to denosylate the amine. PMB deprotection of glycosides, **2.31.A**. ( $\alpha$ -anomer) and **2.31.B**. ( $\beta$ -anomer) proceeded in varying yields (72% and 51%, respectfully) when reacted with DDQ in a biphasic solution of DCM and distilled water to produce **Compounds 2.32.A** ( $\alpha$ -anomer) and **2.32.B** ( $\beta$ -anomer). After purification, **Compounds 2.32.A and 2.32.B** were then

subjected to Fukuyama-deprotection conditions. A mixture of  $\alpha$  and  $\beta$  glycosides (**2.32.A/B**) were dissolved in DMF and reacted with thiophenol in the presence of Hunigs base at 110°C for 4 hours to obtain target compound, **Figure 2-9; 2.7.A/B**, in unsatisfactory yields. The high temperature reaction conditions were determined to be degrading the glycosidic linkage; the high temperatures were employed because no reaction was initially observed due to the starting material and the product having such similar polarities. Reaction monitoring by HPLC-MS revealed complete consumption of the starting anomers at room temperature nearly instantly. Separation of the final deprotected anomers was challenging.

The anomers of the starting material were separated immediately after glycosylation reaction (**Figure 2-9**). Following PMB deprotection, each individual anomer was subjected to Fukuyama deprotection. Upon optimization, the desired C22-*N*-glycoside OSW-1 derivative (**Figure 2-9; 2.7.B**) was obtained with ~15% conversion. This deprotection sequence was later rearranged to do Fukuyama deprotection first followed by PMB deprotection. The sequence prevented excess-DDQ from being used as it degraded the compound.

The bioactivity and importance of the C22-*N*-glycoside OSW-1 compound, **2.7**, has been submitted for biological testing.

### **2.3.Discussion**

Our developed model of OSW-1 as it exists within the OSBP/ORP4 binding pocket provided critical insight in identifying the biologically important structural features of OSW-1 and provided a foundation for the design of new OSW-1 derived scaffolds. We report, in agreement with literature, that the acyl groups (i.e the arabinose C2-acetate and

the xylose C2-benzoate) are critical components for antiproliferative potency. Our model suggests that the acetate itself is not biologically active but plays a critical role in the structural conformation of OSW-1 through a putative intramolecular hydrogen bonding network. No OSW-1 structures lacking only the arabinose C2-acetate have been reported. Presumably, SAR studies of the arabinose C2-acetate have not been conducted due to the synthesis efforts necessary to generate these molecules. However, SAR studies of the acetate group are crucial for further development of our model, especially for greater understanding of the disaccharide component. Importantly, our model suggests that the disaccharide component is structurally influential in the orientation of the biologically essential components of OSW-1 (i.e. C3-hydroxyl, side chain, and acyl groups) but that the disaccharide itself is not critical for activity. This hypothesis of the disaccharide being a spacer unit allowed us to envision replacement of that disaccharide with a simplified, rigid, and robust replacement scaffold. Replacement of the disaccharide would greatly facilitate synthesis efforts toward OSW-1 derivatization for the biological elucidation and therapeutic targeting of OSBP and ORP4.

Our three-component approach combines the steroid body, side chain, and disaccharide, allowing for incremental development of a replacement disaccharide spacer unit. The synthetic complexity of the tedious side chain construction and oxidation steps are circumvented in this approach by introduction of an azacyclic E-ring. The azacyclic E-ring structure compensates for the rigidity of the putative hydrogen bonding network and facilitates a highly flexible synthesis for orientating the side-chain component and acyl groups in relation to one another. A limitation of the azacyclic E-ring structure is accounting for the conformational changes of the overall structure which could drastically

impact its bioactivity. Overcoming this limitation will require methodical and incremental structural changes that facilitate predictable structural conformations.

The scope and flexibility of our three-component approach will be limited by the lack of reactivity of the C22-position. As discussed, functionalizing and glycosylating this position required development of new methodology to overcome the inherent inert nature of the C22-position. Such stability will limit the structural modifications and glycosyl acceptors available for development of OSW-1 derived scaffolds. The inherent lack of reactivity of this position is presumably due to the steroid scaffold which is conformationally rigid and sterically bulky.<sup>83,140–143</sup> The inherent rigidity of steroids limit conformational freedom of the sterol side chain and conformationally lock steroid substituents (i.e. C18-, C19-, and C21-methyl groups).<sup>140,142</sup> Within the context of 22-amino cholesterol (**Compound 2.29**), the distance between CH<sub>3</sub>18, CH<sub>3</sub>21, H20, H22, and H16 were calculated using qNOESY and contribute to a spatially congested scaffold. Based on this information, it is reasonable that nucleophilic attack of the C22-position is sterically blocked by the C18 and C21 methyl groups.<sup>83,143</sup> This would explain why the C22-position was resilient to nitrogen nucleophiles; it is not easily accessible. It also seems plausible that the C22-heteroatom (i.e. C22-hydroxyl and C22-amine) interacts with the C16-C17 pi bond further restricting movement and reducing nucleophilicity of these heteroatoms. This would also explain the challenging glycosylation of 22-aminosterol, which required a strong electron withdrawing substituent. The inherent conformational rigidity of sterols drastically reduces the reactivity of the C22-position and has potential to limit the scope of our three-component approach. **Chapter 3** details additional progress towards overcoming this limitation by developing a method that

would allow the side chain and disaccharide building blocks to be combined prior to being coupled with the steroid.

The Fukuyama-Mitsunobu glycosylation reaction likely does not proceed through an oxonium glycosyl acceptor (**Figure 2-14**) based on the mild selectivity of the anomeric mixture of amino-glycoside products (3:1  $\alpha$ : $\beta$ -anomers). During the glycosylation reaction, formation of a disaccharide oxonium glycosyl donor through ejection of the triphenylphosphine oxide is possible; several glycosylation methods generate the disaccharide oxonium, such as the Schmitt glycosylation, losing any stereochemistry at the anomeric position (**Section 2.2.4.5**).<sup>119,144</sup> The formation of the oxonium intermediate would lead to anchimeric assistance of the neighboring arabinose-C2 acetate group, which would block the axial position (**Section 2.2.4.5**).<sup>119,144</sup> This would lead to a likely high preference of  $\alpha$ -anomers, as is typical with the Schmidt glycosylation of OSW-1 synthesis.<sup>69</sup> The 3:1,  $\alpha$ / $\beta$ - anomeric product ratio, starting from an  $\sim$ 1:1  $\alpha$ / $\beta$ - anomeric starting material ratio, could be consistent with a  $S_N2$  mechanism where the  $\alpha$ -anomer of the TPPO-disaccharide glycosyl donor is preferentially attacked over the  $\beta$ - anomer. Additionally, the TPPO-disaccharide anomers could be epimerizing in the reaction. However, a  $S_N1$  mechanism of glycosylation proceeding through an oxonium intermediate cannot be excluded from this reaction.

A novel glycosylation method was developed for the coupling of functionalized 22-aminosterol (**Compound 2.30**) and disaccharide (**Compound 2.26**) through unique application of a Fukuyama-Mitsunobu reaction with atypical reagents. The lack of reactivity of 22-aminosterols demanded further functionalization of the amine to facilitate its participation within the Fukuyama-Mitsunobu-Glycosylation reaction (**Section 2.2.3**).

The glycosylation was optimized by adding ditertbutyl azaodicarboxylate (DTBAD) into a mixture of diphenyl pyridyl phosphine (Ph<sub>2</sub>PyP) and glycosyl acceptor and donor at ~5°C. These conditions provided for easy purification; a post-reaction acid quench decomposed unreacted DTBAD into isobutene, hydrazine, and carbon dioxide and an acidic workup washed out unreacted Ph<sub>2</sub>PyP.<sup>102,121</sup> Additionally, and more importantly, these two reagents prevented formation of side-product glycosides for reasons that are unclear. DTBAD is a sterically bulkier azadicarboxylate in comparison to typical Mitsunobu reagents, DEAD and DIAD, which should reasonably prevent formation of dicarboxamide glycosides.<sup>102</sup> However, when another phosphine reagent besides Ph<sub>2</sub>PyP was used, the dicarboxamide glycoside side-products still formed. This suggests that the phosphine reagent plays a critical role in the prevention of side-product formation. The role of phosphine within the Mitsunobu is well understood<sup>103,108,145</sup> but a comprehensive account of phosphine electronic effects on the mechanism have not been well reported. Further investigation of heteroatom containing phosphine reagents within the Mitsunobu reaction are needed to better understand its role in product formation.

#### **2.4. Conclusions and future work**

The development of the molecular model of OSW-1 interaction within the oxysterol-binding pocket led to the development of a new, three-component approach to produce an azacycle E-ring OSW-1 analog. The three-component, E-ring OSW-1 approach requires the development of several methods in the context of OSW-1, and this work describes the development of new methods to produce the 22-aminosterol and a novel glycosylation method via Fukuyama-Mitsunobu-glycosylation. Towards the development of new E-ring OSW-1 analogs from a three components method, two new

versatile and scalable OSW-1 analogs were achieved; C22-*O*-glycoside OSW-1 and C22-*N*-glycoside OSW-1 were synthesized. The C22-*N*-glycoside represents the first report of a steroidal *N*-glycoside synthesis in the literature. Extensive screening of Fukuyama-Mitsunobu-glycosylation conditions led to identification of a good yielding reaction with dinitrobenzene sulfonamide that could be easily purified on scale. Future work on development of OSW-1-derived scaffolds, based on these accomplishments, will seek to obtain the fully cyclized azacycle E-ring bridge from the three-component strategy. **Chapter 3** details additional progress towards this goal.

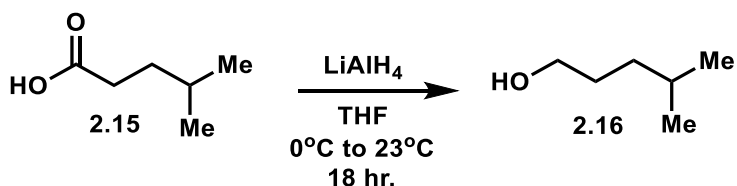
## **2.5. Experimental and supplemental information**

*General synthetic methods:* All reactions were performed in oven-dried glassware under a positive pressure of nitrogen unless noted otherwise. Flash column chromatography was performed as described by Still et al.<sup>146</sup> employing E. Merck silica gel 60 (230-400 mesh ASTM). Thin layer chromatography (TLC) analyses and preparative TLC (pTLC) purification was performed on 250  $\mu\text{m}$  Silica Gel 60 F254 plates purchased from EM Science and Fluka Analytical. All TLC samples were visualized under UV-light and stained using cerium ammonium molybdate stain (CAM stain) unless otherwise noted. All solvents and chemicals were used as purchased without further purification. Solvents used in the reactions were collected under nitrogen atmosphere from a Pure Solv 400-5-MD Solvent Purification System (Innovative Technology). Automated purification columns were performed on Biotage Isolera One purification system using manually packed columns of 5G, 10G, 25G, or 50G as specified of oven dried silica.

All melting points were collected on a SRS DigiMelt MPA160 melting point apparatus and were uncorrected. NMR samples were prepared in 5 mm tubes with noted solvent. NMR data were all collected on a 300 MHz, 400 MHz, or 500 MHz Varian VNMRS DirectDrive spectrometer equipped with an indirect observe probe or 600 MHz 5 mm Nalaroc broad band probe. Chemical shifts for proton and carbon resonances are reported in ppm ( $\delta$ ) relative to the residual proton or the specified carbon in chloroform ( $\delta$  7.26, proton; 77.16, carbon). Data was collected under STP conditions. Pulse sequences were used as supplied by Varian VNMRJ 4.2 software. All 2D data employed non-uniform sampling (NUS). All data was processed in MestreNova v12.0.2 2D gCOSY was collected with 2 scans, 256 increments, a spectral width of 3633.7 Hz, an acquisition time of 0.2818 seconds and a relaxation delay of 1.0182 seconds. Data was zero-filled to 2048 data points with a gaussian fit of 20 Hz and sin bell in F1 then gaussian fit of 10 Hz and  $\text{Cos}^2$  in F2 prior to Fourier Transform. 2D HSQCAD was collected with 8 scans, 256 increments, a spectral width of 3633.7Hz in f2 and 30165.9 Hz in f1, an acquisition time of 0.2818 seconds, a relaxation delay of 1.0182 seconds, and C-H coupling constant of 146 Hz. Data was zero-filled to 2048 data points with a gaussian fit of 20 Hz and sin bell 90 in F1 then gaussian fit of 7.64 Hz and  $\text{Cos}$  90 in F2 prior to Fourier Transform. 2D HMBC was collected with 16 scans, 512 increments, a spectral width of 3633.7Hz in f2 and 30165.9 Hz in f1, an acquisition time of 0.5636 seconds, a relaxation delay of 0.7364 seconds. Data was intensified using zero-filled but not linear predict, a gaussian fit of 40 Hz and sin bell 90 in F1 then gaussian fit of 5 Hz and  $\text{Cos}$  90 in F2 prior to Fourier Transform.



High-resolution mass spectrometry (HRMS) analysis was performed using Agilent 6538 high-mass-resolution QTOF mass spectrometer. HPLC purification was performed on Shimadzu LCMS 2020 system [LC-20AP (pump), SPD-M20A (diode array detector), LCMS-2020 (mass spectrometer)]. Semi-preparative HPLC purification was performed using Phenomenex Luna C-18(2) column, 5 $\mu$ m particle size (250 mm x 4.6 mm), supported by Phenomenex Security Guard cartridge kit C18 (4.0 mm x 3.0 mm); Phenomenex Luna C-8(2) column, 5 $\mu$ m particle size (250 mm x 4.6 mm), supported by Phenomenex Security Guard cartridge kit C8 (4.0 mm x 3.0 mm) and HPLC-grade solvents.



**4-methylpentanol; (2.16):** 4-methylpentanol (**2.16**) was prepared through following a previously reported protocol with no notable modifications.<sup>147</sup> Solid lithium aluminum hydride (6.10 g, 160 mmol, 2.9 equiv.) was added to a 500 ml three-neck round bottom flask along with a large Teflon-coated stir bar. The flask of LiAlH<sub>4</sub> was immediately septa sealed and purged thrice with nitrogen and vacuum and then cooled to 0°C. Dry THF (200 ml) was added to create a suspension which was stirred vigorously. 4-methylpentanoic acid (**Compound 2.15**, 5.00 ml, 40.0 mmol, 1.0 equiv.) was diluted in THF (100 ml) and then slowly added to the LiAlH<sub>4</sub> suspension at 0°C over 1 hour using an addition funnel. The reaction continued for approximately 18 hours and slowly warmed to room temperature. Upon complete addition of the 4-methylpentanoic acid solution, the reaction was stirred for 3 hours, before the ice-water bath was removed and the reaction allowed to warm to room temperature. After 18 hours at room temperature, 100 ml of THF was added and the reaction was cooled to 0°C. A saturated sodium potassium tartrate solution (50 ml) was added slowly to quench the reaction. The quenched solution stirred for an additional 3 hours at room temperature, until it became a bi-phasic slurry of a clear solution with white aluminum oxide solids. The crude mixture was filtered through a

Celite pad to remove the aluminum oxide byproduct. The clear filtrate was then condensed *in vacuo* to produce a crude biphasic solution (~15 ml) which was then transferred to a separatory funnel. The biphasic solution was separated, and the organic phase was then washed twice with brine and dried over sodium sulfate. Vacuum distillation at 90-95°C using house vacuum produced 4.0 g of 4-methylpentanol (**2.16**) as a clear liquid obtained (71% yield). The NMR data agreed with the published reference.<sup>147</sup>  
**4-methylpentanol (2.16):** <sup>1</sup>H-NMR (400 MHz, DMSO-*d*<sub>6</sub>): δ 4.32 (td, *J* = 5.2, 0.4 Hz, 1H), 3.36 (td, *J* = 6.6, 5.2 Hz, 2H), 1.50 (dp, *J* = 13, 6.7 Hz, 1H), 1.45 – 1.34 (m, 2H), 1.21 – 1.08 (m, 2H), 0.85 (d, *J* = 6.6 Hz, 6H). <sup>13</sup>C-NMR (101 MHz, DMSO-*d*<sub>6</sub>) δ 61.0, 34.8, 30.4, 27.3, 22.5.

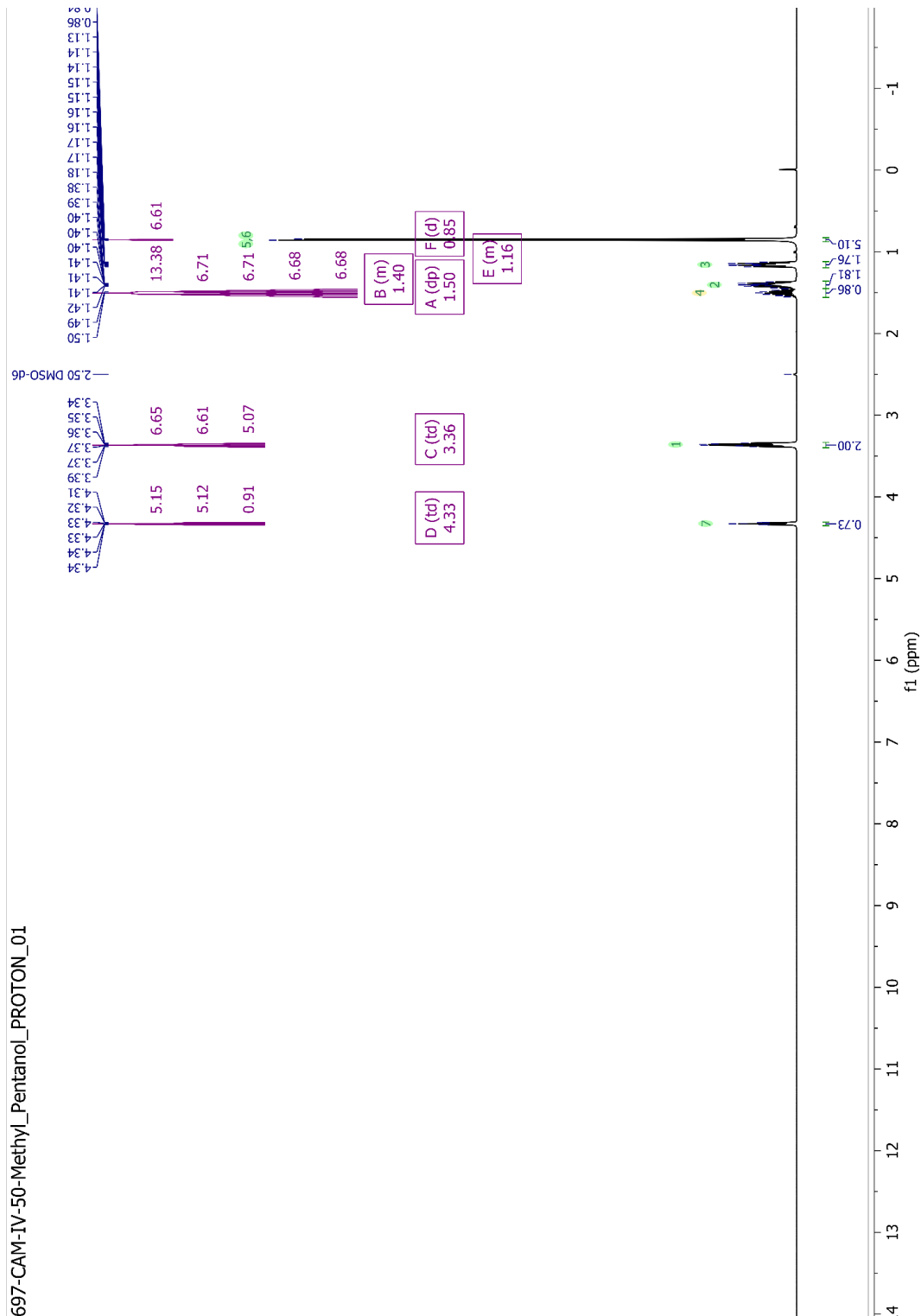


**Figure 2-15.**  $^1\text{H-NMR}$  of 4-methylpentanol (**2.16**) in  $\text{DMSO-}d_6$ .

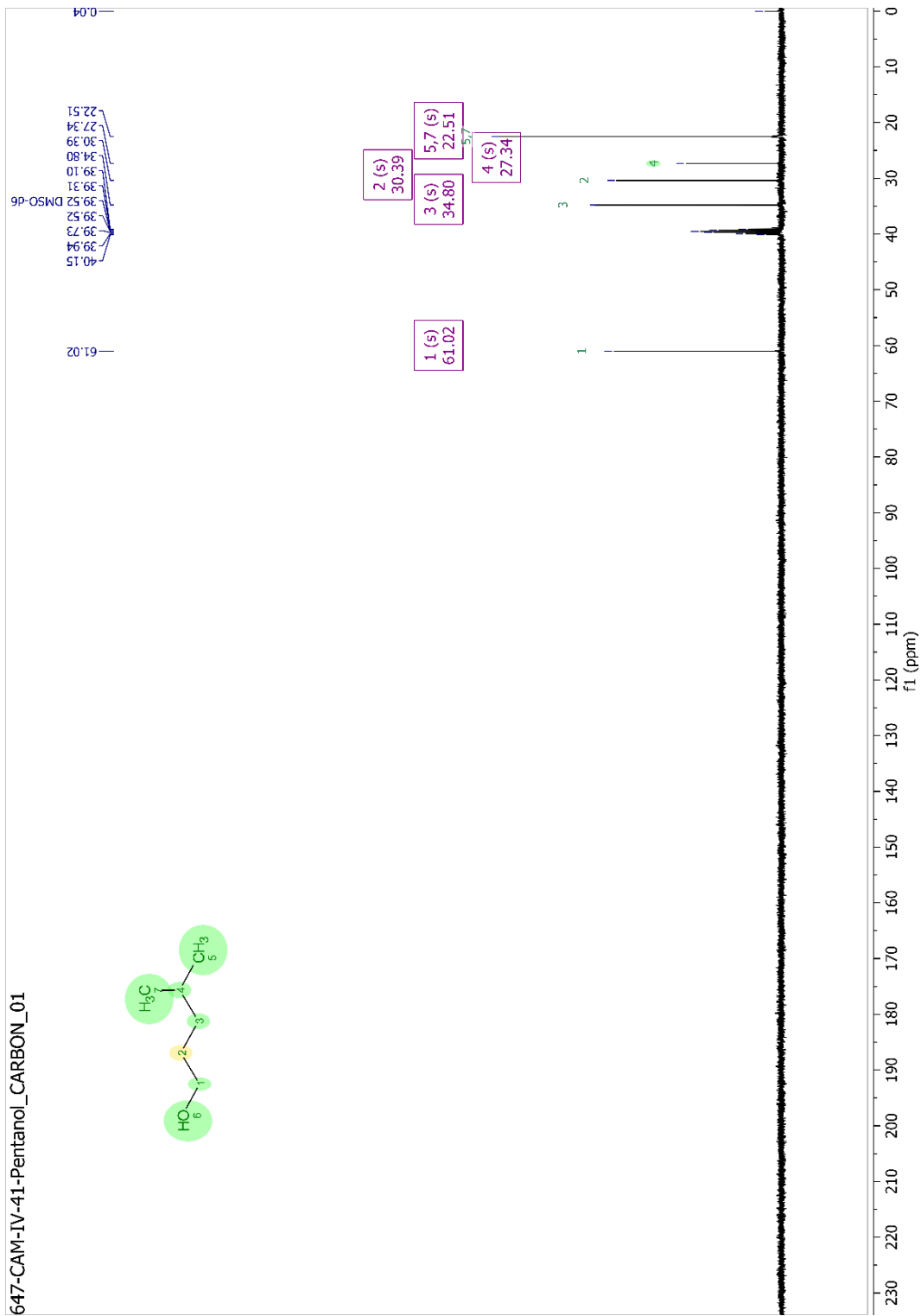
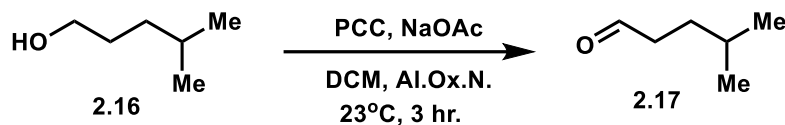


**Figure 2-16.**  $^{13}\text{C}$ -NMR of 4-methylpentanol (2.16) in  $\text{DMSO-}d_6$ .



**4-methylpentanal; (2.17):** 4-methylpentanal (**2.17**) was prepared through following a previously reported protocol with a modified purification procedure.<sup>148</sup> Solid pyridinium chlorochromate (6.88 g, 63.9 mmol, 2.0 equiv.) and neutral alumina oxide (6.90) were combined and ground together to a fine powder in a mortar and pestle. The solid mixture was added to a 50 ml pear-shaped flask with a large Teflon-coated stir bar. Solid sodium acetate anhydride (266 mg, 3.18 mmol, 0.2 equiv.) was added to the reaction flask which was then septa sealed and purged thrice with nitrogen and vacuum. Dry DCM (50 ml) was added to the reaction and the resulting slurry was stirred for thirty minutes at room temperature to create a bright orange suspension. 4-methylpentanol (**Compound 2.16**, 2.00 ml, 15.9 mmol, 1 equiv.) was diluted in DCM (14 ml) and then slowly added to the orange suspension over thirty minutes via addition funnel. Upon complete addition of the alcohol, the suspension turned dark orange/black. The reaction proceeded at room temperature under nitrogen atmosphere for three hours. Then the suspension was diluted with DCM (50 ml) and additional neutral alumina oxide (~7.0 g) was added. The suspension was then added to a flash column containing a 1:1 mixture of oven-dried silica (20 g) and neutral alumina oxide (20 g) packed with dry DCM. 150 ml of dry DCM was used to elute off the desired product. Due to the high volatility of the product, *in vacuo* solvent evaporation was done carefully at relatively low pressure, and residual DCM remained with the desired product as it was carried into the next reaction. The NMR data matched the published reference data.<sup>148</sup>

**4-methylpentanal (2.17):**  $R_f = 0.9$  (30% EtOAc/Hex). <sup>1</sup>H-NMR (400 MHz, DMSO-*d*<sub>6</sub>):  $\delta$  9.68 (t,  $J = 1.7$  Hz, 1H), 2.41 (dt,  $J = 7.6, 1.7$  Hz, 2H), 1.53 (ddq,  $J = 20, 13, 6.2$  Hz, 1H), 1.43 (qd,  $J = 7.1, 0.7$  Hz, 2H), 0.86 (d,  $J = 6.5$  Hz, 6H). <sup>13</sup>C-NMR (101 MHz, DMSO-*d*<sub>6</sub>)  $\delta$  203.6, 41.6, 30.7, 27.5, 22.5.

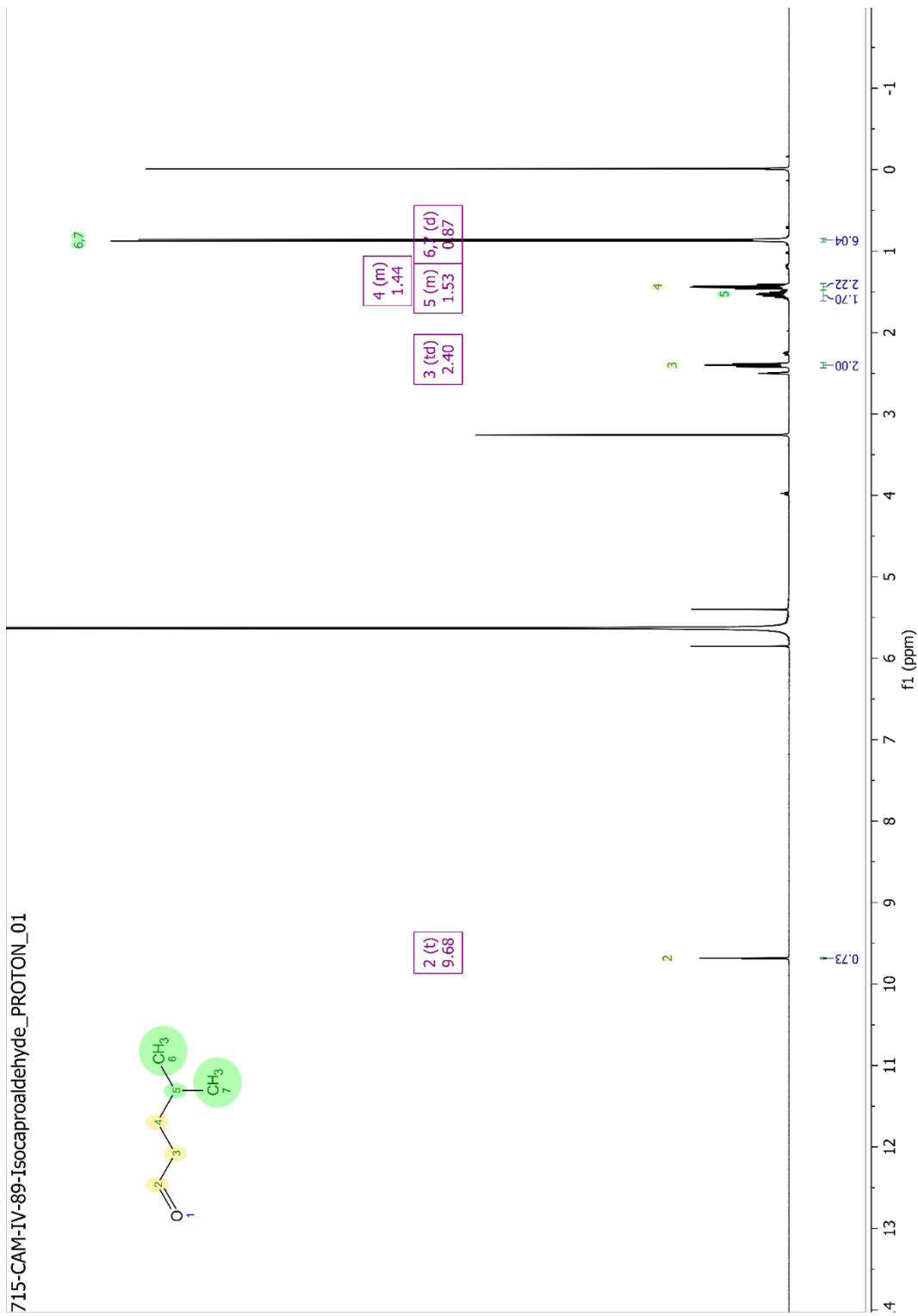


**Figure 2-17.**  $^1\text{H-NMR}$  of crude 4-methylpentanal (2.17) in  $\text{DMSO-}d_6$ .

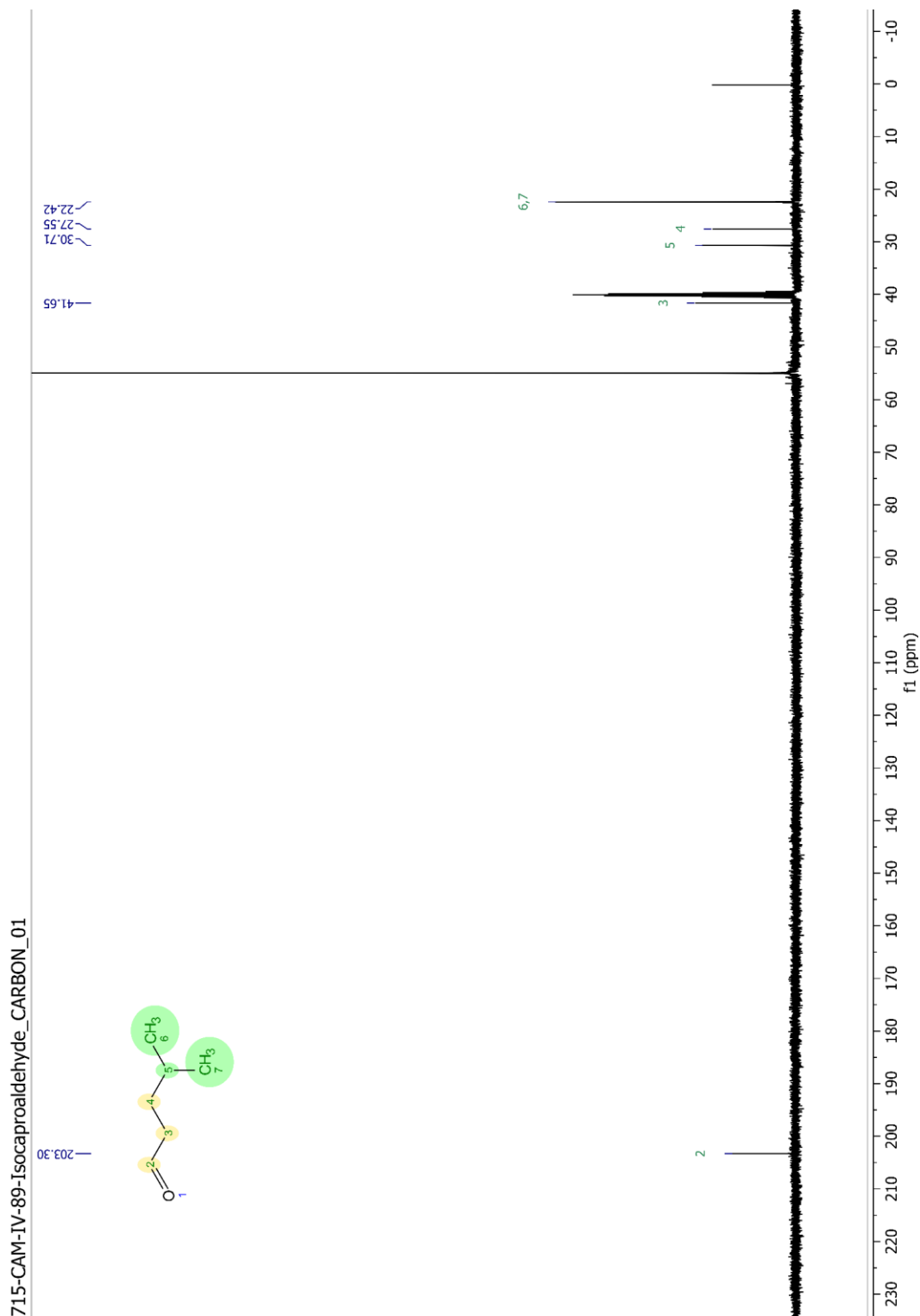
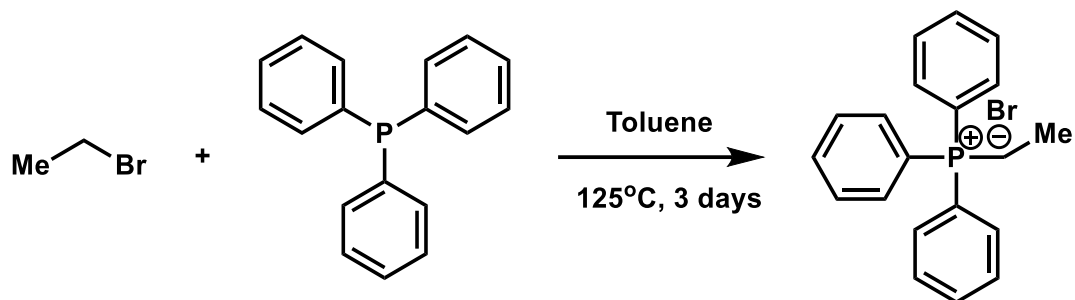


**Figure 2-18.**  $^{13}\text{C}$ -NMR of crude 4-methylpentanal (2.17) in  $\text{DMSO}-d_6$ .



**Ethyltriphenylphosphonium bromide:** Ethyltriphenylphosphonium bromide was prepared through following a previously reported protocol with no modifications.<sup>149</sup> Solid triphenylphosphine (24.1 g, 91.8 mmol, 1.0 equiv.) was added to a 100 ml round-bottom flask with Teflon-coated stir bar. The reaction flask was equipped with a reflux column which was then septa sealed and purged thrice with nitrogen and vacuum. The solid triphenylphosphine was then dissolved in toluene (35 ml, 2.6 M) and vigorously stirred for thirty minutes at room temperature. Liquid ethylbromide (6.85 ml, 91.8 mmol, 1 equiv.) was added via syringe fast dropwise. The reaction was heated to reflux at 125°C for three days. Upon complete conversion of starting material, the reaction turned cloudy with white precipitate. The resulting suspension was cooled to room temperature and then filtered through a Buchner funnel. The white solid was washed twice with cold toluene. The collected solid was then dried in a vacuum oven to afford quantitative yields of a white powder, that was used without further purification (~99% yield). A trace impurity is present as shown in <sup>1</sup>H-NMR at 1.80 ppm. The melting point and NMR data matched the published reference data.<sup>149</sup>

**Ethyltriphenylphosphonium bromide:** <sup>1</sup>H-NMR (500 MHz, Chloroform-*d*): δ 7.87 – 7.73 (m, 3H), 7.68 (tdd, *J* = 7.6, 3.5, 1.6 Hz, 2H), 3.84 (dt, *J* = 12.1, 7.3 Hz, 1H), 1.37 (dtd, *J* = 20.1, 7.5, 1.6 Hz, 1H). m.p. 201-204°C.



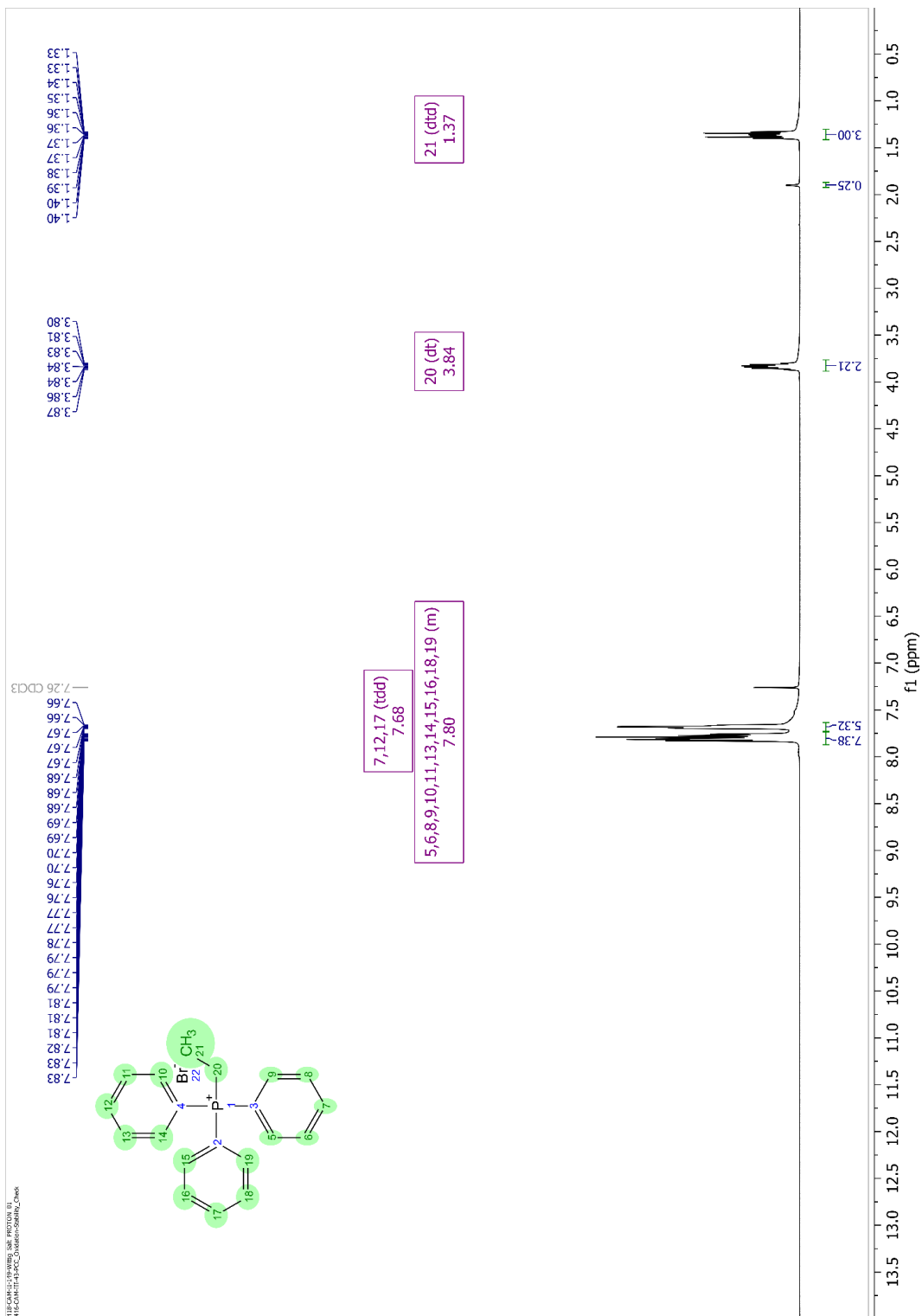
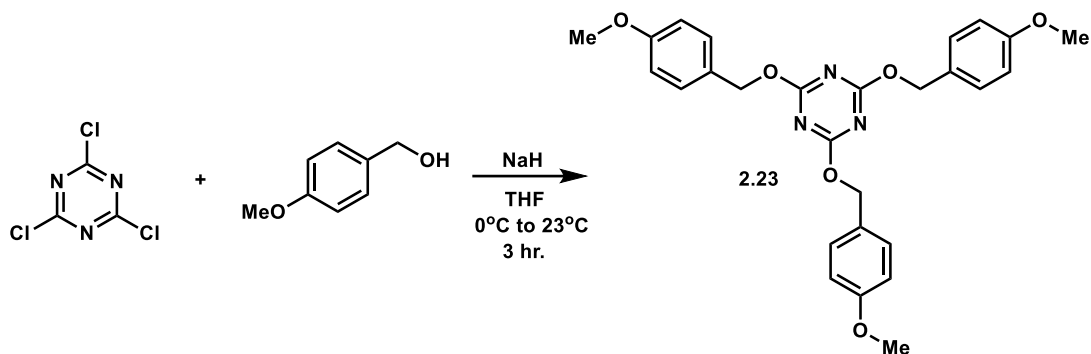


**Figure 2-19.**  $^1\text{H-NMR}$  of ethyltriphenylphosphonium bromide in chloroform- $d$ .



**TriBot-PM; (2.23):** Tribot-PM (**2.23**) was prepared through following a previously reported protocol with no modifications.<sup>96</sup> To a heat treated, two-neck round bottom flask with Teflon-coated stir bead and drop-funnel under nitrogen atmosphere was added solid sodium hydride (60% in mineral oil, 7.90 g, 197 mmol, 3.6 equiv.) followed by dry THF (90.0 ml, 2.2 M). The resulting slurry was vigorously stirred and cooled to 0°C on an ice-water bath for 10 minutes. Anisyl alcohol (22.0 ml, 180 mmol, 3.3 equiv.) was diluted in dry THF (20 ml) and added slow dropwise to the stirring slurry at 0°C over 30 minutes. The temperature was maintained at 0°C for an additional 15 minutes then the reaction was removed from the ice-water bath and warmed to room temperature. After 30 minutes at room temperature, the reaction was cooled to 0°C and a suspension of canuric chloride (**Compound 2.21**, 10.0 g, 54.2 mmol, 1.0 equiv.) in dry THF (90.0 ml, 602 mM) was added over 15 minutes. The reaction was maintained at 0°C for an additional 15 minutes then removed from the ice-water bath and warmed to room temperature. The reaction proceeded over 3 hours under nitrogen atmosphere. The reaction was quenched by pouring the reaction slurry into a 250 ml Erlenmeyer flask containing a stirring solution of ice-cold distilled water. The quenched reaction produced a white precipitate product which was then collected on a stone-frit filter. The collected white precipitate was then washed with ice-cold distilled water (700 ml) followed by hexanes (500 ml) until all yellow color had been removed from the precipitate. The precipitate was dried on high vacuum to afford 25.4 g of product as pure white solid pellets (96.0% yield). Residual water was present in the <sup>1</sup>H-NMR at 1.55 ppm. The NMR data matched the published reference data.<sup>96</sup>

**TriBot-PM (2.23):** <sup>1</sup>H-NMR (500 MHz, Chloroform-*d*): δ 7.37 (d, *J* = 8.6 Hz, 1H), 6.89 (d, *J* = 8.7 Hz, 1H), 5.38 (s, 2H), 3.81 (s, 2H), 1.57 (s, 1H). <sup>13</sup>C-NMR (151 MHz, Chloroform-*d*) δ 206.5, 173.1, 159.9, 130.4, 114.1, 69.9, 55.4.

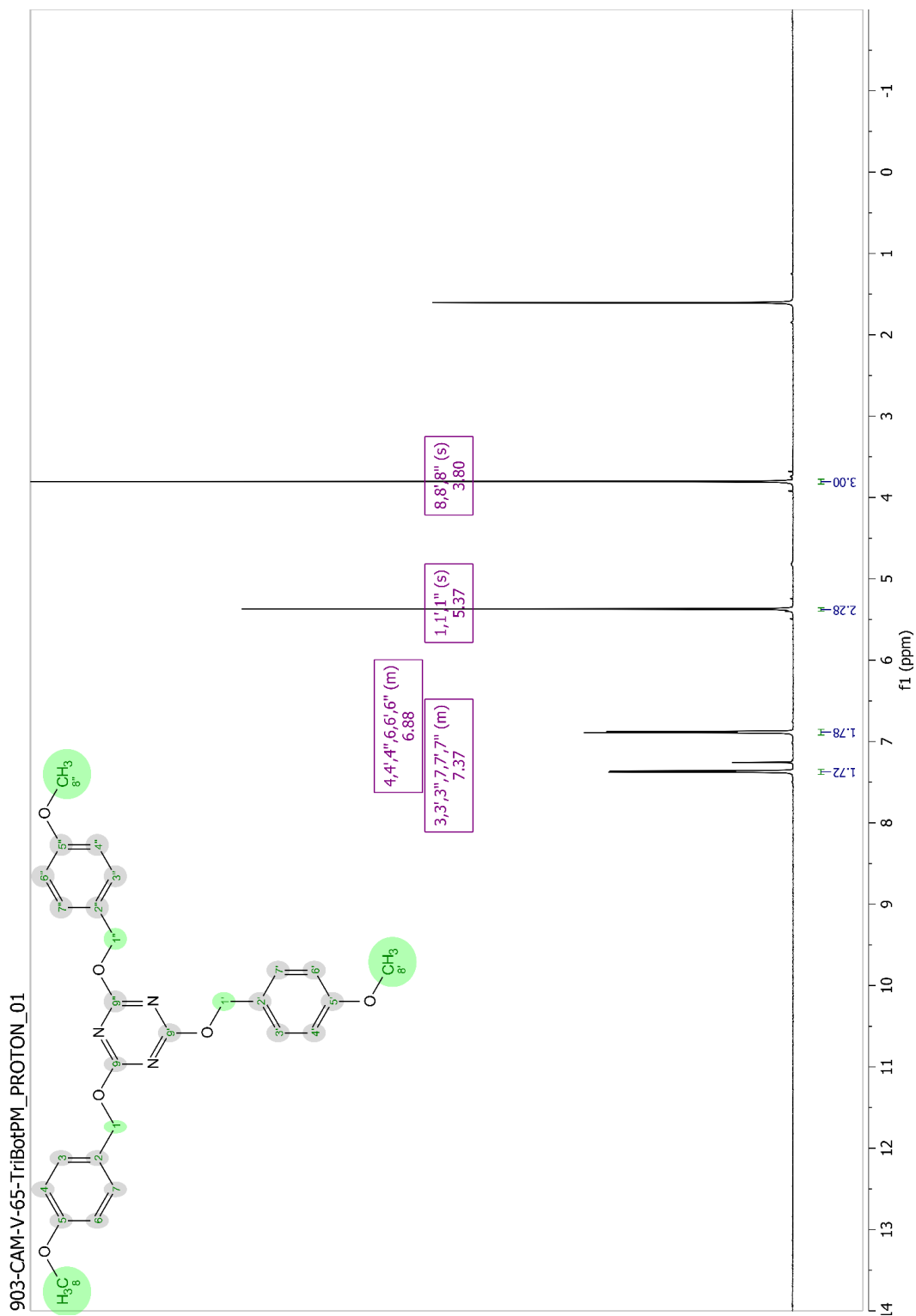


**Figure 2-20.**  $^1\text{H-NMR}$  of TriBot-PM (2.23) in chloroform-*d*.

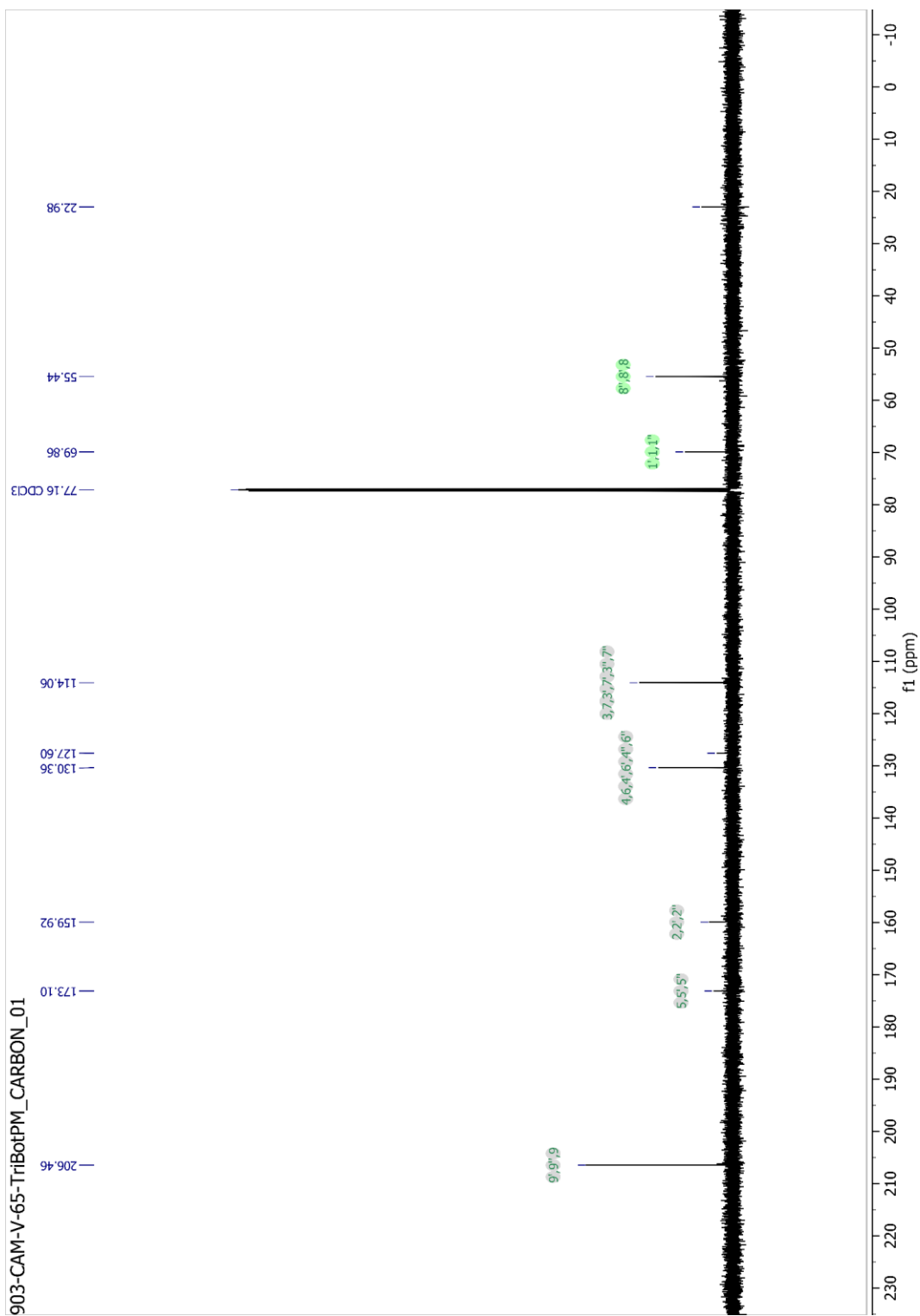
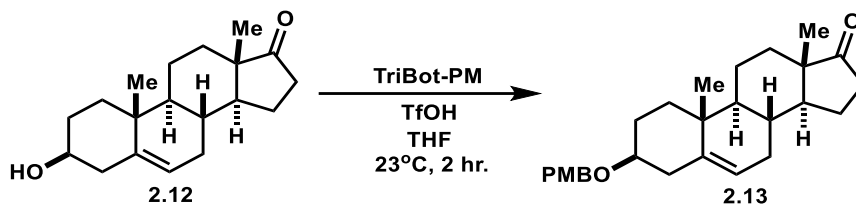


**Figure 2-21.**  $^{13}\text{C}$ -NMR of TriBot-PM (2.23) in chloroform-*d*.



**(3S,8R,9S,10R,13S,14S)-3-((4-methoxybenzyl)oxy)-10,13-dimethyl-1,2,3,4,7,8,9,10,11,12,13,14,15,16-tetradecahydro-17H-cyclopenta[a]phenanthren-17-one; (2.13):** Compound 2.13 was prepared through applying a previously reported general method for TriBOT-PM to *trans*-dehydroandrosterone (Compound 2.12).<sup>64,96</sup> Concentrated trifluoromethane sulfonic acid (90.0  $\mu$ l, 3.0 mol %) was added slowly, dropwise, to a stirring solution of *trans*-dehydroandrosterone (Compound 2.12, 10.0 g, 34.7 mmol, 1.0 equiv.) dissolved in dry THF (48.0 ml, 0.723 M) at room temperature under a nitrogen atmosphere. The reaction was stirred for 5 minutes at room temperature, followed by addition of 10 ml of TriBot-PM (Compound 2.23, 10.2 g, 20.8 mmol, 0.6 equiv.) in dry THF (36.0 ml, 0.572 M) and an additional 5 ml of this solution was added every 30 minutes for 2 hours. The reaction slurry became opaque-white with no yellow color after 2 hours. The reaction was then quenched with 10 ml aqueous saturated sodium carbonate. The reaction was transferred to a separatory funnel, diluted in DCM (100 ml), and washed extensively with sat.  $\text{NaHCO}_{3(\text{aq})}$  (4 x 50 ml). The organic layers were combined and then washed twice with brine and dried over sodium sulfate. The drying agent was then filtered off and the organic solution condensed *in vacuo*. The crude material was recrystallized in fuming isopropanol (200 ml) to afford 8.50 g of desired Compound 2.13 as a white crystalline solid (60% yield). The NMR data matched the published reference data.<sup>64,96</sup>

**Compound 2.13:**  $^1\text{H-NMR}$  (500 MHz, Chloroform-*d*):  $\delta$  7.27 (d,  $J = 8.6$  Hz, 1H), 6.88 (d,  $J = 8.6$  Hz, 1H), 5.44 – 5.30 (m, 1H), 4.50 (s, 2H), 3.80 (s, 3H), 3.27 (tt,  $J = 11, 4.5$  Hz, 1H), 2.52 – 2.44 (m, 2H), 2.42 (dd,  $J = 4.8, 2.3$  Hz, 0H), 2.33 – 2.24 (m, 1H), 2.15 – 2.03 (m, 2H), 1.99 – 1.91 (m, 3H), 1.91 – 1.81 (m, 3H), 1.70 – 1.62 (m, 3H), 1.58 – 1.53 (m, 1H), 1.53 – 1.43 (m, 1H), 1.35 – 1.23 (m, 2H), 1.11 – 1.05 (m, 1H), 1.04 (s, 4H), 1.00 – 0.96 (m, 1H), 0.89 (s, 4H).

1072-CAM-VI-53-PMBAndrosterone-pure\_PROTON\_01

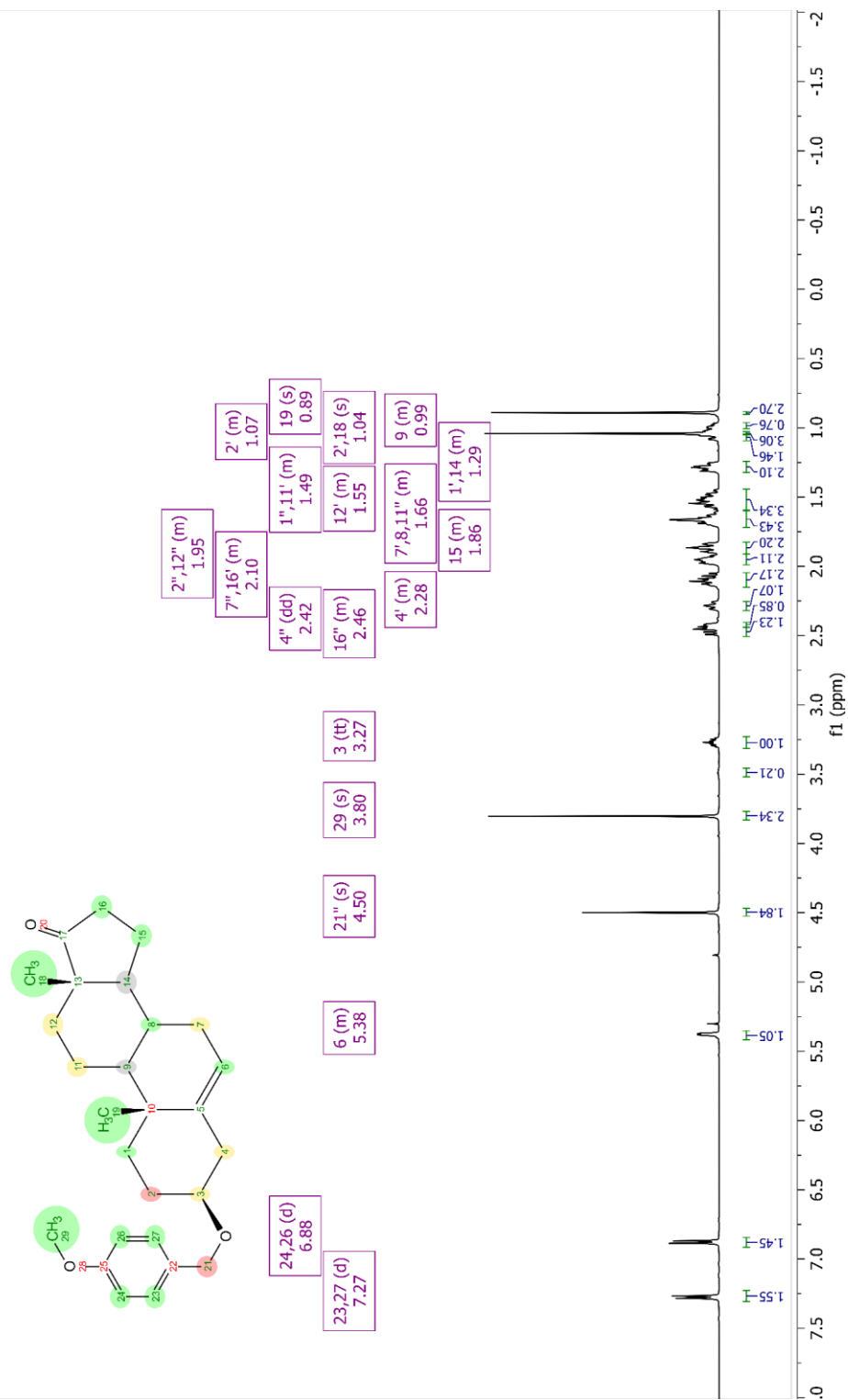
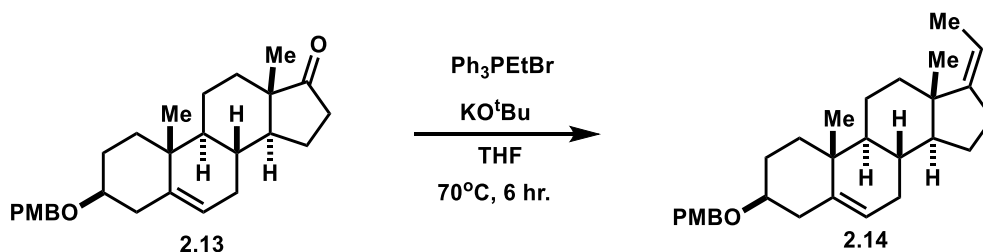


Figure 2-22. <sup>1</sup>H-NMR of Compound 2.13 in chloroform-*d*.



**(3S,8S,9S,10R,13S,14S,Z)-17-ethylidene-3-((4-methoxybenzyl)oxy)-10,13-dimethyl-2,3,4,7,8,9,10,11,12,13,14,15,16,17-tetradecahydro-1H-cyclopenta[a]phenanthrene; (2.14):** Compound 2.14 is a previously reported compound and was prepared through applying a previously reported protocol to transform **Compound 2.13**.<sup>143</sup> To a heat treated 500 ml three-neck round-bottom flask was added potassium tert-butoxide (7.50 g, 66.8 mmol, 3.2 equiv.) and ethyltriphenylphosphonium bromide (27.7 g, 74.9 mmol, 3.6 equiv.). A large Teflon-coated stir bar was added to the flask, and a reflux column assembly attached. The reaction flask was septa sealed and purged thrice with nitrogen and vacuum. Dry THF (270 ml) was added to create an orange/red suspension which was stirred at room temperature for approximately 20 minutes. To the suspension was added a solution of starting steroid, **Compound 2.13**, (8.50 g, 20.8 mmol, 1.0 equiv.) in dry THF (30 ml, 0.700 M) fast dropwise. The reaction was refluxed for 6 hours and upon complete conversion by TLC, the reaction solution was cooled to room temperature and then quenched with saturated aqueous ammonium chloride (~15 ml). The quenched-reaction solution was transferred to a separatory flask and diluted with ethyl acetate (100 ml), washed once with saturated ammonium chloride (75 ml), then twice with distilled water (100 ml each). The aqueous layers were combined and back extracted in ethyl acetate (100 ml). The organic layers were combined and washed once with brine then dried over sodium sulfate. The drying agent was removed, and the clear organic solution was condensed *in vacuo* to a crude white solid. The crude material was recrystallized in fuming isopropanol (175 ml) and the resulting crystalline precipitate was collected on a stone-frit filter and washed with cold isopropanol (750 ml). The collected crystals were dried on high vacuum to afford 7.15 g, with trace impurities of unreacted starting material (~82% yield). The product was used without further purification. NMR data matched literature reference NMR data.<sup>143</sup>

**Compound 2.14:** <sup>1</sup>H-NMR (600 MHz, Chloroform-*d*):  $\delta$  7.55 – 6.91 (m, 4H), 6.87 (d,  $J$  = 8.6 Hz, 2H), 5.35 (d,  $J$  = 5.2 Hz, 1H), 5.28 – 5.00 (m, 1H), 4.49 (d,  $J$  = 2.0 Hz, 2H), 3.80 (s, 3H), 3.26 (td,  $J$  = 11, 5.4 Hz, 1H), 2.44 – 2.39 (m, 1H), 2.33 – 2.24 (m, 2H), 2.18 (dt,  $J$  = 17, 9.0 Hz, 1H), 2.02 (dd,  $J$  = 16, 3.7 Hz, 1H), 1.94 (d,  $J$  = 13 Hz, 1H), 1.87 (dd,  $J$  = 13, 3.6 Hz, 1H), 1.66 (dt,  $J$  = 7.2, 2.0 Hz, 3H), 1.63 – 1.55 (m, 1H), 1.55 (s, 5H), 1.28 – 1.18 (m, 1H), 1.17 – 1.08 (m, 1H), 1.05 (dd,  $J$  = 14, 3.8 Hz, 1H), 0.99 – 0.92 (m, 1H), 0.89 (s, 4H). <sup>13</sup>C-NMR (101 MHz, Chloroform-*d*):  $\delta$  159.0, 150.3, 141.0, 131.1, 129.2, 121.4, 113.8, 113.5, 78.2, 69.6, 56.5, 55.3, 50.2, 44.0, 39.2, 37.2, 37.0, 37.0, 31.8, 31.4, 31.4, 28.4, 24.5, 21.2, 19.4, 16.6, 13.2.

1077-CAM-VI-57-PMBPregnadiene-pure\_PROTON\_01

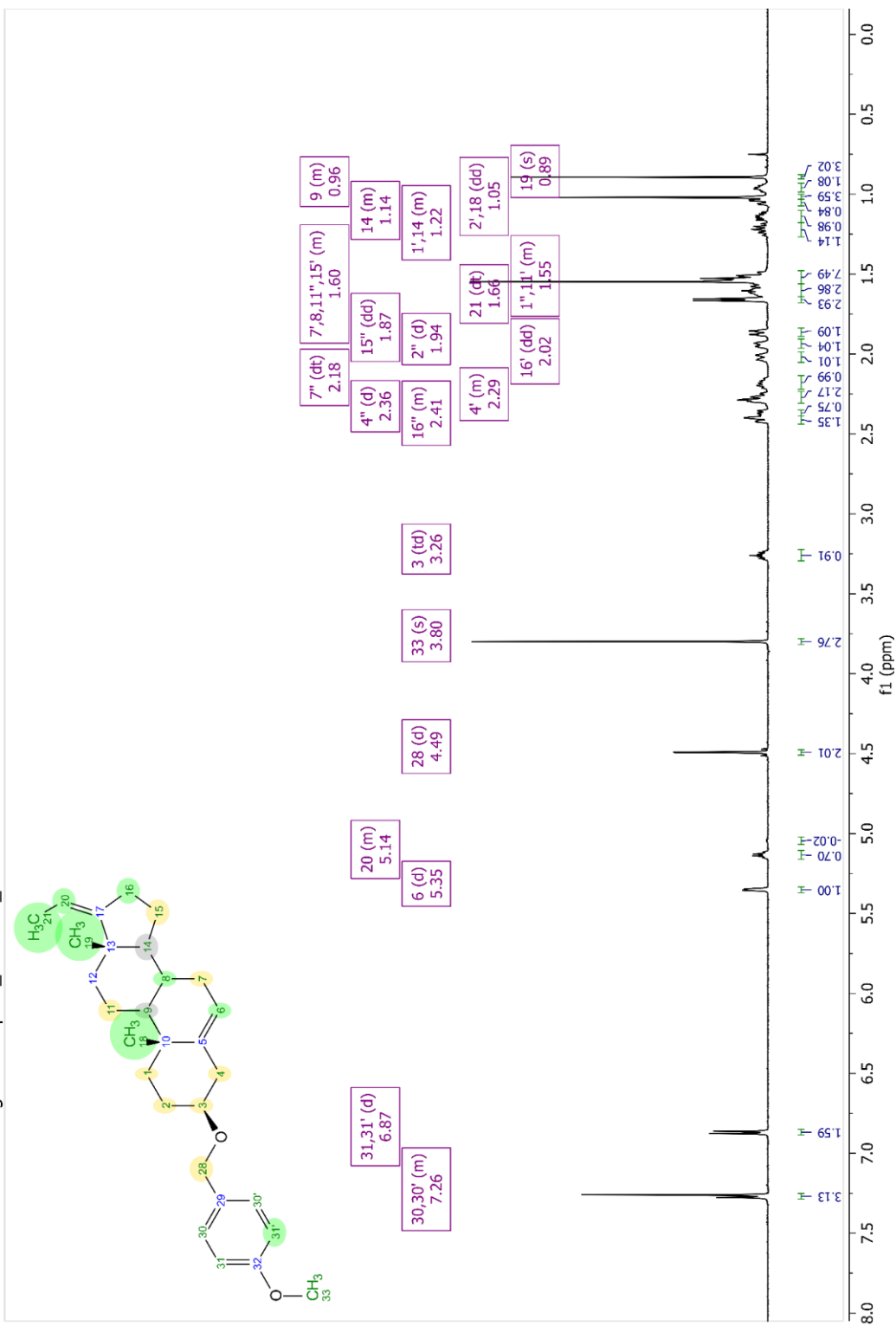
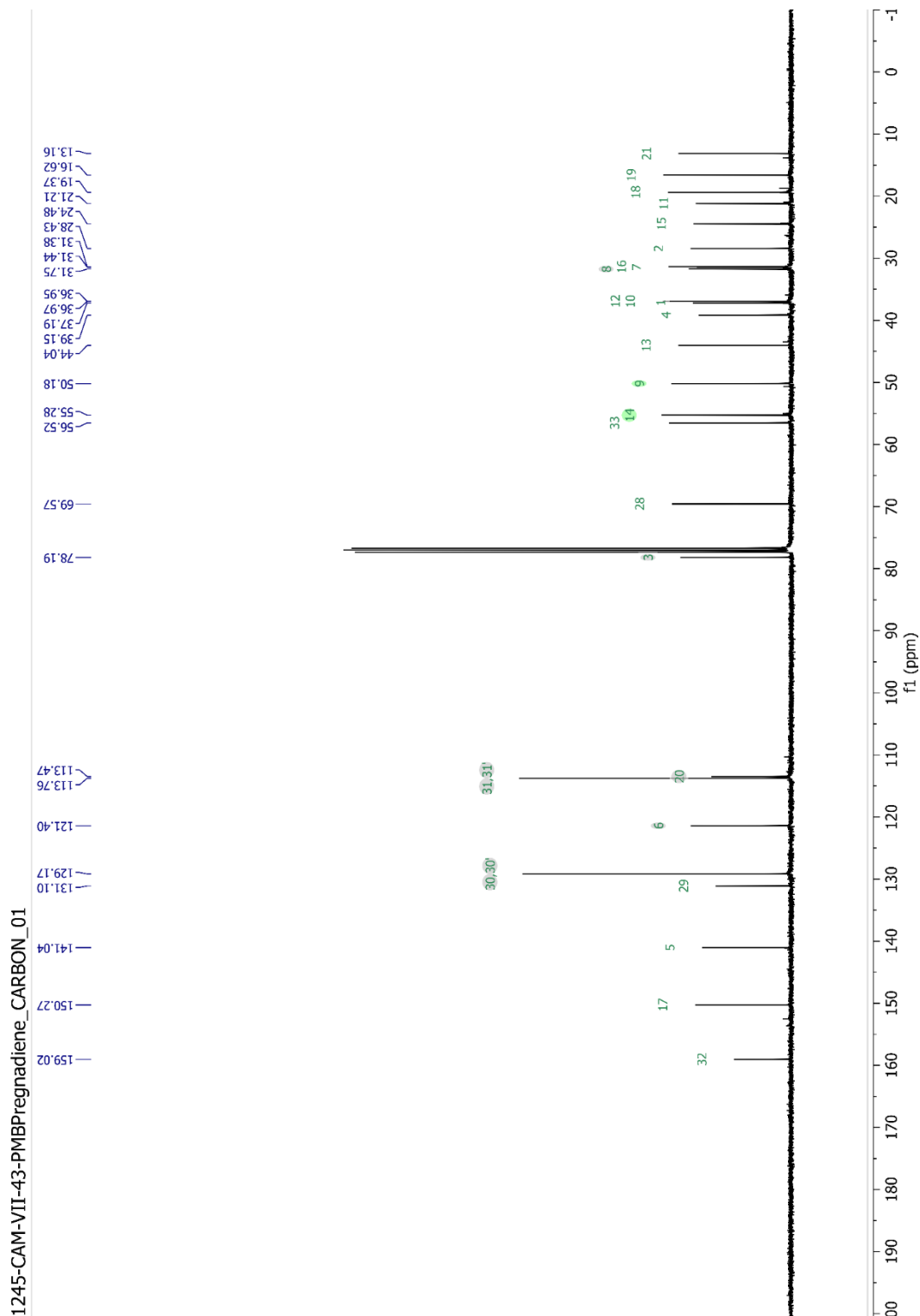
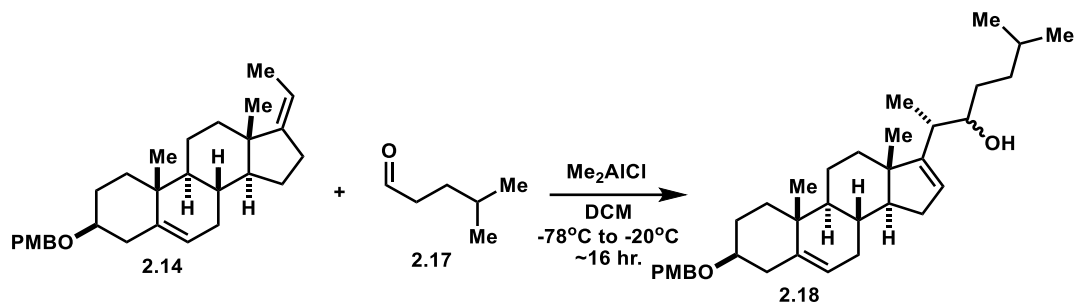


Figure 2-23. <sup>1</sup>H-NMR of Compound 2.14 with trace impurity in chloroform-d.





**Figure 2-24.**  $^{13}\text{C}$ -NMR of **Compound 2.14** with trace impurity, in chloroform-*d*.



(2S)-2-((3S,8R,9S,10R,13S,14S)-3-((4-methoxybenzyl)oxy)-10,13-dimethyl-2,3,4,7,8,9,10,11,12,13,14,15-dodecahydro-1H-cyclopenta[a]phenanthren-17-yl)-6-methylheptan-3-ol; (**2.18**): **Compound 2.18** was formed through a new reaction adapting previously reported reaction protocol.<sup>101</sup> A solution of distilled DCM (10 mL) and freshly prepared 4-methylpentanal (**Compound 2.17**, 2.84 g, 28.3 mmol, 2.9 equiv.) was stirred under nitrogen atmosphere at  $-78^{\circ}\text{C}$  for 10 minutes. A solution of  $\text{Me}_2\text{AlCl}$  (1.0 M solution, 60.0 mL, 60.6 mmol, 6.2 equiv.) was added via addition funnel over 60 minutes dropwise at  $-78^{\circ}\text{C}$ . The reaction was then stirred at  $-78^{\circ}\text{C}$  for an additional 20 minutes. A solution of starting material steroid, **Compound 2.14**, (4.11 g, 9.77 mmol, 1.0 equiv.) in dry DCM (20.0 mL, 0.489 M), was added via additional funnel over 60 minutes dropwise at  $-78^{\circ}\text{C}$ . Upon complete addition of **Compound 2.14**, the reaction was stirred at  $-78^{\circ}\text{C}$  for an additional 30 minutes then was warmed to  $-20^{\circ}\text{C}$  for 14 hours. Then, the reaction was cooled to  $-78^{\circ}\text{C}$  and quenched with a solution of MeOH: DI  $\text{H}_2\text{O}$  (1:1 vol. ratio, 10.0 mL). The reaction mixture was diluted with DI  $\text{H}_2\text{O}$  (70.0 mL) and transferred to a separatory funnel. The biphasic mixture was separated, and the aqueous layer extracted with DCM (3 x 50.0 mL). The combined organic layers were washed with 1N HCl (50.0 mL), saturated solution of  $\text{NaHCO}_3$  (50.0 mL), and DI  $\text{H}_2\text{O}$  (2 x 50.0 mL). The combined aqueous phases were back extracted with DCM (50.0 mL). The combined organic phases were washed with brine then dried over  $\text{Na}_2\text{SO}_4$ . The drying agent was removed, and the crude mixture was condensed *in vacuo* to afford a crude white solid. The crude material was purified via automated column chromatography, using a 50 G Biotage column with oven-dried silica gel as the stationary phase, and the product was eluted with a gradient of 5% to 30% ethyl acetate in hexanes. 4.50 g of purified **Compound 2.18** as a ~1:1 diastereomeric mixture was afforded as a white solid (88% yield). Diagnostic NMR peaks agreed with published reference and contained trace amounts of an oxa-E-ring side product.<sup>101</sup>

**Compound 2.18**:  $^1\text{H-NMR}$  (500 MHz, Chloroform-*d*):  $\delta$  5.51 – 5.48 (m, 1H), 5.41 – 5.37 (m, 1H), 4.61 (tdd,  $J = 10.4, 6.2, 4.3$  Hz, 1H), 3.63 (dtd,  $J = 8.0, 4.7, 3.3$  Hz, 1H, H-22 of major isomer), 3.57 (tt,  $J = 8.7, 2.1$  Hz, 1H, H-22 of minor isomer), 2.39 – 2.25 (m, 4H), 2.19 – 2.06 (m, 2H), 2.06 – 1.96 (m, 5H), 1.95 – 1.83 (m, 4H), 1.82 – 1.74 (m, 1H), 1.75 – 1.59 (m, 3H), 1.59 – 1.48 (m, 4H), 1.49 – 1.41 (m, 2H), 1.41 – 1.31 (m, 3H), 1.31 – 1.24 (m, 1H), 1.23 – 1.16 (m, 1H), 1.15 – 1.10 (m, 1H), 1.08 – 1.05 (m, 4H), 1.02 (dd,  $J = 7.0, 1.7$  Hz, 3H), 1.01 – 0.98 (m, 1H), 0.92 – 0.87 (m, 13H).  $^{13}\text{C-NMR}$  (101 MHz, Chloroform-*d*):  $\delta$  159.0, 158.6, 141.0, 131.1, 129.2, 121.4, 113.8, 78.2, 73.9, 69.6, 57.9, 50.7, 47.0, 38.3, 37.9, 37.1, 37.0, 35.7, 34.8, 32.6, 31.7, 31.4, 30.5, 28.3, 27.9, 22.8, 22.8, 21.6, 20.8, 19.4, 16.9, 14.3.

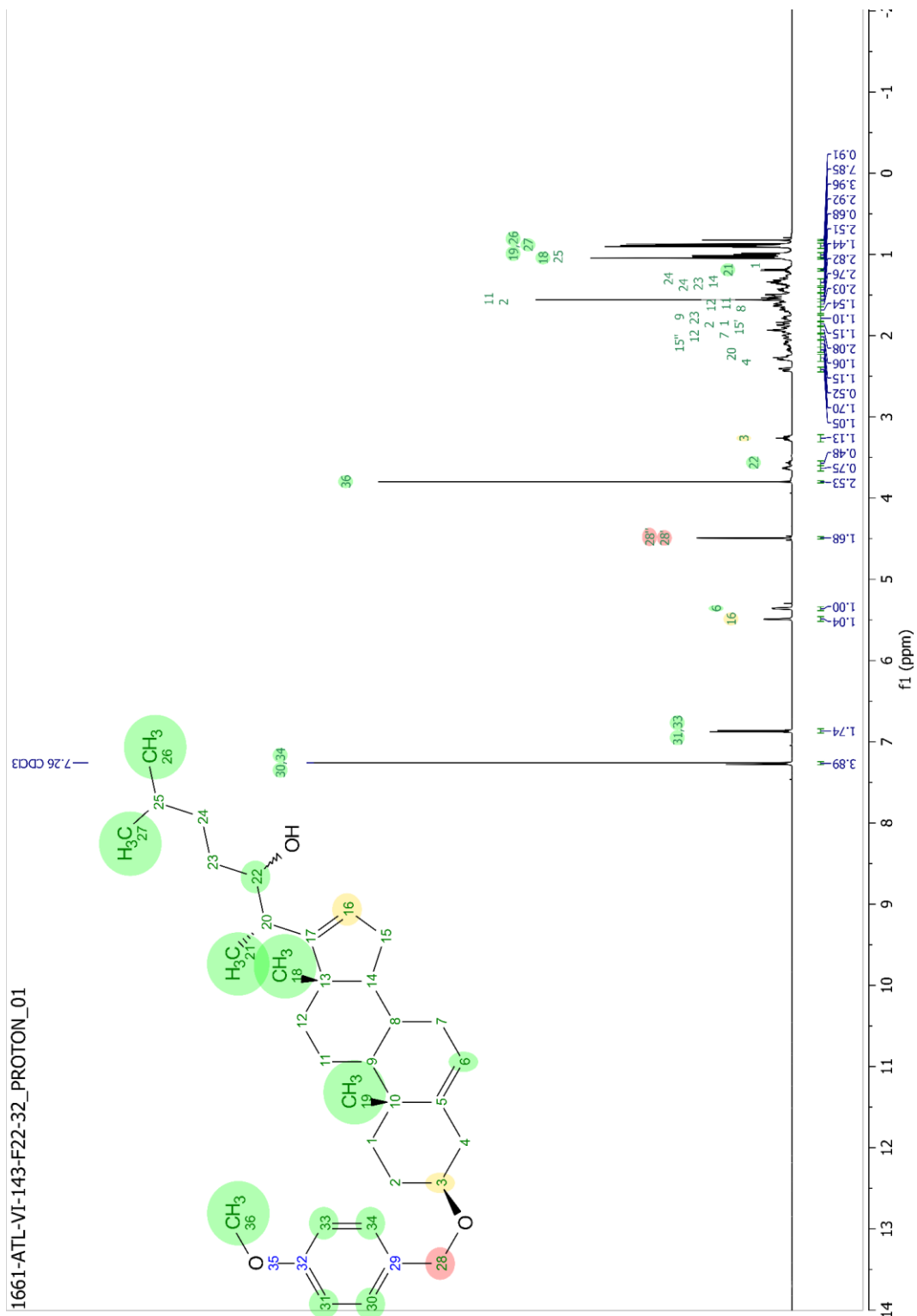


**Figure 2-25.**  $^1\text{H-NMR}$  of **Compound 2.18** as a diastereomeric mixture in chloroform-*d*.

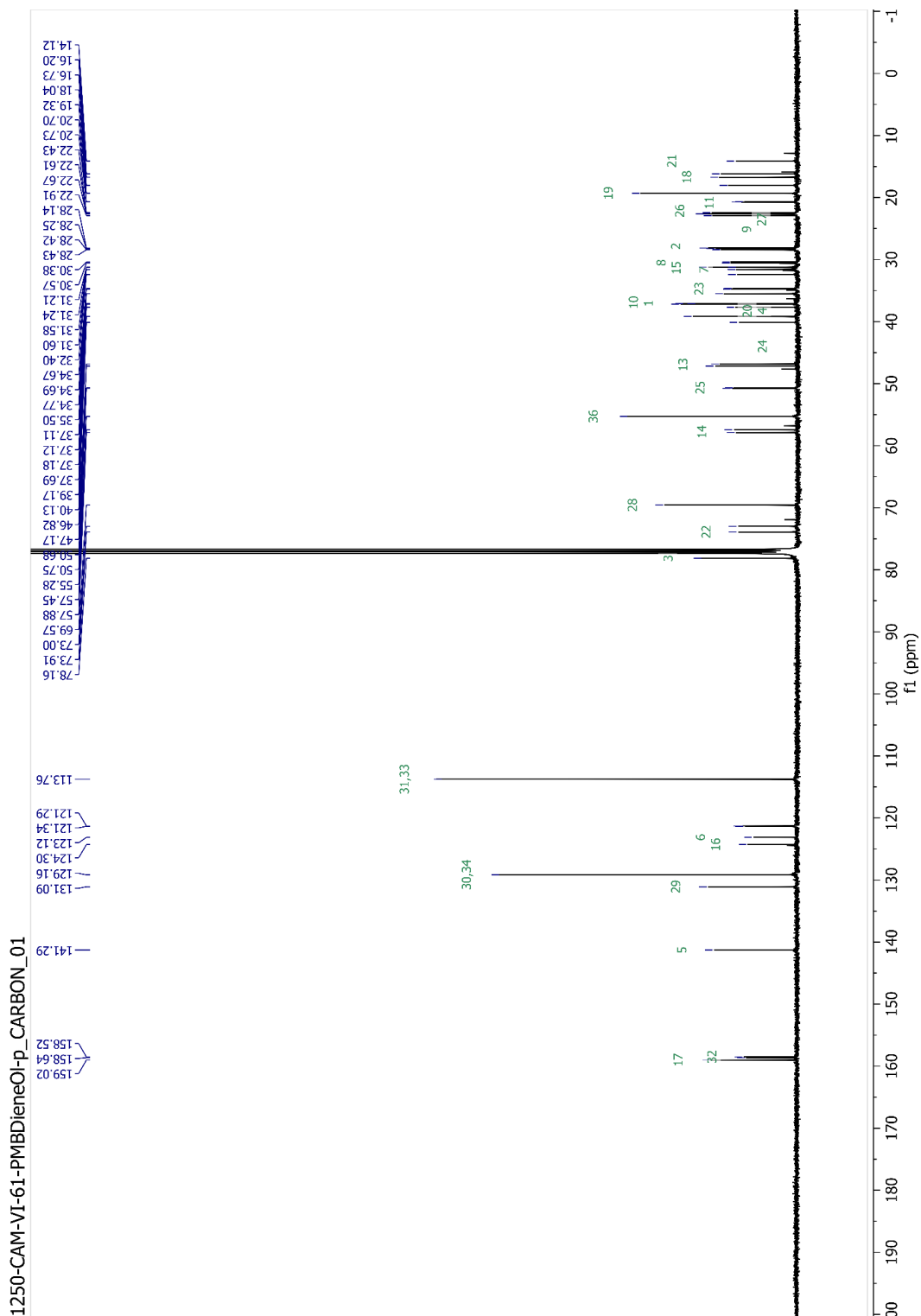
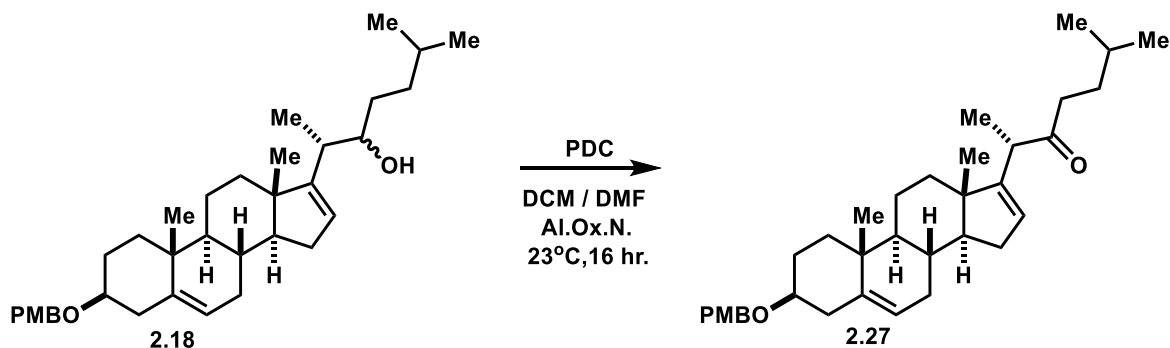


**Figure 2-26.**  $^{13}\text{C}$ -NMR of **Compound 2.18** as a diastereomeric mixture in chloroform-*d* with trace amounts of an oxa-E-ring side product.



**(S)-2-((3S,8R,9S,10R,13S,14S)-3-((4-methoxybenzyl)oxy)-10,13-dimethyl-2,3,4,7,8,9,10,11,12,13,14,15-dodecahydro-1H-cyclopenta[a]phenanthren-17-yl)-6-methylheptan-3-one; (2.27):** Compound 2.27 was prepared through following a previously reported protocol adapted for transforming **Compound 2.18** which had not previously been shown.<sup>57</sup> In a 100 ml two-neck round-bottom flask at room temperature under nitrogen atmosphere was created a slurry of PDC (1.04 g, 2.76 mmol, 2.05 equiv.) and neutral alumina oxide (1.04 g) in dry DCM (30.0 ml) and DMF (2.0 ml). The slurry stirred at room temperature for 10 minutes. To this stirring slurry was added a solution of starting sterol, **Compound 2.18**, (702 mg, 1.35 mmol, 1.0 equiv.) in dry DCM (10.0 ml) fast dropwise. The reaction proceeded over 16 hours and upon complete conversion by TLC, an additional portion of neutral alumina (1.00 g) was added followed by DCM (50 ml). The brown slurry was poured into a flash column containing a 1:1 mixture of oven-dried silica (5.0 g) and neutral alumina oxide (5.0 g), and the desired product was eluted with DCM (350 ml). 536 mg of the desired compound was obtained (77% yield) and carried forward without further purification. The diagnostic NMR data agreed with the published reference.<sup>57</sup>

**Compound 2.27:** <sup>1</sup>H-NMR (600 MHz, Chloroform-*d*):  $\delta$  7.30 – 7.19 (m, 2H), 6.86 (d,  $J$  = 8.2 Hz, 1H), 5.35 (s, 1H), 4.48 (s, 2H), 3.79 (d,  $J$  = 1.2 Hz, 3H), 3.25 (tt,  $J$  = 11.1, 4.5 Hz, 1H), 3.19 (q,  $J$  = 6.9 Hz, 1H), 1.15 (d,  $J$  = 6.8 Hz, 3H), 1.04 (s, 3H), 0.89 – 0.80 (m, 9H).

656-CAM-IV-48-PMBDieneOne-Crude\_PROTON\_01

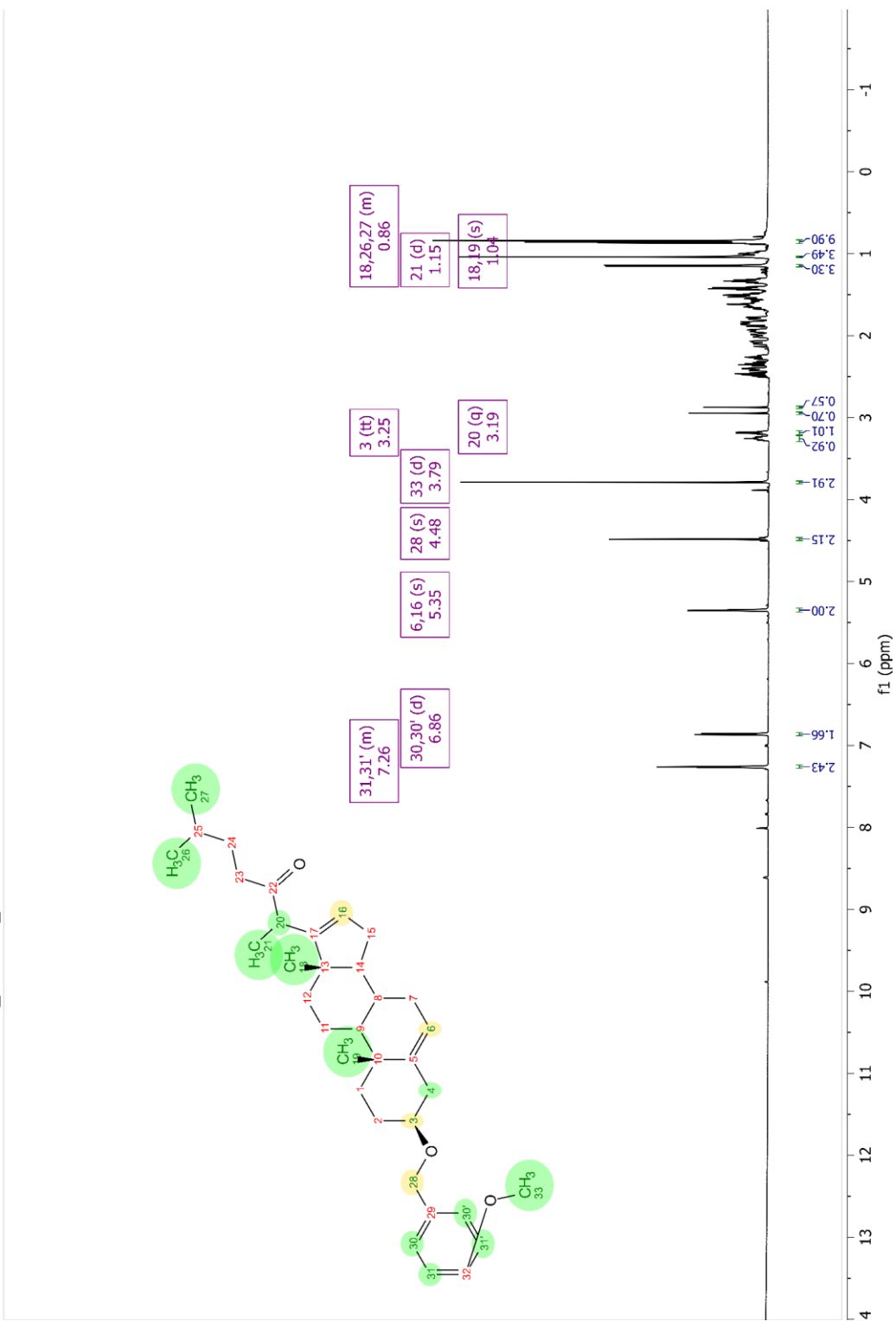
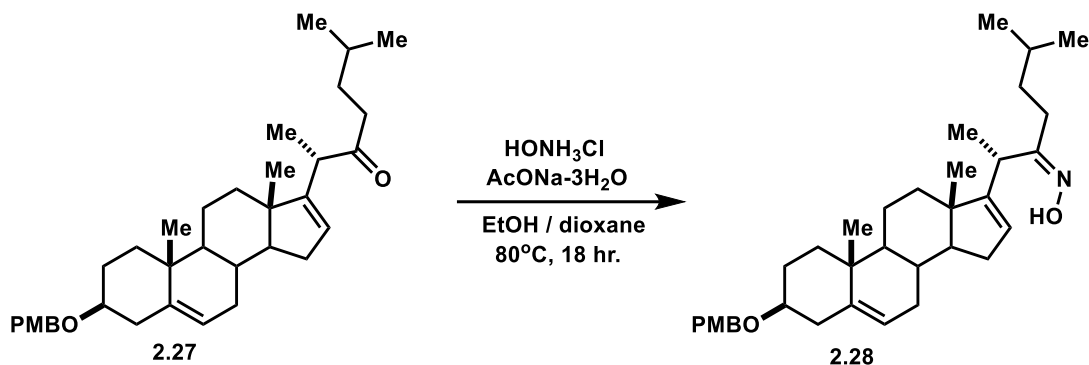


Figure 2-27. <sup>1</sup>H-NMR of Compound 2.27 in chloroform-*d*.



**(S)-2-((3S,8R,9S,10R,13S,14S)-3-((4-methoxybenzyl)oxy)-10,13-dimethyl-2,3,4,7,8,9,10,11,12,13,14,15-dodecahydro-1H-cyclopenta[a]phenanthren-17-yl)-6-methylheptan-3-one oxime; (2.28):** Compound **2.28** was prepared through following a previously reported protocol not previously used on steroidal reactants.<sup>150</sup> Starting steroid **Compound 2.27** (275 mg, 0.530 mmol, 1.0 equiv.) was dissolved in a solution of ethanol (6.0 ml) and dioxane (3 ml,) within a 20 ml round-bottom flask. Solid sodium acetate trihydrate (432 mg, 3.18 mmol, 6.0 equiv.) and solid hydroxylammonium chloride (152 mg, 2.17 mmol, 4.1 equiv.). The resulting slurry was heated to reflux at ~80°C for 18 hours. Then, the reaction mixture was diluted with DI H<sub>2</sub>O (20.0 mL) and then transferred to a separatory funnel. The mixture was extracted with DCM (3 x 30.0 mL) and the organic layers combined. The combined organic layers were washed with brine and dried over Na<sub>2</sub>SO<sub>4</sub>. The drying agent was removed, and the solution condensed *in vacuo* to afford 280 mg of crude white solid (99% yield). The crude material was taken forward without further purification.

**Compound 2.28:** <sup>1</sup>H-NMR (500 MHz, Chloroform-*d*): δ 5.46 (dt, *J* = 2.9, 1.4 Hz, 1H), 5.42 – 5.37 (m, 1H), 4.65 – 4.55 (m, 1H), 3.12 – 3.07 (m, 1H), 2.37 – 2.29 (m, 2H), 2.29 – 2.23 (m, 1H), 2.17 – 2.05 (m, 2H), 2.03 (s, 3H), 2.00 – 1.96 (m, 1H), 1.91 – 1.82 (m, 4H), 1.72 – 1.44 (m, 7H), 1.42 – 1.23 (m, 3H), 1.20 (d, *J* = 7.1 Hz, 3H), 1.18 – 1.09 (m, 1H), 1.07 – 0.99 (m, 4H), 0.90 (dd, *J* = 6.5, 1.8 Hz, 6H), 0.78 (s, 3H). <sup>13</sup>C-NMR (126 MHz, Chloroform-*d*): δ 164.2, 159.0, 155.9, 141.3, 131.1, 129.1, 124.9, 121.3, 113.8, 78.2, 69.6, 57.5, 55.3, 50.7, 46.9, 39.2, 38.5, 38.1, 37.2, 37.1, 35.2, 34.6, 31.6, 31.1, 30.5, 28.7, 28.4, 25.2, 22.4, 22.3, 20.7, 19.3, 17.6, 16.1, 15.7.

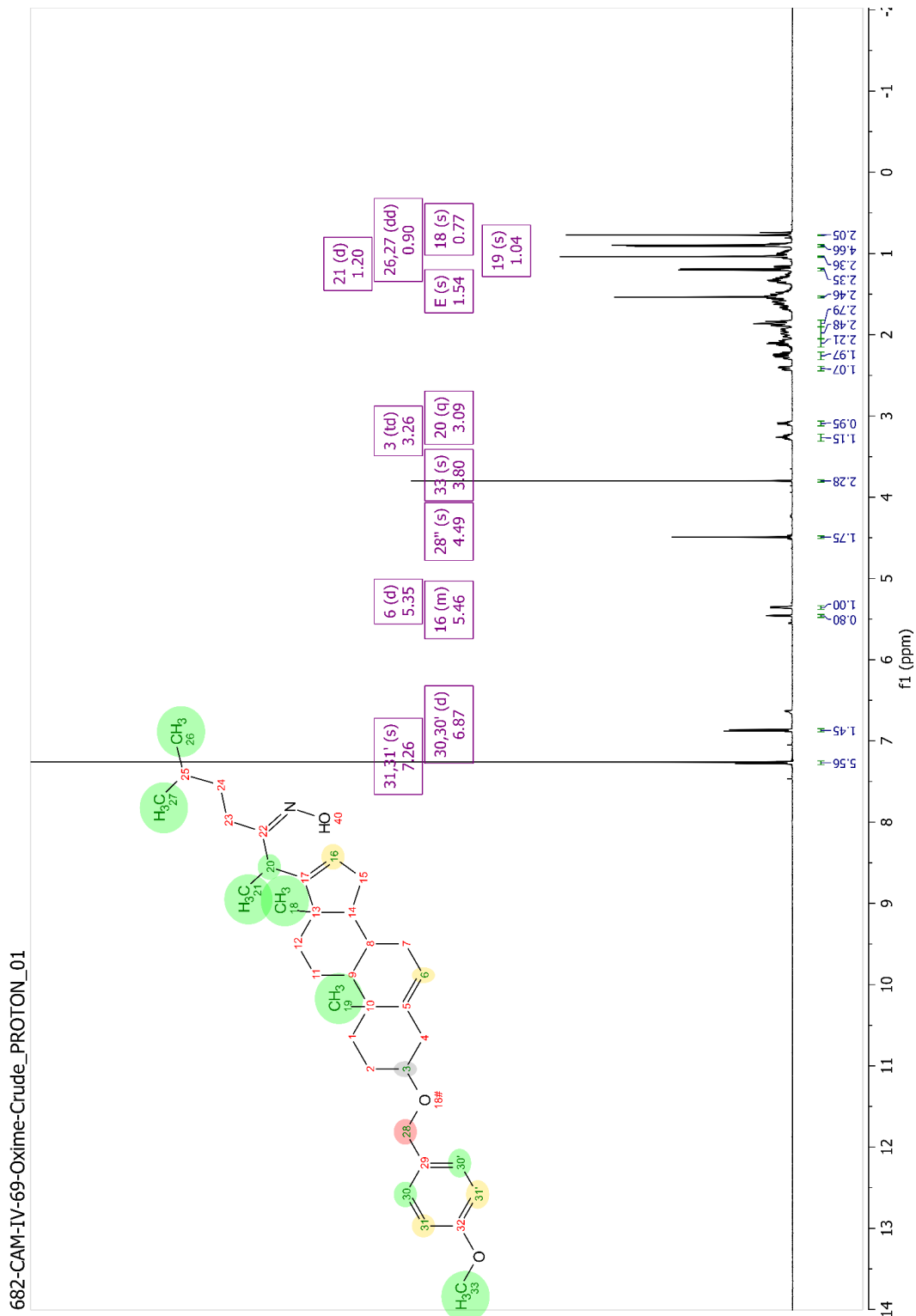
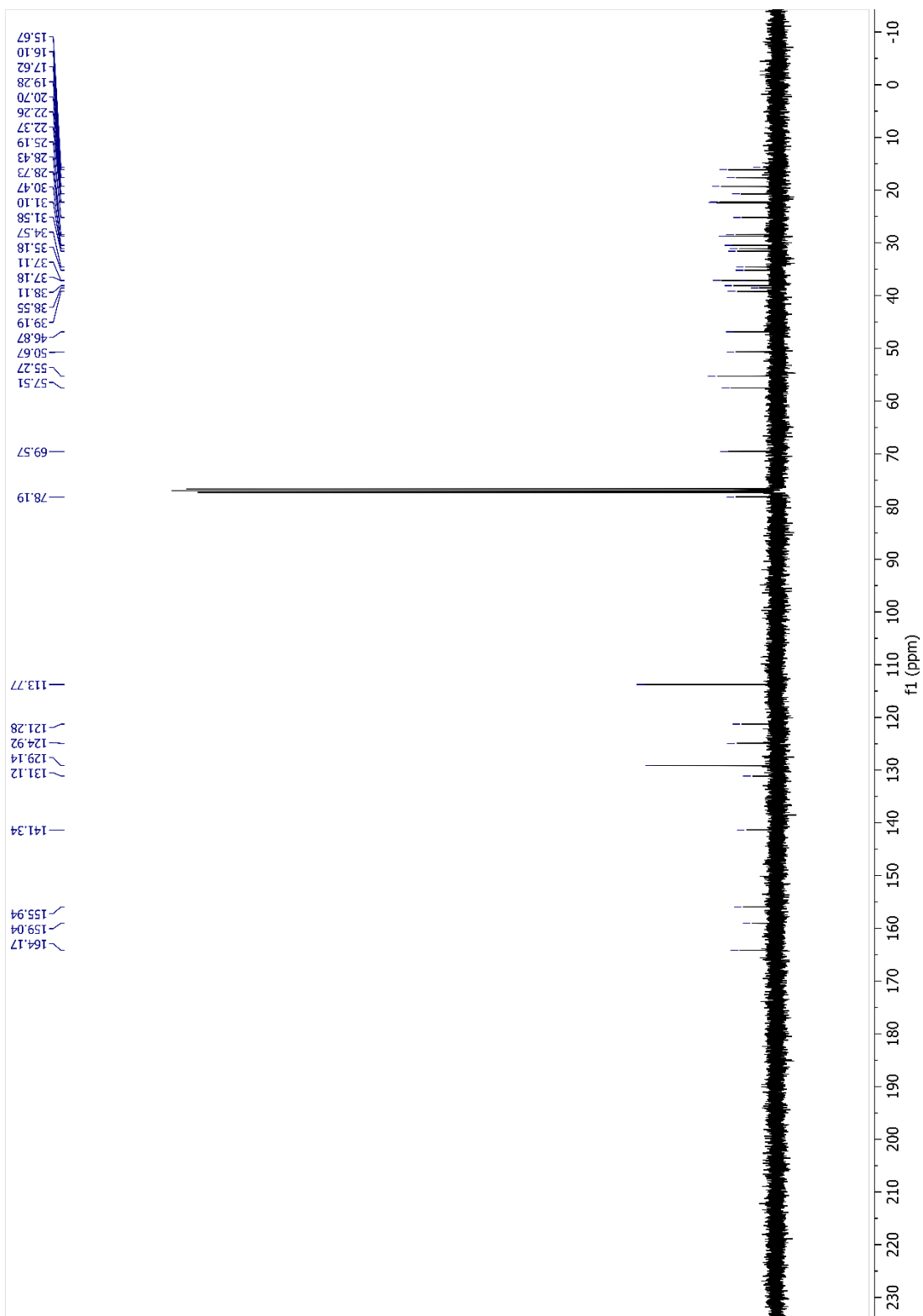
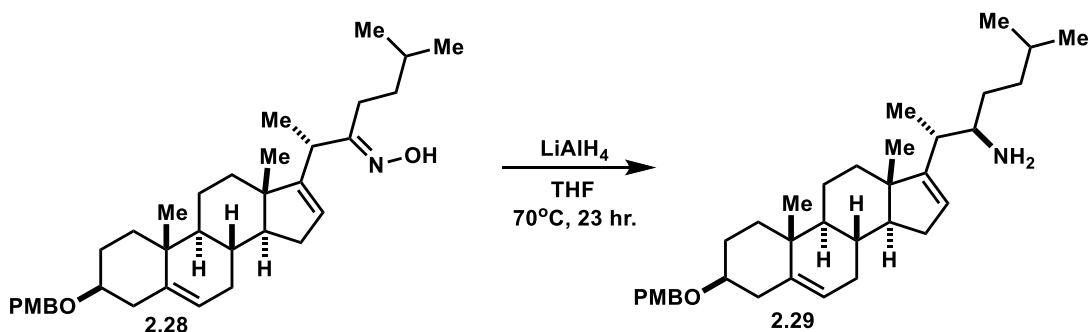


Figure 2-28. <sup>1</sup>H-NMR of Compound 2.28 in chloroform-*d*.





**Figure 2-29.**  $^{13}\text{C}$ -NMR of Compound 2.28 in chloroform-*d*.



**2S,3R)-2-((3S,8R,9S,10R,13S,14S)-3-((4-methoxybenzyl)oxy)-10,13-dimethyl-2,3,4,7,8,9,10,11,12,13,14,15-dodecahydro-1H-cyclopenta[a]phenanthren-17-yl)-6-methylheptan-3-amine; (2.29):** Compound **2.29** was prepared through following a previously reported protocol that had not been demonstrated on steroidal reactants.<sup>151</sup> In a 10 ml round-bottom flask containing a Teflon-coated stir bar, a stirring suspension of lithium aluminum hydride (140 mg, 3.69 mmol, 15 equiv.) in dry THF (1.5 ml) under nitrogen atmosphere was prepared and cooled to 0°C. To the reaction flask, steroid starting material **Compound 2.28**, (121 mg, 0.230 mmol, 1.0 equiv.) in dry THF (1.0 ml) was added slowly dropwise. The flask was equipped with a reflux column and then heated to reflux at 70°C for 23 hours. Then, the reaction was cooled to 0°C, poured into a vigorously stirring solution of 12% NaOH in distilled water at 0°C, followed by warming to room temperature. The quenched solution formed a precipitate as it warmed to room temperature. The reaction mixture was then transferred to separatory funnel and extracted with ethyl acetate (3 x 100 ml). The combined organic phases were washed with brine and then dried over Na<sub>2</sub>SO<sub>4</sub>. The drying agent was removed, and the solvent was evaporated *in vacuo* to afford a crude yellow solid. The crude material was purified via silica gel chromatography and eluted with a gradient of 0% to 15% methanol in DCM to afford 108 mg of desired product as a single stereoisomer (92% yield). The stereochemistry of C20 and C22 was determined via qNOESY by excitation of H23'' to determine distance to H22. H22 was then excited to determine other distances.<sup>112</sup>

**Compound 2.29:** <sup>1</sup>H-NMR (500 MHz, Chloroform-*d*): δ 7.29 (d, *J* = 1.7 Hz, 1H), 6.92 – 6.85 (m, 2H), 5.42 – 5.40 (m, 1H), 5.39 – 5.35 (m, 1H), 4.50 (d, *J* = 1.4 Hz, 3H), 3.81 (s, 3H), 3.27 (tt, *J* = 11, 4.4 Hz, 1H), 2.79 (d, *J* = 8.7 Hz, 1H), 2.43 (ddd, *J* = 13, 4.9, 2.3 Hz, 1H), 2.30 (dddd, *J* = 17, 14, 9.4, 4.3 Hz, 2H), 2.10 (ddd, *J* = 15, 6.5, 3.3 Hz, 1H), 1.75 – 1.62 (m, 2H), 1.65 – 1.55 (m, 2H), 1.58 – 1.50 (m, 2H), 1.46 (ddd, *J* = 28, 11, 5.1 Hz, 1H), 1.42 – 1.33 (m, 1H), 1.36 – 1.25 (m, 1H), 1.28 – 1.08 (m, 2H), 1.06 (s, 3H), 0.99 (d, *J* = 6.7 Hz, 3H), 0.91 (t, *J* = 6.2 Hz, 5H), 0.84 (s, 2H). <sup>13</sup>C-NMR (101 MHz, Chloroform-*d*): δ 159.2, 159.0, 141.3, 131.1, 129.2, 121.9, 121.4, 113.8, 78.2, 69.6, 57.6, 55.3, 54.1, 50.8, 47.0, 40.3, 39.2, 37.2, 37.1, 37.1, 35.3, 34.8, 31.6, 31.5, 31.2, 30.6, 28.4, 23.0, 22.4, 20.8, 19.3, 18.3, 16.2.

1145-CAM-VI-129-PMBDieneAmine-F\_55\_71\_PROTON\_01

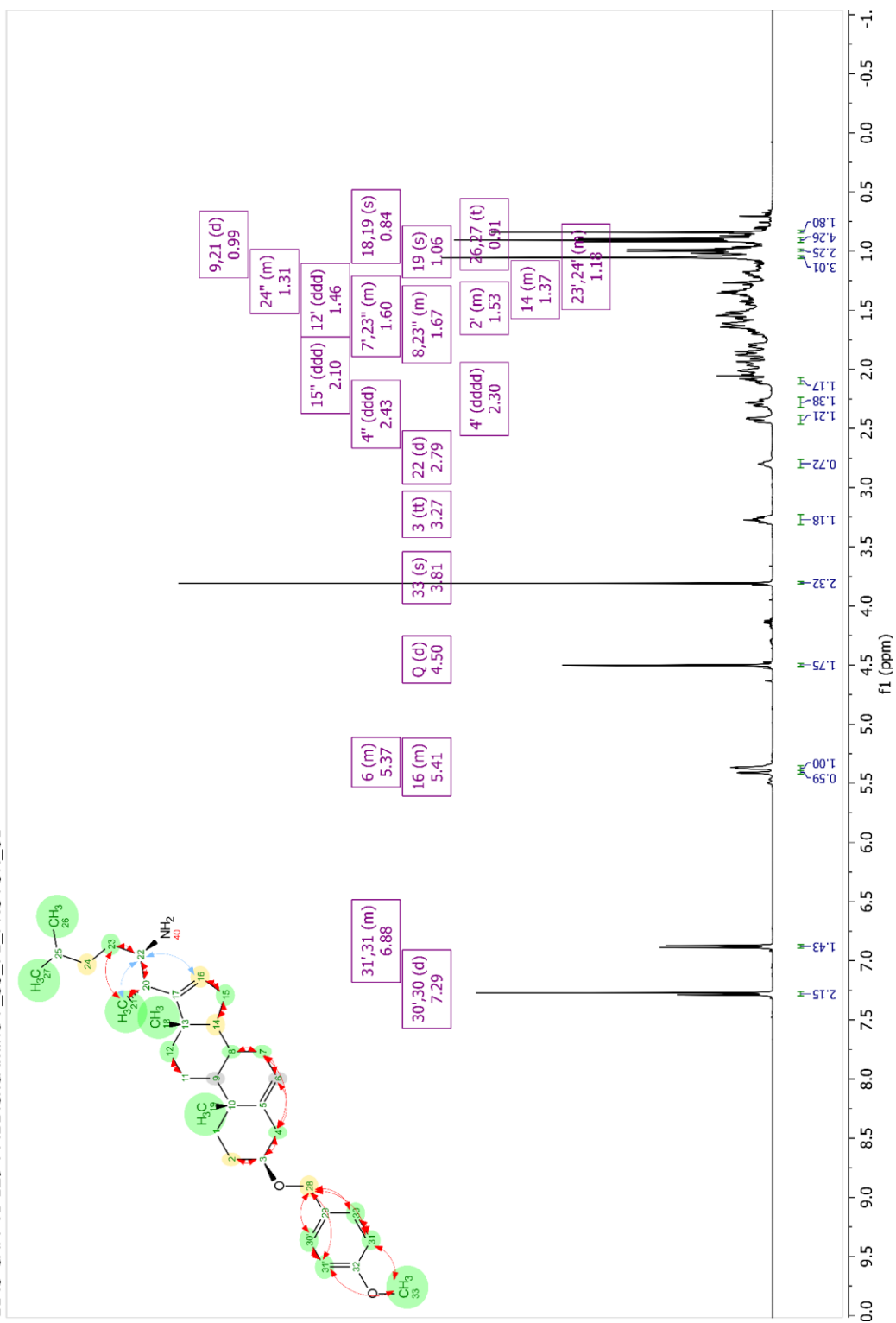


Figure 2-30. <sup>1</sup>H-NMR of Compound 2.29 in chloroform-*d*.

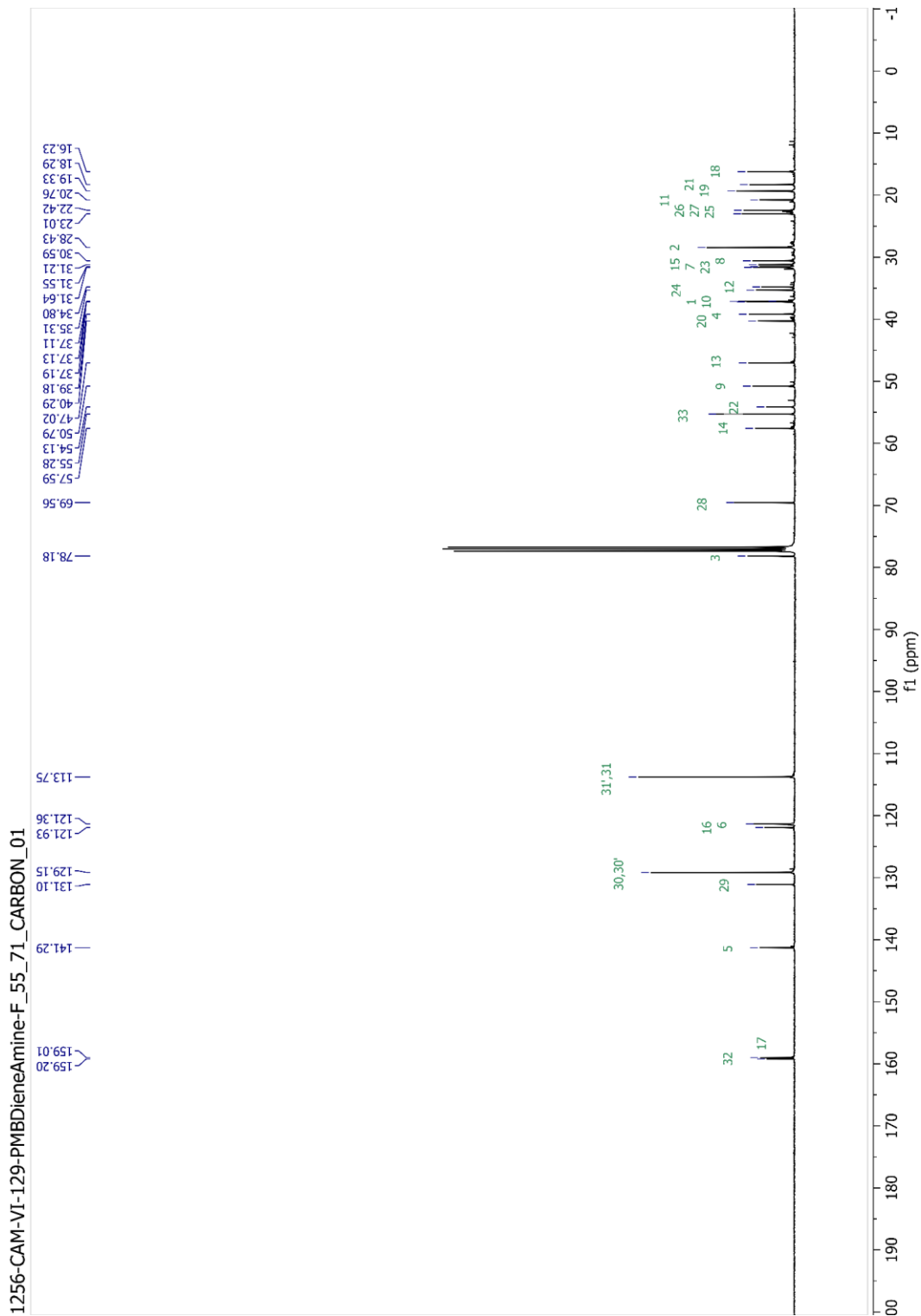


Figure 2-31.  $^{13}\text{C}$ -NMR of Compound 2.29 in chloroform-*d*.

1256-CAM-VII-129-PMBDieneAmine-F\_55\_71\_COSY\_01

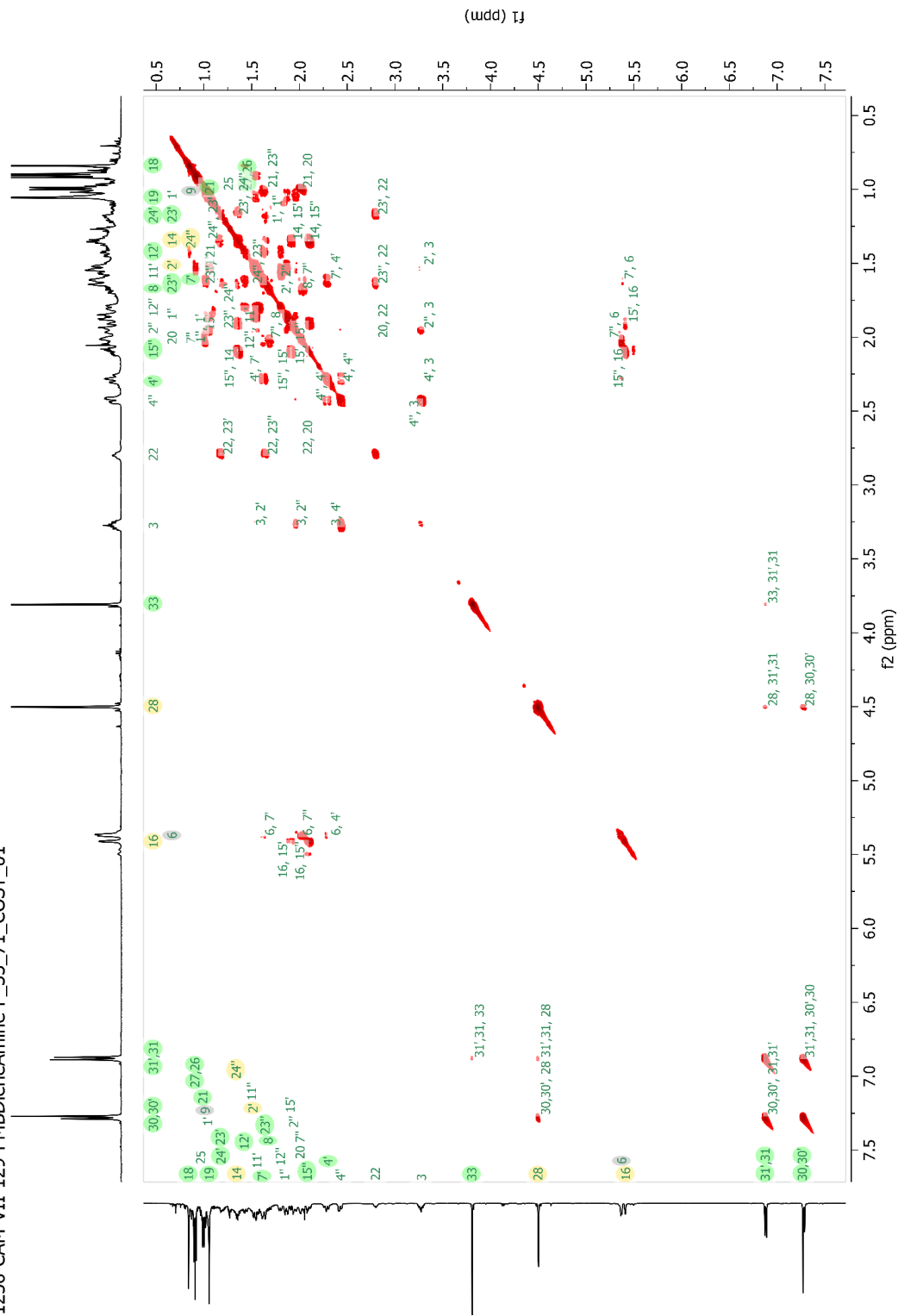


Figure 2-32. COSY of Compound 2.29 in chloroform-*d*.

1256-CAM-VII-129-PMBDieneAmine-F\_55\_71\_HSQCAD\_01

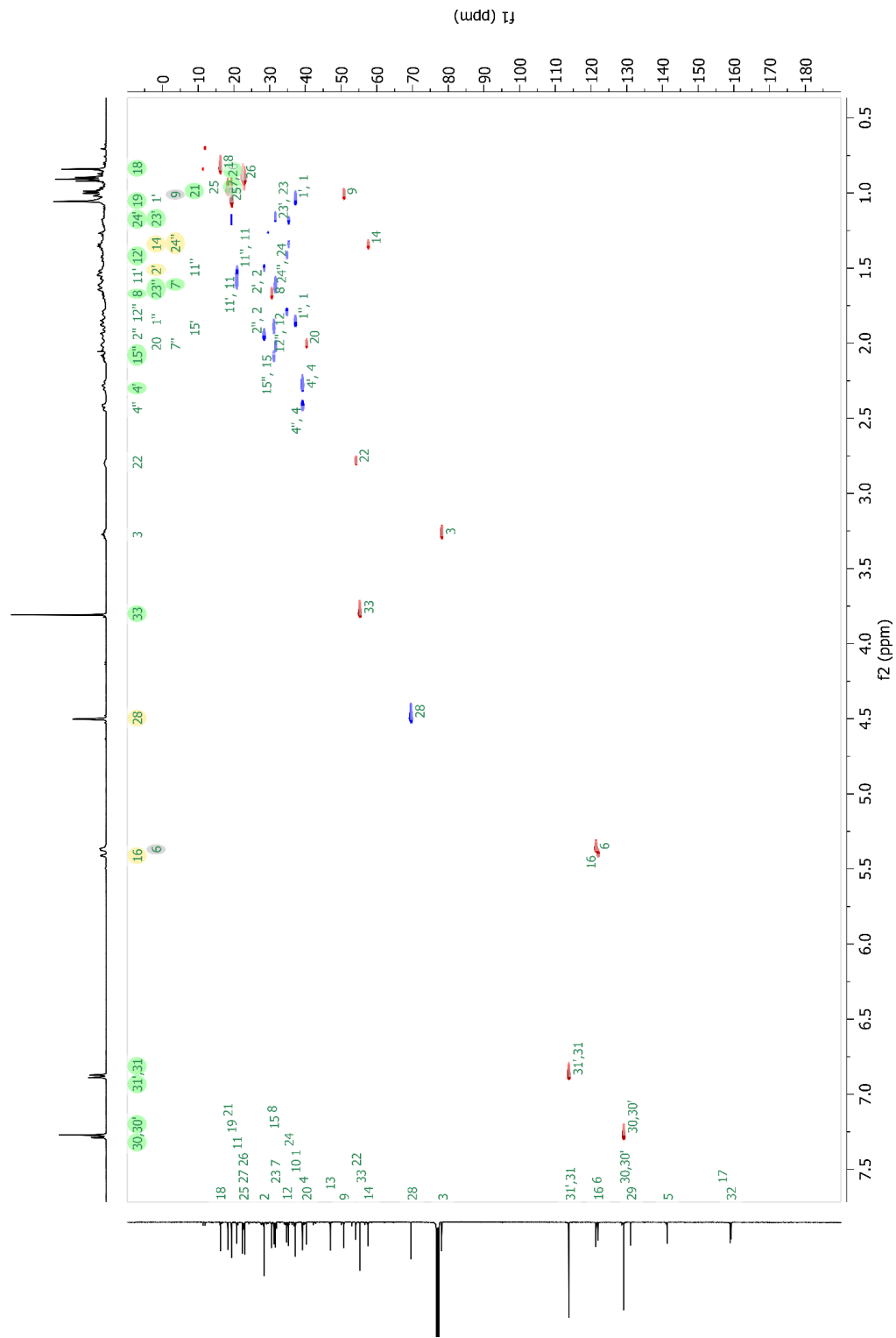
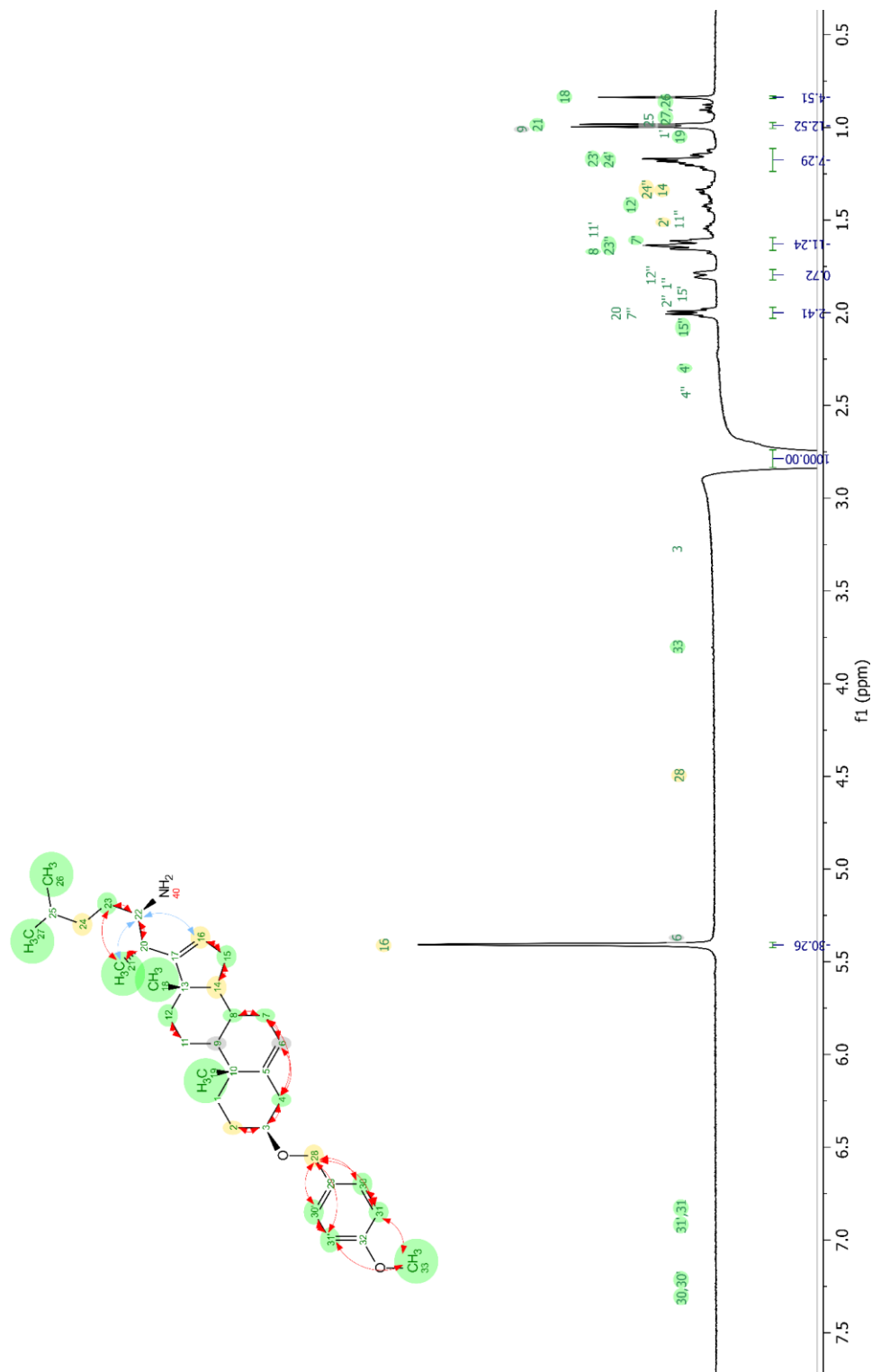


Figure 2-33. HSQC-AD of Compound 2.29 in chloroform-*d*.

1256-CAM-VII-129-PMBDieneAmine-F\_55\_71\_NOESY1D\_01



**Figure 2-34.** 1D-NOESY selective irradiation of H22, of **Compound 2.29** in chloroform-*d*.

1256-CAM-VI-129-PMBDieneAmine-F\_55\_71-C23\_NOESY1D\_01

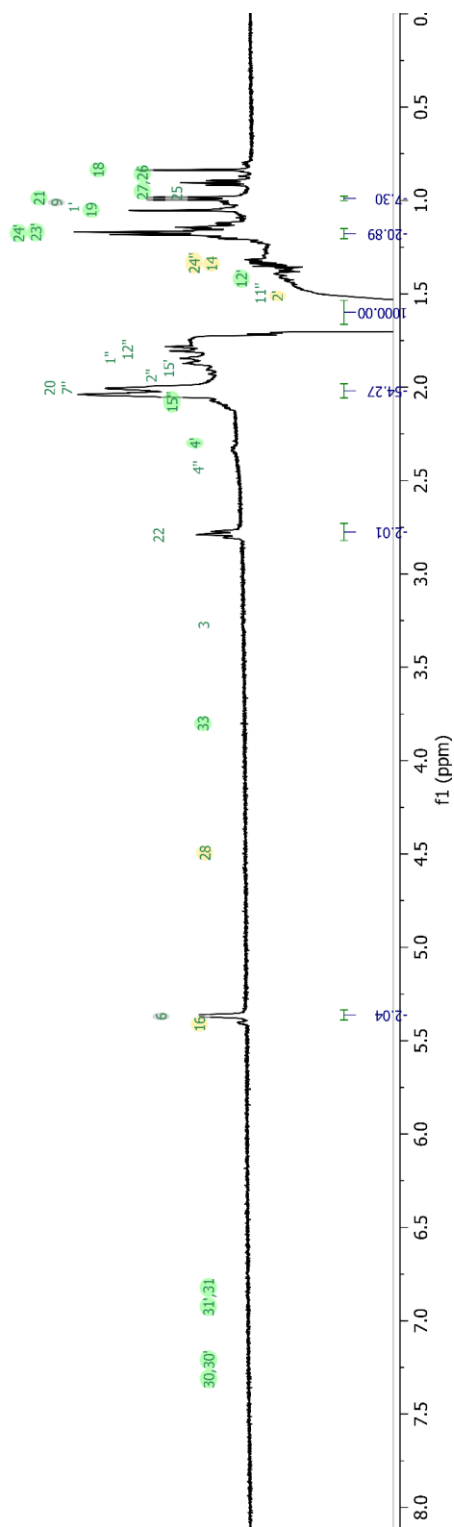


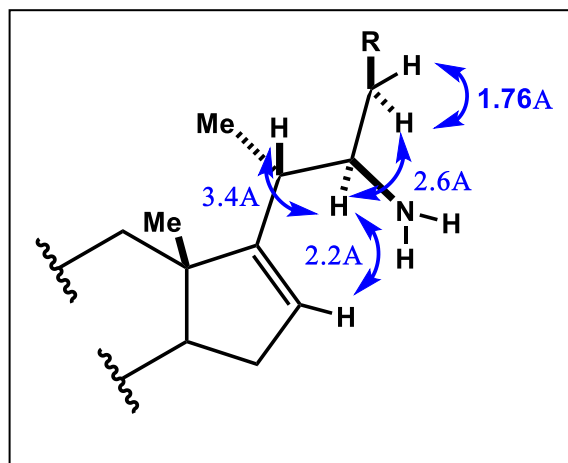
**Figure 2-35.** 1D-NOESY selective irradiation of H<sub>23'</sub>, of **Compound 2.29** in chloroform-*d*.

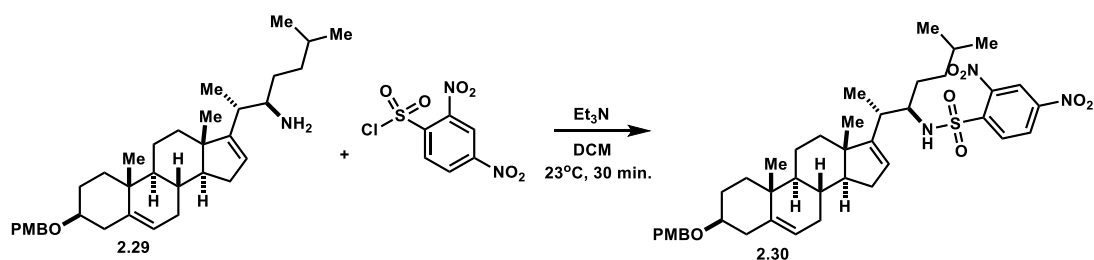


**Table 4.** qNOESY correlations of selective 1D-NOESY irradiations of **Compound 2.29**<sup>112</sup>

Irrad. 1H	Obs 1H	NOE integral	NOE REFERENCE	Reference Distance	Calculated distance to H23''
H23''	H23'	20.89	20.89	1.76	1.76
	H22	2.01	20.89	1.76	<b>2.60</b>
	H21	7.3	20.89	1.76	2.10
	H16	2.04	20.89	1.76	2.60
	H20	54.77	20.89	1.76	1.50

Irrad. 1H	Obs 1H	NOE integral	NOE REFERENCE	Reference Distance	Calculated distance to H22
H22	H23'	7.29	11.24	<b>2.6</b>	2.80
	H23''	11.24	11.24	2.6	2.60
	H21	12.52	11.24	2.6	2.55
	H16	30.26	11.24	2.6	2.20
	H20	2.41	11.24	2.6	3.36
	H18	4.51	11.24	2.6	3.03





**N-((2S,3R)-2-((3S,8R,9S,10R,13S,14S)-3-((4-methoxybenzyl)oxy)-10,13-dimethyl-2,3,4,7,8,9,10,11,12,13,14,15-dodecahydro-1H-cyclopenta[a]phenanthren-17-yl)-6-methylheptan-3-yl)-2,4-dinitrobenzenesulfonamide; (2.30):** Compound **2.30** was prepared through following a previously reported protocol that had not been demonstrated on steroid reactants.<sup>136</sup> Steroid **Compound 2.29**, (150 mg, 0.290 mmol, 1.0 equiv.) and 2,4-dinitrobenzenesulfonyl chloride (155 mg, 0.580 mmol, 2.0 equiv.) were dissolved in DCM (3.0 ml, 290 mM) at room temperature under nitrogen atmosphere. Triethyl amine (80.0  $\mu$ l, 0.580 mmol, 2.0 equiv.) was added. The reaction changed colors from orange to red-orange and was slightly exothermic. After 15 min, the reaction was complete. The reaction was diluted with ethyl acetate then quenched with 1 N HCl<sub>(aq)</sub> (3.0 ml) at 0°C. The reaction was warmed to room temperature and then transferred to a separatory funnel. The biphasic solution was separated, and the organic layer washed with 1 N HCl<sub>(aq)</sub> (3 x 5.0 ml). The organic layer was washed once with brine and dried over Na<sub>2</sub>SO<sub>4</sub>. The drying agent was removed, and the solvent evaporated *in vacuo* to afford a yellow liquor. The crude material was purified via automated column chromatography using a Biotage 10 G silica column and a gradient of 7% to 30% ethyl acetate in hexanes, with 10 column volumes. Desired product (187.0 mg) was isolated as a pure yellow solid (86% yield).<sup>136</sup>

**Compound 2.30:** <sup>1</sup>H-NMR (400 MHz, Chloroform-*d*):  $\delta$  8.68 (ddd, *J* = 14, 8.4, 2.2 Hz, 1H), 8.62 – 8.46 (m, 1H), 8.36 (d, *J* = 8.6 Hz, 1H), 7.26 (s, 4H), 6.87 (d, *J* = 8.7 Hz, 2H), 5.41 (s, 1H), 5.34 (s, 1H), 5.28 (d, *J* = 8.1 Hz, 1H), 4.49 (s, 1H), 3.80 (s, 2H), 3.65 (s, 1H), 3.37 – 3.15 (m, 1H), 2.48 – 2.36 (m, 2H), 2.28 (d, *J* = 12.7 Hz, 1H), 1.55 (s, 1H), 1.04 (s, 2H), 0.97 (d, *J* = 7.0 Hz, 1H), 0.80 (s, 2H), 0.77 (d, *J* = 6.6 Hz, 1H), 0.73 (d, *J* = 6.6 Hz, 2H). <sup>13</sup>C-NMR (101 MHz, Acetonitrile-*d*<sub>3</sub>):  $\delta$  159.0, 156.9, 150.0, 147.6, 141.5, 139.3, 132.1, 131.5, 129.2, 127.3, 125.0, 121.1, 120.4, 113.6, 78.0, 69.0, 58.5, 58.2, 54.8, 50.7, 46.5, 39.0, 38.1, 37.1, 36.9, 34.7, 34.4, 31.3, 30.8, 30.2, 28.3, 27.5, 26.2, 21.9, 21.5, 20.5, 18.8, 16.3, 13.3.

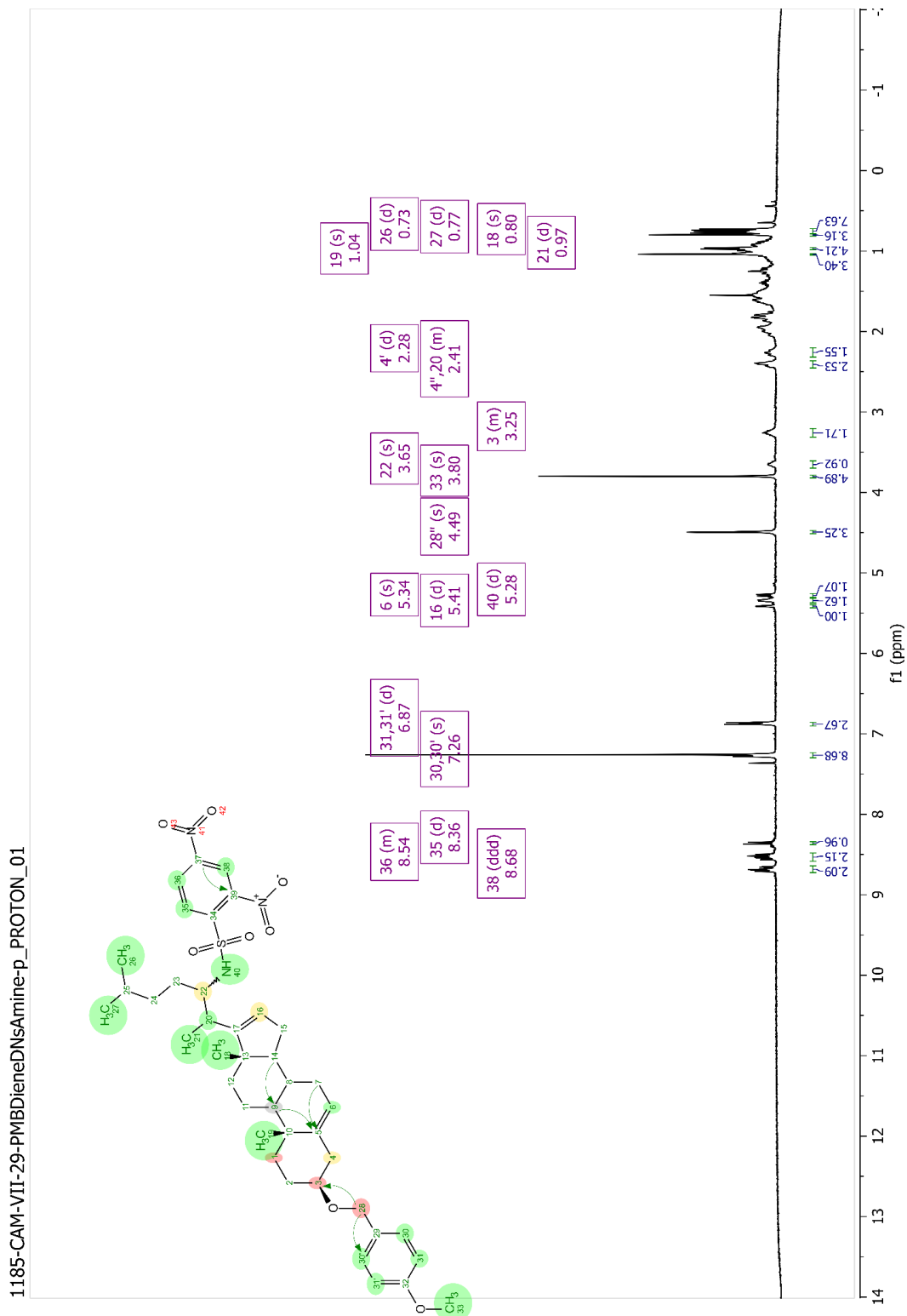


Figure 2-36.  $^1\text{H-NMR}$  of Compound 2.30 in chloroform-*d*.

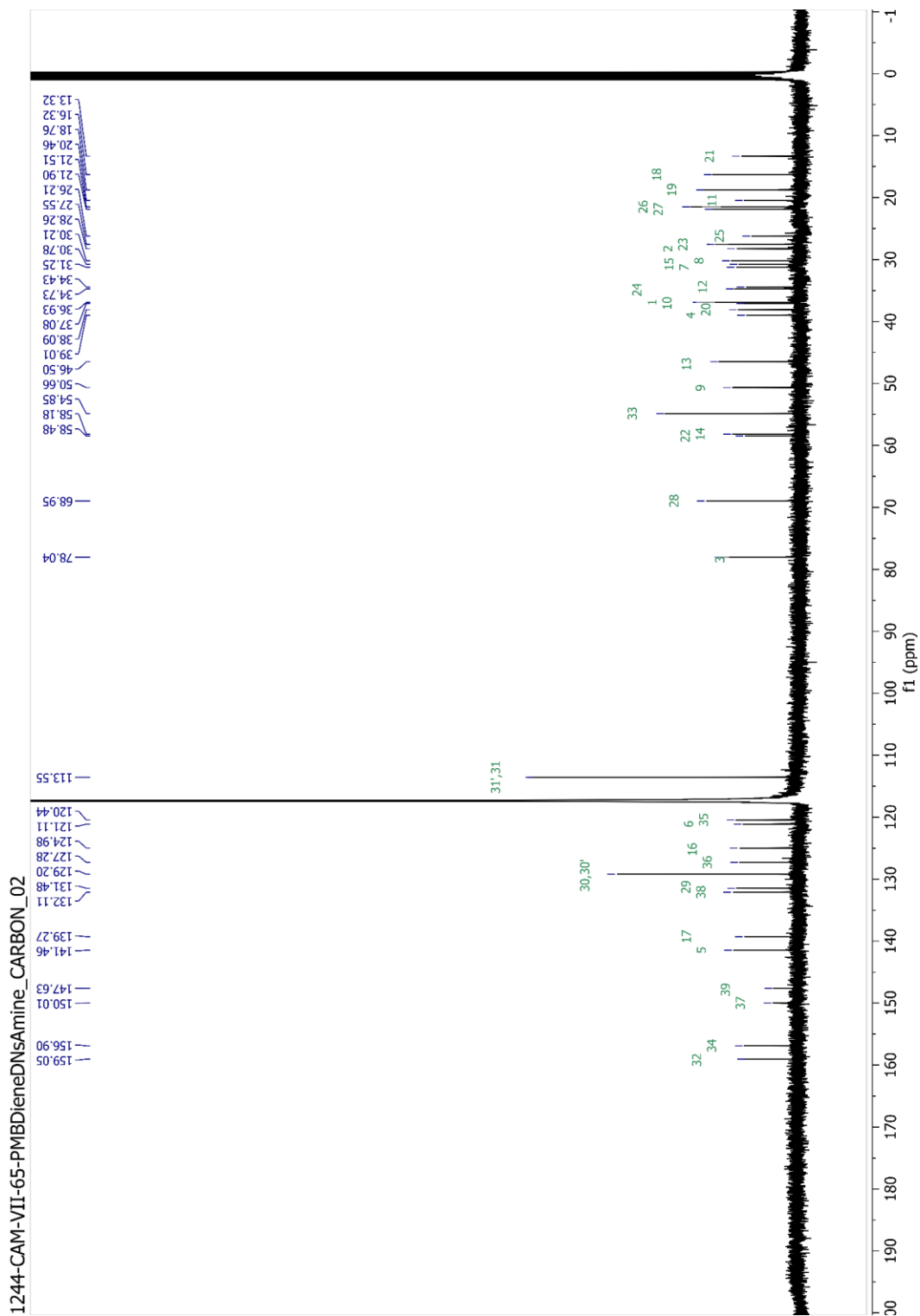
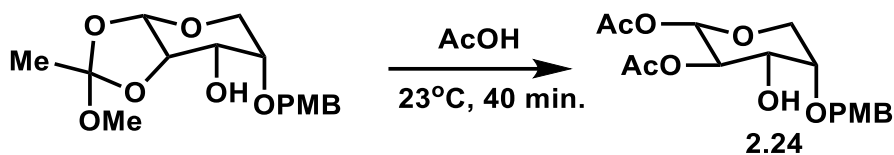


Figure 2-37.  $^{13}\text{C}$ -NMR of Compound 2.30 in acetonitrile- $d_3$ .



**(2S,3R,4S,5R)-4-hydroxy-5-((4-methoxybenzyl)oxy)tetrahydro-2H-pyran-2,3-diyl diacetate; (2.24):** Synthesis of the starting material from L-arabinose was done as reported and not included in this dissertation.<sup>89</sup> **Compound 2.24** was prepared through following a previously reported protocol with no modifications.<sup>89</sup> To a round-bottom flask containing protected L-arabinose moiety starting material (4.22 g, 12.9 mmol, 1.0 equiv.) under nitrogen atmosphere was added glacial acetic acid (13.0 mL). The clear, colorless solution was stirred at room temperature for 40 minutes. The reaction mixture was diluted with ethyl acetate (50 mL) and then transferred to a separatory funnel. The organic phase was washed with DI water until the aqueous phase presented with a neutral pH. The organic layer was then washed with brine and dried over Na<sub>2</sub>SO<sub>4</sub>. Drying agent was removed and the solvent was evaporated *in vacuo* to afford 1.4 g of the crude mixture as an off-white, waxy solid. The crude mixture was purified via automated column chromatography using a Biotage 50 G column with oven-dried silica and eluted with a gradient of 30% to 100% ethyl acetate in hexanes over 10 column volumes. 2.6 g of the desired product (57% yield.) was isolated. The NMR data agreed with the published reference data.<sup>89</sup>

**Compound 2.24:** <sup>1</sup>H-NMR (400 MHz, Chloroform-*d*): δ 5.59 (d, *J* = 6.7 Hz, 0H), 5.21 – 5.02 (m, 0H), 4.57 (dd, *J* = 74.8, 11.4 Hz, 1H), 4.09 (dd, *J* = 12.8, 3.5 Hz, 1H), 3.81 (s, 1H), 3.75 (d, *J* = 3.4 Hz, 1H), 3.59 – 3.48 (m, 1H), 2.45 (d, *J* = 8.8 Hz, 0H), 2.11 (s, 1H), 2.10 (s, 2H).

1087-CAM-VI-73-Final\_Arabinose-p\_PROTON\_01

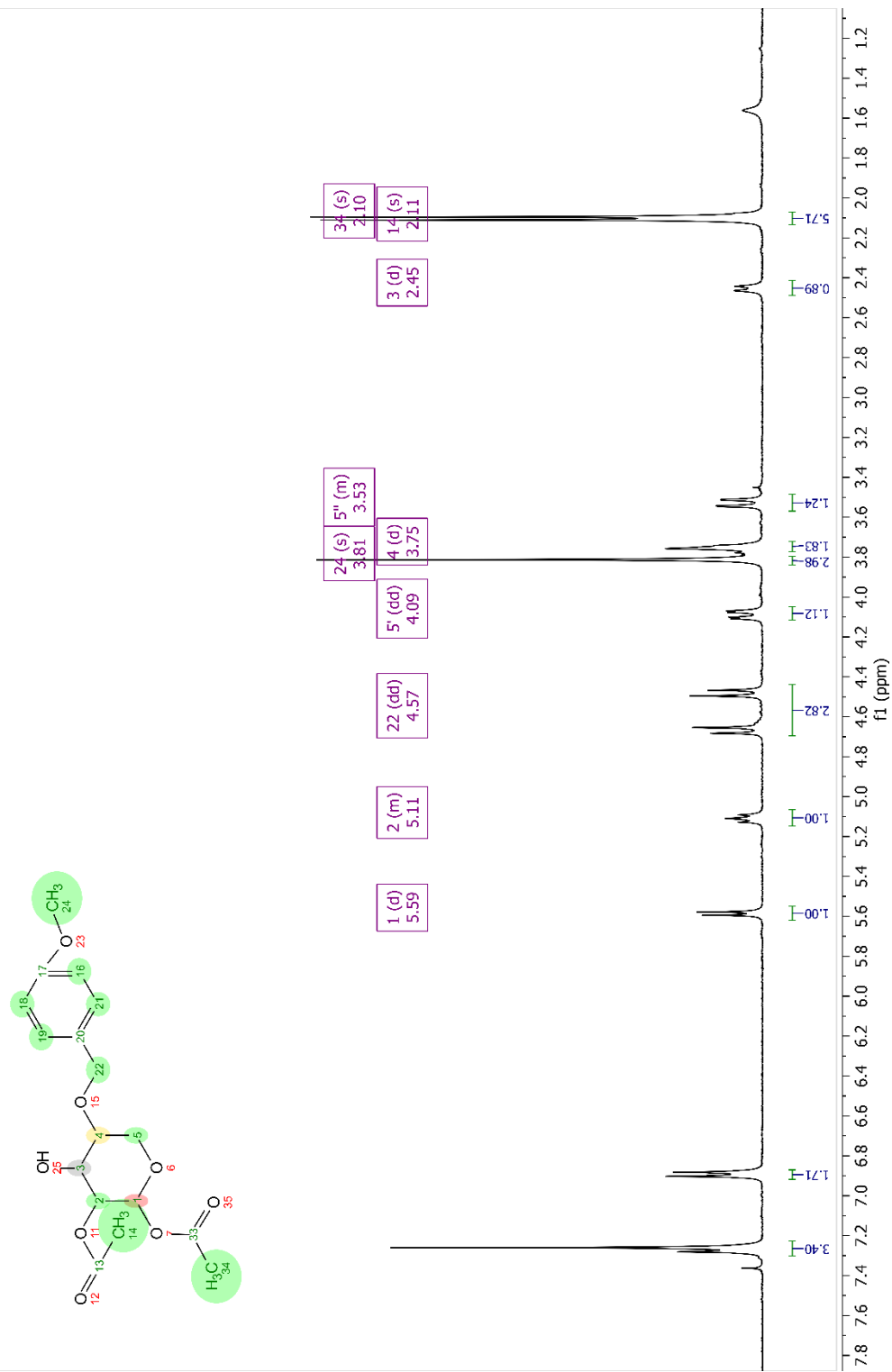
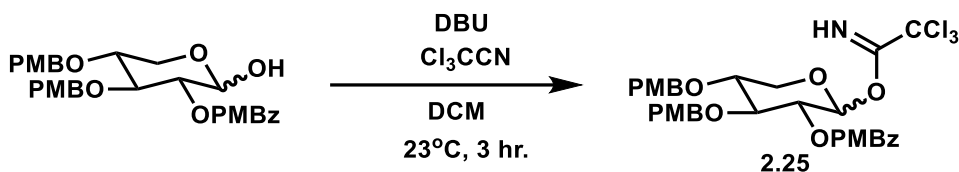


**Figure 2-38.** <sup>1</sup>H NMR of final L-arabinose (2.24) in chloroform-*d*.



**(3R,4S,5R)-4,5-bis((4-methoxybenzyl)oxy)-2-(2,2,2-trichloro-1-iminoethoxy)tetrahydro-2H-pyran-3-yl 4-methoxybenzoate; (2.25):**

Synthesis of the starting material from D-xylose was done as reported and not included in this dissertation.<sup>89</sup> **Compound 2.25** was prepared through following a previously reported protocol with no modifications.<sup>89</sup> Starting material xylose compound (233 mg, 0.440 mmol, 1.0 equiv.) was dissolved in dry DCM (3.0 mL, 0.15 M) under nitrogen atmosphere at room temperature. Trichloroacetonitrile (225  $\mu$ L, 2.22 mmol, 5.0 equiv.) and DBU (4.0  $\mu$ L, 4.4  $\mu$ mol, 10 mol%) were added. The reaction color changed from light yellow to dark yellow. The reaction mixture was stirred at room temperature and progress was monitored via <sup>1</sup>H-NMR. After 3 hours, the solvent was removed *in vacuo* to afford a crude mixture as a yellow gel. The crude mixture was purified by silica gel column and eluted with a gradient of 30% to 100% ethyl acetate in hexanes with 3% NEt<sub>3</sub> to afford 231 mg of a ~2:3  $\alpha/\beta$ -anomer mixture of products as a light-yellow gel (78% yield). The NMR data agreed with the published reference data.<sup>89</sup>

**Compound 2.25:** <sup>1</sup>H-NMR (500 MHz, Chloroform-*d*):  $\delta$  8.58 (s, 1H), 8.00 – 7.77 (m, 1H), 7.23 (d, *J* = 8.6 Hz, 1H), 7.15 (d, *J* = 8.6 Hz, 1H), 6.85 (dd, *J* = 8.8, 3.5 Hz, 2H), 6.72 (d, *J* = 8.7 Hz, 1H), 5.97 (d, *J* = 5.7 Hz, 1H), 5.41 (dd, *J* = 7.0, 5.7 Hz, 1H), 4.68 (d, *J* = 4.2 Hz, 2H), 4.63 – 4.51 (m, 2H), 4.13 (dd, *J* = 12.0, 4.1 Hz, 1H), 3.86 (s, 3H), 3.80 (s, 3H), 3.74 (s, 2H), 3.62 (dd, *J* = 12.0, 7.3 Hz, 1H).

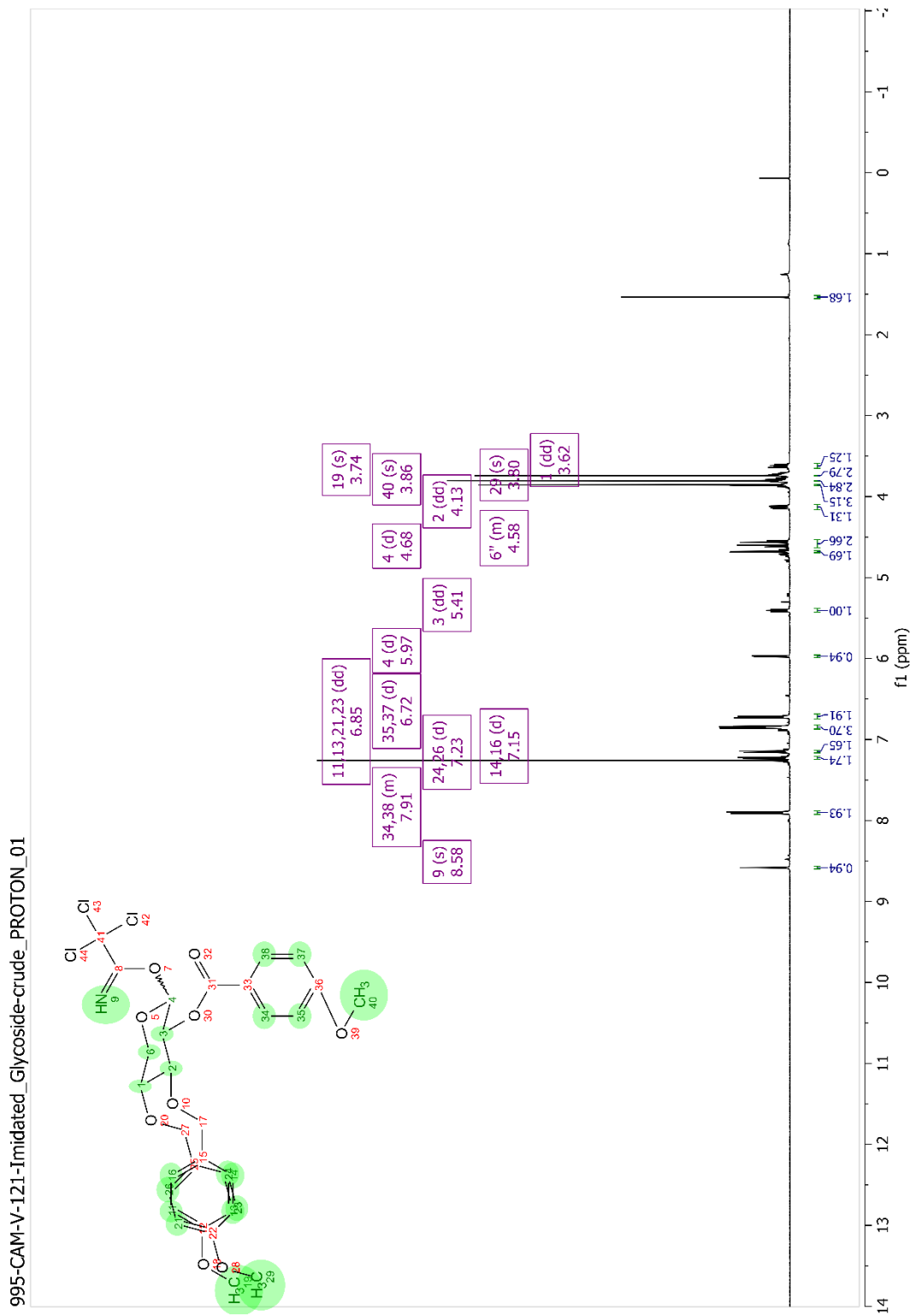
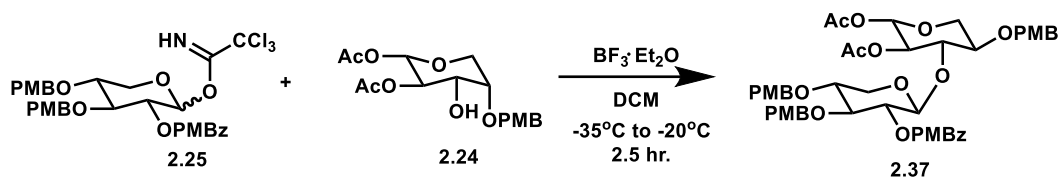


Figure 2-39.  $^1\text{H-NMR}$  of xylose imidate (2.25) in chloroform- $d$ .





**(2S,3R,4S,5R)-4-(((2S,3R,4S,5R)-3-((4-methoxybenzoyl)oxy)-4,5-bis((4-methoxybenzyl)oxy)tetrahydro-2H-pyran-2-yl)oxy)-5-((4-methoxybenzyl)oxy)tetrahydro-2H-pyran-2,3-diyl diacetate; (2.37):** Compound **2.37** was prepared through following a previously reported protocol with no modifications.<sup>89</sup> A ~2:3  $\alpha/\beta$ -anomer mixture of xylose imidate (**Compound 2.25**, 1.08 g, 1.6 mmol, 1.0 equiv.), L-arabinose moiety (**Compound 2.24**, 345 mg, 960  $\mu\text{mol}$ , 0.6 equiv.) and 4 Å molecular sieves powder (550 mg) was dissolved in dry DCM (16 mL, 0.1 M), and stirred at room temperature under a nitrogen atmosphere for 1 hour. Then, the reaction was cooled to  $-35^\circ\text{C}$ , and a solution of  $\text{BF}_3 \cdot \text{Et}_2\text{O}$  (9.0  $\mu\text{L}$ , 0.078 mmol, 0.05 equiv.) in dry DCM (100  $\mu\text{L}$ ) was added. The reaction mixture was stirred at  $-35^\circ\text{C}$  for 30 minutes. After 30 minutes, the reaction mixture was warmed to  $-20^\circ\text{C}$ . After 1 hour at  $-20^\circ\text{C}$ , the reaction was quenched with  $\text{NEt}_3$  (100  $\mu\text{L}$ ). The reaction mixture was warmed to room temperature and filtered through a Celite pad. The filtrate was then condensed down *in vacuo* to afford a crude yellow gel. The crude material was purified by silica gel column chromatography and eluted with a gradient of 0% to 8% acetone in benzene to afford 193 mg of the  $\beta$ -anomer product exclusively, as a white, foamy solid (83% yield). The NMR data agreed with the published reference data.<sup>89</sup>

**Compound 2.37:**  $^1\text{H-NMR}$  (500 MHz, Chloroform-*d*):  $\delta$  7.85 – 7.79 (m, 2H), 7.19 – 7.12 (m, 4H), 7.02 – 6.94 (m, 2H), 6.81 – 6.71 (m, 6H), 6.58 (d,  $J = 8.6$  Hz, 2H), 5.43 (d,  $J = 5.8$  Hz, 1H), 5.08 (ddd,  $J = 13, 7.2, 5.8$  Hz, 2H), 4.62 – 4.49 (m, 6H), 4.48 – 4.42 (m, 1H), 3.88 (dd,  $J = 12, 4.2$  Hz, 1H), 3.83 (dd,  $J = 12, 5.2$  Hz, 1H), 3.78 – 3.72 (m, 4H), 3.71 (s, 3H), 3.70 – 3.66 (m, 4H), 3.65 – 3.55 (m, 6H), 3.40 (dd,  $J = 12, 2.4$  Hz, 1H), 3.23 (dd,  $J = 12, 7.8$  Hz, 1H), 1.86 (s, 3H), 1.69 (s, 3H).

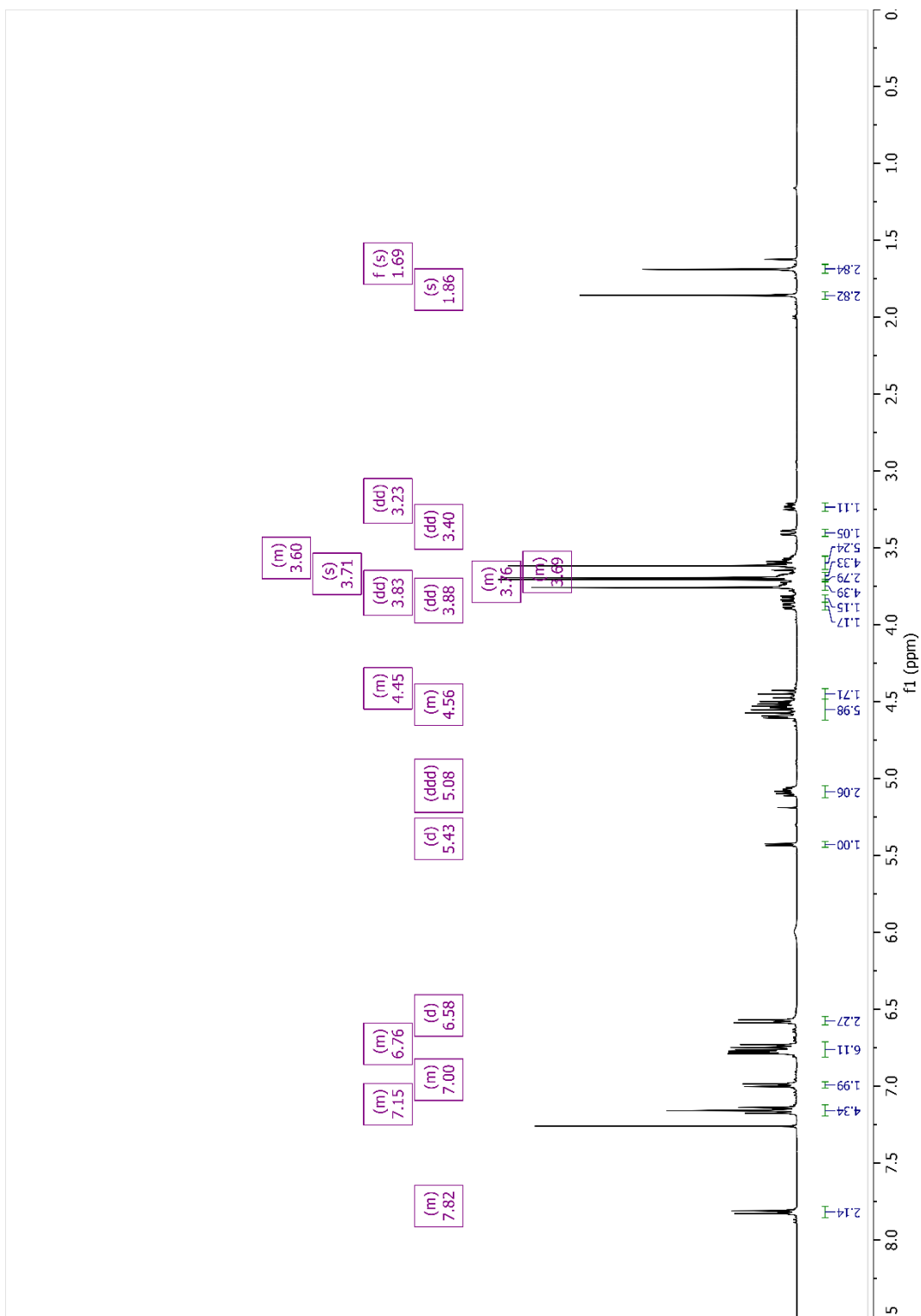
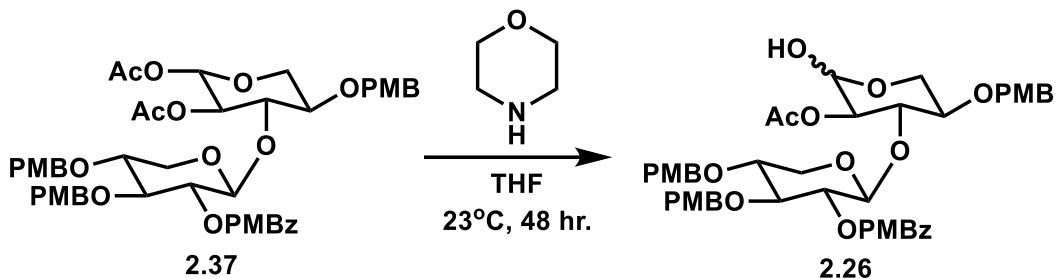


**Figure 2-40.** <sup>1</sup>H-NMR of protected disaccharide in chloroform-*d*.



**(2S,3R,4S,5R)-2-(((3R,4S,5R)-3-acetoxy-2-hydroxy-5-((4-methoxybenzyl)oxy)tetrahydro-2H-pyran-4-yl)oxy)-4,5-bis((4-methoxybenzyl)oxy)tetrahydro-2H-pyran-3-yl 4-methoxybenzoate; (2.26):** **Compound 2.26** was prepared through following a previously reported protocol with no modifications.<sup>89</sup> To a clear, colorless solution of **Compound 2.37** (1.54 g, 1.8 mmol, 1.0 equiv.) in dry THF (18 mL, 0.1 M) at room temperature under nitrogen atmosphere morpholine (1.23 mL, 14.3 mmol, 8.0 equiv.) was added. The reaction mixture was stirred at room temperature and after 19 hours, an additional portion of morpholine (1.0 equiv.) was added. After 48 hours, the solvent was removed *in vacuo* to afford a crude mixture. The crude mixture was purified by silica gel column chromatography and eluted with a gradient of 20% to 100% ethyl acetate in hexanes to afford 960 mg of the desired 2:3  $\alpha/\beta$ -anomer mixture of products as a white powder (66% yield). The NMR data agreed with the published reference data.<sup>89</sup>

**Compound 2.26:** <sup>1</sup>H-NMR (400 MHz, Chloroform-*d*):  $\delta$  7.94 – 7.87 (m, 2H), 7.30 – 7.21 (m, 4H), 7.09 (dd,  $J = 8.9, 2.7$  Hz, 2H), 6.91 – 6.81 (m, 6H), 6.71 – 6.64 (m, 2H), 5.25 – 5.13 (m, 2H), 5.04 (dd,  $J = 9.1, 3.1$  Hz, 1H), 4.94 (td,  $J = 9.1, 8.4, 6.0$  Hz, 1H), 4.78 – 4.47 (m, 9H), 4.11 – 4.06 (m, 1H), 4.02 – 3.86 (m, 2H), 3.87 – 3.83 (m, 4H), 3.81 – 3.80 (m, 3H), 3.79 (s, 6H), 3.75 – 3.69 (m, 6H), 3.68 – 3.57 (m, 1H), 1.76 (s, 3H).

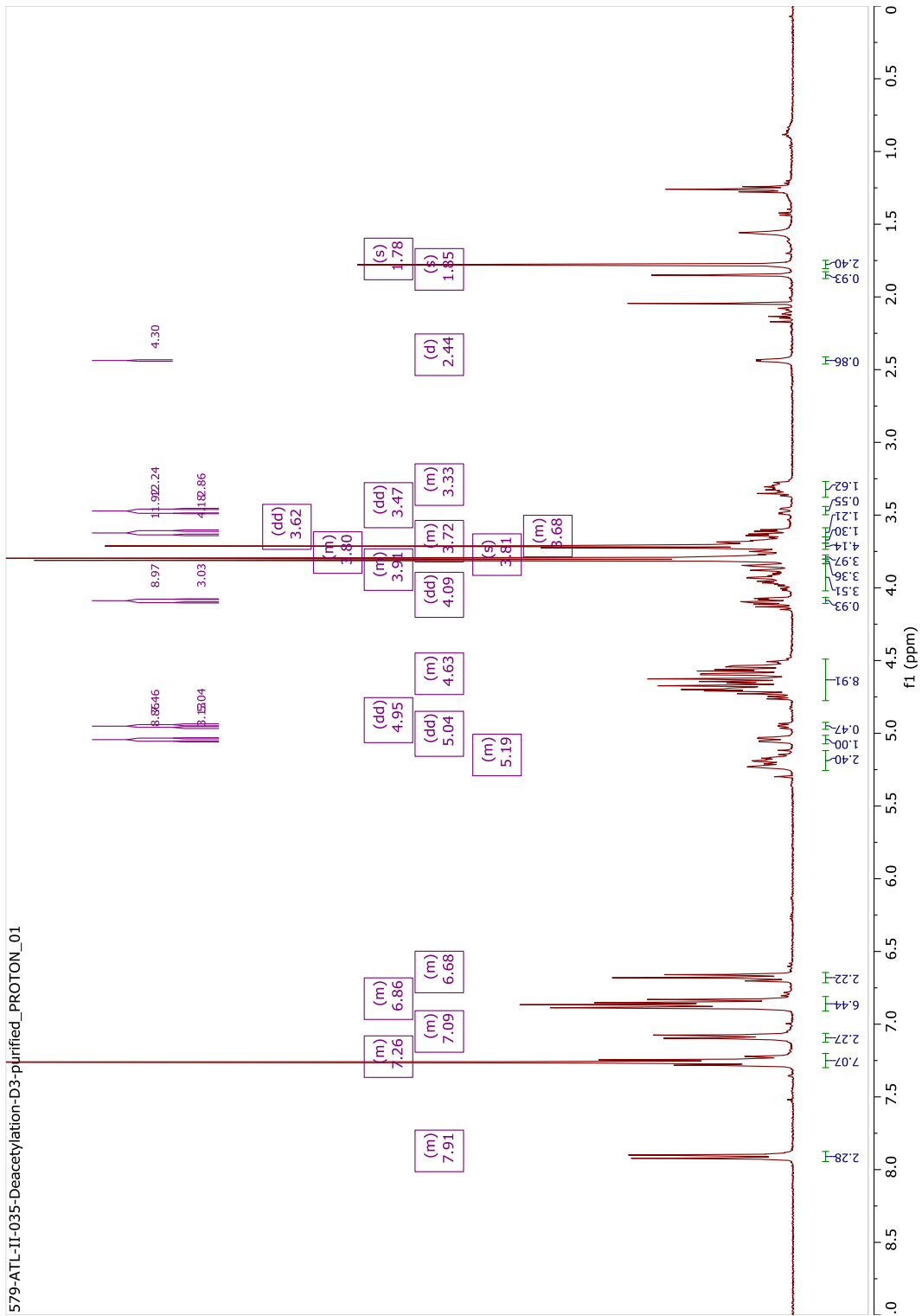
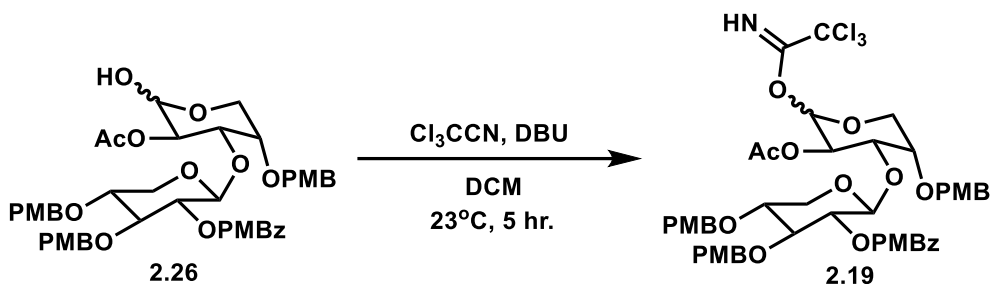


Figure 2-41. <sup>1</sup>H-NMR of Compound 2.26 in chloroform-*d*.



**(2S,3R,5R)-2-(((3R,4S,5S)-3-acetoxy-5-((4-methoxybenzyl)oxy)-2-(2,2,2-trichloro-1-iminoethoxy)tetrahydro-2H-pyran-4-yl)oxy)-4,5-bis((4-methoxybenzyl)oxy)tetrahydro-2H-pyran-3-yl 4-methoxybenzoate; (2.19):**

**Compound 2.19** was prepared through following a previously reported protocol with no modifications.<sup>89</sup> To a solution of disaccharide (**Compound 2.26**, 149 mg, 0.182 mmol, 1.0 equiv.) in dry DCM (1.0 mL, 0.18 M) at room temperature under nitrogen atmosphere was added trichloroacetonitrile (92.0  $\mu\text{L}$ , 0.92 mmol, 5.0 equiv.) and DBU (~1.0  $\mu\text{L}$ , 9.1  $\mu\text{mol}$ , 5.0 mol %). The reaction color changed from light to dark yellow. The reaction was stirred at room temperature. After 5 hours, the solvent was removed *in vacuo* to afford a crude yellow mixture. The crude mixture was purified by silica gel column chromatography and eluted with 50% ethyl acetate in hexanes with 3%  $\text{NEt}_3$  to afford 122.5 mg of a 2:3  $\alpha$ : $\beta$ -anomeric mixture of products as a light yellow, thick gel in a 69% yield. The NMR data agreed with the published reference.<sup>89</sup>

**Compound 2.19:**  $^1\text{H-NMR}$  (400 MHz, Chloroform-*d*):  $\delta$  8.55 (s, 1H), 8.48 (s, 1H), 7.96 – 7.88 (m, 2H), 7.30 – 7.24 (m, 2H), 7.23 – 7.19 (m, 2H), 7.16 – 7.11 (m, 2H), 6.90 – 6.80 (m, 6H), 6.73 – 6.66 (m, 2H), 6.42 (d,  $J = 3.5$  Hz, 1H), 5.72 (d,  $J = 5.9$  Hz, 1H), 5.42 (dd,  $J = 8.0, 5.9$  Hz, 1H), 5.22 (dd,  $J = 6.8, 5.3$  Hz, 1H), 4.80 (d,  $J = 5.3$  Hz, 1H), 4.75 – 4.48 (m, 7H), 4.09 – 4.03 (m, 2H), 3.96 – 3.88 (m, 1H), 3.88 – 3.82 (m, 1H), 3.80 (s, 3H), 3.79 (s, 3H), 3.76 – 3.70 (m, 4H), 3.66 – 3.56 (m, 2H), 3.46 – 3.34 (m, 2H), 1.79 (s, 3H).

1178-CAM-VII-23-Disaccharide\_Imidate-c\_PROTON\_02

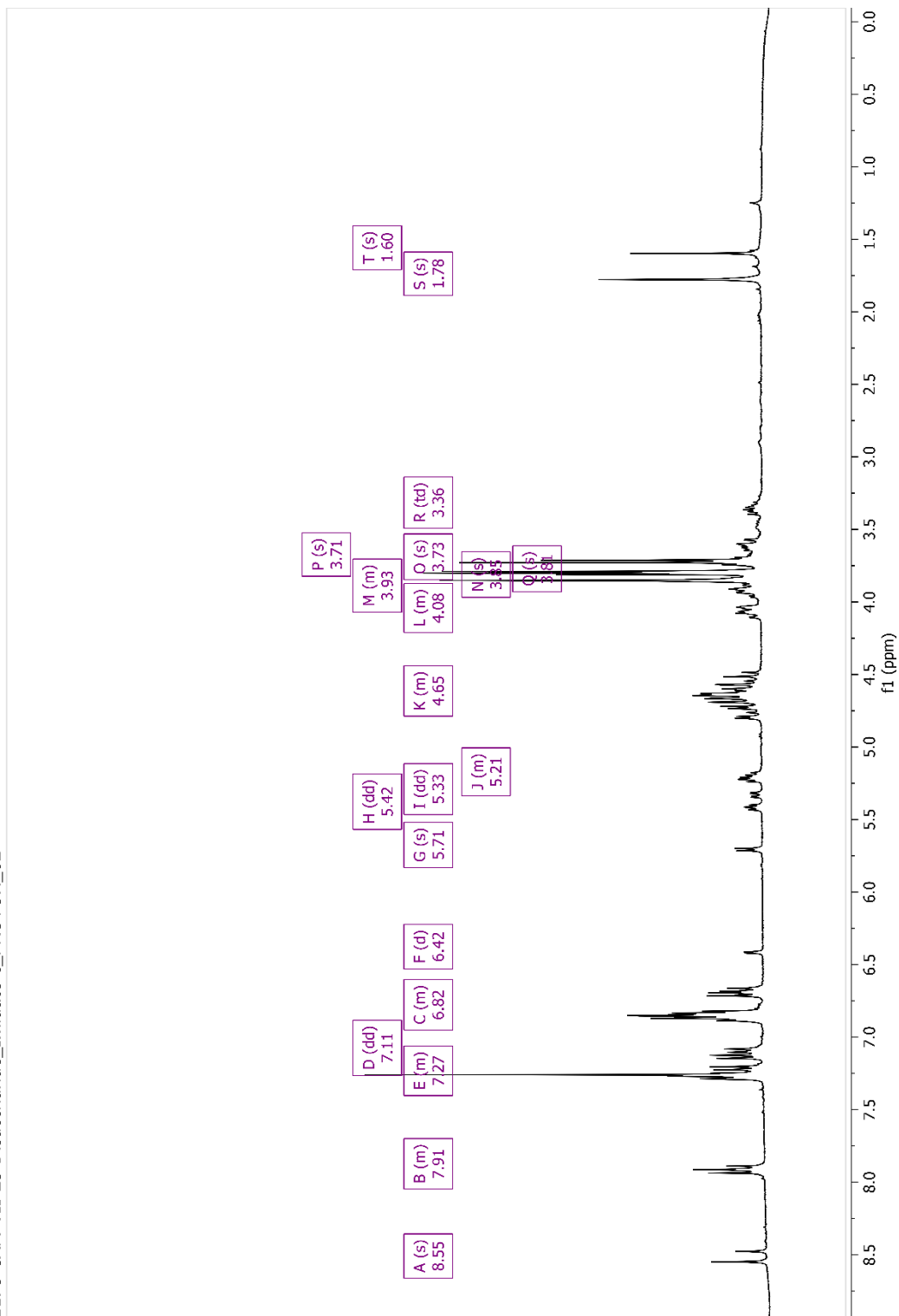
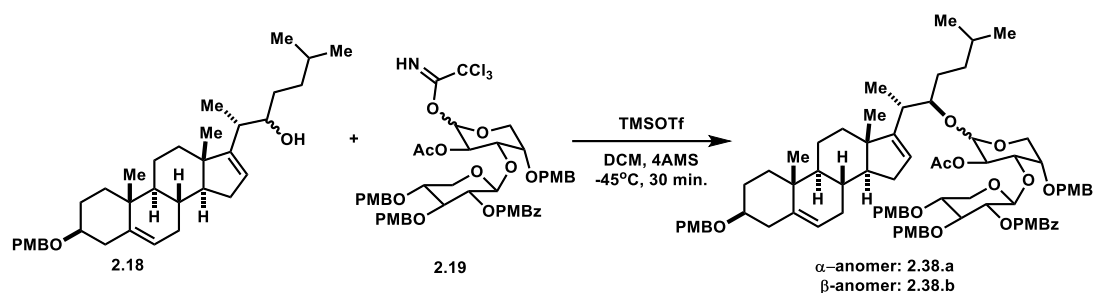


Figure 2-42. <sup>1</sup>H-NMR of Compound 2.19 in chloroform-*d*.



(2S,3R,4S,5R)-2-(((2S,3R,4S,5S)-3-acetoxy-5-((4-methoxybenzyl)oxy)-2-(((2S,3R)-2-((3S,8R,9S,10R,13S,14S)-3-((4-methoxybenzyl)oxy)-10,13-dimethyl-2,3,4,7,8,9,10,11,12,13,14,15-dodecahydro-1H-cyclopenta[a]phenanthren-17-yl)-6-methylheptan-3-yl)oxy)tetrahydro-2H-pyran-4-yl)oxy)-4,5-bis((4-methoxybenzyl)oxy)tetrahydro-2H-pyran-3-yl 4-methoxybenzoate; (**2.38.a**)

(2S,3R,4S,5R)-2-(((2R,3R,4S,5S)-3-acetoxy-5-((4-methoxybenzyl)oxy)-2-(((2S,3R)-2-((3S,8R,9S,10R,13S,14S)-3-((4-methoxybenzyl)oxy)-10,13-dimethyl-2,3,4,7,8,9,10,11,12,13,14,15-dodecahydro-1H-cyclopenta[a]phenanthren-17-yl)-6-methylheptan-3-yl)oxy)tetrahydro-2H-pyran-4-yl)oxy)-4,5-bis((4-methoxybenzyl)oxy)tetrahydro-2H-pyran-3-yl 4-methoxybenzoate; (**2.38.b**):

**Compounds 2.38.a** and **2.38.b** were prepared through following a previously reported protocol adapted for using starting material, **Compound 2.18**, as glycosyl acceptor.<sup>89</sup> Solid aglycone (**Compound 2.18**, 21.2 mg, 41.0  $\mu$ mol, 1.0 equiv.) and a mixture of 2:3  $\alpha/\beta$  disaccharide imidate anomers (39.8 mg, 41.2  $\mu$ mol, 1.0 equiv.) were added to a 5.0 ml conical flask containing activated 4 Å molecular sieves (85.0 mg). The flask was septa sealed then purged with nitrogen and vacuum. The starting materials were dissolved, and sieves suspended in dry DCM (0.7 ml). The reaction was cooled to -45°C using an acetonitrile and dry ice bath. To the reaction was added TMSOTf (73.7  $\mu$ l, 0.4  $\mu$ mol) diluted in dry DCM (0.2 ml) slow dropwise to start the reaction and then 5  $\mu$ l additional TMSOTf in 0.1 ml DCM were added at 30 and 60 minutes. The reaction proceeded over 5 hours and then was quenched at room temperature with 5 ml of sat. NaHCO<sub>3</sub>. The quenched reaction solution was transferred to a separatory funnel, diluted with DCM (15 ml), washed with sat. NaHCO<sub>3(aq)</sub> (2 x 10 ml), distilled water (2 x 10 ml) and brine (1 x 15 ml). Aqueous layers were combined and back extracted with DCM (15 ml). The organic layers were combined and dried over sodium sulfate. The drying agent was removed, and the solvent was condensed down *in vacuo* to produce a white spongy solid. The crude mixture of 10:1  $\alpha/\beta$  anomers was purified via reverse phase HPLC on a Luna 5  $\mu$ m C8(2) 100Å column (Phenomenex) using a gradient mobile phase of 98%-100% acetonitrile/ 0.1% formic acid water. The 10.1 mg (19% yield) of the  $\alpha$  anomer (**2.38A**) was isolated with a retention time of 18.0 min. The 1.6 mg of the  $\beta$  anomer (3% yield) (**2.38B**) was isolated with a retention time of 14.3 min. Only the C22(R)-hydroxysterol reacted; these was no evidence of any C22(S)-hydroxysterol glycosylated material.

**Compound 2.38.a** ( $\alpha$ -anomer, major product):  $^1\text{H-NMR}$  (600 MHz, Chloroform-*d*):  $\delta$  7.93 (d,  $J = 8.8$  Hz, 1H), 7.26 (s, 6H), 7.23 (d,  $J = 8.5$  Hz, 1H), 7.10 (d,  $J = 8.5$  Hz, 1H), 6.89 – 6.84 (m, 3H), 6.82 (d,  $J = 8.5$  Hz, 1H), 6.68 (d,  $J = 8.6$  Hz, 1H), 5.34 (s, 0H), 5.26 (s, 1H), 5.18 (t,  $J = 6.6$  Hz, 1H), 4.72 (d,  $J = 5.9$  Hz, 1H), 4.69 (d,  $J = 12.0$  Hz, 1H), 4.63 (s, 1H), 4.62 – 4.57 (m, 2H), 4.52 (d,  $J = 11.3$  Hz, 1H), 4.49 (s, 1H), 4.34 (d,  $J = 6.3$  Hz, 1H), 3.97 (dd,  $J = 11.9, 4.3$  Hz, 1H), 3.94 – 3.88 (m, 1H), 3.85 (s, 2H), 3.80 (s, 2H), 3.80 (s, 2H), 3.79 (s, 2H), 3.72 (s, 3H), 3.70 (d,  $J = 7.4$  Hz, 1H), 3.66 – 3.60 (m, 1H), 3.50 – 3.44 (m, 1H), 3.34 – 3.31 (m, 1H), 3.30 (d,  $J = 12.1$  Hz, 1H), 3.28 – 3.21 (m, 1H), 2.41 (d,  $J = 12.1$  Hz, 1H), 2.26 (t,  $J = 12.3$  Hz, 1H), 2.08 (d,  $J = 7.1$  Hz, 1H), 2.00 (d,  $J = 14.9$  Hz, 1H), 1.95 (s, 1H), 1.93 (s, 0H), 1.85 (s, 0H), 1.83 (s, 0H), 1.79 (s, 2H), 1.66 (d,  $J = 11.6$  Hz, 1H), 1.62 (dd,  $J = 10.6, 4.5$  Hz, 0H), 1.55 (s, 2H), 1.50 (d,  $J = 8.0$  Hz, 3H), 1.49 (s, 0H), 1.40 (dt,  $J = 13.3, 6.6$  Hz, 1H), 1.24 – 1.20 (m, 0H), 1.15 (t,  $J = 7.6$  Hz, 1H), 1.02 (s, 2H), 0.96 (s, 0H), 0.87 (d,  $J = 6.9$  Hz, 2H), 0.79 (dd,  $J = 8.9, 6.6$  Hz, 4H), 0.75 (s, 2H).  $^{13}\text{C-NMR}$  (151 MHz, Chloroform-*d*):  $\delta$  170.1, 165.6, 164.6, 159.3, 142.7, 132.7, 123.4, 123.3, 121.7, 114.7, 102.8, 83.9, 81.3, 75.7, 74.5, 71.8, 71.2, 70.5, 68.5, 66.5, 65.7, 58.4, 56.3, 51.7, 48.0, 43.0, 38.1, 37.5, 37.4, 35.7, 34.6, 32.4, 32.3, 32.3, 31.8, 31.3, 28.8, 22.9, 22.7, 21.5, 20.8, 19.7, 17.9, 16.8.

**Compound 2.38.b** ( $\beta$ -anomer, minor product):  $^1\text{H-NMR}$  (600 MHz, Chloroform-*d*)  $\delta$  7.94 (dd,  $J = 8.9, 2.6$  Hz, 1H), 7.27 (dd,  $J = 10, 2.6$  Hz, 2H), 7.24 – 7.19 (m, 1H), 7.08 (dd,  $J = 8.7, 2.5$  Hz, 1H), 6.86 (ddd,  $J = 13, 7.5, 2.6$  Hz, 3H), 6.78 – 6.60 (m, 1H), 5.34 (s, 1H), 5.22 (s, 1H), 5.15 – 5.09 (m, 1H), 5.01 (s, 1H), 4.69 (dd,  $J = 6.5, 2.4$  Hz, 1H), 4.67 – 4.63 (m, 1H), 4.53 (dd,  $J = 11, 2.6$  Hz, 1H), 4.49 (s, 1H), 4.40 (d,  $J = 4.9$  Hz, 1H), 3.96 (d,  $J = 12$  Hz, 1H), 3.91 (d,  $J = 9.4$  Hz, 1H), 3.85 (d,  $J = 2.5$  Hz, 2H), 3.80 (d,  $J = 2.8$  Hz, 3H), 3.77 (d,  $J = 6.6$  Hz, 1H), 3.72 (d,  $J = 2.6$  Hz, 2H), 3.71 – 3.66 (m, 0H), 3.65 (s, 1H), 3.45 (s, 1H), 3.41 (d,  $J = 9.3$  Hz, 1H), 3.35 (t,  $J = 10$  Hz, 1H), 3.26 (s, 1H), 2.41 (d,  $J = 13$  Hz, 1H), 2.26 (t,  $J = 13$  Hz, 1H), 2.02 (d,  $J = 7.8$  Hz, 1H), 1.97 (d,  $J = 16$  Hz, 1H), 1.84 (d,  $J = 13$  Hz, 1H), 1.79 (d,  $J = 2.5$  Hz, 2H), 1.76 (d,  $J = 14$  Hz, 1H), 1.65 (d,  $J = 12$  Hz, 1H), 1.57 (s, 1H), 1.52 (d,  $J = 12$  Hz, 1H), 1.46 (s, 1H), 1.41 (d,  $J = 8.1$  Hz, 1H), 1.27 (t,  $J = 12$  Hz, 1H), 1.18 (q,  $J = 11, 7.7$  Hz, 1H), 1.03 (d,  $J = 2.6$  Hz, 2H), 0.95 (s, 0H), 0.82 (s, 1H), 0.81 – 0.77 (m, 2H), 0.74 (d,  $J = 2.5$  Hz, 2H).



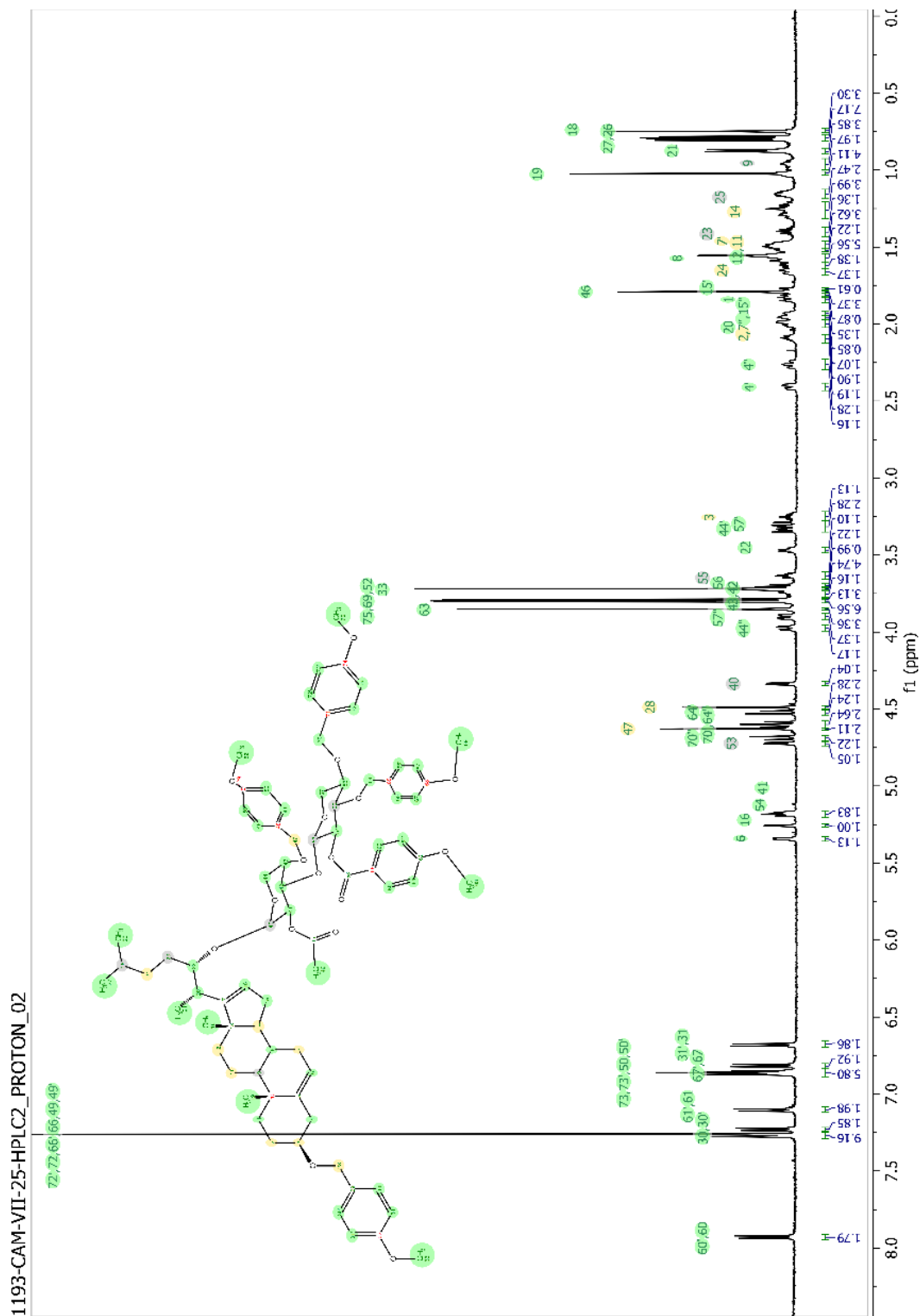


Figure 2-43.  $^1\text{H-NMR}$  of Compound 2.38.a in chloroform-*d*.

1193-CAM-VII-25-HPLC2\_CARBON\_01

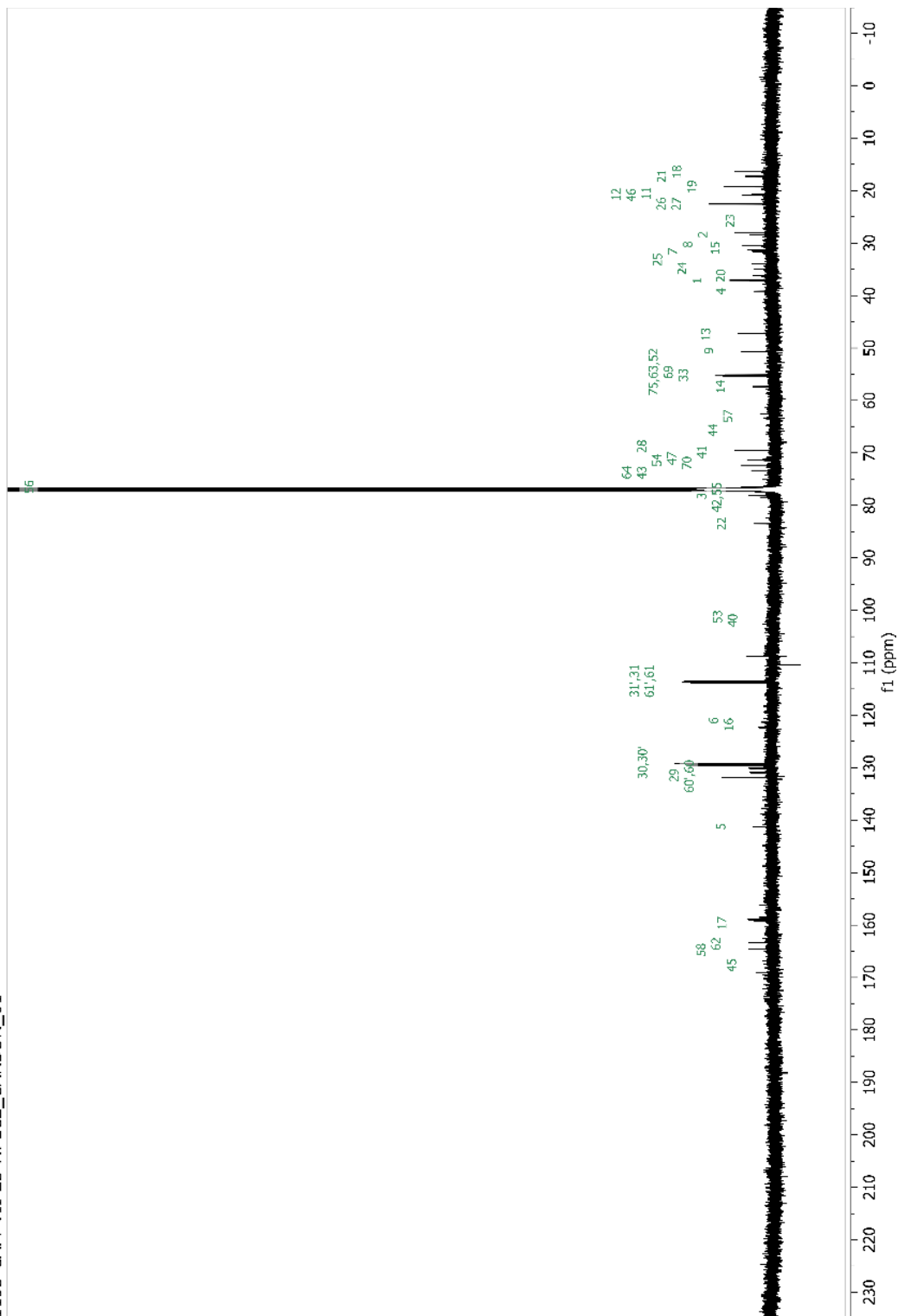
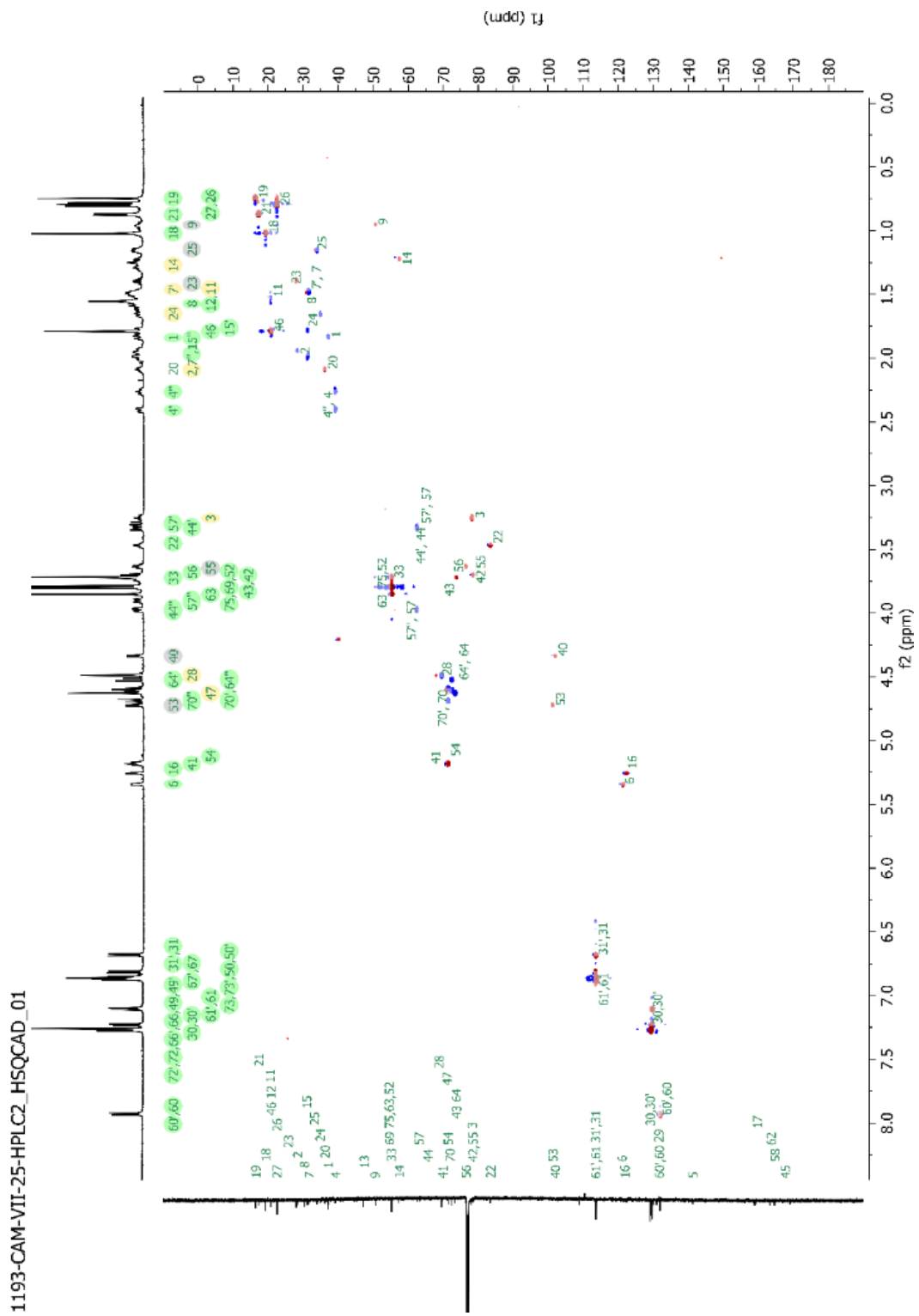


Figure 2-44.  $^{13}\text{C}$ -NMR of Compound 2.38.a in chloroform-*d*.



1192-CAM-VII-25-HPLC1\_PROTON\_02

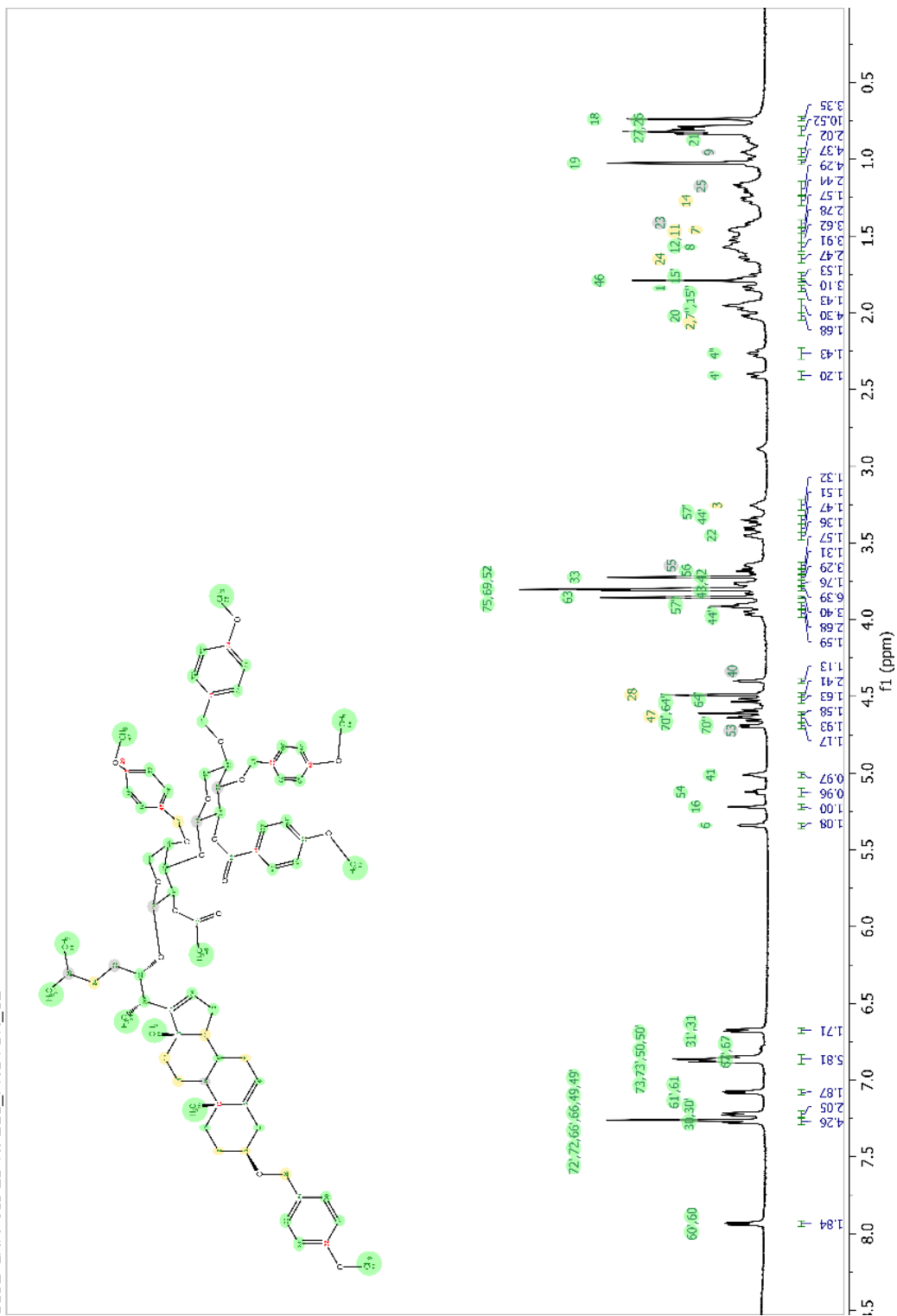
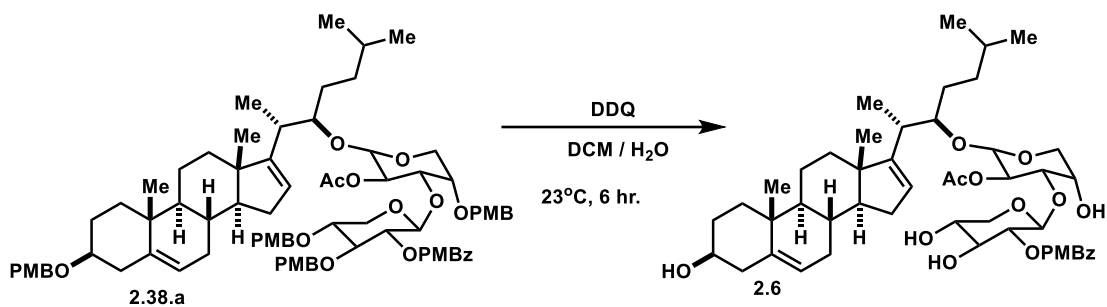


Figure 2-46. <sup>1</sup>H-NMR of Compound 2.38.b in chloroform-*d*.



**(2S,3R,4S,5R)-2-(((2S,3R,4S,5S)-3-acetoxy-5-hydroxy-2-(((2S,3R)-2-((3S,8R,9S,10R,13S,14S)-3-hydroxy-10,13-dimethyl-2,3,4,7,8,9,10,11,12,13,14,15-dodecahydro-1H-cyclopenta[a]phenanthren-17-yl)-6-methylheptan-3-yl)oxy)tetrahydro-2H-pyran-4-yl)oxy)-4,5-dihydroxytetrahydro-2H-pyran-3-yl 4-methoxybenzoate; (2.6):** Compound 2.6 was prepared through following a previously reported protocol adapted for use in transforming the starting material, **Compound 2.38.a**.<sup>89</sup> To a stirring solution of protected steroid aglycone (10.1 mg, 7.6  $\mu\text{mol}$ , 1.0 equiv.) in DCM (0.7 ml, 0.01 M) at room temperature was added distilled water (70  $\mu\text{l}$ ) followed by solid DDQ (15.5 mg, 68.5  $\mu\text{mol}$ , 9.0 equiv.). The biphasic reaction was vigorously stirred and turned yellow/green. After 6 hours, the reaction was quenched at room temperature with sat.  $\text{NaHCO}_{3(\text{aq})}$  (5 ml), then transferred to a separatory funnel, and diluted with DCM (15.0 ml). The biphasic solution was separated, and the organic layer was washed with sat.  $\text{NaHCO}_{3(\text{aq})}$  (4 x 20 ml). The aqueous layers were combined and back extracted with DCM (20 ml). The organic layers were combined and washed with brine and then dried over sodium sulfate. The drying agent was removed, and the solvent evaporated *in vacuo* to afford a crude white solid. The crude material was purified via reverse phase HPLC on a Luna 5  $\mu\text{m}$  C8(2) 100 $\text{\AA}$  column (Phenomenex) with a 90% acetonitrile/0.1% formic acid water mobile phase. 1.5 mg of the desired product (23% yield after HPLC purification) was isolated with a retention time of 11.5 min.  $^1\text{H-NMR}$  contained residual water from HPLC purification.

**Compound 2.6:**  $^1\text{H-NMR}$  (600 MHz, Acetonitrile- $d_3$ ):  $\delta$  7.99 (d,  $J$  = 8.7 Hz, 3H), 7.02 (d,  $J$  = 8.7 Hz, 3H), 5.34 (s, 1H), 5.28 (s, 2H), 4.84 (dt,  $J$  = 16, 8.5 Hz, 3H), 4.64 (d,  $J$  = 7.8 Hz, 2H), 4.34 (d,  $J$  = 7.6 Hz, 2H), 3.95 (s, 2H), 3.91 (dd,  $J$  = 12, 5.2 Hz, 2H), 3.86 (s, 5H), 3.81 (dd,  $J$  = 13, 2.6 Hz, 2H), 3.67 (dd,  $J$  = 9.6, 3.4 Hz, 2H), 3.63 – 3.56 (m, 1H), 3.56 – 3.49 (m, 3H), 3.45 (d,  $J$  = 13 Hz, 2H), 3.33 (s, 2H), 3.27 (t,  $J$  = 11 Hz, 2H), 3.11 (s, 1H), 2.15 (s, 2H), 2.02 – 1.97 (m, 1H), 1.48 (s, 5H), 1.18 (q,  $J$  = 7.5 Hz, 3H), 1.02 (s, 5H), 0.98 (td,  $J$  = 12, 5.4 Hz, 1H), 0.87 (d,  $J$  = 6.9 Hz, 5H), 0.83 (d,  $J$  = 6.6 Hz, 5H), 0.81 (d,  $J$  = 6.7 Hz, 4H), 0.79 (s, 5H).  $^{13}\text{C-NMR}$  (151 MHz, Acetonitrile- $d_3$ ):  $\delta$  170.1, 165.6, 164.6, 159.3, 142.7, 132.7, 123.4, 123.3, 121.7, 114.7, 102.8, 83.9, 81.3, 75.7, 74.5, 71.8, 71.2, 70.5, 68.5, 66.5, 65.7, 58.4, 56.3, 51.7, 48.0, 43.0, 38.1, 37.5, 37.4, 35.7, 34.6, 32.4, 32.3, 32.3, 31.8, 31.3, 28.8, 22.9, 22.7, 21.5, 20.8, 19.7, 17.9, 16.8. HRMS (+ESI, 180V, rt: 0.815 min): calcd for  $\text{C}_{47}\text{H}_{68}\text{O}_{13} + \text{Na}^+$   $[\text{M}+\text{H}]^+$ : 863.45631; found 863.4529,  $\Delta\text{ppm}$  = -3.95 ppm.

1199-CAM-VII-35-C22Oimimetic-HPLC6\_PROTON\_02

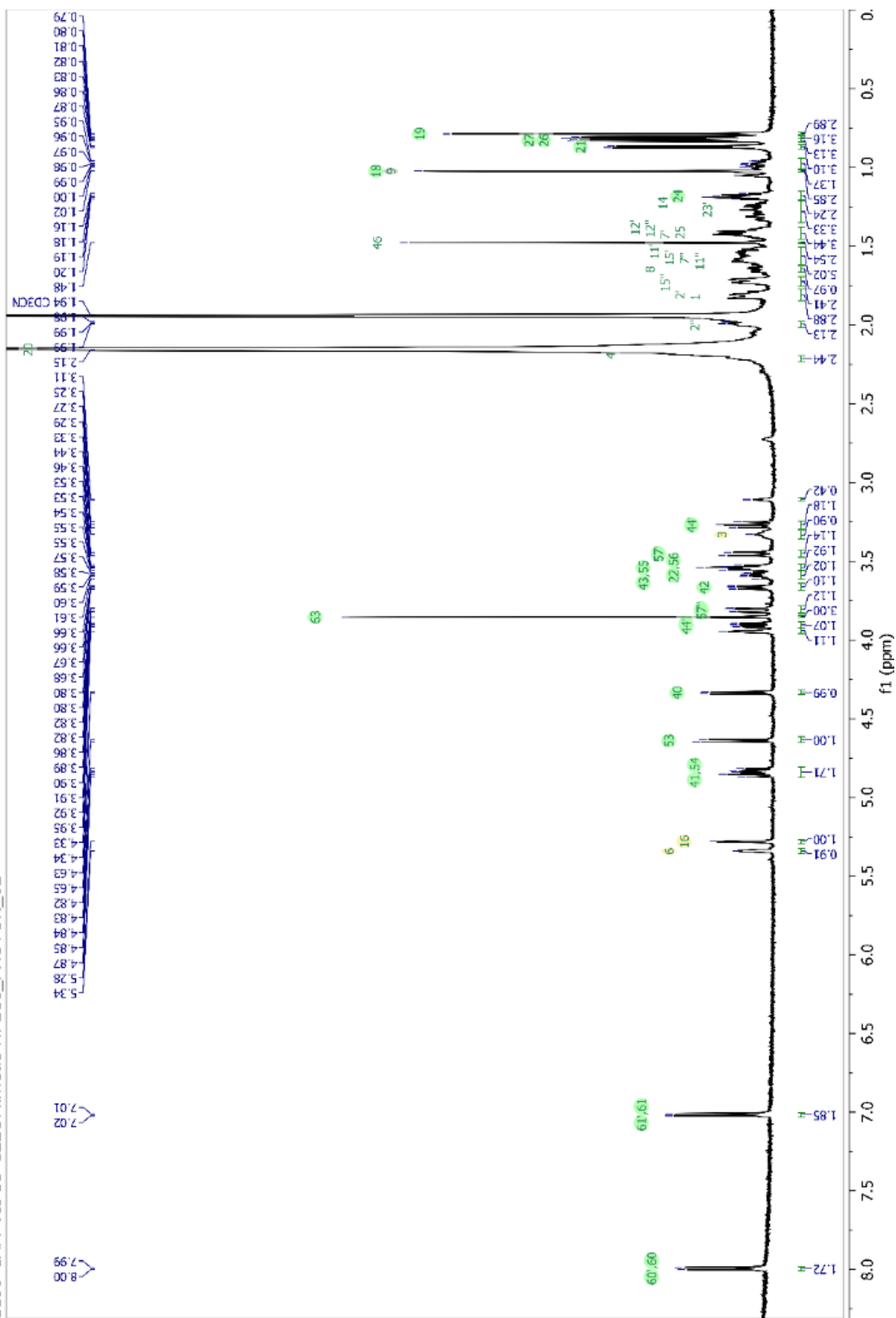


Figure 2-47. <sup>1</sup>H-NMR of  $\alpha$ -anomer C22-O-Glycoside (2.6) in acetonitrile- $d_3$ .

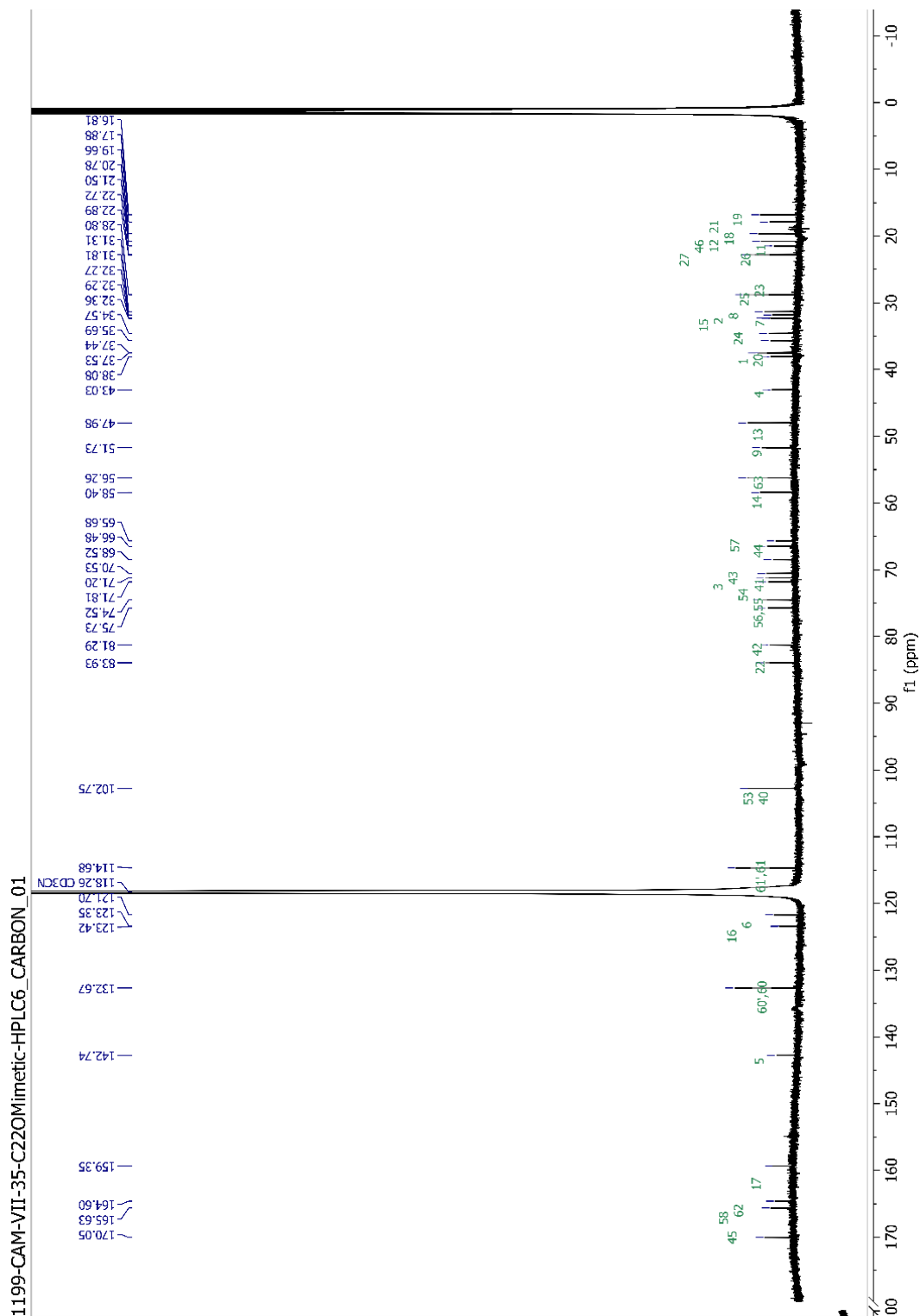


Figure 2-48.  $^{13}\text{C}$ -NMR of  $\alpha$ -anomer C22-O-Glycoside (**2.6**) in acetonitrile- $d_3$ .

1199-CAM-VII-35-C22Omimetic-HPLC6\_HSQCAD\_01

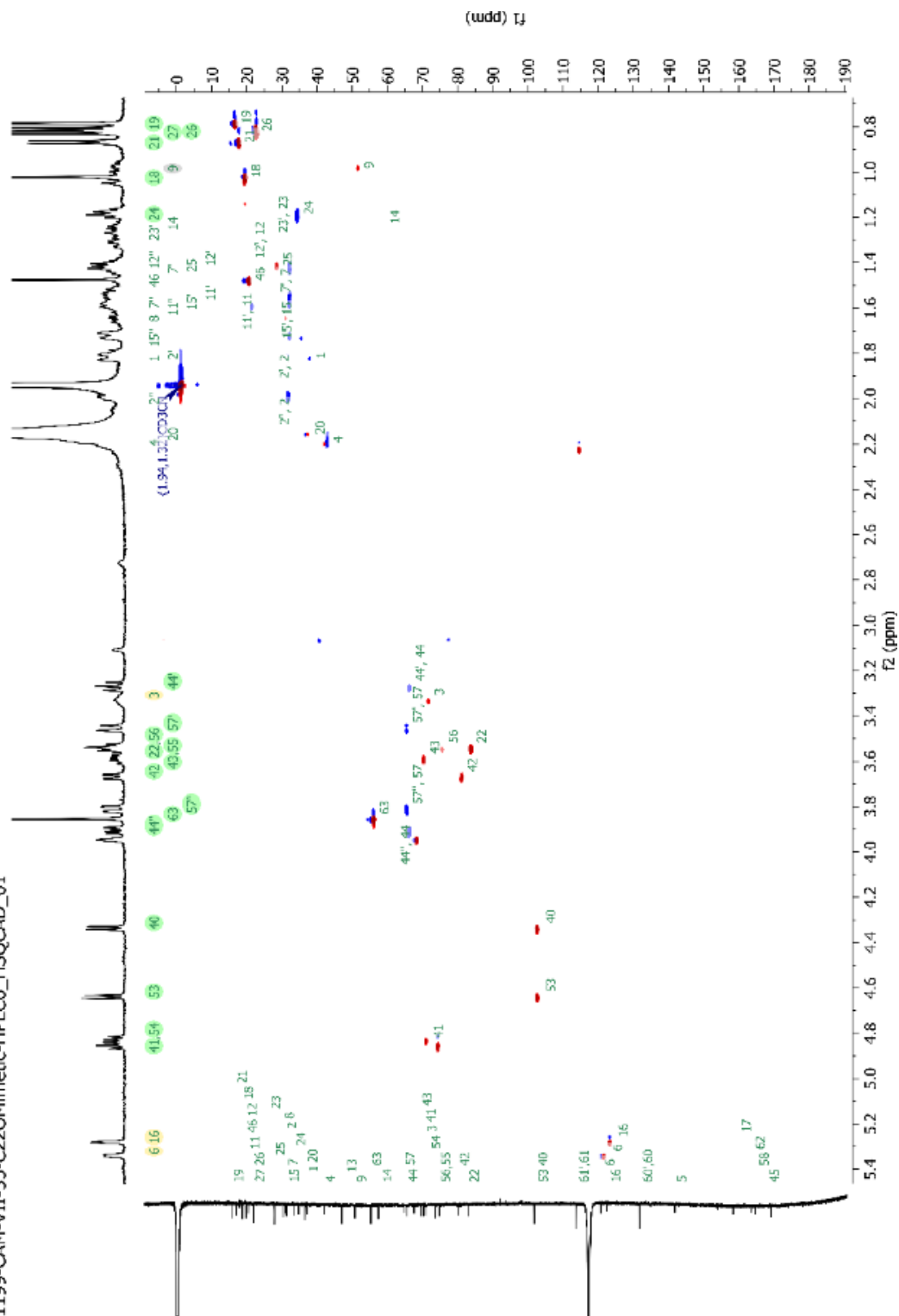
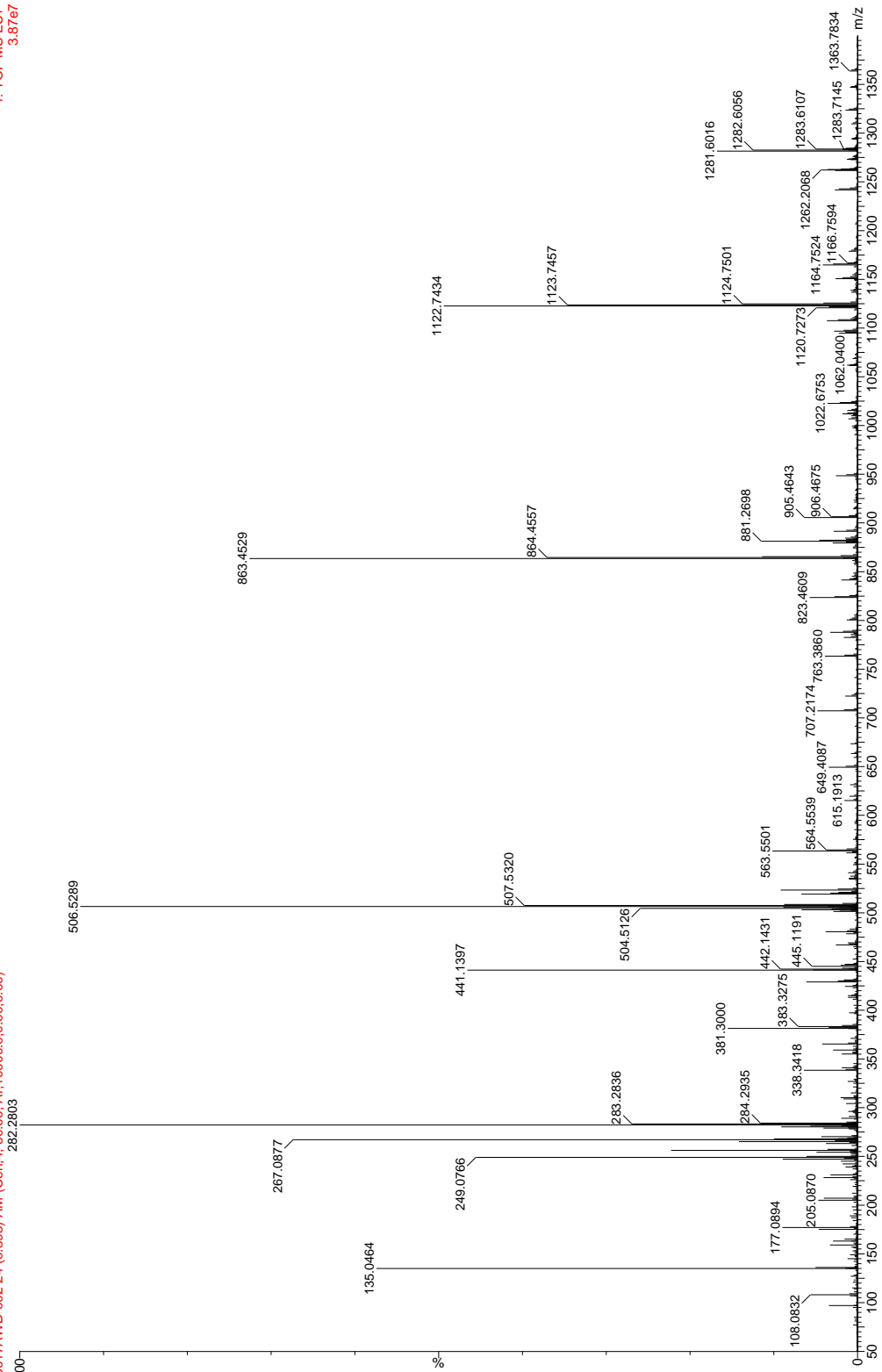


Figure 2-49. HSCQ-AD of  $\alpha$ -anomer C22-O-Glycoside (**2.6**) in acetonitrile- $d_3$ .





**Figure 2-50. Compound 2.6, HRMS (+ESI, 180V, rt: 0.815 min): calcd for  $C_{47}H_{68}O_{13} + Na^+$  -  $[M+H]^+$ : 863.45631; found 863.4529,  $\Delta$ ppm= 3.95ppm.**

05-Dec-2019 13:58:47  
1: TOF MS ES+  
2.8167

SYNAPT2-SI#UGA589

CAM-VII-35-HPLC  
Malinky  
13017AWB-002 24 (0.895) AM (Gen,4, 80.00, Ar,100000.0,0.00,0.00)

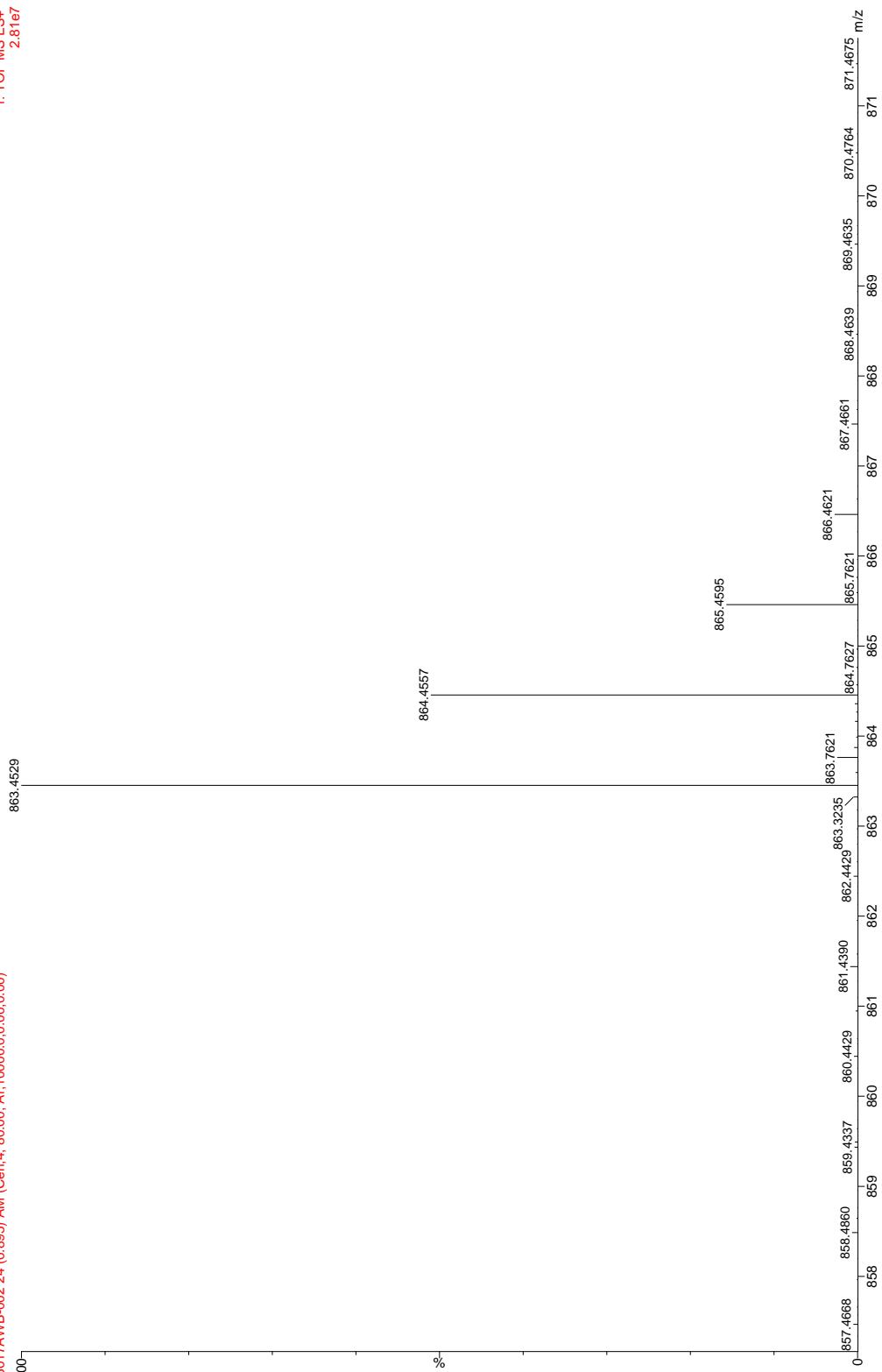
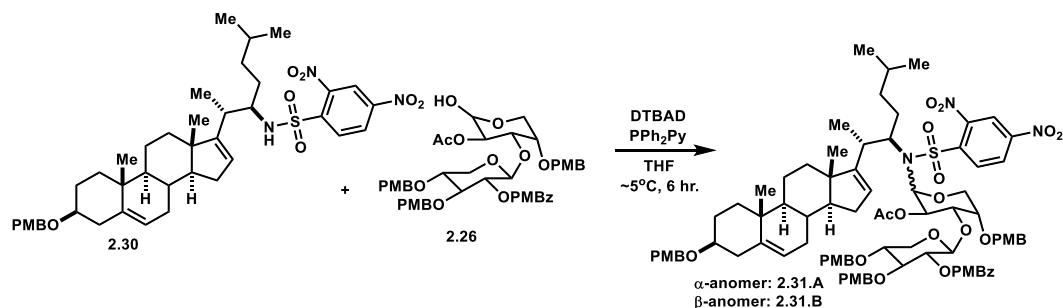


**Figure 2-51. Compound 2.6, HRMS (+ESI, 180V, rt: 0.815 min): calcd for  $C_{47}H_{68}O_{13} + Na^+$   $[M+H]^+$ : 863.45631; found 863.4529,  $\Delta$ ppm= 3.95ppm.**

Fukuyama-Mitsunobu reaction optimization table

Entry	Amine Equiv. (1)	Sugar Equiv. (2)	Phosphine (3)	Phosphine Equiv. (3)	Azodicarb. (4)	Equiv. (4)	Temp	Solvent	Order of addition	Results	Yield	Results
1	NHNs, 1	1.2	Ph <sub>3</sub> P	4	DIAD	4.0	-40 to Rt	THF	1,2 into 3,4	NR; byproduct formed	NR; byproduct formed	NR; byproduct formed
2	NHNs, 1	1.3	Ph <sub>3</sub> P	2	DIAD	2.0	-40 to Rt	THF	1,2 into 3,4	trace	trace	trace
3	NHNs, 1	1.7	(Ph <sub>3</sub> P) <sub>2</sub>	4	TMAD	4.0	RT	THF	1,2 into 3,4	NR; byproduct formed	NR; byproduct formed	NR; byproduct formed
4	NHNs, 1.2	1.0	(Ph <sub>3</sub> P) <sub>2</sub>	2	DIAD	1.5	-40 to Rt	THF	1,2 into 3,4	NR; byproduct formed	NR; byproduct formed	NR; byproduct formed
5	NHNs, 1	1.7	(Ph <sub>3</sub> P) <sub>2</sub>	4	DIAD	4.0	RT	THF	1,2 into 3,4	NR; byproduct formed	NR; byproduct formed	NR; byproduct formed
6	NHNs, 1	1.2	Ph <sub>3</sub> P	4	TMAD	4.0	RT	THF	1,2 into 3,4	NR; byproduct formed	NR; byproduct formed	NR; byproduct formed
7	NHNs, 1	1.2	<sup>n</sup> Bu <sub>3</sub> P	4	TMAD	4.0	-40 to Rt	THF	1,2 into 3,4	Trace	Trace	Trace
8	NHNs, 1	1.2	<sup>n</sup> Bu <sub>3</sub> P	4	TMAD	4.0	-40 to Rt	MePh	1,2 into 3,4	Trace	Trace	Trace
9	NHNs, 1	1.2	Ph <sub>3</sub> PyP	4	TMAD	4.0	RT	DCM	1,2 into 3,4	NR; byproduct formed	NR; byproduct formed	NR; byproduct formed
10	NHNs, 1	1.2	Ph <sub>3</sub> PyP	4	TBAD	4.0	RT	DCM	1,2 into 3,4	Trace	Trace	Trace
11	NHNs, 1	1.2	Ph <sub>3</sub> PyP	4	TBAD	2 then 4	0 to RT	DCM	1,2 into 3,4	trace	trace	trace

Entry	Amine (1), Equiv	Sugar (2), Equiv	Phosphine (3)	Azodicarb. (4)	Equiv.	Temp	Solvent	Order of addition	Results
13	NHNs, 1	1.1	<sup>t</sup> Bu <sub>3</sub> P 1.5	TMAD	1.5	0 to RT	THF	4 into 1,2,3	NR; byproduct formed
14	NHNs, 1	1.2	Ph <sub>2</sub> PyP 2	DTBAD	2.0	-40 to Rt	DCM	4 into 1,2,3	trace
15	NHNs, 1	1.2	Ph <sub>2</sub> PyP 2	DTBAD	2.0	0 to RT	DCM	4 into 1,2,3	~20% BORSM
16	NHNs, 1	1.2	Ph <sub>2</sub> PyP 2	DTBAD	2.0	-10 to RT	DCM	4 into 1,2,3	~20% BORSM
17	NHNs, 2	1.0	Ph <sub>2</sub> PyP 2.5	DTBAD	2.5	-10 to RT	DCM	4 into 1,2,3	~8% BORSM
18	NHNs, 2	1.0	Ph <sub>2</sub> PyP 2.5	DTBAD	2.5	-10 to RT	DCM	1,2 into 3,4	~11% BORSM
19	NHNs, 1	1.5	Ph <sub>2</sub> PyP 2	DTBAD	2.0	-10 to RT	DCM	2 into 1,3,4	~13% BORSu
20	NHNs, 1	1.2	Ph <sub>2</sub> PyP 2	DTBAD	2.0	0 to RT	DCM	1,4 into 2,3	~15% BORSM
21	NHNs, 1	1.2	Ph <sub>2</sub> PyP 2	DTBAD	2.0	0 to RT	THF	4 into 1,2,3	~25% BORSM
22	NHNs, 1	1.2, +1 after 24h	Ph <sub>2</sub> PyP 2, +1.5 after 24h	DTBAD	2, +1.5 after 24h	0 to RT	THF	4 into 1,2,3	~35% BORSM
23	NHNs, 1	1.2	Ph <sub>2</sub> PyP 2	DTBAD	2.0	0 to RT	THF	4 into 1,2,3	~14% BORSM
24	NHNs, 1	4.0	Ph <sub>2</sub> PyP 5.5	DTBAD	5.5	0 to RT	THF	4 into 1,2,3	NR
25	NHNs, 1	4.0	Ph <sub>2</sub> PyP 5.5	DTBAD	5.5	0 to RT	THF	portion addition of 2,3,4 into 1	NR
27	NHDNs, 1	1.2	Ph <sub>2</sub> PyP 2.2	DTBAD	2.0	0 to RT	THF	4 into 1,2,3	~44% yield
28	NHDNs, 1	1.4	Ph <sub>2</sub> PyP 4	DTBAD	4.0	4-5°C	THF	4 into 1,2,3	~61% yield



(2S,3R,4S,5R)-2-(((2R,3R,4S,5S)-3-acetoxy-5-((4-methoxybenzyl)oxy)-2-((N-((2S,3R)-2-((3S,9S,10R,13S,14S)-3-((4-methoxybenzyl)oxy)-10,13-dimethyl-2,3,4,7,8,9,10,11,12,13,14,15-dodecahydro-1H-cyclopenta[a]phenanthren-17-yl)-6-methylheptan-3-yl)-2,4-dinitrophenyl)sulfonamido)tetrahydro-2H-pyran-4-yl)oxy)-4,5-bis((4-methoxybenzyl)oxy)tetrahydro-2H-pyran-3-yl 4-methoxybenzoate; (2.31.A)

(2S,3R,4S,5R)-2-(((2S,3R,4S,5S)-3-acetoxy-5-((4-methoxybenzyl)oxy)-2-((N-((2S,3R)-2-((3S,9S,10R,13S,14S)-3-((4-methoxybenzyl)oxy)-10,13-dimethyl-2,3,4,7,8,9,10,11,12,13,14,15-dodecahydro-1H-cyclopenta[a]phenanthren-17-yl)-6-methylheptan-3-yl)-2,4-dinitrophenyl)sulfonamido)tetrahydro-2H-pyran-4-yl)oxy)-4,5-bis((4-methoxybenzyl)oxy)tetrahydro-2H-pyran-3-yl 4-methoxybenzoate; (2.31.B): Compound 2.321.A (α-anomer) and Compound 2.31.B (β-anomer) were prepared through screening and optimizing previously reported general Mitsunobu-Fukuyama reaction conditions to a new substrate class.<sup>102</sup> Solid starting material nosyl-aminosterol, **Compound 2.30**, (47.2 mg, 62.9 μmol, 1.0 equiv.), disaccharide (**Compound 2.26**, 72.3 mg, 88.1 μmol, 1.4 equiv.), and diphenyl pyridyl phosphine (68.2 mg, 261 μmol, 4.2 equiv.) were added to a 10 ml pear-shaped flask with Teflon-coated spin vane. The reaction flask was purged with nitrogen and vacuum. The solids within the flask were then dissolved in dry THF (2.0 ml, 0.020 M) and the reaction was cooled to ~5°C on an ice-water bath. 400 μl of a stock solution of DTBAD (57.7 mg, 251 μmol, 4.0 equiv.) in THF (1.8 ml, 140 mM) was added to the reaction. Then an additional 200 μl (28.9 mg, 126 μmol, 2.0 equiv.) of this solution was added to the reaction flask every 45 minutes for 4 hours. The reaction proceeded over 6 hours at 5°C, and then the reaction was directly condensed *in vacuo* to afford a crude yellow/orange gel. The crude material was purified via automated column chromatography using a manually packed Biotage 25 G column of oven dried silica eluted with a gradient of 5-20% ethyl acetate in hexanes over 15 column volumes, then 20-40% over 10 column volumes. The products eluted off the column at ~30% ethyl acetate in hexanes. The individual anomers were isolated along with a mixture of α/β-anomer glycoside products: 31.6 mg of **Compound 2.31.A** α-anomer glycoside product (34% yield), 12.5 mg of **Compound 2.31.B** β-anomer glycoside product (14%), and 15.5 mg of an α/β-anomeric mixture of glycoside products (17%). A total 59.6 mg of desired compound was collected (61.2% yield). 59.6 mg of a 2:1 mixture of α/β-anomers was isolated (61.2% yield). Diagnostic NMR peaks were of appropriate chemical shift but characterization at this stage proved to be challenging. A more detailed characterization of the following transformation is described for **Compound 2.32.a.** and **Compound 2.32.b.**

**Compound 2.31:**  $^1\text{H-NMR}$  (400 MHz, Acetonitrile- $d_3$ ):  $\delta$  8.04 – 7.79 (m, 1H), 7.80 (d,  $J$  = 8.5 Hz, 1H), 7.41 (d,  $J$  = 8.4 Hz, 1H), 7.37 – 7.20 (m, 5H), 7.00 (d,  $J$  = 8.8 Hz, 2H), 6.94 – 6.85 (m, 6H), 6.69 – 6.59 (m, 2H), 6.07 (d,  $J$  = 10.0 Hz, 1H), 5.45 (s, 1H), 5.34 (s, 2H), 5.11 – 5.05 (m, 1H), 5.05 – 4.95 (m, 1H), 4.88 (d,  $J$  = 6.6 Hz, 1H), 4.72 – 4.52 (m, 6H), 4.52 – 4.40 (m, 4H), 4.34 (s, 1H), 4.16 – 3.94 (m, 2H), 3.86 (s, 1H), 3.80 – 3.73 (m, 9H), 3.72 – 3.62 (m, 6H), 3.50 (d,  $J$  = 12.7 Hz, 1H), 3.41 (dd,  $J$  = 11.9, 8.5 Hz, 1H), 3.35 – 3.25 (m, 1H), 3.23 – 3.11 (m, 1H), 2.43 – 2.32 (m, 1H), 2.16 (s, 2H), 2.02 – 1.89 (m, 4H), 1.62 (s, 1H), 1.42 (dd,  $J$  = 7.1, 4.5 Hz, 2H), 1.35 – 1.15 (m, 3H), 1.11 – 0.96 (m, 5H), 0.84 – 0.71 (m, 5H), 0.64 – 0.45 (m, 4H).

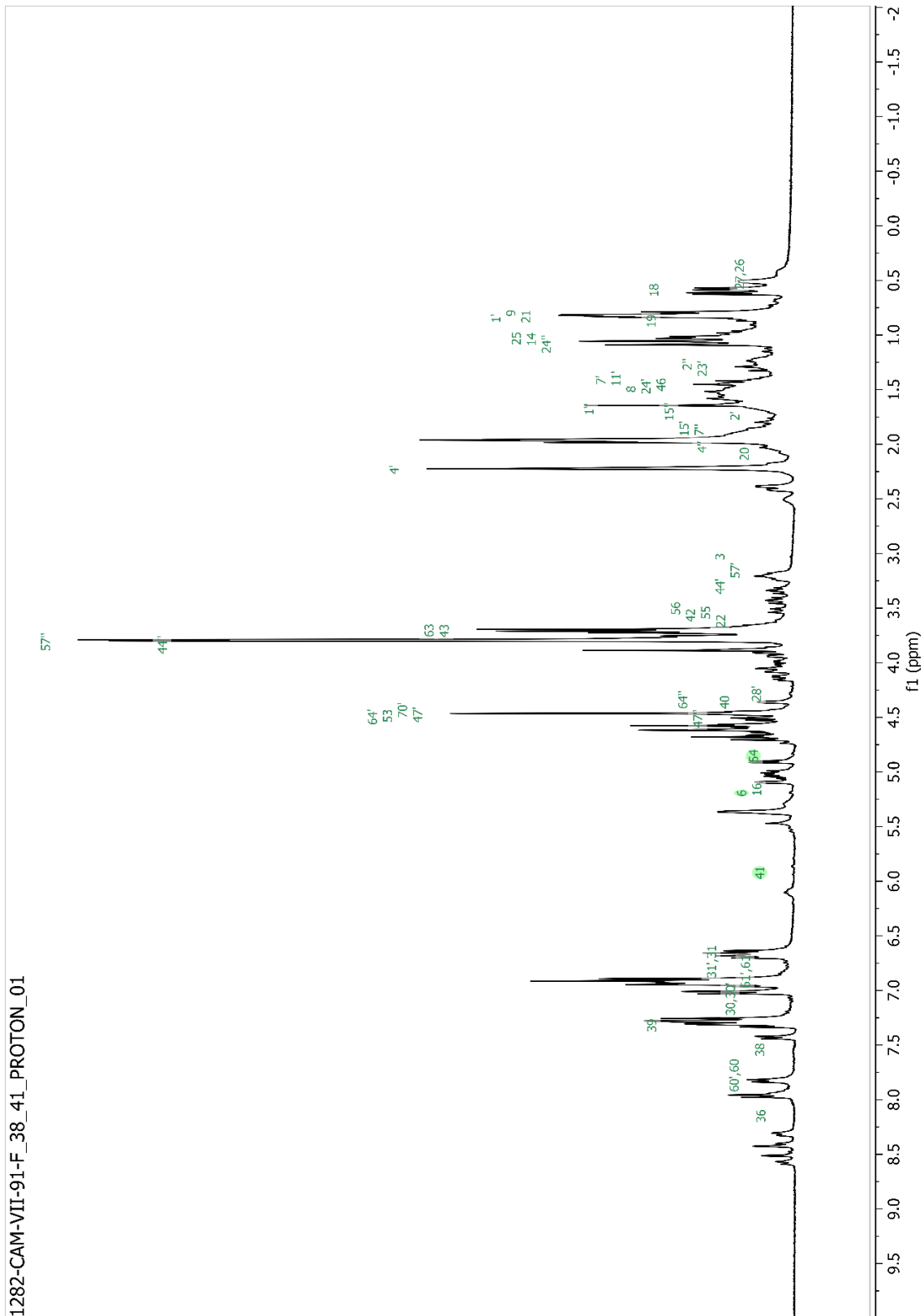


**Figure 2-52.** <sup>1</sup>H-NMR of the mixture of **Compound 2.321.A** (α-anomer) and **Compound 2.31.B** (β-anomer) in acetonitrile-*d*<sub>3</sub>.

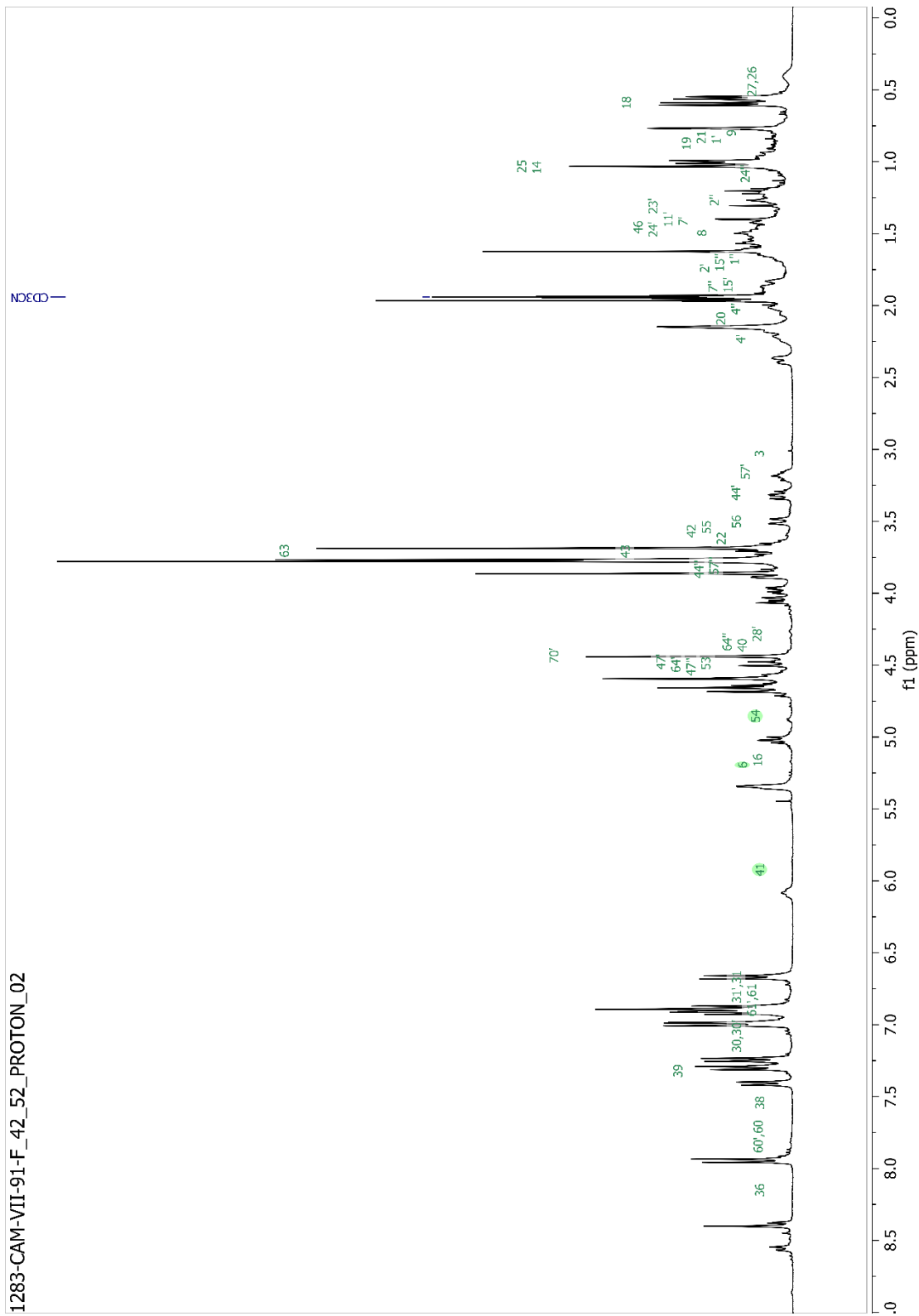


**Figure 2-53.**  $^1\text{H-NMR}$  of **Compound 2.31.A** ( $\alpha$ -anomer) in acetonitrile- $d_3$ .



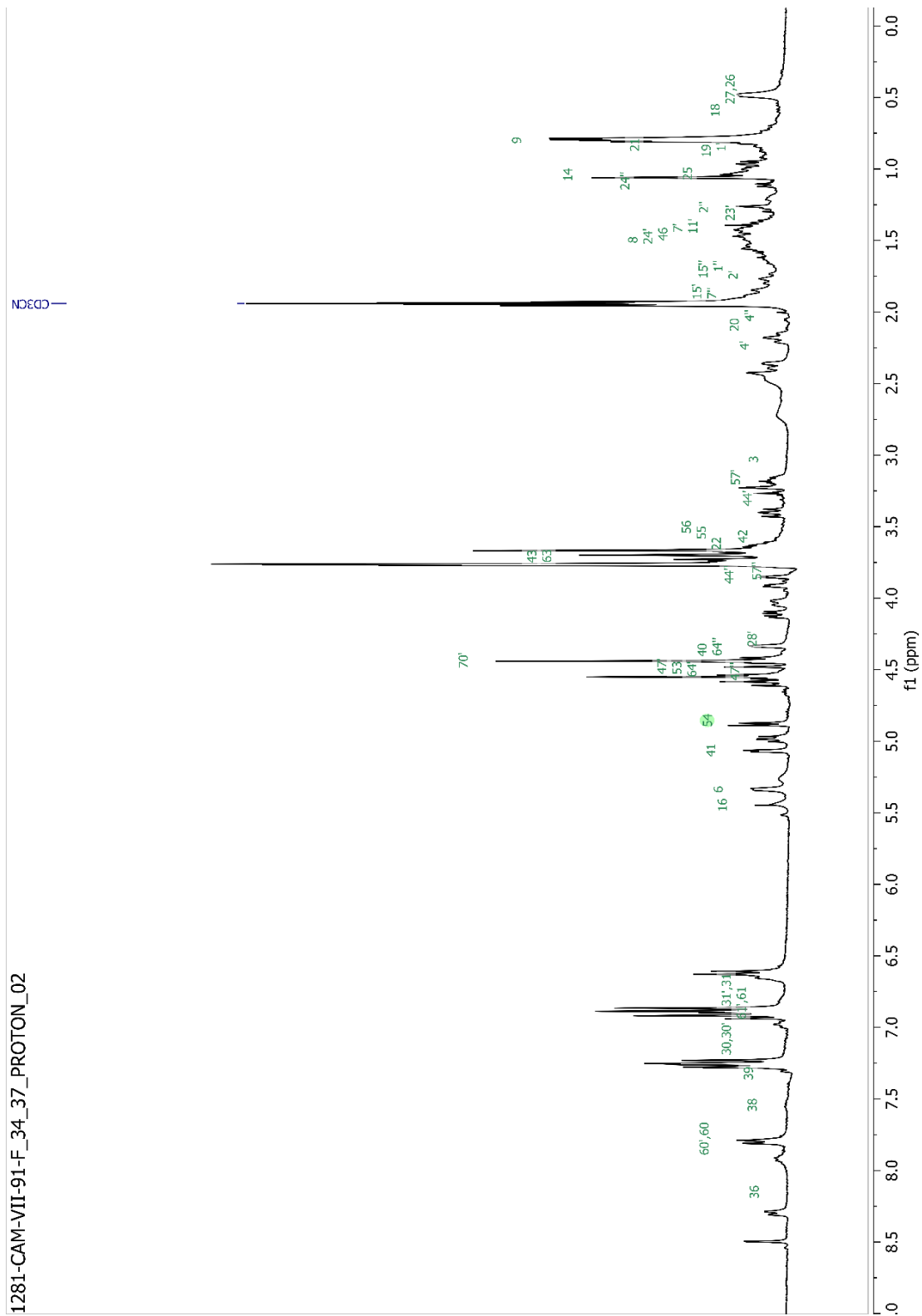
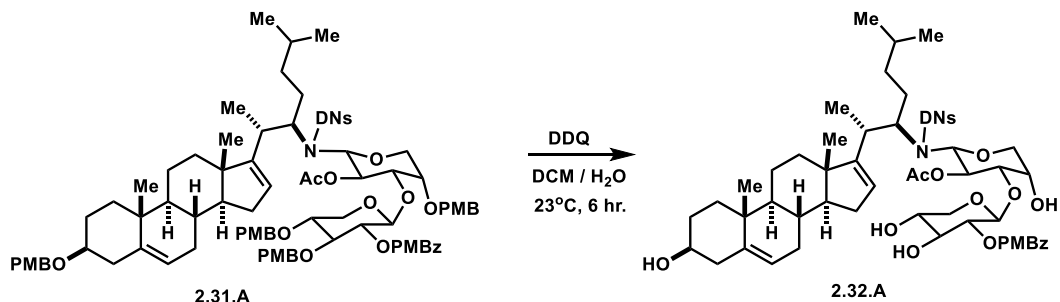


**Figure 2-54.**  $^1\text{H-NMR}$  of **Compound 2.31.B** ( $\beta$ -anomer) in acetonitrile- $d_3$ .



**(2S,3R,4S,5R)-2-(((2R,3R,4S,5S)-3-acetoxy-5-((4-methoxybenzyl)oxy)-2-((N-((2S,3R)-2-((3S,9S,10R,13S,14S)-3-((4-methoxybenzyl)oxy)-10,13-dimethyl-2,3,4,7,8,9,10,11,12,13,14,15-dodecahydro-1H-cyclopenta[a]phenanthren-17-yl)-6-methylheptan-3-yl)-2,4-dinitrophenyl)sulfonamido)tetrahydro-2H-pyran-4-yl)oxy)-4,5-bis((4-methoxybenzyl)oxy)tetrahydro-2H-pyran-3-yl** **4-**

**methoxybenzoate; (2.32.A): Compound 2.32.A** ( $\alpha$ -anomer) was prepared through following a previously reported protocol adapted for use in transforming the starting material, **Compound 2.31.A**.<sup>89</sup> To a 5 ml conical flask containing solid starting material  $\alpha$ -anomer glycoside (**Compound 2.31.A**, 36.4 mg, 23.5  $\mu$ mol, 1.0 equiv.) and solid DDQ (26.6 mg, 117  $\mu$ mol, 5.0 equiv.) under nitrogen atmosphere at room temperature was added dry DCM (2.0 ml, 12.0 mM) followed by DI water (0.4 ml). The biphasic reaction turned immediately black and as the reaction proceeded it turned to a brown/orange mixture. Upon complete conversion of starting material by TLC, the reaction was diluted in ethyl acetate (2.0 ml) then quenched with sat.  $\text{NaHCO}_{3(\text{aq})}$  at room temperature. The reaction mixture was transferred to a separatory funnel and diluted with 20 ml of ethyl acetate. The layers were separated and then the organic layer was washed with sat.  $\text{NaHCO}_{3(\text{aq})}$  (5 x 15.0 ml), followed by water (2 x 15.0 ml). The aqueous layers were combined and back extracted with ethyl acetate (2 x 15.0 ml). The organic layers were combined and washed with brine then dried over  $\text{Na}_2\text{SO}_4$ . The drying agent was then removed, and the solvent was removed *in vacuo* to afford a crude yellow/orange paste. The crude material was purified via oven-dried silica column and eluted with a gradient of 1-12.5% methanol in DCM. 18.1 mg of  $\alpha$ -anomer glycoside product (**2.32.A**) was obtained as a white solid (72%). Assignment of the  $\alpha$ -anomer were made based on characteristic carbon shifts:  $\alpha$ -anomeric carbon at 84.7 ppm,  $\beta$ -anomeric carbon at 99.3 ppm.<sup>120</sup>

**Compound 2.32.a** ( $\alpha$ -anomer):  $^1\text{H-NMR}$  (500 MHz, Methanol- $d_4$ ):  $\delta$  8.75 (d,  $J = 8.9$  Hz, 1H), 8.57 (s, 1H), 8.53 (dd,  $J = 8.9, 2.3$  Hz, 1H), 8.05 (d,  $J = 8.9$  Hz, 1H), 7.17 – 6.92 (m, 1H), 6.21 (t,  $J = 9.5$  Hz, 1H), 5.37 (t,  $J = 4.6$  Hz, 2H), 4.97 (dd,  $J = 8.8, 7.6$  Hz, 1H), 4.72 (dd,  $J = 7.6, 1.3$  Hz, 1H), 4.69 (s, 1H), 4.19 (d,  $J = 2.4$  Hz, 1H), 4.02 – 3.96 (m, 1H), 3.96 – 3.91 (m, 1H), 3.89 (s, 2H), 3.83 (d,  $J = 9.6$  Hz, 1H), 3.72 – 3.58 (m, 2H), 3.40 (tt,  $J = 11, 4.9$  Hz, 1H), 3.37 – 3.33 (m, 1H), 2.33 (d,  $J = 7.4$  Hz, 1H), 2.27 – 2.20 (m, 1H), 2.08 (ddd,  $J = 15, 6.6, 3.3$  Hz, 1H), 2.02 (d,  $J = 11$  Hz, 1H), 1.98 – 1.85 (m, 1H), 1.81 (d,  $J = 12$  Hz, 1H), 1.69 (dd,  $J = 11, 4.5$  Hz, 1H), 1.61 (dd,  $J = 18, 10$  Hz, 1H), 1.55 (s, 2H), 1.51 (d,  $J = 11$  Hz, 0H), 1.34 – 1.20 (m, 1H), 1.07 (s, 2H), 1.06 (d,  $J = 7.1$  Hz, 2H), 0.99 (ddt,  $J = 16, 11, 5.6$  Hz, 1H), 0.83 (s, 2H), 0.61 (d,  $J = 6.6$  Hz, 2H), 0.58 (d,  $J = 6.6$  Hz, 2H), 0.54 – 0.46 (m, 1H). HRMS (+ESI, 180V, rt: 0.896 min): calcd for  $\text{C}_{53}\text{H}_{71}\text{N}_3\text{O}_{18}\text{S} + \text{Na}^+$  -  $[\text{M}+\text{Na}]^+$ : 1092.4357; found 1092.4338, -

1.7 Δ ppm.

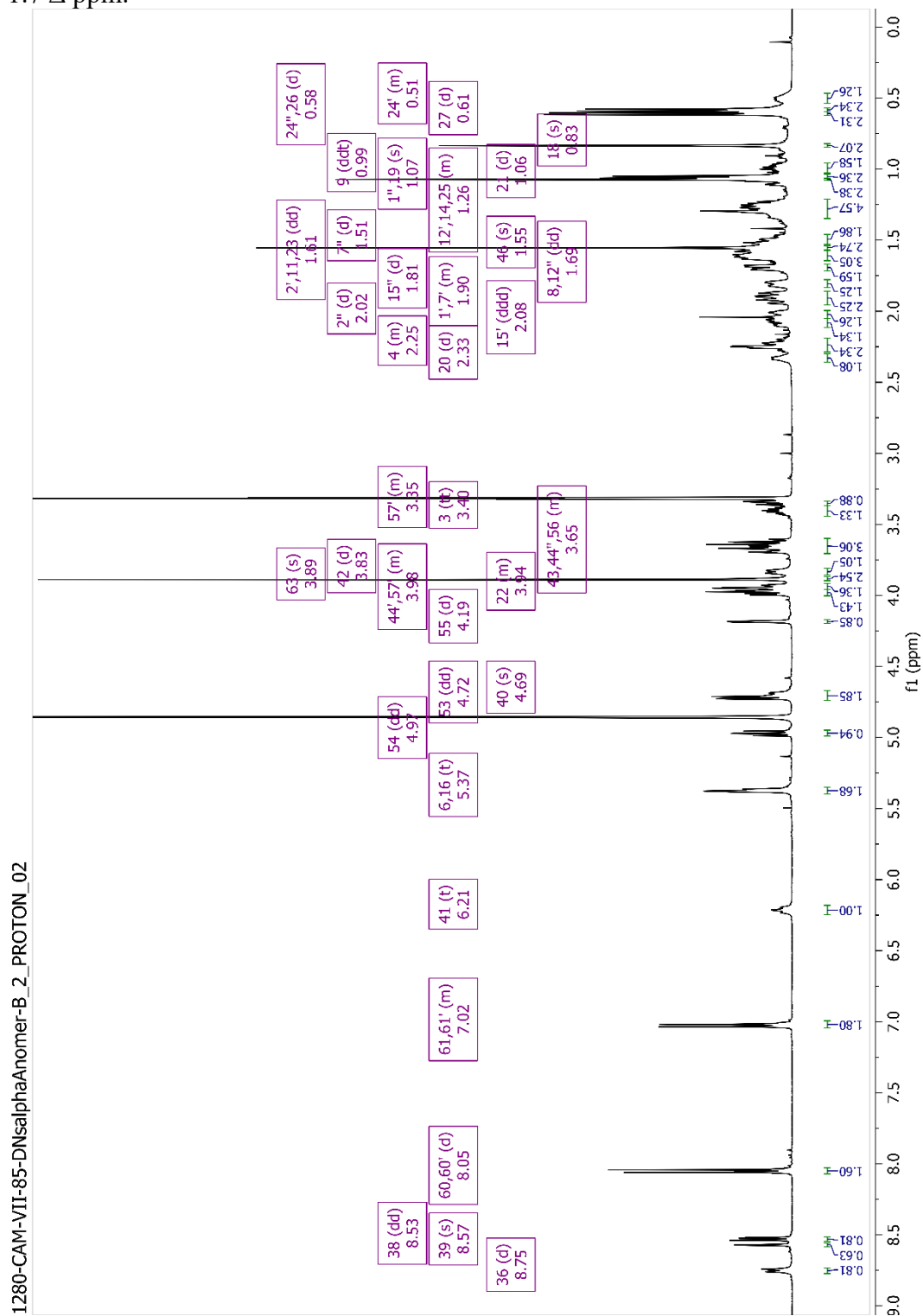
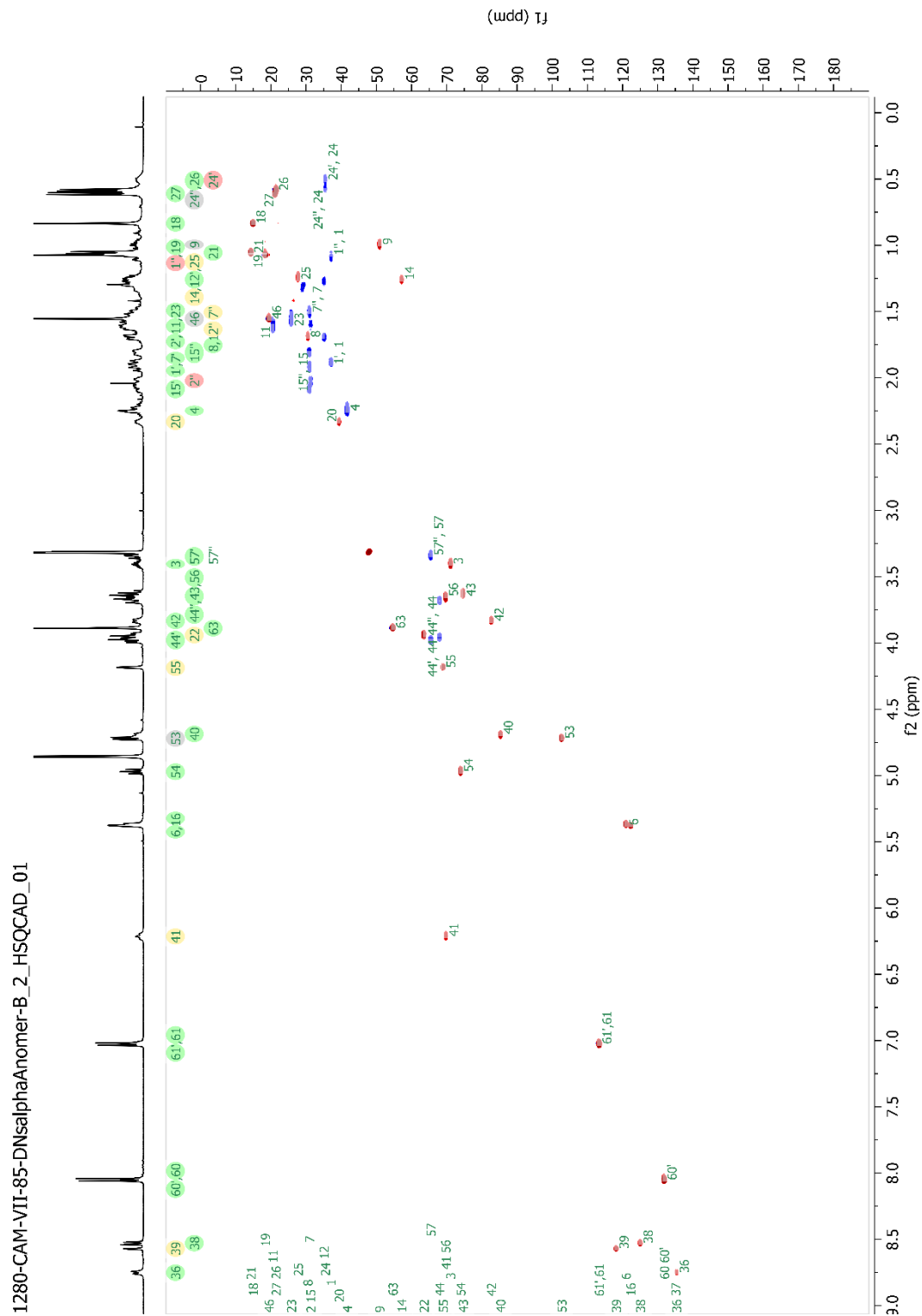


Figure 2-55. <sup>1</sup>H-NMR of Compound 2.32.a (α-anomer) in Methanol-*d*<sub>4</sub>.



12-Feb-2020 16:52:39

SYNAPT G2-S#UJGA589

1249-CAM-VII-71

Malinky

13036AWB-004 24 (0.896) AM (Gen,4, 80.00, At,100000.0,0.00,0.00)

1: TOF MS ES+  
2.2567

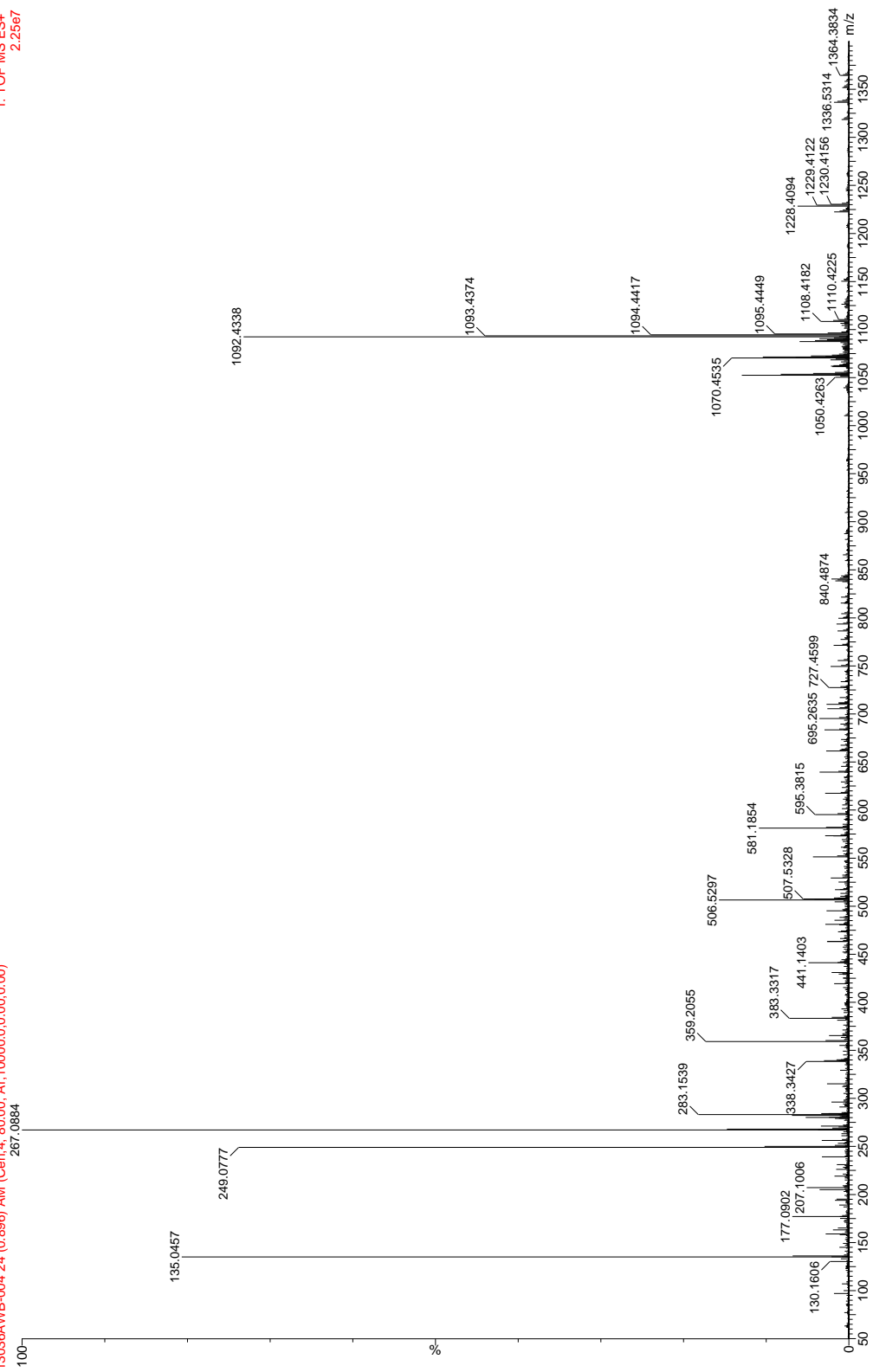


**Figure 2-57.** Compound **2.32.a** ( $\alpha$ -anomer), HRMS (+ESI, 180V, rt: 0.896 min): calcd for  $C_{53}H_{71}N_3O_{18}S + Na^{+}$   $[M+Na]^{+}$ : 1092.4357; found 1092.4338,  $-1.7 \Delta$  ppm.

12-Feb-2020 16:52:39

SYNAPTG2-S#JUGA589

1249-CAM-VII-71

Malinky

13036AWB-004 24 (0.896) AM (Gen,4, 80.00, Ar,10000.0,0.00,0.00)

1: TOF MS ES+  
1.6467

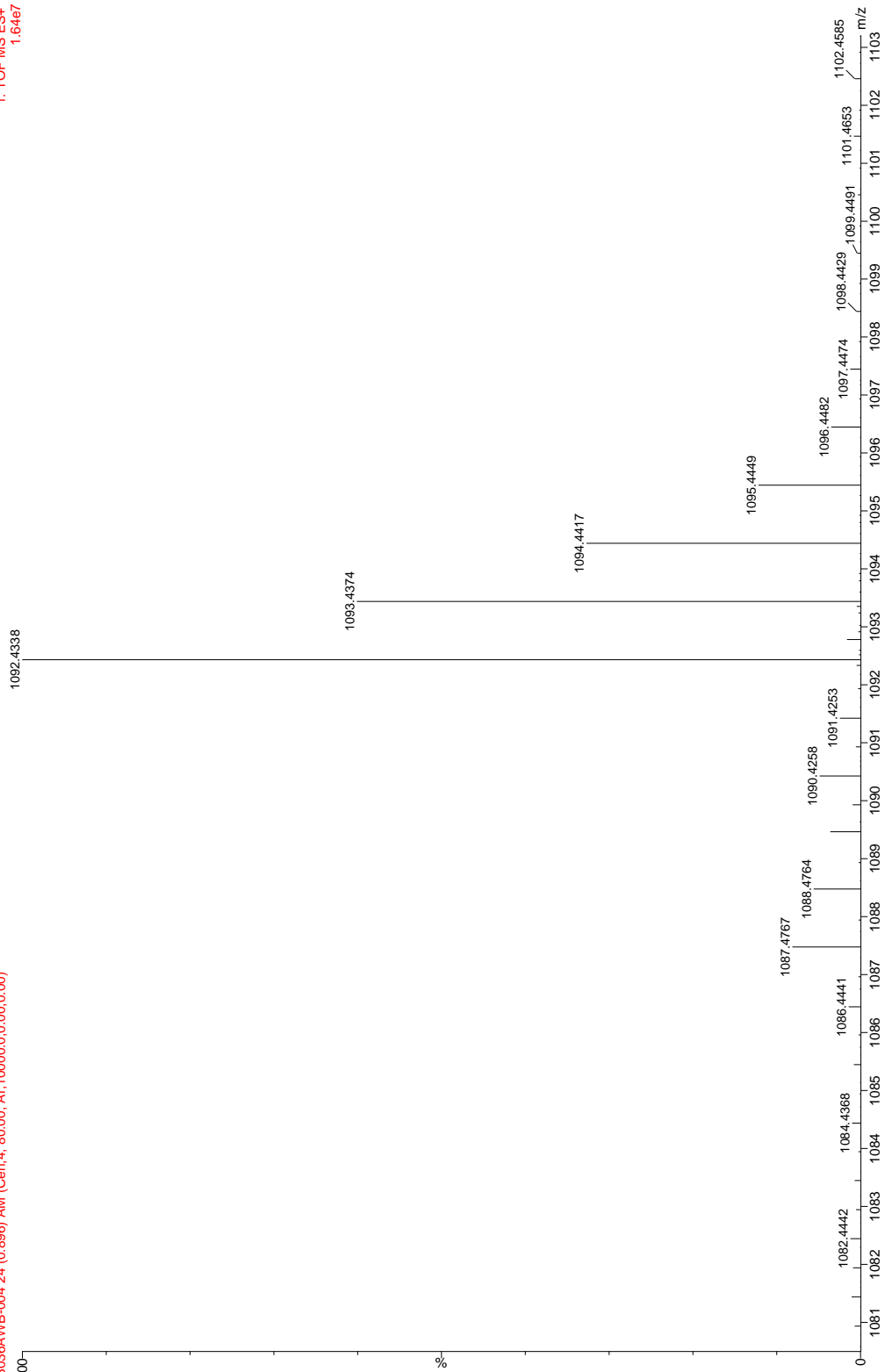
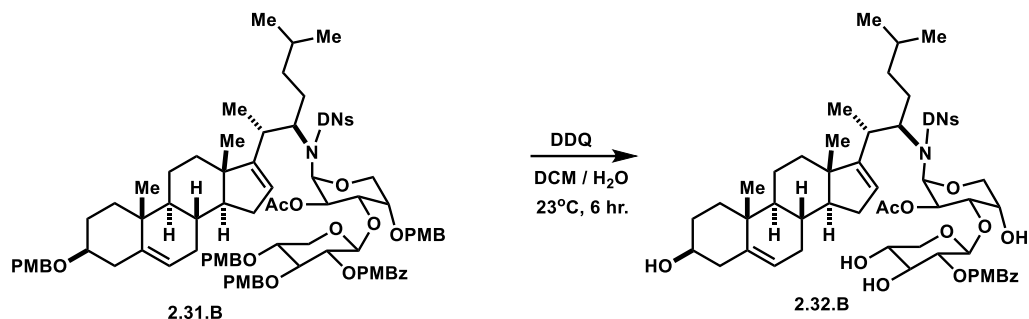


**Figure 2-58.** Compound **2.32.a** ( $\alpha$ -anomer), HRMS (+ESI, 180V, rt: 0.896 min): calcd for  $C_{53}H_{71}N_3O_{18}S + Na^+$   $[M+Na]^+$ : 1092.4357; found 1092.4338, -1.7  $\Delta$  ppm.



**(2S,3R,4S,5R)-2-(((2S,3R,4S,5S)-3-acetoxy-5-((4-methoxybenzyl)oxy)-2-((N-((2S,3R)-2-((3S,9S,10R,13S,14S)-3-((4-methoxybenzyl)oxy)-10,13-dimethyl-2,3,4,7,8,9,10,11,12,13,14,15-dodecahydro-1H-cyclopenta[a]phenanthren-17-yl)-6-methylheptan-3-yl)-2,4-dinitrophenyl)sulfonamido)tetrahydro-2H-pyran-4-yl)oxy)-4,5-bis((4-methoxybenzyl)oxy)tetrahydro-2H-pyran-3-yl 4-methoxybenzoate; (2.32.B):** Compound **2.32.B** ( $\alpha$ -anomer) was prepared through

following a previously reported protocol adapted for use in transforming the starting material, **Compound 2.31.B**.<sup>89</sup> To a 5 ml conical flask containing solid starting material  $\beta$ -anomer glycoside (**Compound 2.31.B**, 16.0 mg, 10.3  $\mu$ mol, 1.0 equiv.) and solid DDQ (11.7 mg, 51.6  $\mu$ mol, 5.0 equiv.) under nitrogen atmosphere at room temperature was added dry DCM (516  $\mu$ l, 20 mM) followed by DI water (100  $\mu$ l). The biphasic reaction turned immediately black and as the reaction proceeded it turned to a brown/orange mixture. Upon complete conversion of starting material by TLC, the reaction was diluted in ethyl acetate (2.0 ml) then quenched with sat.  $\text{NaHCO}_{3(\text{aq})}$  at room temperature. The reaction mixture was transferred to a separatory funnel and diluted with 20 ml of ethyl acetate. The layers were separated and then the organic layer was washed with sat.  $\text{NaHCO}_{3(\text{aq})}$  (5 x 15.0 ml), followed by water (2 x 15.0 ml). The aqueous layers were combined and back extracted with ethyl acetate (2 x 15.0 ml). The organic layers were combined and washed with brine then dried over  $\text{Na}_2\text{SO}_4$ . The drying agent was then removed, and the solvent was removed *in vacuo* to afford a crude yellow/orange paste. The crude material was purified via oven-dried silica column and eluted with a gradient of 1-12.5% methanol in DCM. 5.66 mg of  $\beta$ -anomer glycoside product (**2.32.B**) was obtained as a white solid (51%). Assignment of the  $\beta$ -anomer were made based on characteristic carbon shifts:  $\alpha$ -anomeric carbon at 84.7 ppm,  $\beta$ -anomeric carbon at 99.3 ppm.<sup>120</sup>

**Compound 2.32.B** ( $\beta$ -anomer):  $^1\text{H-NMR}$  (500 MHz, Acetonitrile- $d_3$ ):  $\delta$  8.58 (d,  $J = 2.3$  Hz, 1H), 8.40 (dd,  $J = 8.8, 2.3$  Hz, 2H), 7.92 (d,  $J = 8.3$  Hz, 3H), 6.72 (s, 3H), 5.39 – 5.26 (m, 2H), 5.06 (dd,  $J = 4.0, 1.4$  Hz, 2H), 4.91 (t,  $J = 8.3$  Hz, 2H), 4.83 (d,  $J = 7.6$  Hz, 2H), 4.28 – 4.18 (m, 2H), 4.19 (d,  $J = 2.4$  Hz, 1H), 4.02 – 3.96 (m, 1H), 3.96 – 3.91 (m, 1H), 3.89 (s, 2H), 3.83 (d,  $J = 9.6$  Hz, 1H), 3.72 – 3.58 (m, 2H), 3.40 (tt,  $J = 11, 4.9$  Hz, 1H), 3.37 – 3.33 (m, 1H), 2.33 (d,  $J = 7.4$  Hz, 1H), 2.27 – 2.20 (m, 1H), 2.08 (ddd,  $J = 15, 6.6, 3.3$  Hz, 1H), 2.02 (d,  $J = 11$  Hz, 1H), 1.98 – 1.85 (m, 1H), 1.81 (d,  $J = 12$  Hz, 1H), 1.69 (dd,  $J = 11, 4.5$  Hz, 1H), 1.61 (dd,  $J = 18, 10$  Hz, 1H), 1.55 (s, 2H), 1.51 (d,  $J = 11$  Hz, 0H), 1.34 – 1.20 (m, 1H), 1.07 (s, 2H), 1.06 (d,  $J = 7.1$  Hz, 2H), 0.99 (ddt,  $J = 16, 11, 5.6$  Hz, 1H), 0.83 (s, 2H), 0.61 (d,  $J = 6.6$  Hz, 2H), 0.58 (d,  $J = 6.6$  Hz, 2H), 0.54 – 0.46 (m, 1H).

1272-CAM-VII-81-C22DNsNGlycoside-p\_PROTON\_02

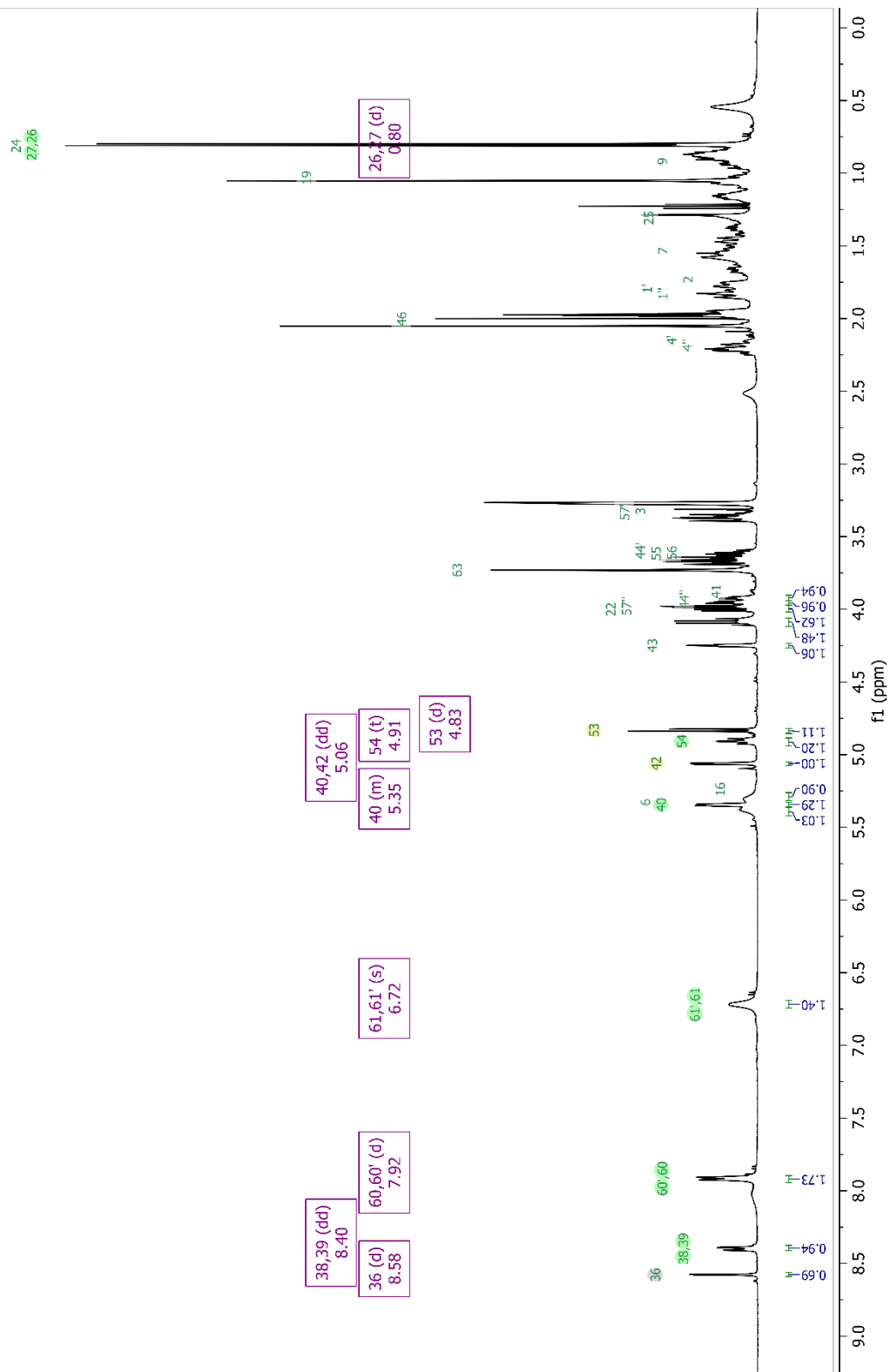


Figure 2-59.  $^1\text{H-NMR}$  of Compound 2.32.b ( $\beta$ -anomer) in acetonitrile- $d_3$ .



**Reaction also performed on a mixture of anomer starting materials; mixture of Compound 2.32.A ( $\alpha$ -anomer) and Compound 2.32.B ( $\beta$ -anomer):**  $^1\text{H-NMR}$  (500 MHz, Acetonitrile- $d_3$ ):  $\delta$  8.64 (d,  $J = 8.9$  Hz, 1H), 8.50 (dd,  $J = 8.9, 2.3$  Hz, 1H), 8.46 – 8.32 (m, 2H), 8.04 (d,  $J = 8.9$  Hz, 2H), 7.94 (d,  $J = 8.4$  Hz, 2H), 7.05 (d,  $J = 8.9$  Hz, 2H), 6.78 (s, 2H), 6.04 (t,  $J = 9.7$  Hz, 1H), 5.46 – 5.29 (m, 2H), 5.02 (dd,  $J = 3.9, 1.4$  Hz, 1H), 4.95 – 4.87 (m, 2H), 4.82 (d,  $J = 7.6$  Hz, 1H), 4.70 (d,  $J = 7.8$  Hz, 1H), 4.60 (d,  $J = 9.5$  Hz, 1H), 4.23 (d,  $J = 3.7$  Hz, 1H), 4.13 – 4.04 (m, 3H), 3.98 – 3.94 (m, 1H), 3.89 (s, 4H), 3.77 (s, 4H), 3.71 – 3.55 (m, 7H), 3.46 – 3.10 (m, 5H), 2.31 – 2.14 (m, 6H), 2.07 (d,  $J = 20$  Hz, 2H), 2.02 – 1.95 (m, 4H), 1.94 – 1.90 (m, 1H), 1.85 (ddt,  $J = 16, 8.3, 4.0$  Hz, 2H), 1.79 – 1.74 (m, 3H), 1.69 (td,  $J = 11, 4.8$  Hz, 1H), 1.65 – 1.58 (m, 4H), 1.57

1249-CAM-VII-71-PMDBprotect-F\_31\_39\_PROTON\_02

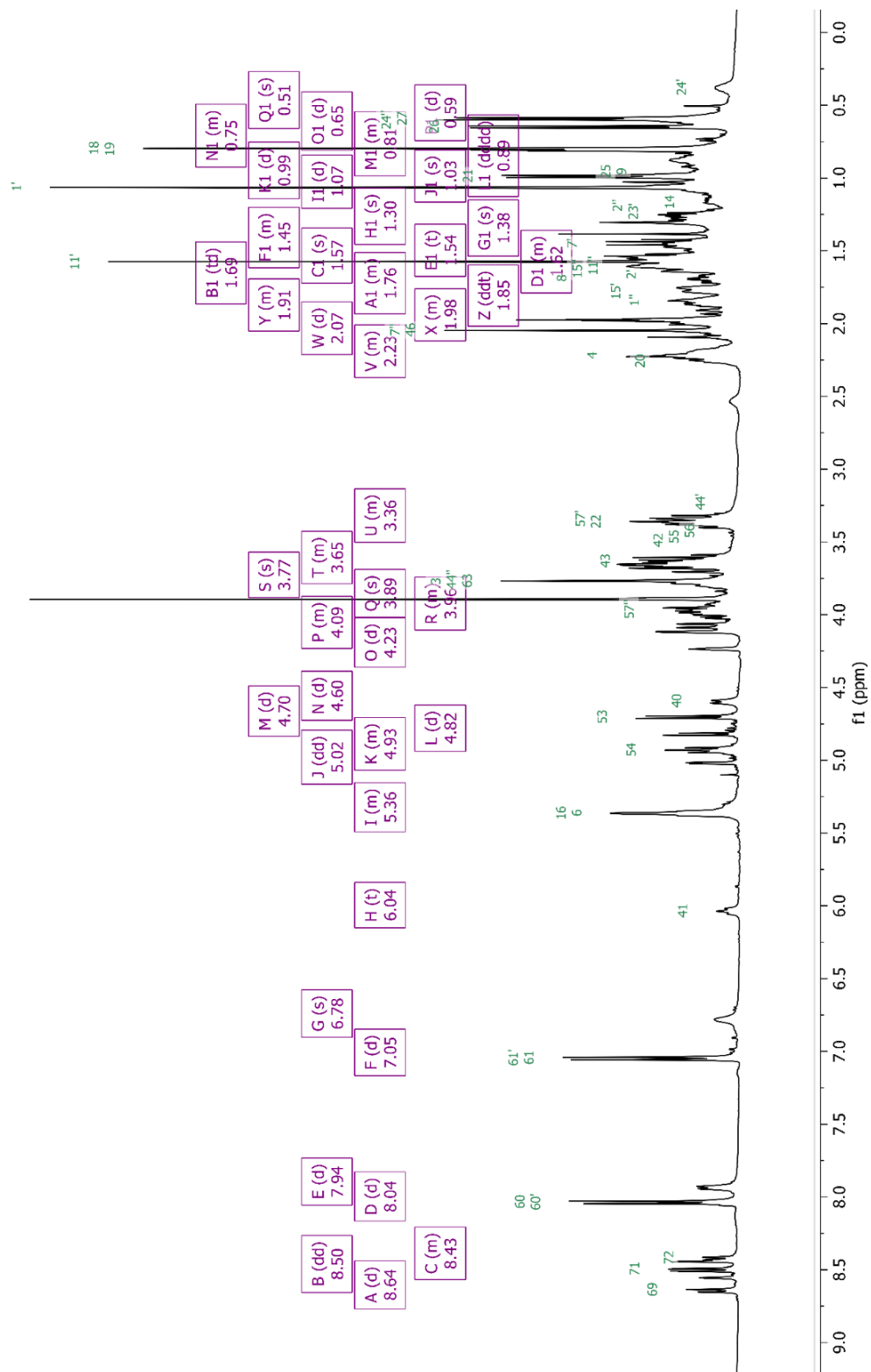
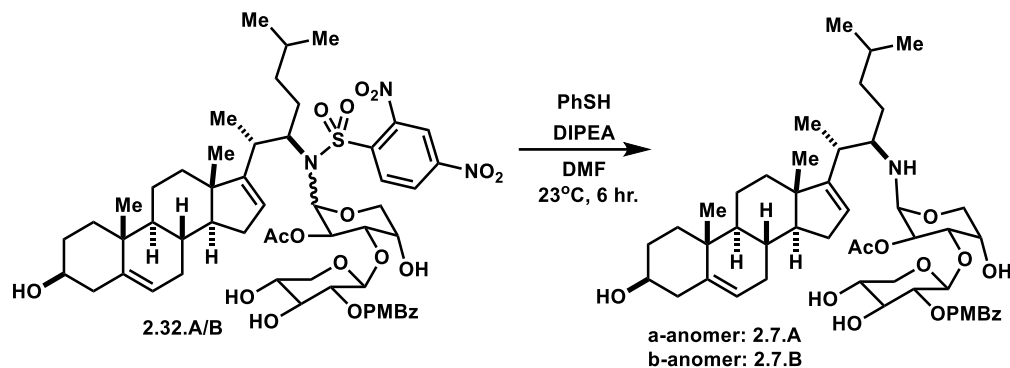


Figure 2-60. <sup>1</sup>H-NMR of the mixture of Compound 2.32.A ( $\alpha$ -anomer) and Compound 2.32.B ( $\beta$ -anomer) in acetonitrile-*d*<sub>3</sub>.



(2S,3R,4S,5R)-2-(((2R,3R,4S,5S)-3-acetoxy-5-hydroxy-2-(((2S,3R)-2-((3S,8R,9S,10R,13S,14S)-3-hydroxy-10,13-dimethyl-2,3,4,7,8,9,10,11,12,13,14,15-dodecahydro-1H-cyclopenta[a]phenanthren-17-yl)-6-methylheptan-3-yl)amino)tetrahydro-2H-pyran-4-yl)oxy)-4,5-dihydroxytetrahydro-2H-pyran-3-yl 4-methoxybenzoate; (2.7.A),

(2S,3R,4S,5R)-2-(((2S,3R,4S,5S)-3-acetoxy-5-hydroxy-2-(((2S,3R)-2-((3S,8R,9S,10R,13S,14S)-3-hydroxy-10,13-dimethyl-2,3,4,7,8,9,10,11,12,13,14,15-dodecahydro-1H-cyclopenta[a]phenanthren-17-yl)-6-methylheptan-3-yl)amino)tetrahydro-2H-pyran-4-yl)oxy)-4,5-dihydroxytetrahydro-2H-pyran-3-yl 4-methoxybenzoate; (2.7.B): Deprotection of **Compound 2.32A/B** ( $\alpha/\beta$ -anomeric mixture) was done with standard conditions.<sup>102</sup> To a translucent yellow solution of starting material glycosides, **Compound 2.32A/B** (2:1  $\alpha/\beta$ -anomeric mixture), (10.2 mg, 9.53  $\mu\text{mol}$ , 1.0 equiv.) in DMF (480  $\mu\text{l}$ , 2.0 mM) at room temperature under nitrogen atmosphere was added thiophenol (6.6  $\mu\text{l}$ , 64.8  $\mu\text{mol}$ , 8.0 equiv.) followed by Hunigs base (13.0  $\mu\text{l}$ , 76.3  $\mu\text{mol}$ , 8.0 equiv.). The solution became dark yellow/orange in color indicating the formation of the Meisenheimer complex. The reaction was stirred at room temperature for 6 hours, then the reaction was diluted with ethyl acetate (10 ml) and transferred to a separatory funnel. The organic layer was then washed with water (3 x 7.0 ml). The aqueous layers were combined and back extracted with ethyl acetate (2 x 7.0 ml). The organic layers were combined and washed with brine then dried over  $\text{Na}_2\text{SO}_4$ . The drying reagent was removed, and the solvent was evaporated *in vacuo* to afford a crude brown paste. The crude material was purified via oven-dried-silica pipet column and eluted with a gradient of 1% to 12.5% methanol in DCM. The desired glycoside products eluted off the column ~10%. The fractions were collected and condensed *in vacuo* to afford 10.7 mg of semi-pure material which was further purified via HPLC to afford ~1.0 mg of pure  $\beta$ -anomer glycoside product (7.5 %). The product was poorly soluble in all organic solvents screened, which likely accounted for the poor overall yield. NMR analysis were performed in a 10:1 solution of acetonitrile- $d_3$ : methanol- $d_3$  due to the poor solubility.

**Compound 2.7.B:**  $^1\text{H-NMR}$  (500 MHz, Acetonitrile- $d_3$ ):  $\delta$  7.99 (d,  $J = 8.6$  Hz, 1H), 6.99 (d,  $J = 8.8$  Hz, 1H), 5.36 (s, 1H), 5.33 (t,  $J = 5.0$  Hz, 1H), 5.28 (s, 1H), 5.10 (d,  $J = 7.1$  Hz, 1H), 4.88 (t,  $J = 8.1$  Hz, 1H), 4.70 (d,  $J = 7.7$  Hz, 0H), 3.95 (dd,  $J = 12, 4.8$  Hz, 0H), 3.84 (s, 1H), 3.75 (d,  $J = 8.1$  Hz, 1H), 3.09 (t,  $J = 6.9$  Hz, 1H), 2.52 (s, 1H), 1.62 (d,  $J = 7.4$  Hz, 1H), 0.89 – 0.79 (m, 6H).

<b>Table 5</b>			Ato	Chemic	HSQ	Ato	Chemic	HSQ	Ato	Chemic	HSQ
m	al Shift	C	m	al Shift	C	m	al Shift	C	m	al Shift	C
1 C	37.2	1	13 C	47.4		25 C	33.2	25	55 C	71.2	55
H2	1.84	1	14 C	57.4	14	H	1.15	25	H	3.56	55
2 C	28.4	2	H	1.27	14	26 C	13.2	26	56 C	70.9	56
H2	1.97	2	15 C	31.0	15', 15"	H3	0.87	26	H	3.34	56
3 C	83.4	3	H'	1.76	15	27 C	13.2	27	57 C	62.5	57', 57"
H	3.55	3	H''	1.97	15	H3	0.87	27	H'	3.44	57
4 C	39.2	4', 4"	16 C	121.1	16	40 C	129.7	40	H''	3.47	57
H'	2.41	4	H	5.28	16	H	5.33	40	58 C	164.7	
H''	2.26	4	17 C	159.6		41 C	117.7	41	59 C		
5 C	141.2		18 C	19.3	18	H	5.11	41	60 C	131.8	60
6 C	120.7	6	H3	1.02	18	42 C	53.0	42	H	7.99	60
H	5.37	6	19 C	18.6	19	H	3.75	42	60'	131.8	60'
7 C	31.6	7', 7"	H3	0.97	19	43 C	70.2	43	C	113.8	61'
H'	1.46	7	20 C	36.2	20	H	3.75	43	H	7.99	60'
H''	1.97	7	H	2.08	20	44 C	65.6	44', 44"	61 C	113.0	61
8 C	30.28	8	21 C	12.7	21	H'	3.27	44	H	6.99	61
H	1.57	8	H3	1.62	21	H''	3.97	44	61'	113.8	61'
9 C	50.52	9	22 C	74.6	22	45 C	167.6		C	6.99	61'
H	0.95	9	H	3.56	22	46 C	21.9	46	H	6.99	61'
10 C			23 C	25.8	23	H3	1.89	46	62 C	163.6	
11 C	20.5	11	H2	1.41	23	53 C	101.9	53	63 C	55.1	63
H2	1.52	11	24 C	34.8	24	H	4.70	53	H3	3.85	63
12 C	20.8	12	H2	1.65	24	54 C	74.1	54			
H2	1.52	12				H	4.89	54			

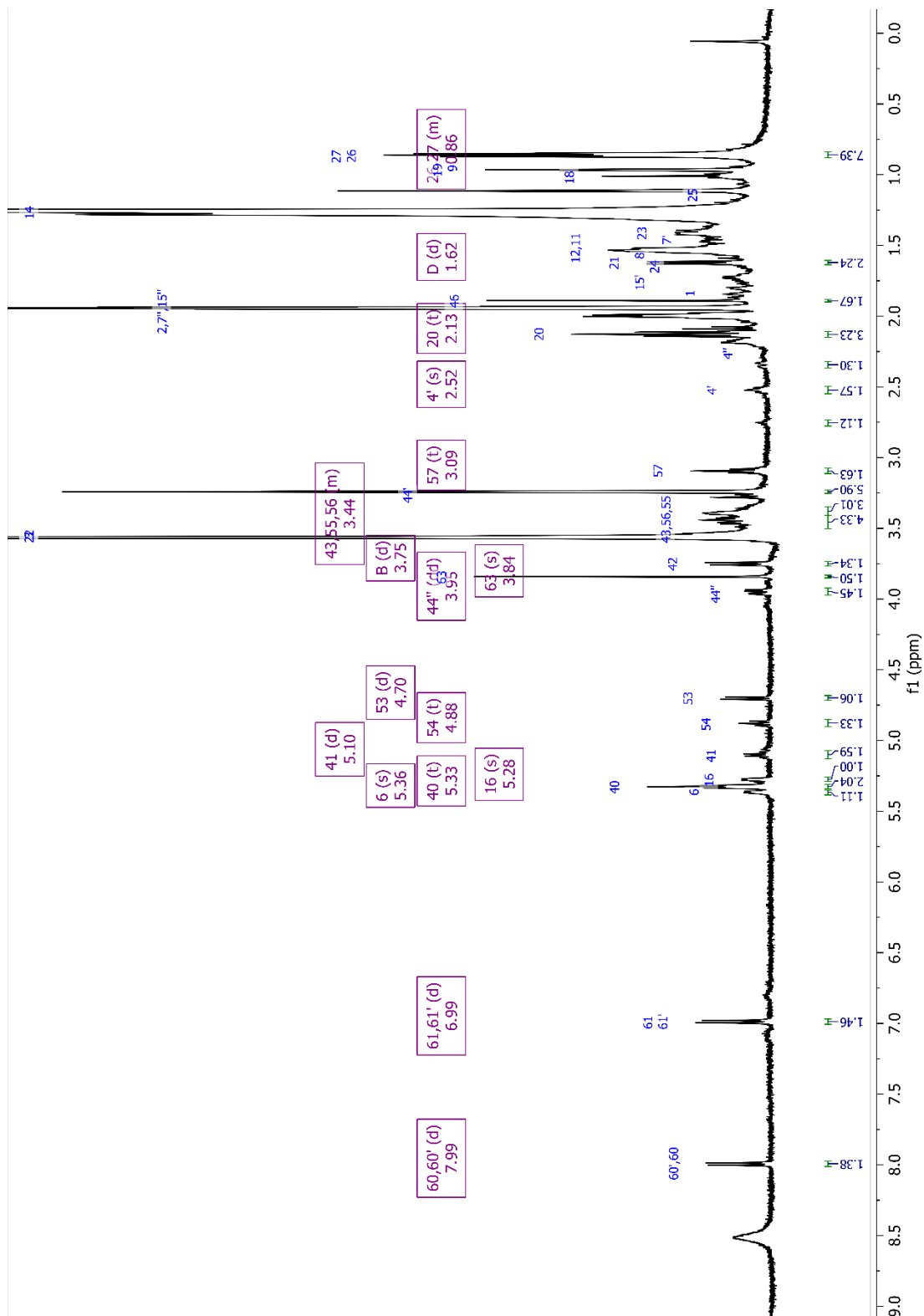


**Figure 2-61.** <sup>1</sup>H-NMR of C22-N-Glycoside OSW-1 derived analog (2.33) in 10:1 acetonitrile-*d*<sub>3</sub>/methanol-*d*<sub>4</sub>.

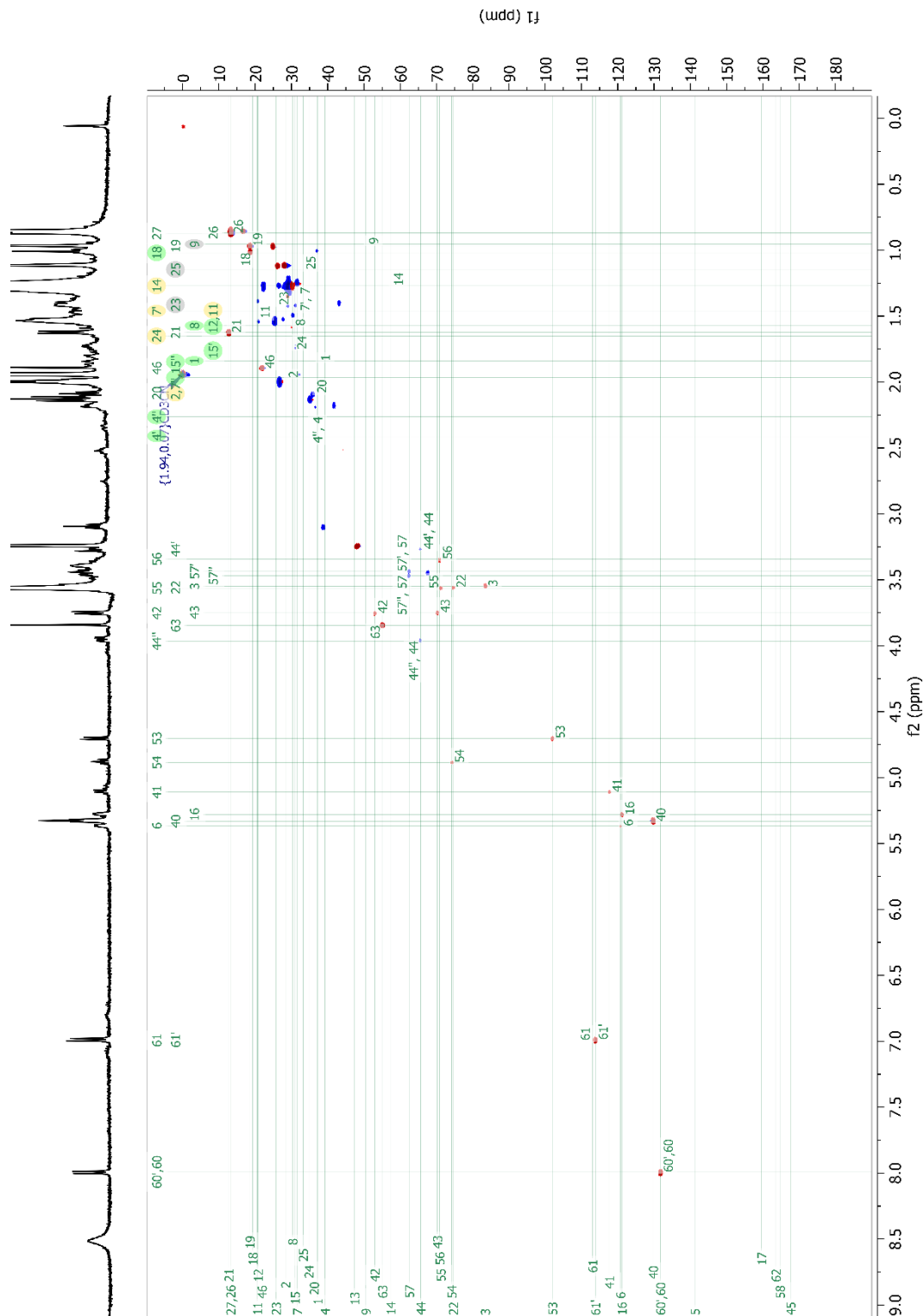


**Figure 2-62.** HSQC of C22-N-Glycoside OSW-1 derived analog (**2.33**) in 10:1 acetonitrile- $d_3$ /methanol- $d_4$ .



### **Chapter 3: A convenient two-component approach to functionalized 22-aminosterols**

**Abstract:** Sterol scaffolds containing nitrogen functionality provide synthetic handles for derivation, affect chemical properties, and can produce useful alteration in the biological activities of structurally complex molecules. The methods and approaches to rationally design aminosterol scaffolds through the introduction of one or more nitrogen atoms directly on the steroidal side-chain component are currently limited. Herein, a direct, two-component approach to the stereoselective formation of either C16-C17-ene-22-aminosterol or the 17-hydroxyl-22-aminosterol has been developed. The elaboration to 22-aminosterols combines *exo*-olefin steroidal scaffold with N-aryl sulfonyl alkyl imines through an imino-ene/aza-Prins reaction. The versatile reaction is highly tunable through use of specific Lewis acids and tolerates the introduction of alkyl side chains possessing varying electronic N-aryl substituents. The convenience and versatility of this directional two-component approach to both functionalized 22-aminosterols and/or 17-hydroxy-22-aminosterols provides synthetic access to derivation for further biological elucidation. The reported 22-aminosterols provide useful synthetic handles for the synthesis of complex molecular compounds, such as OSW-1.

**Contributions:** Gianni Manginelli assisted with the synthesis of steroid and N-aryl sulfonyl alkyl imine starting materials and performed the aza-Prins reaction on *p*Ns-N-pentylimine for his capstone research project.



### **3.1. Introduction**

This chapter details further investigation into the synthetic methodology and approaches to aminosterols through imino-ene/aza-Prins reactivity of pregnadiene. As discussed in **Chapter 2:**, making steroidal 22-amine functionality is a critical part of our proposed synthesis of new OSW-1 derived compounds for drug development, but the synthesis of 22-aminosterols presented an unexpected challenge (**Section 2.2.4.4**). Much to my surprise, there are few reported methods to establish amine functionality on the side chain of sterols.<sup>78-83</sup> The lack of established methods granted an opportunity to pioneer methods and approaches to aminosterols that could be utilized in the synthesis of complex molecular scaffolds such as, OSW-1 derived analogs.

Herein, a practical and convenient imino-ene/aza-Prins reaction method to directionally synthesize functionalized C16-C17-ene-22-aminosterols and/or 17-hydroxy-22-aminosterols is reported. The reaction combines aryl sulfonyl N-alkyl imines with C17-C20 olefin pregnadiene to make, in one high yielding step, 22-aminosterols. A previously reported computational study of the imino-ene reaction,<sup>152</sup> was the basis of our investigation into Lewis acid mediated imino-ene/aza-Prins reactivity. The developed method allows for switchable synthesis of either C16-C17-ene-22-aminosterols or 17-hydroxy-22-aminosterols depending on the chosen Lewis acid. To explore the mechanism and increase the synthesis scope of this reaction on complex molecular scaffolds, an investigation into the formation and reactivity of different aryl sulfonyl N-alkyl imines was performed. Collectively, this body of work provides convenient access to aminosterols with synthetically useful functional handles for further derivation and for

use in the synthesis of complex molecular targets, including OSW-1-derived analog compounds.

### **3.1.1. Importance of developing approaches and methods toward aminosterol scaffolds**

Sterols with amine-containing side chains are present in many natural products and synthetically made compounds that feature numerous biological activities, including antibiotic agent tomatidine, the antifungal agents solacongestidine and solafloridine, and toxic agents like solanine and  $\alpha$ -chaconine.<sup>81,82,122,153</sup> These natural product aminosterols have inspired the synthesis and development of amino-modified steroids to identify novel compounds of pharmacological value.<sup>81,82,122,153</sup> The replacement of heteroatoms, especially nitrogen to steroidal scaffolds, provide synthetic handles for derivation, affect chemical properties, and can produce useful alteration in biological activities.<sup>81,82,122,153</sup> Rationally designed synthetic aminosterols possess great potential as therapeutic agents, but the methods and approaches to introduce one or more nitrogen atoms directly on the steroidal side-chain component are currently limited.<sup>56,78-80,154,155</sup>

Through synthesis of the C22-*N*-glycoside OSW-1 analog (**Compound 2.7**), a novel approach to 22-aminosterol was reported (**Section 2.2.4.4**). The desired C22-amine functionality was obtained by first reacting pregnadiene with 4-methyl pentanal in the presence of dimethyl aluminum chloride, under ene reaction conditions, to generate 22-hydroxysterol (**Section 2.2.4.2,**

**Figure 2-7**). Then through a series of oxidations and reductions the desired functionalized 22-aminosterol was generated (**Section 2.2.4.4,**

**Figure 2-9).** The difficulty in creating the desired C22-amine functionality was considerable (see **Section 2.2.4.4** and **2.3**), and this difficulty provides the opportunity to develop new methodology to concisely synthesize the desired 22-aminosterol. Through use of an imino-ene/aza-Prins reaction, pregnadiene can be reacted with functionalized alkyl imines in the presence of different Lewis acids, to conveniently access functionalized aminosterols. Depending on the chosen Lewis acid, functionalized 22-aminosterols and/or 17-hydroxy-22-aminosterols can be rapidly generated. This reaction is versatile, proceeds in the presence of many different Lewis acids and tolerates various imine functionality. Herein, a convenient two-component approach to functionalized 22-aminosterol and/or 17-hydroxy-22-aminosterol scaffolds is reported.

### **3.1.2. The ene and Prins reactions**

The ene and Prins reactions are synthetically powerful methods for C-C bond formation that are mechanistically distinct, but both reactions are often operable in similar reaction settings.<sup>156–158</sup> An ene reaction occurs between an allylic hydrogen and a  $\pi$ -bond system (i.e. alkene, alkyne, carbonyl) that are merged in a pericyclic, concerted fashion to transform one  $\sigma$  bond and two  $\pi$  bonds into two new  $\sigma$  bonds and one new  $\pi$  bond.<sup>158</sup> This pericyclic reaction is analogous to the Diels-Alder reaction although the activation energy required to initiate an ene reaction is significantly higher.<sup>158</sup> Due to the higher activation energy, ene-reaction conditions are typically carried out in the presence of a Lewis acid.<sup>158</sup> The Lewis acid coordinates to the enophile to lower the energy of the HOMO to facilitate a pericyclic reaction.<sup>158</sup> A Prins reaction occurs under the same circumstances; an allylic hydrogen reacts with a  $\pi$ -bond system to transform one  $\sigma$  bond and two  $\pi$  bonds into two new  $\sigma$  bonds and one new  $\pi$  bond.<sup>156–158</sup> However, the Prins

reaction is not pericyclic and therefore not concerted.<sup>156–158</sup> The Prins reaction occurs stepwise through a carbocation intermediate which is quenched via deprotonation to form a new  $\pi$  bond.<sup>158–160</sup> However, the carbocation can be trapped by nucleophiles to form useful synthetic functional handles. The ene and Prins reaction mechanisms can occur with the same reactants under the same reaction conditions, and can occur within one reaction flask.<sup>156–158</sup> Specific modification of the reaction conditions, including temperature effects, the addition of Lewis acids, or addition of coORDinating adducts,

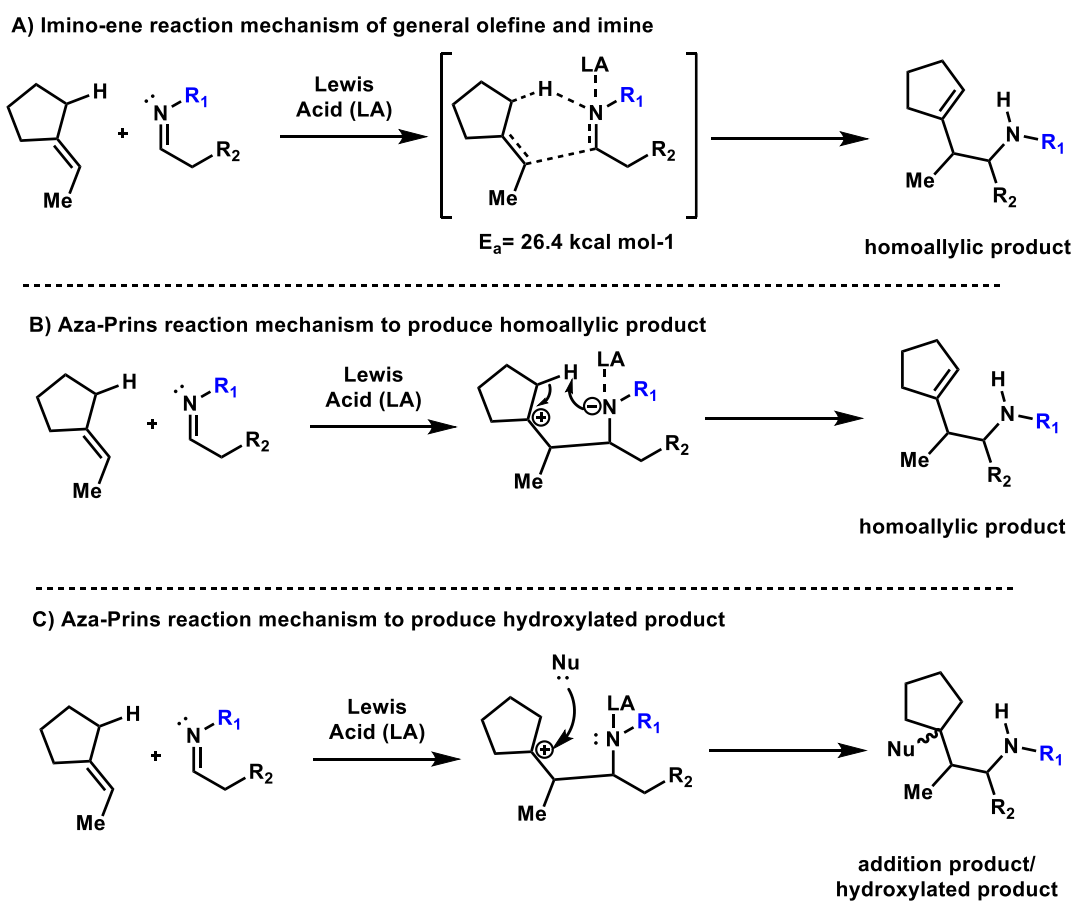


**Figure 3-1.** Proposed mechanistic pathways of the imino-ene (A) and aza-prins (B and C) reactions to obtain homoallylic and hydroxylated 22-aminosterol products. Activation energies computationally calculated by Yang, Q., et. al.<sup>152</sup>

can be employed to ensure that one reaction (i.e. ene versus Prins reaction) predominates to generate a desired product.<sup>156–158,161</sup>

There are different variations of the ene and Prins reactions based on the reactants, such as, oxo-ene/oxo-Prins reactions which react ketones or aldehydes or the imino-ene/aza-Prins reaction which react imines.<sup>162</sup> These two variations are operably and mechanistically similar with only the difference of the reactants.<sup>152,158,162–164</sup> A thorough and detailed theoretical investigation of Lewis acid mediated imino-ene reactivity was reported by Yang, Q., et. al.<sup>152</sup> In this report, the ene mechanism is computationally examined; energetics of each transition state and intermediates as well as influencing factors of catalysts, substituents, and solvents are taken into consideration. This report provided an in-depth computational analysis of the effects of Lewis acids, electron-withdrawing (EWG), and electron-donating groups (EDG) on the imino-ene mechanistic route. By inference, we applied these computational results to our investigation of the imino-ene/aza-Prins reaction.

As shown in **Figure 3-1**, three mechanisms are possible in our proposed reaction to combine an exo-cyclic olefin and functionalized imine: A) a concerted imino ene pathway to produce homoallylic amines, B) a stepwise aza-Prins mechanism with a coORDinating Lewis acid, or C) a stepwise aza-Prins mechanism with nucleophilic addition of water.<sup>152</sup> The imino-ene reaction goes through a cyclic transition state and stereochemical outcomes are established based on formation of that transition state (**Figure 3-1, Mechanism A**).<sup>152,158</sup> In contrast, the stepwise aza-Prins mechanism creates an intermediate possessing zwitterionic character, as shown by carbocation and anionic nitrogen (**Figure 3-1, Mechanism B**).<sup>165,166</sup> Due to the zwitterionic character, stereochemical outcomes are uncertain.<sup>166</sup> The stepwise Prins mechanism has two potential outcomes depending on the selected Lewis acid. When a coORDinating Lewis

acid that does not form a formal amino metallic bond is used, the nitrogen can perform an intramolecular deprotonation to quench both charges and afford homoallylic amines. When a formal amino metallic bond is formed, a carbocation intermediate is formed and the cation can be trapped by a nucleophilic anion that was ejected by the Lewis acid, which is then hydrolyzed during work up (**Figure 3-1, Mechanism C**).<sup>158,162,165</sup> These mechanisms are not mutually exclusive; it is possible that both the imino-ene and aza-Prins mechanisms occur within one reaction pot, therefore leading to the formation of multiple products.<sup>156-158</sup> The conditions of the reaction can guide which mechanism predominates and therefore which potential product (i.e. homoallylic or hydroxylated products) predominates

### 3.1.3. Lewis acid effects on the imino-ene and aza-Prins reactions

The role of the Lewis acid to catalyze both the imino-ene and the aza-Prins reactions is through coORDination to the imine lone pair, thereby rendering the imine carbonyl carbon more electrophilic.<sup>152</sup> In the reported computational analysis of the imino-ene reaction,<sup>152</sup> the influence of various Lewis acids on the activation energy and on the electronics of the transition state are examined. The electronics of the transition state vary based on the induced partial positive and negative charges (i.e. zwitterionic character).<sup>152</sup> Intuitively, an inverse relationship of the Lewis acid's effect on the energy barrier and its effect on zwitterionic character within the ene reaction was proposed by Yang, Q., et. al.;<sup>152</sup> Lewis acids that induce greater zwitterionic character have low activation energies (Lewis acids calculated: Al(OMe)<sub>3</sub>, SnCl<sub>2</sub>, AlMe<sub>2</sub>O, SnCl<sub>4</sub>, YCl<sub>3</sub>, BCl<sub>3</sub>, GaCl<sub>3</sub>, AlCl<sub>3</sub>),<sup>152</sup> Lewis acids that induce minimal zwitterionic character have high activation energies

(Lewis acids calculated: TiCl<sub>4</sub>, ZnCl<sub>2</sub>, MgCl<sub>2</sub>, AlMe<sub>2</sub>Cl, HCOOAg, HCOOCu, AlMe<sub>3</sub>, CuCl).<sup>152</sup>

The extent to which the reaction mechanism could be influenced toward the aza-Prins reaction mechanism is thought to be dependent on two properties of the Lewis acid: 1) the leaving group ability of its substituents in order to form a formal bond with the nitrogen,<sup>167,168</sup> and 2) orbital overlap with the nitrogen of the selected N-aryl sulfonyl alkyl imine.<sup>163,164</sup> A formal amino-metallic bond between the nitrogen and the selected Lewis acid (**Figure 3-1; Mechanism C**) prevents the imino-ene reaction mechanism by preventing intramolecular deprotonation and forcing a non-paracyclic reaction mechanism. In order for a formal amino-metallic bond to form, the Lewis acid must have an orbital in which the nitrogen lone pair can occupy. The ejected leaving group of the Lewis acid, if nucleophilic, can attack the carbocation carbon and, if labile, the newly added substituent can then be hydrolyzed during aqueous work up.<sup>162</sup> The orbital overlap between the selected Lewis acid and the nitrogen delves into hard-soft acid-base theory (HSAB).<sup>163,164</sup> HSAB theory suggests that *hard* Lewis acids will preferentially bond to *hard* atoms, and *soft* Lewis acids will preferentially bond to *soft* atoms.<sup>163,164</sup> The periodic trend of *hard* and *soft* properties is that hardness increases along a period but decreases along a group (i.e. fluorine is the *hardest* atom and francium is the *softest*).<sup>163,164</sup> More specifically, a *hard* atom will have a larger HOMO/LUMO gap than a *soft* atom, and atoms with similar HOMO/LUMO gaps have beneficial orbital overlap.<sup>163,164</sup>

Different imino electron-donating groups or electron-withdrawing groups affect the atomic-HOMO/LUMO gap of the nitrogen and can be finely tuned to facilitate optimal orbital overlap with the chosen Lewis acid.<sup>152,158,163,164</sup> EDG render the imine carbonyl

carbon more electron dense, increasing the atomic-HOMO/LUMO gap, and increasing the activation energy required for the imino-ene and aza-Prins for the reaction to occur.<sup>152,158</sup> EWG render the imine carbonyl carbon less electron dense with enhanced electrophilicity, decreasing the atomic-HOMO/LUMO gap, and lowering the activation energy.<sup>152,158</sup> These observations within the literature in combination with the computational studies on the imino-ene reaction by Yang, Q., et. al.<sup>152</sup> provided the theoretical foundation to develop an imino-ene/aza-Prins method to form aminosterols.

## **3.2. Results**

### **3.2.1. Atypical synthesis of functionalized N-alkyl aryl sulfonyl imines**

To develop the new imino-ene/aza-Prins approach to aminosterols, a better route to functionalized N-aryl alkyl imines also needed to be developed. Aryl imines generated from aromatic aldehydes are easy to prepare but alkyl imines are much more difficult to synthesize due to their high reactivities.<sup>109,169,170</sup> Initial attempts to synthesize the desired N-aryl alkyl imines reacted alkyl aldehydes with toluene sulfonamide in the presence of strong Lewis acids such as  $\text{BF}_3\text{-Et}_2\text{O}$  or  $\text{TiCl}_4$ ; no desired product was observed. Formation of the desired N-aryl alkyl imine required an approach with more finesse. As shown in **Figure 3-2**, a two-step synthetic approach to imine formation was employed.<sup>170</sup> The general reaction combines aryl sulfonyl amides with alkyl aldehydes to generate aminals in an acidic aqueous reaction environment. The aminal is then transformed into the desired functionalized alkyl imine under biphasic basic conditions. Preliminary results were obtained by reacting toluene sulfonamide, sodium toluene sulfinate, and pentylaldehyde in a 1:1 ratio of formic acid to water to generate bis-tosyl-N-pentylaminal. This aminal was then transformed in the presence of saturated sodium bicarbonate to



produce the desired *N*-sulfonamide alkyl imine (**Figure 3-2; Entry A**) at a reproducible 75% yield. The majority of iminals made were shelf stable over multiple weeks and then could be converted to the desired imine through vigorously stirring in biphasic basic conditions for 2 hours. Following an aqueous work up, the imine was condensed down and immediately ready for use in the imino-ene/aza-Prins reaction.

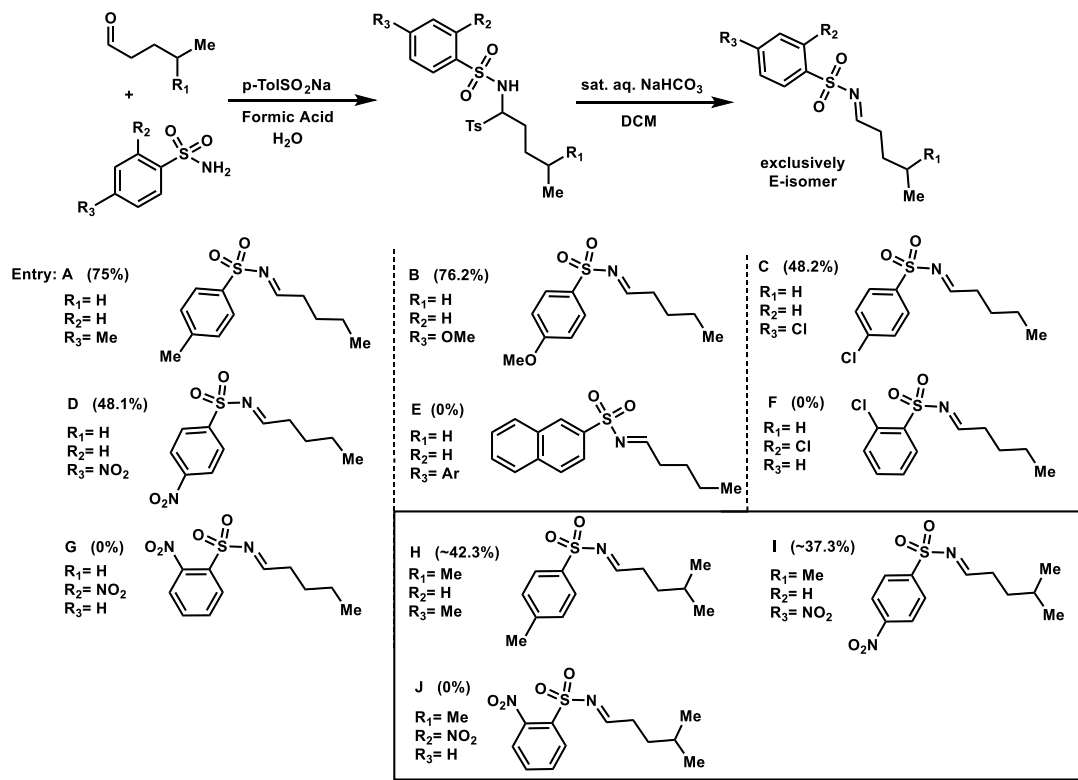


**Figure 3-2.** Formation of functionalized *N*-aryl alkyl imines of various electron donating and electron withdrawing properties. Isohexylimine yields (**Entries H-J**) are reported after two steps from isohexanol.

The literature source of this reaction investigated a variety of alkyl aldehydes reacting with toluene sulfonamide to produce a library of functionalized alkyl imines.<sup>170</sup> These alkyl aldehydes ranged from cyclic and straight chain alkyl groups to aromatic and sterically-encumbered alkyl groups.<sup>170</sup> In Order to develop methods for the generation of complex, functionalized 22-aminosterols, various *N*-aryl groups with differing electron

withdrawing (EWG) or electron donating groups (EDG) needed to be incorporated in the N-aryl alkyl imines. Following the initial satisfactory result in synthesizing Nosyl-N-pentylimine, multiple aryl sulfonyl N-alkyl imines of varying electronics were generated, as shown in **Figure 3-2**. In all cases, only a single geometric isomer, assigned as the E-isomer, was observed, as is consistent with the literature.<sup>170</sup> As an overview, only *para* substituted aryl sulfonamides were tolerated. *Ortho*- or *meta*- substituted aryl sulfonamides did not form the corresponding imines. Electron rich aryl sulfonamides were sluggish to form the amins but rapidly formed the corresponding imines, whereas electron deficient aryl sulfonamides rapidly produced the amins but were slow to form the corresponding imines.

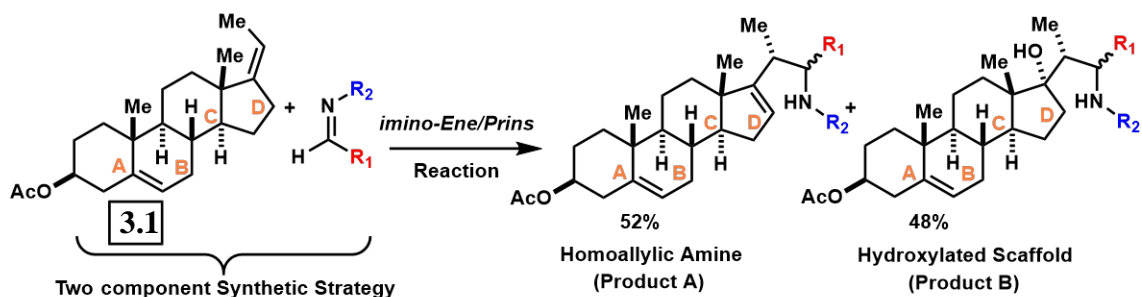
Formation of electron rich anisole aryl sulfonamides (**Figure 3-2; Entry B**), was sluggish and required extended reaction time lengths but did produce sufficient amounts of aminal. The aminal rapidly transformed into its corresponding imine, anisole sulfonyl N-pentylimine (**Entry B**). Formation of electron deficient aryl sulfonamides (**Entries C, D, I, and J**) had the opposite trend; aminal formation occurred rapidly whereas imine formation was sluggish in comparison to the tosyl imine (**Entry A**). Interestingly, *ortho* substituted aryl sulfonamides failed to produce corresponding amins (**Figure 3-2; Entries F, G, and J**). These results indicate that aromatic substitution patterns hinder aminal formation.

The results of this study on N-aryl sulfonamide alkyl imine formation suggests electron density of the aryl sulfonamides directly impact the yields of the corresponding imine formation. Sulfonamides consisting of higher electron density (**Figure 3-2; Entries A and B**) afforded higher yields than electron deficient sulfonamides (**Figure 3-2;**

**Entries C, D, I, and J).** Additionally, *ortho*-substituted aryl sulfonamides failed to form the amination product, likely due to steric effects. With synthetic access to a variety of N-alkyl aryl sulfonyl imines, the study continued with generation of 22-amino cholesterol derivatives through the imino-ene/aza-Prins reaction.

### 3.2.2. Two-component approach to functionalized 22-aminosterols

A) Preliminary Imino-Ene results with 97% conversion of starting materials.



B) 22-amino cholesterol and spiro-E-ring azasteroidal products generated

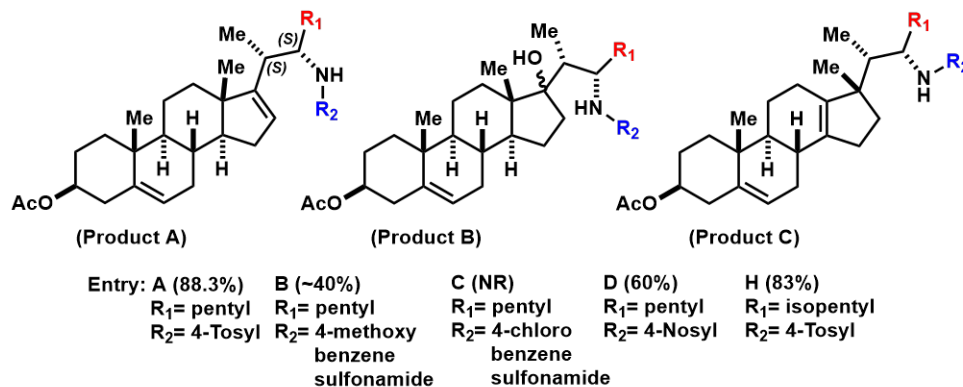


**Figure 3-3. A.** Preliminary imino-ene/aza-Prins reaction using  $\text{BF}_3\text{-Et}_2\text{O}$  with 97% conversion of pregnadiene to hydroxylated and homoallylic 22-aminosterol scaffolds. **B.** Mixture of homoallylic, hydroxylated, and rearranged products afforded during the reaction of various imines to pregnadiene in the presence of  $\text{BF}_3\text{-Et}_2\text{O}$ .

Having established a reliable synthetic approach to both protected pregnadiene (Section 2.2.3) and N-aryl sulfonamide alkyl imine (Section 3.2.1), development of an imino-ene/aza-Prins reaction toward 22-aminosterols commenced. Initial attempts reacted protected pregnadiene (Figure 3-3; Compound 3.1) with N-tosyl pentylamine (Figure 3-2; Entry A) in the presence of  $\text{BF}_3\text{-Et}_2\text{O}$  at cryogenic temperatures to produce

a mixture of both homoallylic 22-aminosterols (54% yield, **Figure 3-3; Product A**) and 17-hydroxy-22-aminosterols (48% yield, **Figure 3-3; Product B**). With satisfactory preliminary results, various N-aryl sulfonamide alkyl imines (**Figure 3-2**) were subjected to these imino-ene/aza-Prins conditions. Three products were formed from the imino-ene/aza-Prins reactions in various ratios (**Figure 3-3**), homoallylic aminosterols (**Product A**), 17-hydroxyl-22-aminosterols (**Product B**), and Wagner-Meerwein rearranged aminosterols (**Product C**). The imino-ene/aza-Prins reaction is stereoselective, producing only C20(*S*) and C22(*S*) stereochemistry. Stereochemical assignments determined by 1D and 2D NMR comparison to previously synthesized 22-aminosterols (**Section 2.2.4.4**) as well as crystal structures of the homoallylic aminosterols (**Product A**). The production of 17-hydroxyl-22-aminosterol (**Figure 3-3; Product B**) as well as Wagner-Meerwein rearranged aminosterol (**Product C**), indicated carbocation formation through the aza-Prins mechanistic pathway. Upon nucleophilic attack of the activated imine by the exo-olefin of pregnadiene (**Compound 3.1**), the carbocation is localized to the C17-position. C18 methyl group can then undergo a 1,2-rearrangement (i.e Wagner-Meerwein rearrangement). The resulting C13 carbocation is quenched upon workup to produce the C13-C14 endo-olefin aminosterol (**Product C**). Alternatively, the C17 carbocation is quenched upon aqueous workup to form the 17-hydroxyl-22-aminosterol (**Product B**). It was not clear whether the homoallylic aminosterols (**Product A**) were also formed through the aza-Prins mechanistic pathway, or if it proceeded via the imino-ene mechanism.

Of the aryl sulfonyl N-alkylimines tested (**Figure 3-2, Entries A-D, and H**) only 4 provided products (**Figure 3-3**). Toluene sulfonyl N-pentylimine (**Entry A**) afforded the

highest yield at 88% product formation, with a near 1:1 ratio of **Products A** and **B**, no trace amounts of **Product C** were observed. **Entries B, D, and H** afforded approximately similar ratios: nearly 1:1 of **Products A** and **B** with trace amounts of rearranged **Product C**. In comparison to an electron rich system, anisole sulfonyl N-pentylimine (**Entry B**) was particularly interesting because it afforded significantly more hydroxylated sterol amine (**Products B**) than homoallylic amine (**Products A**). No azacycle E-ring was observed in any of the imino-ene/aza-Prins reactions. This is in contrast to the analogs oxo-ene reaction between pregnadiene (**Compound 2.14**) and alkyl aldehydes, formed both four and five membered heterocyclic E-rings.<sup>84</sup>

### **3.2.3. Probing mechanism of imino-ene/aza-Prins reaction through Lewis acid screening**

The properties of different Lewis acids were predicted, via computational modeling, to directly influence the activation energy and zwitterionic character of the transition states within the imino-ene reaction (**Section 3.1.3**).<sup>152</sup> The extent to which the reaction mechanism could be influenced is thought to be dependent on two properties of the Lewis acid: 1) the leaving group ability of its substituents,<sup>167,168</sup> and 2) orbital overlap with the nitrogen of the selected N-aryl sulfonamide alkyl imine.<sup>163,164</sup> My hypothesis that Lewis acids with a good leaving group and greater orbital overlap with the nitrogen would establish a formal bond with the selected N-aryl sulfonamide alkyl imine, thereby leading to carbocation formation through the aza-Prins reaction mechanism seems plausible (**Figure 3-1**). The putative controlling influence of Lewis acids was experimentally tested in aminosterol-forming imino-ene/aza-Prins reaction between acetylated pregnadiene (**Compound 3.1**) and N-tosyl pentylamine (**Figure 3-2, Entry A**).

Screening of the Lewis acids was done under standard reaction conditions; toluene sulfonyl N-pentylimine (**Figure 3-2, Entry A.**) was reacted with various Lewis acids, either 1 or 3 equivalence, at cryogenic temperatures followed by slow addition of acetylated pregnadiene (**Compound 3.1**). Reactions quenched with a 1:1 mixture of

**Table 3-1.** Effect of various Lewis acids on product ratios formed from imino-Ene and aza-Prins mechanism pathways, arranged in Order of increasing zwitterionic character (CT/e value) as calculated by Yang, Q., et. al.<sup>152</sup>

	Entry	Catalyst	Eq.	Product Ratio (A : B & C)	
← Increasing CT/e value	1	CuCl	1	NR	methanol and
	2	CuCl	3	NR	deionized water at
	3	ZnCl <sub>2</sub>	3	NR	cryogenic
	4	TiCl <sub>4</sub>	1	degradation	temperatures.
	5	BF <sub>3</sub> Et <sub>2</sub> O	1	NR	Product ratios
	6	BF <sub>3</sub> Et <sub>2</sub> O	3	2:1	were determined
	7	PdCl <sub>2</sub>	0.05	NR	by percent areas
	8	AlCl <sub>3</sub>	1	2:1	of product peaks
	9	AlCl <sub>3</sub>	3	1:33	on C-18 reverse
ncalculated CT/e value	10	FeCl <sub>3</sub>	1	2:1	phase semi-prep
	11	FeCl <sub>3</sub> :TMSCl (3:1)	3	1.5:1	column. BF <sub>3</sub> -
	12	Cu(OTf) <sub>3</sub>	3	NR	
	13	Sc(OTf) <sub>3</sub>	3	4:1	

Et<sub>2</sub>O (3 equiv.) was consistently shown to produce a ratio of ~0.52:0.48 of **Products A:B** in several experimental replications. The published computational modeling studies of the imino-ene/aza-Prins reaction predicted that CuCl would induce the least amount of zwitterionic character within the reaction mechanism, thereby favoring the imino-ene mechanism.<sup>152</sup> In contrast, AlCl<sub>3</sub> was expected to induce the most amount of zwitterionic character, leading to the aza-Prins mechanism.<sup>152</sup> Other Lewis acids were chosen based on availability and literature precedent (**Table 3-1**).<sup>171-177</sup> Interestingly, not all Lewis acids investigated promoted product formation which prevents clear correlation between

the computationally calculated values and the mechanism pathway from being determined.<sup>152</sup> Of the six Lewis acids tested with calculated CT/e values, only two of the acids afforded product: the control, BF<sub>3</sub>-Et<sub>2</sub>O, and the outerlimit Lewis acid, AlCl<sub>3</sub>.<sup>152</sup> The Lewis acid predicted to induce the most zwitterionic character within the reaction mechanism, AlCl<sub>3</sub>, did in fact produce the highest ratio of Product B to Product A (33:1, **Table 3-1; Entry 9**). Furthermore, scandium (III) triflate produced the lowest ratio of Product B to Product A (0.27:1, **Table 3-1; Entry 13**). The computationally calculated activation energy and CT/e value of scandium (III) triflate was not reported<sup>152</sup> but it is a borderline-*hard* acid with a relatively poor leaving group in comparison to metal halides.<sup>163,164</sup> The Lewis acid screening did establish reaction conditions capable of selectively producing either the C16-C17-ene-22-aminosterol (**Product A**) or the 17-hydroxyl-22-aminosterol (**Product B**) in high yields through varying the Lewis acid in the reaction.

### **3.3. Discussion**

The imino-ene/aza-Prins two-component approach to functionalized 22-aminosterols provides convenient access to the OSW-1 cholestane scaffold through the direct combining of the sterol core and sterol side chain. Introduction of the steroidal 22-amine functionality is a critical part of our proposed synthesis of new OSW-1 derived compounds for drug development, but the synthesis of 22-aminosterol presented an unexpected challenge (**Section 2.2.4.4**) that granted opportunity to pioneer this new imino-ene/aza-Prins two-component approach. Through combination of pregnadiene and functionalized N-aryl sulfonyl alkyl imines, I was able to produce *p*nosyl, *p*tosyl, and anisol sulfonyl protected 22-amino cholesterols and 17-hydroxy-22amino cholesterols.

Tosyl protected 22-amino cholesterol was deprotected under harsh conditions, 100°C reflux in the presence of sodium naphthelide, without affecting any other functional group of the 22-amino cholesterol. Nosyl protected 22-aminosterol was easily deprotected with thiophenol and a mild base at elevated temperatures, providing synthetic access to 22-aminosterols which can be further manipulated. This synthesis pathway provides convenient access to 22-amino cholesterol for the three-component approach to new OSW-1 derived scaffolds (see **Chapter 2**).

My initial hypothesis that different Lewis acids could directionally synthesize different 22-aminosterols was correct. This hypothesis is based on computational calculations of the imino-ene reaction which provided critical theoretical understanding of the role of Lewis acids and N-substituents.<sup>152</sup> Not all Lewis acids investigated promoted product formation which prevents clear correlations between the computationally calculated values and the mechanism pathway from being determined. Interestingly, of the Lewis acids investigated, only relatively *hard* Lewis acids reacted (i.e. BF<sub>3</sub>-Et<sub>2</sub>O, AlCl<sub>3</sub>, and Sc(OTf)<sub>3</sub>).<sup>163,164</sup> The main characteristic of these Lewis acids that leads to different ratios of product formation is the substituents of the leaving group. BF<sub>3</sub>-Et<sub>2</sub>O is a *hard*, strong coORDinating Lewis acid that does not have a good leaving group but still produced a near 1:1 ratio of 17-hydroxy-22-aminosterol (**Product B**) and 22-aminosterol (**Product A**). This indicates that the reaction strictly follows an aza-Prins mechanism that, upon work up, affords both possible products in equal amounts (**Figure 3-1, B and C**). AlCl<sub>3</sub> is a *hard*, strong Lewis acid with a good leaving group that afforded a 33:1 ratio of 17-hydroxy-22-aminosterol (**Product B**) and 22-aminosterol (**Product A**). This is likely because the chlorine quenches the C17 carbocation and is then hydrolyzed



during work up (**Figure 3-1, Mechanism C**). Interestingly,  $\text{Sc}(\text{OTf})_3$  deselected formation of 17-hydroxy-22-aminosterol (**Product B**) in favor of 22-aminosterol (**Product A**) in a 0.27:1 ratio. This suggests that the ejected triflate anion may behave as a counterion to the C17 carbocation, essentially blocking nucleophilic addition, until the nitrogen deprotonates C16 to form the alkene (**Product A**). These results all indicate that an aza-Prins reaction predominates.

Only one stereoisomeric product with the C20(*S*) and C22(*S*) stereochemistry was isolated. The stereoselectivity of these reactions was surprising, especially when considering that the aza-Prins reaction likely predominates. Aza-Prins reactions are typically not stereoselective due to the carbocation intermediate.<sup>172</sup> The stereoselectivity at the C20 position makes sense due to known reactivity of that position in steroids.<sup>140,142</sup> The inherent rigidity of steroids conformationally locks steroid substituents (i.e. C18-, C19-methyl groups) which leads to C21-methyl group typically adopting one stereochemical orientation. (see **Section 2.3**).<sup>140,142</sup> However, the stereoselectivity of the C22 position is unexpected. One possible explanation for the C22 stereoselectivity is due to the restrictions on how the imine approaches the olefin to facilitate the initiating nucleophilic step of the aza-Prins reaction. Due to the steric interaction of the C19-methyl group, the imine would presumably approach from the bottom face of the steroid.<sup>140,142</sup> The N-aryl sulfonyl alkyl imine can then approach the olefin either with the aryl group pointed into the steroid (endo approach) or with the aryl sulfonyl group pointed away from the steroid (exo approach). In a polar aprotic solvent (DCM), the E-isomer N-aryl sulfonyl alkyl imine would likely conform to an exo approach with the polar aryl sulfonyl group pointed away from the lipophilic steroid and into the polar aprotic solvent.

### **3.4. Conclusions and future work**

A direct, two-component approach to the stereoselective formation of either C16-C17-ene-22-aminosterol or the 17-hydroxyl-22-aminosterol has been developed, which can be applied to the three-component approach to generate new OSW-1 derived compounds. These 22-aminosterols are formed in one step from a tunable Lewis acid mediated imino-ene/aza-Prins reaction between pregnadiene and N-aryl sulfonyl alkyl imines. A method to produce a range of N-aryl sulfonyl alkyl imines through a robust and scalable two-step process from alkyl aldehydes and aryl sulfonamides, proceeding through an aminal intermediate was further developed based on previously established protocol.<sup>170</sup> The reaction scope of aryl groups in the formation of the N-aryl sulfonyl alkylamine was limited to *para*-substituted aryl sulfonamides and tolerated various electro donating and with drawing substituents. Furthermore, aryl sulfonamides with electron donating groups were sluggish in aminal formation but rapidly transformed into the corresponding imine. Aryl sulfonamides with electron withdrawing groups had the inverse relationship.

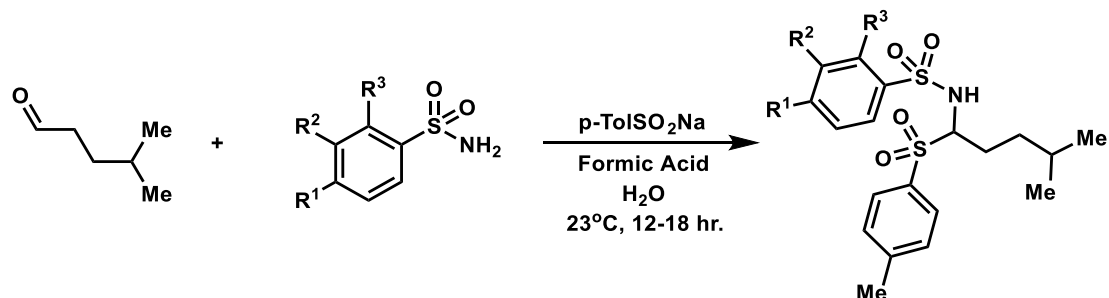
Various functionalized aryl sulfonyl N-alkylimines were reacted with pregnadiene in the presence of different Lewis acids to stereoselectively produce two aminosterol scaffolds in a highly tunable fashion, depending on the chosen Lewis acid. In agreement with the computational models<sup>152</sup> this work shows that imine electron withdrawing groups increase product yields whereas imine electron donating groups decrease yields.

Within this work, a new concise method to synthesize 22-aminosterols was developed. This new synthesis pathway to 22-aminosterols replaces the four-step synthesis to 22-aminosterols described in **Section 2.2.4.4** with a directional one-step

synthesis to C16-C17-ene-22-aminosterol or C17-hydroxy-22-aminosterol. Future work to further develop this approach should be focused on heteroatom nucleophilic addition to the C17-carbocation intermediate formed in the aza-Prins mechanistic pathway. Nucleophilic addition, if possible, can be optimized to product C17-functionalized 22-aminosterols and potentially to produce E-ring azaterols.

The imino-ene/aza-Prins two-component approach to functionalized 22-aminosterols provides convenient access to the OSW-1 cholestane scaffold through the direct combining of the sterol core and sterol side chain. This approach eliminates four synthetic steps from previous total syntheses of 22-aminosterols (**Section 2.2.4.4**), while introducing maximum diversification of the side chain and steroid components. The capability to rapidly make various 22-aminosterols, combined with the new capability to glycosylate the C22-amine (see **Section 2.2.3**), provides further achievements towards the three-component synthesis of OSW-1 analogs (see **Section 2.2.3, Scheme 2-4**). This body of work provides easier access to not only OSW-1 derived scaffolds but even further establishes a convenient approach to functionalized aminosterols that previously required numerous synthetic steps to obtain.

### 3.5. Experimental and supporting information



**General Procedure for the synthesis of N-arylsulfonyl alkylaminal compounds:** The N-arylsulfonyl alkylaminal compounds were made through adapting a previously reported protocol.<sup>170</sup> To a stirring mixture of aryl sulfonamide (1 equiv.) and sodium p-

toluenesulfinate (1.1 equiv.) in distilled water (6.0 ml) and formic acid (6.0 ml) at room temperature, the alkylaldehyde (1 equiv.) was added slowly dropwise. The solution was vigorously stirred for 12 hours. The resulting white precipitate was collected in a fritted filter then washed with cold DI water (2 x 20 ml) and cold hexanes (2 x 20 ml). Residual solvent was evaporated *in vacuo* to afford the desired N-aryl alkyl sulfonyl aminal compound which were carried forward without further purification. Diagnostic NMR data agreed with published reference data.<sup>170</sup>

**N-(1-tosylpentyl)-p-toluenesulfonamide; (Figure 3-2; Entry A):** <sup>1</sup>H-NMR (600 MHz, Chloroform-*d*): δ 7.69 (d, *J* = 8.2 Hz, 2H), 7.54 (d, *J* = 8.2 Hz, 2H), 7.28 (d, *J* = 8.0 Hz, 2H), 7.21 (d, *J* = 8.0 Hz, 2H), 5.23 (d, *J* = 10 Hz, 1H), 4.53 (td, *J* = 10, 3.7 Hz, 1H), 2.44 (s, 3H), 2.41 (s, 3H), 2.22 – 2.09 (m, 1H), 1.64 (dtd, *J* = 14, 10, 4.1 Hz, 1H), 1.21 (dddd, *J* = 22, 10, 7.1, 2.7 Hz, 3H), 1.11 (dtt, *J* = 14, 5.6, 3.1 Hz, 1H), 0.76 (t, *J* = 7.0 Hz, 3H). <sup>13</sup>C-NMR (151 MHz, Chloroform-*d*): δ 145.2, 143.7, 137.8, 132.8, 129.7, 129.6, 129.5, 126.8, 77.2, 77.0, 76.8, 73.7, 28.1, 27.1, 22.1, 21.7, 21.5, 13.6

**N-(1-tosylpentyl)-p-methoxybenzenesulfonamide; (Figure 3-2; Entry B):** <sup>1</sup>H-NMR (600 MHz, Chloroform-*d*): δ 7.69 (d, *J* = 8.3 Hz, 2H), 7.59 (d, *J* = 9.0 Hz, 2H), 7.33 – 7.26 (m, 2H), 6.86 (d, *J* = 9.0 Hz, 2H), 5.24 (d, *J* = 10 Hz, 1H), 4.53 (td, *J* = 10, 3.7 Hz, 1H), 3.85 (s, 3H), 2.44 (s, 1H), 2.21 – 2.07 (m, 1H), 1.71 – 1.61 (m, 1H), 1.34 – 1.18 (m, 2H), 1.19 – 1.09 (m, 1H), 0.78 (t, *J* = 6.9 Hz, 3H). <sup>13</sup>C-NMR (151 MHz, Chloroform-*d*): δ 129.7, 129.6, 128.9, 114.1, 73.7, 55.6, 27.1, 22.1, 21.7.

**(N-(1-tosylpentyl)-p-chlorobenzenesulfonamide; (Figure 3-2; Entry C):** <sup>1</sup>H-NMR (600 MHz, Chloroform-*d*): δ 7.63 (d, *J* = 8.2 Hz, 2H), 7.57 (d, *J* = 8.6 Hz, 2H), 7.36 (d, *J* = 8.6 Hz, 2H), 7.25 (d, *J* = 9.1 Hz, 2H), 5.23 (d, *J* = 10 Hz, 1H), 4.56 (td, *J* = 10.3, 3.6 Hz, 1H), 2.45 (s, 3H), 2.22 – 2.14 (m, 1H), 1.68 (dq, *J* = 10, 5.7, 5.3 Hz, 2H), 1.40 – 1.29 (m, 2H), 1.29 – 1.19 (m, 2H), 0.83 (t, *J* = 6.8 Hz, 3H). <sup>13</sup>C-NMR (151 MHz, Chloroform-*d*): δ 139.3, 129.8, 129.4, 129.2, 128.1, 73.7, 27.1, 22.1.

**N-(1-tosylpentyl)-p-nitrobenzenesulfonamide; (Figure 3-2; Entry D):** <sup>1</sup>H-NMR (600 MHz, Chloroform-*d*): δ 8.17 (d, *J* = 8.9 Hz, 2H), 7.83 (d, *J* = 8.9 Hz, 2H), 7.53 (d, *J* = 8.3 Hz, 2H), 7.16 (d, *J* = 7.9 Hz, 2H), 6.08 (s, 1H), 4.52 (td, *J* = 10, 3.3 Hz, 1H), 2.32 (s, 2H), 2.09 – 1.93 (m, 1H), 1.62 – 1.52 (m, 1H), 1.20 (dp, *J* = 12, 4.4, 4.0 Hz, 2H), 1.13 (ddd, *J* = 13, 7.5, 4.7 Hz, 2H), 0.70 (t, *J* = 6.8 Hz, 3H).

**N-(1-tosylpentyl)-1-naphthalenesulfonamide; (Figure 3-2; Entry E):** <sup>1</sup>H-NMR (600 MHz, Acetone-*d*<sub>6</sub>): δ 8.43 (d, *J* = 8.9 Hz, 1H), 8.37 (d, *J* = 8.9 Hz, 2H), 8.27 – 8.12 (m, 1H), 7.99 (d, *J* = 8.9 Hz, 2H), 7.82 – 7.76 (m, 2H), 7.63 (d, *J* = 8.3 Hz, 2H), 7.33 (d, *J* = 7.9 Hz, 2H), 6.97 (s, 1H), 4.75 (t, *J* = 10 Hz, 1H), 2.41 (s, 3H), 2.12 (td, *J* = 9.5, 4.5 Hz, 1H), 1.75 – 1.59 (m, 1H), 1.30 (td, *J* = 11, 10., 5.5 Hz, 2H), 1.27 – 1.22 (m, 2H), 0.79 (t, *J* = 6.4 Hz, 3H).

**N-(4-methyl-1-tosylpentyl)-p-toluenesulfonamide; (Figure 3-2; Entry H):** <sup>1</sup>H-NMR (500 MHz, Chloroform-*d*): δ 7.70 (d, *J* = 8.3 Hz, 2H), 7.54 (d, *J* = 8.4 Hz, 2H), 7.29 (d, *J* = 8.0 Hz, 2H), 7.21 (d, *J* = 8.0 Hz, 2H), 5.02 (d, *J* = 10 Hz, 1H), 4.48 (td, *J* = 10.2, 3.7 Hz, 1H), 2.45 (s, 2H), 2.41 (s, 2H), 2.17 (dddd, *J* = 14, 9.7, 7.8, 3.7 Hz, 1H), 1.62 (dtd, *J* = 14, 9.8, 7.5 Hz, 1H), 1.43 (dp, *J* = 13, 6.7 Hz, 1H), 1.07 – 0.96 (m, 2H), 0.75 (dd, *J* = 6.6, 3.0 Hz, 6H).

**N-(4-methyl-1-tosylpentyl)-p-nitrobenzenesulfonamide; (Figure 3-2; Entry I):** <sup>1</sup>H-NMR (500 MHz, Chloroform-*d*): δ 8.25 (d, *J* = 8.9 Hz, 1H), 8.12 (d, *J* = 8.9 Hz, 1H), 7.86 (d, *J* = 8.8 Hz, 1H), 7.61 (d, *J* = 8.4 Hz, 2H), 7.25 (d, *J* = 8.0 Hz, 2H), 5.58 (d, *J* = 10 Hz, 1H), 4.57 (td, *J* = 10, 3.4 Hz, 1H), 2.14 (ddt, *J* = 17, 10, 3.3 Hz, 1H), 1.77 – 1.62 (m, 1H), 1.52 (dt, *J* = 13, 6.7 Hz, 0H), 1.24 – 1.13 (m, 2H), 0.82 (dd, *J* = 9.0, 6.7 Hz, 6H).



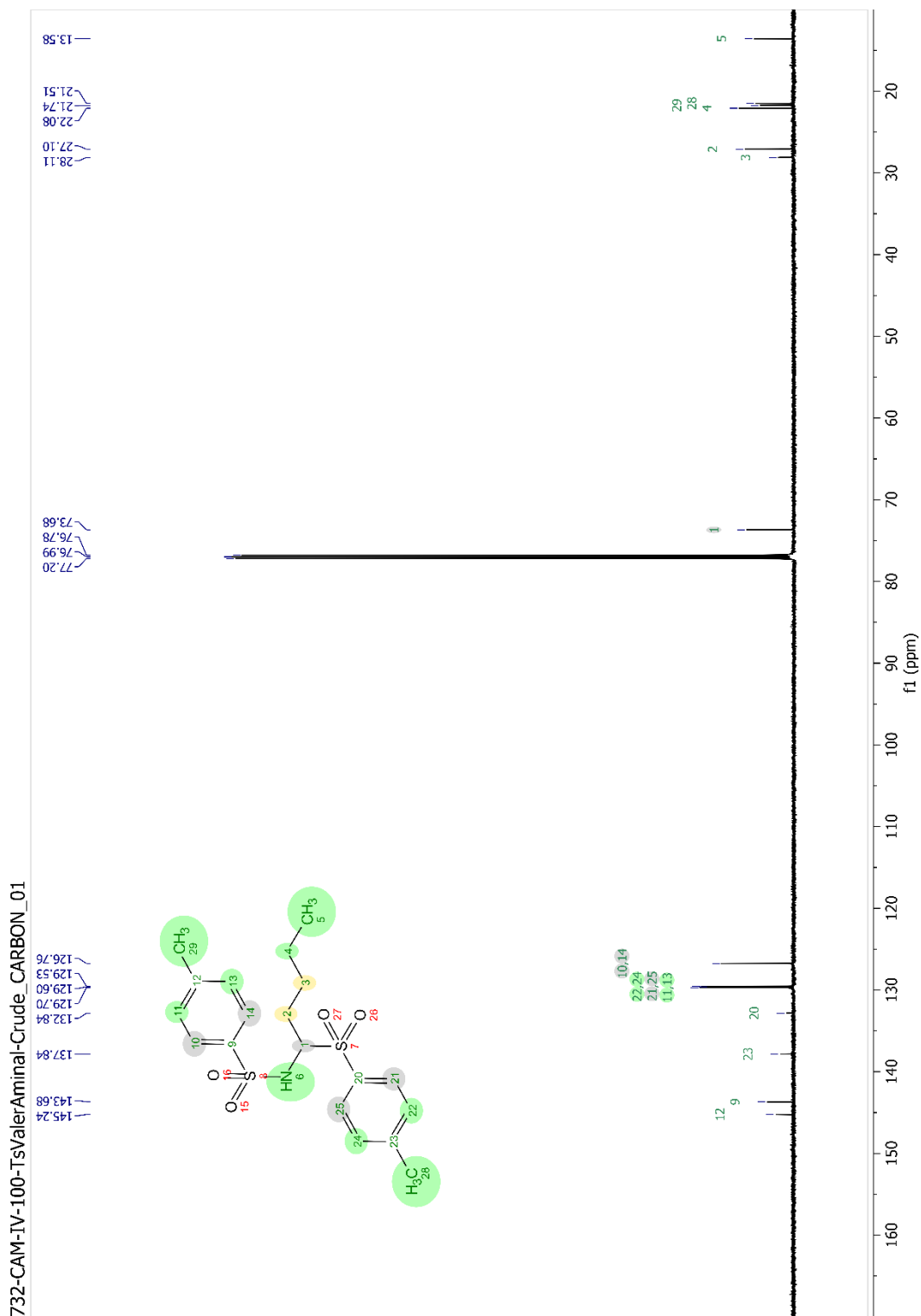


**Figure 3-5.** <sup>13</sup>CNMR of N-(1-tosylpentyl)-p-toluenesulfonamide (**Figure 3-2; Entry A**) in chloroform-*d*.

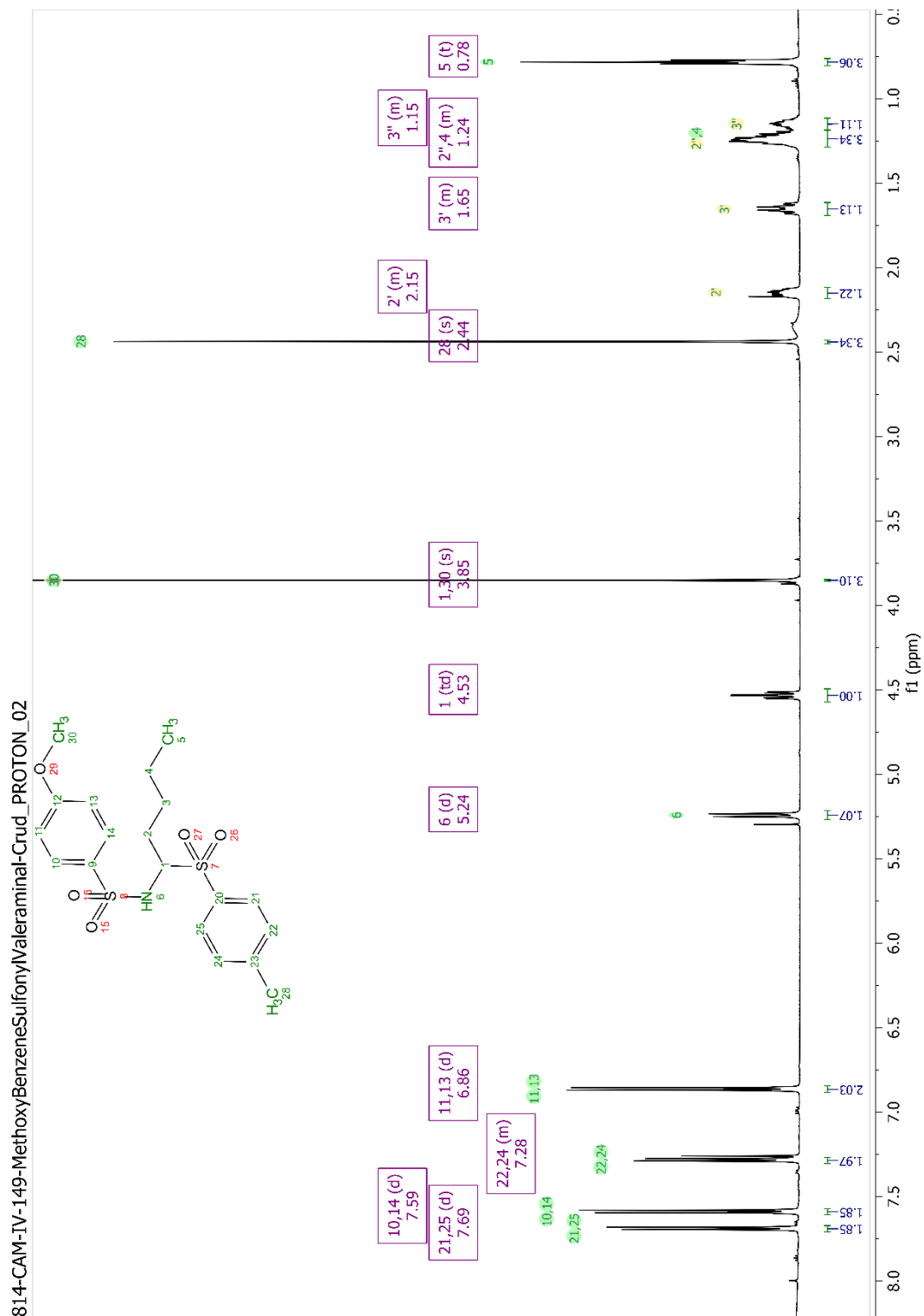


**Figure 3-6.**  $^1\text{H-NMR}$  of N-(1-tosylpentyl)-p-methoxybenzenesulfonamide (**Figure 3-2; Entry B**) in chloroform-*d*.



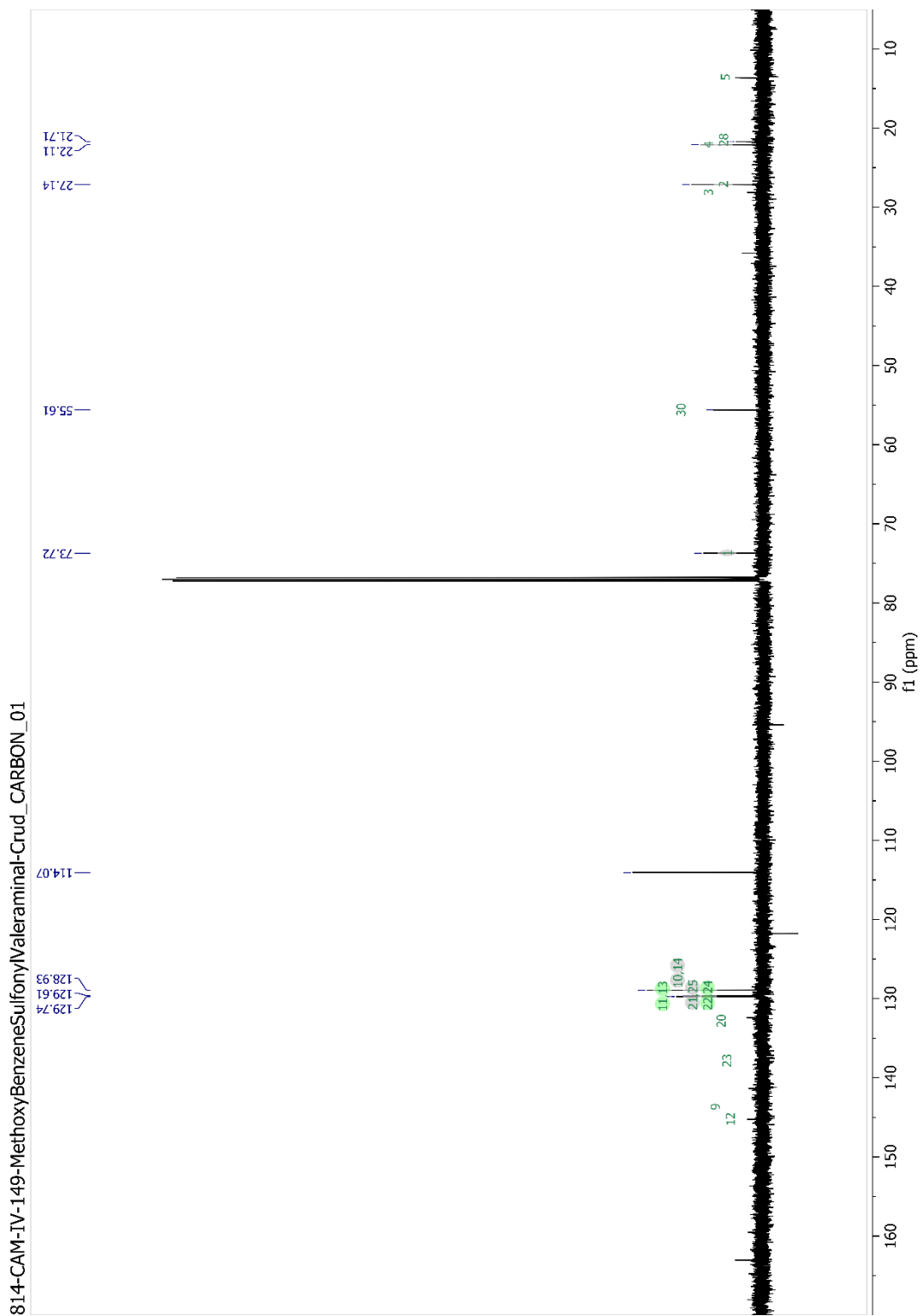


**Figure 3-7.**  $^{13}\text{C}$ -NMR of N-(1-tosylpentyl)-p-methoxybenzenesulfonamide (**Figure 3-2; Entry B**) in chloroform-*d*.

817-CAM-IV-149-4ChloroBenzeneSulfonylValeramin-Crud\_PROTON\_02

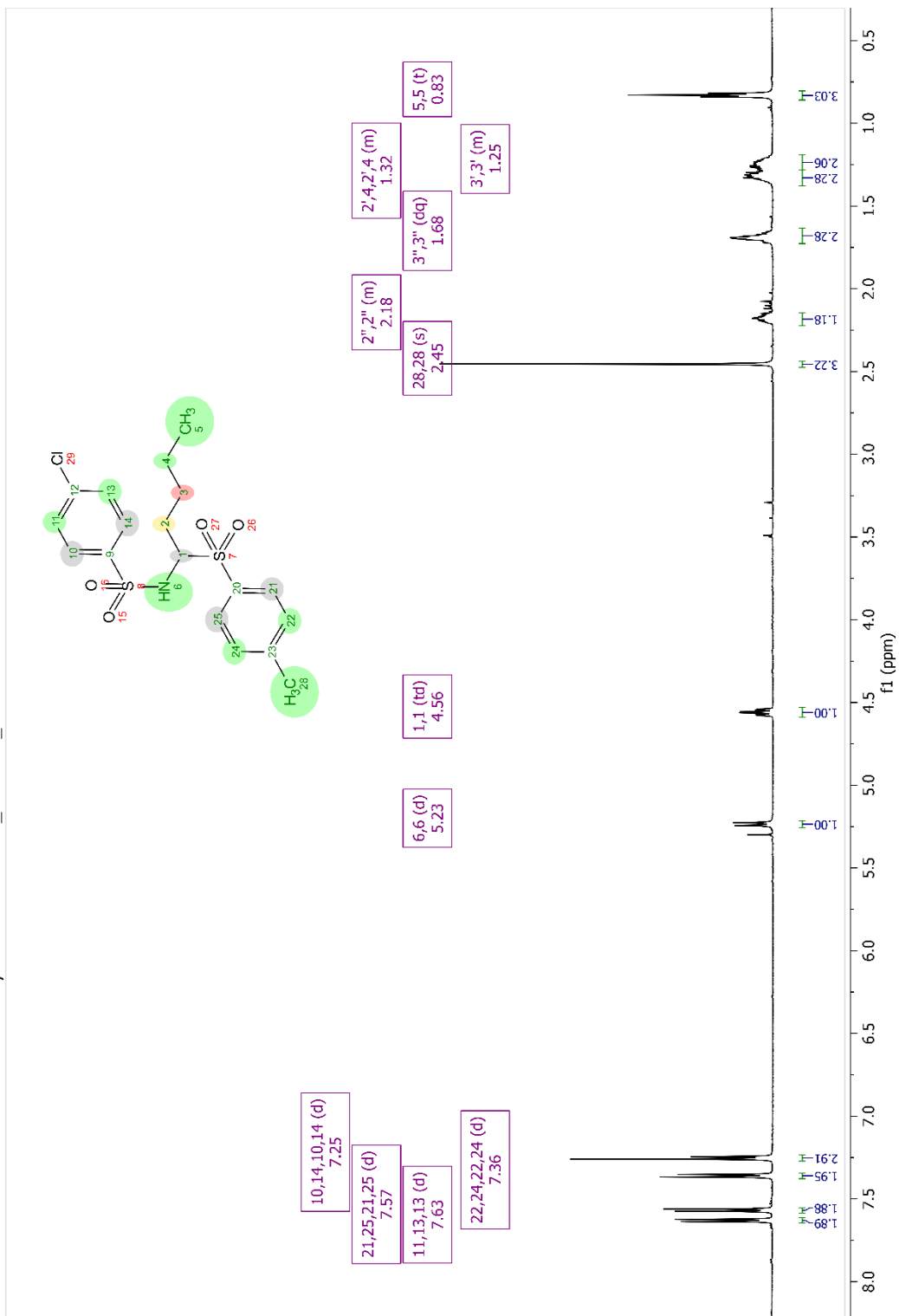


**Figure 3-8.** <sup>1</sup>H-NMR of N-(1-tosylpentyl)-p-chlorobenzenesulfonamide (**Figure 3-2; Entry C**) in chloroform-*d*.

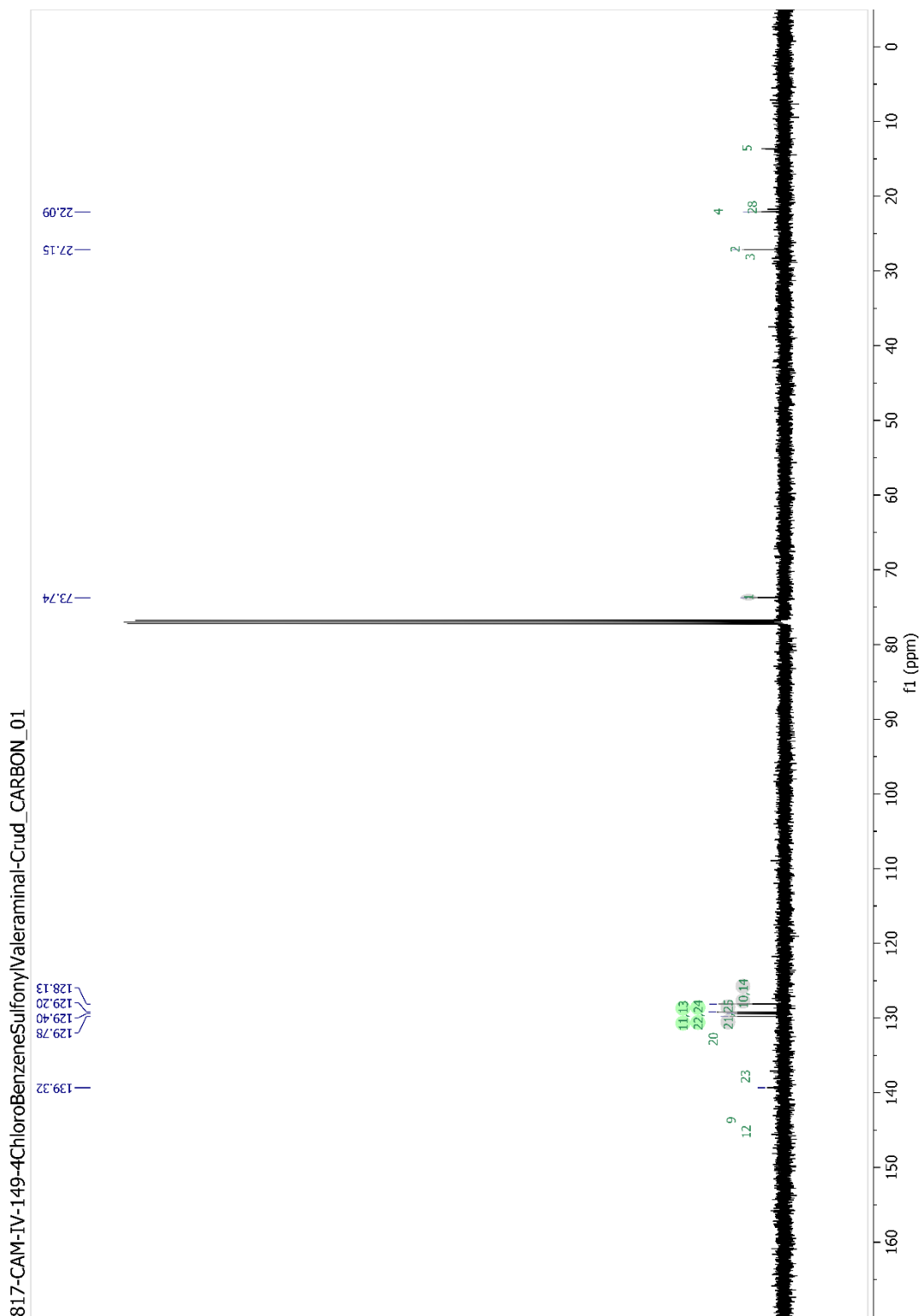


**Figure 3-9.**  $^{13}\text{C}$ -NMR of N-(1-tosylpentyl)-p-chlorobenzenesulfonamide (**Figure 3-2; Entry C**) in chloroform-*d*.

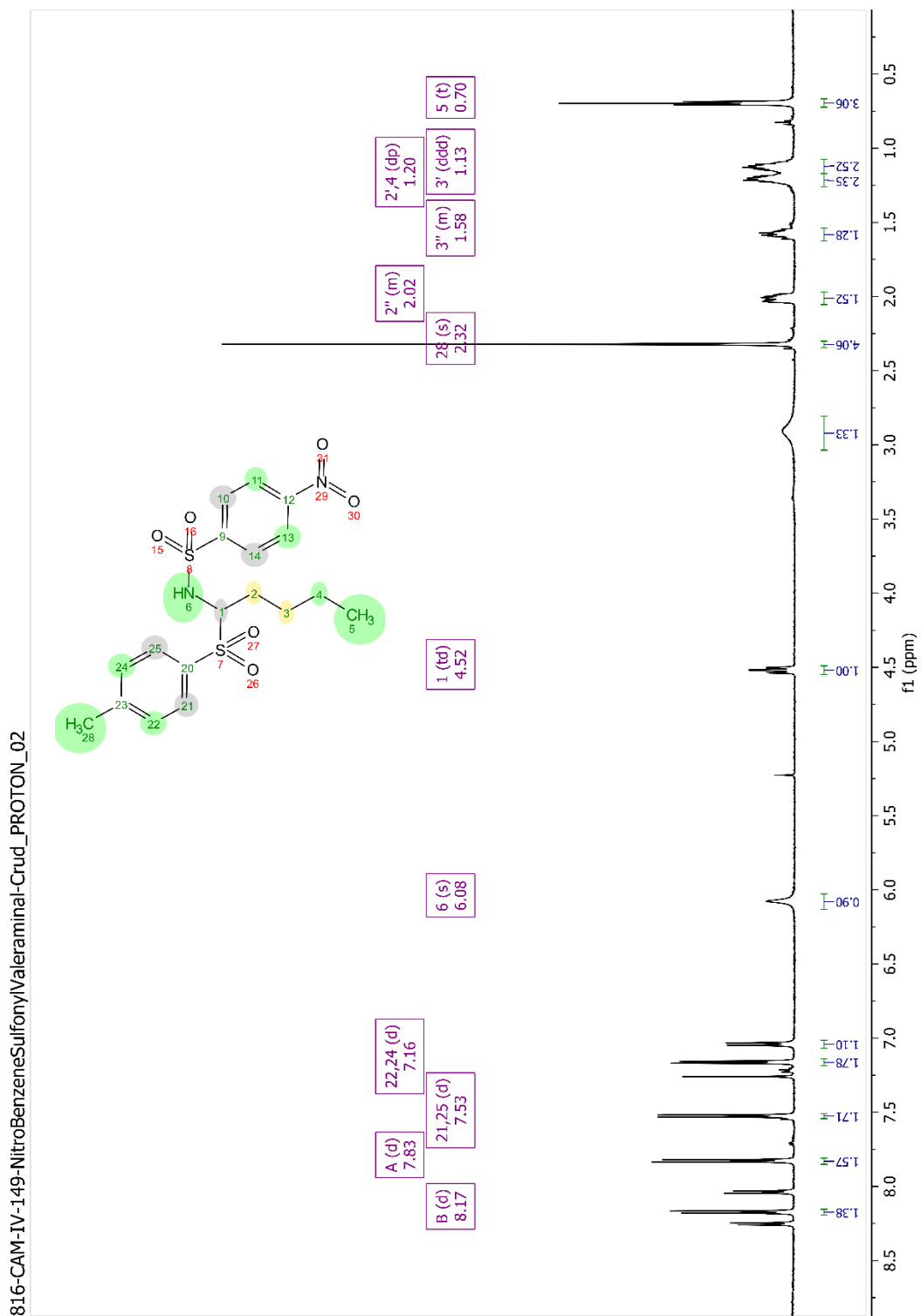


**Figure 3-10.**  $^1\text{H-NMR}$  of N-(1-tosylpentyl)-p-nitrobenzenesulfonamide (**Figure 3-2; Entry D**) in chloroform-*d*.

815-CAM-IV-149-NaphthaleneSulfonylValerimine-Crude\_PROTON\_02

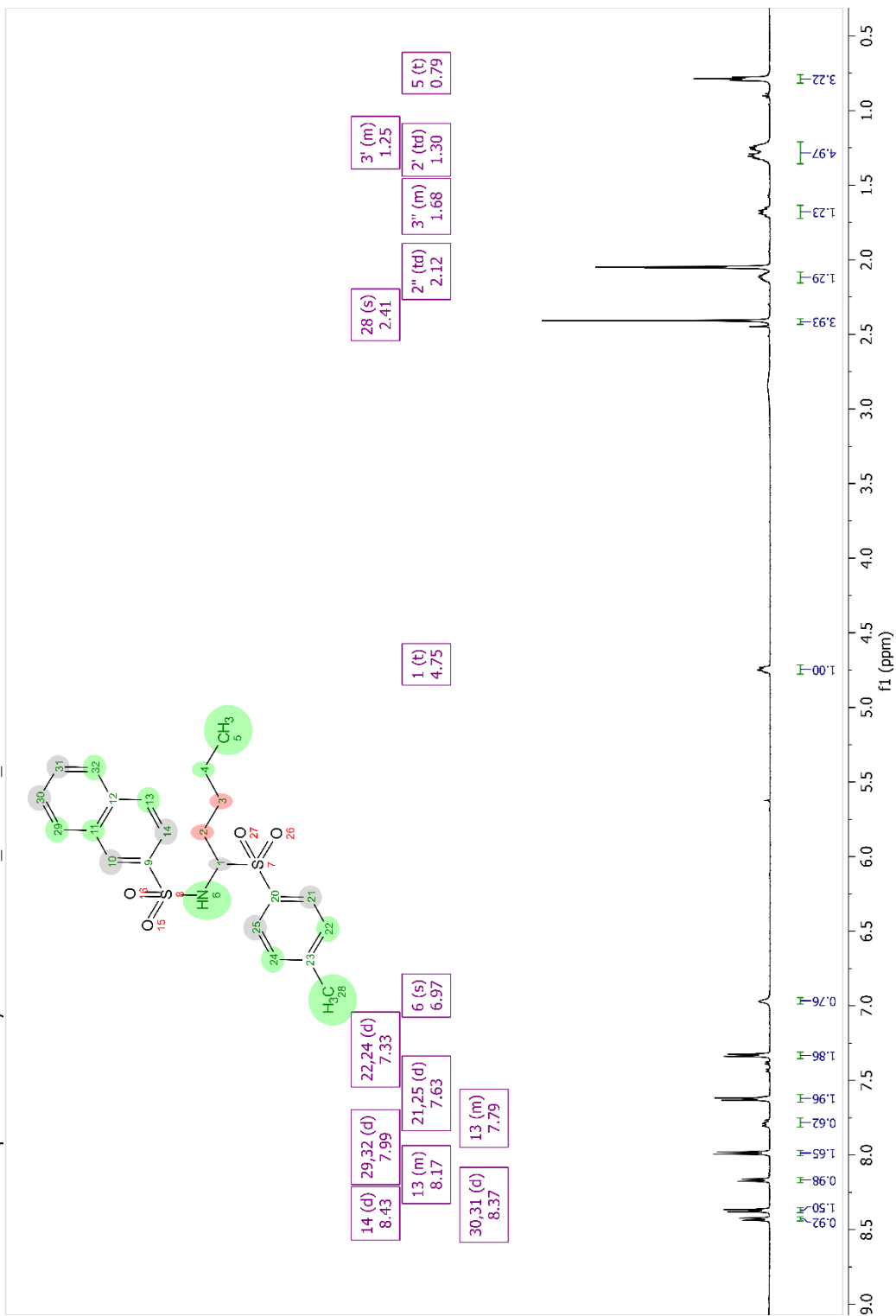


**Figure 3-11.** <sup>1</sup>H-NMR of N-(1-tosylpentyl)-1-naphthalenesulfonamide (**Figure 3-2; Entry E**) in acetone-*d*<sub>6</sub>.

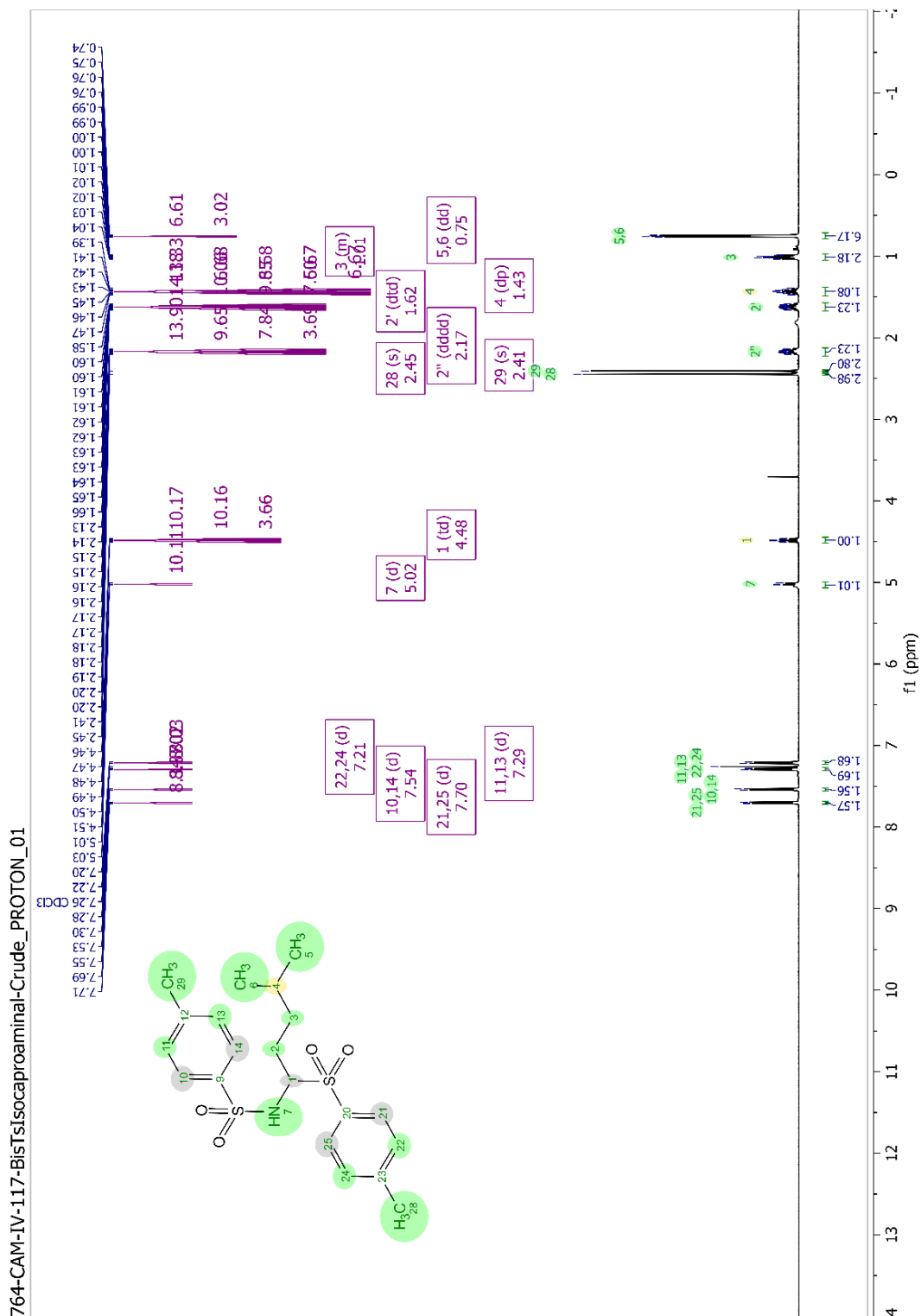


**Figure 3-12.**  $^1\text{H-NMR}$  of -(4-methyl-1-tosylpentyl)-p-toluenesulfonamide (**Figure 3-2; Entry H**) in chloroform-*d*.

836-CAM-V-13-pNsIsocaproAminal\_PROTON\_01

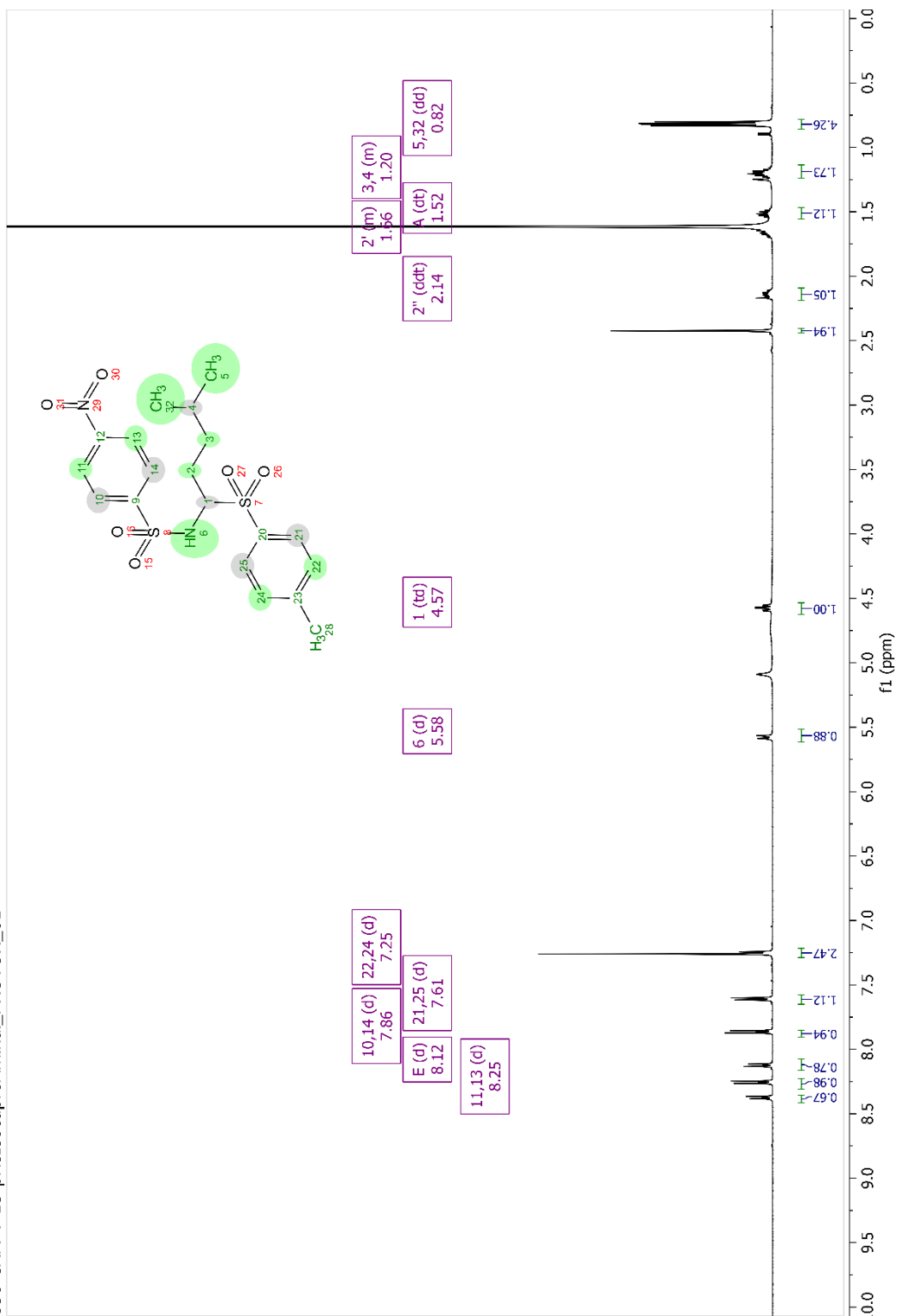
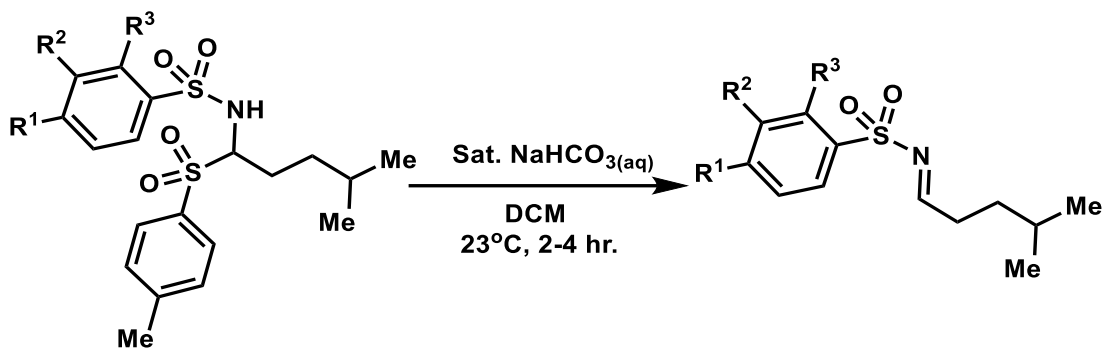


**Figure 3-13.** <sup>1</sup>H-NMR of N-(4-methyl-1-tosylpentyl)-p-nitrobenzenesulfonamide (**Figure 3-2; Entry I**) in chloroform-*d*.



**General procedure for the synthesis of N-arylsulfonyl alkylidene compounds:** The N-arylsulfonyl **alkylidene** compounds were made through adapting a previously reported protocol.<sup>170</sup> Starting material, N-arylsulfonyl alkylamine compound (1 equiv.) was dissolved in a mixture of DCM (20 ml) and sat. NaHCO<sub>3(aq)</sub>. The reaction proceeded over two hours and was monitored via <sup>1</sup>H-NMR. Upon complete transformation of the starting material as indicated by <sup>1</sup>H-NMR, the biphasic mixture was transferred to a separatory funnel. The biphasic mixture was separated, and the aqueous layer was extracted with DCM (2 x 20 ml). The organic layers were combined and washed with sat. NaHCO<sub>3(aq)</sub> (1 x 20 ml) and then DI water (2 x 20 ml). The organic solution was then washed with brine and dried over sodium sulfate. The drying reagent was removed, and the solvent was evaporated *in vacuo* to afford a white solid which was immediately used in the following reaction without further purification. Diagnostic NMR peaks agreed with published reference.<sup>170</sup>

**(E)-N-(pentylidene)-p-toluenesulfonamide; (Figure 3-2; Entry A):** <sup>1</sup>H NMR (500 MHz, Chloroform-*d*): δ 8.59 (t, *J* = 4.6 Hz, 0H), 7.80 (d, *J* = 8.2 Hz, 0H), 7.33 (dd, *J* = 8.4, 1.0 Hz, 1H), 2.50 (td, *J* = 7.5, 4.6 Hz, 1H), 2.43 (s, 1H), 1.59 (p, *J* = 7.5 Hz, 1H), 1.34 (h, *J* = 7.4 Hz, 1H), 0.89 (t, *J* = 7.3 Hz, 1H).

**(E)-N-(pentylidene)-p-nitrobenzenesulfonamide; (Figure 3-2; Entry D):** <sup>1</sup>H NMR (300 MHz, Chloroform-*d*): δ 8.72 (t, *J* = 4.5 Hz, 1H), 8.36 (d, *J* = 9.1 Hz, 2H), 8.11 (d, *J* = 9.1 Hz, 2H), 2.56 (ddd, *J* = 7.8, 7.3, 4.5 Hz, 2H), 1.66 – 1.51 (m, 5H), 1.43 – 1.24 (m, 2H), 0.88 (t, *J* = 7.3 Hz, 3H).

**(E)-N-(4-methylpentylidene)-p-toluenesulfonamide; (Figure 3-2; Entry H):** <sup>1</sup>H NMR (400 MHz, Chloroform-*d*): δ 8.59 (t, *J* = 4.6 Hz, 1H), 7.81 (d, *J* = 8.3 Hz, 2H), 7.30 (d, *J* = 8.1 Hz, 2H), 2.44 (s, 3H), 1.62 – 1.55 (m, 1H), 1.54 – 1.45 (m, 2H), 0.88 (d, *J* = 6.4 Hz, 6H). <sup>13</sup>C-NMR (151 MHz, Chloroform-*d*): δ 129.8, 129.7, 128.1, 126.5, 34.01, 33.3, 27.7, 22.2.



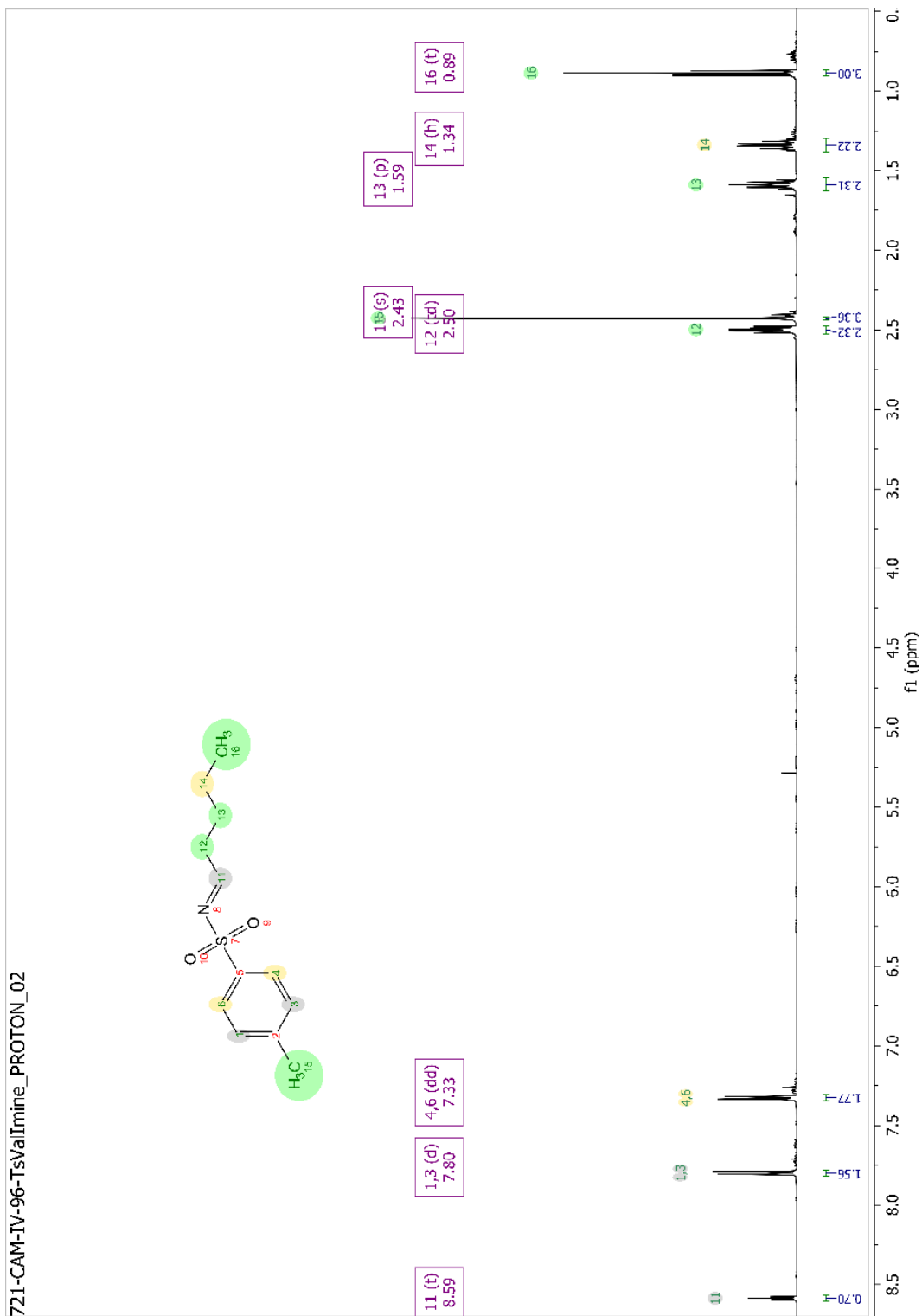


**Figure 3-14.** <sup>1</sup>H-NMR of (E)-N-(pentylidene)-p-toluenesulfonamide (**Figure 3-2; Entry A**) in chloroform-*d*.

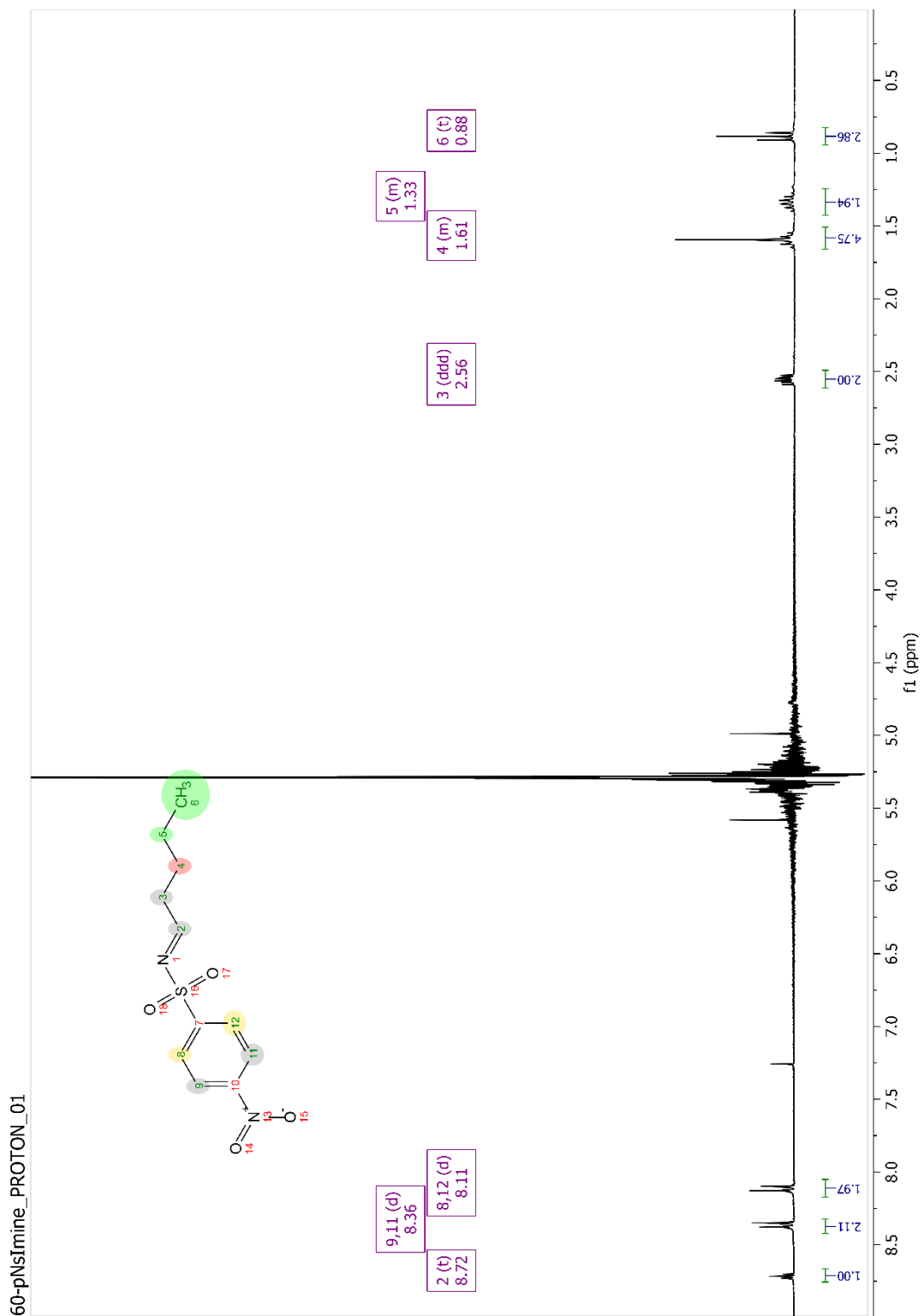


**Figure 3-15.** <sup>1</sup>H-NMR of (E)-N-(pentylidene)-p-nitrobenzenesulfonamide (**Figure 3-2; Entry D**) in acetone-*d*<sub>6</sub>.

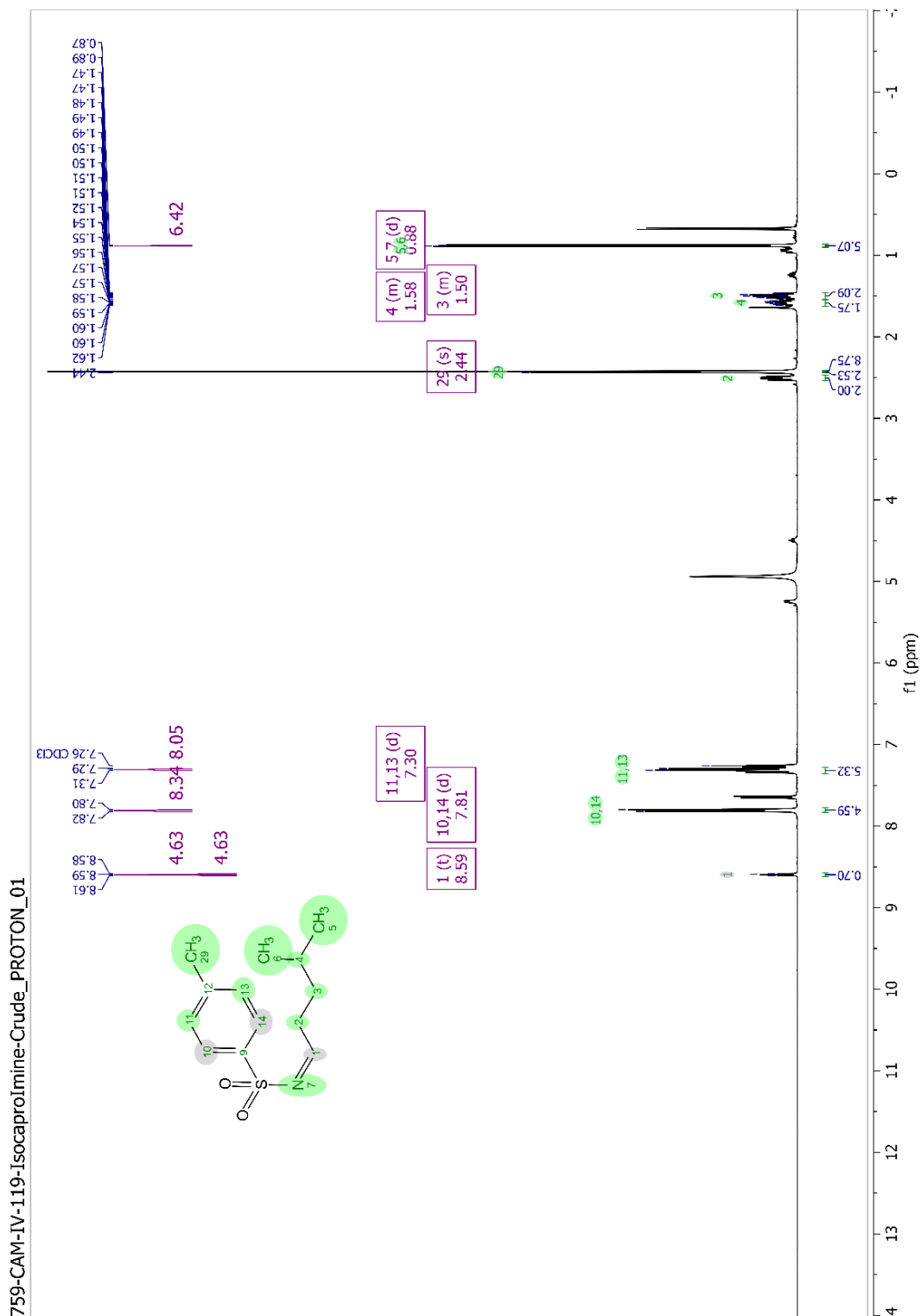


**Figure 3-16.** <sup>1</sup>H-NMR of (E)-N-(4-methylpentylidene)-p-toluenesulfonamide (**Figure 3-2; Entry H**) in chloroform-*d*.

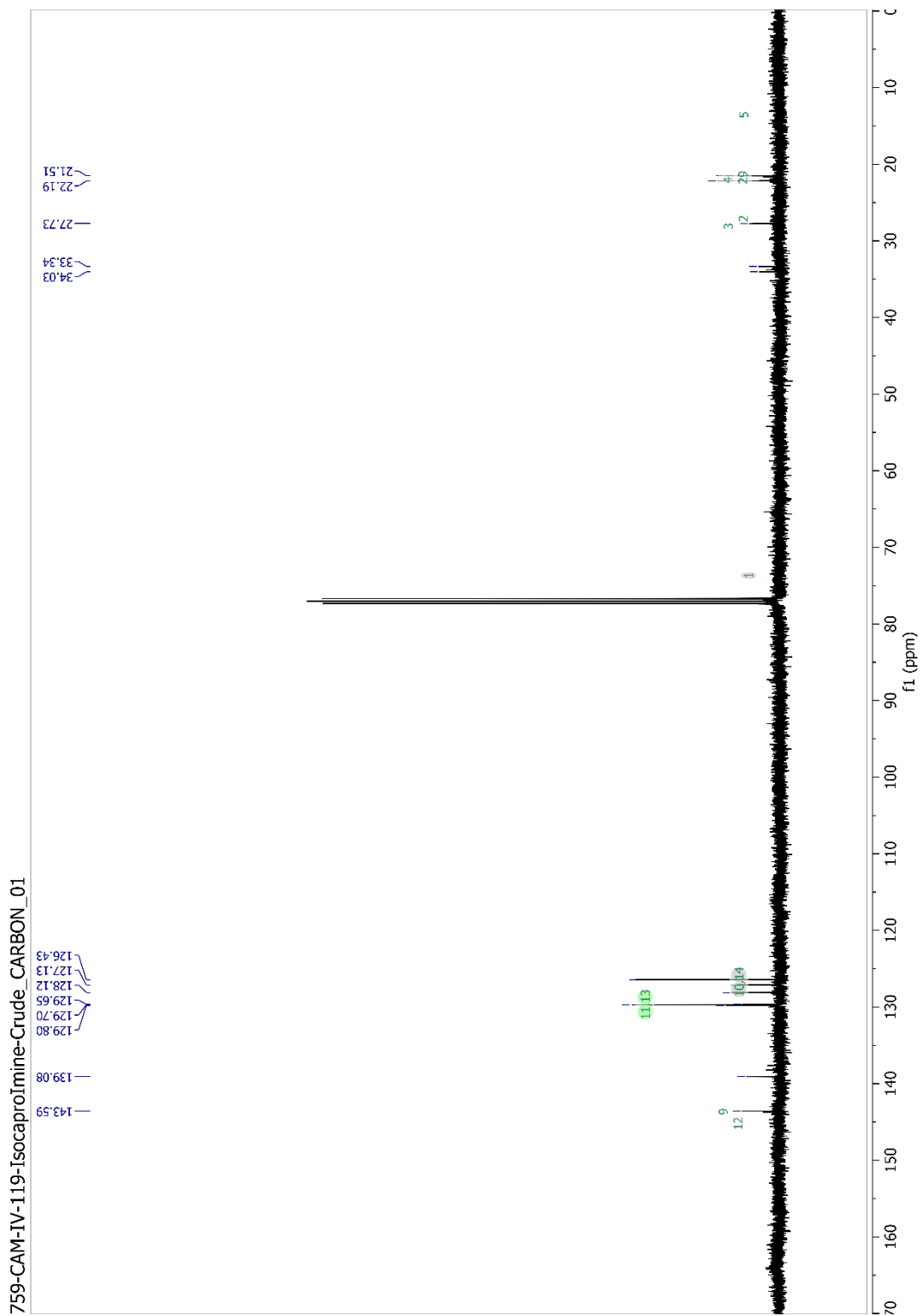
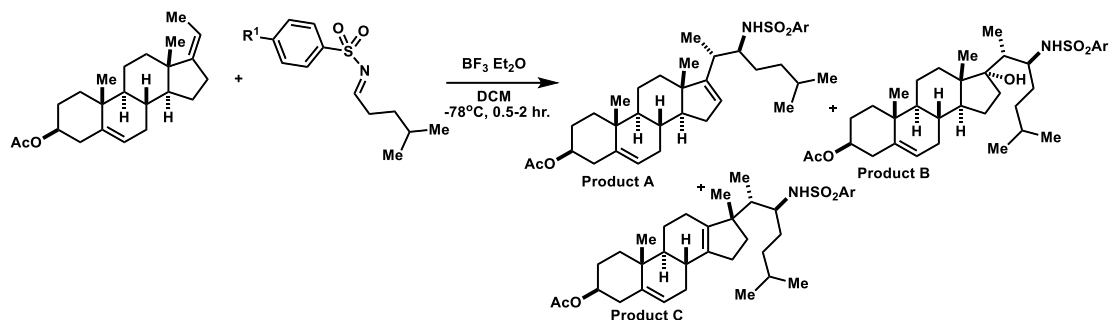


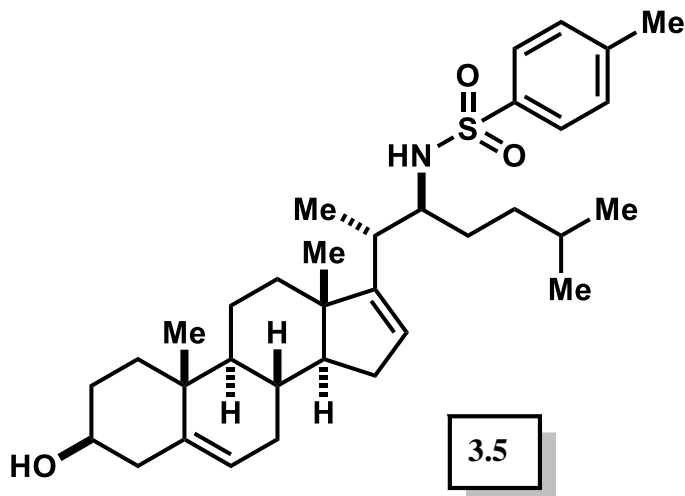
**Figure 3-17.**  $^{13}\text{C}$ -NMR of (E)-N-(4-methylpentylidene)-p-toluenesulfonamide (**Figure 3-2; Entry H**) in chloroform-*d*.



**General procedure for the synthesis of various aminosterol compounds:** A solution of freshly prepared N-arylsulfonyl alkylimine (3 equiv.) in dry DCM (100 mM) in a round-bottom flask was cooled to  $-40^\circ\text{C}$  using dry ice and acetonitrile bath. To this solution was added boron trifluoride diethyl etherate (either 1, 3, or 5 equiv.) slowly dropwise, and the reaction was stirred at  $-40^\circ\text{C}$  for 20 minutes. A solution of the acetylated pregnadiene (1 equiv.) in DCM (200 mM) was added slowly dropwise to the reaction. The reaction proceeded between 0.5- 2 hours. Up to three aminosterol products (**A**, **B** and **C**) were formed depending on the N-arylsulfonyl alkylamine starting material used. Upon complete transformation of the starting material as indicated by TLC, the reaction was quenched with a solution of methanol (5 ml) and distilled water (5 ml) at  $-40^\circ\text{C}$  then warmed to room temperature. The reaction solution was transferred to a separatory funnel and washed once with sat.  $\text{NaHCO}_3(\text{aq})$  followed by two washes of distilled water. The aqueous layers were combined and back extracted with DCM. The organic layers were combined and washed once with brine then dried over sodium sulfate. The drying agent was removed, and the solvent evaporated *in vacuo* to afford crude material as a white solid. The crude material was purified via silica gel chromatography and eluted with a 5-20% ethyl acetate in hexanes gradient afford the desired aminosterol products **A**, **B**, and **C**.

**General procedure for the synthesis of various aminosterol compounds varying the Lewis-acid:** A solution of freshly prepared (*E*)-*N*-(pentylidene)-*p*-toluenesulfonamide (3 equiv.) in dry DCM (100 mM) in a round-bottom flask was cooled to  $-40^\circ\text{C}$  in a dry ice/acetonitrile bath. To this solution was added the selected Lewis-acid (1 or 3 equiv.) slow dropwise and the reaction stirred at  $-40^\circ\text{C}$  for 20 minutes. To the reaction was added a solution of acetylated pregnadiene (1 equiv.) in DCM (200 mM) slowly dropwise. The reaction proceeded over 0.5 to 2 hours. Up to three aminosterol products were formed depending on the selected Lewis acid. Upon complete transformation of the starting material as indicated by TLC, the reaction was quenched with a solution of methanol (5 ml) and distilled water (5 ml) at  $-40^\circ\text{C}$  then warmed to room temperature. The reaction solution was transferred to a separatory funnel and washed once with sat.  $\text{NaHCO}_3(\text{aq})$  followed by two washes of distilled water. The aqueous layers were combined and back extracted with DCM. The organic layers were combined and washed once with brine then dried over sodium sulfate. The drying agent was removed, and the solvent evaporated *in vacuo* to afford crude material as a white solid. The crude material was analyzed via

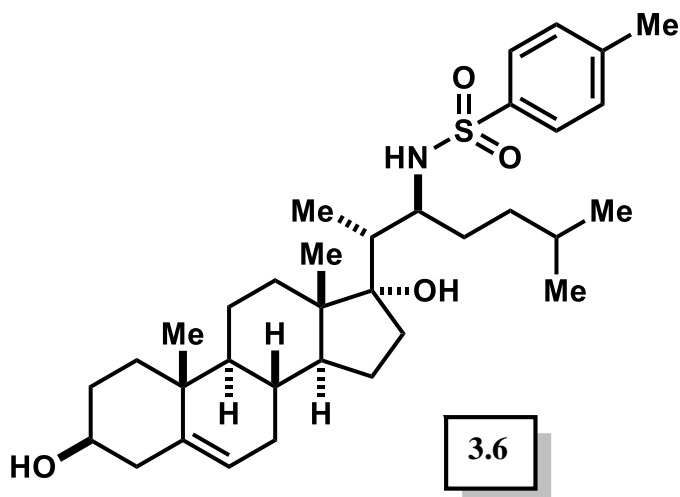
HPLC-MS on a Luna 5  $\mu\text{m}$  C8(2) 100 $\text{\AA}$  (Phenomenex) column and a 90% isocratic mobile phase of acetonitrile to 0.1% formic acid/water. The ratios of product formation were calculated from percent area of the UV-Vis chromatogram.



**Reaction with (E)-N-(pentylidene)-p-toluenesulfonamide; (Figure 3-2; Entry A), to form Compound 3.5:**  $^1\text{H-NMR}$  (600 MHz, Chloroform-*d*):  $\delta$  7.74 (d,  $J = 8.2$  Hz, 1H), 7.30 – 7.26 (m, 2H), 5.38 (d,  $J = 5.4$  Hz, 1H), 5.37 (s, 1H), 4.60 (tt,  $J = 11, 5.1$  Hz, 1H), 4.19 (d,  $J = 8.4$  Hz, 1H), 3.49 (s, 2H), 3.33 (p,  $J = 7.1$  Hz, 1H), 2.41 (s, 3H), 2.33 (d,  $J = 4.8$  Hz, 1H), 2.24 (p,  $J = 7.0$  Hz, 1H), 2.03 (s, 3H), 2.00 (s, 1H), 1.97 (s, 1H), 1.95 – 1.81 (m, 1H), 1.78 (d,  $J = 14$  Hz, 1H), 1.69 (d,  $J = 12$  Hz, 1H), 1.60 (d,  $J = 12$  Hz, 1H), 1.49 (ddd,  $J = 14, 11, 4.5$  Hz, 1H), 1.30 (dtd,  $J = 23, 12, 11, 4.9$  Hz, 2H), 1.13 (dt,  $J = 15, 7.1$  Hz, 3H), 1.04 (s, 2H), 1.03 – 0.96 (m, 1H), 0.93 (d,  $J = 7.0$  Hz, 2H), 0.74 (d,  $J = 4.0$  Hz, 3H).  $^{13}\text{C-NMR}$  (151 MHz, Chloroform-*d*):  $\delta$  170.5, 157.0, 142.9, 139.9, 129.4, 127.0, 123.9, 122.4, 73.9, 57.8, 57.3, 50.9, 50.5, 47.1, 38.1, 36.9, 36.8, 36.5, 34.8, 32.7, 31.5, 31.2, 30.4, 27.7, 27.6, 22.4, 21.44 21.4, 20.6, 19.2, 17.9, 16.3, 13.8.

Atom	Chemical Shift	COSY	HSQC	Atom	Chemical Shift	COSY	HSQC	Atom	Chemical Shift	COSY	HSQC
1 C	36.5		1'	13 C				26 C	13.8		26
H'	1.83	1''	1	14 C	57.3		14	H3	0.74		26
H''	1.13	1'		H	1.30	8	14	28 C	170.5		
2 C	27.55		2', 2''	15 C	23.25		15	29 C	21.45		29
H'	1.83		2	H2	1.78	16	15	H3	2.03		29
H''	1.60		2	16 C	122.4		16	34 C	143.0		
3 C	74.5		3	H	5.38	15	16	35 C	127.0		35
H	4.57	4	3	17 C	157.0			H	7.74		35
4 C	378.0		4	18 C	16.3		18	36 C	129.5		36
H2	2.33	3, 6	4	H3	0.74		18	H	7.27		36
5 C	127.2			19 C	19.2		19	37 C	139.9		
6 C	124.0		6	H3	1.04		19	38 C	129.5		38
H	5.36	4	6	20 C	36.5		20	H	7.27		38
7 C	35.4		7	H	2.24	21, 22	20	44 C	127.0		44

H2	2.33		7	21 C	18.0		21	H	7.74		44
8 C			8	H3	0.93		20	21	45 C	21.5	45
H	1.69		14	8	22 C	57.9		22	H3	2.41	45
9 C	50.6		9	H	3.33		20, 46	22	46 N		
H	1.00		9	23 C	29.7			23	H	4.19	22
10 C				H2	1.30			23			
11 C	32.7		11	24 C	31.8			24			
H2	1.49		11	H2	2.00			24			
12 C	20.7		12	25 C	31.2			25			
H2	1.60		12	H2	1.97			25			

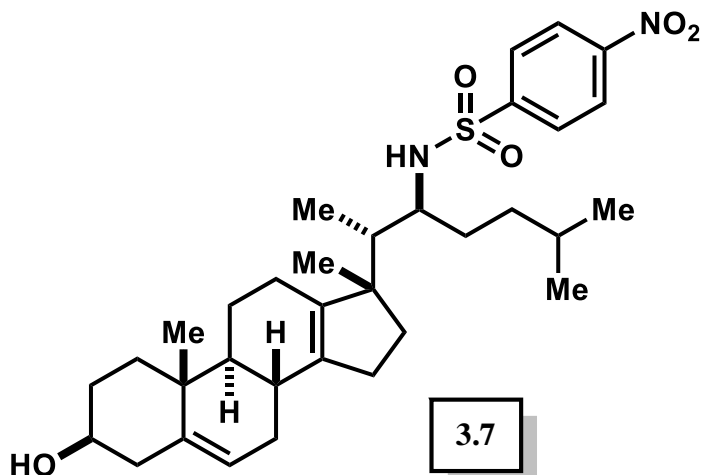


**Reaction with (E)-N-(pentylidene)-p-toluenesulfonamide; (Figure 3-2; Entry A) to form Compound 3.6:**  $^1\text{H-NMR}$  (600 MHz, Chloroform-*d*):  $\delta$  7.68 (d,  $J = 8.2$  Hz, 2H), 7.23 (d,  $J = 7.9$  Hz, 2H), 5.58 – 5.17 (m, 1H), 4.73 – 4.49 (m, 1H), 3.74 – 3.60 (m, 1H), 2.68 (t,  $J = 7.7$  Hz, 1H), 2.62 – 2.49 (m, 1H), 2.40 (s, 4H), 2.36 (dd,  $J = 13, 4.6$  Hz, 1H), 2.28 (t,  $J = 12$  Hz, 1H), 2.16 (d,  $J = 15$  Hz, 3H), 1.92 – 1.82 (m, 3H), 1.76 (q,  $J = 7.0$  Hz, 1H), 1.73 – 1.69 (m, 4H), 1.68 – 1.67 (m, 1H), 1.60 (s, 1H), 1.42 (dtd,  $J = 26, 13, 6.6$  Hz, 2H), 1.33 (d,  $J = 9.0$  Hz, 1H), 1.30 – 1.23 (m, 5H), 1.23 – 1.20 (m, 1H), 1.17 (s, 3H), 1.12 (dd,  $J = 13, 6.5$  Hz, 1H), 0.92 (s, 3H), 0.90 – 0.81 (m, 5H).  $^{13}\text{C-NMR}$  (151 MHz, Chloroform-*d*):  $\delta$  170.4, 142.0, 141.3, 138.9, 129.2, 126.4, 122.2, 80.6, 73.8, 64.8, 54.4, 50.6, 46.4, 45.5, 41.5, 37.8, 36.8, 36.4, 34.8, 34.2, 33.5, 32.2, 29.9, 27.6, 26.5, 23.8, 22.9, 22.0, 21.4, 18.9, 13.9, 10.8.

Ato	Chemic	COS	HSQ	HMB	Ato	Chemic	COS	HSQ	HMB	Ato	Chemic	COS	HSQ	HMB
m	al	Y	C	C	m	al	Y	C	C	m	al	Y	C	C
1 C	36.5		1', 1''	19	24 C	33.5		14,	14	24 C	33.5		24'	24'
H'	1.87		1		12 C	41.6		12	14,	H'	1.67		24	24
H''	1.20	2', 2''	1		H2	1.40	11',	12	14,	H''				
2 C	27.6		2', 2''	4'			11''		17, 20	25 C	33.5		25	25
H'	1.88	1'', 2''	2		13 C	54.5			18,	H2	1.64		25	25
H''	1.58	1'', 2'	2						20, 21	26 C	10.8		26	26
3 C	73.8		3	4'	14 C	50.6		14	12	H3	0.86		26	26







**Reaction with (E)-N-(pentylidene)-p-nitrobenzenesulfonamide; (Figure 3-2; Entry D) to form Compound 3.7:**  $^1\text{H-NMR}$  (500 MHz, Chloroform-*d*)  $\delta$  8.34 (d,  $J = 8.5$  Hz, 2H), 8.01 (d,  $J = 8.5$  Hz, 2H), 5.51 (s, 1H), 4.70 – 4.61 (m, 1H), 4.31 (d,  $J = 9.4$  Hz, 1H), 3.56 (s, 1H), 2.42 – 2.30 (m, 2H), 2.21 (d,  $J = 18$  Hz, 1H), 2.07 – 1.99 (m, 5H), 1.94 (dd,  $J = 29, 14$  Hz, 4H), 1.81 (s, 1H), 1.79 – 1.73 (m, 1H), 1.68 – 1.62 (m, 1H), 1.40 – 1.35 (m, 1H), 1.27 – 1.24 (m, 2H), 1.20 (d,  $J = 11$  Hz, 3H), 1.10 – 1.05 (m, 3H), 1.01 (s, 4H), 0.97 (s, 4H), 0.89 (d,  $J = 7.1$  Hz, 3H), 0.74 (t,  $J = 6.7$  Hz, 3H).

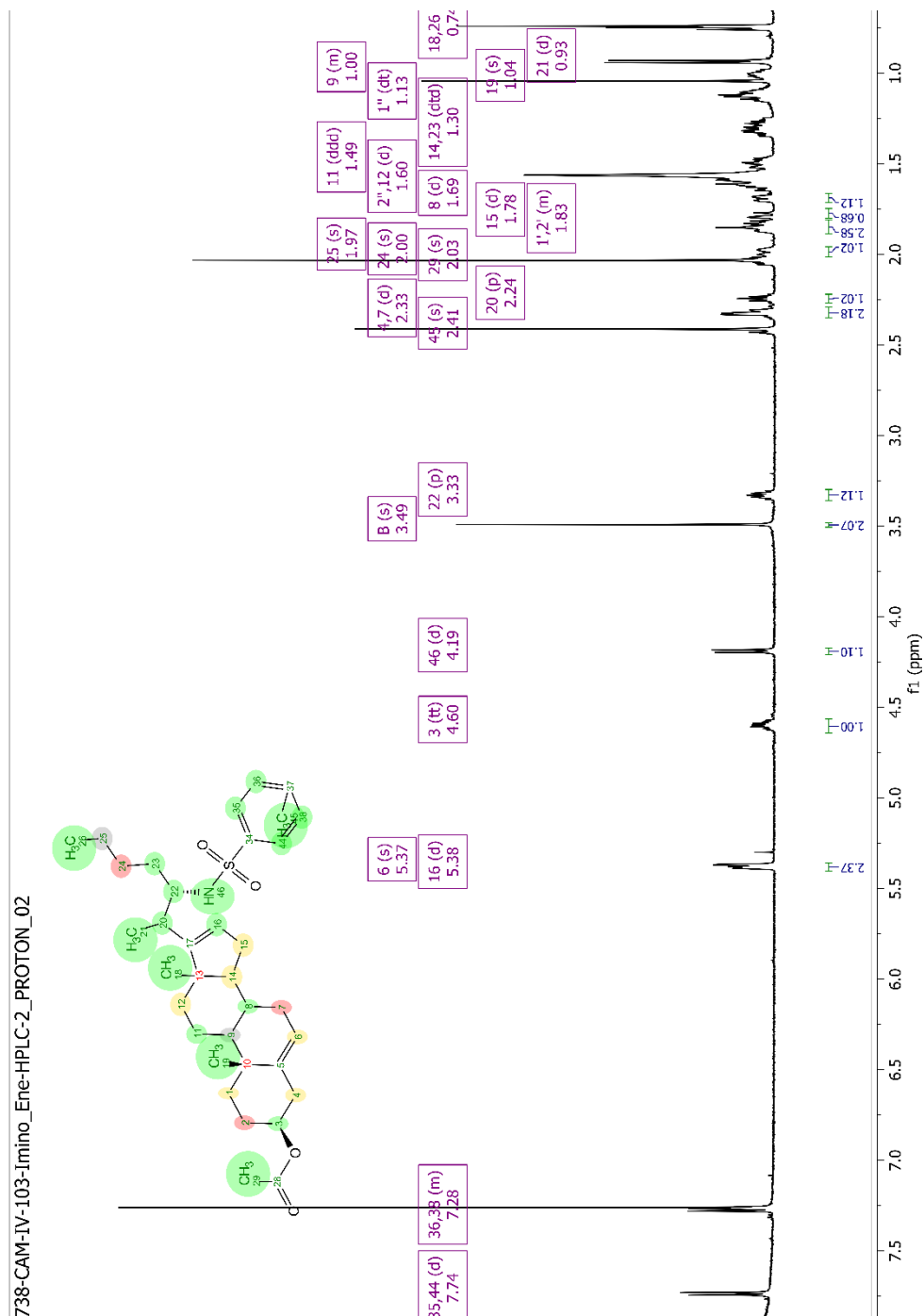


Figure 3-18. <sup>1</sup>H-NMR of Compound 3.5 in chloroform-*d*.

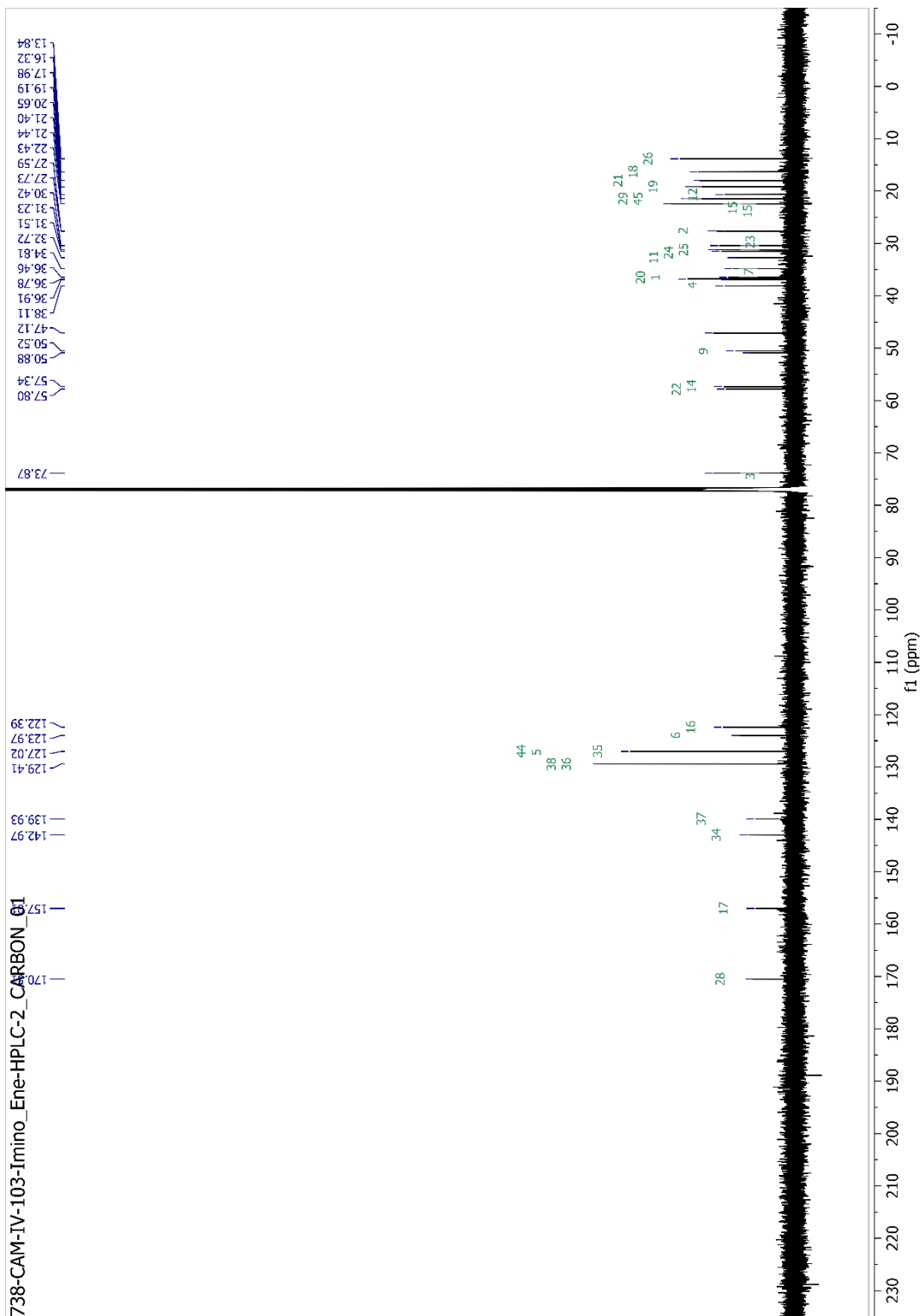
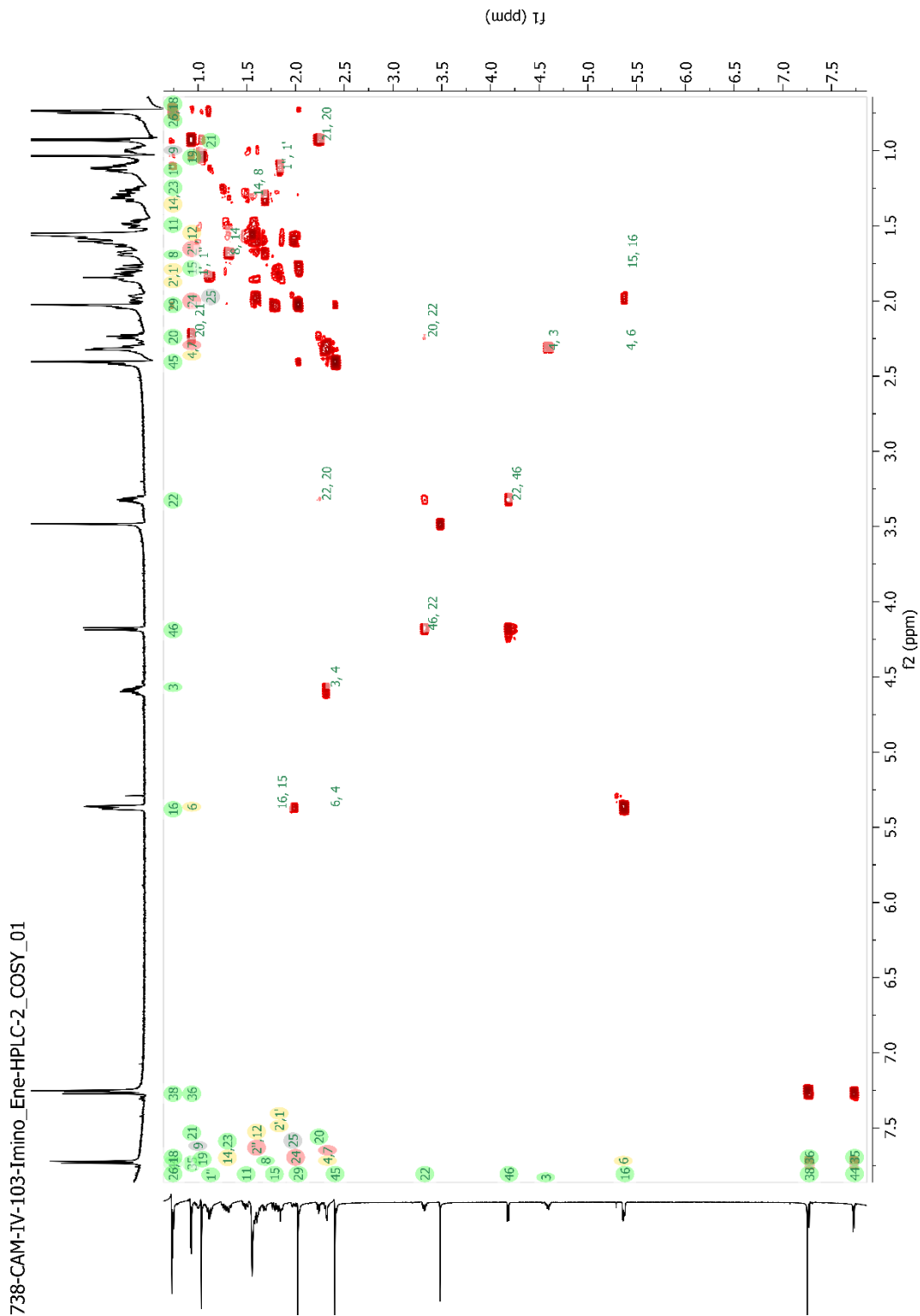


Figure 3-19.  $^{13}\text{C}$ -NMR of Compound 3.5 in chloroform-*d*.



738-CAM-IV-103-Imino\_Ene-HPLC-2\_HSQCAD\_01

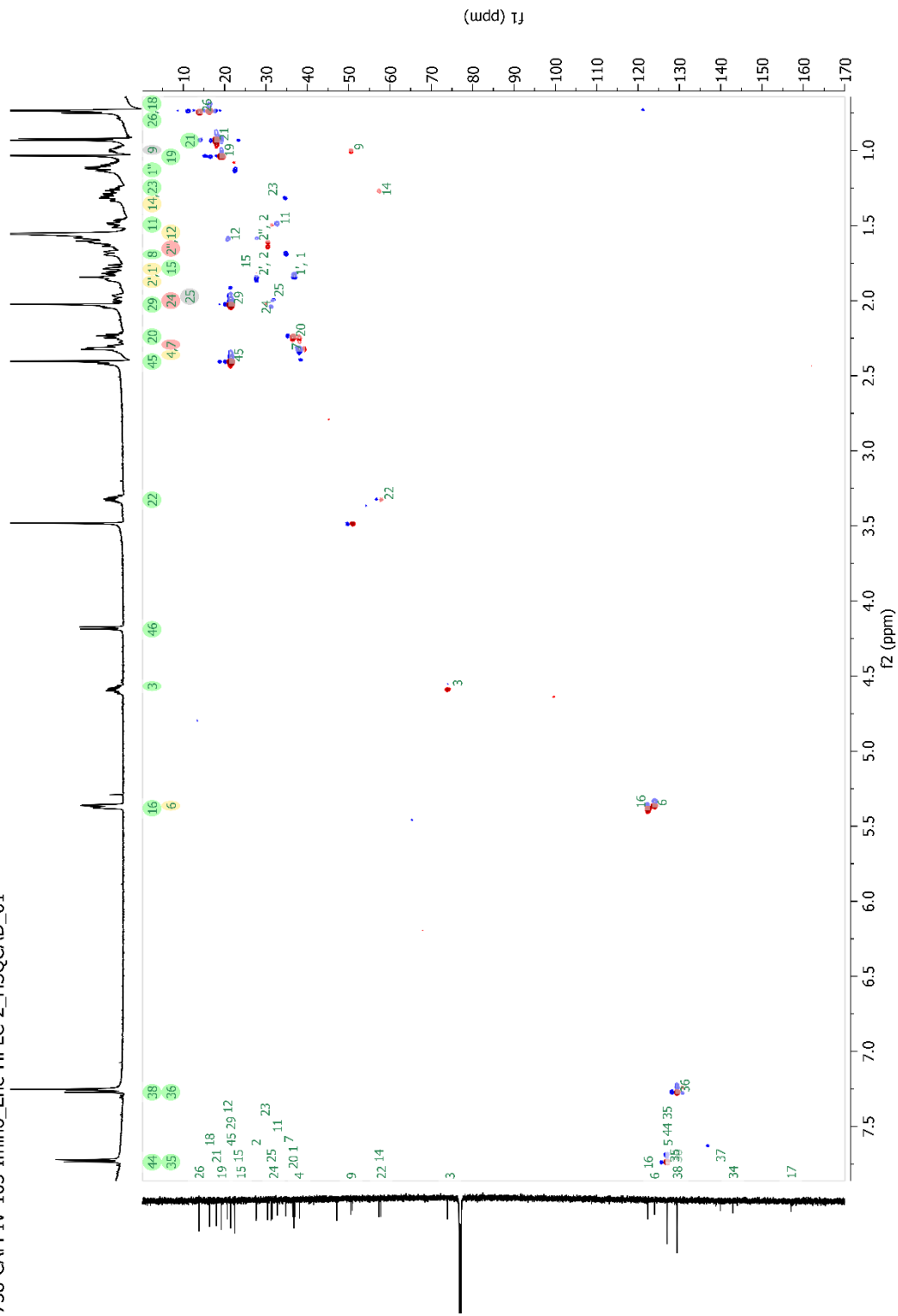
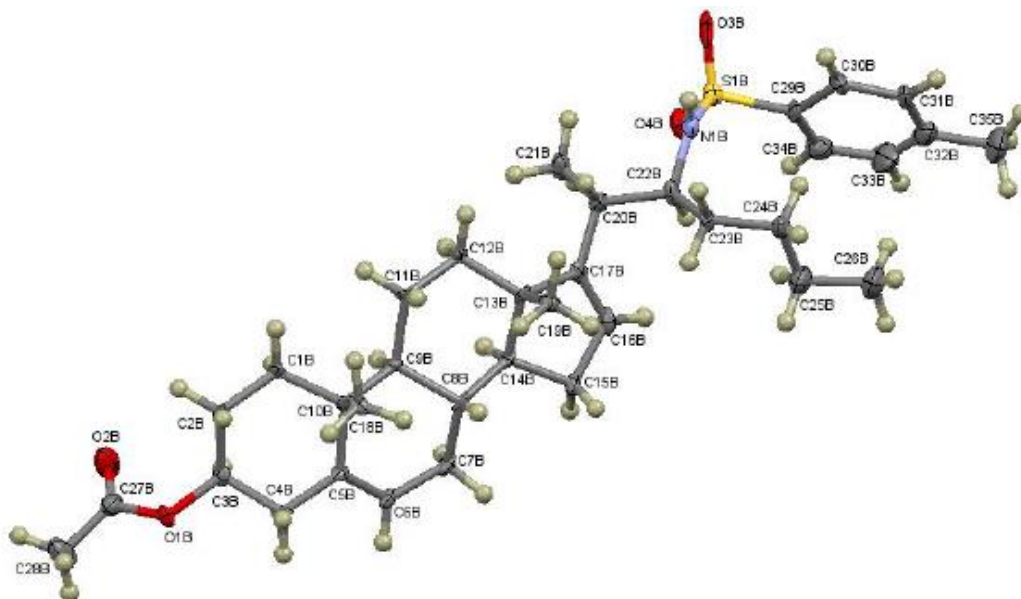


Figure 3-21. HSQC of Compound 3.5 in chloroform-*d*.



**Figure 3-22.** Crystal structure of **Compound 3.5**.

### Experimental

A colorless, block-shaped crystal of dimensions 0.052 x 0.164 x 0.220 mm was selected for structural analysis. Intensity data for this compound were collected using a D8 Quest k-geometry diffractometer with a Bruker Photon II cpad area detector (1) and an Incoatec I $\mu$ s microfocus Mo K $\alpha$  source ( $\lambda = 0.71073 \text{ \AA}$ ). The sample was cooled to 100(2) K. Cell parameters were determined from a least-squares fit of 9394 peaks in the range  $2.23 < \theta < 25.69^\circ$ . A total of 278681 data were measured in the range  $2.188 < \theta < 25.681^\circ$  using  $\phi$  and  $\omega$  oscillation frames. The data were corrected for absorption by the empirical method (2) giving minimum and maximum transmission factors of 0.6581 and 0.7456. The data were merged to form a set of 25381 independent data with  $R(\text{int}) = 0.0824$  and a coverage of 99.9 %.

The monoclinic space group  $P21$  was determined by systematic absences and statistical tests and verified by subsequent refinement. The structure was solved by direct methods and refined by full-matrix least-squares methods on  $F^2$  (3). The positions of hydrogens bonded to carbons and nitrogens were initially determined by geometry and were refined using a riding model. Hydrogens bonded to water oxygens were estimated from possible hydrogen bonds, and their positions were refined with a riding model. Non-hydrogen atoms were refined with anisotropic displacement parameters. Hydrogen atom displacement parameters were set to 1.2 (1.5 for methyl) times the isotropic equivalent displacement parameters of the bonded atoms. A total of 1520 parameters were refined against 1383 restraints and 25381 data to give  $wR(F^2) = 0.1726$  and  $S = 1.008$  for weights of  $w = 1/[\sigma^2(F^2) + (0.1340 P)^2 + 2.8000 P]$ , where  $P = [Fo^2 + 2Fc^2] / 3$ . The final  $R(F)$  was 0.0649 for the 24170 observed,  $[F > 4\sigma(F)]$ , data. The largest shift/s.u. was 0.021 in the final refinement cycle. The final difference map had maxima and minima of 1.657 and  $-0.612 \text{ e/\AA}^3$ , respectively. The absolute structure was determined by refinement of 7 the Flack parameter(4).

### Comment

There were 4 steroid molecules and 2 water molecules in the asymmetric unit. After initial refinement, the structure was shown to exhibit twinning by merohedry with a refined twin ratio of 0.4643(17). Restraints on the displacement parameters of all steroid atoms were required. The displacement ellipsoids were drawn at the 50% probability level.

## References

- (1) (a) Data Collection: APEX3 (2018) Bruker AXS Inc., Madison, Wisconsin, USA. (b) Data Reduction: SAINT (2016) Bruker AXS Inc., Madison, Wisconsin, USA.  
 (2) L. Krause, R. Herbst-Irmer, G. M. Sheldrick, and D. Stalke (2015). *J. Appl. Cryst.*, *48*, 3-10.  
 (3) (a) G. M. Sheldrick (2015). *Acta Cryst.*, *A71*, 3-8. (b) G. M. Sheldrick (2015). *Acta Cryst.*, *C71*, 3-8.  
 (4) S. Parsons, H. D. Flack, and T. Wagner (2013). *Acta Cryst.*, *B69*, 249-259.

Table 7. Crystal data and structure refinement for homoallylic tosyl amine with pentyl side chain

<b>Empirical formula</b>	<b>2(C<sub>30</sub> H<sub>51</sub> N O<sub>4</sub> S) · (C<sub>2</sub> H<sub>3</sub> N) · (H<sub>2</sub>O)</b>	
	<b>C<sub>70</sub> H<sub>104</sub> N<sub>2</sub> O<sub>9</sub> S<sub>2</sub></b>	
<b>Formula weight</b>	<b>1181.67</b>	
<b>Crystal system</b>	<b>monoclinic</b>	
<b>Space group</b>	<b>P2<sub>1</sub></b>	
<b>Unit cell dimensions</b>	<b>a = 12.0830(4) Å</b>	<b>α = 90°</b>
	<b>b = 11.3592(5) Å</b>	<b>β = 97.072(13)°</b>
	<b>c = 49.0680(18) Å</b>	<b>γ = 90°</b>
<b>Volume</b>	<b>6683.5(4) Å<sup>3</sup></b>	
<b>Z, Z'</b>	<b>4, 1</b>	
<b>Density (calculated)</b>	<b>1.174 Mg/m<sup>3</sup></b>	
<b>Wavelength</b>	<b>0.71073 Å</b>	
<b>Temperature</b>	<b>100(2) K</b>	
<b>F(000)</b>	<b>2568</b>	
<b>Absorption coefficient</b>	<b>0.136 mm<sup>-1</sup></b>	
<b>Absorption correction</b>	<b>semi-empirical from equivalents</b>	
<b>Max. and min. transmission</b>	<b>0.7456 and 0.65816</b>	
<b>Theta range for data collection</b>	<b>2.188 to 25.681°</b>	
<b>Reflections collected</b>	<b>278681</b>	
<b>Independent reflections</b>	<b>25381 [R(int) = 0.0824]</b>	
<b>Data / restraints / parameters</b>	<b>25381 / 1383 / 1520</b>	

<b><math>wR(F^2 \text{ all data})</math></b>	<b><math>wR2 = 0.1726</math></b>
<b><math>R(F \text{ obsd data})</math></b>	<b><math>R1 = 0.0649</math></b>
<b>Goodness-of-fit on <math>F^2</math></b>	<b>1.008</b>
<b>Observed data [<math>I &gt; 2 \sigma(I)</math>]</b>	<b>24170</b>
<b>Absolute structure parameter</b>	<b>0.031(18)</b>
<b>Extinction coefficient</b>	<b>n/a</b>
<b>Largest and mean shift / s.u.</b>	<b>0.021 and 0.003</b>
<b>Largest diff. peak and hole</b>	<b>1.657 and -0.612 e/Å<sup>3</sup></b>



739-CAM-IV-103-Imino\_Ene-HPLC-3\_PROTON\_02

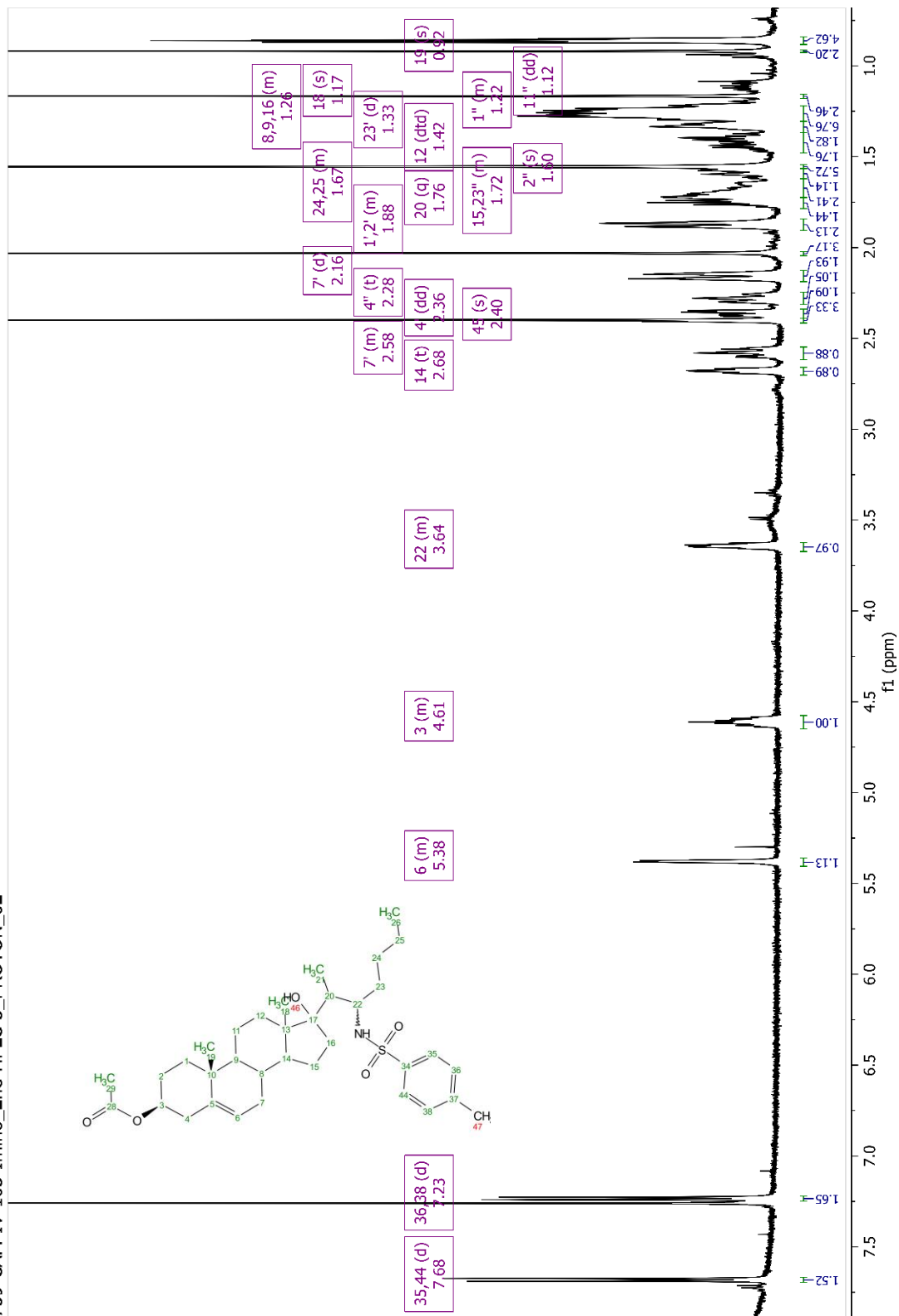


Figure 3-23. <sup>1</sup>H-NMR of Compound 3.6 in chloroform-*d*.

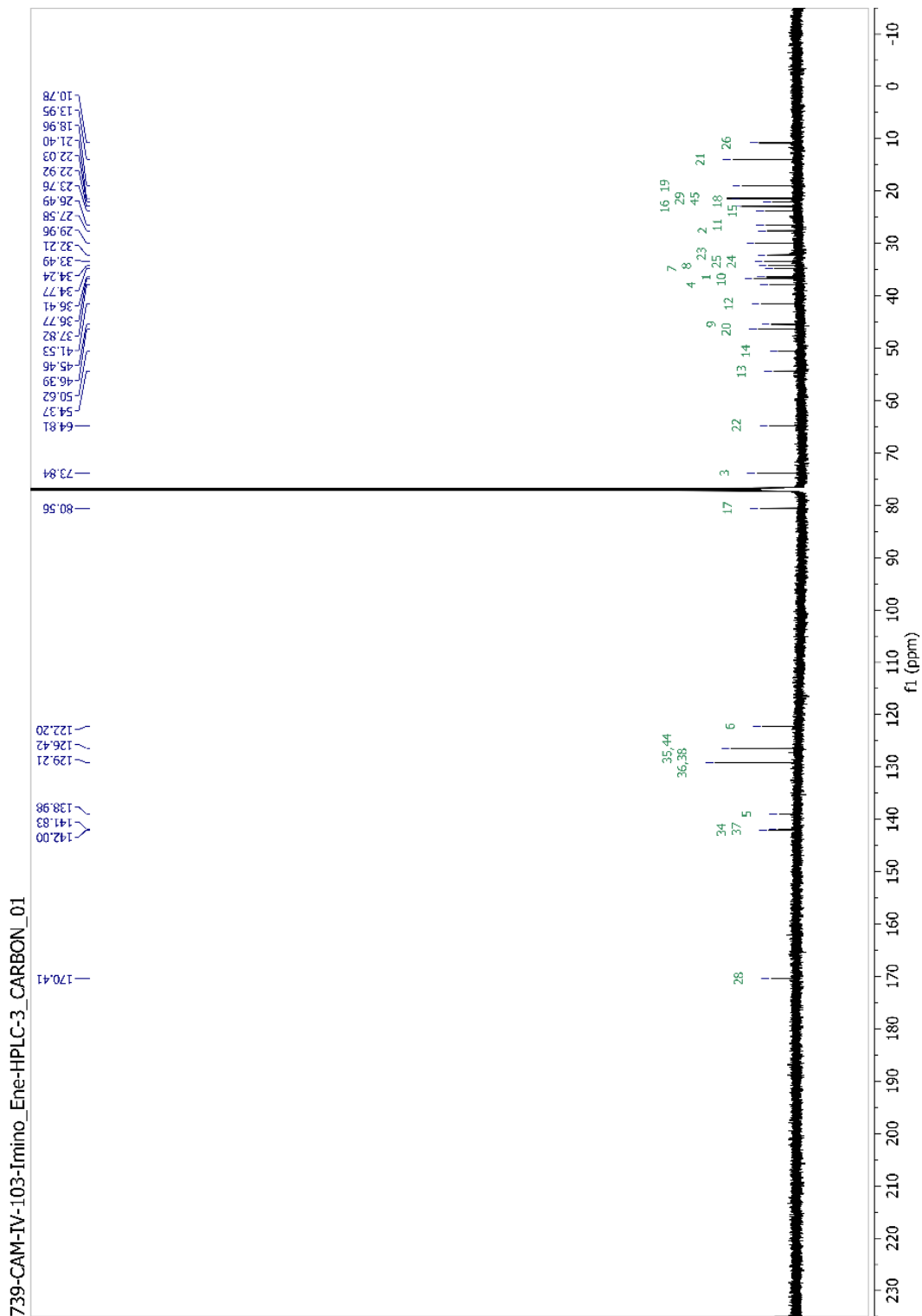


Figure 3-24.  $^{13}\text{C}$ -NMR of Compound 3.6 in chloroform-*d*.

739-CAM-IV-103-Imino\_Ene-HPLC-3\_COSY\_01

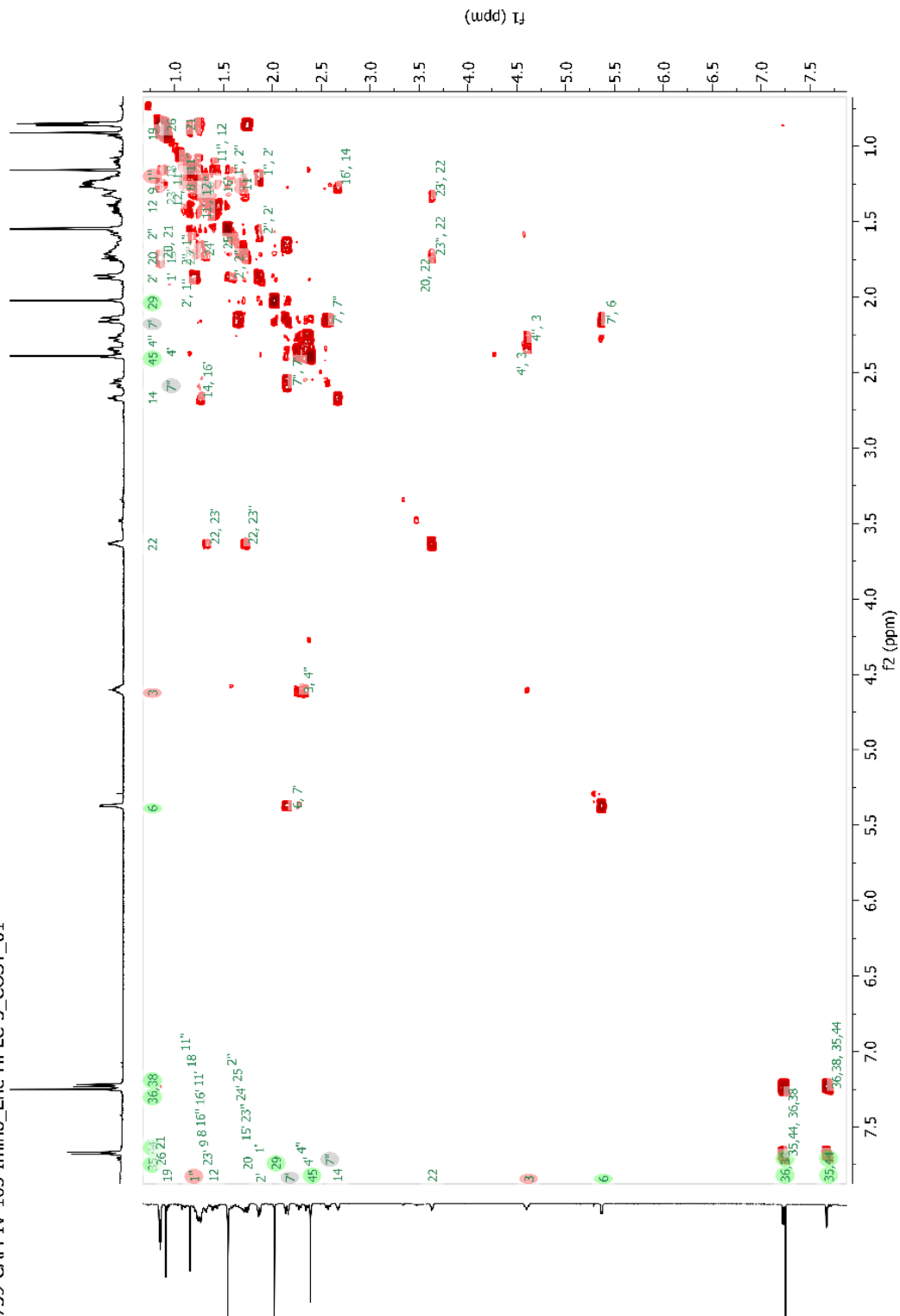


Figure 3-25. COSY of Compound 3.6 in chloroform-*d*.

739-CAM-IV-103-Imino\_Ene-HPLC-3\_HSQCAD\_01

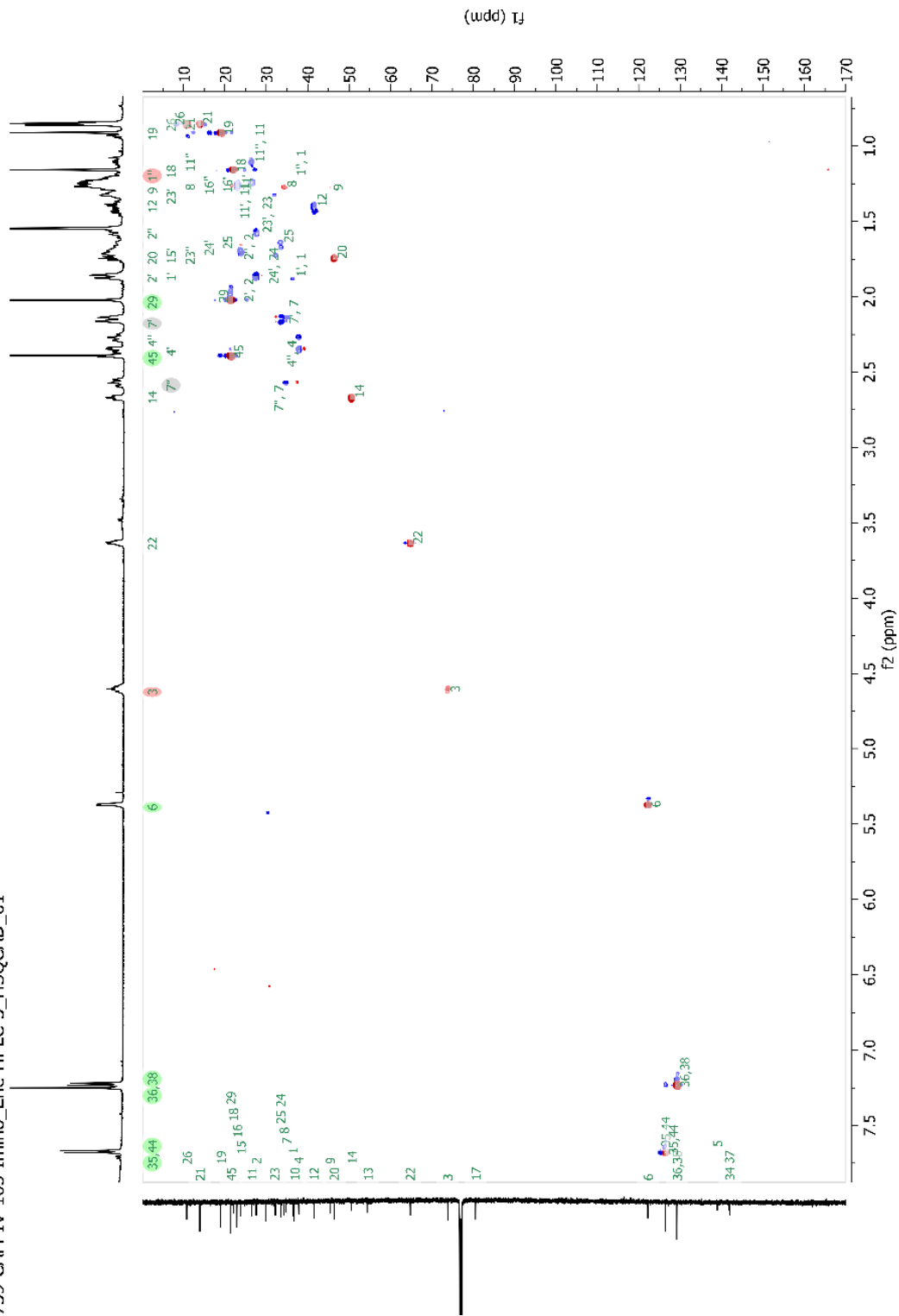


Figure 3-26. HSQC of Compound 3.6 in chloroform-*d*.

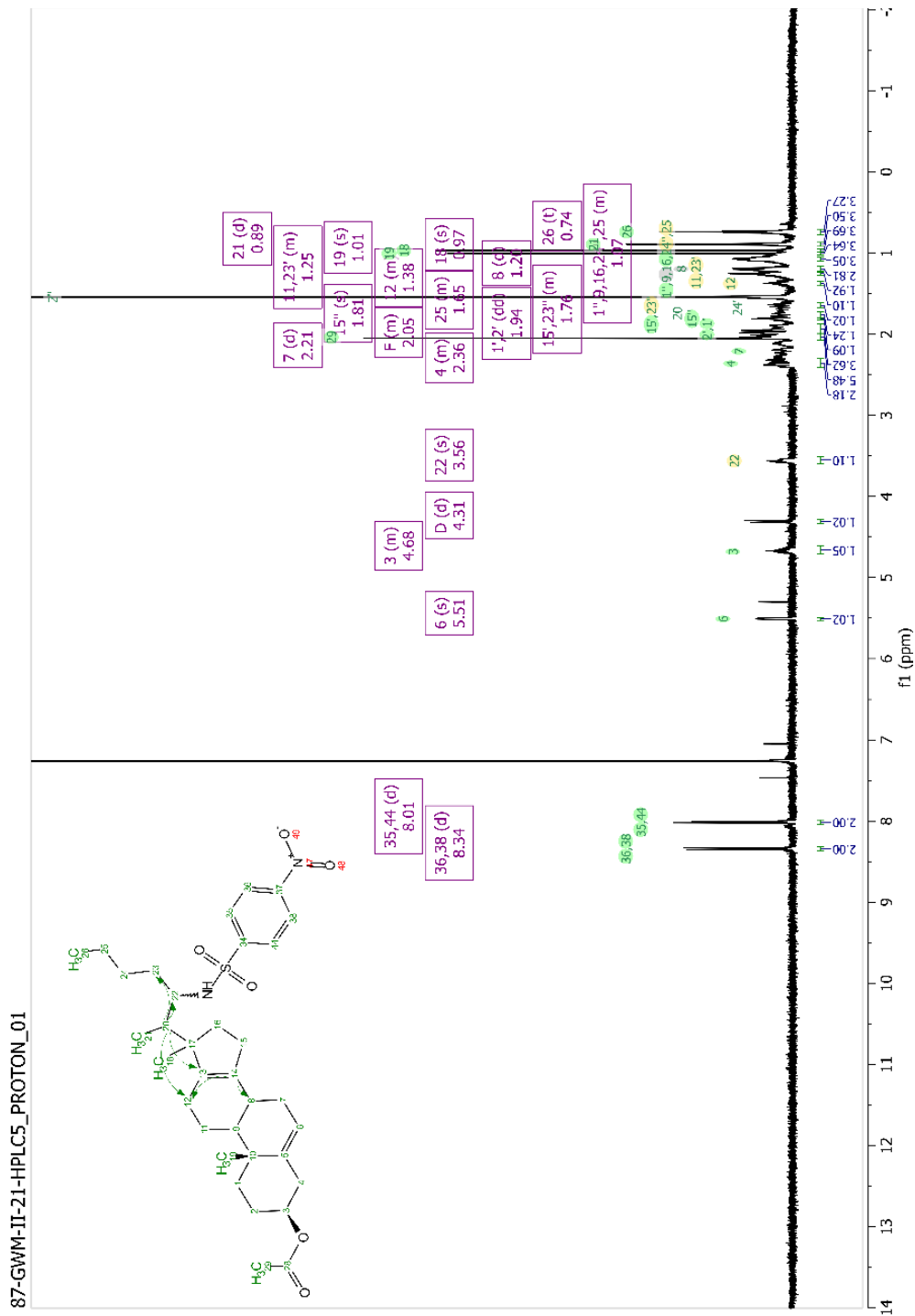


Figure 3-27.  $^1\text{H-NMR}$  of Compound 3.7 in chloroform- $d$ .



## **Chapter 4: Structure-activity relationships of ligand binding to oxysterol-binding protein (OSBP) and OSBP-related protein 4 (ORP4)**

**Abstract:** Oxysterol-binding protein (OSBP) and OSBP-related protein 4 (ORP4) have emerged as potentially druggable targets in antiviral and precision cancer drug development. The oxysterol-binding proteins were discovered based on their ability to bind oxysterols *in vitro*, including 25-hydroxycholesterol. Multiple biologically active, structurally diverse small molecules function through targeting the OSBP/ORP family of proteins, including the antiviral steroidal compounds, OSW-1. The structure-activity relationship (SAR) of oxysterol binding to OSBP and ORP4 have not been extensively characterized. Within this research project, a library of 20(*S*)-hydroxycholesterol analogs with varying aliphatic side chains were prepared and characterized to provide the first comprehensive report of human OSBP and ORP4 oxysterol SAR. The side chain analogs reveal that the sterol isohexyl side chain is required for oxysterol binding to OSBP and ORP4, and alterations of the side chain length or branching is not tolerated for OSBP and ORP4 binding. The characterization of ligand binding to OSBP and ORP4 will allow for the development of small molecule antiviral and anticancer compounds operating through multiple modes of interaction.

**Contributions:** I synthesized (*R/S*)-*n*-octyl- and (*R/S*)-*n*-butyl-pregnenolol analogs, synthesized all 22-hydroxysterol analogues, assembled the supporting information, and assisted with the management of the undergraduate syntheses. Dr. Anh Le-McClain developed the synthesis routes of starting materials and managed the undergraduate syntheses. Mr. Zach Severance and Mr. Ryan Bensen performed all biological evaluations of the screened oxysterol compounds. Gianni Manginelli, Sophia Sakers, and Hailee Rau each contributed two oxysterol compounds to the generated compound library.

## **4.1. Introduction**

### **4.1.4. Oxysterol derivation to better define OSBP/ORP ligand binding**

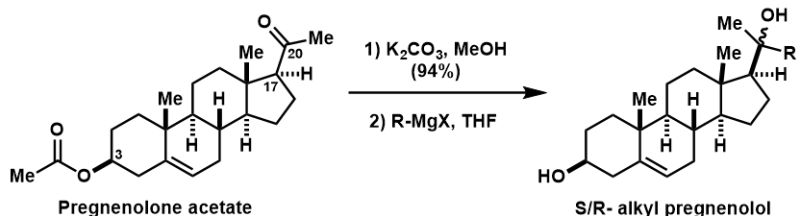
Several structurally-diverse small molecules have been shown to interact with both OSBP and ORP4, including the natural product compound OSW-1 (**Compound 1.1**).<sup>4</sup> The potential druggability of the protein family is highlighted by the evident roles of OSBP and ORP4 in viral replication and cancer cell proliferation respectively, as described in detail in **Section 1.1**.<sup>1-3</sup> OSBP and ORP4 are obvious and attractive therapeutic targets due to the ability of small molecules to bind and affect the cellular function of these proteins.<sup>8,9,32-35,37</sup> However, the potential drug development of OSBP and ORP4 is limited by the undefined structure activity relationships (SAR) of ligand binding. The ligand binding SAR is especially important for the development of small molecules, such as OSW-1, into selective ligands that bind OSBP for antiviral drug targeting, or ORP4 for anticancer drug targeting.<sup>32-35 8,9,37 1-3</sup>

25-hydroxycholesterol (25-OHC) is a high affinity ligand of OSBP and ORP4.<sup>178,179</sup> 25-OHC has a reported  $K_D$  ten-fold lower than cholesterol, indicating hydroxylation of the sterol side chain may be a critical component of OSBP/ORP binding.<sup>9</sup> Many other OSBP and ORP4 targeting small-molecules are structurally modified oxysterols including, OSW-1 (**Compound 1.1**), cephalostatin 1 (**Compound 1.2**), ritterzaine B, and T-00127-HEV2 (THEV).<sup>8,9,11,50,180</sup> These compounds have all been shown to inhibit [<sup>3</sup>H]-25-OHC binding to OSBP and ORP4.<sup>8,9,11,50,180</sup> The binding of oxysterols to OSBP and ORP4 has not been extensively characterized, particularly using human OSBP and ORP4. Therefore, understanding the SAR of oxysterol binding to human OSBP and ORP4,



particularly of the side-chain component, will be important in developing improved lead compounds for drug development, especially for OSW-1-derived compounds.

A) General synthetic route



B) Alkyl Pregnenolol analogues

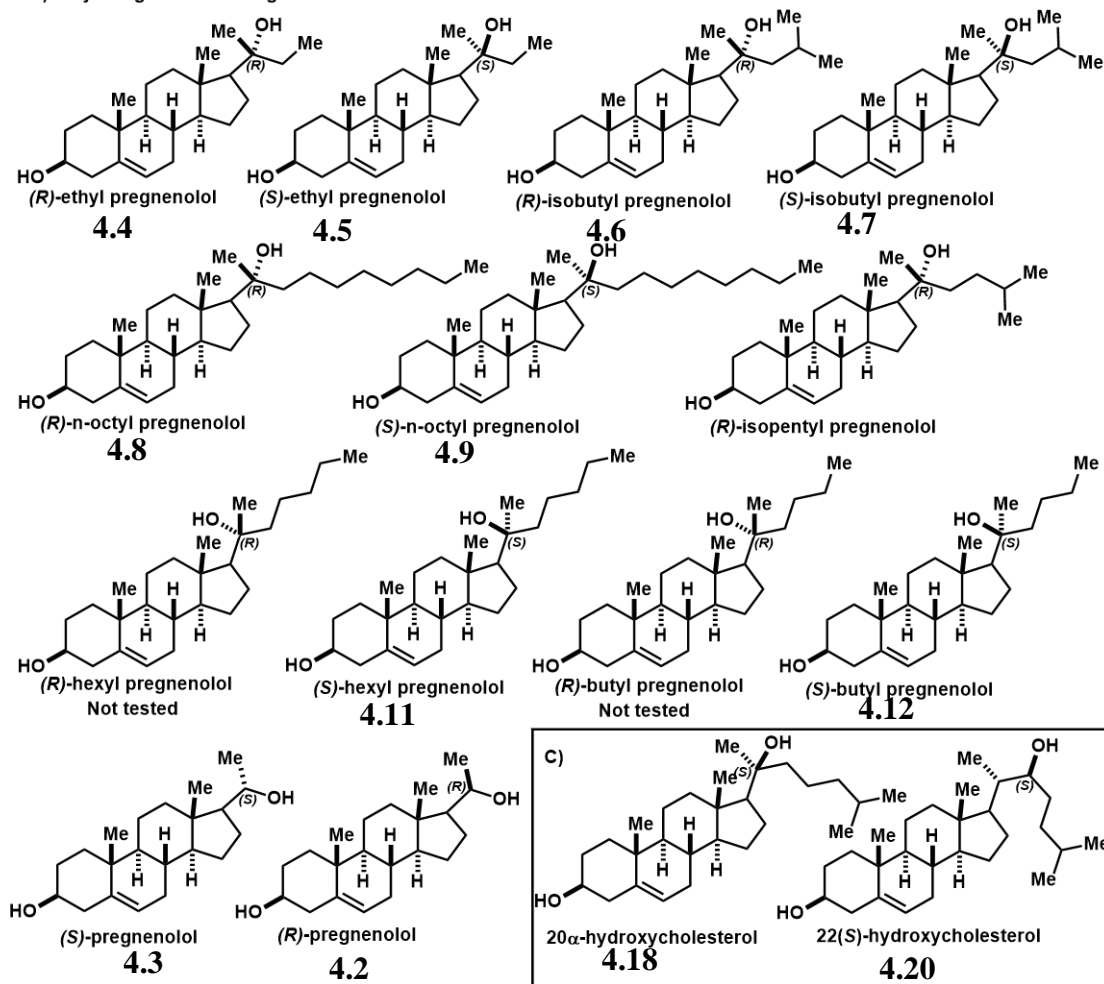


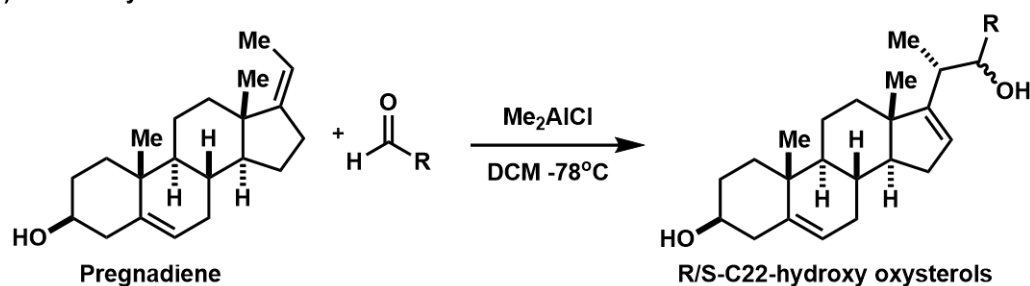
**Figure 4-1.** A. General synthetic route to generate alkyl pregnenolol analogs from pregnenolone acetate. B. Generated pregnenolol analogs consisting of changes to the alkyl side-chain component by varying the lengths and branching points. C. Commercially purchased hydroxycholesterols.

## 4.2. Results:

### 4.2.5. Synthesis of structurally modified oxysterol derivatives

To better define the ligand binding SAR of the oxysterol side chain, an oxysterol-derived scaffold library consisting of synthesized 20(*S*)-OHC derivatives with truncated and structurally modified alkyl side chains (**Figure 4-1** and **Figure 4-2**) were prepared. Thirteen C20-hydroxy oxysterol derivatives (**Figure 4-1**) were prepared through alkyl Gignard reactions with pregnenolol. Pregnenolone acetate was saponified in the presence

#### A) General synthetic route



#### B) Synthesized C22-hydroxy Oxysterols

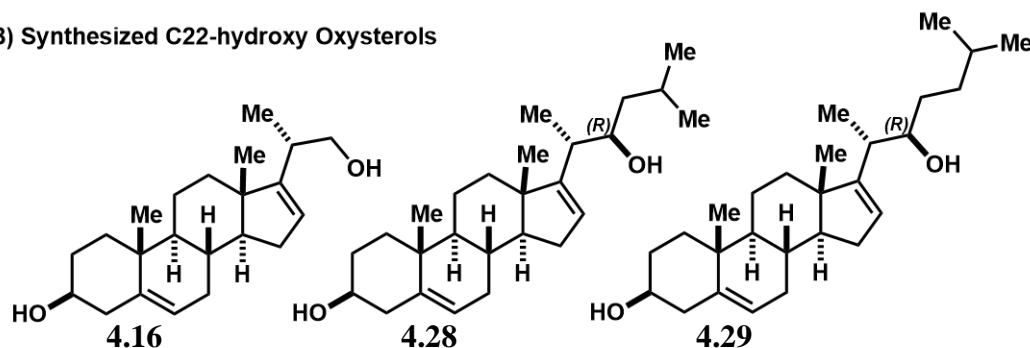


**Figure 4-2. A.** General synthetic route to generate 22-hydroxy oxysterol analogs from pregnenolone **B.** Synthesized (*R*)-22-hydroxy oxysterol of varying side chain length and branching.

of potassium carbonate in methanol to generate gram quantities of pregnenolol. The Grignard reagents (i.e., alkylmagnesium halide) used were either commercially available, or generated *in situ* through the reaction of magnesium metal turnings and alkyl halides with iodine as an activator.<sup>181</sup> Both *R* and *S* C20-stereoisomers were produced, but in all examples, the *S*-stereoisomer predominated the mixture. This is presumably due to the

steric nature of steroids, especially the C19-methyl group which blocks *Re* face approach to the carbonyl while allowing the Grignard nucleophile to access to *Si* face.<sup>140,142</sup> In some instances, 20(*R*)-epimer oxysterol analogs were produced in sufficient quantities for isolation and biological testing (**Figure 4-1**).

Three (*R*)-22-hydroxy oxysterol derivatives were also made (**Figure 4-2**) through reacting pregnadiene with commercially purchased alkyl aldehydes in the presence of dimethyl aluminum chloride at cryogenic temperatures. The C22(*R*)-stereoisomer was then purified for biological evaluation. **Compound 2.11**, required the synthesis of 4-methyl pentanal (**2.17**) which was prepared through the reduction of 4-methyl valeric acid (**2.15**) to produce 4-methyl pentanol (**2.16**). The resulting alcohol which was then oxidized to arrive at the desired 4-methyl-pentanal, as described in **Section 2.2.4.2**.

#### **4.2.6. OSBP and ORP4 binding activity of structurally modified oxysterol side chain derivatives**

The produced oxysterol library of compounds (**Figure 4-1** and **Figure 4-2**) were evaluated for OSBP and ORP4 binding to develop the first comprehensive report of human OSBP and ORP4 oxysterol SAR. The well-established radioactive 25-hydroxy cholesterol (<sup>3</sup>H]-25-OHC) competitive binding assays were performed by Mr. Zach Severance to measure binding affinity of the generated oxysterols.<sup>4</sup> A panel of commercially available oxysterols were also tested for OSBP and ORP4 binding (**Table 4-1, Compounds 4.19-4.27**). These binding results present three new discoveries of oxysterol binding SAR to OSBP and ORP4. First, the side chain component is critical for oxysterol binding to OSBP and ORP4. Comparing (*S*)-pregnenolol (**4.3**) to C20-(*S*)-hydroxysterol (**4.18**) the absence of the alkyl side chain reduces binding to OSBP and

ORP4 several hundred-fold, as measured by  $K_i$  (**Table 4-1**). Second, the library of C-20(*S*)-oxysterols (**Compounds 4.3, 4.5, 4.7, 4.9, 4.10, 4.11, and 4.12**) show that modifications of the isoheptyl side chain structure is not tolerated for OSBP and ORP4

**Table 4-1.** [ $^3\text{H}$ ]-25-OHC competitive binding  $K_i$  values for OSBP and ORP4 of OHC Endogenous ligands as generated by Zack Severance. \*indicates non-sigmoidal.

Compound:	OSBP $K_i$ (nM):	ORP4 $K_i$ (nM):
OSW-1 (1.1)	11 ± 7	55 ± 8
( <i>R</i> )-pregnenolol (4.2)	-	-
( <i>S</i> )-pregnenolol (4.3)	-	-
( <i>R</i> )-ethyl pregnenolol (4.4)	-	-
( <i>S</i> )-ethyl pregnenolol (4.5)	>100,000	>100,000
( <i>R</i> )-isobutyl pregnenolol (4.6)	>100,000	>100,000
( <i>S</i> )-isobutyl pregnenolol (4.7)	>30,000	>30,000
( <i>R</i> )- <i>n</i> -octyl-pregnenolol (4.8)	>100,000	>100,000
( <i>S</i> )- <i>n</i> -octyl-pregnenolol (4.9)	>10,000	>20,000
( <i>S</i> )-isopentyl-pregnenolol (4.10)	1,300 ± 600	>2,000
( <i>S</i> )-hexyl-pregnenolol (4.11)	600 ± 10	780 ± 180
( <i>S</i> )-pentyl-pregnenolol (4.12)	>10,000	>30,000
25-hydroxy cholesterol (4.14)	24 ± 16	51 ± 26
Hydroxymethylpregnadiene (4.16)	>100,000	>100,000
22-hydroxy-isopentyl pregnadiene (4.28)	-	-
22-hydroxy -isoheptyl pregnadiene (4.29)	-	-
20( <i>R</i> )-hydroxycholesterol (4.17)	>12,000	>16,000
20( <i>S</i> )-hydroxycholesterol (4.18)	130 ± 35	320 ± 90
22( <i>R</i> )-hydroxycholesterol (4.19)	>50,000	>50,000
22( <i>S</i> )-hydroxycholesterol (4.20)	>10,000	>3,000

Figure 4-1 and Figure 4-2

binding (**Table 4-1**). Shortening the length of the side chain (**Compounds 4.2-4.7**) or extending the length of the side chain beyond six carbons (**Compounds 4.8 and 4.9**)

produced weak OSBP and ORP4 binding (**Table 4-1**). The isopentyl side chain analog (**4.10**) showed a ~6-fold loss of binding affinity for OSBP and ORP4, compared to 20(*S*)-hydroxycholesterol (**4.18**). Transforming the isohexyl side chain into a n-pentyl (**4.12**), where the branched methyl has been removed, resulted in a 3-4-fold increase in OSBP and ORP4  $K_i$  values, compared to 20(*S*)-hydroxycholesterol (**4.18**). Additionally, both (*R*) and (*S*) C22-hydroxycholesterol epimers showed weak binding to OSBP and ORP4.

### **4.3. Discussion**

The result of testing the oxysterol side chain analogs for OSBP and ORP4 binding (**Figure 4-2** and **Table 4-1**) suggests that the structure of the alkyl isohexyl side chain cannot be modified to produce high affinity interactions. This would suggest a hydrophobic binding pocket designed to fit the alkyl isohexyl side chain is present in OSBP and ORP4. However, side chain hydroxylations at both the C25 and the C20 positions, but not C22, provide high affinity binding to OSBP and ORP4. This would seem to contradict the possible existence of a hydrophobic side chain binding pocket present in OSBP and ORP4. One explanation that could explain both C20-hydroxycholesterol (**4.17**) and C-25 hydroxycholesterol (**4.14**) binding with high affinity, while not allowing changes to the isohexyl side chain, would be the existence of multiple side chain binding pockets in OSBP and ORP4.

These oxysterol-binding SAR results will be potentially useful in guiding the development of OSW-1 derived lead compounds by providing critical insight into ligand binding interactions within the OSBP and ORP4 ligand-binding domain. However, these results are not consistent with OSW-1 phenotypic SAR studies. Specifically, elongation of the side-chain component of OSW-1 appears to be well tolerated, exhibiting equivalent

growth inhibition within cancer cell lines (**Section 1.2.1**).<sup>68</sup> This inconsistency may be further evidence of the existence of multiple binding modes in OSBP and ORP4.

#### **4.4. Conclusions and future work**

In this study, a library of oxysterols with side chain modifications were generated and testing for binding to OSBP and ORP4, producing the first comprehensive report of oxysterol side chain binding SAR. Evaluation of the produced 20(*S*)-hydroxycholesterol analog compounds showed that the side chain is required for high-affinity binding to OSBP and ORP4, and any modifications of the isohexyl side chain were not well tolerated. Additionally, although C20(*S*)- and C25-hydroxycholesterols bound with high affinity to OSBP and ORP4, C22(*S*)-hydroxycholesterol and C22(*R*)-hydroxycholesterol showed weak binding to OSBP and ORP4. These results are somewhat contradictory, indicating flexibility in side hydroxylation positions but not flexibility in the hydrophobic isohexyl side chain.

These oxysterol-binding SAR results will be potentially useful in guiding the development of sterol-derived lead compounds targeting OSBP and ORP4, including OSW-1 derived lead compounds.

#### **4.5. Experimental and supporting information**

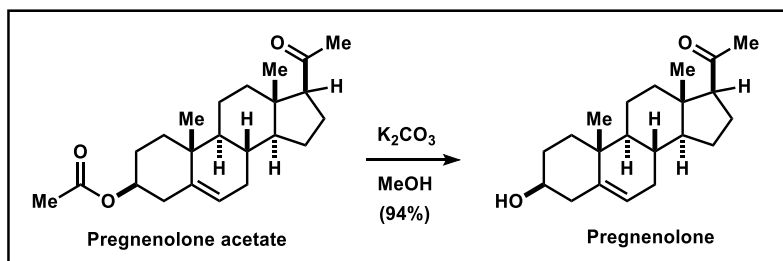


**Figure 4-3.** Saponification of commercially available pregnenolone acetate to pregnenolone

**Pregnenolone:** Pregnenolone was prepared through following a previously reported protocol.<sup>182</sup> To a solution of pregnenolone acetate (1.00 g, 2.79 mmol, 1.0 equiv.) in MeOH (15.0 mL) was added  $K_2CO_3$  (193.0 mg, 1.39 mmol) in one portion. The cloudy reaction mixture was stirred at room temperature for 16 hours. Then, the solvent was removed *in vacuo* to afford a crude mixture as a white solid. The crude solid was then dissolved in DCM (50 mL) and transferred to a separatory funnel. The organic phase was washed with 1N  $HCl_{(aq)}$  (2 x 20 mL), saturated  $NaHCO_3$  solution (2 x 20 mL), and DI  $H_2O$  (2 x 20 mL). The aqueous layers were combined and back extracted with DCM (2 x 15 mL). The organic layers were combined and washed with brine then dried over  $Na_2SO_4$ . The drying agent was removed and the solvent was evaporated *in vacuo* to afford crude product as a white solid, which was purified via silica gel column chromatography and eluted with 30% ethyl acetate in hexanes to afford pure pregnenolone (830.0 mg, 94% yield). The NMR data was consistent with the literature reported data.<sup>182</sup>  $^1H$ -NMR (400 MHz, Chloroform-*d*)  $\delta$  5.35 (dt,  $J = 4.5, 1.9$  Hz, 1H), 3.52 (tt,  $J = 9.8, 5.0$  Hz, 1H), 2.53 (t,  $J = 8.9$  Hz, 1H), 2.36 – 2.16 (m, 3H), 2.12 (s, 2H), 2.09 – 2.01 (m, 1H), 2.01 – 1.95 (m, 0H), 1.90 – 1.80 (m, 2H), 1.74 – 1.57 (m, 2H), 1.55 (s, 1H), 1.54 – 1.40 (m, 3H), 1.30 – 1.04 (m, 2H), 1.01 (s, 4H), 0.63 (s, 3H).

**General procedure for Grignard reactions of pregnenolone:**

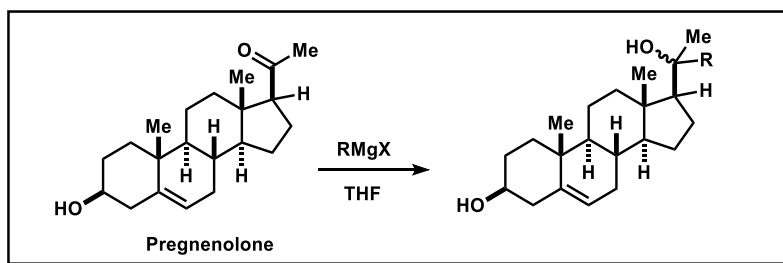


**Figure 4-4.** General synthesis of 20-hydroxycholesterol analogs via Grignard reaction

**20-hydroxy pregnenolol compounds:** The general procedure for Grignard reactions was adapted from a previously reported protocol, modified only by use of different alkyl Grignard reagents.<sup>183</sup> Grignard reagents (i.e., alkylmagnesium halides) used were either commercially available, or generated *in situ* through the reaction of magnesium metal turnings and alkyl halide with iodine as an activator, based on established literature protocol.<sup>181</sup>

Pregnenolone (1.0 equiv.) was dissolved in either anhydrous THF or  $Et_2O$  (0.16 M) and cooled to  $0^\circ C$  under nitrogen. A solution of alkylmagnesium bromide or chloride was added slowly dropwise over 10 minutes. The reaction mixture was stirred at room temperature, and the reaction progress was monitored via TLC. When the reaction reached completion, or no further progress was observed by TLC, the reaction mixture was cooled to  $0^\circ C$ . The reaction was quenched with saturated solution of  $NH_4Cl_{(aq)}$  and the mixture was stirred for 30 minutes at room temperature. The reaction mixture was transferred to a separatory funnel and then extracted with ethyl acetate (3 times). The organic layers were combined, washed with brine, and then dried over anhydrous  $Na_2SO_4$ . The drying agent was removed and the solvent was evaporated *in vacuo* to afford crude solid material. The crude material was purified via silica gel column chromatography and eluted with a gradient of 10-80% ethyl acetate in hexanes to provide the 20-

hydroxycholesterol analog as a mixture of diastereomers. This mixture was then subjected to reverse-phase HPLC purification (C(8)-Phenomenex column with MeCN/0.1% formic acid water to yield the pure compounds. In all cases, the distribution of products favored formation of the C22(*S*)-isomer.

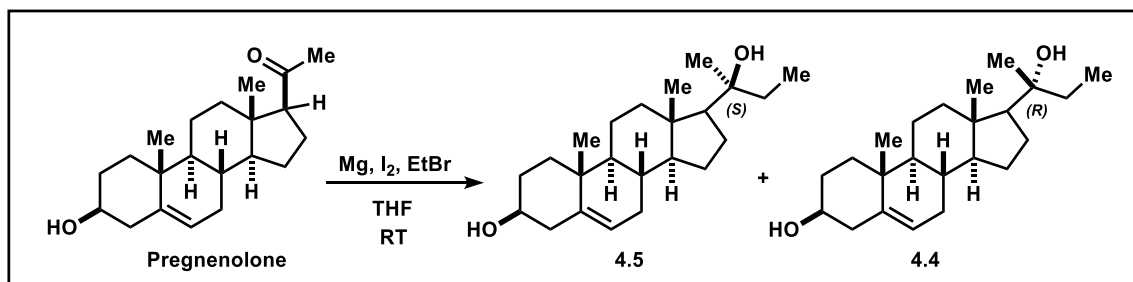


**Figure 4-5.** Synthesis of stereoisomers **Compound 4.4** and **Compound 4.5**; Grignard reagent was generated *in situ*.

**C22-(*S*)-20-OHC-ethyl (4.5) and C22-(*R*)-20-OHC-ethyl (4.4):** Grignard reagent was generated *in situ* following established protocol.<sup>181</sup> Magnesium turnings (115 mg, 4.79 mmol) were ground to a fine powder with mortar and pestle, and solid iodine (0.2 mg, 0.8 mmol) were put into an oven-dried 25-mL two-necked flask connected to a reflux condenser. The reaction flask was purged with nitrogen and vacuum and was then heated with a heat gun until a purple vapor was observed. After the reaction cooled, dry THF (100  $\mu$ L) was added, and the reaction mixture was stirred at room temperature for 5 minutes. A solution of ethylbromide (71  $\mu$ L, 0.95 mmol, dissolved in 0.95 mL dry THF) was slowly added to the reaction flask at 40°C. The reaction mixture became cloudy, and gas bubbles were observed. The reaction mixture was then reflux at 70°C for one hour, and then cooled to room temperature. To the reaction mixture was added a solution of pregnenolone (100 mg, 0.320 mmol) in 3.5 mL of dry THF. The reaction mixture was stirred at room temperature for 12 hours. When the reaction showed no further progress, it was quenched with sat.  $\text{NH}_4\text{Cl}_{(\text{aq})}$ . The mixture was stirred for 30 minutes and then transferred to a separatory funnel. The reaction mixture was then extracted with ethyl acetate (3x 5 mL). The organic layers were combined, washed with brine, and then dried over anhydrous  $\text{Na}_2\text{SO}_4$ . The drying agent was removed, and the solvent was evaporated *in vacuo* to afford a solid crude material. The crude material was purified via silica gel column chromatography and eluted with a gradient of 10-80% in ethyl acetate in hexanes to provide a crude mixture of product diastereomers. This mixture was then subjected to reverse-phase HPLC purification (C(8)-Phenomenex column, MeCN/0.1% formic acid in  $\text{H}_2\text{O}$  gradient) to yield the pure diastereomers **Compound 4.4** (18.0 mg, 16 %) and **Compound 4.5** (1.9 mg, 1.7 %).

**Compound 4.5:**  $^1\text{H-NMR}$  (500 MHz, Chloroform-*d*):  $\delta$  5.37 – 5.33 (m, 1H), 3.52 (tdd,  $J = 11, 5.2, 4.1$  Hz, 1H), 2.30 (ddd,  $J = 13, 5.1, 2.2$  Hz, 1H), 2.27 – 2.19 (m, 1H), 2.09 (dt,  $J = 12, 3.5$  Hz, 1H), 2.01 – 1.94 (m, 1H), 1.87 – 1.80 (m, 2H), 1.79 – 1.69 (m, 1H), 1.69 – 1.61 (m, 2H), 1.61 – 1.55 (m, 2H), 1.55 – 1.53 (m, 1H), 1.53 – 1.43 (m, 6H), 1.39 (dt,  $J = 13, 7.4$  Hz, 1H), 1.25 (s, 3H), 1.21 (td,  $J = 12, 5.3$  Hz, 1H), 1.17 – 1.11 (m, 1H), 1.11 – 1.06 (m, 1H), 1.06 – 1.02 (m, 1H), 1.01 (s, 3H), 0.92 (td,  $J = 11, 5.7$  Hz, 1H), 0.88 – 0.82 (m, 6H).  $^{13}\text{C-NMR}$  (75 MHz, Chloroform-*d*):  $\delta$  140.9, 121.8, 75.5,



71.9, 57.3, 57.0, 50.2, 42.7, 42.4, 40.2, 37.4, 36.6, 36.3, 31.9, 31.8, 31.5, 25.9, 23.9, 22.4, 21.1, 19.5, 13.7, 8.7.

**Compound 4.4:**  $^1\text{H-NMR}$  (500 MHz, Chloroform-*d*):  $\delta$  5.38 – 5.31 (m, 1H), 3.57 – 3.47 (m, 1H), 2.30 (ddd,  $J = 13, 5.1, 2.1$  Hz, 1H), 2.23 (tq,  $J = 13, 2.6$  Hz, 1H), 2.10 (dt,  $J = 12, 3.5$  Hz, 1H), 2.02 – 1.95 (m, 1H), 1.84 (dtd,  $J = 9.2, 5.4, 4.3, 3.0$  Hz, 2H), 1.80 – 1.67 (m, 2H), 1.67 – 1.63 (m, 1H), 1.60 (t,  $J = 7.5$  Hz, 2H), 1.57 – 1.56 (m, 1H), 1.55 (s, 3H), 1.53 – 1.48 (m, 4H), 1.48 – 1.40 (m, 2H), 1.30 – 1.22 (m, 2H), 1.18 – 1.13 (m, 1H), 1.11 (s, 3H), 1.09 – 1.02 (m, 1H), 1.01 (s, 3H), 1.00 – 0.94 (m, 1H), 0.92 (t,  $J = 7.4$  Hz, 3H), 0.87 (s, 3H).  $^{13}\text{C-NMR}$  (101 MHz, Chloroform-*d*):  $\delta$  140.8, 121.6, 75.9, 71.8, 57.9, 56.9, 50.0, 42.9, 42.3, 40.2, 37.2, 36.5, 34.9, 31.8, 31.6, 31.3, 26.3, 23.8, 23.2, 20.9, 19.39, 13.7, 8.4.

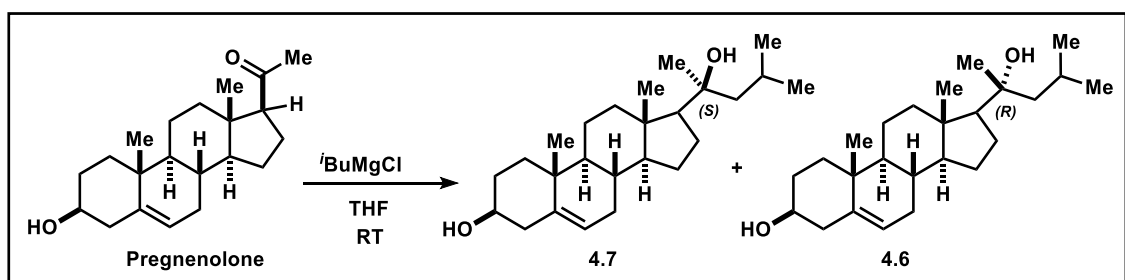
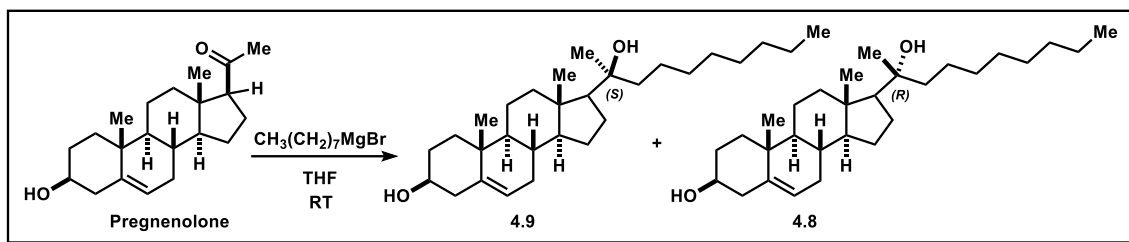


Figure 4-6. Synthesis of stereoisomers **Compounds 4.6** and **4.7**

**C22-(S)-20-OHC-*i*-butyl (4.7) and C22-(R)-20-OHC-*i*-butyl (4.6):** Following the general procedure, **Compounds 4.6** and **4.7** were obtained from pregnenolone (101.8 mg, 0.32 mmol) and isobutylmagnesium chloride (0.97 mL of 2.0 M solution in Et<sub>2</sub>O, 6 equiv. added over 2 hours) in dry THF (3.4 mL) as a mixture. Further reverse-phase HPLC separation yielded the pure diastereomers (**Compounds 4.7**: 10.0 mg, 8 % and **Compounds 4.6**: 2.1 mg, 1.7 %) as white solids.

**Compounds 4.7:**  $^1\text{H-NMR}$  (500 MHz, Chloroform-*d*):  $\delta$  5.37 – 5.32 (m, 1H), 3.52 (tdd,  $J = 11, 5.2, 4.2$  Hz, 1H), 2.30 (ddd,  $J = 13, 5.2, 2.1$  Hz, 1H), 2.27 – 2.19 (m, 1H), 2.11 (dt,  $J = 12, 3.5$  Hz, 1H), 2.00 – 1.94 (m, 1H), 1.87 – 1.80 (m, 2H), 1.79 – 1.67 (m, 3H), 1.67 – 1.58 (m, 1H), 1.57 – 1.47 (m, 4H), 1.47 – 1.41 (m, 2H), 1.39 (dd,  $J = 14, 4.4$  Hz, 1H), 1.31 (s, 3H), 1.28 (dd,  $J = 14, 7.1$  Hz, 1H), 1.21 (td,  $J = 12, 5.3$  Hz, 1H), 1.17 – 1.03 (m, 2H), 1.01 (s, 3H), 0.96 (d,  $J = 6.6$  Hz, 3H), 0.92 (d,  $J = 6.7$  Hz, 3H), 0.86 (s, 3H).  $^{13}\text{C-NMR}$  (126 MHz, Chloroform-*d*):  $\delta$  140.9, 121.7, 75.9, 71.9, 59.1, 57.1, 52.4, 50.2, 42.9, 42.4, 40.4, 37.4, 36.6, 31.9, 31.8, 31.5, 26.8, 25.5, 24.7, 24.3, 23.9, 22.7, 21.1, 19.5, 13.7. HRMS calcd for C<sub>25</sub>H<sub>41</sub>O: 357.3152 [M - OH]<sup>+</sup>, found 357.3155,  $\Delta$ ppm = 0.84 ppm.

**Compounds 4.6:**  $^1\text{H-NMR}$  (500 MHz, Chloroform-*d*):  $\delta$  5.38 – 5.33 (m, 1H), 3.52 (tt,  $J = 11, 4.5$  Hz, 1H), 2.30 (ddd,  $J = 13, 5.2, 2.1$  Hz, 1H), 2.27 – 2.19 (m, 1H), 2.14 (dt,  $J = 12, 3.5$  Hz, 1H), 2.00 – 1.94 (m, 1H), 1.90 – 1.80 (m, 3H), 1.75 – 1.67 (m, 2H), 1.67 – 1.58 (m, 1H), 1.58 – 1.41 (m, 8H), 1.23 (td,  $J = 12, 5.0$  Hz, 1H), 1.16 (s, 3H), 1.15 – 1.03 (m, 2H), 1.01 (s, 3H), 0.99 (d,  $J = 6.6$  Hz, 3H), 0.94 (d,  $J = 6.7$  Hz, 3H), 0.87 (s, 3H).  $^{13}\text{C-NMR}$  (126 MHz, Chloroform-*d*):  $\delta$  140.9, 121.7, 76.7, 71.9, 60.3, 57.0, 51.4, 50.2, 43.1, 42.4, 40.7, 37.4, 36.7, 31.9, 31.8, 31.5, 26.6, 25.5, 24.7, 24.2, 23.9, 23.4, 21.1, 19.5, 13.9. HRMS calcd for C<sub>25</sub>H<sub>41</sub>O: 357.3152 [M - OH]<sup>+</sup>, found 357.3156,  $\Delta$ ppm = 1.12 ppm.



**Figure 4-7.** Synthesis of **Compound 4.8** and **4.9**.

**C22-(S)-20-OHC-octyl (4.9) and C22-(R)-20-OHC-octyl (4.8):** Following the general procedure, compound **Compound 4.8 and 4.9** were obtained from pregnenolone (100.0 mg, 0.31 mmol) and octylmagnesium bromide (0.63 mL of 2.0 M solution in Et<sub>2</sub>O, 4 equiv added over 70 minutes) in anhydrous THF (3.4 mL) as a mixture. Further reverse-phase HPLC separation yielded the pure diastereomers (**Compound 4.9**: 15.2 mg, 11 % and **Compound 4.8**: 2.5 mg, 1.8 %) as white solids.

**Compound 4.9:** <sup>1</sup>H-NMR (500 MHz, Chloroform-*d*): δ 5.41 – 5.32 (m, 1H), 3.59 – 3.49 (m, 1H), 2.31 (ddd, *J* = 13, 5.1, 2.1 Hz, 1H), 2.28 – 2.21 (m, 1H), 2.11 (dt, *J* = 12, 3.5 Hz, 1H), 1.99 (ddt, *J* = 14, 5.1, 1.9 Hz, 1H), 1.89 – 1.81 (m, 2H), 1.81 – 1.72 (m, 1H), 1.72 – 1.61 (m, 2H), 1.54 – 1.49 (m, 3H), 1.49 – 1.42 (m, 2H), 1.36 – 1.23 (m, 14H), 1.23 – 1.16 (m, 2H), 1.16 – 1.05 (m, 2H), 1.03 (s, 3H), 1.00 – 0.92 (m, 1H), 0.92 – 0.87 (m, 6H). <sup>13</sup>C-NMR (75 MHz, Chloroform-*d*): δ 121.8, 75.4, 71.9, 57.7, 57.0, 50.2, 44.2, 42.8, 42.4, 40.2, 37.4, 36.6, 32.0, 31.9, 31.8, 31.5, 30.5, 29.8, 29.5, 26.6, 24.5, 23.9, 22.8, 22.5, 21.1, 19.5, 14.3, 13.8. HRMS calcd for C<sub>29</sub>H<sub>49</sub>O: 413.3778 [M - OH]<sup>+</sup>, found 413.3767, Δppm = -2.66 ppm.

**Compound 4.8:** <sup>1</sup>H-NMR (500 MHz, Chloroform-*d*): δ 5.35 (dt, *J* = 5.5, 1.9 Hz, 1H), 3.57 – 3.47 (m, 1H), 2.28 (dd, *J* = 5.1, 2.1 Hz, 1H), 2.23 (ddq, *J* = 13, 11.1, 2.6 Hz, 1H), 2.09 (dt, *J* = 12, 3.5 Hz, 1H), 1.98 (dtd, *J* = 167, 4.8, 2.5 Hz, 1H), 1.88 – 1.80 (m, 2H), 1.80 – 1.67 (m, 2H), 1.67 – 1.59 (m, 1H), 1.55 (d, *J* = 6.2 Hz, 5H), 1.53 – 1.42 (m, 4H), 1.38 – 1.31 (m, 1H), 1.31 – 1.19 (m, 10H), 1.18 – 1.13 (m, 1H), 1.12 (s, 3H), 1.10 – 1.02 (m, 1H), 1.01 (s, 3H), 1.00 – 0.90 (m, 1H), 0.90 – 0.85 (m, 6H). <sup>13</sup>C-NMR (75 MHz, Chloroform-*d*): δ 140.9, 121.8, 75.9, 71.9, 58.3, 57.0, 50.2, 43.0, 42.4, 40.2, 37.4, 36.6, 32.0, 31.9, 31.8, 31.5, 30.5, 29.8, 29.5, 27.2, 24.2, 23.9, 23.3, 22.8, 21.1, 19.5, 14.3, 13.9.

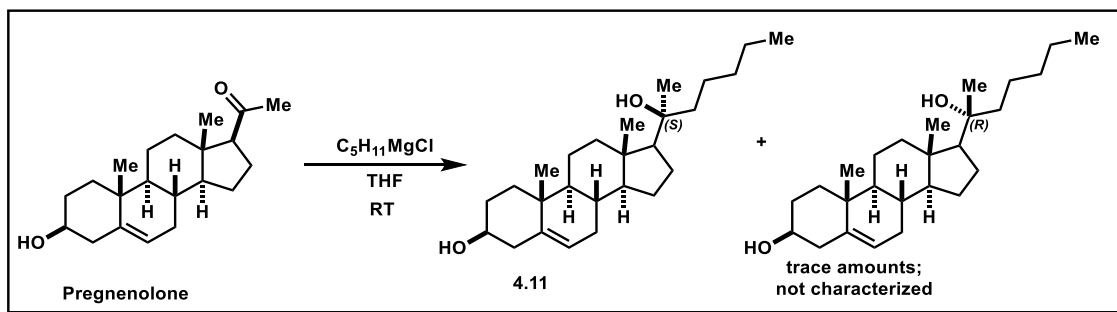


**Figure 4-8.** Synthesis of **Compound 4.11**.

**C22-(S)-20-OHC-pentyl (4.11):** Following the general procedure, compound **Compound 4.11** was obtained from pregnenolone (50.5 mg, 159.6  $\mu\text{mol}$ ) and pentyl magnesium chloride (480  $\mu\text{l}$  of 1 M solution, 480  $\mu\text{mol}$ , 3 equiv. added over 40 min.) in dry THF (3.4 mL) as a mixture. Further reverse-phase HPLC separation yielded the pure diastereomer (**Compound 4.11**: 52.4 mg, 85%) as a white solid.

**Compound 4.11:**  $^1\text{H-NMR}$  (500 MHz, Chloroform-*d*):  $\delta$  5.48 – 5.26 (m, 0H), 3.57 – 3.46 (m, 0H), 2.34 – 2.28 (m, 0H), 2.27 – 2.18 (m, 0H), 2.09 (dt,  $J = 12.6, 3.6$  Hz, 0H), 2.01 – 1.92 (m, 0H), 1.89 – 1.81 (m, 1H), 1.75 (d,  $J = 11.6$  Hz, 0H), 1.64 (d,  $J = 7.7$  Hz, 0H), 1.59 – 1.47 (m, 2H), 1.31 (dd,  $J = 10.4, 4.5$  Hz, 0H), 1.27 (s, 1H), 1.13 – 1.03 (m, 0H), 1.01 (s, 1H), 0.89 (t,  $J = 7.1$  Hz, 1H), 0.87 (s, 1H).  $^{13}\text{C-NMR}$  (151 MHz, Acetone-*d*<sub>6</sub>):  $\delta$  206.9, 140.9, 121.2, 74.9, 71.4, 57.6, 56.8, 50.0, 43.9, 42.5, 42.2, 40.1, 37.2, 36.4, 32.4, 31.7, 31.5, 31.3, 26.3, 23.8, 23.7, 22.5, 22.2, 20.8, 19.2, 13.9, 13.4.

**Compound 4.11 (R-isomer):** Isolated minimal amount, not characterized.

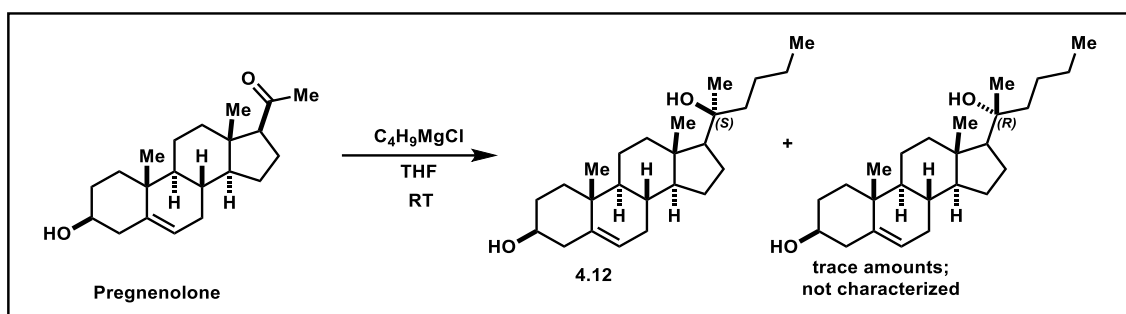


**Figure 4-9.** Synthesis of **Compound 4.12**

**C22-(S)-20-OHC-butyl (4.12):** Following the general procedure, compound **Compound 4.12** was obtained from pregnenolone (49.5 mg, 156.4  $\mu\text{mol}$ ) and butyl magnesium chloride (240  $\mu\text{l}$  of 2 M solution, 481  $\mu\text{mol}$ , 3 equiv. added over 40 min.) in dry THF. Further reverse-phase HPLC separation yielded the pure diastereomer (**Compound 4.12**: 55.7 mg, 95%) as a white solid.

**Compound 4.12:**  $^1\text{H-NMR}$  (500 MHz, Chloroform-*d*):  $\delta$  5.39 – 5.20 (m, 1H), 3.52 (s, 1H), 2.33 – 2.27 (m, 1H), 2.24 (d,  $J = 12$  Hz, 1H), 2.13 – 2.07 (m, 1H), 2.04 (s, 1H), 2.01 – 1.92 (m, 0H), 1.88 – 1.81 (m, 2H), 1.76 (q,  $J = 10.7, 9.6$  Hz, 1H), 1.65 (dt,  $J = 17.7, 9.3$  Hz, 1H), 1.52 – 1.42 (m, 5H), 1.27 (s, 2H), 1.01 (s, 2H), 0.90 (t,  $J = 7.0$  Hz, 3H), 0.87 (s, 2H).  $^{13}\text{C-NMR}$  (151 MHz, Chloroform-*d*):  $\delta$  140.8, 121.6, 75.2, 71.8, 56.9, 50.0, 43.7, 42.6, 42.3, 40.1, 37.2, 36.5, 31.8, 31.6, 31.3, 26.5, 26.4, 23.7, 23.3, 22.3, 20.9, 19.4, 14.1, 13.6.

**Compound 4.12 (R-isomer):** Isolated minimal amount, not characterized.

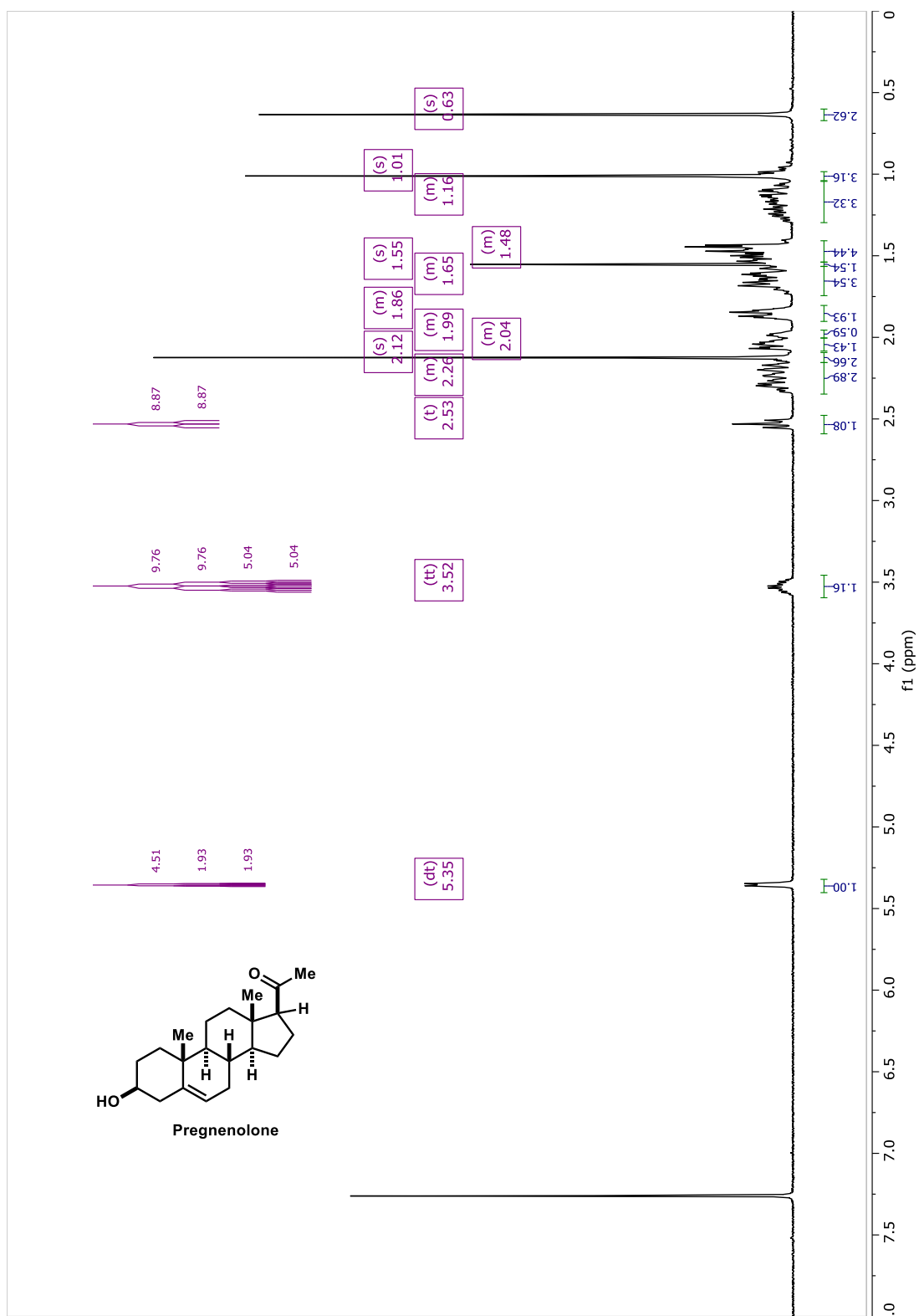


**Figure 4-10.** <sup>1</sup>H-NMR of starting material pregnenolone in chloroform-*d*.

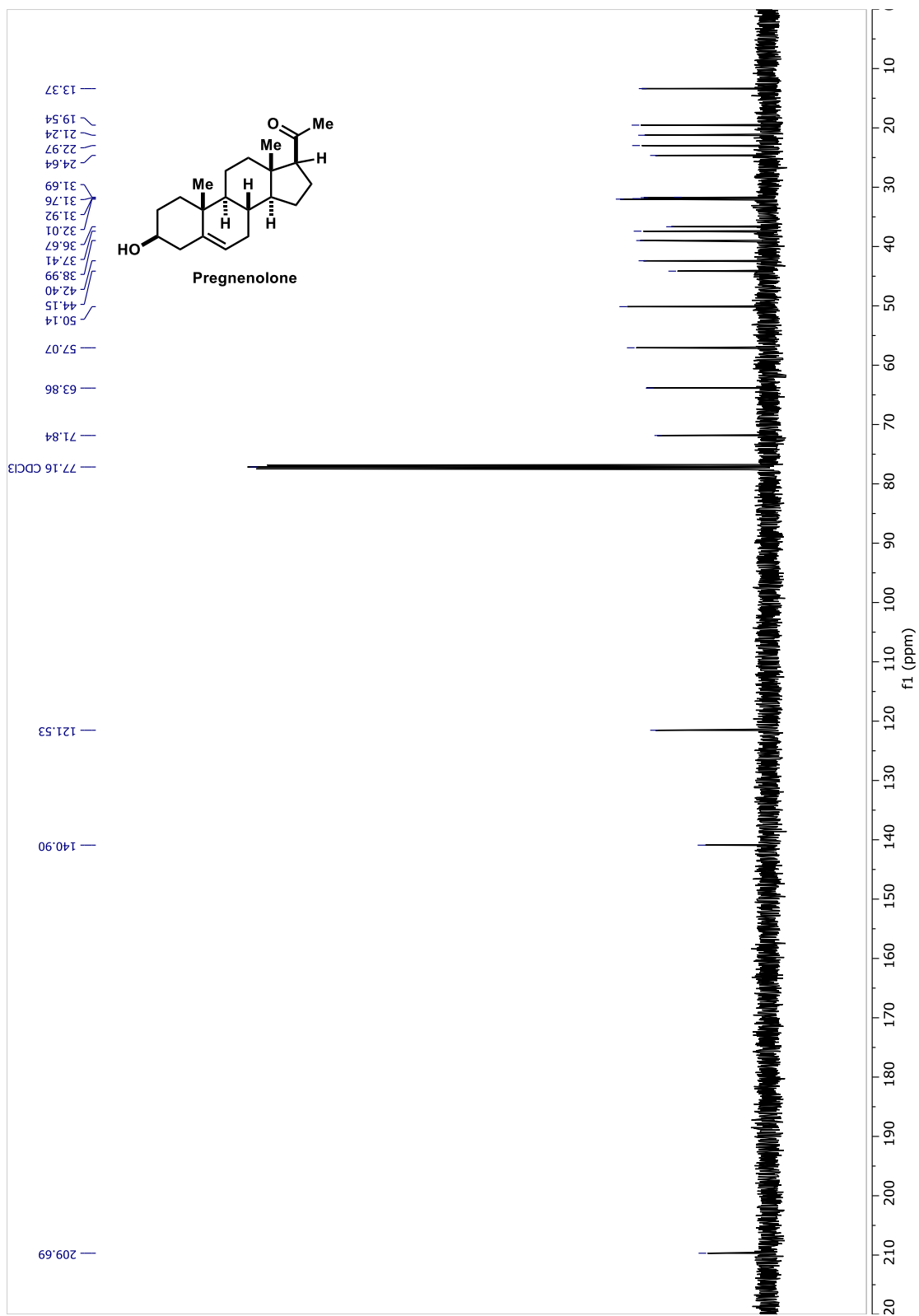


**Figure 4-11.**  $^{13}\text{C}$ -NMR of starting material Pregnenolone in chloroform-*d*.

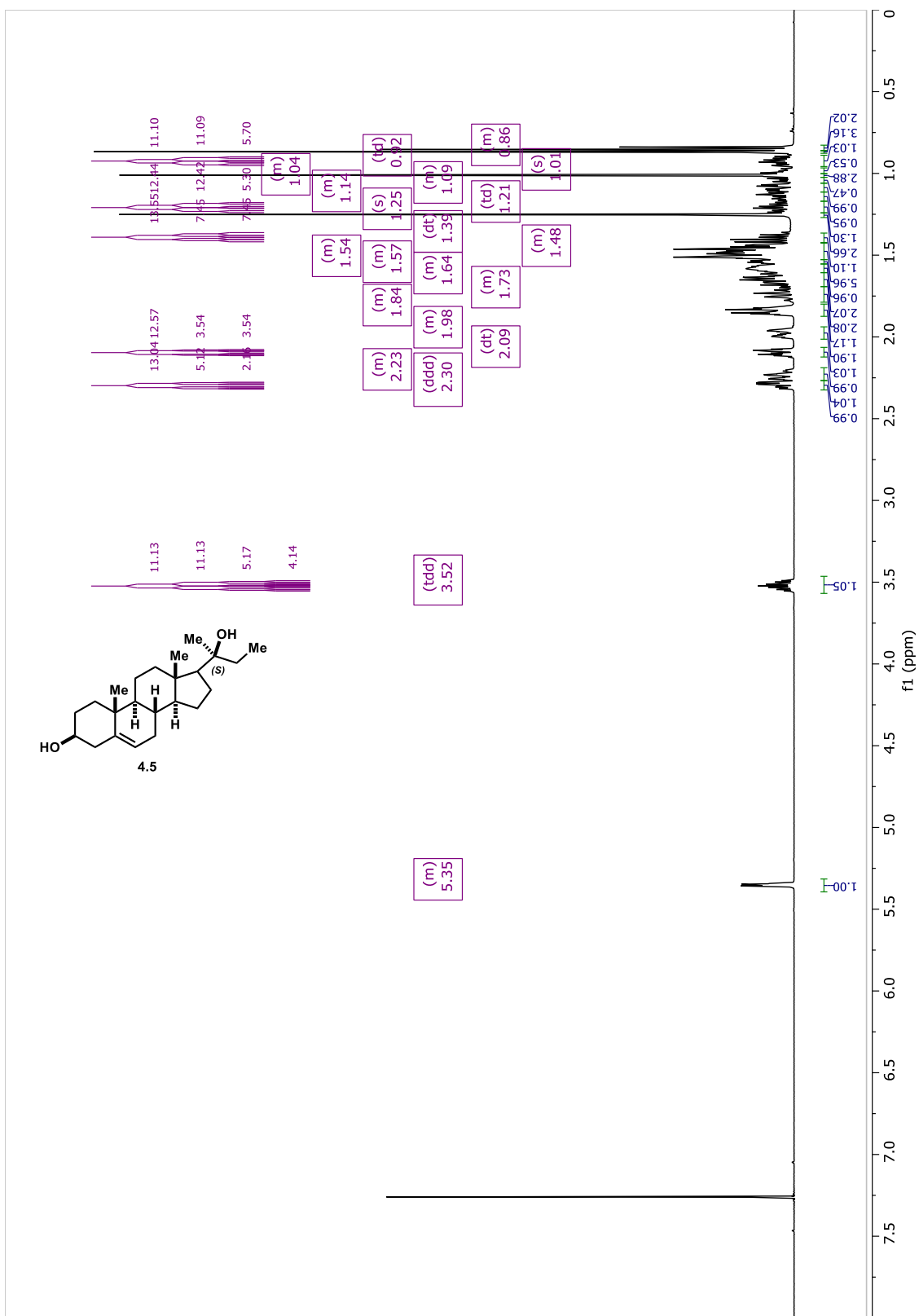
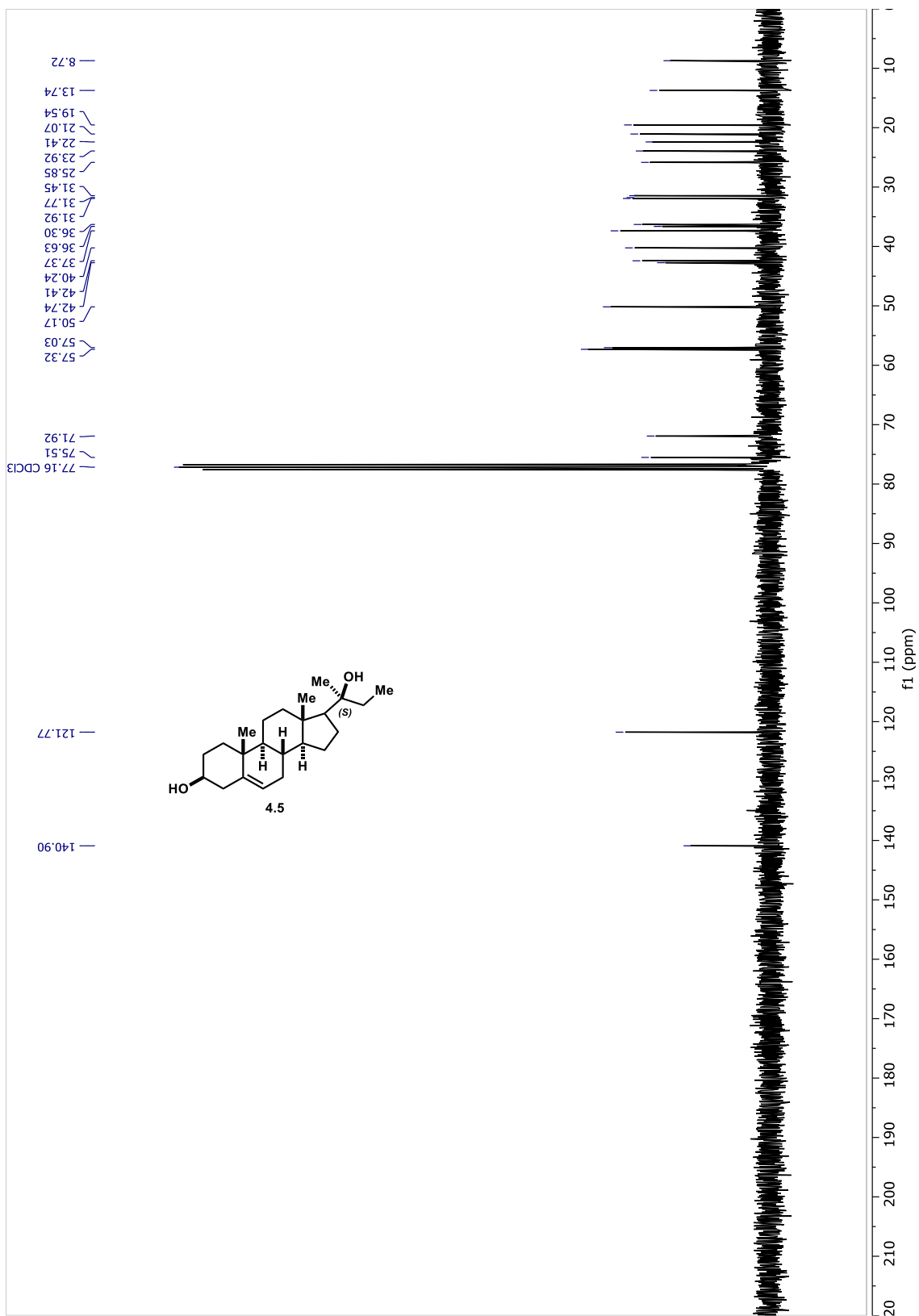
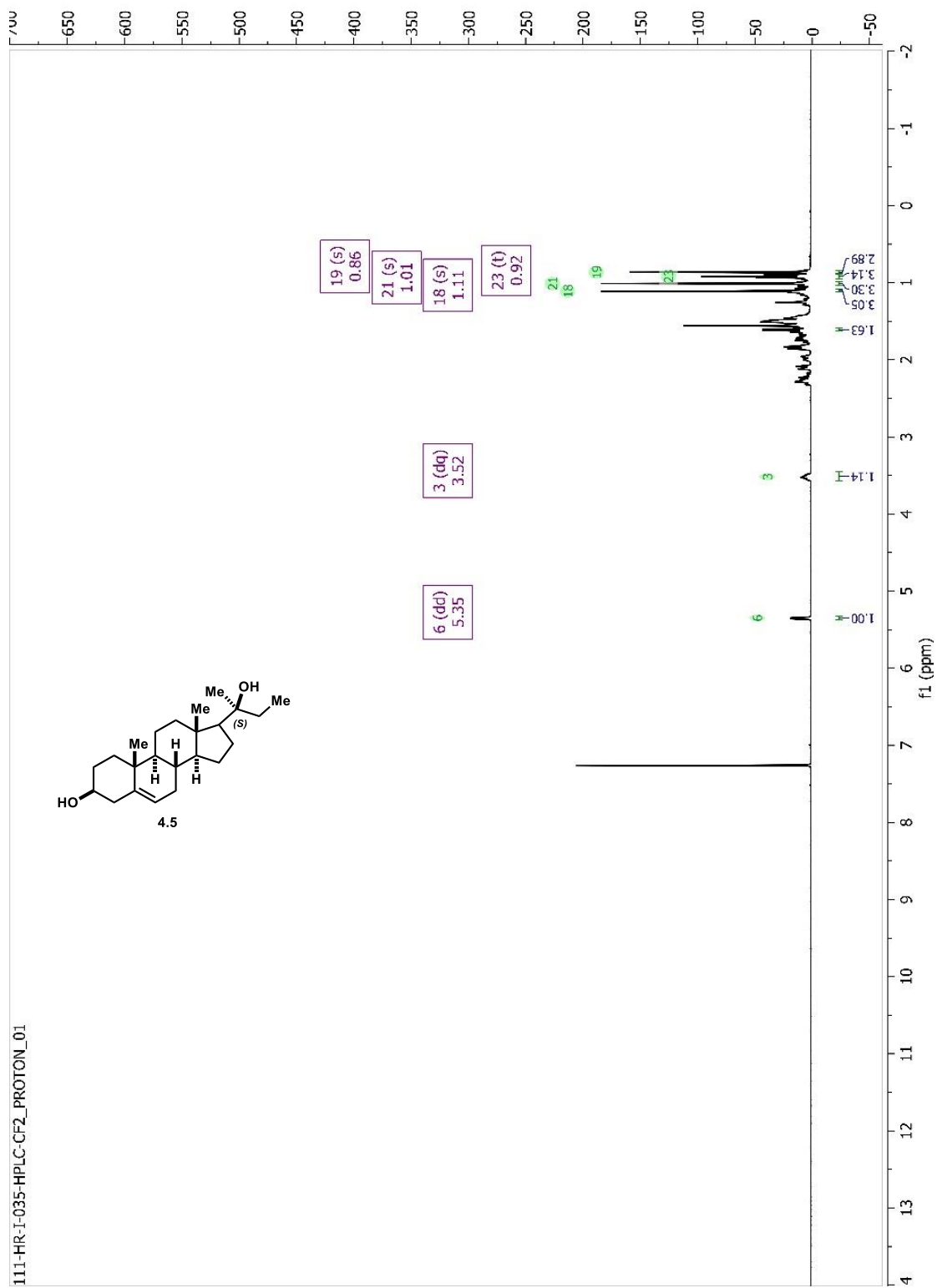


Figure 4-12. <sup>1</sup>H-NMR of (S)-ethyl-pregnenolol analog (4.5) in chloroform-*d*.



**Figure 4-13.**  $^{13}\text{C}$ -NMR of *(S)*-ethyl-pregnenolol analog (4.5) in chloroform-*d*.



**Figure 4-14.** <sup>1</sup>H-NMR of (*S*)-ethyl-pregnenolol analog (**4.5**) in chloroform-*d*.



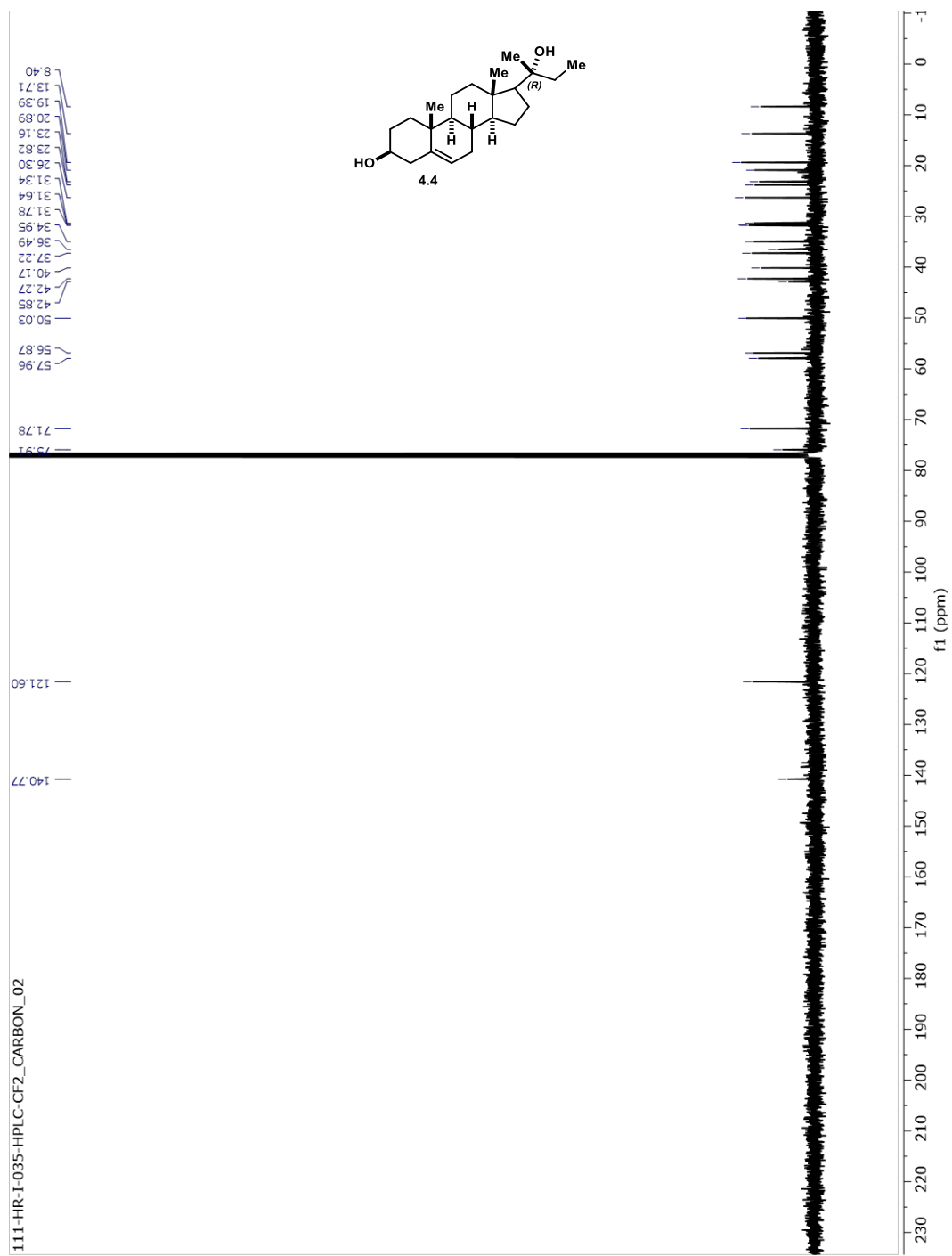


**Figure 4-15.** <sup>13</sup>C-NMR of (*R*)-ethyl-pregnenolol analog (**4.4**) in chloroform-*d*.

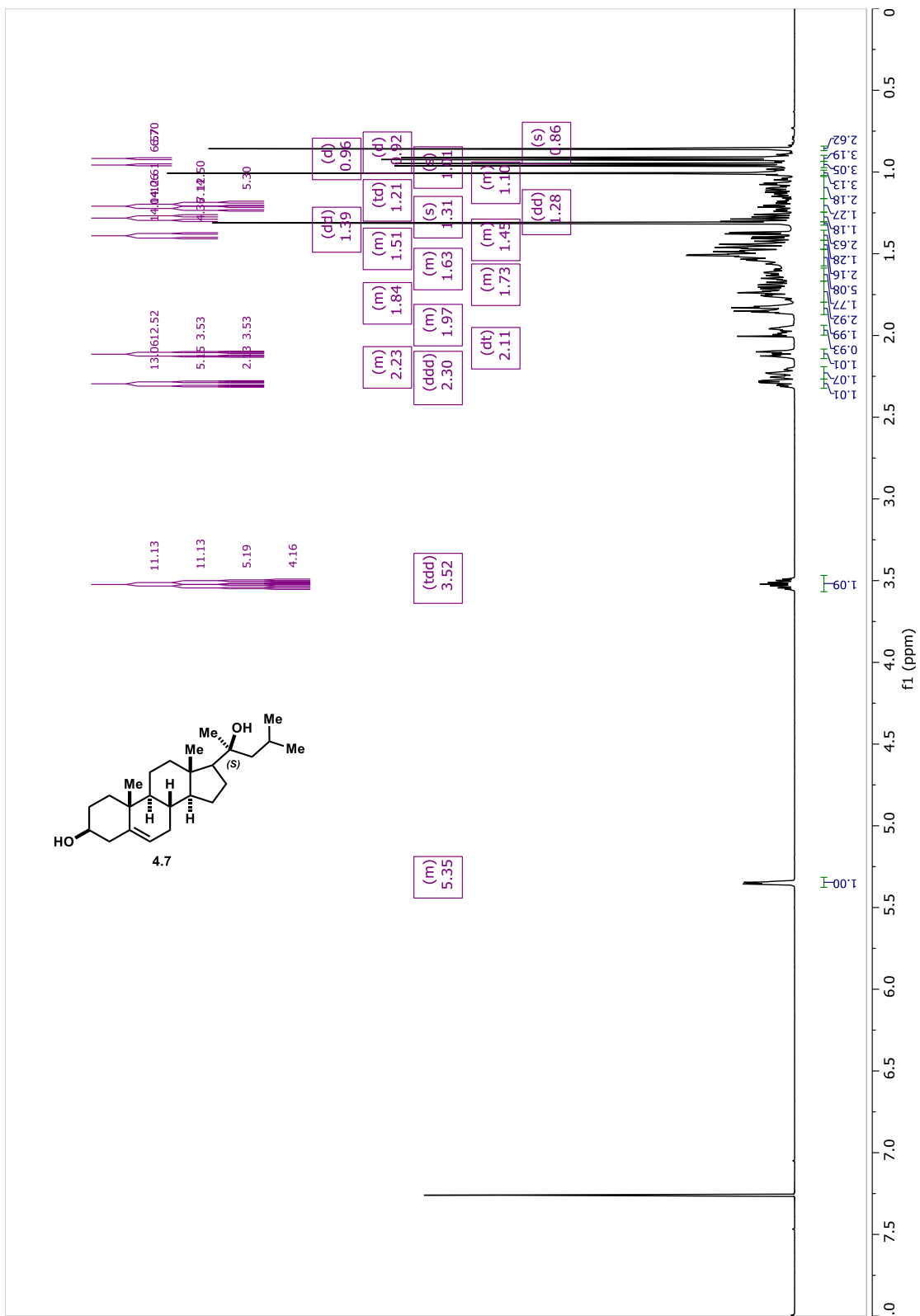
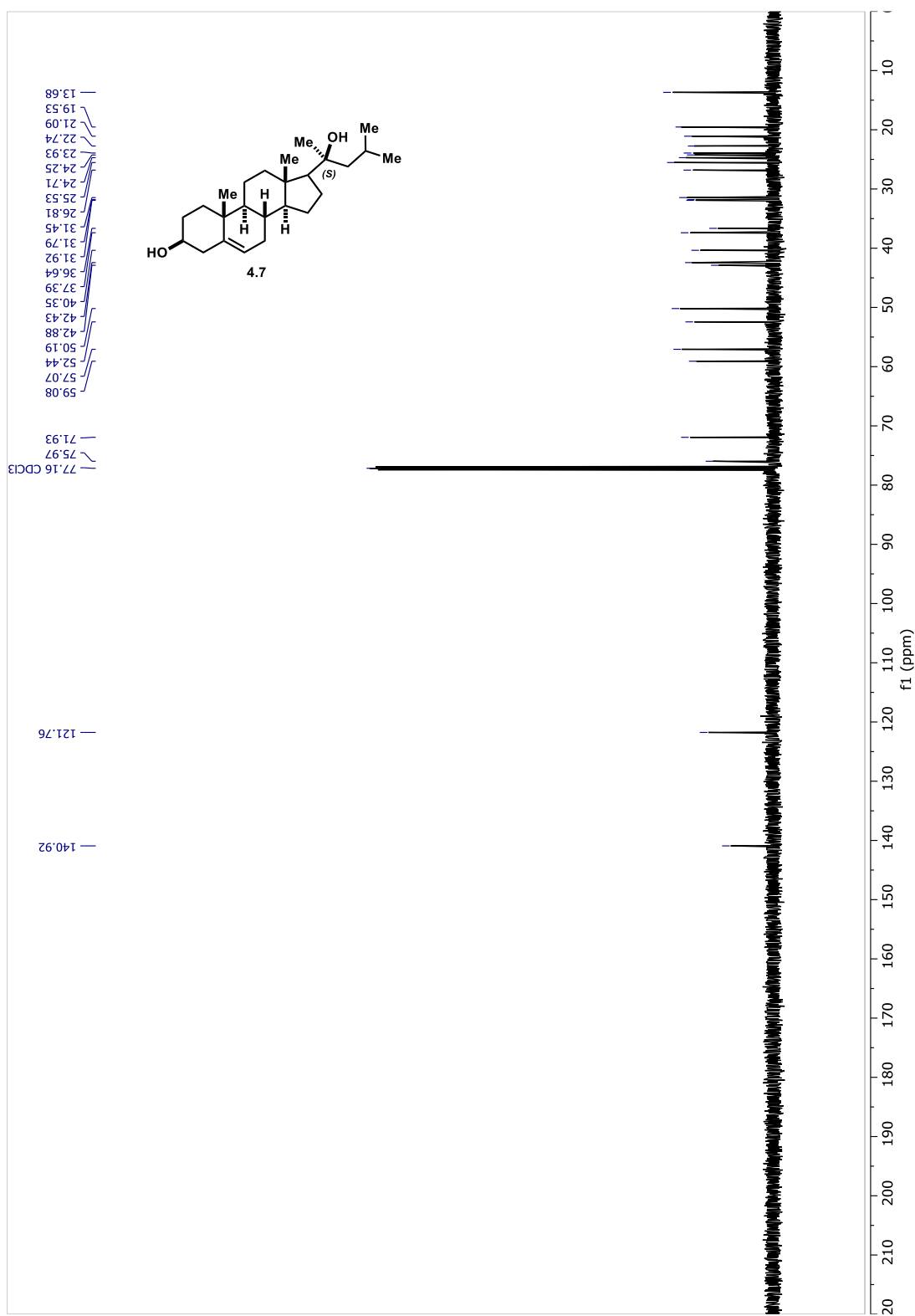
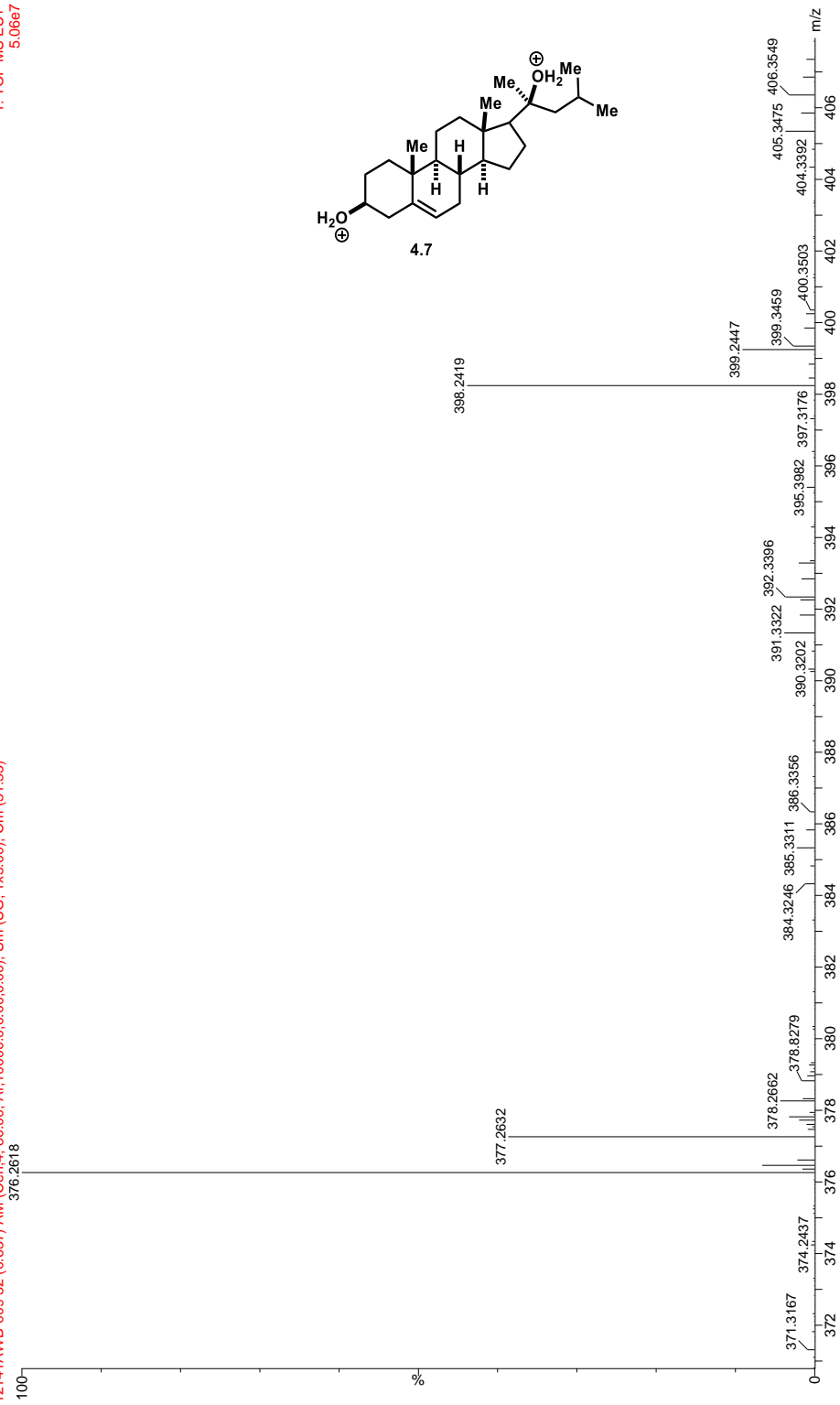


Figure 4-16. <sup>1</sup>H-NMR of (S)-isobutyl-pregnenolol analog (4.7) in chloroform-*d*.



**Figure 4-17.**  $^{13}\text{C}$ -NMR of *(S)*-isobutyl-pregnenolol analog (4.7) in chloroform-*d*.



**Figure 4-18.** HRMS (+ESI) of 4.7: calculated  $C_{25}H_{44}O_2$   $2+$   $[M + 2H]^+$ : 376.3347 m/z, found 376.2618 m/z,  $\Delta$ ppm = 190 ppm, a significant difference as the compound did not ionize well.

20-Dec-2017 12:29:18

1: TOF MS ES+  
7.7766

SYNAPT G2-Si#JUGA589

SA-11 (0.1x)

Le

12141AWB-009 32 (0.637) AM (Cen,4, 80.00, Ar,100000.0,0.00,0.00); Sm (31.33)

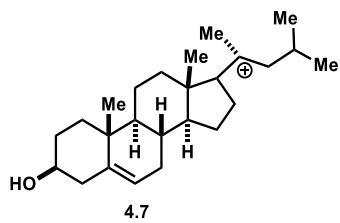
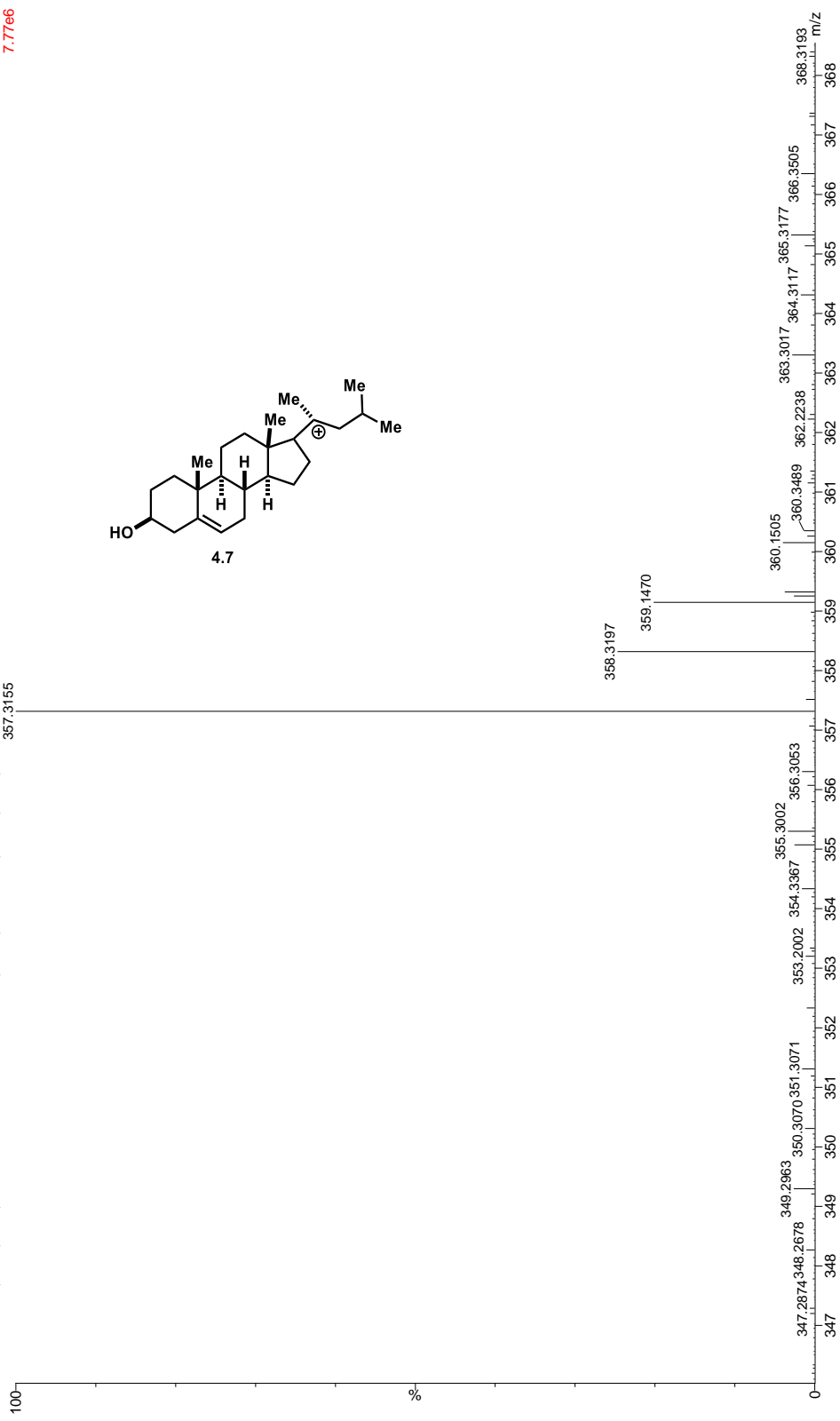


**Figure 4-19.** HRMS (+ESI) of **Compound 4.7**: calculated  $C_{25}H_{41}O + [M - OH]^-$ : 357.3152 m/z, observed 357.3155m/z,  $\Delta$ ppm = 0.86 ppm

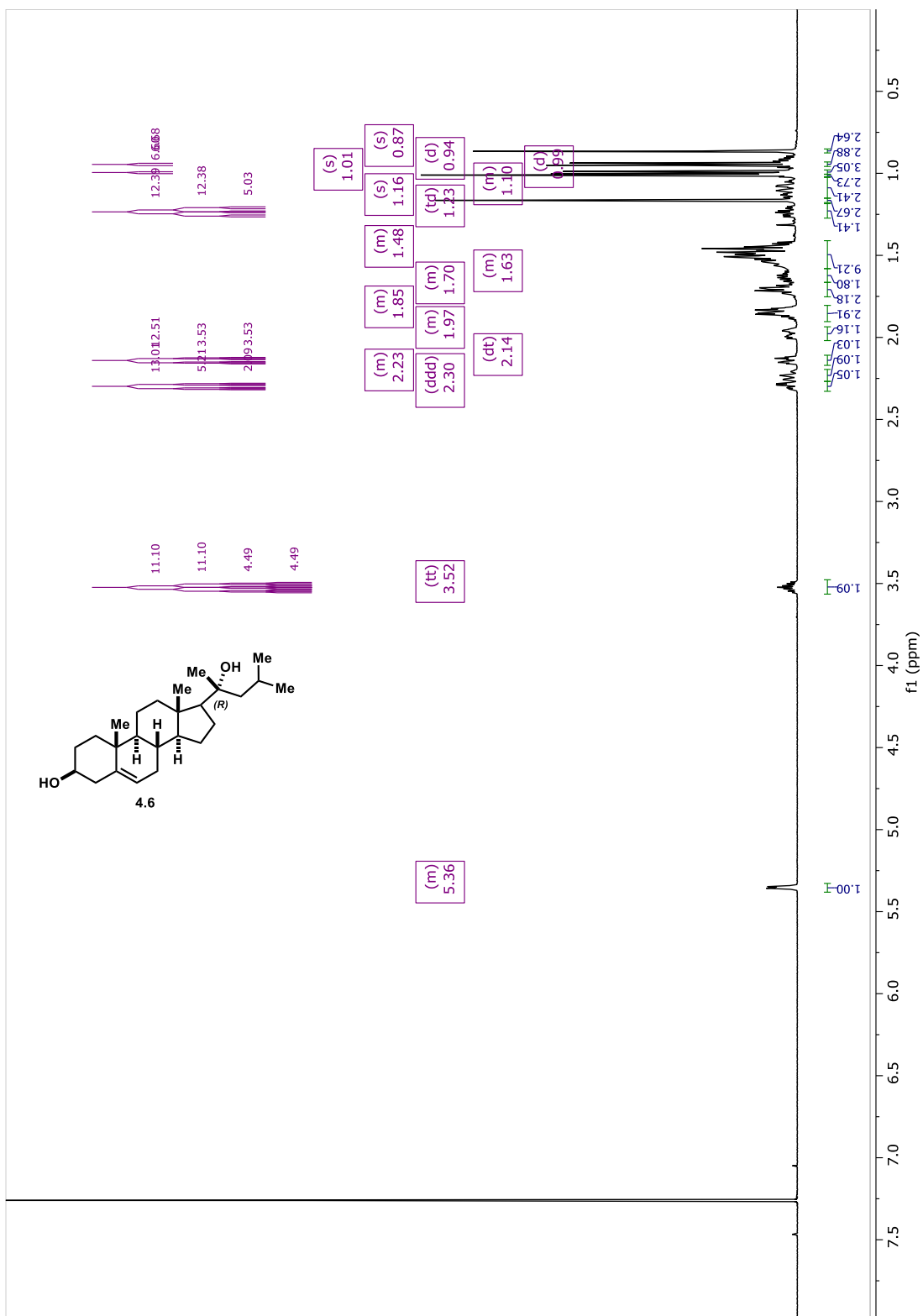


**Figure 4-20.** <sup>1</sup>H-NMR of (*R*)-isobutyl-pregnenolol analog (**4.6**) in chloroform-*d*.

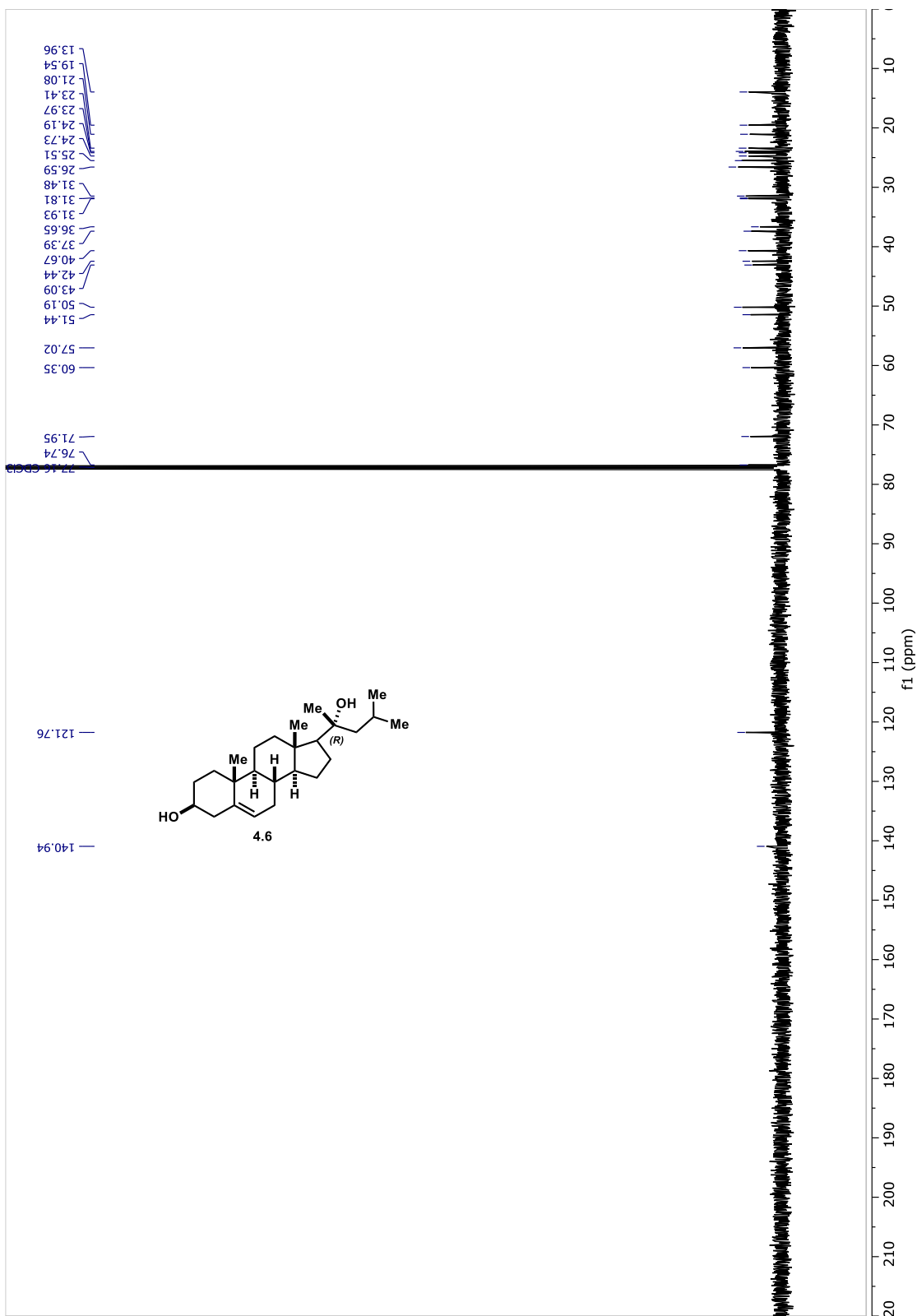


**Figure 4-21.**  $^{13}\text{C}$ -NMR of *(R)*-isobutyl-pregnenolol analog (4.6) in chloroform-*d*.

20-Dec-2017 12:45:29

1: TOF MS ES+  
1.25e7

SYNAPT G2-Si#UGA589

SA-12 (0.1x)

Le

12.142AWB-003 32 (0.637) AM (Cen:4, 80.00, Ar:100000.0,0.00,0.00); Sm (SG, 1x5.00); Cm (30:34)

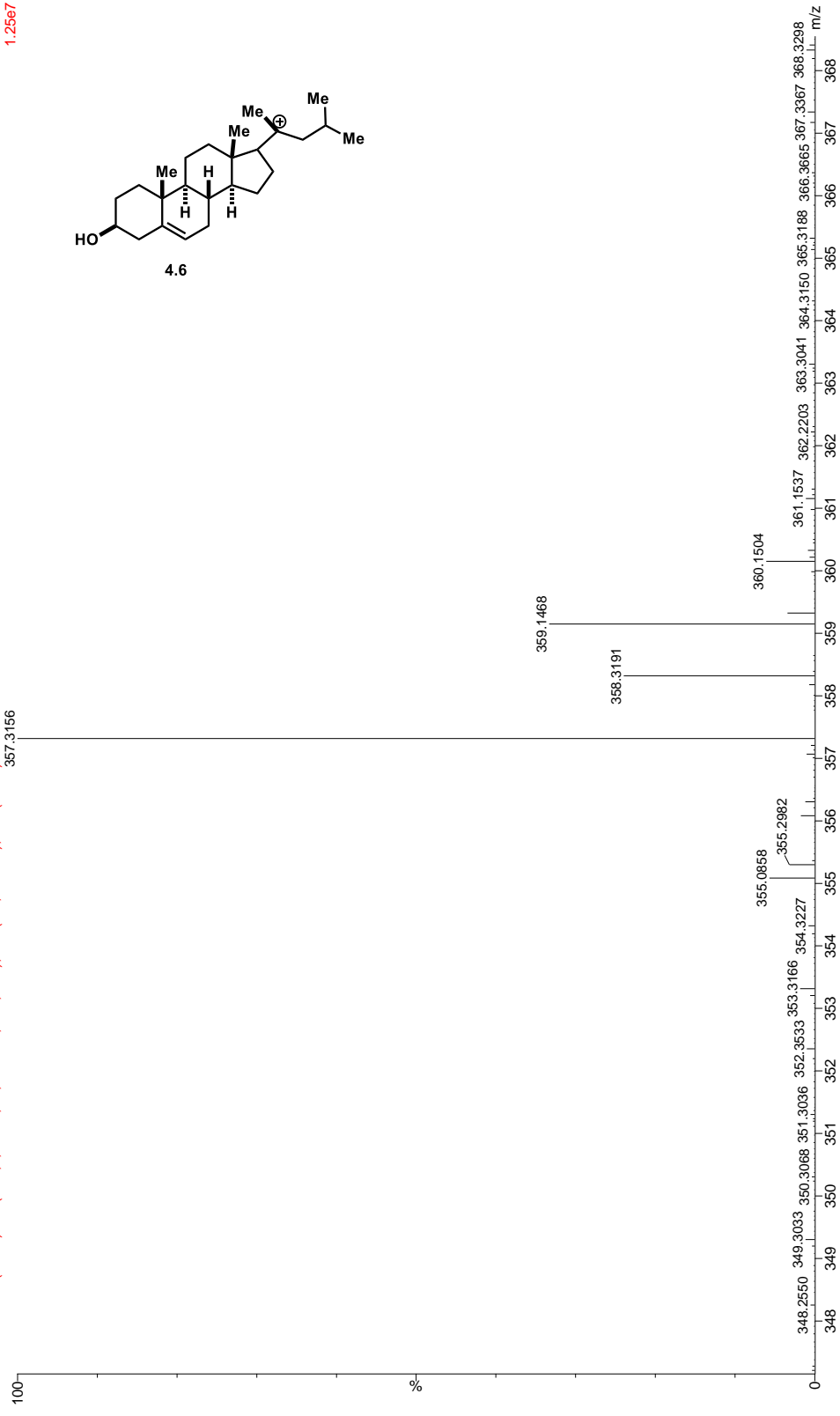


**Figure 4-22.** HRMS (+ESI) of **Compound 4.6**: calculated  $C_{25}H_{41}O + [M - OH]^-$ : 357.3152 m/z, observed 357.3156 m/z,  $\Delta ppm = 1.1 ppm$



SA-12 (0.1x)

SYNAPT G2-Si#UGA589

20-Dec-2017 12:45:29

Le

12142AWB-003.32 (0.637) AM (Cen.4, 80.00, Ar,10000.0,0.00,0.00); Sm (SG, 1x5.00); Cm (30:34)

1: TOF MS ES+  
1.99e7

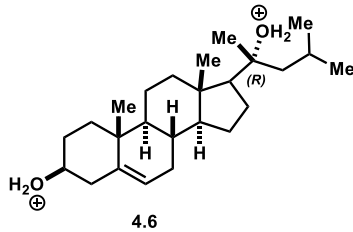
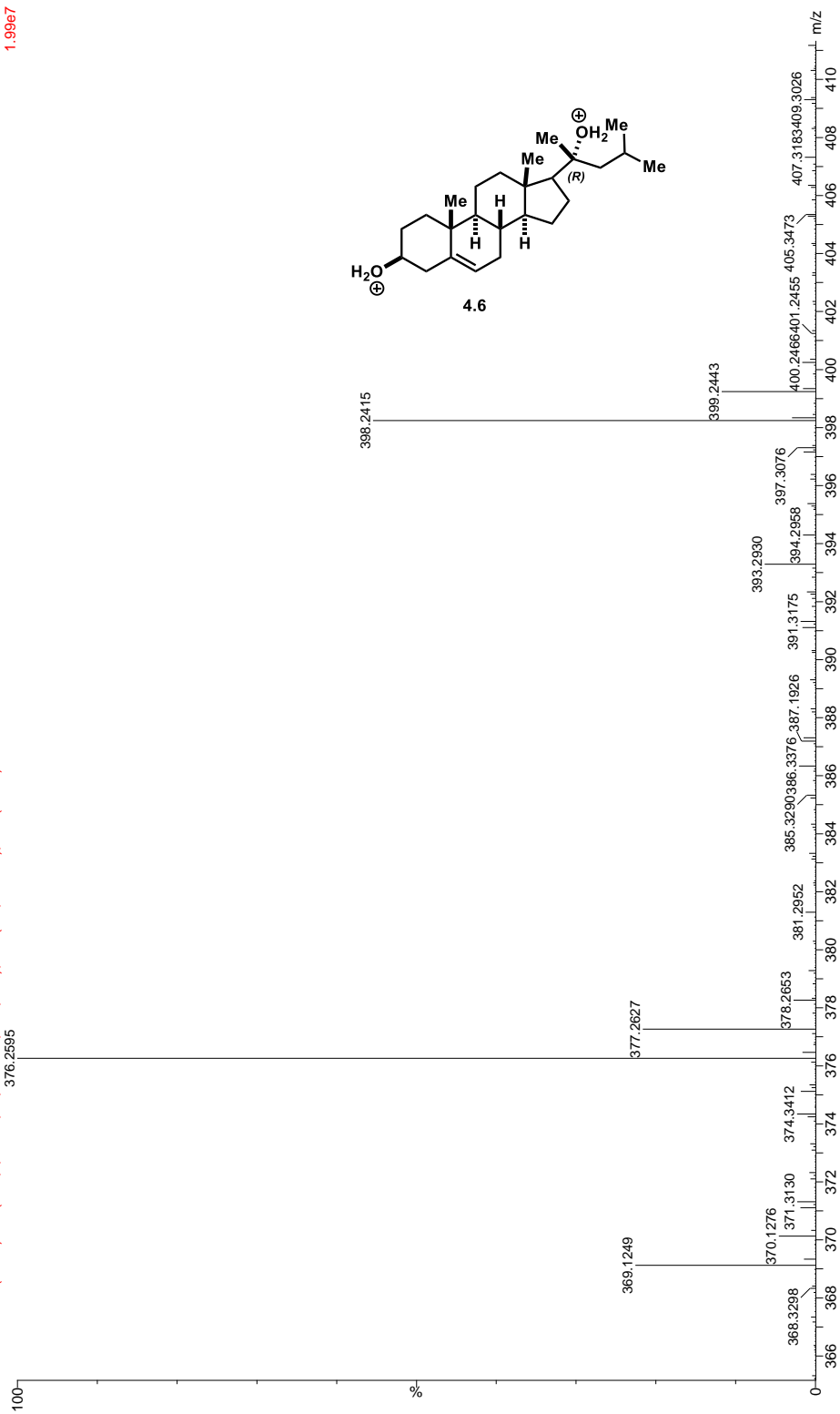


**Figure 4-23.** HRMS (+ESI) of **Compound 4.6**: calculated C<sub>25</sub>H<sub>44</sub>O<sub>2</sub> 2+ [M + 2H<sup>+</sup>]: 376.3347 m/z, observed 376.2595 m/z,  $\Delta = 200$  ppm, a significant difference as the compound did not ionize well.

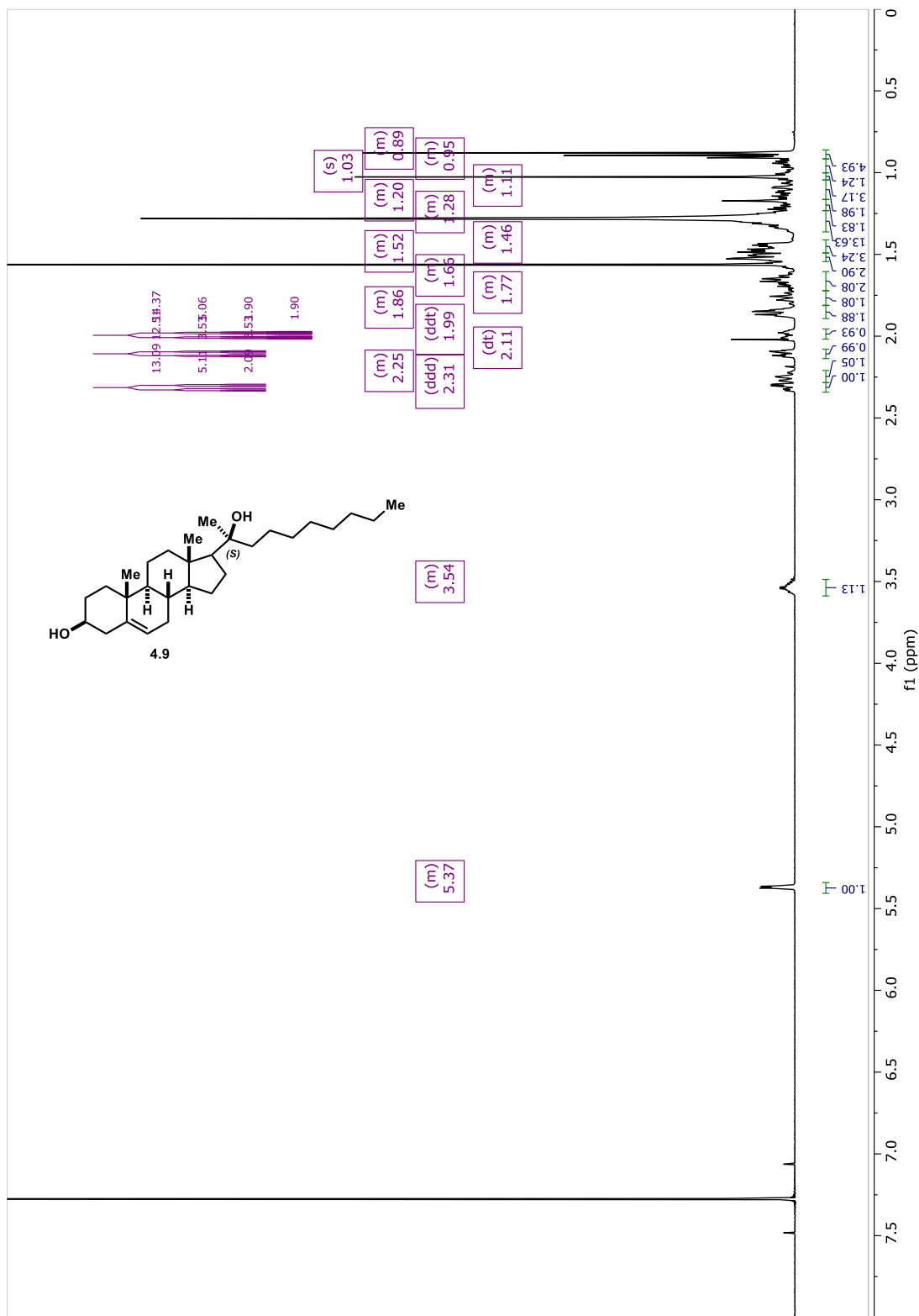
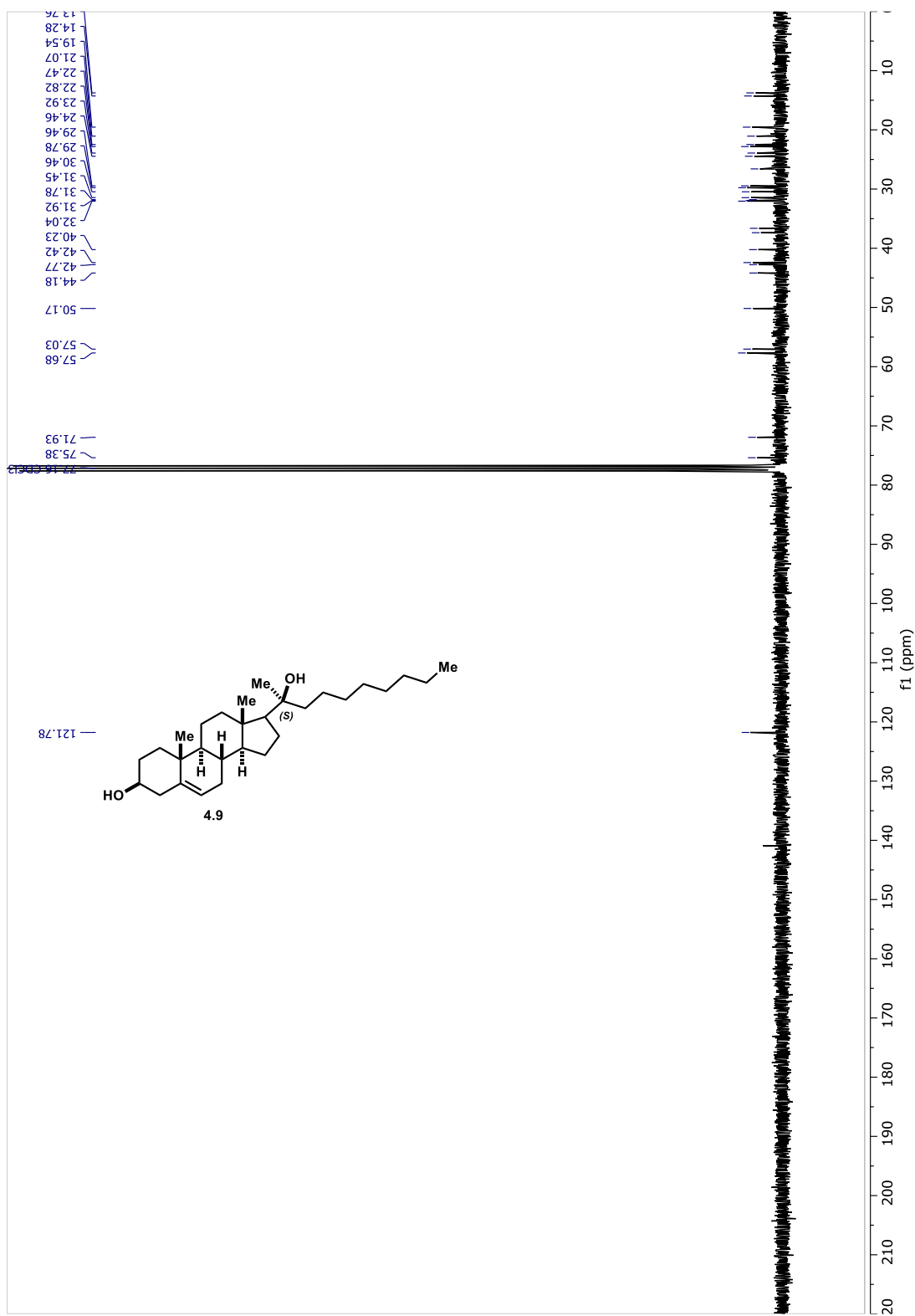
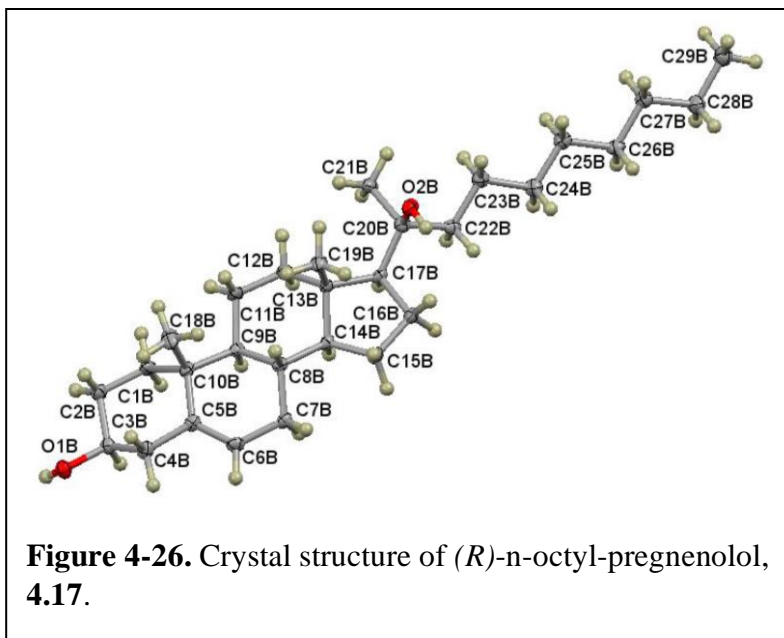


Figure 4-24. <sup>1</sup>H-NMR of (S)-n-octyl-pregnenolol analog (4.9) in chloroform-*d*.



**Figure 4-25.**  $^{13}\text{C}$ -NMR of *(S)*-n-octyl-pregnenolol analog (**4.9**) in chloroform-*d*.



## Crystallography Experimental

A colourless, rod-shaped crystal of dimensions 0.05 x 0.05 x 0.46 mm was selected for structural analysis. Intensity data for this compound were collected using a diffractometer with a Bruker APEX ccd area detector (1) and graphite-monochromated Mo K $\alpha$  radiation ( $\lambda = 0.71073$  Å). The sample was cooled to 100(2) K. Cell parameters were

determined from a least-squares fit of 3454 peaks in the range  $2.51 < \theta < 21.32^\circ$ . A total of 31764 data were measured in the range  $1.368 < \theta < 27.528^\circ$  using  $\omega$  oscillation frames. The data were corrected for absorption by the empirical method (2) giving minimum and maximum transmission factors of 0.6726 and 0.7456. The data were merged to form a set of 12648 independent data with  $R(\text{int}) = 0.0595$  and a coverage of 100.0 %.

The monoclinic space group P21 was determined by systematic absences and statistical tests and verified by subsequent refinement. The structure was solved by direct methods and refined by full-matrix least-squares methods on F<sup>2</sup> (3). The positions of hydrogens bonded to carbons were initially determined by geometry and were refined using a riding model. Hydrogens bonded to oxygens were located on a difference map, and their positions were refined independently. Non-hydrogen atoms were refined with anisotropic displacement parameters. Hydrogen atom displacement parameters were set to 1.2 (1.5 for methyl) times the isotropic equivalent displacement parameters of the bonded atoms. A total of 622 parameters were refined against 1 space group restraint and 12648 data to give  $wR(F^2) = 0.1149$  and  $S = 0.955$  for weights of  $w = 1/[\sigma^2(F^2) + (0.0520 P)^2]$ , where  $P = [F_o^2 + 2F_c^2] / 3$ . The final  $R(F)$  was 0.0518 for the 8968 observed,  $[F > 4 \sigma(F)]$ , data. The largest shift/s.u. was 0.000 in the final refinement cycle. The final difference map had maxima and minima of 0.200 and -0.219 e/Å<sup>3</sup>, respectively. The absolute structure was determined by the known stereochemistry at atoms C8, C10, and C13. The polar axis restraint was taken from Flack and Schwarzenbach.

**Table 2.** Crystal data and structure refinement for (*R*)-*n*-octyl-pregnenolol, **4.17**.

<b>Empirical formula</b>	<b>2(C<sub>29</sub> H<sub>50</sub> O<sub>2</sub>) · (C<sub>2</sub> H<sub>3</sub> N) · (H<sub>2</sub>O)</b>	
	<b>C<sub>60</sub> H<sub>105</sub> O<sub>5</sub></b>	
<b>Formula weight</b>	<b>920.44</b>	
<b>Crystal system</b>	<b>monoclinic</b>	
<b>Space group</b>	<b><i>P</i>2<sub>1</sub></b>	
<b>Unit cell dimensions</b>	<b><i>a</i> = 14.888(3) Å</b>	<b><i>α</i> = 90°</b>
	<b><i>b</i> = 7.6221(15) Å</b>	<b><i>β</i> = 90.959(4)°</b>
	<b><i>c</i> = 24.343(5) Å</b>	<b><i>γ</i> = 90°</b>
<b>Volume</b>	<b>2762.0(10) Å<sup>3</sup></b>	
<b>Z, Z'</b>	<b>2, 1</b>	
<b>Density (calculated)</b>	<b>1.107 Mg/m<sup>3</sup></b>	
<b>Wavelength</b>	<b>0.71073 Å</b>	
<b>Temperature</b>	<b>100(2) K</b>	
<b><i>F</i>(000)</b>	<b>1024</b>	
<b>Absorption coefficient</b>	<b>0.068 mm<sup>-1</sup></b>	
<b>Absorption correction</b>	<b>semi-empirical from equivalents</b>	
<b>Max. and min. transmission</b>	<b>0.7456 and 0.6726</b>	
<b>Theta range for data collection</b>	<b>1.368 to 27.528°</b>	
<b>Reflections collected</b>	<b>31764</b>	
<b>Independent reflections</b>	<b>12648 [R(int) = 0.0595]</b>	
<b>Data / restraints / parameters</b>	<b>12648 / 1 / 622</b>	
<b><i>wR</i>(<i>F</i><sup>2</sup> all data)</b>	<b><i>wR</i>2 = 0.1149</b>	
<b><i>R</i>(<i>F</i> obsd data)</b>	<b><i>R</i>1 = 0.0518</b>	
<b>Goodness-of-fit on <i>F</i><sup>2</sup></b>	<b>0.955</b>	
<b>Observed data [<i>I</i> &gt; 2 σ (<i>I</i>)]</b>	<b>8968</b>	
<b>Absolute structure parameter</b>	<b>-0.6(8)</b>	
<b>Extinction coefficient</b>	<b>n/a</b>	
<b>Largest and mean shift / s.u.</b>	<b>0.000 and 0.000</b>	
<b>Largest diff. peak and hole</b>	<b>0.200 and -0.219 e/Å<sup>3</sup></b>	

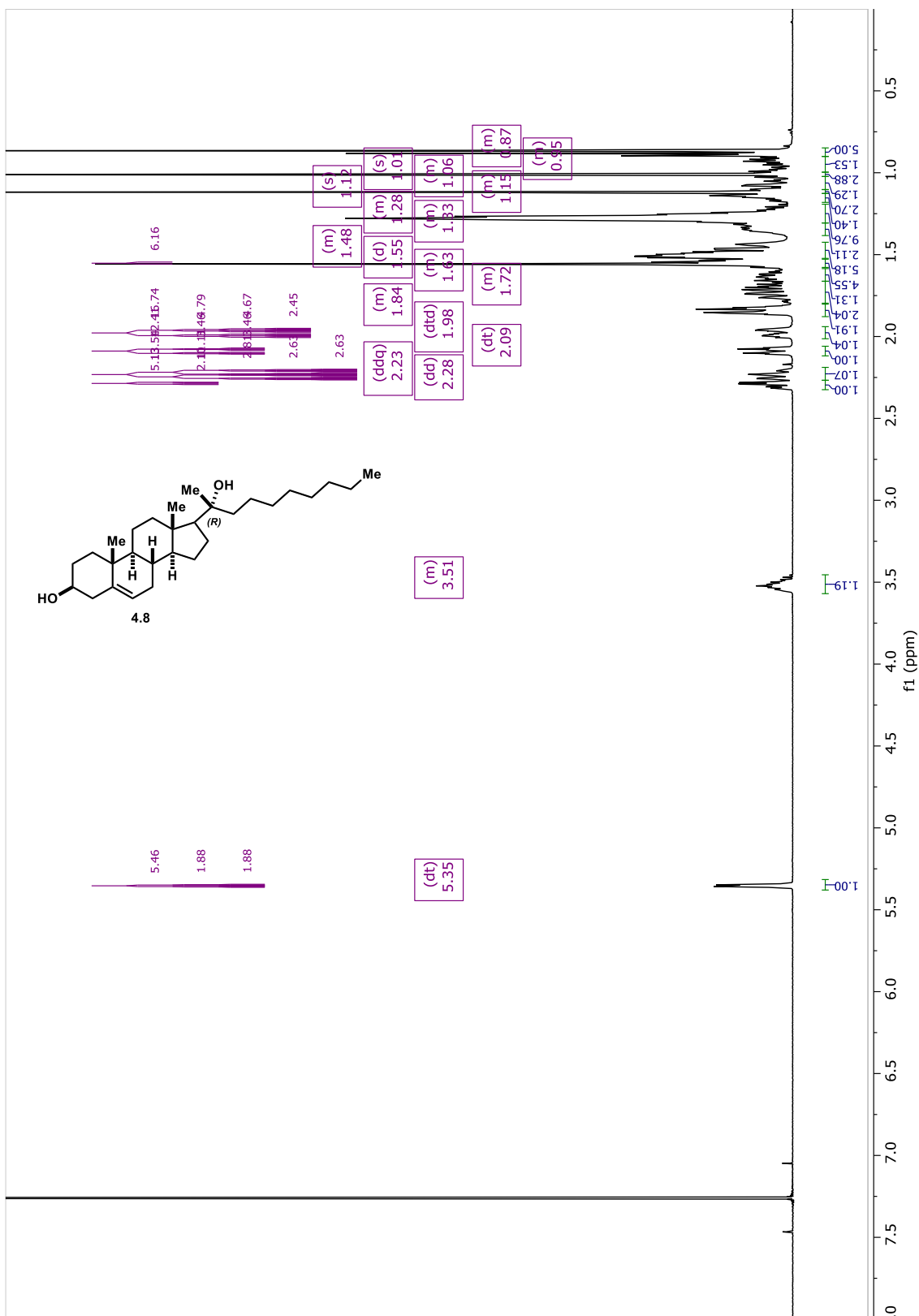


Figure 4-27. <sup>1</sup>H-NMR of (*R*)-n-octyl-pregnenolol analog (**4.8**) in chloroform-*d*.

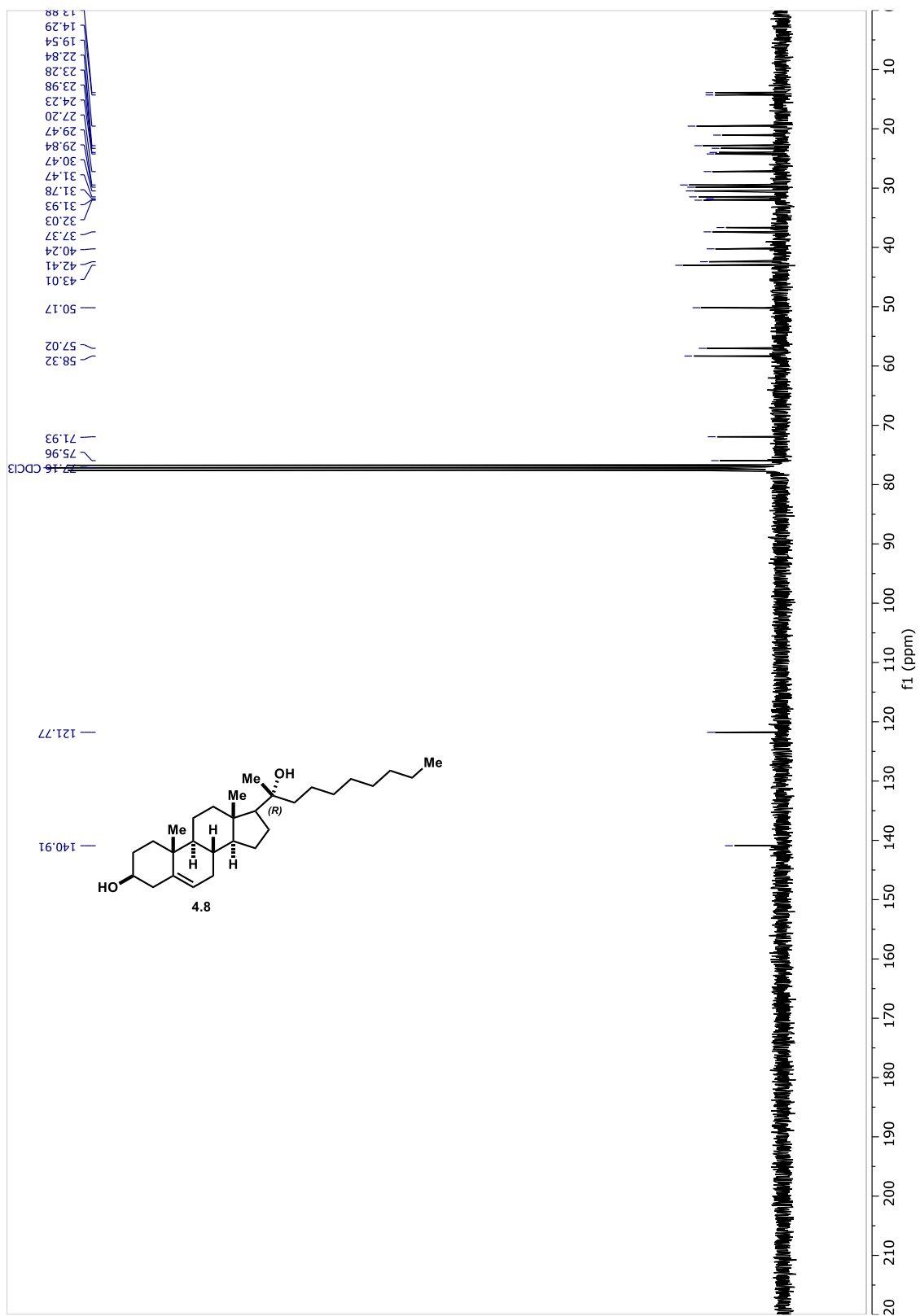
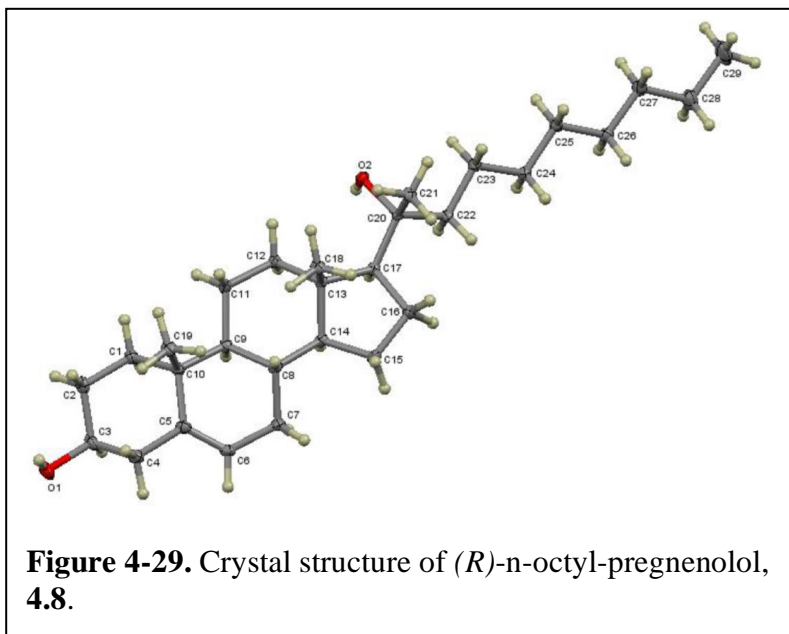


Figure 4-28. <sup>13</sup>C-NMR of (*R*)-n-octyl-pregnenolol analog (4.8) in chloroform-*d*.



### Crystallography Experimental

A colorless, block-shaped crystal of dimensions 0.115 x 0.120 x 0.214 mm was selected for structural analysis. Intensity data for this compound were collected using a diffractometer with a Bruker APEX ccd area detector and graphite-monochromated Mo K $\alpha$  radiation ( $\lambda = 0.71073$  Å). The sample was cooled to 100(2) K. Cell parameters were

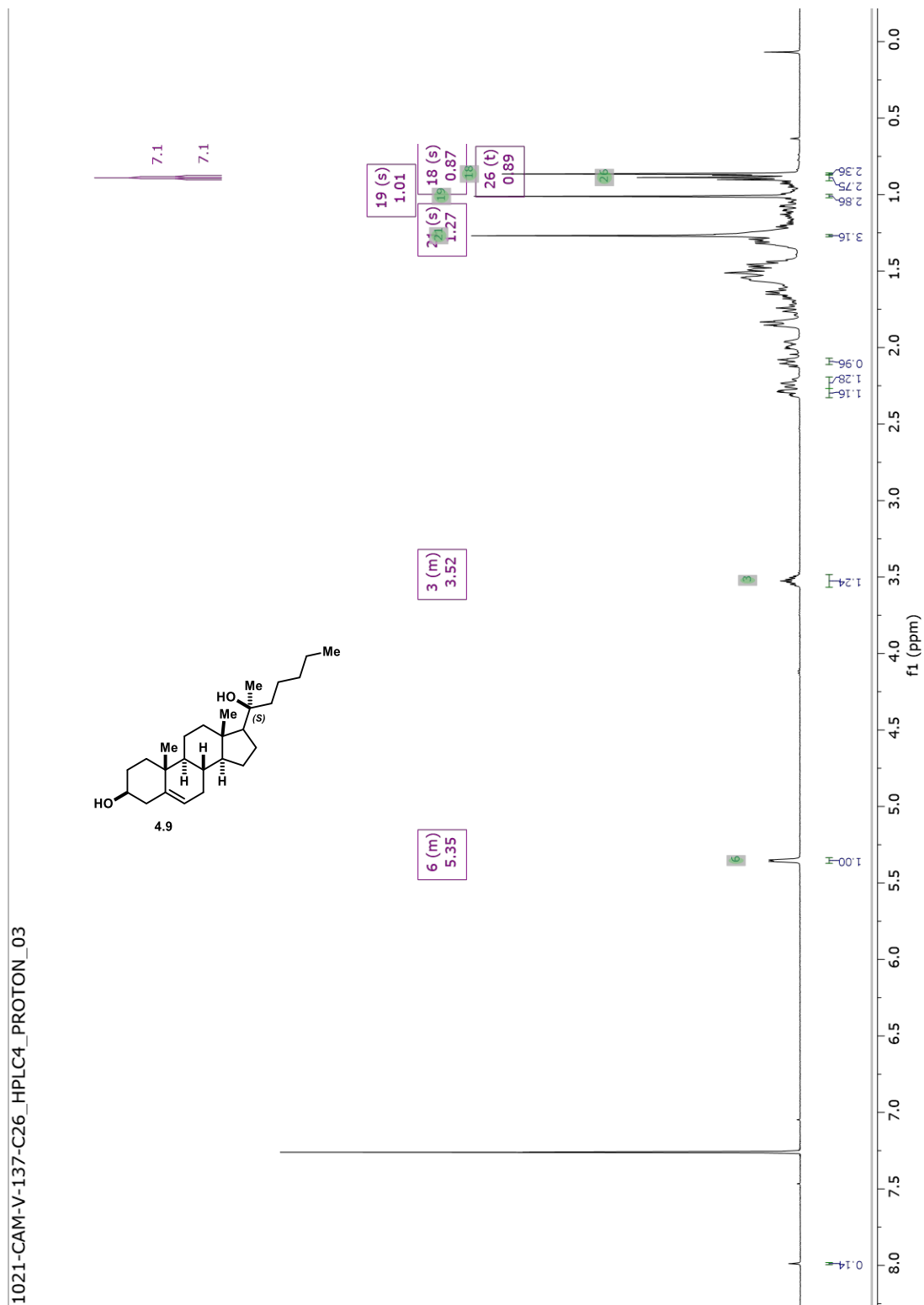
determined from a least-squares fit of 3468 peaks in the range  $2.25 < \theta < 29.45^\circ$ . A total of 13920 data were measured in the range  $1.804 < \theta < 29.693^\circ$  using  $\phi$  and  $\omega$  oscillation frames. The data were corrected for absorption by the empirical method giving minimum and maximum transmission factors of 0.6404 and 0.7459. The data were merged to form a set of 7036 independent data with  $R(\text{int}) = 0.0383$  and a coverage of 99.9 %.

The monoclinic space group  $P2_1$  was determined by systematic absences and statistical tests and verified by subsequent refinement. The structure was solved by direct methods and refined by full-matrix least-squares methods on  $F^2$ . The positions of hydrogens bonded to carbons were initially determined by geometry and were refined using a riding model. Hydrogens bonded to the oxygens were located on a difference map, and their positions were refined independently. Non-hydrogen atoms were refined with anisotropic displacement parameters. Hydrogen atom displacement parameters were set to 1.2 (1.5 for methyl) times the isotropic equivalent displacement parameters of the bonded atoms. A total of 286 parameters were refined against 1 space group restraint and 7036 data to give  $wR(F^2) = 0.1098$  and  $S = 0.976$  for weights of  $w = 1/[\sigma^2(F^2) + (0.0600 P)^2]$ , where  $P = [F_o^2 + 2F_c^2] / 3$ . The final  $R(F)$  was 0.0466 for the 5896 observed,  $[F > 4\sigma(F)]$ , data. The largest shift/s.u. was 0.000 in the final refinement cycle. The final difference map had maxima and minima of 0.293 and -0.243 e/Å<sup>3</sup>, respectively. The absolute structure was determined by the chirality of the ring system. The polar axis restraints were taken from Flack and Schwarzenbach.



**Table 3.** Crystal data and structure refinement for (*R*)-n-octyl-pregnenolol, **4.8**.

<b>Empirical formula</b>	<b>C<sub>29</sub> H<sub>50</sub> O<sub>2</sub></b>
<b>Formula weight</b>	<b>430.69</b>
<b>Crystal system</b>	<b>monoclinic</b>
<b>Space group</b>	<b><i>P</i>2<sub>1</sub></b>
<b>Unit cell dimensions</b>	<b><i>a</i> = 9.5537(14) Å      <math>\alpha = 90^\circ</math> <i>b</i> = 5.9587(9) Å      <math>\beta = 94.985(3)^\circ</math> <i>c</i> = 22.658(4) Å      <math>\gamma = 90^\circ</math></b>
<b>Volume</b>	<b>1285.0(4) Å<sup>3</sup></b>
<b>Z, Z'</b>	<b>2, 1</b>
<b>Density (calculated)</b>	<b>1.113 Mg/m<sup>3</sup></b>
<b>Wavelength</b>	<b>0.71073 Å</b>
<b>Temperature</b>	<b>100(2) K</b>
<b><i>F</i>(000)</b>	<b>480</b>
<b>Absorption coefficient</b>	<b>0.067 mm<sup>-1</sup></b>
<b>Absorption correction</b>	<b>semi-empirical from equivalents</b>
<b>Max. and min. transmission</b>	<b>0.7459 and 0.6404</b>
<b>Theta range for data collection</b>	<b>1.804 to 29.693°</b>
<b>Reflections collected</b>	<b>13920</b>
<b>Independent reflections</b>	<b>7036 [R(int) = 0.0383]</b>
<b>Data / restraints / parameters</b>	<b>7036 / 1 / 286</b>
<b><i>wR</i>(<i>F</i><sup>2</sup> all data)</b>	<b><i>wR</i>2 = 0.1098</b>
<b><i>R</i>(<i>F</i> obsd data)</b>	<b><i>R</i>1 = 0.0466</b>
<b>Goodness-of-fit on <i>F</i><sup>2</sup></b>	<b>0.976</b>
<b>Observed data [I &gt; 2 σ (I)]</b>	<b>5896</b>
<b>Absolute structure parameter</b>	<b>0.0(8)</b>
<b>Extinction coefficient</b>	<b>n/a</b>
<b>Largest and mean shift / s.u.</b>	<b>0.000 and 0.000</b>
<b>Largest diff. peak and hole</b>	<b>0.293 and -0.243 e/Å<sup>3</sup></b>



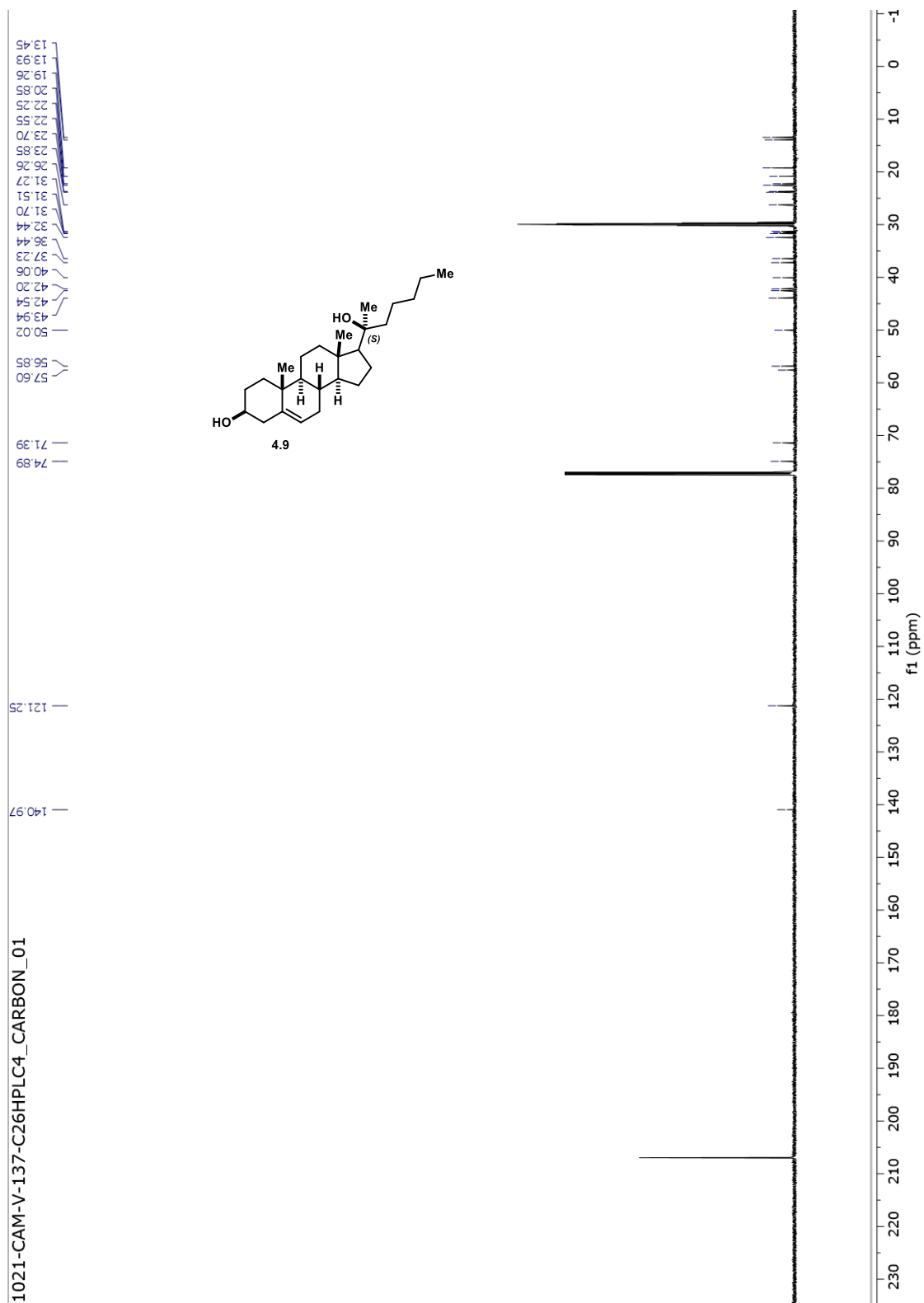


**Figure 4-31.**  $^{13}\text{C}$ -NMR of (*S*)-*n*-octyl-pregnenolol analog (**4.9**) in 10:1 chloroform-*d* : acetone-*d*<sub>6</sub>.

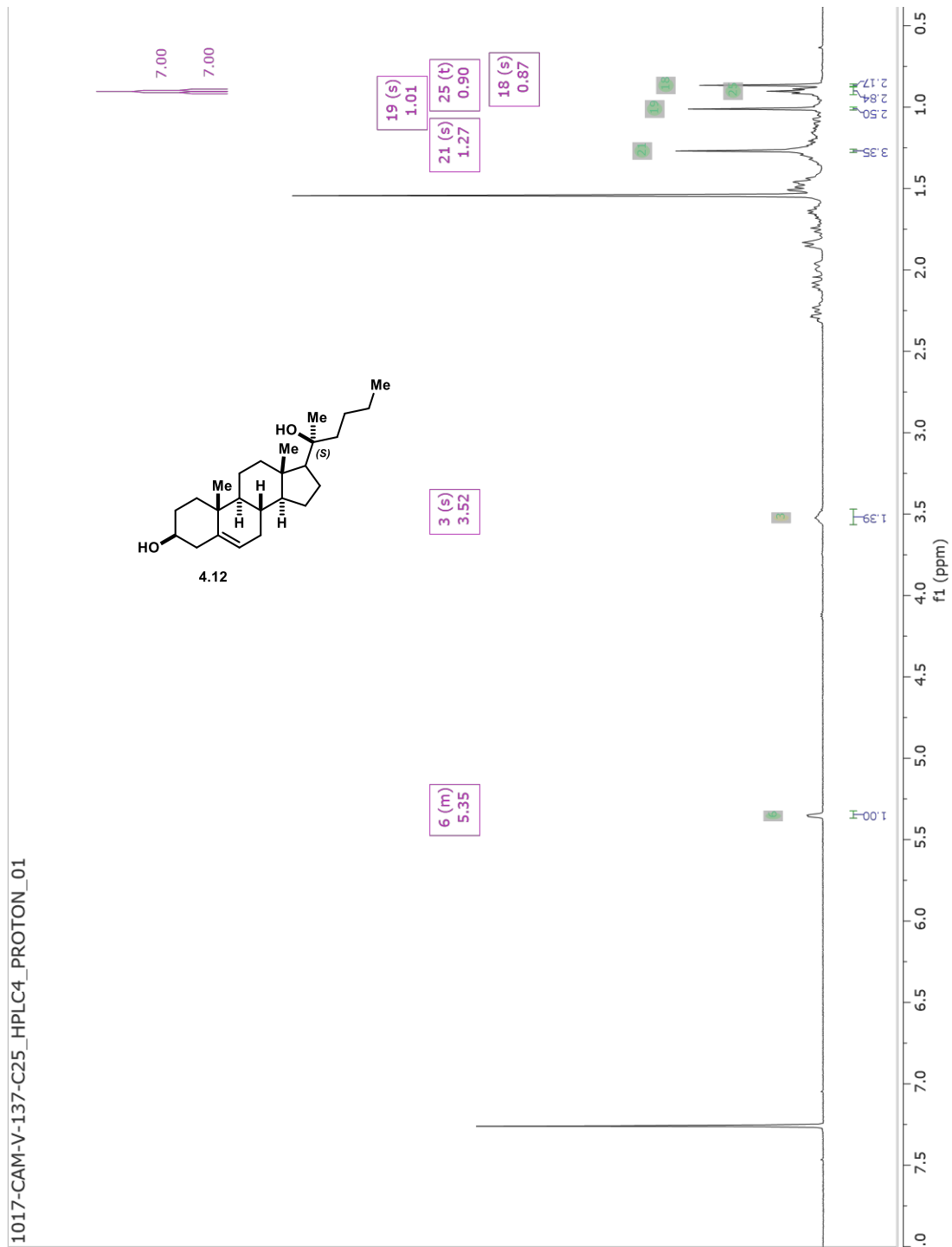


**Figure 4-32.**  $^1\text{H}$ -NMR of (*S*)-*n*-butyl-pregnenolol analog (**4.12**) in chloroform-*d*.

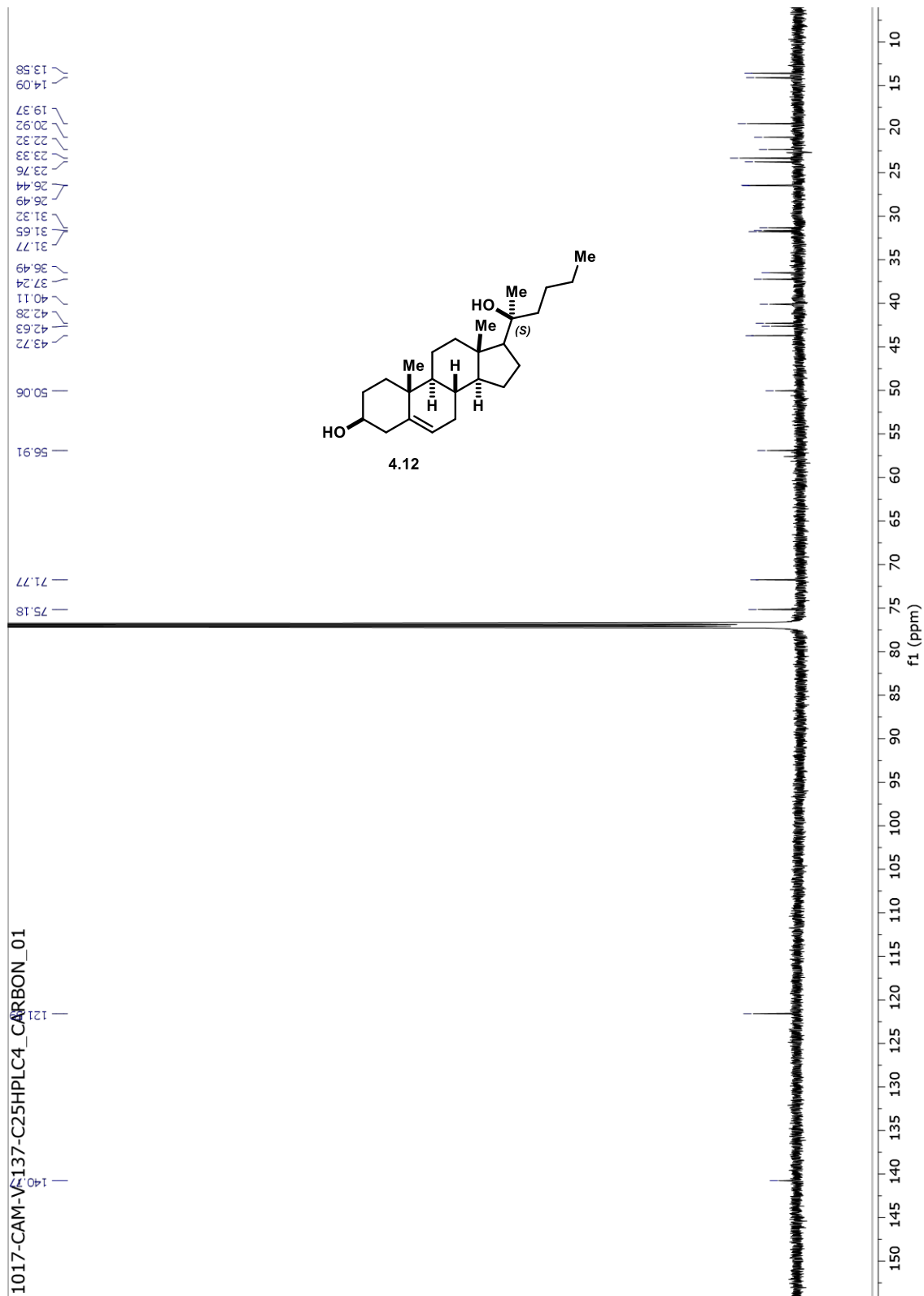


**Figure 4-33.**  $^{13}\text{C}$ -NMR of (*S*)-n-butyl-pregnenolol analog (**4.12**) in chloroform-*d*.



## **Chapter 5: Synthesis of characterization of Oxysterol-binding protein (OSBP) targeting anti-viral compound, TTP-8307**

**Abstract:** TTP-8307 was identified as a dose-dependent potent inhibitor of viral RNA synthesis that did not affect cellular protein synthesis or processing. Multiple mutational studies have conferred that TTP-8307 likely targets either PI4KIII $\beta$  or OSBP. Evidence has recently emerged that showed the antiviral activity of TTP-8307 was exerted through targeting of OSBP, not PI4KIII $\beta$ . TTP-8307 was produced in our laboratory for use in our research into the molecular pharmacology of OSBP-targeting antiviral compounds. Discrepancies found between the reported TTP-8307 molecular characterization data and our data suggests that an incorrectly identified derivative of TTP-8307 was used in the reported identification of its anti-viral activity through targeting OSBP. The first complete small-molecule structural elucidation of TTP-8307 is reported. Synthesis and characterization of oxazole containing TTP-8307 derivative are also reported and biological evaluation will be communicated elsewhere.

**Contributions:** Mr. Zack Severance performed all biological evaluations of the generated compounds.

## **5.1. Introduction**

### **5.1.1. TTP-8307 as OSBP-targeting anti-viral compound**

TTP-8307 (TTP) was identified as a dose-dependent potent inhibitor of viral RNA synthesis and our lab became interested in TTP due to recent literature evidence that it likely exerts its antiviral activity through the targeting of OSBP.<sup>44,50,184,185</sup> Our lab has recently reported that short-term exposure of low doses of OSW-1 induces reduction of cellular OSBP level by 90% and the reduction is inherited in multiple generations of cells after OSW-1 treatment.<sup>10</sup> Our research group has demonstrated that OSW-1 is an OSBP targeting compound that produces a prophylactic anti-viral effect and that OSW-1 is the only OSBP-targeting anti-viral compound that causes a prophylactic cellular response. Multiple other OSBP-targeting anti-viral compounds, including TTP, were biologically screened to compare the cellular response and it was found that TTP does not induce reduce cellular OSBP levels.<sup>10,44,50,184,185</sup> During this comparative study, inconsistencies within the reported TTP syntheses led to the first reported full characterization of TTP and the first reported synthesis and characterization of an oxazole-containing TTP derivative.

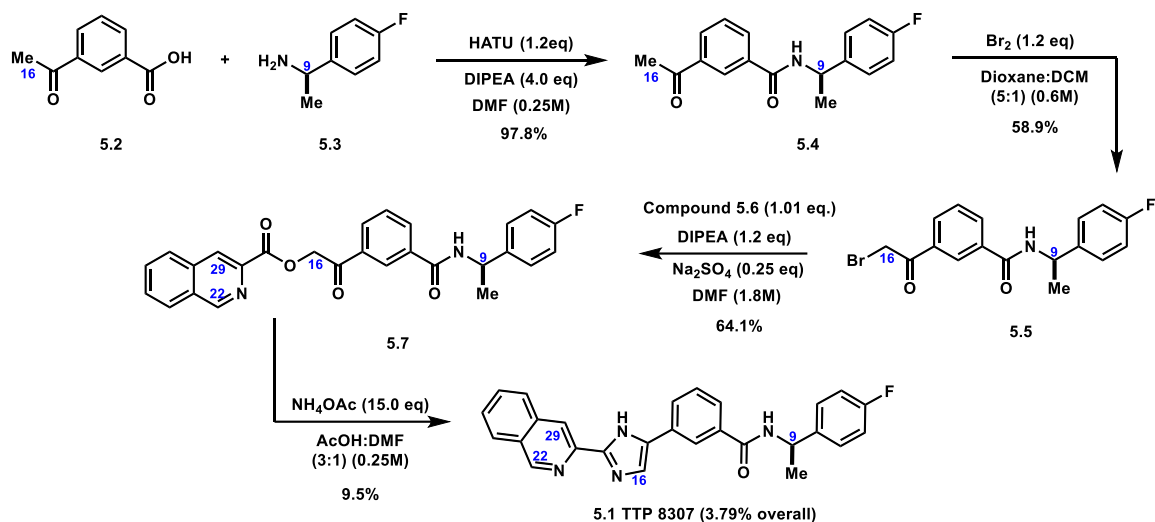
## **5.2. Results**

### **5.2.2. Synthesis and first full characterization of TTP**

A four-step linear synthesis of TTP was carried out with a 3.8% overall yield after HPLC purification. The synthesis began with coupling 3-acetylbenzoic acid (**5.1**) to 4-fluoro methyl benzyl amine (**5.3**) with coupling reagent HATU and N,N-diisopropylethylamine (DIPEA), to afford diaryl amide (**5.4**). Amide **5.4** then underwent  $\alpha$ -bromination at the acetyl position to produce diaryl bromo amide, **5.5**, which was then



coupled to isoquinoline-3-carboxylic acid (**5.6**) via base mediated nucleophilic substitution, to afford oxoaryl isoquinolate intermediate, **5.7**. The terminating step forms the imidazole ring through two subsequent imine formations that eliminate water upon cyclization to arrive at title compound, TTP-8307 (**5.1**).<sup>50,186,187</sup>



The literature reports of TTP (**5.1**), do not provide a complete characterization of the small molecule.<sup>50,187</sup> The article reporting that TTP exerts its antiviral cellular activity through the targeting of OSBP only reported a final <sup>1</sup>H-NMR spectra and a low resolution mass spectrum.<sup>50</sup> My synthesis of TTP produced a <sup>1</sup>H-NMR spectra that did not match the literature NMR spectrum, particularly in the aromatic region (>8.0 ppm).<sup>11</sup> Additionally, the reported literature <sup>1</sup>H-NMR spectra was taken in acetone-D<sub>6</sub> however, my synthesized compound was poorly soluble in acetone-D<sub>6</sub>.<sup>11,50</sup> Furthermore, the low-resolution mass spectrum of the reported TTP compound was not consistent with the high-resolution mass spectrum of my synthesized TTP compound.<sup>11,50</sup> The discrepancy between the synthesized TTP compound here and the literature reported structural characterizations led to the full structural characterization of the TTP compound, including <sup>13</sup>C-NMR, HSQC, and high-resolution mass spec. (Table 5-1). The

characterization data confer that the TTP compound synthesized here, was successfully made. This is most evident by the high-resolution mass spec which revealed an observed mass of 437.1761 m/z, in comparison to the calculated C<sub>27</sub>H<sub>21</sub>FN<sub>4</sub>O [M + H<sup>+</sup>] of 437.1772 m/z with a  $\Delta = 2.5$  ppm.

Analysis of the reported <sup>1</sup>H-NMR data for the compound reported as TTP indicates the possibility of an oxazole containing TTP derivative.<sup>50</sup> The last reaction of the TTP synthesis forms an imidazole ring in the presence of sodium acetate and acetic acid at 150°C. These conditions are also known to form oxazole rings.<sup>186,188–190</sup> Based on the literature low-resolution mass spec data that reports a 437.87 m/z peak and is more similar to the oxazole containing derivative of TTP, it is likely that the recent literature reports synthesized an oxazole containing derivative of TTP. The carbon shifts of imidazole and oxazoles are similar enough as to not be conclusively distinguishing. HSQC data on the synthesized compound reported here, did not show a C16 to H16 correlation because imidazole coupling of J(C16-H16) ~210 Hz.<sup>191</sup> was outside of the HSQC NMR C-H coupling constant setting, of 146 Hz.<sup>192</sup>

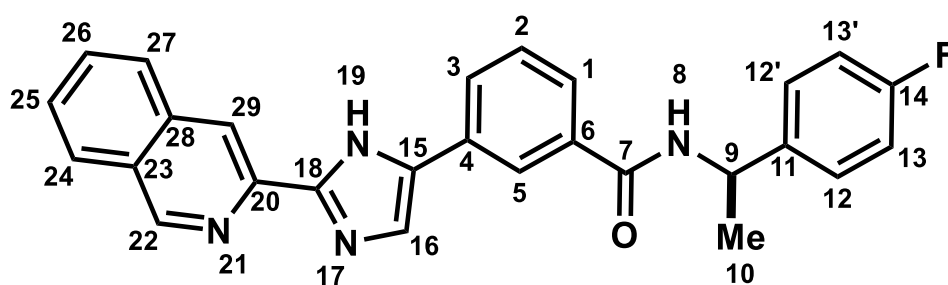


**Table 5-1.** <sup>1</sup>H-NMR, <sup>13</sup>C-NMR, COSY, and HSQC characterization of TTP-8307 (5).  
\*HSQC correlation not observed for C16-H16 because of the coupling constant of imidazole being outside of the NMR acquisition parameters.

Atom	Chemical Shift	COSY	HSQC	Atom	Chemical Shift	COSY	HSQC
------	----------------	------	------	------	----------------	------	------

<b>1 C</b>	127.92		1	<b>13' C</b>	114.70		13'
<b>1 H</b>	7.96	2, 5	1	<b>13' H</b>	7.07	12, 12'	13'
<b>2 C</b>	129.32		2	<b>14 C</b>	163.11, 160.69		
<b>2 H</b>	7.68	1, 3	2	<b>15 C</b>	124.28		
<b>3 C</b>	128.43		3	<b>16 C</b>	117.22		*
<b>3 H</b>	8.04	2	3	<b>16 H</b>	8.17		*
<b>4 C</b>	130.11			<b>18 C</b>	147.29		
<b>5 C</b>	124.88		5	<b>19 N</b>			
<b>5 H</b>	8.33	1	5	<b>19 H</b>			
<b>6 C</b>	130.11			<b>20 C</b>	143.82		
<b>7 C</b>	167.56			<b>22 C</b>	146.19		22
<b>8 N</b>				<b>22 H</b>	9.43	29	22
<b>8 H</b>				<b>23 C</b>	137.25		
<b>9 C</b>	49.03		9	<b>24 C</b>	127.85		24
<b>9 H</b>	5.27	10	9	<b>24 H</b>	8.17	25, 26	24
<b>10 C</b>	20.81		10	<b>25 C</b>	133.19		25
<b>10 H<sub>3</sub></b>	1.60	9	10	<b>25 H</b>	8.00	24, 26, 27	25
<b>11 C</b>	139.95			<b>26 C</b>	128.64		26
<b>12 C</b>	127.70		12	<b>26 H</b>	7.82	24, 25, 27	26
<b>12 H</b>	7.44	13, 13'	12	<b>27 C</b>	128.86		27
<b>12' C</b>	127.70		12'	<b>27 H</b>	8.17	25, 26	27
<b>12' H</b>	7.44	13, 13'	12'	<b>28 C</b>	135.34		
<b>13 C</b>	114.70		13	<b>29 C</b>	137.68		29
<b>13 H</b>	7.07	12, 12'	13	<b>29 H</b>	9.04	22	29

### 5.2.3. Synthesis and characterization of oxazole containing TTP-8307 derivative

In Order to more conclusively confirm that the previously reported TTP compound was in fact the oxazole compound (**5.8**) the deliberate synthesis of oxazole-containing TTP derivative was undertaken.<sup>188</sup> The reported Radziszweski reaction conditions of ammonium acetate and acetic acid at high temperatures are known to afford both oxazole and imidazole structures from dicarbonyl compounds.<sup>162</sup> In the synthesis of TTP reported here, these conditions afforded only a 9.6% yield, and the oxazole-TTP was not observed. To deliberately form the oxazole TTP compound, oxoaryl isoquinolate (**5.7**) was reacted

with acetamide and BF<sub>3</sub>-Et<sub>2</sub>O in xylenes at 150°C for 19 hours, according to established protocol, to afford oxazole TTP derivative in a 3.5% yield.<sup>188</sup>

High-resolution mass spectroscopy confirmed the presence of the oxazole-TTP compound; calculated C<sub>27</sub>H<sub>20</sub>FN<sub>3</sub>O<sub>2</sub> [M<sup>+</sup>] 438.1612 m/z, found 438.1630 m/z Δppm = 4.035. NMR characterization supported the oxazole-TTP structure. The <sup>1</sup>HNMR of the oxazole derivative in comparison to the imidazole containing TTP was different; many small chemical shifts of the aromatic protons drastically changed the overall spectra. Unlike the imidazole however, the oxazole derivative was readily soluble in acetone-D<sub>6</sub> solvent

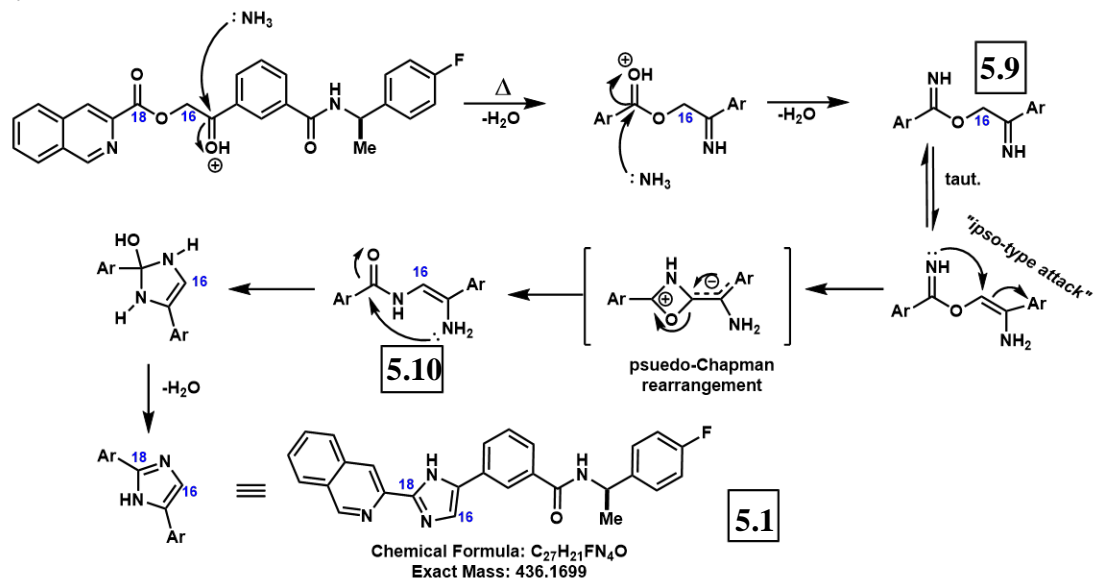
### **5.3.Discussion**

#### **5.3.4.Mechanistic analysis of imidazole and oxazole under Radziszweski reaction conditions**

The last synthetic step of the TTP-8307 synthesis forms the imidazole ring under Radziszweski reaction conditions (**Figure 5-2**), which are known to produce both imidazole and oxazole products.<sup>186,188–190</sup> The more typical Radziszweski reaction is performed on α-diketones at room temperature.<sup>162</sup> However, the TTP synthesis is not the first report of an imidazole formation from oxoaryl esters such as oxoaryl isoquinolate (**5.7**), at high temperatures.<sup>186</sup> **Figure 5-2 A and B** presents proposed mechanisms for both imidazole and oxazole formation based on mechanisms discussed with the literature.<sup>186,188–190</sup> These conditions are appropriate to produce an imidate intermediate (**5.9**). Intermediate **5.9** is then believed to undergo an *ipso*-type attack followed by a *psuedo*-Chapman rearrangement which transforms the imidate into an amide.<sup>188</sup> Species **5.10** then undergoes cyclization through nucleophilic attack of the enamine on the amide

carbonyl. Subsequent elimination of water forms, TTP (**5.1**). Although there is no agreed upon general mechanism cited in literature, the proposed mechanism is plausible and agrees with proposed mechanisms reported.<sup>186,188–190</sup>

**A) Possible Imidazole Formation**



**B) Possible Oxazole Formation**

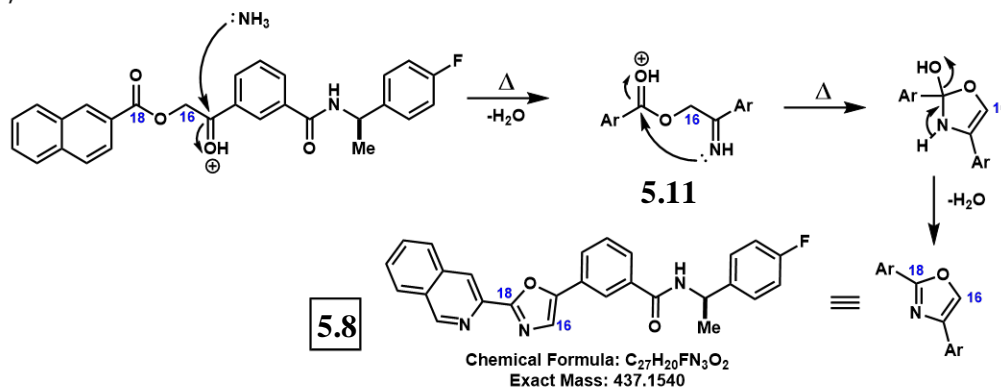


**Figure 5-2.** Mechanism of possible Radziszweski reactions to form **A)** imidazole containing TTP-8307, and **B)** oxazole containing TTP-8307.

Imidazole formation under the conditions discussed in **Figure 5-2.**, are known to be plagued by a common side-product, ring closure to an oxazole.<sup>162,188</sup> A similar mechanism under Radziszweski reaction conditions can form an oxazole from oxoaryl isoquinolate (**Figure 5-2.**, **Compound 5.7**). If the imino imide intermediate **5.9** fails

to form before intramolecular attack of the imine on the activated ester (**5.11**), then cyclization to form the hydroxyoxazoline occurs. Elimination of water produces oxazole-TTP derivative (**5.8**).

Presumably, reaction conditions can be manipulated to preferentially form the imidazole or the oxazole from Radziszewski reactions on oxoaryl esters.<sup>186,188–190</sup> Insufficient ammonium acetate or reaction temperatures that fail to drive formation of the imino imidate **5.9**, should favor oxazole formation. Experimental studies to explore oxazole formation under these modified conditions, i.e. lower equivalents of ammonium acetate as well as lowering the reaction temperatures to 120°C, resulted only in unreacted starting material. Since the successful formation of the imidazole-TTP compound at 150°C were low yielding (9.6%), the failure of milder reaction conditions to afford the oxazole-TTP compound were expected. Literature reports of oxoaryl ester compounds, such as oxoaryl isoquinolate **5.7**, subjected to Radziszewski reaction conditions also report <30% yield.<sup>186</sup> The lack of reactivity of oxoaryl isoquinolate (**5.7**) might explain the lack of oxazole formation under milder conditions (i.e. cooler reaction temperature, less ammonium acetate).

Characterization of both TTP-8307 and oxazole derivative reveals substantially different chemical shifts, splitting, and solubility. None of which seem to correspond to the literature reported characterization. The reported characterization of TTP-8307 was performed in acetone-D<sub>6</sub>. The experimental TTP-8307 did not readily dissolve in acetone-D<sub>6</sub> but the oxazole derivative did. However, neither the imidazole nor the oxazole containing molecule were consistent with the literature reported <sup>1</sup>H-NMR spectra.<sup>50</sup> <sup>1</sup>H-NMR of unreacted starting material, oxoaryl isoquinolate (**5.7**), in acetone-D<sub>6</sub> also did not

match the literature  $^1\text{H-NMR}$  spectra.<sup>50</sup> It is difficult to conclude exactly what structure the reported literature used in their biologically evaluations.

#### 5.4. Conclusions and future work

To enable investigation of OSBP-targeting antiviral compounds, TTP-8307 was synthesized. The synthesis of TTP-8307 produced characterization data not consistent with the limited characterization available in the literature. Based on the analysis, the literature reported TTP-8307 used in a previous OSBP antiviral paper is inconsistent with both the imidazole- and oxazole-containing TTP-8307 compounds. Synthesis of an oxazole containing TTP-8307 derivative for  $^1\text{H-NMR}$  comparison to the literature eliminated it as a possible structure. However, our confirmed TTP-8307 compound seemed to have similar effects on OSBP and similar antiviral activity as the miss assigned TTP-8307 described in the literature, indicating that both compounds might have similar biological activity.

#### 5.5. Experimental and supporting information

##### TTP-8307 (5) Compound Synthesis

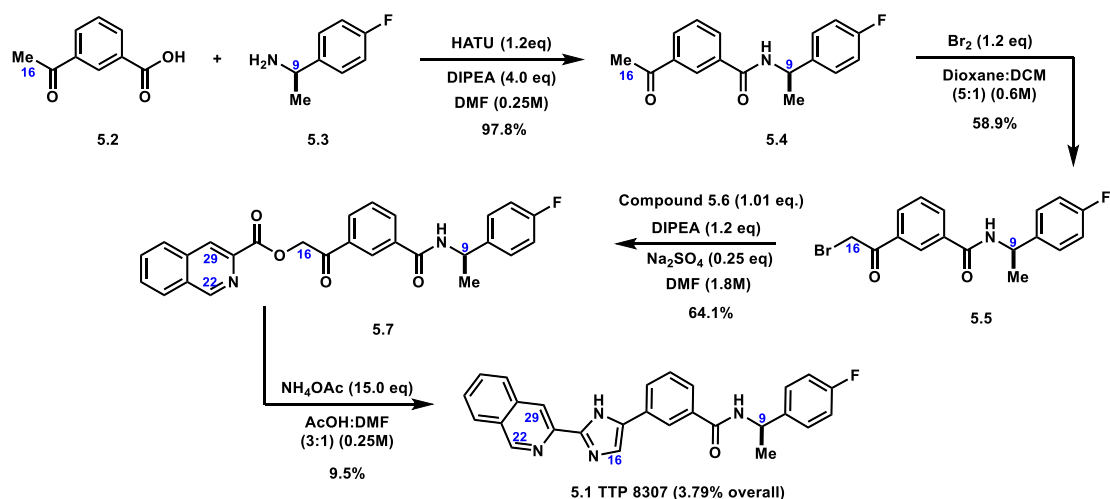
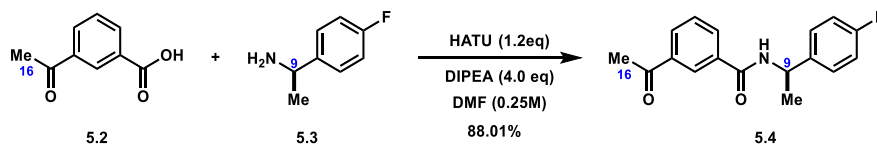


Figure 5-3. Synthesis of TTP-8307 (5.1) compound

A four-step linear synthesis of TTP-8307 (**5.1**). was carried out based on established literature protocol, with a 3.8% overall yield after HPLC purification.<sup>11,50</sup> The synthesis began with coupling 3-acetylbenzoic acid (**5.2**) to 4-fluoro methyl benzyl amine (**5.3**) with coupling reagent HATU and N,N-diisopropylethylamine (DIPEA), to afford diaryl amide (**5.4**). Amide **5.4** then underwent  $\alpha$ -bromination at the acetyl position to produce diaryl bromo amide, **5.5**, which was then coupled to isoquinoline-3-carboxylic acid (**5.6**) via base mediated nucleophilic substitution, to afford oxoaryl isoquinolate intermediate, **5.7**. The terminating step forms the imidazole ring through two subsequent imine formations that eliminate water upon cyclization to arrive at the target compound, TTP-8307 (**5.1**). The TTP-8307 compound was confirmed via <sup>1</sup>H-NMR, <sup>13</sup>C-NMR, 2D-NMR, and HRMS.

2D COSY was collected with 8 scans, 512 increments, a spectral width of 5367.7 Hz, an acquisition time of 0.1908 seconds and a relaxation delay of 1.0 seconds. Data was not intensified using zero-filled or linear predict, sin square II applied in both F1 and F2 prior to Fourier Transform. 2D HSQC-AD was collected with 8 scans, 256 increments, a spectral width of 5000.0 Hz in f2 and 17597.9 Hz in f1, an acquisition time of 0.2048 seconds, a relaxation delay of 1.0952 seconds, and C-H coupling constant of 146 Hz. Data was not intensified using zero-filled or linear predict, sin square II applied in both F1 and F2 prior to Fourier Transform.



**(R)-3-acetyl-N-(1-(4-fluorophenyl)ethyl)benzamide (5.4):** Compound **5.4** was prepared through following a previously reported protocol with no modifications.<sup>50</sup> 3-acetyl benzoic acid (Compound **5.2**, 1.00 g, 6.09 mmol, 1 equiv.) was dissolved in DMF (2.0 ml) under nitrogen atmosphere. A solution of the HATU coupling agent (278 mg, 7.31 mmol, 4 equiv.) in DMF (4.0 ml) was added fast dropwise. N,N-diisopropylethylamine (DIPEA, 425  $\mu$ l, 2.44 mmol, 4.0 equiv.) was then added slowly dropwise to the reaction over 15 minutes. The reaction turned yellow in color and progressively became a dark brown color over 10 min. 4-fluoro methyl benzyl amine (Compound **5.3**, 823  $\mu$ L, 6.09 mmol, 1 equiv.) was added to the reaction via syringe fast dropwise. The reaction proceeded over 2 hours. Then, the reaction was diluted with distilled water (10 ml) and transferred to a separatory funnel. The biphasic mixture was separated, and the aqueous phase was back extracted with ethyl acetate (4 x 10 ml). The organic layers were combined and washed with brine and dried over sodium sulfate. The drying agent was removed and the solvent evaporated *in vacuo* to afford 1.54 g of crude Compound **5.4** as a white solid (88% yield) which was carried forward into the next reaction without further purification.

**Compound 5.4:** <sup>1</sup>H-NMR (500 MHz, Chloroform-*d*)  $\delta$  1.61 (d,  $J$  = 6.9 Hz, 3H), 2.64 (s, 3H), 5.32 (p,  $J$  = 7.1 Hz, 1H), 6.57 (s, 1H), 7.04 (t,  $J$  = 8.7 Hz, 2H), 7.37 (t,  $J$  = 8.6, 6.7 Hz, 2H), 7.54 (t,  $J$  = 7.8 Hz, 1H), 8.02 (dt,  $J$  = 5.8, 1.4 Hz, 1H), 8.07 (dt,  $J$  = 7.8, 1.4 Hz,



1H), 8.33 (s, 1H). Residual DMF peaks at: 2.87 (dt,  $J = 7.79$ , 3H), 2.95 (s, 2H, 4), 8.02 (s, 1H), Residual ethyl acetate peaks at: 1.25 (td,  $J = 7.14$ , 0.77 Hz, 1H), 2.04 (s, 1H, 3), 4.11 (q,  $J = 7.12$  Hz, 1H). HRMS (-ESI):  $m/z$  calculated  $C_{17}H_{16}FNO_2 \cdot H^+$  [ $M - H^+$ ]: 284.1092  $m/z$ , observed 284.1089  $m/z$ ,  $\Delta ppm = 1.1 ppm$ .

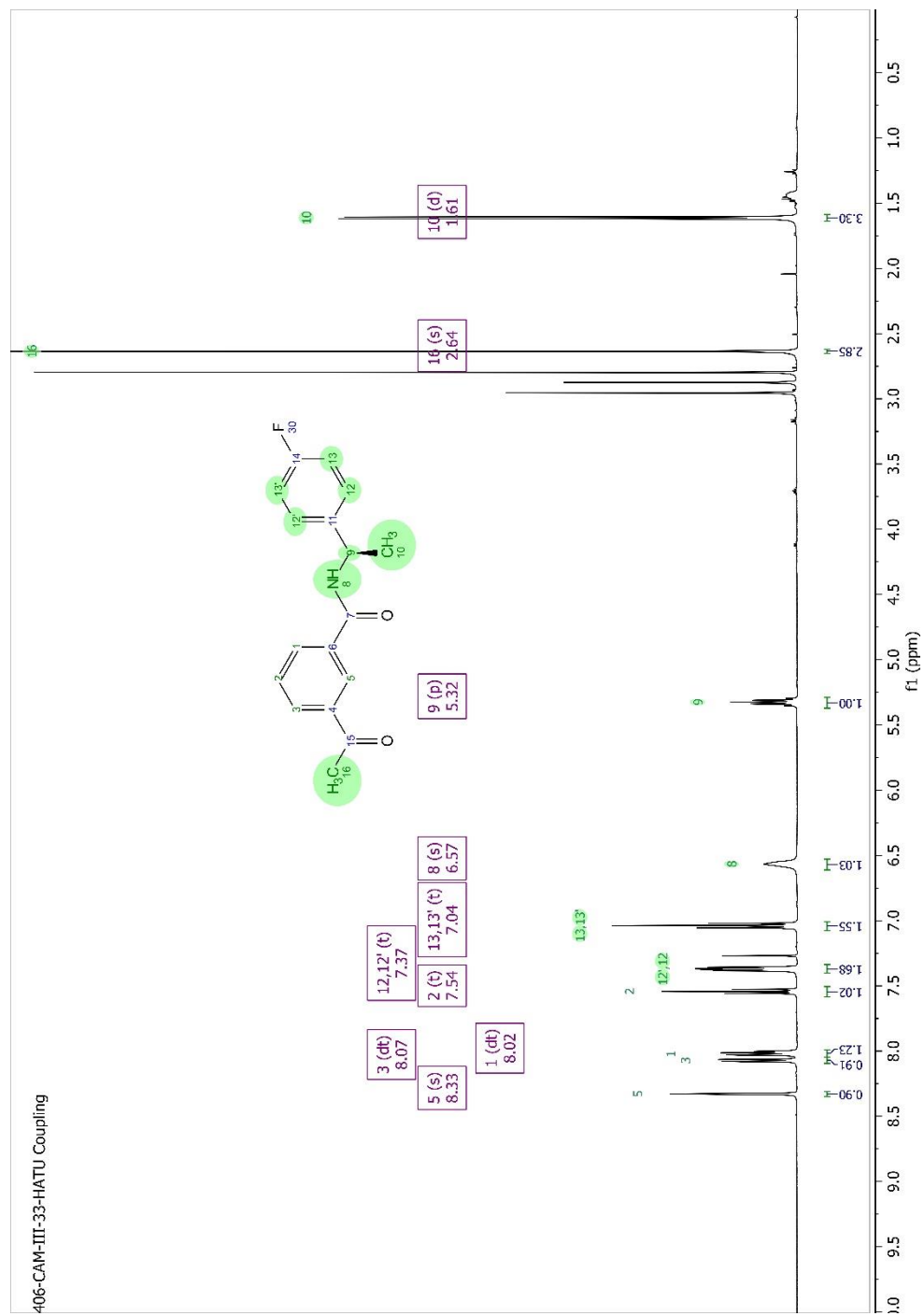
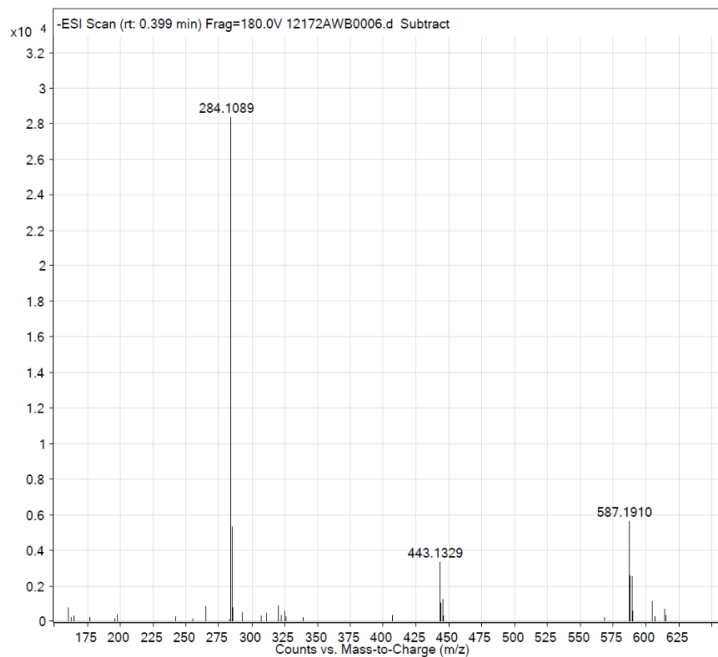
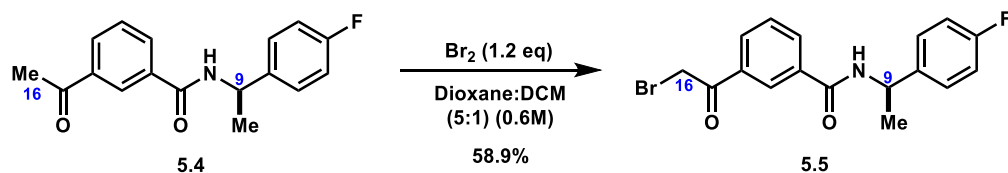


Figure 5-4. <sup>1</sup>H-NMR of amide (5.4) in chloroform-*d*.



**Figure 5-5. Compound 5.4, HRMS (-ESI) of compound 5.4: calculated C<sub>17</sub>H<sub>16</sub>FNO<sub>2</sub> -H<sup>+</sup> [M - H<sup>+</sup>]: 284.1092 m/z, observed 284.1089 m/z,  $\Delta$  = 1.1 ppm.**



**(R)-3-(2-bromoacetyl)-N-(1-(4-fluorophenyl)ethyl)benzamide (5.5)** : **Compound 5.5** was prepared through following a previously reported protocol with no modifications.<sup>50</sup> To a stirring solution of **Compound 5.4** (1.74 g, 6.10 mmol, 1.0 equiv.) in dry DCM (2.0 mL) and dioxane (10 ml) at 0°C was added a solution of bromine (344  $\mu\text{L}$ , 6.71 mmol, 1.1 equiv.) fast dropwise. The reaction was warmed to room temperature and proceeded for 18 hours. Upon complete conversion of the starting material, as indicated by TLC, the reaction was condensed *in vacuo* to afford an orange/yellow crude semisolid. The crude material was dissolved in hot DCM and the desired product crashed out upon cooling. The white precipitate was then filtered to afford 1.53g of **Compound 5.5** which was carried forward into the next reaction without further purification (68.9% yield).

**Compound 5.5:**  $^1\text{H-NMR}$  (500 MHz, Chloroform-*d*)  $\delta$  1.61 (d,  $J = 7.0$  Hz, 3H), 4.46 (s, 2H), 5.31 (p,  $J = 7.1$  Hz, 1H), 6.45 (d,  $J = 7.4$  Hz, 1H), 7.04 (td,  $J = 8.7, 2.04$  Hz, 2H), 7.36 (dd,  $J = 8.6, 5.4$  Hz, 2H), 7.50 – 7.66 (m, 1H), 8.04 (dd,  $J = 8.3, 1.23$  Hz), 8.09 (ddd,  $J = 7.8, 1.8, 1.13$  Hz, 1H), 8.34 (t,  $J = 1.82$  Hz, 1H). HRMS (-ESI): calculated  $\text{C}_{17}\text{H}_{16}\text{BrFNO}_2$  -H+ [M - H+]: 365.0250 m/z, observed 362.0196 m/z,  $\Delta\text{ppm} = 0.28$  ppm.

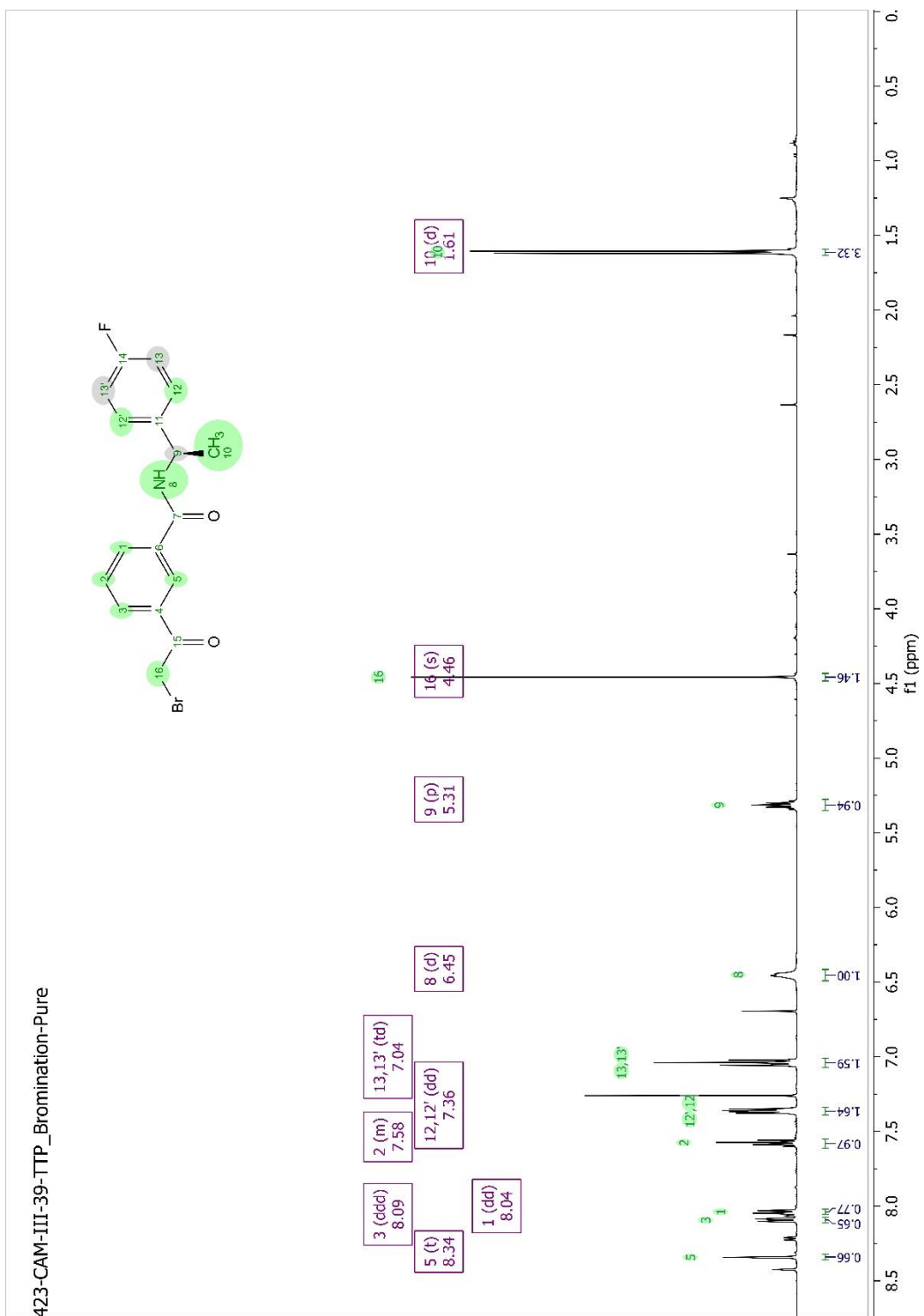


**Figure 5-6.** <sup>1</sup>H-NMR of alpha mono brominated amide (5.5) in chloroform-*d*.



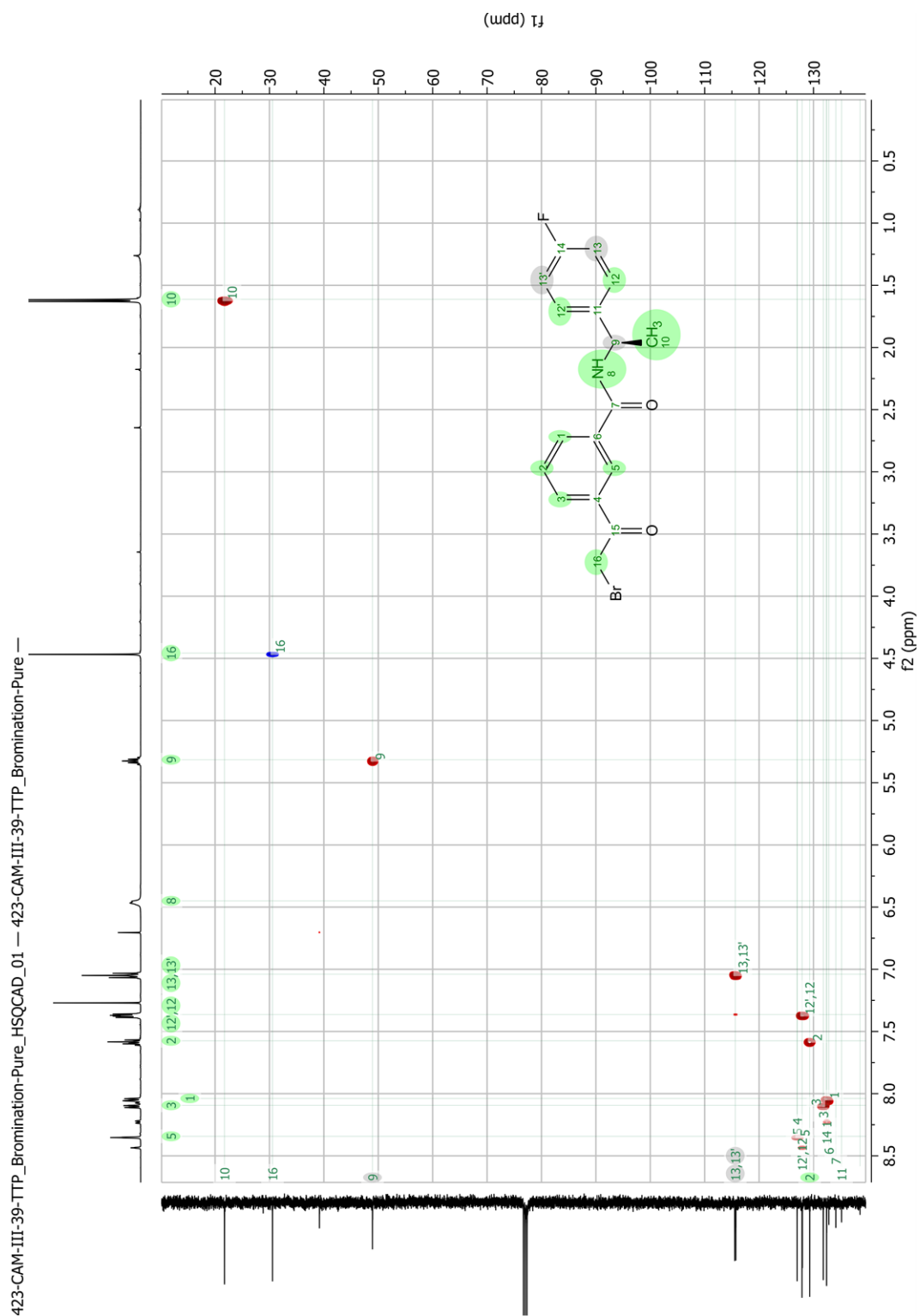


**Figure 5-8.** HSQC correlations of alpha mono brominated amide (5.5) in chloroform-*d*.

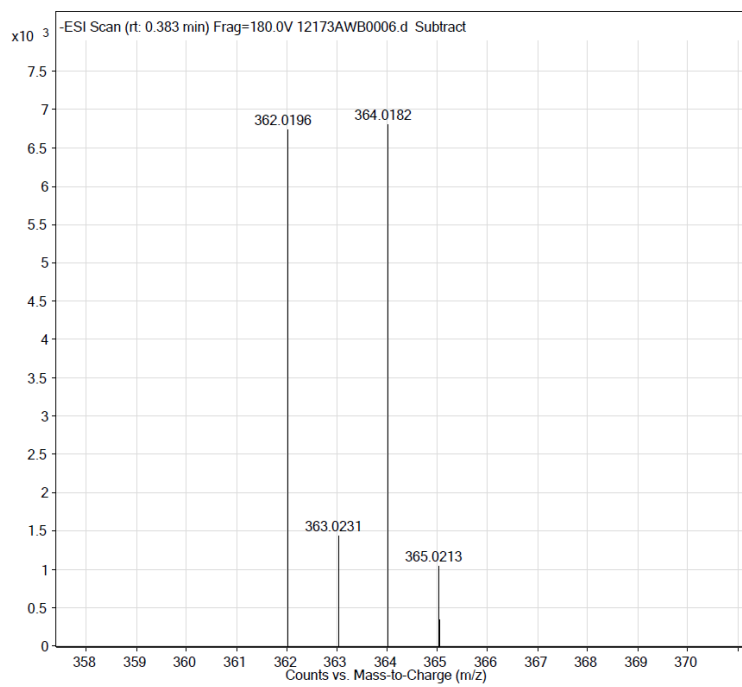
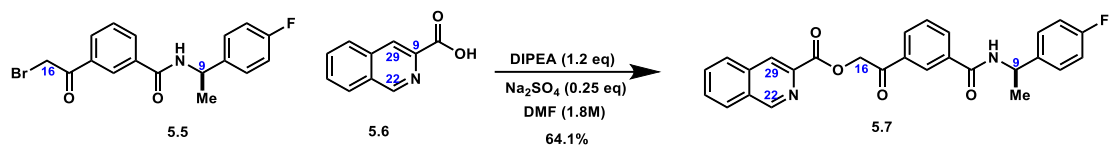


**Figure 5-9. Compound 5.5, HRMS (-ESI) of compound 5.3: calculated  $C_{17}H_{16}BrFNO_2 -H^+ [M - H^+]$ : 365.0250 m/z, observed 362.0196 m/z,  $\Delta$ ppm = 0.28 ppm.**



**(R)-2-(3-((1-(4-fluorophenyl)ethyl)carbamoyl)phenyl)-2-oxoethyl isoquinoline-3-carboxylate (5.7):** Compound **5.7** was prepared through following a previously reported protocol with no modifications.<sup>50</sup> To a stirring solution of isoquinoline-1-carboxylic acid (**Compound 5.6**, 211  $\mu$ l, 380  $\mu$ mol, 1.0 equiv.) and sodium sulfate (13.4 mg, 94.0  $\mu$ mol, 1.0 equiv.) in DMF (1.0 mL, 0.46 M) at room temperature was added N,N-diisopropylethylamine (78.63  $\mu$ L). The reaction was cooled to 0°C on an ice-water bath. A solution of **Compound 5.5** (137 mg, 376  $\mu$ mol, 1.0 equiv.) in DMF (1.0 mL, 0.38 M) was added to the reaction slow dropwise via syringe. The reaction proceeded over 90 minutes. No further progress was indicated by TLC after 60 minutes. The reaction was quenched with DI water (2 ml) and a white precipitate formed within the solution. The precipitate was collected via filtration and washed with cold DI water (50 ml). The white solid was then dissolved in ethyl acetate (10 ml) and transferred to a separatory funnel. The organic solution was washed with saturated sodium bicarbonate (2 x 10 ml). The aqueous layers were combined and back extracted with ethyl acetate (2 x 10 ml). The organic layers were combined, washed with brine, and then dried over sodium sulfate. The drying agent was removed, and the solvent evaporated *in vacuo* afford a crude white solid. The crude material was purified via silica gel column chromatography and eluted with 30% acetone in hexanes as mobile phase to afford 117 mg of white solid **Compound 5.7** (69% yield).

**Compound 5.7:** <sup>1</sup>H-NMR (500 MHz, Chloroform-*d*)  $\delta$  1.63 (d,  $J$  = 6.9 Hz, 3H), 5.33 (p,  $J$  = 7.08 Hz, 1H), 5.69 (d,  $J$  = 0.95 Hz, 2H), 6.38 (d,  $J$  = 7.8 Hz, 1H), 7.05 (t,  $J$  = 8.6 Hz, 2H), 7.37 (t,  $J$  = 6.7 Hz, 2H), 7.62 (t,  $J$  = 7.75 Hz, 1H), 7.65 (ddd,  $J$  = 8.1, 6.9, 1.18 Hz, 1H), 7.87 (ddd,  $J$  = 8.5, 6.9, 1.4 Hz, 1H), 7.97 (d,  $J$  = 8.1 Hz, 1H), 8.07 (dd,  $J$  = 8.9, 1.4 Hz, 1H), 8.11 (dt,  $J$  = 7.7, 1.4 Hz, 1H), 8.20 (dd,  $J$  = 8.6, 1.1 Hz, 1H), 8.37 (t,  $J$  = 1.7 Hz, 1H), 8.97 (d,  $J$  = 1.9 Hz, 1H), 9.53 (d,  $J$  = 2.1 Hz, 1H). HRMS (-ESI): calculated C<sub>27</sub>H<sub>21</sub>FN<sub>2</sub>O<sub>4</sub>-H<sup>+</sup> [M - H<sup>+</sup>]: 455.1413 m/z, observed 455.1417 m/z,  $\Delta$ ppm = 0.88 ppm.



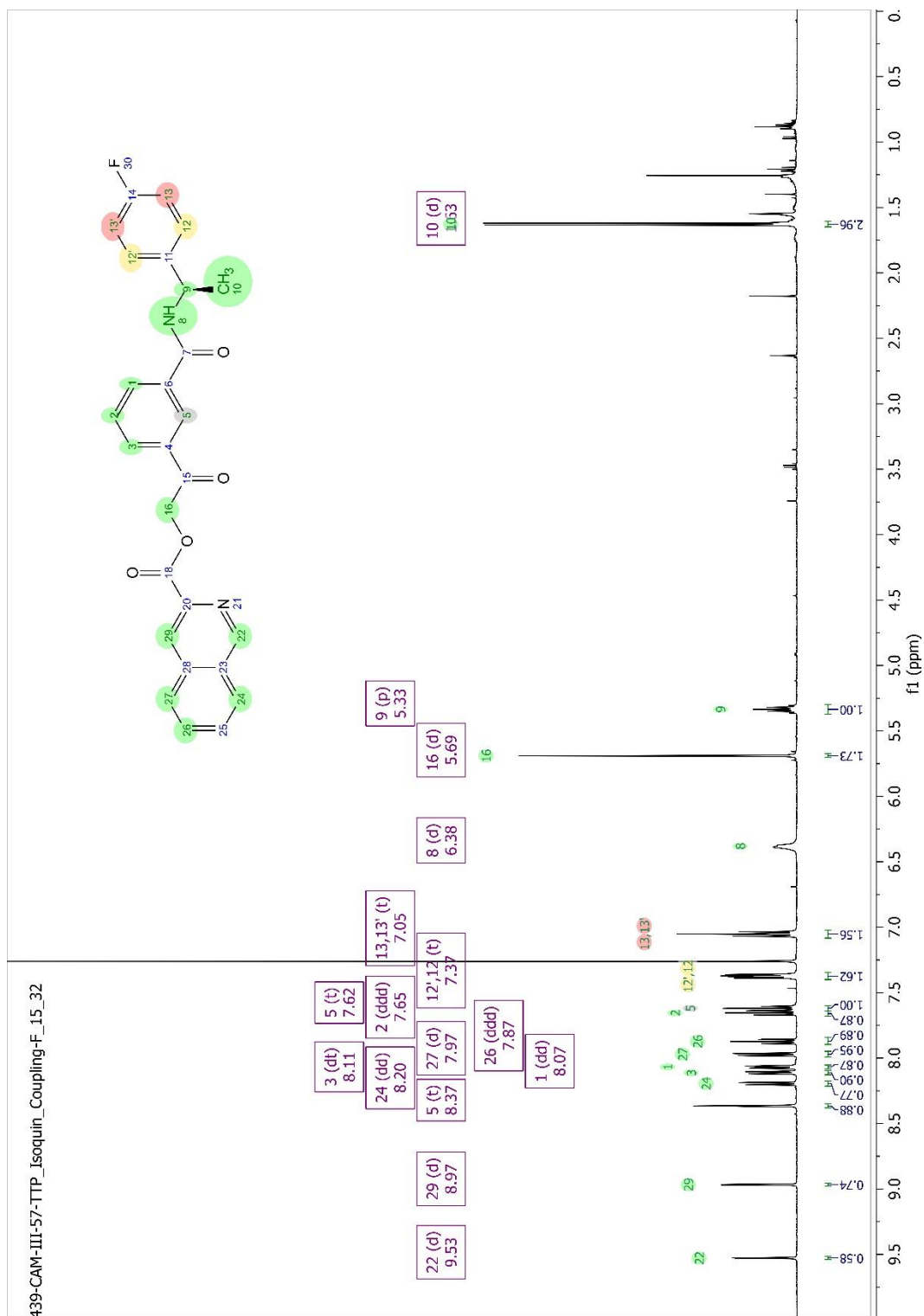
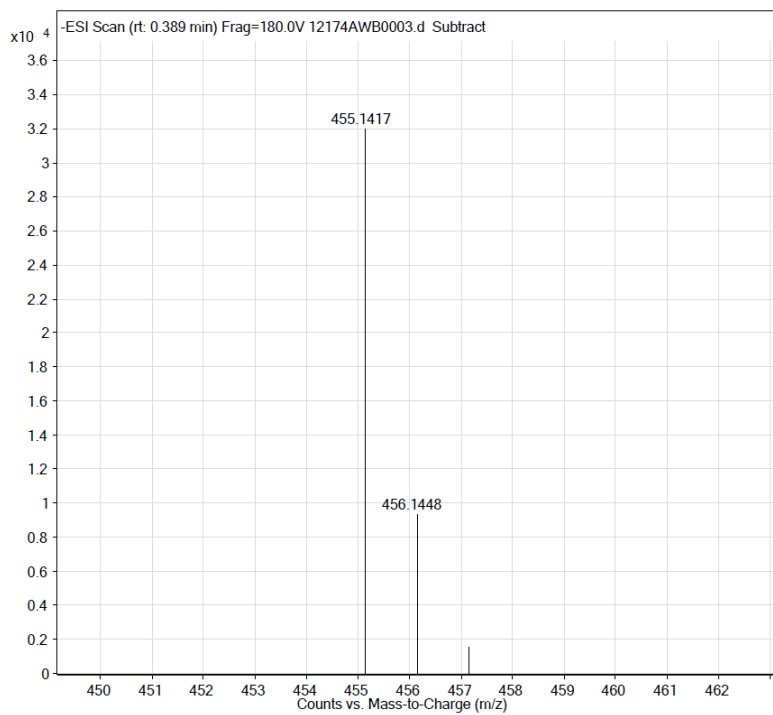
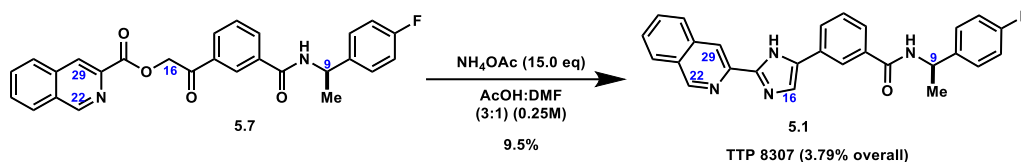


Figure 5-10. <sup>1</sup>H-NMR of Compound 5.7 in chloroform-*d*.



**Figure 5-11.** HRMS (-ESI) of **Compound 5.7**: calculated  $C_{27}H_{21}FN_2O_4-H^+$   $[M - H^+]$ : 455.1413  $m/z$ , observed 455.1417  $m/z$ ,  $\Delta = 0.88$  ppm.

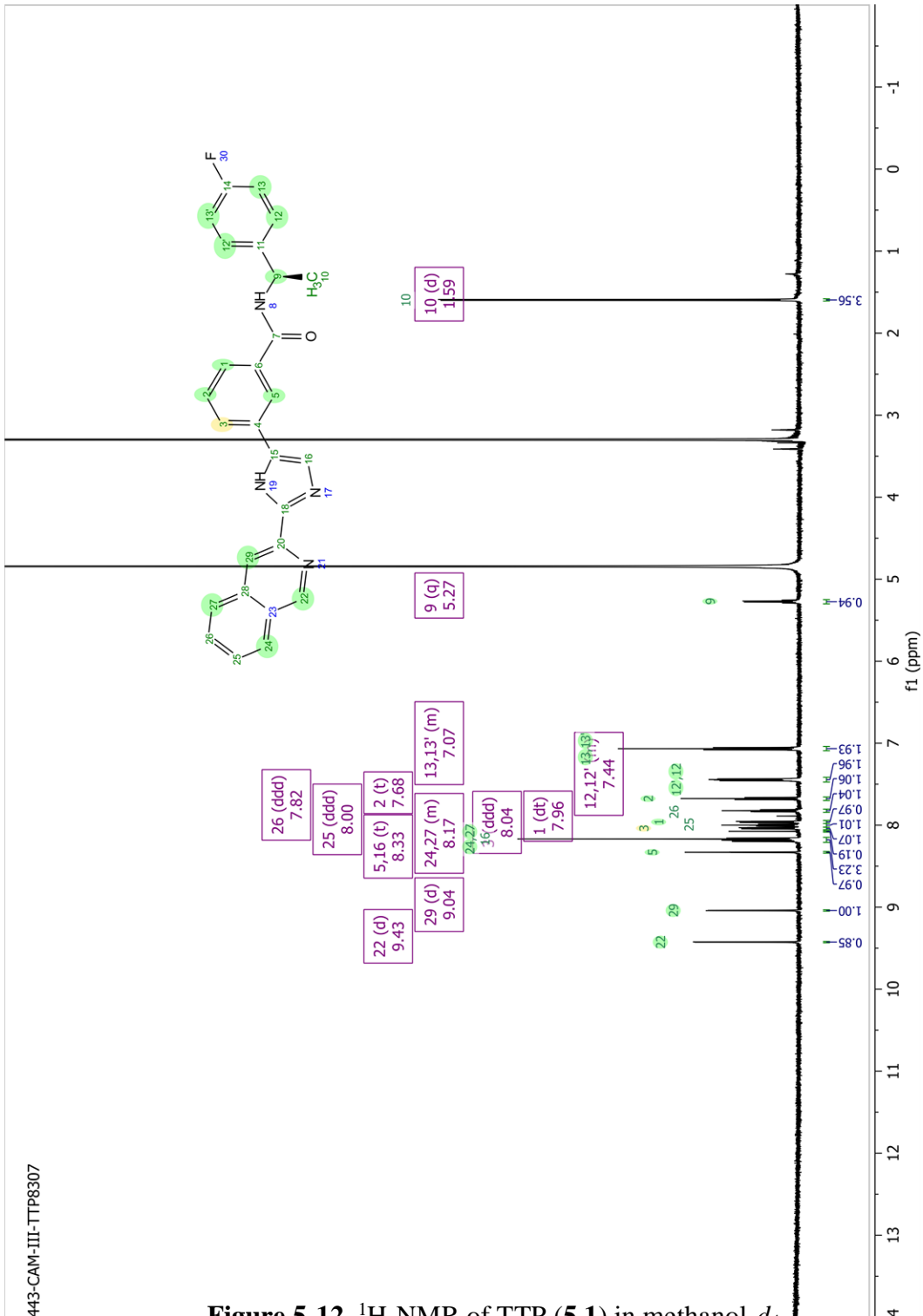


**TTP-8307 (5.1):** Compound **5.1** was prepared through following a previously reported protocol with no modifications.<sup>50</sup> To a stirring solution of **Compound 5.7** (110 mg, 240  $\mu\text{mol}$ , 1 equiv.) dissolved in DMF (0.5 mL, 0.5M) at room temperature was added glacial acetic acid (1.4 mL) followed by solid ammonium acetate (279 mg, 3.61 mmol, 15 equiv.). The reaction flask was equipped with a water jacketed condenser and then warmed to 150°C for 90 minutes. Upon complete conversion of starting material, as indicated by TLC, the reaction was cooled to room temperature and then quenched with cold DI water (10 ml). The quenched reaction was transferred to a separatory funnel and diluted ethyl acetate (10 ml). The solution was washed with saturated sodium bicarbonate (2 x 10 ml). The aqueous layers were combined and back extracted with ethyl acetate (2 X 10 ml). The organic layers were combined and then vigorously shaken in 4N HCl<sub>(aq)</sub> to precipitate a white/yellow solid. The precipitate was collected via filtration and residual solvent evaporated *in vacuo* to afford a crude light-yellow solid. The crude mixture was purified via HPLC-MS using Shimadzu UFLC instrumentation equipped with Luna 5  $\mu\text{m}$  C8(2) 100 Å column and isocratic 80% methanol to 0.1% formic acid/water. 10.0 mg of **Compound 5.1** were obtained and fully characterized as shown in **Table 18**, Purity determined via HPLC chromatogram as shown in **Figure 5-20** and **Table 19** (9.5%).

**TTP-8307 (5.1):** <sup>1</sup>H-NMR (600 MHz, Methanol-*d*<sub>4</sub>)  $\delta$  1.59 (d,  $J = 7.0$  Hz, 3H), 5.27 (q,  $J = 7.2$  Hz, 1H), 7.01 – 7.13 (m, 2H), 7.41 – 7.52 (m, 2H), 7.68 (t,  $J = 7.8$  Hz, 1H), 7.82 (ddd,  $J = 8.2, 6.9, 1.1$  Hz, 1H), 7.96 (dt,  $J = 8.2, 1.2$  Hz, 1H), 8.00 (ddd,  $J = 8.4, 6.89, 1.4$  Hz, 1H), 8.04 (ddd,  $J = 7.77, 1.89, 1.00$  Hz, 1H, 3), 8.14 – 8.23 (m, 3H, 16, 24, 27), 8.33 (t,  $J = 1.76$  Hz, 1H), 9.04 (d,  $J = 2.3$  Hz, 1H), 9.43 (d,  $J = 2.3$  Hz, 1H). <sup>13</sup>C-NMR (101 MHz, Methanol-*d*<sub>4</sub>)  $\delta$  167.6, 163.1, 160.7, 147.3, 147.0, 140.0, 139.9, 135.3, 134.6, 131.5, 130.1, 129.0, 128.6, 128.1, 128.1, 127.8, 127.8, 127.7, 127.4, 126.8, 124.3, 117.7, 114.8, 114.6, 48.9, 20.8. HRMS (+ESI): calculated C<sub>27</sub>H<sub>21</sub>FN<sub>4</sub>O [M + H]<sup>+</sup>: 437.1772 m/z, observed 437.1761 m/z,  $\Delta\text{ppm} = 2.5$  ppm.

**Table 15.**  $^1\text{H}$ -NMR,  $^{13}\text{C}$ -NMR, COSY, & HSQC characterization of **TTP-8307 (5.1)**. \*HSQC correlation not observed for C16-H16 because of the coupling constant of imidazole being outside of the NMR acquisition parameters.<sup>192</sup>

Atom	Chemical	COSY	HSQC	Atom	Chemical	COSY	HSQC
1 C	127.92		1	13' C	114.70		13'
H	7.96	2, 5	1	H	7.07	12, 12'	13'
2 C	129.32		2	14 C			
H	7.68	1, 3	2	15 C			
3 C	128.43		3	16 C	117.22		*
H	8.04	2	3	H	8.17		*
4 C				18 C			
5 C	124.88		5	19 N			
H	8.33	1	5	H			
6 C				20 C			
7 C				22 C	146.19		22
8 N				H	9.43	29	22
H				23 C			
9 C	49.03		9	24 C	127.85		24
H	5.27	10	9	H	8.17	25, 26	24
10 C	20.81		10	25 C	133.19		25
H3	1.60	9	10	H	8.00	24, 26,	25
11 C				26 C	128.64		26
12 C	127.70		12	H	7.82	24, 25,	26
H	7.44	13, 13'	12	27 C	128.86		27
12' C	127.70		12'	H	8.17	25, 26	27
H	7.44	13, 13'	12'	28 C			
13 C	114.70		13	29 C	137.68		29
H	7.07	12, 12'	13	H	9.04	22	29



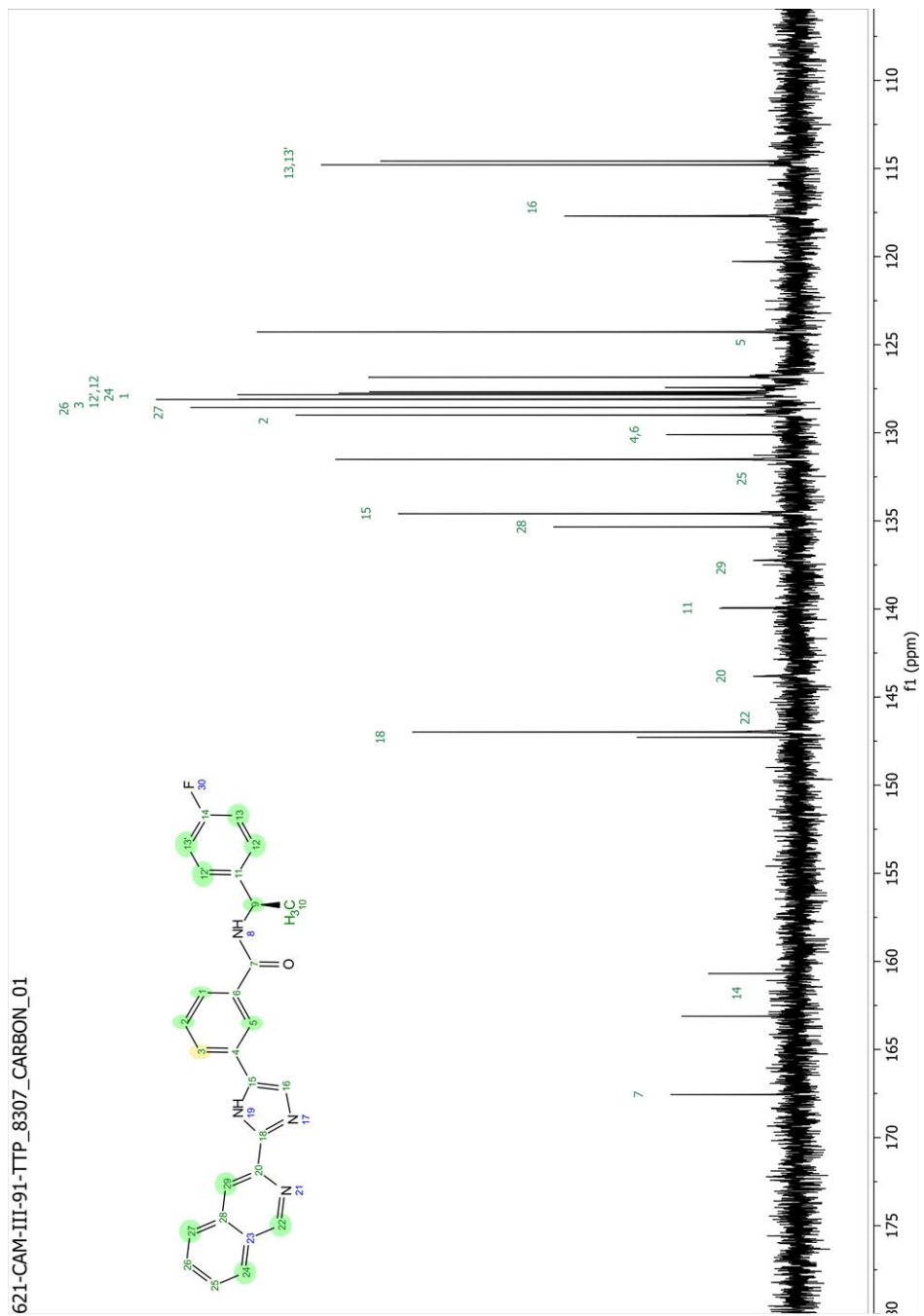


**Figure 5-13.**  $^{13}\text{C}$ -NMR of TTP (5.1) in methanol- $d_4$ .

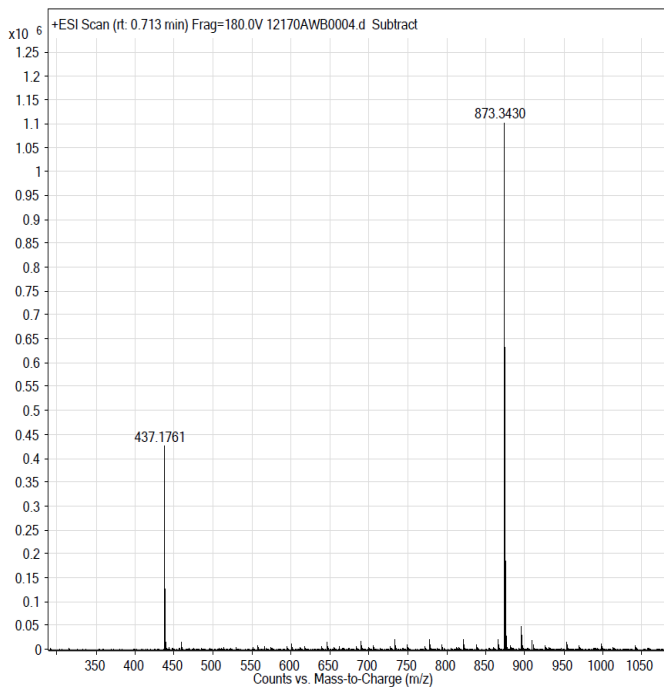


**Figure 5-14. TTP (5.1), HRMS (+ESI) of TTP-8307 (5):** calculated  $C_{27}H_{21}FN_4O$  [M + H<sup>+</sup>]: 437.1772 m/z, observed 437.1761 m/z,  $\Delta$ ppm = 2.5 ppm.

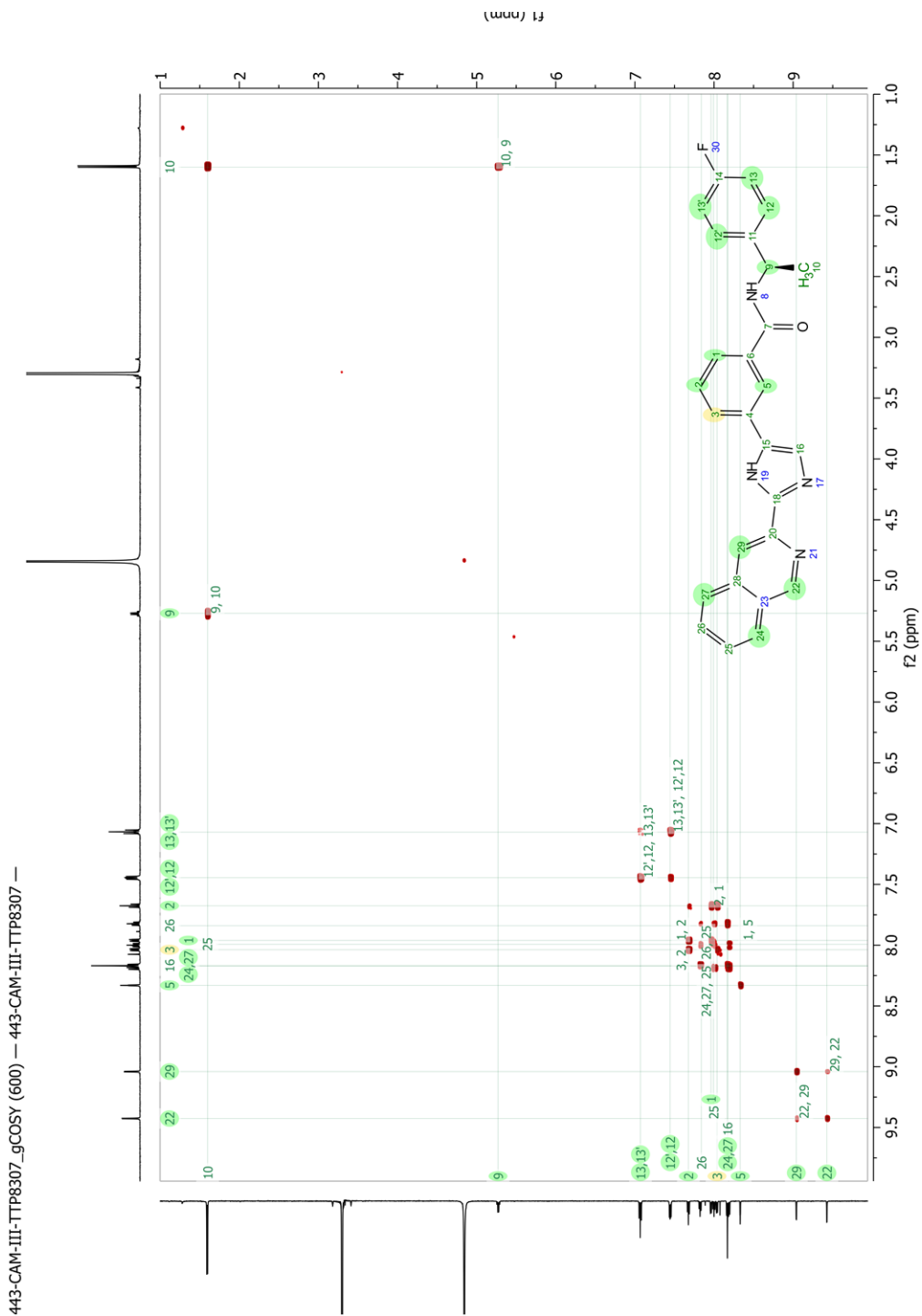


**Figure 5-15.** COSY correlation of TTP (**5.1**) in methanol-*d*<sub>4</sub>.



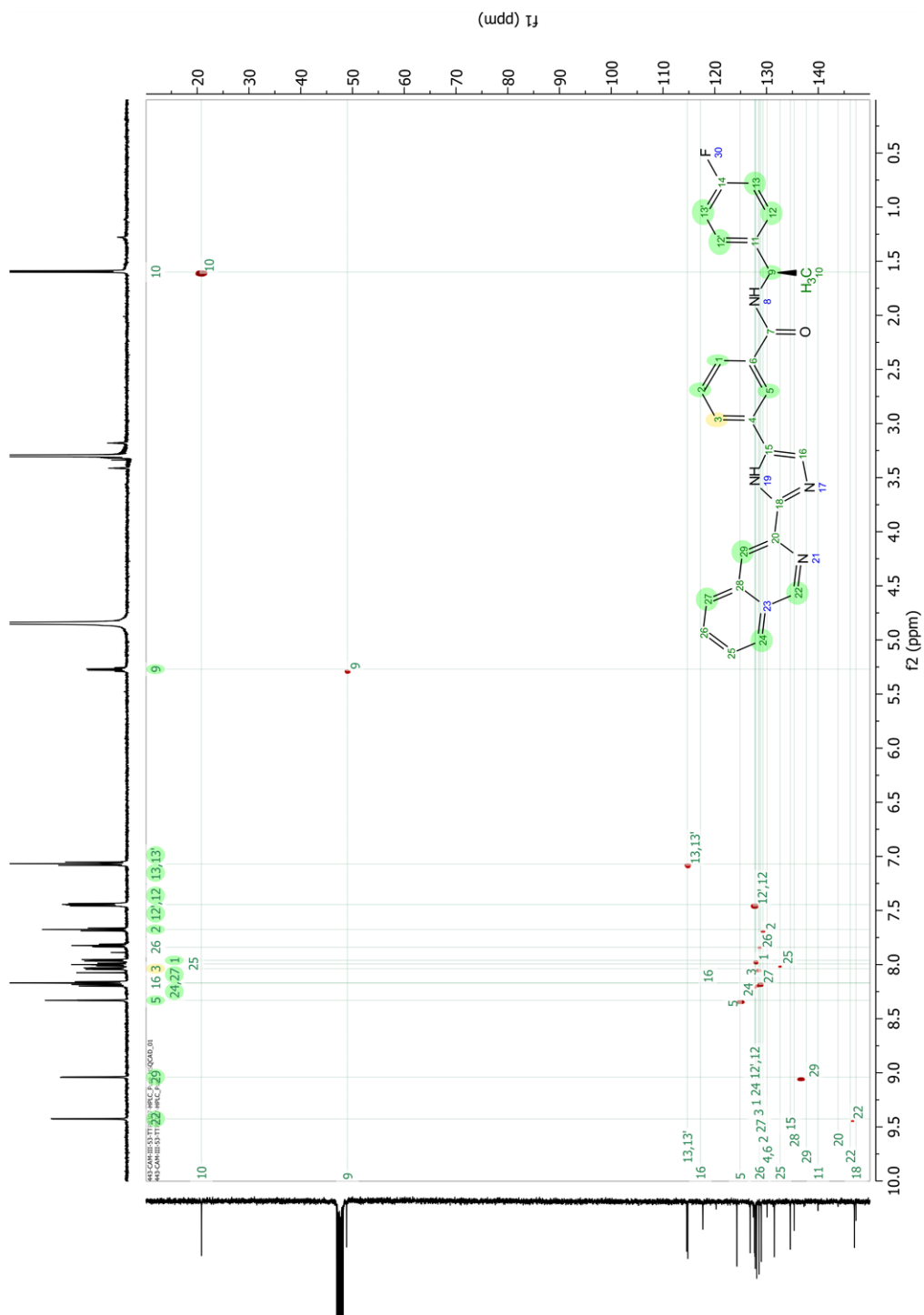
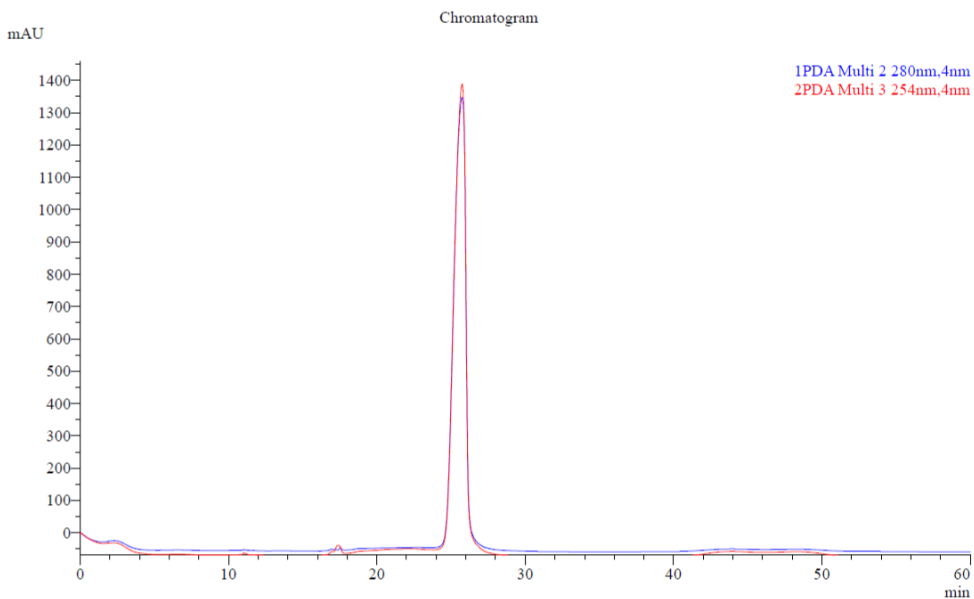


Figure 5-16. HSQC correlation of TTP (5.1) in methanol- $d_4$ .



**Figure 5-17.** Multi-Chromatogram analysis of TTP-8307 (5.1) at max absorbance 280nm (shown in blue) and 254nm (shown in red).

**Table 3. TTP (5.1),** Tabulated multi-chromatogram analysis. At 280 nm, concentration of TTP (5.1) is 98.3%. At 254 nm, concentration of TTP (5.1) is 95.8%.

Peak Table

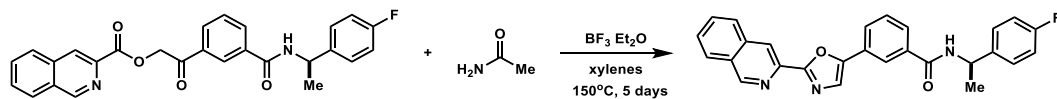
FRC Signal				
Peak#	Ret. Time	Area	Height	Conc.
Total				

PDA Ch2 280nm				
Peak#	Ret. Time	Area	Height	Conc.
1	2.288	877946	11408	1.094
2	6.293	1652	59	0.002
3	11.027	42452	2982	0.053
4	11.673	7005	499	0.009
5	13.301	5679	285	0.007
6	16.982	114538	5023	0.143
7	17.228	29067	2978	0.036
8	17.536	92803	7931	0.116
9	18.783	77174	2402	0.096
10	20.597	109585	381	0.137
11	21.931	12073	325	0.015
12	22.773	31134	816	0.039
13	25.748	78831210	1397048	98.254
Total		80232317	1432136	100.000

PDA Ch3 254nm				
Peak#	Ret. Time	Area	Height	Conc.
1	2.240	823032	10530	0.991
2	11.031	142094	8004	0.171
3	11.160	82195	5614	0.099
4	11.670	54131	2124	0.065
5	13.292	4315	205	0.005
6	17.000	210389	9872	0.253
7	17.383	690872	27340	0.832
8	21.280	422617	521	0.509
9	25.749	79634715	1448529	95.848
10	48.289	1019685	6040	1.227
Total		83084043	1518777	100.000



**(R)-N-(1-(4-fluorophenyl)ethyl)-3-(2-(isoquinolin-3-yl)oxazol-5-yl)benzamide (5.8):**

**Compound 5.8** was prepared through adaption of a previously reported protocol for use in transforming **Compound 5.7**.<sup>188</sup> To a stirring suspension of isoquinoline ester intermediate (**Compound 5.7**, 50.4 mg, 110  $\mu$ mol, 1 equiv.) in xylenes (4.4 ml, 25 mM) was added solid acetamide (36.9 mg, 624  $\mu$ mol, 5.65 equiv.) followed by a solution of  $\text{BF}_3 \cdot \text{Et}_2\text{O}$  (15  $\mu$ l, 122  $\mu$ mol, 1.1 equiv.) diluted in xylenes (400  $\mu$ l). The reaction flask was equipped with a reflux condenser and then warmed to 150°C for five days. The reaction was cooled to room temperature and then diluted in ethyl acetate (45 ml) and transferred to a separatory funnel. The reaction was washed with 1 N  $\text{HCl}_{(\text{aq})}$  (2 x 25 ml), sat.  $\text{NaHCO}_{3(\text{aq})}$  (3 x 25 ml), and DI water (2 x 25 ml). The organic layer was then washed with brine and dried over sodium sulfate. The drying agent was removed, and the solvent evaporated *in vacuo* to afford 62 mg of crude yellow/orange semisolid. The crude mixture was purified via HPLC on a Luna 5  $\mu$ m C8(2) 100Å column using a isocratic 85% methanol/0.1% formic acid water mobile phase. Isoquinoline starting material eluted at a 14.5 min retention time. The desired oxazole product eluted at Rt 20.266 and afforded 1.43 g of desired **Compound 5.8** (3.5%).

**Compound 5.8:**  $^1\text{H-NMR}$  (500 MHz, Methanol- $d_4$ )  $\delta$  9.58 (d,  $J = 2.2$  Hz, 1H), 9.05 (d,  $J = 2.2$  Hz, 1H), 8.56 (d,  $J = 6.5$  Hz, 7H), 8.40 (t,  $J = 1.8$  Hz, 1H), 8.16 – 8.12 (m, 3H), 8.11 – 8.07 (m, 1H), 7.90 (ddd,  $J = 8.5, 6.9, 1.4$  Hz, 1H), 7.86 – 7.83 (m, 1H), 7.74 (ddd,  $J = 8.1, 6.9, 1.1$  Hz, 1H), 7.59 (t,  $J = 7.7$  Hz, 1H), 7.47 (dd,  $J = 8.6, 5.4$  Hz, 2H), 7.09 (t,  $J = 8.8$  Hz, 2H), 5.29 (q,  $J = 7.1$  Hz, 1H), 1.62 (d,  $J = 7.1$  Hz, 5H). HRMS (+ESI, 180V, rt: 0.963 min): calculated  $\text{C}_{27}\text{H}_{20}\text{FN}_3\text{O}_2$  [ $\text{M}^+$ ] 438.1612 m/z, found 438.1630 m/z  $\Delta$ ppm = 4.0 ppm



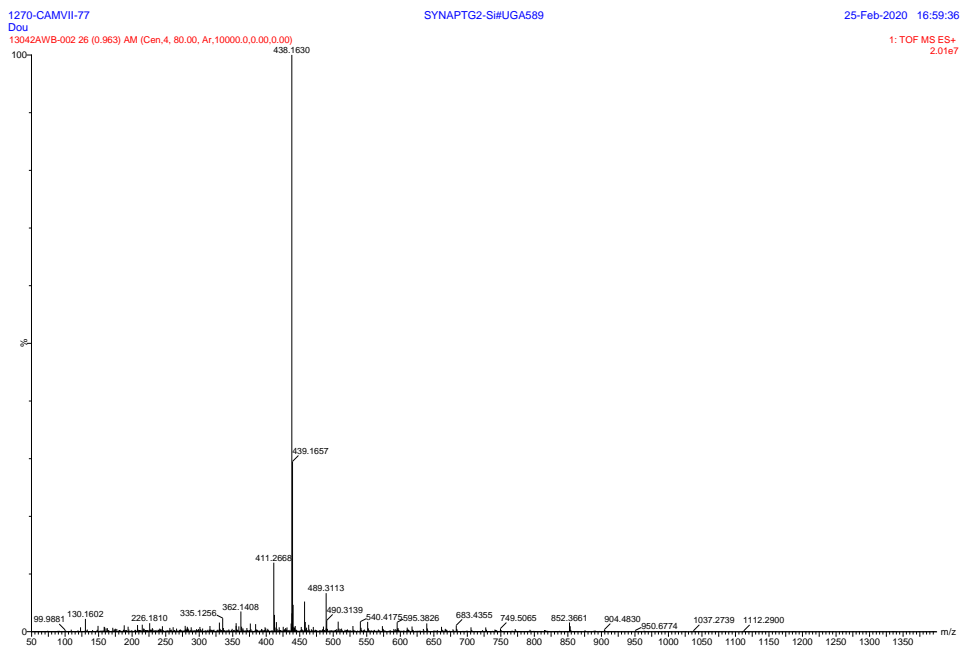


**Figure 5-19. Compound 5.8, HRMS (+ESI):** calculated  $C_{27}H_{20}FN_3O_2$  [ $M^+$ ] 438.1612 m/z, found 438.1630 m/z  $\Delta$ ppm = 4.0 ppm



## **Chapter 6: Closing remarks and future work**

## **6.1. Development of three-component approach to OSW-1-derived scaffolds**

OSW-1 has been of great interest since it was first identified as a potent antiproliferative compound and recently, the discovery of OSW-1's inhibition of RNA virus proliferation has made the compound a focus of antiviral drug development as well.<sup>1,10,11,54</sup> Nearly a dozen phenotypic structure-activity relationship studies have been conducted for OSW-1. These studies largely focused on the modification of three main structural components of the OSW-1 scaffold: the side chain, the xylosyl benzoate, and the disaccharide. Although these SAR studies provide critical insight into the biologically active structural components of OSW-1, there has yet to be a practical synthesis reported for OSW-1. The lack of a practical synthesis to OSW-1 is presumably due to the structural and synthetic complexities inherent to saponin compounds.

The work described here has largely been dedicated to the development of a simplified synthesis to generate lead compounds of therapeutic value from the OSW-1 structure. This pursuit has required developing fundamental understanding of OSW-1 interactions with OSBP and ORP4 as well as the development of synthesis methods and approaches to make accessible new OSW-1-derived scaffolds.

Our three-component synthesis approach to OSW-1-derived scaffolds is through the generation of three building blocks that can conveniently be merged into a high-atom economy structure (**Chapter 2**). The synthesis of C22-N-glycoside OSW-1 derived scaffold (**2.7**) required the synthesis of three components (steroid body, sterol side chain, and disaccharide) as well as new method development for merging these components together (**Chapter 2**). The initial approach to 22-aminosterols was through combining functionalized steroid with sterol side chain component in the form of an alkyl aldehyde



followed by a three-step oxidation/ reduction sequence (**Chapter 2:**). This synthesis was then improved upon through development of a directional aza-Prins mechanism for the direct construction of C16-C17-ene-22-aminosterol or 17-hydroxy-22-aminosterol (**Chapter 3:**). Through this developed aza-Prins reaction, 22-aminosterols are readily accessible for derivatization or as building blocks in the synthesis of other complex molecular scaffolds, such as OSW-1 (**Chapter 3:**). When applied to the three-component synthesis approach to OSW-1 derived scaffolds, this aza-Prins reduces the overall synthesis by four steps and allows C22-*N*-glycoside OSW-1-derived scaffolds to be synthesized within seven total steps from dehydroandrosterone (**Chapter 3:**).

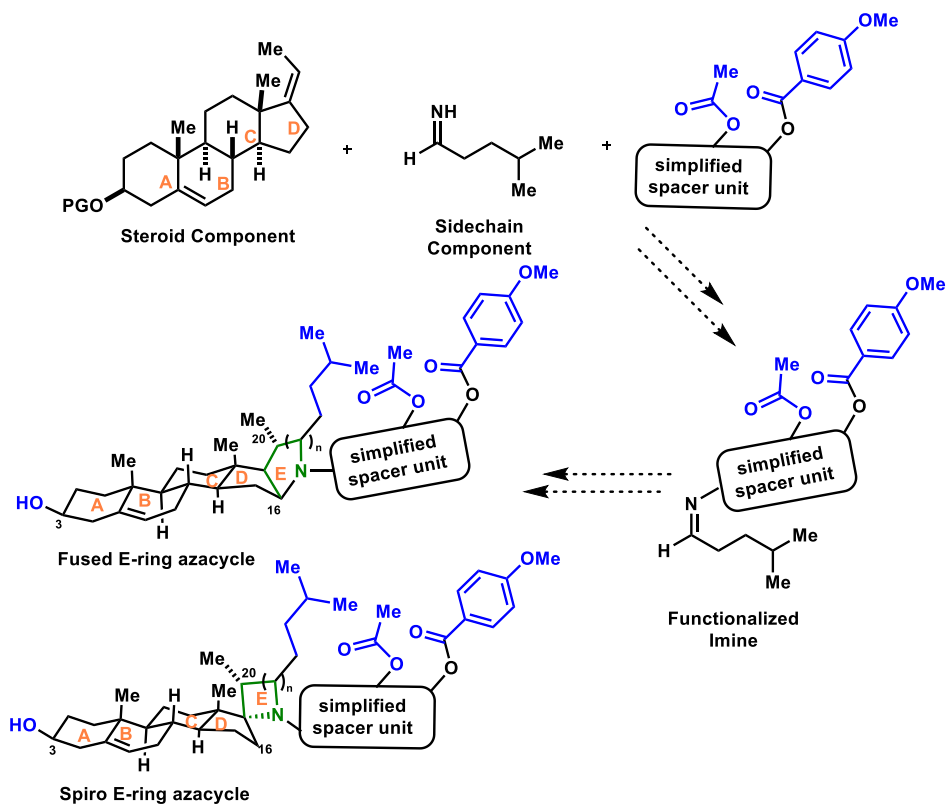
Glycosylation of aminosterols required the optimization of a new glycosylation technique using an atypical Fukuyama-Mitsunobu reaction to overcome the inert characteristics of the C22-steroid position (**Chapter 2:**). The atypical conditions of this developed Fukuyama-Mitsunobu-glycosylation reaction employed diphenyl pyridyl phosphine (Ph<sub>2</sub>PyP) and ditertmethyl azadicarboxamide (DTBAD) at ~5°C which reduced byproduct hydrazine glycoside formation and optimized steroidal *N*-glycoside production. Additionally, these atypical conditions facilitated an easy purification strategy because both the Ph<sub>2</sub>PyP and DTBAD could be washed away from the product in an acidic workup. This optimized method will facilitate future *N*-glycosylations as well as Mitsunobu reactions of inert nitrogen nucleophiles in the presence of over-reactive electrophiles. These methods and improved approaches have facilitated the development of our three-component approach to OSW-1-derived scaffolds and have already produced the first scaffold in a reduced number of synthesis steps with higher total yields.

Through the synthesis of C22-*N*-Glycoside OSW-1 derivative (**Chapter 2**;, **Section 2.2.4.4**) a fundamental understanding of the complexities inherent to steroid synthesis was gained. The three-component approach through first combining the steroid and side-chain components then merging to the disaccharide component revealed limitations of the scope and flexibility of this synthesis route. Specifically, the limited reactivity surrounding the C22-position of the elaborated sterol skeleton. The inherent rigidity of steroids limits conformational freedom of the sterol side chain and conformationally lock steroid substituents, contributing to the highly spatially congested scaffold about the C22-position. These characteristics negatively impacted the available transformations of this position and required extensive reaction development for each synthesis step.

## **6.2. Future development of three-component approach to OSW-1-derived scaffolds**

The development of the methods and approaches within this work have provided the fundamental synthesis tools necessary for further development of this three-component approach to OSW-1-derived scaffolds. The inherent limited reactivity of the elaborated sterol has guided the future development of the three-component approach. The future pathway will first combine the side-chain component and disaccharide, or disaccharide replacement spacer unit, before merging with the steroid component (**Scheme 6-1**). This new pathway to azacyclic E-ring OSW-1-derived scaffolds foregoes the inherent complexities of the sterol scaffold thereby granting access to previously inaccessible transformations. This new pathway will require further development of methods and approaches to access the functionalized imine which can be guided by the two-step synthesis approach to *N*-aryl sulfonyl alkyl imines (**Section 3.2.1**) as well as the developed Fukuyama-Mitsunobu-Glycosylation method (**Section 2.2.3**). Merging the

functionalized imines to the steroid will then build upon the developed imino-ene/aza-Prins reaction (**Sections 3.2.2 and 3.2.3**) to facilitate [2+2] and [3+2] cycloaddition reactions to produce azacyclic E-ring OSW-1-derived scaffolds.



**Scheme 6-1.** Future pathway of the three-component approach to azacyclic E-ring OSW-1-derived scaffolds.

## List of Compounds

1. Chapter 1:
  - 1.1. OSW-1
  - 1.2. Cephalostatin 1
  - 1.3. Schweinfurthen A
  - 1.4. LYZ-81
2. Chapter 2:
  - 2.1. General Protected Pregnadiene
  - 2.2. General carbonyl
  - 2.3. General C22 sterol
  - 2.4. General disaccharide
  - 2.5. General C22-glycoside
  - 2.6. C22-O-Glycoside
  - 2.7. C22-N-Glycoside
  - 2.8. E-ring-N-Glycoside
  - 2.9. C22-hydroxy cmpnd 1
  - 2.10. C22-hydroxy cmpnd 2
  - 2.11. C22-hydroxy cmpnd 3
  - 2.12. Dehydroandrosterone
  - 2.13. PMBDehydroandrosterone
  - 2.14. PMBPregnadiene
  - 2.15. 4-methyl valeric acid
  - 2.16. 4-methyl pentanol
  - 2.17. 4-methyl pentanal
  - 2.18. PMB C22-hydroxy cholesterol
  - 2.19. Disaccharide imidate
  - 2.20. BnDehydroandrosterone
  - 2.21. Cyanuric chloride
  - 2.22. TriBot
  - 2.23. TriBot-PM
  - 2.24. L-arabinose
  - 2.25. D-xylose
  - 2.26. Arb-Xyl-Disaccharide
  - 2.27. PMB-C22-keto Cholesterol
  - 2.28. PMB-C22-Oxime Cholesterol
  - 2.29. PMB C22-amino cholesterol
  - 2.30. PMB C22-DNs amino cholesterol
  - 2.31. PMB, DNs C22-N-Glycoside
  - 2.32. DNs C22-N-Glycoside
  - 2.33. C22-N-Glycoside
  - 2.34. PMB, C22-NsAmine-Cholesterol
  - 2.35. PMB, C22-NsN-Glycoside
  - 2.36. C22-NsN-Glycoside
  - 2.37. Protected disaccharide
  - 2.38. Protected C22-O-glycoside
3. Chapter 3:
  - 3.1. AcPregnadiene
  - 3.2. C22- aminosterol
  - 3.3. Spiro E-ring azasterol
  - 3.4. Wagner-Meerwein rearranged aminosterol
  - 3.5. Tosy N-pentylimine Product A
  - 3.6. Tosyl N-pentylimine Product B
  - 3.7. Nosyl N-pentylimine Product C
4. Chapter 4:
  - 4.1. OSW-1
  - 4.2. (*R*)-Pregnenolol
  - 4.3. (*S*)-Pregnenolol
  - 4.4. (*R*)-ethyl Pregnenolol
  - 4.5. (*S*)-ethyl Pregnenolol
  - 4.6. (*R*)-isobutyl Pregnenolol
  - 4.7. (*S*)-isobutyl Pregnenolol
  - 4.8. (*R*)-n-octyl-Pregnenolol
  - 4.9. (*S*)-n-octyl-Pregnenolol
  - 4.10. (*S*)-isopentyl-Pregnenolol
  - 4.11. (*S*)-hexyl-Pregnenolol
  - 4.12. (*S*)-pentyl-Pregnenolol
  - 4.13. THEV truncated
  - 4.14. 25-hydroxy Cholesterol
  - 4.15. 25-hydroxy Cholesterol (reduced)
  - 4.16. Hydroxymethylpregnadiene (2.4)
  - 4.17. 20(*R*)-hydroxy Cholesterol
  - 4.18. 20(*S*)-hydroxy Cholesterol
  - 4.19. 22(*R*)-hydroxy Cholesterol
  - 4.20. 22(*S*)-hydroxy Cholesterol
  - 4.21. 24(*R*)-hydroxyCholesterol
  - 4.22. 24(*S*)-hydroxyCholesterol
  - 4.23. 25(*R*),27-dihydroxy Cholesterol
  - 4.24. 25(*S*),27-dihydroxyCholesterol
  - 4.25. (20(*R*),22(*R*)-dihydroxy cholesterol
  - 4.26. 7 $\alpha$ ,25-dihydroxycholesterol
  - 4.27. 5 $\alpha$ -hydroxy-6-ketocholesterol
  - 4.28. 22-hydroxy-isopentyl pregnadiene
  - 4.29. 22-hydroxy-isohexyl pregnadiene
5. Chapter 5:
  - 5.1. TTP 8307
  - 5.2. 3-acetylbenzoic acid
  - 5.3. 4-fluoro methyl benzyl amine

- 5.4. diaryl amide**
- 5.5. diaryl bromo amide**
- 5.6. isoquinoline-3-carboxylic acid**
- 5.7. oxoethyl ketone isoquinolate**

- 5.8. Oxazole TTP Derivative**
- 5.9. Imine & imidate intermediate**
- 5.10. Amide intermediate**
- 5.11. Activated ester intermediate**

## References

- (1) Burgett, A. W. G.; Poulsen, T. B.; Wangkanont, K.; Anderson, D. R.; Kikuchi, C.; Shimada, K.; Okubo, S.; Fortner, K. C.; Mimaki, Y.; Kuroda, M.; et al. Natural Products Reveal Cancer Cell Dependence on Oxysterol- Binding Proteins. *Nat. Chem. Biol.* **2011**, *7* (9), 639–647. <https://doi.org/10.1038/nchembio.625>.Natural.
- (2) Shoemaker, R. H. The NCI60 Human Tumour Cell Line Anticancer Drug Screen. *Nat. Rev. Cancer* **2006**, *6* (10), 813–823. <https://doi.org/10.1038/nrc1951>.
- (3) Rabow, A. a.; Shoemaker, R. H.; Sausville, E. a.; Covell, D. G. Mining the National Cancer Institute’s Tumor-Screening Database: Identification of Compounds with Similar Cellular Activities. *J. Med. Chem.* **2002**, *45* (4), 818–840. <https://doi.org/10.1021/jm010385b>.
- (4) Burgett, A. W. G.; Poulsen, T. B.; Wangkanont, K.; Anderson, D. R.; Kikuchi, C.; Shimada, K.; Okubo, S.; Fortner, K. C.; Mimaki, Y.; Kuroda, M.; et al. Natural Products Reveal Cancer Cell Dependence on Oxysterol-Binding Proteins. *Nat. Chem. Biol.* **2011**, *7* (9), 639–647. <https://doi.org/10.1038/nchembio.625>.
- (5) Mesmin, B.; Bigay, J.; Polidori, J.; Jamecna, D.; Lacas-Gervais, S.; Antonny, B.; Lacas-Gervais, S.; Antonny, B. Sterol Transfer, PI4P Consumption, and Control of Membrane Lipid Order by Endogenous OSBP. *EMBO J.* **2017**, *36* (21), e201796687. <https://doi.org/10.15252/emboj.201796687>.
- (6) Amako, Y.; Sarkeshik, A.; Hotta, H.; Yates, J.; Siddiqui, A. Role of Oxysterol Binding Protein in Hepatitis C Virus Infection. *J. Virol.* **2009**, *83* (18), 9237–9246. <https://doi.org/10.1128/JVI.00958-09>.
- (7) Bao, X.; Zheng, W.; Sugi, N.; Agarwala, K.; Xu, Q.; Wang, Z.; Tendyke, K.; Lee, W.; Parent, L.; Li, W.; et al. Small Molecule Schweinfurthins Selectively Inhibit Cancer Cell Proliferation and MTOR/AKT Signaling by Interfering with Trans-Golgi-Network Trafficking. *Cancer Biol. Ther.* **2015**, *16* (4), 589–601. <https://doi.org/10.1080/15384047.2015.1019184>.
- (8) Strating, J. R. P. M.; Van Der Linden, L.; Albuлесcu, L.; Bigay, J.; Arita, M.; Delang, L.; Leyssen, P.; Van Der Schaar, H. M.; Lanke, K. H. W.; Thibaut, H. J.; et al. Itraconazole Inhibits Enterovirus Replication by Targeting the Oxysterol-Binding Protein. *Cell Rep* **2015**, *10* (4), 600–615. <https://doi.org/10.1016/j.celrep.2014.12.054>.

- (9) Albuлесcu, L.; Strating, J. R. P. M.; Thibaut, H. J.; van der Linden, L.; Shair, M. D.; Neyts, J.; van Kuppeveld, F. J. M. Broad-Range Inhibition of Enterovirus Replication by OSW-1, a Natural Compound Targeting OSBP. *Antiviral Res.* **2015**, *117*, 110–114. <https://doi.org/10.1016/J.ANTIVIRAL.2015.02.013>.
- (10) Roberts, B. L.; Severance, Z. C.; Bensen, R. C.; Le, A. T.; Kothapalli, N. R.; Nuñez, J. I.; Ma, H.; Wu, S.; Standke, S. J.; Yang, Z.; et al. Transient Compound Treatment Induces a Multigenerational Reduction of Oxysterol-Binding Protein (OSBP) Levels and Prophylactic Antiviral Activity. *ACS Chem. Biol.* **2019**, *14* (2), 276–287. <https://doi.org/10.1021/acschembio.8b00984>.
- (11) Roberts, B. L. B. L.; Severance, Z. C.; Bensen, R. C. R. C.; Le-McClain, A. T. A. T.; Malinky, C. A. C. A.; Mettenbrink, E. M. E. M.; Nuñez, J. I. J. I.; Reddig, W. J. W. J.; Blewett, E. L. E. L.; Burgett, A. W. G. A. W. G. Differing Activities of Oxysterol-Binding Protein (OSBP) Targeting Anti-Viral Compounds. *Antiviral Res.* **2019**, *170* (April), 104548. <https://doi.org/10.1016/j.antiviral.2019.104548>.
- (12) Weber-Boyvat, M.; Zhong, W.; Yan, D.; Olkkonen, V. M. Oxysterol-Binding Proteins: Functions in Cell Regulation beyond Lipid Metabolism. *Biochem. Pharmacol.* **2013**, *86* (1), 89–95. <https://doi.org/10.1016/j.bcp.2013.02.016>.
- (13) Kentala, H.; Weber-Boyvat, M.; Olkkonen, V. M. OSBP-Related Protein Family: Mediators of Lipid Transport and Signaling at Membrane Contact Sites. In *International Review of Cell and Molecular Biology*; 2016; Vol. 321. <https://doi.org/10.1016/bs.ircmb.2015.09.006>.
- (14) Pietrangelo, A.; Ridgway, N. D. Bridging the Molecular and Biological Functions of the Oxysterol-Binding Protein Family. *Cell. Mol. Life Sci.* **2018**, *75* (17), 3079–3098. <https://doi.org/10.1007/s00018-018-2795-y>.
- (15) Olkkonen, V. M.; Li, S. Oxysterol-Binding Proteins: Sterol and Phosphoinositide Sensors Coordinating Transport, Signaling and Metabolism. *Prog. Lipid Res.* **2013**, *52* (4), 529–538. <https://doi.org/10.1016/j.plipres.2013.06.004>.
- (16) Im, Y. J.; Raychaudhuri, S.; Prinz, W. A.; Hurley, J. H. Structural Mechanism for Sterol Sensing and Transport by OSBP-Related Proteins. *Nature* **2005**, *437* (7055), 154–158.

<https://doi.org/10.1038/nature03923>.

- (17) Maeda, K.; Anand, K.; Chiapparino, A.; Kumar, A.; Poletto, M.; Kaksonen, M.; Gavin, A.-C. Interactome Map Uncovers Phosphatidylserine Transport by Oxysterol-Binding Proteins. *Nature* **2013**, *501* (7466), 257–261. <https://doi.org/10.1038/nature12430>.
- (18) Raychaudhuri, S.; Im, Y. J.; Hurley, J. H.; Prinz, W. a. Nonvesicular Sterol Movement from Plasma Membrane to ER Requires Oxysterol-Binding Protein–Related Proteins and Phosphoinositides. *J. Cell Biol.* **2006**, *173* (1), 107–119. <https://doi.org/10.1083/jcb.200510084>.
- (19) Tong, J.; Yang, H. H.; Yang, H. H.; Eom, S. H.; Im, Y. J. Article Structure of Osh3 Reveals a Conserved Mode of Phosphoinositide Binding in Oxysterol-Binding Proteins. *Struct. Des.* **2013**, *21* (7), 1203–1213. <https://doi.org/10.1016/j.str.2013.05.007>.
- (20) Wang, H.; Ma, Q.; Qi, Y.; Dong, J.; Du, X.; Rae, J.; Wang, J.; Wu, W. F.; Brown, A. J.; Parton, R. G.; et al. ORP2 Delivers Cholesterol to the Plasma Membrane in Exchange for Phosphatidylinositol 4, 5-Bisphosphate (PI(4,5)P<sub>2</sub>). *Mol. Cell* **2019**, *73* (3), 458-473.e7. <https://doi.org/10.1016/j.molcel.2018.11.014>.
- (21) Dong, J.; Du, X.; Wang, H.; Wang, J.; Lu, C.; Chen, X.; Zhu, Z.; Luo, Z.; Yu, L.; Brown, A. J.; et al. Allosteric Enhancement of ORP1-Mediated Cholesterol Transport by PI(4,5)P<sub>2</sub>/PI(3,4)P<sub>2</sub>. *Nat. Commun.* **2019**, *10* (1), 829. <https://doi.org/10.1038/s41467-019-08791-0>.
- (22) Sakurai, K.; Hiraizumi, M.; Isogai, N.; Komatsu, R.; Shibata, T.; Ohta, Y. Synthesis of a Fluorescent Photoaffinity Probe of OSW-1 by Site-Selective Acylation of an Inactive Congener and Biological Evaluation. *Chem. Commun.* **2017**, *53* (3), 517–520. <https://doi.org/10.1039/C6CC08955K>.
- (23) Sakurai, K.; Fukumoto, T.; Noguchi, K.; Sato, N.; Asaka, H.; Moriyama, N.; Yohda, M. Three-Dimensional Structures of OSW-1 and Its Congener. *Org. Lett.* **2010**, *12* (24), 5732–5735. <https://doi.org/10.1021/ol1025519>.
- (24) Raychaudhuri, S.; Prinz, W. A. The Diverse Functions of Oxysterol-Binding Proteins. *Annu. Rev. Cell Dev. Biol.* **2010**, *26* (1), 157–177. <https://doi.org/10.1146/annurev.cellbio.042308.113334>.
- (25) Goto, A.; Charman, M.; Ridgway, N. D. Oxysterol-Binding Protein Activation at Endoplasmic Reticulum-Golgi Contact Sites



- Reorganizes Phosphatidylinositol 4-Phosphate Pools. *J. Biol. Chem.* **2016**, *291* (3), 1336–1347. <https://doi.org/10.1074/jbc.M115.682997>.
- (26) Mesmin, B.; Bigay, J.; Moser Von Filseck, J.; Lacas-Gervais, S.; Drin, G.; Antonny, B.; Moser von Filseck, J.; Lacas-Gervais, S.; Drin, G.; Antonny, B. A Four-Step Cycle Driven by PI(4)P Hydrolysis Directs Sterol/PI(4)P Exchange by the ER-Golgi Tether OSBP. *Cell* **2013**, *155* (4), 830–843. <https://doi.org/10.1016/j.cell.2013.09.056>.
- (27) Antonny, B.; Bigay, J.; Mesmin, B. The Oxysterol-Binding Protein Cycle: Burning Off PI(4)P to Transport Cholesterol. *Annu. Rev. Biochem.* **2018**, *87* (1). <https://doi.org/10.1146/annurev-biochem-061516-044924>.
- (28) Wyles, J. P.; Perry, R. J.; Ridgway, N. D. Characterization of the Sterol-Binding Domain of Oxysterol-Binding Protein (OSBP)-Related Protein 4 Reveals a Novel Role in Vimentin Organization. *Exp. Cell Res.* **2007**, *313* (7), 1426–1437. <https://doi.org/10.1016/j.yexcr.2007.01.018>.
- (29) Zhong, W.; Pan, G.; Wang, L.; Li, S.; Ou, J.; Xu, M.; Li, J.; Zhu, B.; Cao, X.; Ma, H.; et al. ORP4L Facilitates Macrophage Survival via G-Protein-Coupled Signaling. *Circ. Res.* **2016**, *119* (12), 1296–1312. <https://doi.org/10.1161/CIRCRESAHA.116.309603>.
- (30) Zhong, W.; Xu, M.; Li, C.; Zhu, B.; Cao, X.; Li, D.; Chen, H.; Hu, C.; Li, R.; Luo, C.; et al. ORP4L Extracts and Presents PIP 2 from Plasma Membrane for PLC $\beta$ 3 Catalysis: Targeting It Eradicates Leukemia Stem Cells. *Cell Rep.* **2019**, *26* (8), 2166-2177.e9. <https://doi.org/10.1016/j.celrep.2019.01.082>.
- (31) Pan, G.; Cao, X.; Liu, B.; Li, C.; Li, D.; Zheng, J.; Lai, C.; Olkkonen, V. M.; Zhong, W.; Yan, D. OSBP-Related Protein 4L Promotes Phospholipase C $\beta$ 3 Translocation from the Nucleus to the Plasma Membrane in Jurkat T-Cells. *J. Biol. Chem.* **2018**, *293* (45), 17430–17441. <https://doi.org/10.1074/jbc.RA118.005437>.
- (32) Fournier, M. V; Guimarães da Costa, F.; Paschoal, M. E.; Ronco, L. V; Carvalho, M. G.; Pardee, a B.; Giumaraes, F. C. Identification of a Gene Encoding a Human Oxysterol-Binding Protein-Homologue: A Potential General Molecular Marker for Blood Dissemination of Solid Tumors. *Cancer Res.* **1999**, *59* (15), 3748–3753.
- (33) Henriques Silva, N.; Vasconcellos Fournier, M.; Pimenta, G.;

- Pulcheri, W. A.; Spector, N.; da Costa Carvalho, M. da G. HLM/OSBP2 Is Expressed in Chronic Myeloid Leukemia. *Int. J. Mol. Med.* **2003**, *12* (4), 663–666.  
<https://doi.org/10.3892/ijmm.12.4.663>.
- (34) Charman, M.; Colbourne, T. R.; Pietrangelo, A.; Kreplak, L.; Ridgway, N. D. Oxysterol-Binding Protein (OSBP)-Related Protein 4 (ORP4) Is Essential for Cell Proliferation and Survival. *J. Biol. Chem.* **2014**, *289* (22), 15705–15717.  
<https://doi.org/10.1074/jbc.M114.571216>.
- (35) Zhong, W.; Yi, Q.; Xu, B.; Li, S.; Wang, T.; Liu, F.; Zhu, B.; Hoffmann, P. R.; Ji, G.; Lei, P.; et al. ORP4L Is Essential for T-Cell Acute Lymphoblastic Leukemia Cell Survival. *Nat. Commun.* **2016**, *7* (1), 12702. <https://doi.org/10.1038/ncomms12702>.
- (36) Zheng, D.; Zhou, L.; Guan, Y.; Chen, X.; Zhou, W.; Chen, X.; Lei, P. Synthesis of Cholestane Glycosides Bearing OSW-1 Disaccharide or Its 1→4-Linked Analogue and Their Antitumor Activities. *Bioorg. Med. Chem. Lett.* **2010**, *20* (18), 5439–5442.  
<https://doi.org/10.1016/J.BMCL.2010.07.085>.
- (37) Baggen, J.; Thibaut, H. J.; Strating, J. R. P. M.; Van Kuppeveld, F. J. M. The Life Cycle of Non-Polio Enteroviruses and How to Target It. *Nat. Rev. Microbiol.* **2018**. <https://doi.org/10.1038/s41579-018-0005-4>.
- (38) Tapparel, C.; Siegrist, F.; Petty, T. J.; Kaiser, L. Picornavirus and Enterovirus Diversity with Associated Human Diseases. *Infect. Genet. Evol.* **2013**, *14*, 282–293.  
<https://doi.org/10.1016/J.MEEGID.2012.10.016>.
- (39) Lugo, D.; Krogstad, P.; Opin, C.; Author, P. Enteroviruses in the Early 21 St Century: New Manifestations and Challenges. *Curr Opin Pediatr* **2016**, *28* (1), 107–113.  
<https://doi.org/10.1097/MOP.0000000000000303>.
- (40) Abzug, M. J. The Enteroviruses: Problems in Need of Treatments. *J. Infect.* **2014**, *68*, S108–S114.  
<https://doi.org/10.1016/J.JINF.2013.09.020>.
- (41) Ledford, R. M.; Collett, M. S.; Pevear, D. C. Insights into the Genetic Basis for Natural Phenotypic Resistance of Human Rhinoviruses to Pleconaril. *Antiviral Res.* **2005**, *68* (3), 135–138.  
<https://doi.org/10.1016/j.antiviral.2005.08.003>.

- (42) Takano, T.; Akiyama, M.; Doki, T.; Hohdatsu, T. Antiviral Activity of Itraconazole against Type I Feline Coronavirus Infection. *Vet. Res.* **2019**, *50* (1), 1–6. <https://doi.org/10.1186/s13567-019-0625-3>.
- (43) Amako, Y.; Syed, G. H.; Siddiqui, A. Protein Kinase D Negatively Regulates Hepatitis C Virus Secretion through Phosphorylation of Oxysterol-Binding Protein and Ceramide Transfer Protein. *J. Biol. Chem.* **2011**, *286* (13), 11265–11274. <https://doi.org/10.1074/jbc.M110.182097>.
- (44) Dorobantu, C. M.; Albulescu, L.; Lyoo, H.; van Kampen, M.; De Francesco, R.; Lohmann, V.; Harak, C.; van der Schaar, H. M.; Strating, J. R. P. M.; Gorbalenya, A. E.; et al. Mutations in Encephalomyocarditis Virus 3A Protein Uncouple the Dependency of Genome Replication on Host Factors Phosphatidylinositol 4-Kinase III $\alpha$  and Oxysterol-Binding Protein. *mSphere* **2016**, *1* (3), 1–17. <https://doi.org/10.1128/msphere.00068-16>.
- (45) Meutiawati, F.; Bezemer, B.; Strating, J. R. P. M.; Overheul, G. J.; Žusinaite, E.; van Kuppeveld, F. J. M.; van Cleef, K. W. R.; van Rij, R. P. Posaconazole Inhibits Dengue Virus Replication by Targeting Oxysterol-Binding Protein. *Antiviral Res.* **2018**, *157* (February), 68–79. <https://doi.org/10.1016/j.antiviral.2018.06.017>.
- (46) Dorobantu, C. M.; Albulescu, L.; Harak, C.; Feng, Q.; van Kampen, M.; Strating, J. R. P. M.; Gorbalenya, A. E.; Lohmann, V.; van der Schaar, H. M.; van Kuppeveld, F. J. M. Modulation of the Host Lipid Landscape to Promote RNA Virus Replication: The Picornavirus Encephalomyocarditis Virus Converges on the Pathway Used by Hepatitis C Virus. *PLOS Pathog.* **2015**, *11* (9), e1005185. <https://doi.org/10.1371/journal.ppat.1005185>.
- (47) Nchoutmboube, J.; Ford-Siltz, L. A.; Belov, G. A. Enterovirus Replication: Go with the (Counter)Flow. *Trends Microbiol.* **2015**, *23* (4), 183–184. <https://doi.org/10.1016/J.TIM.2015.02.008>.
- (48) Arita, M. Phosphatidylinositol-4 Kinase III Beta and Oxysterol-Binding Protein Accumulate Unesterified Cholesterol on Poliovirus-Induced Membrane Structure. *Microbiol. Immunol.* **2014**, *58* (4), 239–256. <https://doi.org/10.1111/1348-0421.12144>.
- (49) Mesmin, B.; Kovacs, D.; D'Angelo, G. Lipid Exchange and Signaling at ER–Golgi Contact Sites. *Curr. Opin. Cell Biol.* **2019**, *57*, 8–15. <https://doi.org/10.1016/j.ceb.2018.10.002>.

- (50) Albulescu, L.; Bigay, J.; Biswas, B.; Weber-Boyvat, M.; Dorobantu, C. M.; Delang, L.; van der Schaar, H. M.; Jung, Y. S.; Neyts, J.; Olkkonen, V. M.; et al. Uncovering Oxysterol-Binding Protein (OSBP) as a Target of the Anti-Enteroviral Compound TTP-8307. *Antiviral Res.* **2017**, *140*, 37–44. <https://doi.org/10.1016/j.antiviral.2017.01.008>.
- (51) Arita, M.; Kojima, H.; Nagano, T.; Okabe, T.; Wakita, T.; Shimizu, H. Oxysterol-Binding Protein Family I Is the Target of Minor Enviroxime-Like Compounds. *J. Virol.* **2013**, *87* (8), 4252–4260. <https://doi.org/10.1128/JVI.03546-12>.
- (52) Shim, A.; Song, J.-H.; Kwon, B.-E.; Lee, J.-J.; Ahn, J.-H.; Kim, Y.-J.; Rhee, K.-J.; Chang, S.-Y.; Cha, Y.; Lee, Y.-S.; et al. Therapeutic and Prophylactic Activity of Itraconazole against Human Rhinovirus Infection in a Murine Model. *Sci. Rep.* **2016**, *6*, 23110. <https://doi.org/10.1038/srep23110>.
- (53) Zhou, Y.; Garcia-Prieto, C.; Carney, D. A.; Xu, R. hua; Pelicano, H.; Kang, Y.; Yu, W.; Lou, C.; Kondo, S.; Liu, J.; et al. OSW-1: A Natural Compound with Potent Anticancer Activity and a Novel Mechanism of Action. *J. Natl. Cancer Inst.* **2005**, *97* (23), 1781–1785. <https://doi.org/10.1093/jnci/dji404>.
- (54) Science, E.; Britain, G.; Mimaki, Y.; Kuroda, M.; Kameyama, A.; Sashida, Y.; Hirano, T.; Oka, K.; Mafkawa, R.; Wada, T.; et al. Cholestane Glycosides with Potent Cytostatic Activities on Various Tumor Cells from *Ornithogalum Saundersiae* Bulbs. *Bioorg. Med. Chem. Lett.* **1997**, *7* (5), 633–636.
- (55) Kubo, S.; Mimaki, Y.; Terao, M.; Sashida, Y. Acylated Cholestane Glycosides from the Bulbs of *Ornithogalum Saundersiae*. *Phytochemistry* **1992**, *31* (11), 3969–3973.
- (56) Sun, L.; Wang, R.; Wang, X.; Dang, Y.; Li, W.; Yu, B. Synthesis and Antiproliferative Activities of OSW-1 Analogues Bearing 2-Acylamino-Xylose Residues. *Org. Chem. Front.* **2019**, *6* (14), 2385–2391. <https://doi.org/10.1039/C9QO00462A>.
- (57) Deng, S.; Yu, B.; Lou, Y.; Hui, Y. First Total Synthesis of an Exceptionally Potent Antitumor Saponin, OSW-1. *J. Org. Chem.* **1999**, *64* (1), 202–208. <https://doi.org/10.1021/jo981685c>.
- (58) Wojtkielewicz, A.; Długosz, M.; Maj, J.; Morzycki, J. W.; Nowakowski, M.; Renkiewicz, J.; Strnad, M.; Swaczynová, J.;

- Wilczewska, A. Z.; Wójcik, J. New Analogues of the Potent Cytotoxic Saponin OSW-1. *J. Med. Chem.* **2007**, *50* (15), 3667–3673. <https://doi.org/10.1021/jm0613572>.
- (59) Morzycki, J. W.; Wojtkielewicz, A.; Wołczyński, S. Synthesis of Analogues of a Potent Antitumor Saponin OSW-1. *Bioorg. Med. Chem. Lett.* **2004**, *14* (12), 3323–3326. <https://doi.org/10.1016/j.bmcl.2004.03.102>.
- (60) Deng, L.; Wu, H.; Yu, B.; Jiang, M.; Wu, J. Synthesis of OSW-1 Analogs with Modified Side Chains and Their Antitumor Activities. *Bioorganic Med. Chem. Lett.* **2004**, *14* (11), 2781–2785. <https://doi.org/10.1016/j.bmcl.2004.03.081>.
- (61) Morzycki, J. W.; Wojtkielewicz, A. Synthesis of a Cholestane Glycoside OSW-1 with Potent Cytostatic Activity. *Carbohydr. Res.* **2002**, *337* (14), 1269–1274. [https://doi.org/10.1016/S0008-6215\(02\)00126-X](https://doi.org/10.1016/S0008-6215(02)00126-X).
- (62) Shi, B.; Wu, H.; Yu, B.; Wu, J. 23-Oxa-Analogues of OSW-1: Efficient Synthesis and Extremely Potent Antitumor Activity. *Angew. Chemie - Int. Ed.* **2004**, *43* (33), 4324–4327. <https://doi.org/10.1002/anie.200454237>.
- (63) Yu, W. S.; Jin, Z. D. Total Synthesis of the Anticancer Natural Product OSW-1. *J. Am. Chem. Soc.* **2002**, *124* (3), 6576–6583. [https://doi.org/Doi 10.1021/Ja012119t](https://doi.org/Doi%2010.1021/Ja012119t).
- (64) Shi, B.; Tang, P.; Hu, X.; Liu, J. O.; Yu, B. OSW Saponins: Facile Synthesis toward a New Type of Structures with Potent Antitumor Activities. *J. Org. Chem.* **2005**, *70* (25), 10354–10367. <https://doi.org/10.1021/jo051536b>.
- (65) Xu, Q. H.; Peng, X. W.; Tian, W. S. A New Strategy for Synthesizing the Steroids with Side Chains from Steroidal Sapogenins: Synthesis of the Aglycone of OSW-1 by Using the Intact Skeleton of Diosgenin. *Tetrahedron Lett.* **2003**, *44* (52), 9375–9377. <https://doi.org/10.1016/j.tetlet.2003.09.227>.
- (66) Lapitskaya, M. A.; Vasiljeva, L. L.; Pivnitsky, K. K. Practical Synthesis of 16,22-Diketocholesterol Acetate, a Precursor of Anticancer Saponin OSW-1, from Diosgenin. *Mendeleev Commun.* **2010**, *20* (6), 318–320. <https://doi.org/10.1016/j.mencom.2010.11.005>.
- (67) Zheng, D.; Guan, Y.; Chen, X.; Xu, Y.; Chen, X.; Lei, P. Synthesis of

- Cholestane Saponins as Mimics of OSW-1 and Their Cytotoxic Activities. *Bioorganic Med. Chem. Lett.* **2011**, *21* (11), 3257–3260. <https://doi.org/10.1016/j.bmcl.2011.04.030>.
- (68) Maj, J.; Morzycki, J. W.; Rárová, L.; OklešťKová, J.; Strnad, M.; Wojtkielewicz, A. Synthesis and Biological Activity of 22-Deoxo-23-Oxa Analogues of Saponin OSW-1. *J. Med. Chem.* **2011**, *54* (9), 3298–3305. <https://doi.org/10.1021/jm101648h>.
- (69) Tang, Y.; Li, N.; Duan, J. A.; Tao, W. Structure, Bioactivity, and Chemical Synthesis of OSW-1 and Other Steroidal Glycosides in the Genus *Ornithogalum*. *Chem. Rev.* **2013**, *113* (7), 5480–5514. <https://doi.org/10.1021/cr300072s>.
- (70) Komatsu, R.; Sakurai, K. Development of Chemical Probes for Functional Analysis of Anticancer Saponin OSW-1. *Chem. Rec.* **2019**, 1–9. <https://doi.org/10.1002/tcr.201900042>.
- (71) Ma, X.; Yu, B.; Hui, Y.; Miao, Z.; Ding, J. Synthesis of Steroidal Glycosides Bearing the Disaccharide Moiety of OSW-1 and Their Antitumor Activities. *Carbohydr. Res.* **2001**, *334* (2), 159–164. [https://doi.org/10.1016/S0008-6215\(01\)00171-9](https://doi.org/10.1016/S0008-6215(01)00171-9).
- (72) Tang, P.; Mamdani, F.; Hu, X.; Liu, J. O.; Yu, B. Synthesis of OSW Saponin Analogs with Modified Sugar Residues and Their Antiproliferative Activities. *Bioorganic Med. Chem. Lett.* **2007**, *17* (4), 1003–1007. <https://doi.org/10.1016/j.bmcl.2006.11.032>.
- (73) Guan, Y.-Y.; Song, C.; Lei, P.-S. Synthesis of Three OSW-1 Analogs with Maltose Side Chains Bearing Different Protection Groups. *J. Asian Nat. Prod. Res.* **2014**, *16* (1), 43–52. <https://doi.org/10.1080/10286020.2013.863185>.
- (74) Liu, C.; Wang, A. peng; Jin, L.; Guo, Y.; Li, Y.; Zhao, Z.; Lei, P. Synthesis, Conformational Analysis and SAR Research of OSW-1 Analogues. *Tetrahedron* **2016**, *72* (27–28), 4091–4102. <https://doi.org/10.1016/j.tet.2016.05.049>.
- (75) Sakurai, K.; Takeshita, T.; Hiraizumi, M.; Yamada, R. Synthesis of OSW-1 Derivatives by Site-Selective Acylation and Their Biological Evaluation. *Org. Lett.* **2014**, *16* (24), 6318–6321. <https://doi.org/10.1021/ol503044j>.
- (76) Yamada, R.; Takeshita, T.; Hiraizumi, M.; Shinohe, D.; Ohta, Y.; Sakurai, K. Fluorescent Analog of OSW-1 and Its Cellular Localization. *Bioorganic Med. Chem. Lett.* **2014**, *24* (7), 1808–1811.

<https://doi.org/10.1016/j.bmcl.2014.02.009>.

- (77) Hiraizumi, M.; Komatsu, R.; Shibata, T.; Ohta, Y.; Sakurai, K. Dissecting the Structural Basis for the Intracellular Delivery of OSW-1 by Fluorescent Probes. *Org. Biomol. Chem.* **2017**, *15* (17), 3568–3570. <https://doi.org/10.1039/c7ob00486a>.
- (78) Uhle, F. C.; Sallmann, F. The Synthesis and Transformations of a Steroid Pyrroline Derivative. *J. Am. Chem. Soc.* **1960**, *82* (5), 1190–1199. <https://doi.org/10.1021/ja01490a041>.
- (79) Sheehan, J. C.; Young, R. L.; Cruickshank, P. A. C(16)-C(18) Rearrangements of Steroid Alkaloids. *J. Am. Chem. Soc.* **1960**, *82* (23), 6147–6153. <https://doi.org/10.1021/ja01508a044>.
- (80) Mueller, G. P.; Jiu, J. The Synthesis of Steroid Ring-E Pyrroles and Pyrrolidines. *J. Org. Chem.* **1961**, *26* (5), 1611–1614. <https://doi.org/10.1021/jo01064a074>.
- (81) Chung, S. K.; Ryoo, C. H.; Yang, H. W.; Shim, J. Y.; Kang, M. G.; Lee, K. W.; King, H. II. Synthesis and Bioactivities of Steroid Derivatives as Antifungal Agents. *Tetrahedron* **1998**, *54* (52), 15899–15914. [https://doi.org/10.1016/S0040-4020\(98\)01000-X](https://doi.org/10.1016/S0040-4020(98)01000-X).
- (82) Renard, D.; Perruchon, J.; Giera, M.; Müller, J.; Bracher, F. Side Chain Azasteroids and Thiasteroids as Sterol Methyltransferase Inhibitors in Ergosterol Biosynthesis. *Bioorganic Med. Chem.* **2009**, *17* (23), 8123–8137. <https://doi.org/10.1016/j.bmc.2009.09.037>.
- (83) Shingate, B. B.; Hazra, B. G. A Concise Account of Various Approaches for Stereoselective Construction of the C-20(H) Stereogenic Center in Steroid Side Chain. *Chem. Rev.* **2014**, *114* (12), 6349–6382. <https://doi.org/10.1021/cr4004083>.
- (84) Le, A. Design and Synthesis of OSW-1 Analogs and Other Bioactive Small Molecules for Potential Therapeutic Applications. **2018**, 300.
- (85) Morzycki, J. W.; Wojtkielewicz, A. Synthesis of a Highly Potent Antitumor Saponin OSW-1 and Its Analogues. *Phytochem. Rev.* **2005**, *4* (2–3), 259–277. <https://doi.org/10.1007/s11101-005-1233-6>.
- (86) Minato, D.; Li, B.; Zhou, D.; Shigeta, Y.; Toyooka, N.; Sakurai, H.; Sugimoto, K.; Nemoto, H.; Matsuya, Y. Synthesis and Antitumor Activity of Des-AB Analogue of Steroidal Saponin OSW-1. *Tetrahedron* **2013**, *69* (37), 8019–8024. <https://doi.org/10.1016/j.tet.2013.06.105>.

- (87) Morzycki, J. W.; Gryszkiewicz, A.; Ābska, I. J. Neighboring Group Participation in Epoxide Ring Cleavage in Reactions of Some 16a,17a-Oxidosteroids with Lithium Hydroperoxide. *Tetrahedron* **2001**, No. 57, 2185–2193.
- (88) Tsubuki, M.; Matsuo, S.; Honda, T. A New Synthesis of Potent Antitumor Saponin OSW-1 via Wittig Rearrangement. *Tetrahedron Lett.* **2008**, 49 (2), 229–232.  
<https://doi.org/10.1016/j.tetlet.2007.11.087>.
- (89) Xue, J.; Liu, P.; Pan, Y.; Guo, Z.; State, W.; Uni, V.; Cass, A. V. A Total Synthesis of OSW-1. *J. Org. Chem.* **2008**, 2007 (2), 157–161.  
<https://doi.org/10.1021/jo7018812>.
- (90) Fukaya, K.; Urabe, D.; Hiraizumi, M.; Noguchi, K.; Matsumoto, T.; Sakurai, K. Computational and Experimental Analysis on the Conformational Preferences of Anticancer Saponin OSW-1. *J. Org. Chem.* **2020**, 85 (2), 339–344.  
<https://doi.org/10.1021/acs.joc.9b02085>.
- (91) Tschamber, T.; Adam, S.; Matsuya, Y.; Masuda, S.; Ohsawa, N.; Maruyama, S.; Kamoshita, K.; Nemoto, H.; Eustache, J. OSW-1 Analogues: Modification of the Carbohydrate Moiety. *Bioorganic Med. Chem. Lett.* **2007**, 17 (18), 5101–5106.  
<https://doi.org/10.1016/j.bmcl.2007.07.017>.
- (92) C Sarma, J.; Borbaruah, M.; N Sarma, D.; C Barua, N.; P Sharma, R. Cleavages of Ethers by Chlorotrimethylsilane and Acetic Anhydride. *Tetrahedron* **1986**, 42 (14), 3999–4006.  
[https://doi.org/10.1016/S0040-4020\(01\)87555-4](https://doi.org/10.1016/S0040-4020(01)87555-4).
- (93) Deutsch, J.; Jang, H. G.; Mansur, N.; Ilovich, O.; Shpolansky, U.; Galili, D.; Feldman, T.; Rosen, H.; Lichtstein, D. 4-(3'α15'β-Dihydroxy-5'β-Estran-17'β-Yl)Furan-2-Methyl Alcohol: An Anti-Digoxin Agent with a Novel Mechanism of Action. *J. Med. Chem.* **2006**, 49 (2), 600–606. <https://doi.org/10.1021/jm0505819>.
- (94) Xu, Y.; Yan, G.; Ren, Z.; Dong, G. Diverse Sp<sup>3</sup> C-H Functionalization through Alcohol β-Sulfonyloxylation. *Nat. Chem.* **2015**, 7 (10), 829–834. <https://doi.org/10.1038/nchem.2326>.
- (95) Yamada, K.; Fujita, H.; Kunishima, M. A Novel Acid-Catalyzed O-Benzylating Reagent with the Smallest Unit of Imidate Structure. *Org. Lett.* **2012**, 14 (19), 5026–5029.  
<https://doi.org/10.1021/ol302222p>.



- (96) Yamada, K.; Fujita, H.; Kitamura, M.; Kunishima, M. A Practical Method for p -Methoxybenzylation of Hydroxy Groups Using 2,4,6-Tris(p-Methoxybenzyloxy)-1,3,5-Triazine (TriBOT-PM). *Synthesis (Stuttg)*. **2013**, *45* (Scheme 2), 2989–2997. <https://doi.org/10.1055/s-0033-1339713>.
- (97) Kunishima, M.; Asao, R.; Yamada, K.; Kitamura, M.; Fujita, H. Development of Acid-Catalyzed Fluorous Benzylating Reagents Based on a Triazinedione Core. *J. Fluor. Chem.* **2016**, *190*, 68–74. <https://doi.org/10.1016/j.jfluchem.2016.09.003>.
- (98) Yamada, K.; Hayakawa, N.; Fujita, H.; Kitamura, M. Development of a Triazine-Based Tert -Butylating Reagent , TriAT- t Bu. **2016**, No. Table 1, 4093–4098. <https://doi.org/10.1002/ejoc.201600663>.
- (99) Yamada, K.; Hayakawa, N.; Fujita, H.; Kitamura, M.; Kunishima, M. Study of O -Allylation Using Triazine-Based Reagents. **2017**, *65* (1), 112–115.
- (100) Yamada, K.; Kota, M.; Takahashi, K.; Fujita, H.; Kitamura, M.; Kunishima, M. Development of Triazinone-Based Condensing Reagents for Amide Formation. *J. Org. Chem.* **2019**, *84* (23), 15042–15051. <https://doi.org/10.1021/acs.joc.9b01261>.
- (101) Houston, T. A.; Tanaka, Y.; Koreeda, M. Stereoselective Construction of 22-Oxygenated Steroid Side Chains by Dimethylaluminum Chloride-Mediated Ene Reactions of Aldehydes. *J. Org. Chem.* **1993**, *58* (16), 4287–4292. <https://doi.org/10.1021/jo00068a024>.
- (102) Fletcher, S. The Mitsunobu Reaction in the 21st Century. *Org. Chem. Front.* **2015**, *2* (6), 739–752. <https://doi.org/10.1039/C5QO00016E>.
- (103) Varasi, M.; Walker, K. A. M. M.; Maddox, M. L. A Revised Mechanism for the Mitsunobu Reaction. *J. Org. Chem.* **1987**, *52* (19), 4235–4238. <https://doi.org/10.1021/jo00228a016>.
- (104) Fukuyama, T.; Jow, C. K.; Cheung, M. 2- and 4-Nitrobenzenesulfonamides: Exceptionally Versatile Means for Preparation of Secondary Amines and Protection of Amines. *Tetrahedron Lett.* **1995**, *36* (36), 6373–6374. [https://doi.org/10.1016/0040-4039\(95\)01316-A](https://doi.org/10.1016/0040-4039(95)01316-A).
- (105) Vidrna, L.; Černý, I.; Pouzar, V.; Borovská, J.; Vyklický, V.; Vyklický, L.; Chodounská, H. Azido Analogs of Neuroactive

Steroids. *Steroids* **2011**, 76 (10–11), 1043–1050.  
<https://doi.org/10.1016/j.steroids.2011.04.008>.

- (106) Mahdi, K. M.; Abdul-Reda, N. A.; Al-Masoudi, N. A. Exploration of New 3 $\alpha$ -Pregnenolone Ester Analogues via Mitsunobu Reaction, Their Anti-HIV Activity and Molecular Modeling Study. *Eur. J. Chem.* **2015**, 6 (1), 1–7. <https://doi.org/10.5155/eurjchem.6.1.1-7.1139>.
- (107) Bordwell, F. G.; Fried, H. E.; Hughes, D. L.; Lynch, T. Y.; Satish, A. V.; Whang, Y. E. Acidities of Carboxamides, Hydroxamic Acids, Carbohydrazides, Benzenesulfonamides, and Benzenesulfonohydrazides in DMSO Solution. *J. Org. Chem.* **1990**, 55 (10), 3330–3336. <https://doi.org/10.1021/jo00297a063>.
- (108) Swamy, K. C. K.; Kumar, N. N. B.; Balaraman, E.; Kumar, K. V. P. Mitsunobu and Related Reactions : Advances and Applications Mitsunobu and Related Reactions : Advances and Applications. *Chem. Rev.* **2009**, No. April, 2551–2651.  
<https://doi.org/10.1021/cr800278z>.
- (109) Hirner, S.; Westmeier, J.; Gebhardt, S.; Müller, C.; von Zezschwitz, P. Convenient Access to Cycloalk-2-Enone-Derived N-Sulfonyl Imines. *Synlett* **2014**, 25 (12), 1697–1700. <https://doi.org/10.1055/s-0034-1378203>.
- (110) Mattson, R. J.; Pham, K. M.; Leuck, D. J.; Cowen, K. A. An Improved Method for Reductive Alkylation of Amines Using Titanium(IV) Isopropoxide and Sodium Cyanoborohydride<sup>1</sup>. *J. Org. Chem.* **1990**, 55 (8), 2552–2554.  
<https://doi.org/10.1021/jo00295a060>.
- (111) Abdel-Magid, A. F.; Carson, K. G.; Harris, B. D.; Maryanoff, C. A.; Shah, R. D. Reductive Amination of Aldehydes and Ketones with Sodium Triacetoxyborohydride. Studies on Direct and Indirect Reductive Amination Procedures<sup>1</sup>. *J. Org. Chem.* **1996**, 61 (11), 3849–3862. <https://doi.org/10.1021/jo960057x>.
- (112) Butts, C. P.; Jones, C. R.; Towers, E. C.; Flynn, J. L.; Appleby, L.; Barron, N. J. Interproton Distance Determinations by NOE - Surprising Accuracy and Precision in a Rigid Organic Molecule. *Org. Biomol. Chem.* **2011**, 9 (1), 177–184.  
<https://doi.org/10.1039/c0ob00479k>.
- (113) Chini, M. G.; Jones, C. R.; Zampella, A.; D'Auria, M. V.; Renga, B.;

- Fiorucci, S.; Butts, C. P.; Bifulco, G. Quantitative NMR-Derived Interproton Distances Combined with Quantum Mechanical Calculations of  $^{13}\text{C}$  Chemical Shifts in the Stereochemical Determination of Conicasterol F, a Nuclear Receptor Ligand from *Theonella Swinhoei*. *J. Org. Chem.* **2012**, *77* (3), 1489–1496. <https://doi.org/10.1021/jo2023763>.
- (114) Gil, R. R.; Navarro-Vázquez, A. Chapter 1. Application of the Nuclear Overhauser Effect to the Structural Elucidation of Natural Products; 2016; pp 1–38. <https://doi.org/10.1039/9781849734684-00001>.
- (115) Jones, C. R.; Butts, C. P.; Harvey, J. N. Accuracy in Determining Interproton Distances Using Nuclear Overhauser Effect Data from a Flexible Molecule. *Beilstein J. Org. Chem.* **2011**, *7*, 145–150. <https://doi.org/10.3762/bjoc.7.20>.
- (116) Butts, C. P.; Jones, C. R.; Song, Z.; Simpson, T. J. Accurate NOE-Distance Determination Enables the Stereochemical Assignment of a Flexible Molecule - Arugosin C. *Chem. Commun.* **2012**, *48* (72), 9023–9025. <https://doi.org/10.1039/c2cc32144k>.
- (117) Di Micco, S.; Zampella, A.; D'Auria, M. V.; Festa, C.; De Marino, S.; Riccio, R.; Butts, C. P.; Bifulco, G. Plakilactones G and H from a Marine Sponge. Stereochemical Determination of Highly Flexible Systems by Quantitative NMR-Derived Interproton Distances Combined with Quantum Mechanical Calculations of  $^{13}\text{C}$  Chemical Shifts. *Beilstein J. Org. Chem.* **2013**, *9*, 2940–2949. <https://doi.org/10.3762/bjoc.9.331>.
- (118) Bame, J.; Hoeck, C.; Carrington, M. J.; Butts, C. P.; Jäger, C. M.; Croft, A. K. Improved NOE Fitting for Flexible Molecules Based on Molecular Mechanics Data—a Case Study with: S - Adenosylmethionine. *Phys. Chem. Chem. Phys.* **2018**, *20* (11), 7523–7531. <https://doi.org/10.1039/c7cp07265a>.
- (119) Dimakos, V.; Taylor, M. S. Site-Selective Functionalization of Hydroxyl Groups in Carbohydrate Derivatives. **2018**. <https://doi.org/10.1021/acs.chemrev.8b00442>.
- (120) Reich, H. J. (University of W. The University of Wisconsin NMR Database, C-13 Chemical Shifts of Common Sugars <https://www.chem.wisc.edu/areas/reich/chem605/index.htm>.
- (121) Guisado, C.; Waterhouse, J. E.; Price, W. S.; Jorgensen, R.; Miller,

- A. D. The Facile Preparation of Primary and Secondary Amines. *Society* **2005**, 1049–1057.
- (122) Birudukota, N.; Mudgal, M. M.; Shanbhag, V. Discovery and Development of Azasteroids as Anticancer Agents. *Steroids* **2019**, *152* (September 2018), 108505. <https://doi.org/10.1016/j.steroids.2019.108505>.
- (123) Martin-Smith, M.; Alauddin, M. Biological Activity in Steroids Possessing Nitrogen Atoms; Part I. Synthetic Nitrogenous Steroids. *Int. J. Canada's J. Glob. Policy Anal.* **1962**, *13* (1), 325–349. <https://doi.org/10.1177/002070205801300106>.
- (124) Martin-Smith, M.; Alauddin, M. Biological Activity in Steroids Possessing Nitrogen Atoms; Part II: Steroidal Alkaloids. *SciFed J. Immunol.* **1962**, *1* (1), 469–495. <https://doi.org/10.23959/sfji-1000003>.
- (125) Petermichl, M.; Loscher, S.; Schobert, R. Total Synthesis of Aurantoside G, an N- $\beta$ -Glycosylated 3-Oligoenoyltetramic Acid from *Theonella Swinhoei*. *Angew. Chemie - Int. Ed.* **2016**, *55* (34), 10122–10125. <https://doi.org/10.1002/anie.201604912>.
- (126) Angawi, R. F.; Bavestrello, G.; Calcinai, B.; Dien, H. A.; Donnarumma, G.; Tufano, M. A.; Paoletti, I.; Grimaldi, E.; Chianese, G.; Fattorusso, E.; et al. Aurantoside J: A New Tetramic Acid Glycoside from *Theonella Swinhoei*. Insights into the Antifungal Potential of Aurantosides. *Mar. Drugs* **2011**, *9* (12), 2809–2817. <https://doi.org/10.3390/md9122809>.
- (127) Wu, Y.; Wu, R. W. K.; Cheu, K. W.; Williams, I. D.; Krishna, S.; Slavic, K.; Gravett, A. M.; Liu, W. M.; Wong, H. N.; Haynes, R. K. Methylene Homologues of Artemisone: An Unexpected Structure–Activity Relationship and a Possible Implication for the Design of C10-Substituted Artemisinins. *ChemMedChem* **2016**, *11* (13), 1469–1479. <https://doi.org/10.1002/cmdc.201600011>.
- (128) Li, L.; Chang, K. C.; Zhou, Y.; Shieh, B.; Ponder, J.; Abraham, A. D.; Ali, H.; Snow, A.; Petrash, J. M.; Labarbera, D. V. Design of an Amide N-Glycoside Derivative of  $\beta$ -Glucogallin: A Stable, Potent, and Specific Inhibitor of Aldose Reductase. *J. Med. Chem.* **2014**, *57* (1), 71–77. <https://doi.org/10.1021/jm401311d>.
- (129) Abd El-Gaber, M. K.; Yasuda, S.; Iida, E.; Mukai, C. Enantioselective Total Synthesis of (+)-Sieboldine A. *Org. Lett.*

- 2017, *19* (2), 320–323. <https://doi.org/10.1021/acs.orglett.6b03416>.
- (130) El-Sayed, W. A.; Abbas, H. A. S.; Abdel Mageid, R. E.; Magdziarz, T. Synthesis, Antimicrobial Activity and Docking Studies of New N-Ethyl-3-Indolyl Heterocycles. *Med. Chem. Res.* **2016**, *25* (2), 339–355. <https://doi.org/10.1007/s00044-015-1488-4>.
- (131) El-Ebiary, N. M.; Swellem, R. H.; Nawwar, G. A. M. Design, Synthesis and Anticancer Activity of Aza Heterocycles Containing Gallate Moiety (Part III). *Pharm. Chem. J.* **2017**, *51* (1), 39–48. <https://doi.org/10.1007/s11094-017-1554-y>.
- (132) Shubina, L. K.; Makarieva, T. N.; Yashunsky, D. V.; Nifantiev, N. E.; Denisenko, V. A.; Dmitrenok, P. S.; Dyshlovoy, S. A.; Fedorov, S. N.; Krasokhin, V. B.; Jeong, S. H.; et al. Pyridine Nucleosides Neopetrosides A and B from a Marine Neopetrosia Sp. Sponge. Synthesis of Neopetroside A and Its  $\beta$ -Riboside Analogue. *J. Nat. Prod.* **2015**, *78* (6), 1383–1389. <https://doi.org/10.1021/acs.jnatprod.5b00256>.
- (133) Gervay, J.; Hadd, M. J. Anionic Additions to Glycosyl Iodides: Highly Stereoselective Syntheses of C-, N-, and O-Glycosides 1. **1997**. <https://doi.org/10.1021/jo970922t>.
- (134) Belkhadem, F.; Othman, A. A. Synthesis and Antibacterial Evaluation of New N- and S-Glycosides Analogues with Dinitrophenyl-Substituted Heterocyclic Bases. *Mol. Divers.* **2017**, *21* (1), 115–124. <https://doi.org/10.1007/s11030-016-9704-9>.
- (135) Li, B.; Zhang, B.; Zhang, X.; Fan, X. Synthesis of 3 - Cyano - 1 H - Indoles and Their 2' -Deoxyribonucleoside Derivatives through One-Pot Cascade Reactions. **2016**, 3–11. <https://doi.org/10.1021/acs.joc.6b01612>.
- (136) Fukuyama, T.; Cheung, M.; Jow, C. K.; Hidai, Y.; Kan, T. 2,4-Dinitrobenzenesulfonamides: A Simple and Practical Method for the Preparation of a Variety of Secondary Amines and Diamines. *Tetrahedron Lett.* **1997**, *38* (33), 5831–5834. [https://doi.org/10.1016/S0040-4039\(97\)01334-8](https://doi.org/10.1016/S0040-4039(97)01334-8).
- (137) Kan, T.; Fukuyama, T. Ns Strategies: A Highly Versatile Synthetic Method for Amines. *Chem. Commun.* **2004**, *4* (4), 353–359. <https://doi.org/10.1039/b311203a>.
- (138) Bordwell, F. G.; Harrelson, J. A.; Lynch, T. Y. Homolytic Bond Dissociation Energies for the Cleavage of .Alpha.-Nitrogen-

Hydrogen Bonds in Carboxamides, Sulfonamides, and Their Derivatives. The Question of Synergism in Nitrogen-Centered Radicals. *J. Org. Chem.* **1990**, *55* (10), 3337–3341. <https://doi.org/10.1021/jo00297a064>.

- (139) Evans. PKa\_table. 1–6. <https://doi.org/10.1098/rspa.2005.1600>.
- (140) Cody, V.; Duax, W. L.; Yasuda, K.; Osawa, Y.; Norton, D. A. Steroid Conformations in Solid and Solution. *Tetrahedron* **1972**, *28* (23), 5683–5687. [https://doi.org/10.1016/S0040-4020\(01\)88912-2](https://doi.org/10.1016/S0040-4020(01)88912-2).
- (141) Jacobs, H. J. C.; Havinga, E. Cotton Effects and Conformations of Skeletally Isomeric Saturated 3-Oxo-Steroids. *Tetrahedron* **1972**, *28* (1), 135–153. [https://doi.org/10.1016/0040-4020\(72\)80063-2](https://doi.org/10.1016/0040-4020(72)80063-2).
- (142) Fishman, J. Bromination of 16-Keto Steroids. Conformation of Ring D. *J. Org. Chem.* **1962**, *27* (5), 1745–1749. <https://doi.org/10.1021/jo01052a061>.
- (143) Houston, T. A.; Tanaka, Y.; Koreeda, M. Stereoselective Construction of 22-Oxygenated Steroid Side-Chains by Dimethylaluminum Chloride-Mediated Ene Reactions of Aldehydes. *J. Org. Chem.* **1993**, *58* (16), 4287–4292. <https://doi.org/Doi.10.1021/Jo00068a024>.
- (144) Wang, Z. Organic Name Reactions and Reagents-Schmidt Glycosylation. *John Wiley Sons, Inc.* **2010**, 2498–2502.
- (145) Tsunoda, T.; Kaku, H.; Itô, S. New Mitsunobu Reagents. *Tcimail* **2005**, *123* (123), 1–10.
- (146) Still, W. C.; Kahn, M.; Mitra, A. Rapid Chromatographic Technique for Preparative Separations with Moderate Resolution. *J. Org. Chem.* **1978**, *43* (14), 2923–2925. <https://doi.org/10.1021/jo00408a041>.
- (147) Tate, D. J.; Anémian, R.; Bushby, R. J.; Nanan, S.; Warriner, S. L.; Whitaker, B. J. Improved Syntheses of High Hole Mobility Phthalocyanines: A Case of Steric Assistance in the Cyclo-Oligomerisation of Phthalonitriles. *Beilstein J. Org. Chem.* **2012**, *8*, 120–128. <https://doi.org/10.3762/bjoc.8.14>.
- (148) Schmidt, Y.; Breit, B. Stereoselective Synthesis of Trisubstituted Olefins by a Directed Allylic Substitution Strategy. *Chem. - A Eur. J.* **2011**, *17* (42), 11780–11788. <https://doi.org/10.1002/chem.201100843>.
- (149) Byrne, P. A.; Gilheany, D. G. Unequivocal Experimental Evidence

for a Unified Lithium Salt-Free Wittig Reaction Mechanism for All Phosphonium Ylide Types: Reactions with  $\beta$ -Heteroatom-Substituted Aldehydes Are Consistently Selective for Cis-Oxaphosphetane-Derived Products. *J. Am. Chem. Soc.* **2012**, *134* (22), 9225–9239. <https://doi.org/10.1021/ja300943z>.

- (150) Mo, X.; Morgan, T. D. R.; Ang, H. T.; Hall, D. G. Scope and Mechanism of a True Organocatalytic Beckmann Rearrangement with a Boronic Acid/Perfluoropinacol System under Ambient Conditions. *J. Am. Chem. Soc.* **2018**, *140* (15), 5264–5271. <https://doi.org/10.1021/jacs.8b01618>.
- (151) Milan, M.; Bietti, M.; Costas, M. Highly Enantioselective Oxidation of Nonactivated Aliphatic C-H Bonds with Hydrogen Peroxide Catalyzed by Manganese Complexes. *ACS Cent. Sci.* **2017**, *3* (3), 196–204. <https://doi.org/10.1021/acscentsci.6b00368>.
- (152) Yang, Q.; Liu, Y.; Zhang, W. A Theoretical Study of Imine-Ene Reaction Influencing Factors. *Org. Biomol. Chem.* **2011**, *9* (18), 6343–6351. <https://doi.org/10.1039/c1ob05493g>.
- (153) Burbiel, J.; Bracher, F. Azasteroids as Antifungals. *Steroids* **2003**, *68* (7–8), 587–594. [https://doi.org/10.1016/S0039-128X\(03\)00080-1](https://doi.org/10.1016/S0039-128X(03)00080-1).
- (154) Scheer, I.; Thompson, M. J.; Mosbttig, E. C-22 Isomeric Dihydrosapogenins from Kryptogenin. *J. Am. Chem. Soc.* **1957**, *79* (12), 3218–3222. <https://doi.org/10.1021/ja01569a060>.
- (155) Atencio, R.; Visbal, G.; Pekerar, S.; Papale, J.; Urbina, J. A. Studies of Molecular Structure Parameters of 20-Piperidin-2-Yl-5 $\alpha$ -Pregnan-3 $\beta$ ,20-Diol and Its N-Methyl Derivative: Two Inhibitors of  $\Delta$ 24(24) Sterol Methyl Transferase and  $\Delta$ 24(24') Sterol Methyl Reductase of *Trypanosoma Cruzi*. *Acta Crystallogr. Sect. B Struct. Sci.* **2001**, *57* (5), 714–721. <https://doi.org/10.1107/S0108768101013234>.
- (156) Saha, P.; Saikia, A. K. Ene Cyclization Reaction in Heterocycle Synthesis. *Org. Biomol. Chem.* **2018**, *16* (16), 2820–2840. <https://doi.org/10.1039/C8OB00429C>.
- (157) Hack, D.; Blü Mel, M.; Chauhan, P.; Philipps, A. R.; Enders, D. Catalytic Conia-Ene and Related Reactions. *Chem. Soc. Rev.* **2015**, *44* (44), 6059–6093. <https://doi.org/10.1039/c5cs00097a>.
- (158) Snider, B. B. Lewis-Acid Catalyzed Ene Reactions. *Acc. Chem. Res.* **1980**, *13* (11), 426–432. <https://doi.org/10.1021/ar50155a007>.
- (159) Yamabe, S.; Fukuda, T.; Yamazaki, S. A New Intermediate in the

- Prins Reaction. *Beilstein J. Org. Chem.* **2013**, *9*, 476–485.  
<https://doi.org/10.3762/bjoc.9.51>.
- (160) Alder, R. W.; Carta, F.; Reed, C. A.; Stoyanova, I.; Willis, C. L. Searching for Intermediates in Prins Cyclisations: The 2-Oxa-5-Adamantyl Carbocation. *Org. Biomol. Chem.* **2010**, *8* (7), 1551.  
<https://doi.org/10.1039/b921957a>.
- (161) Kočovský, P.; Ahmed, G.; Šrogl, J.; Malkov, A. V.; Steele, J. New Lewis-Acidic Molybdenum(II) and Tungsten(II) Catalysts for Intramolecular Carbonyl Ene and Prins Reactions. Reversal of the Stereoselectivity of Cyclization of Citronellal. *J. Org. Chem.* **1999**, *64* (8), 2765–2775. <https://doi.org/10.1021/jo9821675>.
- (162) E. J. Corey, K. C. N. *Comprehensive Organic Name Reactions and Reagents*; 2010. <https://doi.org/10.1002/9780470638859>.
- (163) Pearson, R. G. Hard and Soft Acids and Bases—the Evolution of a Chemical Concept. *Coord. Chem. Rev.* **1990**, *100* (C), 403–425.  
[https://doi.org/10.1016/0010-8545\(90\)85016-L](https://doi.org/10.1016/0010-8545(90)85016-L).
- (164) Chattaraj, P. K.; Sarkar, U.; Roy, D. R. Electrophilicity Index. *Chem. Rev.* **2006**, *106* (6), 2065–2091. <https://doi.org/10.1021/cr040109f>.
- (165) Naredla, R. R.; Klumpp, D. A. Contemporary Carbocation Chemistry: Applications in Organic Synthesis. *Chem. Rev.* **2013**, *113* (9), 6905–6948. <https://doi.org/10.1021/cr4001385>.
- (166) Jasti, R.; Rychnovsky, S. D. Racemization in Prins Cyclization Reactions. *J. Am. Chem. Soc.* **2006**, *128* (41), 13640–13648.  
<https://doi.org/10.1021/ja064783l>.
- (167) Cheng, X.; Xia, Y.; Wei, H.; Xu, B.; Zhang, C.; Li, Y.; Qian, G.; Zhang, X.; Li, K.; Li, W. Lewis Acid Catalyzed Intermolecular Olefin Hydroamination: Scope, Limitation, and Mechanism. *European J. Org. Chem.* **2008**, *2008* (11), 1929–1936.  
<https://doi.org/10.1002/ejoc.200701080>.
- (168) Colonna, P.; Bezenine, S.; Gil, R.; Hannedouche, J. Alkene Hydroamination via Earth-Abundant Transition Metal (Iron, Cobalt, Copper and Zinc) Catalysis: A Mechanistic Overview. *Adv. Synth. Catal.* **2020**, adsc.201901157.  
<https://doi.org/10.1002/adsc.201901157>.
- (169) Fan, R.; Pu, D.; Wen, F.; Ye, Y.; Wang, X. A Facile Synthesis of N -Sulfonyl and N -Sulfinyl Aldimines under Barbier-Type Conditions. *J. Org. Chem.* **2008**, *73* (9), 3623–3625.



<https://doi.org/10.1021/jo800009t>.

- (170) Chemla, F.; Hebbe, V.; Normant, J.-F. An Easy Synthesis of Aliphatic and Aromatic N-Sulfonyl Aldimines. *Synthesis (Stuttg)*. **2000**, *2000* (01), 75–77. <https://doi.org/10.1055/s-2000-6232>.
- (171) Subba Reddy, B. V.; Nair, P. N.; Antony, A.; Lalli, C.; Grée, R. The Aza-Prins Reaction in the Synthesis of Natural Products and Analogues. *European J. Org. Chem.* **2017**, *2017* (14), 1805–1819. <https://doi.org/10.1002/ejoc.201601411>.
- (172) Dobbs, A. P.; Guesné, S. J. J.; Parker, R. J.; Skidmore, J.; Stephenson, R. A.; Hursthouse, M. B. A Detailed Investigation of the Aza-Prins Reaction. *Org. Biomol. Chem.* **2010**, *8* (5), 1064. <https://doi.org/10.1039/b915797b>.
- (173) Bondalapati, S.; Indukuri, K.; Ghosh, P.; Saikia, A. K. Stereoselective Synthesis of Tetrahydroquinolines through an Imino-Ene Cyclization Reaction. *European J. Org. Chem.* **2013**, No. 5, 952–956. <https://doi.org/10.1002/ejoc.201201363>.
- (174) Zhao, E.; Zhou, F.; Zhao, Y. Lewis Acids Promoted 3 + 2 Cycloaddition of Oxaziridines and Cyclic Allylic Alcohols through Carbonyl Imine Intermediates. *J. Org. Chem.* **2019**, *84* (7), 4282–4293. <https://doi.org/10.1021/acs.joc.9b00246>.
- (175) Yamago, S. [3+2] Cycloaddition of Trimethylenemethane and Its Synthetic Equivalents. 2002.
- (176) Dobbs, A. P.; Guesné, S. J. J.; Hursthouse, M. B.; Coles, S. J. The Aza-Silyl-Prins Reaction: A Novel Method for the Synthesis of Trans-2,6-Tetrahydropyridines. *Synlett* **2003**, No. 11, 1740–1742. <https://doi.org/10.1055/s-2003-41434>.
- (177) Yamanaka, M.; Nishida, A.; Nakagawa, M. Imino Ene Reaction Catalyzed by Ytterbium(III) Triflate and TMSCl or TMSOTf. *J. Org. Chem.* **2003**, *68* (8), 3112–3120. <https://doi.org/10.1021/jo0268153>.
- (178) Kandutsch, A. A.; Thompson, E. B. Cytosolic Proteins That Bind Oxygenated Sterols. Cellular Distribution, Specificity, and Some Properties. *J. Biol. Chem.* **1980**, *255* (22), 10813–10821.
- (179) Taylor, F. R.; Kandutsch, A. A. Oxysterol Binding Protein. *Chem. Phys. Lipids* **1985**, *38* (1–2), 187–194. [https://doi.org/10.1016/0009-3084\(85\)90066-0](https://doi.org/10.1016/0009-3084(85)90066-0).
- (180) Bauer, L.; Lyoo, H.; van der Schaar, H. M.; Strating, J. R.; van

- Kuppeveld, F. J. Direct-Acting Antivirals and Host-Targeting Strategies to Combat Enterovirus Infections. *Curr. Opin. Virol.* **2017**, *24*, 1–8. <https://doi.org/10.1016/j.coviro.2017.03.009>.
- (181) Eckert, T. S. An Improved Preparation of a Grignard Reagent. *J. Chem. Educ.* **1987**, *64* (2), 179. <https://doi.org/10.1021/ed064p179>.
- (182) Lao, K.; Sun, J.; Wang, C.; Wang, Y.; You, Q.; Xiao, H.; Xiang, H. Design, Synthesis and Biological Evaluation of Novel 3-Oxo-4-Oxa-5 $\alpha$ -Androst-17 $\beta$ -Amide Derivatives as Dual 5 $\alpha$ -Reductase Inhibitors and Androgen Receptor Antagonists. *Bioorg. Med. Chem. Lett.* **2017**, *27* (17), 4212–4217. <https://doi.org/10.1016/j.bmcl.2017.05.078>.
- (183) Nedelcu, D.; Liu, J.; Xu, Y.; Jao, C.; Salic, A. Oxysterol Binding to the Extracellular Domain of Smoothed in Hedgehog Signaling. *Nat. Chem. Biol.* / **2013**, *9*. <https://doi.org/10.1038/nChEMBio.1290>.
- (184) De Palma, A. M.; Thibaut, H. J.; Van Der Linden, L.; Lanke, K.; Heggermont, W.; Ireland, S.; Andrews, R.; Arimilli, M.; Al-Tel, T. H.; De Clercq, E.; et al. Mutations in the Nonstructural Protein 3A Confer Resistance to the Novel Enterovirus Replication Inhibitor TTP-8307. *Antimicrob. Agents Chemother.* **2009**, *53* (5), 1850–1857. <https://doi.org/10.1128/AAC.00934-08>.
- (185) van der Schaar, H. M.; Leyssen, P.; Thibaut, H. J.; de Palma, A.; van der Linden, L.; Lanke, K. H. W.; Lacroix, C.; Verbeken, E.; Conrath, K.; MacLeod, A. M.; et al. A Novel, Broad-Spectrum Inhibitor of Enterovirus Replication That Targets Host Cell Factor Phosphatidylinositol 4-Kinase III $\beta$ . *Antimicrob. Agents Chemother.* **2013**, *57* (10), 4971–4981. <https://doi.org/10.1128/AAC.01175-13>.
- (186) Pavel, H.; Martin, G.; Jan, H.; Antonin, L. The Study of Cyclization of N-Acylphenacyl Anthranilates with Ammonium Salts under Various Conditions. *Heterocycles* **2007**, *71* (2), 269–280.
- (187) Kr, D.; Artemov, V. US 2012/0184582 A1. **2012**, *1* (19).
- (188) Huang, W.; Pei, J.; Chen, B.; Pei, W.; Ye, X. A Novel Improved Procedure for the Synthesis of Oxazoles. *Tetrahedron* **1996**, *52* (30), 10131–10136. [https://doi.org/10.1016/0040-4020\(96\)00552-2](https://doi.org/10.1016/0040-4020(96)00552-2).
- (189) Bertram, A.; Maulucci, N.; New, O. M.; Mohd Nor, S. M.; Pattenden, G. Synthesis of Libraries of Thiazole, Oxazole and Imidazole-Based Cyclic Peptides from Azole-Based Amino Acids. A New Synthetic Approach to Bistratamides and Didmolamides. *Org. Biomol. Chem.* **2007**, *5* (10), 1541–1553.

<https://doi.org/10.1039/b701999h>.

- (190) Hwang, H. I.; Hartman, T. G.; Ho, C. T. Relative Reactivities of Amino Acids in the Formation of Pyridines, Pyrroles, and Oxazoles. *J. Agric. Food Chem.* **1995**, *43* (11), 2917–2921.  
<https://doi.org/10.1021/jf00059a027>.
- (191) Reich, H. J. (University of W. University of Wisconsin NMR Database, JC-H Aromatic heterocycles  
<https://www.chem.wisc.edu/areas/reich/nmr/c13-data/c-coupling.htm>.
- (192) Pachler, K. G. R.; Pachter, R.; Wessels, P. L. Carbon-13  $\square$ proton Coupling Constants in N-substituted Imidazoles. A  $^{13}\text{C}$  NMR Study and MO Calculations. *Org. Magn. Reson.* **1981**, *17* (4), 278–284.  
<https://doi.org/10.1002/mrc.1270170411>.

## Vitae

Cori Alan Malinky was born on the morning of March 11<sup>th</sup>, 1990. Cori and his older sister, Bobbie, were raised together by their mother, Barbara Bowman, in the small town of Madison, Ohio. His mother managed a local restaurant and his father, Norman Malinky, was a drywaller by trade. When he turned 18, Cori enlisted in the Ohio Army National Guard and served in the 135<sup>th</sup> Military Police Company, 2<sup>nd</sup> platoon for seven years. For the first four years of his enlistment, Cori simultaneously earned a Bachelor of Science degree in chemistry from Miami University of Oxford, Ohio. As a first-generation scholar, Cori found guidance and friendship from the Dean of Libraries, Jerome Conley, whom continued to mentor Cori throughout his adult life. In the last year of his enlistment, Cori lost a close friend to suicide which inspired him to continue his education at the graduate level in pursuit of proactive diagnostic tests, treatment, and fundamental understanding of depression. Cori matriculated to the University of Oklahoma, where he has been investigating pharmacologically active compounds under the guidance of Dr. Anthony Burgett. Upon graduation, Cori will begin his post-doctoral position at the Vanderbilt Center for Neurotherapeutic Drug Discovery (VCNDD).

*The ruck march is the great equalizer. The pace or distance do not matter; all that is necessary is having the fortitude to push beyond perceived limitations.*

© Copyright by CORI MALINKY, 2020  
All Rights Reserved.